1991

Enhancement Of Gas-liquid And Particle-liquid Mass Transfer In Bubble Columns And Three-phase Fluidized Beds

Anand Prakash

ENHANCEMENT OF GAS-LIQUID AND PARTICLE-LIQUID MASS TRANSFER IN BUBBLE COLUMNS AND THREE-PHASE FLUIDIZED BEDS

Volume-1

by

Anand Prakash

Faculty of Engineering Science

Department of Chemical and Biochemical Engineering

A thesis submitted in partial fulfilment of
the requirements for the degree of
Doctor of Philosophy

Faculty of Graduate Studies
The University of Western Ontario
London, Ontario
March 1991

ISBN 0-315-66335-9

ABSTRACT

Mass transfer is an important consideration in the design of multiphase contactors. While gas-liquid mass transfer is important for two-phase contactors, both gas-liquid and liquid-solid mass transfer need to be considered for the design three-phase contactors. Many industrial processes such as coal liquefaction, petrochemical, waste water treatment or fermentation processes involve gas absorption in a liquid with or without the presence of inert or catalyst solid particles. When mass transfer is the rate limiting step, the overall rate can be improved by enhancing the rate of mass transfer. This study investigated gas-liquid and liquid-solid mass transfer in bubble columns and three-phase fluidized beds using different types of distributors and coalescence inhibitors. A systematic study was conducted to investigate the effects of molecular structure of various types of coalescence inhibitors. Hydrodynamic parameters such as phase holdups, liquid mixing and flow regimes were also determined. Available literature correlations were tested and their limitations were pointed out. Suitable new correlations were developed based on the data of this study.

ACKNOWLEDGEMENTS

Research can be both frustrating and enlightening experience. The research team of Prof. C.L. Briens and Prof. M.A. Bergougnou at UWO provided me with the opportunity to conduct my research program with fewer frustations. I am thankful to Prof. C.L. Briens for his constructive suggestions, criticisms and guidance during this work. I am also thankful to Prof. Bergougnou for his helpful suggestions and criticisms. He was a constant source of encouragement.

The Ontario Graduate Scholarship awards, awarded to me during the course of my study are gratefully acknowledged.

The financial supports of the National Sciences and Engineering Council of Canada and Imperial Oil Company are also acknowledged gratefully.

I am grateful to Dr. Kosaric for lending the UV spectrophotometer.

I would like to express my sincere appreciation for the staff of the mechanical shop and to Mr. Afara for their co-operation.

My thanks are also due to the graduate students in the department, who provided the necessary break through the ordeal.

Lastly I wish to thank my wife for her patience during my endeavor to complete this work.

TABLE OF CONTENTS

Volume-1

TABLE OF CONTENTS (Cont'd)

TABLE OF CONTENTS (Cont'd)

TABLE OF CONTENTS (Cont'd)

TABLE OF CONTENTS (Cont'd)

TABLE OF CONTENTS (Cont'd)

TABLE OF CONTENTS (Cont'd)

TABLE OF CONTENTS (Cont'd)

TABLE OF CONTENTS (Cont'd)

TABLE OF CONTENTS (Cont'd)

TABLE OF CONTENTS (Cont'd)

TABLE OF CONTENTS (Cont'd)

TABLE OF CONTENTS (Cont'd)

LIST OF TABLES

LIST OF TABLES (Cont'd)

LIST OF FIGURES

LIST OF FIGURES (Cont'd)

Page

LIST OF FIGURES (Cont'd)

LIST OF FIGURES (Cont'd)

LIST OF APPENDICES

LIST OF APPENDICES (Cont'd)

NOMENCLATURE

a	gas-liquid interfacial area per unit volume (m^2/m^3)
a_1, b_1, c_1	coefficients in Equations 2.3.38 and 2.3.39
a_2, b_2	coefficients in Equation 2.3.42
a_{m1}	activity of component 1
a_s	particle-liquid interfacial area per unit volume (m-1)
A	total interfacial area for mass transfer (m^2)
A_1, A_2	coefficients in Equation 3.1.24
A_c	column cross-sectional area (m^2)
A_s	total interfacial area for particle-liquid mass Transfer (m2)
C	carbon number in alcohol molecules
C_1	coefficient in Equation 2.2.7
C_2	coefficient in Equation 2.2.19
C_4, C_5	constants in Equation 2.3.1
C_6	a coefficient in Equation 2.3.57
C_7	a coefficient in Equation 2.3.60
C_8	a coefficient in Equation 4.2.11
C_{Ab}	solute concentration in the bulk of liquid (moles/ m3).
C_A^*	solubility of solute in the liquid ($moles/m^3$)
C_{Ai}	solute concentration at the interface ($moles/M^3$)
C_c	concentration of carbon dioxide in the liquid phase (moles/m3)
C_{cat}	concentration of the catalyst (kg/m^3)
C_{cb}	bulk concentration of carbon dioxide in the liquid phase (moles/m3)

c_c^* solubility of carbon dioxide in the liquid phase (moles/m3)

c_{hi} concentration of hydroxyl ions in the liquid film (moles/m3)

c_{ho} initial bulk concentration of hydroxyl ions (moles/m3)

c_{hb} concentration of hydroxyl ions in the bulk of liquid (moles/m3)

c_m $\dfrac{2a_{m1}}{RT}\dfrac{d\sigma}{da_{m1}}\dfrac{d\sigma}{dC_{nb}}\dfrac{1}{1+(x_{m1}/x_{m2})(V_{m1}/V_{m2})}$

c_{nb} bulk concentration of liquid in the liquid phase (moles/m3)

c_o^- oxygen concentration in the liquid flowing into column (moles/m3)

c_o^+ oxygen concentration in the liquid elements above column inlet (moles/m3)

c_o oxygen concentration in the liquid (moles/m^3)

c_o^* solubility of oxygen in the liquid (moles/m^3)

c_{o1} inlet oxygen concentration in the liquid (moles/m3)

c_{o2} outlet oxygen concentration in the liquid (moles/m3)

c_{pl} specific heat of liquid (J/kg .K)

c_{or} oxygen concentration in liquid at a given radial location (moles/m3)

c_{oc} oxygen concentration in liquid at the column centre (moles/m_3)

c_s bulk concentration of the dissolving solute (moles/m3)

c_{s1} dissolving solute concentration at bed inlet (moles/m3)

c_{s2} dissolving solute concentration at bed outlet (moles/m3)

c_s^* solubility of the dissolving solute in the liquid (moles/m3)

C_t	tracer concentration in the liquid phase (moles/m3)
C_{to}	tracer concentration at the column exit (moles/m^3)
C_z	radial distribution parameter defined by Zuber and Findley; Equation 2.2.3a
d_{bo}	bubble size in the distributor region (m)
d_c	diameter of pore (m)
d_e	equivalent particle diameter (m)
d_m	thickness of monolayer (A)
d_o	diameter of sparger hole (m).
d_p	particle diameter (m)
d_{vs}	sauter mean bubble diameter (m).
D_A	diffusion coefficient for component A (m^2/s)
D_c	column diameter (m)
D_d	diameter of porous plate (m)
D_{co}	diffusivity of carbon dioxide in the liquid phase (m2/s)
D_l	liquid phase diffusity (m^2/s)
D_l'	local liquid phase diffusivity (m^2/s)
D_o	diffusivity of oxygen in the liquid phase (m^2/s)
D_{oh}	diffusivity of hydroxyl ion in water (m^2/s)
D_r	liquid phase radial dispersion coefficient (m^2/s)
D_z	liquid phase axial dispersion coefficient (m^2/s)
D_θ	liquid phase angular dispersion coefficient (m^2/s)
E	local energy dissipation rate (W/kg)
E_a	asymptotic value of the enhancement factor at infinite reaction rate
E_g, E_l	energy dissipation in gas and liquid streams (W)
E_i	energy input rate (W)

E_n enhancement factor for mass transfer with chemical reaction

E_t total energy dissipation in the bed (W)

f_o fraction of distributor pores which are active

f_1 coefficient in correlation of Akita and Yoshida (1973); Table 2.2.1

f_2 coefficient in correlation of Hikita et al. (1980)

F_c absorption rate of carbon dioxide in the liquid phase (moles/m3.s).

g acceleration due to gravity (m/ s^2)

h heat transfer coefficient (W/m^2 . K)

h_2 heat transfer coefficient in liquid-solid systems(W/m2.K)

h_3 heat transfer coefficient in three-phase systems (W/m2.K)

h_f film thickness between two touching bubbles (m)

h_w apparent wall heat transfer coefficient (W/m^2.K)

Δh manometer reading (m)

ΔH height between a pressure tap and zero manometer reading (m)

H_b effective bed height (m)

H_c column height (m)

H_{do} initial gas-liquid dispersion height at t=0.0 (m)

H_{d1} gas-liquid dispersion height as shown in Figure 3.1.5 (m)

H_{d2} gas-liquid dispersion height at the end of large bubbles disengagement (m)

H_{d3} dispersion height which accounts for the disengagement of small bubbles (m); Equation 3.1.46

$(dH_d/dt)_{1,s}$ drop in dispersion height which is due to disengagement of small bubbles during period 1 (Figure 3.1.5)

$(dH_d/dt)_2$ drop in dispersion height in period 2 (Figure 3.1.5)

H_d height of gas-liquid dispersion in a batch bubble column (m)

H_{ec} Henery's law constant for carbon dioxide in aqueous solution (pa.m3/moles)

H_{eo} Henery's law constant for oxygen in aqueous solution (pa.m3/moles).

H_L height of liquid in bubble column with no gas flow (m)

H_m Hamakar constant (J)

H_o static bed height (m)

H_G liquid level in column after gas escape (m)

I' light intensity received in the presence of the bubbles.

I_o light intensity received in the absence of the bubbles.

j as defined in equation 3.1.10a

k_b ratio of wake volume to bubble volume

k' relative wake holdup for single bubble

K_f a constant in Equation 5.2.15

k_l liquid film mass transfer coefficient for gas liquid mass transfer (m/s)

k_m $(12\pi\sigma/H_m r_b)^{1/3}$

k_r second order reaction rate constant (m^3/moles.s)

k_r' first order reaction rate constant (s_{-1})

k_s liquid-solid mass transfer coefficient (m/s)

k_{s2} liquid-solid mass transfer coefficient in two phase fluidized bed (m/s)

k_{s3} liquid-solid mass transfer coefficient in three phase fluidized beds (m/s)

$k_l a$ volumetric mass transfer coefficient for gas-liquid mass transfer (s-1)

$(k_l a)_c$ volumetric mass transfer coefficient for carbon dioxide (s-1)

$(k_l a)_d$ volumetric mass transfer coefficient based on axial dispersion model (s-1)

$(k_l a)_o$ volumetric mass transfer coefficient for oxygen (s-1)

K constant in Equation 2.2.20

L length (m)

l_l thermal conductivity of liquid (W/m.K)

l_o path length for light transmission (m)

Δl average centre to centre distance between neighbouring pores on a porous plate (m)

m exponent in Equation 2.2.7

m' exponent in Equation 5.2.15

m1,m2 coefficients in Equation 3.1.24

m3,m4 exponents in Equation 4.2.11

M_s molecular weight of dissolving solute

n exponent in the Richrdson-Zaki equation

n1 exponent in the correlation by Griffith and Wallis (1961); Table 2.2.2

n2 exponent in the correlation by Kara et al. (1981); Table 2.2.2

n3 exponent in equation 2.2.19

n4 a correction factor; Equation 2.3.16a

n5 exponent in Equation 2.3.51

n_c number of molecules per square meter of surface

n_T total number of data points

N_A local mass transfer flux (moles/m^2.s)

N_{Ao} Avegadro Number

N_g molar flow rate of gas (moles/s)

$N_{g,in}$	molar flow rate of gas at column inlet (moles/s)
$N_{g,out}$	molar flow rate of gas at column outlet (moles/s)
N_o	total number of pores in porous plate distributor
N_p	number of active pores in a porous distributor
N_s	local mass transfer flux (moles/m^2.s)
p_c	partial pressure of carbon dioxide (Pa)
p_o	partial pressure of oxygen (Pa.)
$p_{o,av}$	average partial pressure of oxygen in column (Pa.)
$p_{o,in}$	partial pressure of oxygen in the inlet gas (Pa.)
$p_{o,out}$	partial pressure of oxygen in the outlet gas (Pa.)
ΔP_{bed}	pressure drop inside the bed (Pa)
ΔP_d	pressure drop across a particle (Pa)
ΔP_{dh}	total pressure drop in the column (Pa)
ΔP_w	frictional pressure drop due to wall (Pa)
$\Delta P/\Delta H$	pressure gradient inside the bed (Pa/m)
$\Delta P/\Delta z$	pressure gradient along column wall (Pa/m)
$(\Delta P/L)_l$	pressure drop per unit length due to liquid flow (Pa/m)
$(\Delta P/L)_g$	pressure drop per unit length due to gas flow (Pa/m)
$P_{f,1}$	pressure drop across dry porous distributor PR1 in empty column (Pa)
$\Delta P_{f,2}$	pressure drop across dry porous distributor PR2 in empty column (Pa)
ΔP_{dl}	pressure drop across distributor in presence of liquid (Pa)
ΔP_f	pressure drop due to friction (Pa)
ΔP_h	local reduction of hydrostatic head above developing bubble (Pa)

ΔP_{ft}	net pressure gradient along the radial direction of the liquid film between two touching bubbles (Pa);(Equation 5.1.3)
ΔP_m	pressure created by intermolecular attraction inside a liquid film between two touching bubbles (Pa)
ΔP_p	the capillary pressure (Pa)
ΔP_s	pressure due to surface tension force (Pa)
P_T	total pressure in column (Pa).
$P_{T,av}$	average total pressure in the column (Pa.)
$P_{T,in}$	total pressure at column inlet (Pa.)
$P_{T,out}$	total pressure at column outlet (Pa.)
Q	gas effect term for particle-liquid mass transfer in three-phase fluidized bed (Equation 2.3.68)
Q_g	volumetric flow rate of gas (m^3/s)
Q_l	volumetric flow rate of liquid (m^3/s)
r	radial distance from centre of column (m)
r_{avg}	radial distance corresponding to average concentration in a given horizontal plane (m)
r_b	bubble radius (m)
r_{bf}	final bubble radius (m)
r_{bi}	initial bubble radius (m)
r_c	radius of pore in the porous plate (m)
r_p	radius of particle (m)
R	radius of column (m)
R_A	specific absorption rate of component A (moles/m2.s); Equation 2.1.9
R_g	gas law constant (0.000082 atm.m^3/mole.K)
s	fractional rate of the surface renewal (s^{-1})
Δt	duration of active particles in bed (sec)

t	gas absorption time (s)
t_1	time at the end of large bubbles disengagement (s)
t_2	time at the end of small bubbles disengagement (s)
t_c	contact time (in Equation 2.1.2)
T	temperature (^oK)
v	superficial velocity (m/s)
V_b	bubble volume (m_3)
V_c	average velocity of liquid circulation defined by Equation 2.2.17a
V_e	characteristic velocity based on the energy dissipation rate in bed (Equation 2.3.70a)
V_{bi}	initial bubble volume (m^3)
V_{bf}	final bubble volume (m^3)
V_{bo}	terminal single bubble rise velocity (m/s)
V_{br}	rise velocity of bubble swarm (m/s)
ΔV_b	change in bubble volume (m^3)
V_{gl}	drift flux velocity (m/s)
V_{go}	gas velocity through sparger orifice (m/s)
V_j	velocity of gas jet (m/s)
V_{lr}	radial component of liquid velocity (m/s)
$V_{l\theta}$	angular component of liquid velocity (m/s)
V_{lz}	axial component of liquid velocity (m/s)
V_R	reactor volume (m^3)
V_s	slip velocity between gas bubbles and liquid flow (m/s)
V_t	particle terminal velocity in gas-liquid medium.
V_T	total velocity of homogeneous gas-liquid flow (m/s)
V_{rel}	relative liquid-solid velocity in the liquid/solid fluidized bed (bubble wake model) (m/s)

V_{lmfo} minimum fluidization velovity for liquid-solid system (m/s)

V_{lmf} minimum fluidization velocity in a three-phase system (m/s)

$(V_{lmf})_1$ incipient fluidization velocity of the floatsam particles (m/s)

$(V_{lmf})_2$ incipient fluidization velocity of jetsam particles (m/s)

V_{m1} molar volume of component 1

V_{m2} molar volume of component 2

Δw weight lost by the particle during a run (kg)

W_s bed mass (kg)

x_1, y_1, z_1 coefficients in equation 2.3.28

x_{m1} mole fraction of component 1

x_{m2} mole fraction of component 2

y_c mole fraction of carbon dioxide in the gas phase

$y_{c,in}$ mole fraction of carbon dioxide in the inlet gas

$y_{c,out}$ mole fraction of carbon dioxide in the outlet gas

X_2 weight fraction of the jetsam particles

y_e activation energy of adsorption of surface active molecules (kcal/mol)

Z axial distance along the column (m)

Dimensionless Groups

Ar Archimedes number $(d_p^3 \rho_1 (\rho_s - \rho_1) g / \mu_1^2$

Bo Bond number $(\rho_1 d_p^2 g/\sigma)$

F as defined in equation 2.3.19a

Fr_g gas Froude number $(V_g^2 / d_p g)$

Fr'_g	gas Froude number based on column diameter $(V_g 2/d_g g)$
Fr_l	liquid Froude number $(V_l^2 / d_p g)$
Ga	Galileo number $(d_p^3 \rho_l^2 g / \mu_l^2)$
J	as defined by Equation 3.1.10a
J_d	Colburn factor for particle mass transfer $[(K_s / V_l)/(\mu_l / \rho_l D_l)2/3]$
j'_H	modified j-factor for wall heat transfer $(h_w/\rho_l C_{pl} V_l)\epsilon_l . Pr2/3$
k_o	as defined in Equation 2.3.36c $(\rho_l V_g^4/g\sigma)$
M	Morton number $(g\mu_l^4/\rho_l\sigma^3)$
M_1	Hatta number for first order reaction
M_2	Hatta number for second order reaction
Mv	density number $(\rho_s - \rho_l) / \rho_l$
Nu'	modified Nuselt number $\{(h d_p \epsilon / [l_l(1-\epsilon)]\}$
Pe	Peclet number based on column diameter $(V_l D_c/A_l)$
Pe'	Peclet number based on particle diameter $(V_l d_p/A_l)$
Pr	Prandtl number $(C_{pl} \mu_l / l_l)$
Re_e	particle Reynolds number based on characteristic velocity (V_e); as defined by Equation 2.3.71a $(V_e d_p \rho_l/\mu_l)$
Re_{go}	Reynolds number based on orifice gas velocity $(V_{go} D_c \rho_l/\mu_l)$
Re_{mf}	particle Reynolds number at minimum liquid fluidization velocity $(V_{lmfo} d_p \rho_l/\mu_l)$
Re_g	particle Reynolds number for gas $(V_g d_p \rho / \mu_l)$
Re_l	particle Reynolds number for liquid $(V_l d_p \rho_l/\mu_l)$
Re'_l	modified Reynolds number defined as $V_l d_p \rho_l/\epsilon_l\mu_l$.
Re''_l	modified Reynolds number defined as $V_l d_p \rho_l / (1-\epsilon_l)\mu_l)$.
Re_{lg}	modified Reynolds number defined as $\{Re_l [(\epsilon_g + \epsilon_l) / \epsilon_l(1-\epsilon_g-\epsilon_l)]\}$

Re_{m2}	modified Reynolds number as used in equation 2.3.57 $V_l\rho_l/a_s(1-\epsilon_{l2})\mu_l$
Re_t	Reynold number based on particle terminal velocity $V_t\rho_l d_p/\mu_l$
Sc	Schmidt number $\mu_l/(\rho\ D_l)$
Sh	Sherwood number $(k_s\ d_p\ /\ D_l)$
St_{m2}	modified Stanton number in liquid-solid systems $h_2\epsilon_{l2}/C_{pl}\rho_l\mu_l$
St_{m3}	modified Stanton number in three-phase systems $h_3\epsilon_{l3}/C_{pl}\rho_l\mu_l$
W	as defined by Equation 2.3.30a
We_{crit}	critical Weber number as defined by Equation 2.3.10
We_{crit}	modified critical Weber number as defined by Equation 2.3.11

Greek Symbols

ϵ	void fraction of fluidized bed
ϵ_g	gas-phase hold-up
$\epsilon_{g,l}$	gas holdup due to large bubbles (Equation 3.1.36)
$\epsilon_{g,s}$	gas holdup due to small bubbles (Equation 3.1.37)
ϵ_{gr}	local gas holdup at a given radial position
$\epsilon_{g,B}$	gas holdup in bubble column above the fluidized bed
ϵ_l	liquid-phase hold-up
ϵ_{l2}	liquid holdup in liquid-solid fluidized bed
ϵ_{l3}	liquid holdup in gas-liquid-solid fluidized bed
ϵ_{lf}	liquid holdup in the liquid-solid fluidized region of the three-phase fluidized bed
ϵ_{lw}	liquid holdup in the wake region

ϵ_o	as defined by Equation 2.3.25a
ϵ_s	solid-phase hold-up
ϵ_w	bubble wake holdup
ϵ_{sw}	solid holdup in the wake region
ϵ_{sf}	solid holdup in the liquid-solid fluidized region
μ	fluid viscosity (kg/m/s)
α,β	coefficients in Equation 2.3.68
γ	electrical conductivity of the bed
γ_o	electrical conductivity of the liquid alone
λ	characteristic dimension of the elementry cell as in Equation 2.3.70a
ζ	parameter in Equations 3.1.30a and 3.1.30b
δ	thickness of stagnant film (m)
η	effectiveness factor for catalyst
ρ	density (kg/m^3)
ρ_e	equivalent density (kg/m^3)
σ	surface tension (N/m)
ϕ	dimensionless radial position (r/R)
ψ	angle of wetting between liquid and solid particles (radians)
ϕ_s	particle sphericity
θ	angle of wetting of the distributor material by water (degrees)
Φ	particle shape factor
Γ	surface concentration of the additive per unit area ($moles/m^2$)

Subscripts / Superscripts

g	gas
l	liquid
p	particle
s	solid
w	water
2	two phase (liquid-solid) system
"	two phase (liquid-solid) system
3	three-phase (gas-liquid-solid) system
"'	three-phase (gas-liquid-solid) system

1. INTRODUCTION

1.1 Bubble Columns

Bubble columns are contactors of simple construction in which a discontinuous gas phase in the form of bubbles rises up in a continuous liquid or slurry phase of relatively fine particles. The bubble column can be operated in a batch or continuous mode and in a cocurrent or countercurrent mode. A good comprehensive review for bubble columns has been presented by Shah et al. (1982).

The main advantages of bubble columns are simple construction and low maintenance due to absence of moving parts. Bubble columns can also be designed to achieve high heat and mass transfer rates.

The bubble columns, however, have complex hydrodynamics and are sensitive to changes in physico-chemical properties of the liquid phase. There is also considerable amount of backmixing of liquid in bubble columns which make them less efficient for certain reactions.

Although several design variations are available (i.e. loop reactor, horizontally sparged columns) vertically sparged bubble columns are the most commonly used bubble columns in the industry.

1.1.1 Industrial Applications of Bubble Columns

Bubble columns are frequently used as absorbers, strippers and reactors in various chemical and petrochemical processes (Shah et al., 1982). The applications of bubble columns include biological oxidation of waste water, removal of acid gases (i.e. H_2S, SO_2, CO_2) from gaseous mixtures, and a number of liquid phase oxidation, chlorination, and hydrogenation processes.

Biological oxidation of waste water is one of the most important applications of bubble columns. The aeration system in these units has to ensure that the biomass is efficiently supplied with oxygen. Two of the more recently developed processes for waste water treatment are the ICI "Deep Shaft Process" and the "Bayer Tower Biology" process (Zlokarnik, 1983). The "Deep Shaft Process" consists of a shaft with a concentric inner tube (50-200 m deep). Air is introduced into the riser and downcomer in equal amounts. The performance of these devices is stated to be 1 kg BOD_5/kg O_2 and 3 kg BOD_5/kWh. The "Bayer Tower Biology" process was developed to achieve high oxygen uptake from bubbling air (upto 80 % utilization of O_2) at maximum possible performance (kg O_2/kWh). For this process special slot injectors, which generate fine gas bubbles, were developed. These injectors were then used in towers of height upto 30 m with

performance between 3 to 4 kg O_2/kWh.

1.2 Three-Phase Fluidization

Fluidization is an operation in which a bed of solid particles is transformed into a fluid-like state through contact with a gas and/or a liquid. In three-phase fluidization the solid particles are fluidized with a gas phase and a liquid phase. The industrial applications of three-phase fluidized systems are growing. Several reviews of hydrodynamic and mass transfer characteristics of three-phase fluidized are available in literature (Ostergaard, 1968 and 1971; Epstein, 1981 and 1983; Wild et al., 1984; Muroyama and Fan, 1985; Fan et al., 1987).

Gas-liquid fluidization can be classified into four modes of operation (Muroyama and Fan, 1985):

I. Cocurrent three-phase fluidization with liquid as the continuous phase.

II. Cocurrent three-phase fluidization with gas as the continuous phase.

III. Counter-current flow of gas moving up and liquid flowing down with the liquid as continuous phase (inverse three-phase fluidization).

IV. Counter-current flow of gas moving up and liquid flowing down with the gas as a continuous phase.

The most widely studied mode of operation is the

cocurrent three-phase fluidization with liquid as the continuous phase (Mode I). This is also the manner in which three-phase fluidized bed reactors are generally operated. However, when the particle density is lower than that of the liquid, the inverse mode is applied.

Three-phase fluidized beds offer a number of advantages which include:

- High heat transfer rates and uniform temperature throughout the bed which prevents the formation of hot spots.

- Continuous operation is ensured even in case of catalyst poisoning since catalyst particles can be withdrawn continuously there by eliminating costly shutdowns for catalyst withdrawl and replacement.

- The plug-free operation of three-phase fluidized beds makes them specially attractive for biological processes. There is no packing of solids and clogging of the reactor by biomass. Moreover, relatively small solid particles can be used to provide large surface area for the growth of microbes.

As discussed below, three-phase fluidized beds have some drawbacks as well:

1) The complex hydrodynamics of three-phase fluidized beds makes it difficult to simulate them by

mathematical models. This makes difficult the task of scaling up a pilot plant.

2) Effective solids mixing in the bed means that a mixture of active and deactivated particles is removed and a further separation is therefore required.

3) Particle movements also cause particle to particle friction as well as particle to internals friction. Friction leads to erosion of the equipment, as well as particle attrition and loss of fines by entrainment.

1.2.1 Industrial Applications of Three-Phase Fluidized Beds

On commercial scale, three-phase fluidized beds have been successfully used for hydrotreatment and conversion of petroleum resid, coal liquefaction and biological processing. Since about 70 % of the world oil reserves consist of heavy oil (Parkinson, 1985), the importance of resid processing technology would continue to grow. The two available processes for hydrotreatment of heavy petroleum fractions are the H-Oil process(Mounce et al., 1971) and Hy-Cracking process (Chervenak et al., 1963). In the H-Oil process sulfur containing compounds are removed from the oil by catalytic hydrogenation. Here, a cocurrent flow of oil and hydrogen entering at the bottom of the reactor expands the bed. In the Hy-Cracking

process, virgin and cracked gas oils (a mixture of aromatic, paraffinic and naphthenic hydrocarbons boiling between 130 and 300^{o}C), are cracked to lower boiling more valuable products such as gasoline, kerosene and diesel oil. The two processes are basically similar, their main difference lies in the type of catalyst used. The Hy-Cracking process uses a catalyst with a more highly developed acidic function than the H-Oil process.

Another industrial application of three-phase fluidized bed reactor is the H-Coal process in which coal is converted to liquid products by catalytic hydrogenation. Its product is light crude oil which can, then, be converted to gasoline by conventional refinery operations.

In both H-Oil and H-Coal processes the liquid product is recycled from reactor freeboard through an inner column back to the reactor plenum chamber to provide the main support for the catalyst bed. Since the catalyst expansion takes place the annular region of the fluidized bed, the operation can be more precisely termed "annular three-phase fluidization".

Three-phase fluidized bed reactors have also been applied to the production of "calcium bisulphite" liquors which are used as leaching agents in the paper industry (Volpicelli and Massimilla, 1970). The process is based on contacting limestone particles, water and sulphurous gas in a three-phase fluidized bed reactor. Volpicelli and

Massimilla reported that intensive production of bisulphite liquors is obtained by contacting particulate limestone, water and sulphurous gas. With their system, the rate of calcium carbonate dissolution was found to be two orders of magnitude greater than that obtained in the jenssen tower, a fixed bed absorber with limestone packing.

Biological processes such as biological waste water treatment are relatively new areas of application for three-phase fluidized beds. The "Oxitron Process" being licensed by Dorr Oliver Inc. (Sutton et al., 1981) is based on a fluidized bed bioreactor for waste water treatment. The fluidized bed provides over 93.0 m^2 of surface area for biological growth/m^3 of reactor volume. The volumetric BOD loading for either domestic or industrial sewage treatment in fluidized bed bioreactors can be as high as 15 kg-BOD/m^3-day. The biomass concentration (15 to 40 kg/m^3) and the volumetric BOD loading can be as high as 10 to 20 times higher than in the conventional activated sludge aeration tanks (Fujie et al., 1983).

Some of the latest developments in the application of three-phase fluidized bed reactors have been reported by Fan et al. (1987). These include fermentation processes (Venkatasubramnian and Karkare, 1983), production of amino acids, enzymes and antibiotics (e.g. the production of Patullin by immobilized Penicillium utrica (Berk et al.,

1984a, 1984b) and of pencillin by immobilized Becillus sp. (Morikowa et al., 1980; Endo et al., 1986, Kalogerakis et al., 1986).

1.3 Objectives of the Study

Gas-liquid mass transfer is the rate controlling step in a number of gas-liquid and gas-liquid-solid reactors The mass transfer rate can be enhanced if the resistance for mass transfer is reduced and/or interfacial area for mass transfer is increased. The variables which can affect gas-liquid mass transfer rate in bubble columns include gas distribution, gas and liquid flowrates and coalescing behavior of the liquid. Significant improvements in mass transfer rate can be obtained by increasing the interfacial area for mass transfer since mass transfer rates are directly proportional to the interfacial area. The interfacial area for gas-liquid mass transfer can be enhanced by reducing the average bubble size in gas-liquid dispersion. This can be achieved by generating small gas bubbles using fine gas distributors. However, as the concentration of bubbles in the dispersion increases, their coalescence rate also increases which leads to the formation of larger bubbles. The bubble coalescence rate can, however, be reduced by using suitable coalescence inhibitors.

Although a number of researchers have studied gas-

liquid mass transfer in bubble columns (see section 2.2.5), very little work has been done to systematically investigate the effects of coalescence inhibitors on mass transfer rates, specially at low concentrations (below 50 ppm). Although a number of surface active molecules are known to have coalescence inhibition effect in gas-liquid dispersions (see section 2.2.5.2.4), it is important to know how the effectiveness of the additives is affected by the molecular structure of the additive molecules (i.e. the polar group and hydrocarbon backbones). Therefore, one objective of this study was to systematically investigate the coalescence inhibition effects of various surface active molecules for various concentrations in the liquid phase. Since the mass transfer rates are also affected by other variables such as gas distribution and gas and liquid flow rates, it was decided to study how the effectiveness of the additives varied with the change of these variables.

Gas-liquid mass transfer in three-phase fluidized beds has been investigated by several researchers (see section 2.3.6). No work, however, has been done so far to investigate the effects of coalescence inhibitors on gas-liquid mass transfer rate in three-phase fluidized beds. A number of industrial processes have impurities in the liquid phase which can alter the coalescing behavior of the liquid (i.e. waste water treatment and coal liquefaction processes). An effective additive, based on

bubble column study was used to investigate the effects of coalescence inhibition on gas-liquid mass transfer rate in three-phase fluidized beds. The effects of gas and liquid flow rates, particle size and gas distribution were investigated both in coalescing and noncoalescing liquid phases.

Liquid-solid mass transfer in three-phase fluidized beds was also investigated in this study. No study had been reported in the literature, when particle-liquid mass transfer in three-phase fluidized beds was investigated for this study. However, a few studies on liquid-solid mass transfer in three-phase fluidized beds have appeared in the literature in recent years (see section 2.3.7.3). Knowledge of particle-liquid mass transfer in three-phase fluidized beds is important for both design and analysis of these reactors. A new experimental technique was developed in this study to measure particle-liquid mass transfer without altering the coalescing behavior of the liquid. This technique was then used to investigate the effects of gas and liquid flowrates, liquid viscosity and changes in coalescing behavior of liquid on particle-liquid mass transfer rate.

2.0 LITERATURE REVIEW

2.1 Mass Transfer Theories

2.1.1 Film Theory

Several models have been developed to describe mass transfer mechanisms. The film theory which was originally proposed by Whitman (1923) is the simplest of them all. According to this theory, all the resistance to mass transfer lies in a stagnant film next to the boundary of the fluid. The remainder of the fluid is well mixed so that the concentration gradient is restricted to the stagnant film and the mass transfer is therefore limited by the diffusion across this film (Figure 2.1.1). The distance δ is the thickness of the equivalent film for molecular diffusion. The steady state flux across this film in terms of the mass transfer coefficient is expressed as:

$$N_A = k_l (C_{Ai} - C_{Ab}) = \frac{D_A}{\delta} (C_{Ai} - C_{Ab}) \quad ....(2.1.1)$$

The stagnant film thickness can be determined indirectly from mass transfer measurements with a given solute.

The film theory predicts that the mass transfer coefficient is directly proportional to the diffusion coefficient D_A. This prediction, however, is not in agreement with the majority of the experimental data which show the mass transfer coefficient as being proportional

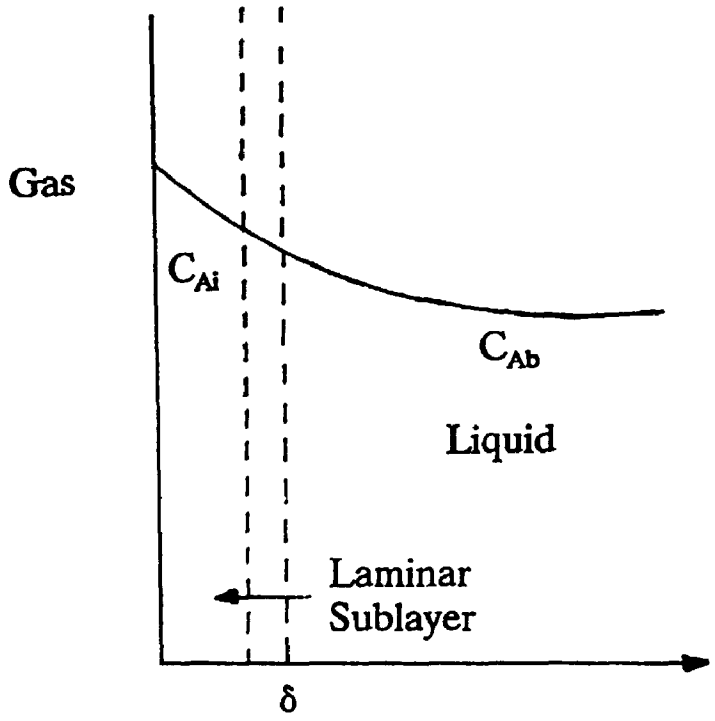

Figure 2.1.1

The film theory for mass transfer.

to $D_A^{2/3}$. Obviously the film theory is limited in its ability to predict turbulent mass transfer rate. The main advantage of film theory is its simplicity. It has been found useful in describing complex situations and in cases where diffusion and chemical reaction occur simultaneously.

2.1.2 Penetration Theory

The penetration theory, originally proposed by Higbie (1935) can be considered to be more realistic than the film theory which does not account for the unstable nature of a fluid-fluid interface. The penetration theory assumes that the surface of a flowing liquid consists of small fluid elements that come in contact with the interface where they remain for a short but constant time before being carried back to the bulk fluid by turbulent eddies. Each element is then replaced by another element from the bulk liquid phase. The solute is assumed to penetrate into each element by unsteady state molecular diffusion (Figure 2.1.2). The mass transfer coefficient is given by:

$$k_l = [\ 4D_A/\pi t_c]^{0.5} \qquad \text{.....(2.1.2)}$$

Where t_c is the contact time between a fluid element and the interface. This theory thus predicts that the mass transfer coefficient varies as the square root of the diffusivity ($D_A^{0.5}$).

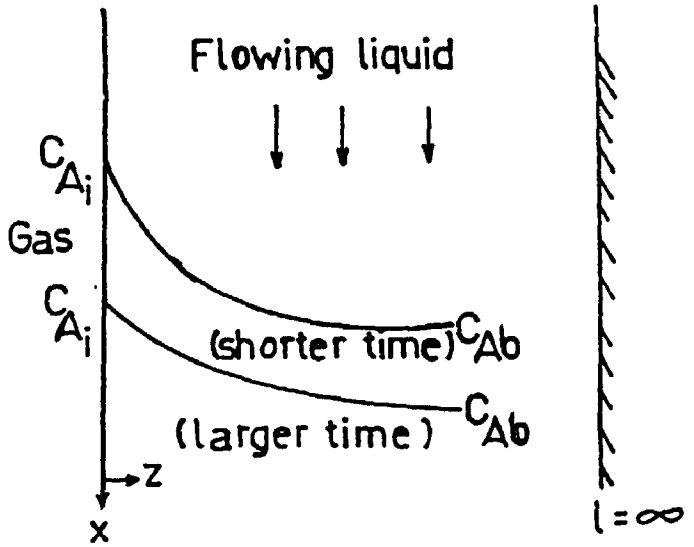

Figure 2.1.2

The penetration theory for mass transfer (Cussler,1984).

2.1.3 Surface Renewal Theory

This theory was proposed by Danckwerts (1951) to improve the penetration theory. According to this theory, the liquid is pictured as two regions (Figure 2.1.3), a large well mixed bulk regions of uniform concentration and a surface region that is renewed so slowly that it behaves as a thick film. The surface renewal is caused by liquid eddies from turbulent core and the contact time (t_c) is not assumed to be the same for all fluid elements. The probability of an element being replaced by fresh eddies is considered to be independent of the time which it has already spent at the interface. As in the penetration theory the mass transfer coefficient is predicted to be proportional to the square root of the molecular diffusivity:

$$k_l = \sqrt{D_A s} \qquad \text{.....(2.1.3)}$$

Where s is the surface renewal factor (s^{-1}).

2.1.4 Chilton-Colborn's "J-factor" anology

Most experimental studies have found that the mass transfer coefficient is neither proportional to $D_A^{1.0}$ as assumed by the film theory nor to $D_A^{0.5}$ as assumed by the penetration and surface renewal theories but to $D_A^{2/3}$. Chilton and Calburn (1934) therefore assumed that the " J-factor" (J_d) given below is a function only of the system

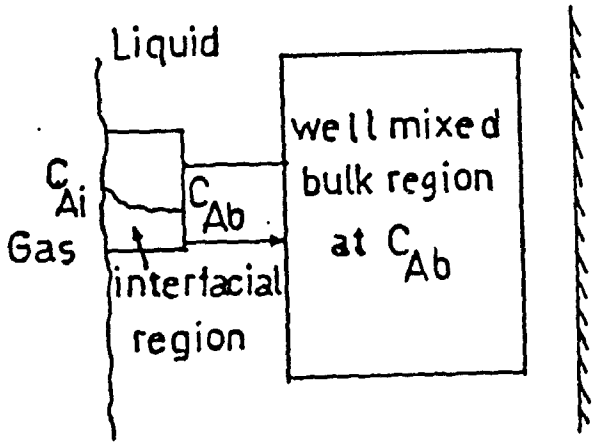

Figure 2.1.3

The surface renewal theory for mass transfer,

(Cussler, 1984)

hydrodynamics:

$$J_d = [(k_l/V_l)(\mu_l/\rho_l D_A)^{2/3}] \quad \text{.....(2.1.4)}$$

2.1.5 Mass Transfer with Chemical Reaction

The theories of mass transfer accompanied by chemical reaction have been discussed in details by Danckwerts (1971) and Astarita (1967). In this section some basic aspects of the theory of mass transfer accompanied by a single step irreversible chemical reaction is discussed.

The following equation of continuity can be written for a gas A being absorbed into a liquid which contains a reactive species B (Bird et al., 1960). For a dilute solution of A, we can assume constant density and diffusivity.

$$\frac{\delta C_A}{\delta t} + (V.\nabla C_A) - D_A \nabla^2 C_A = r_A \quad \text{.....(2.1.5)}$$

For steady state $\delta C_A/\delta t = 0$. For dilute solutions the bulk flow can be neglected ($V = 0.0$). The reaction rate for a first order reaction is $r_A = - k'_r C_A$.

The film theory is used for the analysis of mass transfer process. If the gas phase resistance is assumed negligible, we can now write equation 2.1.5 as:

$$D_A \frac{d^2 C_A}{dz^2} = k'_r C_A \quad \text{.....(2.1.6)}$$

The boundary conditions are

at $z = 0$ $\quad C_A = C_{Ai}$ .....(2.1.7)

at $z = \delta$ $\quad C_A = C_{Ab}$ .....(2.1.7A)

From film theory $\quad \delta = D_A/k_l$

The solution of equation 2.1.6, which is an ordinary second order differential equation is:

$$C_A = \frac{1}{\text{Sinh}\sqrt{M_1}} [C_{Ab}\text{Sinh}z\sqrt{k'_r/D_A} + C_{Ai}\text{Sinh}(\sqrt{M_1} - \sqrt{k'_r/D_A}z)] \quad .....(2.1.8)$$

Where $\sqrt{M_1} = \sqrt{D_A k'_r}/k_l$

$\sqrt{M_1}$ is also called Hatta number (Ha)

The specific rate of absorption of A is given by:

$$R_A = -D_A\left(\frac{dC_A}{dz}\right)_{z=0} \quad .....(2.1.9)$$

$$= k_l\left(C_{Ai} - \frac{C_{Ab}}{\text{Cosh}\sqrt{M_1}}\right)\frac{\sqrt{M_1}}{\tanh\sqrt{M_1}} \quad .....(2.1.9a)$$

It can be noted that in this case R_A is not proportional to $(C_{Ai} - C_{Ab})$ as in physical absorption (Equation 2.1.1). This is usually the case when the bulk concentration of A is not negligible. When $\sqrt{M_1} > 3$ the bulk concentration of A tends to zero and the term $\tanh\sqrt{M_1}$ tends to unity. The Equation 2.1.9a becomes:

$$R_A = C_{Ai}\sqrt{D_A k'_r} \quad .....(2.1.10)$$

The enhancement factor E_A for A can be written as:

$$E_A = R_A/k_1 C_{Ai} \qquad \text{.....(2.1.11)}$$

Where E_A is the factor by which the chemical reaction enhances the rate of absorption compared to physical absorption (with $C_{Ab} = 0$). When $\sqrt{M_1} > 3$, we get from equations 2.1.10 and 2.1.11

$$E_A = \sqrt{M_1} \qquad \text{.....(2.1.12)}$$

2.1.6 Gas Absorption in Three-Phase reactors

As reviewed in section 1.2.1, a number of chemical and biochemical processes use three-phase reactors in which the solid particles (reactant or catalyst) are suspended in a liquid. A three-phase catalytic reactor can be designed using the concept of resistances in series (Figure 2.1.4).

For a first order reaction and enhancement factor of one, we can write

$$\frac{C_{Ai}}{N_A a} = \frac{1}{k_1 a} + \frac{1}{k_s a_s} + \frac{1}{\eta k'_r C_{cat}} \qquad \text{.....(2.1.13)}$$

It can be seen from Equation 2.1.13 that the global rate is dependent upon various mass transfer resistances plus a kinetic resistance.

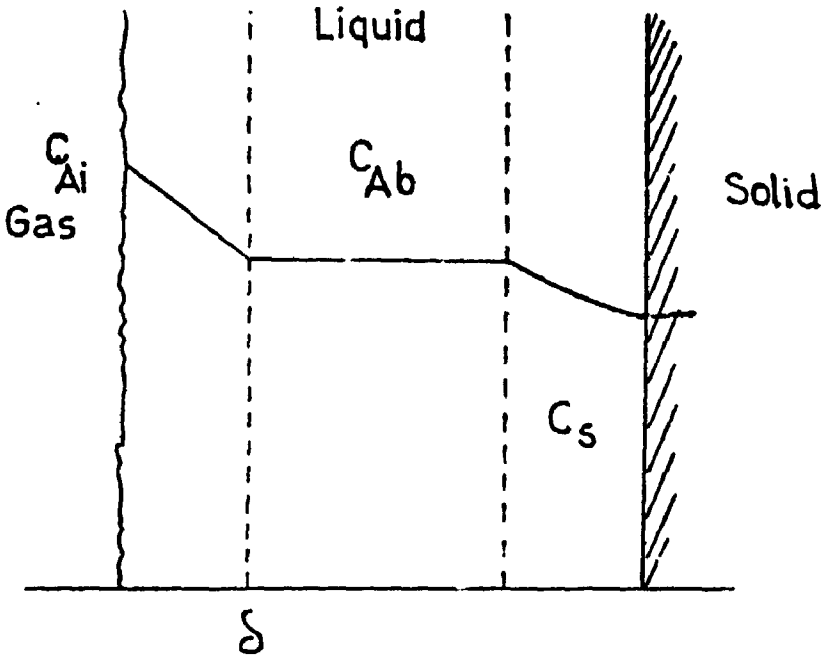

Figure 2.1.4
Concentration distribution of gaseous reactant in a three-phase catalytic reactor

2.2 Bubble Columns

2.2.1 Flow Regimes

The hydrodynamics and mass transfer characteristics in bubble columns depend on the nature of the flow pattern prevailing in the bubble column. The various flow patterns have been described with the help of flow regime maps. (Figure 2.2.1). Researchers have outlined different criteria to differentiate the flow regimes (Wallis, 1969; Hills, 1976; Kawagoe et al., 1976). The flow regimes and their boundaries have often been determined based on visual observations and therefore cannot be quantified. Three types of flow regimes have been observed in multiphase mixtures, these are: 1) Bubble flow regime 2) churn turbulent regime and 3) slug flow regime.

2.2.1.1 Bubble Flow Regime

This regime is characterized by bubbles of uniform size which are distributed over the entire cross sectional area of the column. This regime has been reported to exist at superficial gas velocities less than 0.05 m/s in batch bubble columns (Fair, 1967; Hills, 1974). The values of gas holdup obtained in this regime are generally of the order of 15-25 %. In the bubbly flow regime, the gas holdup increases very rapidly with increase in superficial

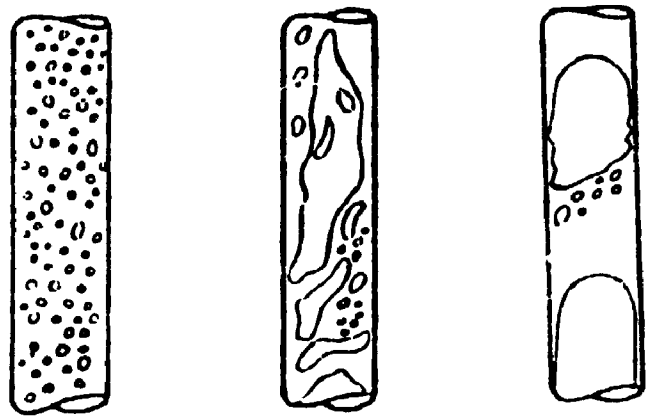

Figure 2.2.1
Flow regimes for bubble columns

gas velocity. Kawagoe et al. (1976) found that the gas holdup in the bubbly flow regime was proportional to the superficial gas velocity.

2.2.1.2 Churn Turbulent Regime

At higher gas velocities the pseudo homogeneous gas in liquid dispersion can no longer be maintained and an unsteady flow pattern with violent and turbulent motion caused by the formation of large bubbles is obtained. This heterogeneous flow regime is characterized by rapid coalescence and break up, resulting in a wide bubble size distribution. This flow regime has been found to exist at superficial gas velocities higher than 0.05 m/s in a batch bubble column (Hills, 1976).

2.2.1.3 Slug Flow Regime

This regime has been observed in small diameter columns, at high gas flow rates when large bubbles are stabilized by the column wall leading to the formation of bubble slugs. Bubble slugs have been observed in columns of diameter up to 0.15 m (Hills, 1976; Miller, 1980).

The boundary between the flow regimes depends on several factors, such as design of gas distributor, physico-chemical properties of liquid, gas and liquid velocities and column diameter. The interactions of all these factors precludes the accurate prediction of the boundaries between flow regimes. Anderson and Quinn (1970)

found that minute traces of contaminants in tap water could change the transition between flow regimes. Ohki and Inoue (1970) and Yamashita and Inoue (1975) found that the transition between bubble flow regime and the churn turbulent regime was more distinct when the distributor hole size was less than 1.0 mm. Moreover the transition gas velocity changed with the distributor hole size.

2.2.1.4 Flow Regime Charts

Some researchers have prepared flow regime charts for bubble columns (Cichy et al., 1969; Oshinowo and Charles, 1974; Govier and Aziz, 1972). However, as found by Miller (1980), the different charts provided different flow regimes for his data, moreover the range of flow covered by these researchers was also narrow.

The concept of drift flux as introduced by Wallis (1969) has proved useful in identifying the flow transition. The drift flux is defined as the volumetric flux of the gas relative to a surface moving with the average velocity of the dispersion. If the volume-average velocity of the dispersion is defined as,

$$V_T = V_g + V_l \quad \ldots\ldots\ldots\ldots\ldots\ldots \quad (2.2.1)$$

Then drift flux is given as,

$$V_{gl} = V_g - \epsilon_g V_T \quad \ldots\ldots\ldots\ldots\ldots\ldots (2.2.2)$$

or

$$V_{gl} = V_g (1-\epsilon_g) - V_l \epsilon_g \quad \ldots\ldots\ldots\ldots (2.2.2a)$$

A plot of V_{gl} vs. ϵ_g can show at which gas velocity the bubble flow switches over into the churn turbulent regime, since at that point the drift flux increases sharply (Kelkar et al., 1983a).

Zuber and Findley (1963) modified Equation 2.2.2a to account for the radial distribution of gas holdup observed in the churn turbulent regime. The following equation was proposed for cocurrent flow:

$$\frac{\langle V_g \rangle}{\langle \epsilon_g \rangle} = \frac{\langle V_{gl} \rangle}{\langle \epsilon_g \rangle} + C_z \langle V_T \rangle \qquad \text{.....(2.2.3)}$$

where

$$C_z = \frac{\langle \epsilon_g V_T \rangle}{\langle \epsilon_g \rangle \langle V_T \rangle} \qquad \text{.....(2.2.3a)}$$

C_z here represents the radial distribution parameter introduced by Zuber and Findley (1963) and the < > sign corresponds to radially averaged values. A plot of V_g/ϵ_g as a function of V_T, provides an estimate of C_z and the intercept gives an indication of the bubble rise vlocity since as $V_g \rightarrow 0$, $V_{gl}/\epsilon_g \rightarrow V_{bo}$.

Zuber and Findley (1963) found the value of C_z to be 1.6 for the air-water system, which indicated that the bubble concentration was considerably larger at the centre than at the wall. This approach is suitable only for the churn turbulent regime. Clark and Flemmer (1985) applied the Zuber and Findley model to down flow bubble column. In the case of down flow the slip velocity (V_{gl}/ϵ_g) will change in sign. Clark and Flemmer (1985) found a value of

1.16 for both up and down flow.

The heterogeneous distribution of bubbles in the churn turbulent regime is attributed to bubble coalescence which leads to the formation of large bubbles or bubble clusters with high rise velocities causing high rates of circulation in the liquid phase.

2.2.2 Phase Holdups

In multiphase flow systems, each phase has a velocity which is different from that of other phase. As a result of the relative velocity between the two phases, the ratio of the volumes occupied by each phase is different from the ratio of the entering volumetric flowrates. The holdup of a phase is defined as the fraction of the column volume which is occupied by this phase.

In two phase gas-liquid systems, the individual holdups satisfy the following expression

$$\epsilon_g + \epsilon_l = 1 \quad \text{.....(2.2.4)}$$

And the static pressure gradient, neglecting the frictional pressure drop is given by:

$$\Delta P = g\Delta H \ (\epsilon_g \rho_g + \epsilon_l \rho_l) \quad \text{.....(2.2.5)}$$

2.2.2.1 Measurement of Phase Holdups

Various techniques have been used in the literature for the measurement of phase holdups in two phase and

three-phase systems. Following is a critical review of the techniques most commonly used in two-phase bubble columns.

2.2.2.1.1 Simultaneous Closure of the Gas and Liquid Flows

This is a relatively simple technique and is based on the recording of gas-liquid dispersion height (H_d) and the liquid height (H_L) after gas and liquid shut off and gas escape. The difference between the initial dispersion height and the recorded liquid level corrosponds to the volume of the gas present in the column at operating conditions. The gas holdup can be obtained as shown below:

$$H_d A_c \epsilon_g = (H_d - H_L) A_c \quad \text{.....(2.2.6)}$$

$$\epsilon_g = \frac{(H_d - H_L)}{H_d} \quad \text{.....(2.2.6a)}$$

In continuous bubble columns the dispersion height (H_d) has usually been assumed to correspond to the column height (H_c) while in batch bubble columns the dispersion height would vary with the initial liquid height.

A number of researchers have used this technique for phase holdup measurement in bubble columns (Akita and Yoshida, 1973; Peschke et al., 1980; Pal et al., 1980; Grover et al., 1986; Ozturk et al., 1987). Although relatively easy to use, there are several sources of

errors which can reduce the accuracy of results obtained with this technique. The main sources of errors are discussed below:

1) In batch bubble columns, it is difficult to determine the accurate height of the gas-liquid dispersion when there are large fluctuations at the interface or when foam is formed at the surface of the liquid. In continuous bubble columns, assuming a dispersion height equal to the column height would be inaccurate due to the weir effects.
2) When the gas is flowing into the column, the pressure inside the distributor is higher than the column pressure which can cause some flow of gas into the column after the gas is shut off until the pressures have equilibrated. Moreover liquid may also drain into the gas sparger and its line. These errors can be minimized by suitable design of the distributors.
3) In continuous bubble columns, the surface waves created by the escaping gas bubbles, after gas shut-off, may entrain some liquid out of the column.

2.2.2.1.2 Phase Holdups from Pressure Gradient

This is the most commonly used technique for phase holdup measurement in bubble columns (Hikita et al., 1980; Miller, 1980; Reilly et al., 1986; Wachi et al., 1987). The pressure gradient along the column height can be obtained by the measurement of static pressure at two or more points. The phase holdups can be obtained using

Equations 2.2.4 and 2.2.5.

This technique is quite accurate for low gas flow rates when fluctuations in the manometer levels are small and accurate readings of the static pressure can be obtained. At high gas flowrates however the column is in churn turbulent regime and there are large fluctuations of liquid levels in the manometers which could reduce the accuracy of measurements (a solution is provided in section 3.1.1).

2.2.2.1.3 Electroconductivity Technique

This technique is based on the measurement of the electrical conductivity which depends on the concentration of each phase in the column. This technique can be used to measure average or local holdups.

Its reliability for local holdup measurements can, however, be affected by the interference of the electroconductive probe with the local hydrodynamics and especially with bubble motion. The other major limitation of the technique is that it fails to detect very small bubbles and large bubbles which avoid the probe (Gardner, 1969-70).

For average holdup measurements, various relationships are available to obtain gas holdup from the average dispersion conductivity (Turner, 1976; Sigrist et al., 1979). In bubble columns this technique has been used by several researchers (Ivanov and Bykov, 1970; Hills,

1974; Kato et al., 1975; Sigrist et al., 1979). Bouman et al. (1974) have shown that the conductivity method is very sensitive to the type of flow. For the same average conductivity, the liquid holdup was about 0.15 in mist flow, about 0.3 in annular flow, about 0.75 in bubble flow and about 0.8 in slug flow.

2.2.2.1.4 Gamma Ray Attenuation

Lockett and Kirkpatrick (1975) used the gamma ray attenuation technique to obtain the mean gas holdup in gas-liquid dispersion. These authors also obtained the mean gas holdup by shutting off the gas and water flows. The results obtained with the two techniques were found to be in good agreement. Compared to other techniques for phase holdup measurements this technique requires more elaborate arrangements and additional precautions of handling radiations. The gamma ray attenuation technique has been discussed in detail by Hewitt (1978).

2.2.2.1.5 Optical Probe Technique

Recently optical probes have been developed to detect the change in the index of refraction in the medium to provide local values of phase holdup (Ishida and Tanaka, 1982; Delhaye, 1983; Nottenkaemper et al., 1983; Lee et al., 1984,1987; Kitano and Fan, 1986; Wachi et al., 1987). Delhaye (1983) reviewed the optical probes which have been developed for the measurement of void fraction

in two phase flow. De Lasa et al. (1984) and Lee et al. (1984,1986) used a silica optical fiber probe with a U-shaped tip sensor. The average gas holdup was obtained from the summation of all the gas bubbles contact time with the probe. Nottenkaemper et al. (1983) used a U-shape fibre optic probe to measure local gas holdup in bubble columns. The area average gas holdup obtained with the probe were about 10% lower than the ones obtained with the manometric method. Wachi et al. (1986), however, reported that the average gas holdup obtained with optical probe was about 30% smaller than the value obtained with the manometric method. These results indicate that the fibre optic technique fails to detect all the gas bubbles in the dispersion, and hence underestimates the mean gas holdup.

The main advantage of optical probes is that they can be used in non-conductive liquids and at high temperatures e.g. in hyderogenation reactors. The main drawbacks of the probes are their higher cost and failure to detect all sizes of bubbles (usually smaller than 1.0 mm).

2.2.2.1.6 Laser Holography

The laser holography technique can provide at the same time the diameter, shape and position of every gas bubble (Peterson, 1985). This is the only technique which can provide such information without interfering with the bubble motion. It is, however, very expensive, hard to set up and difficult to use at higher gas velocities.

From the above review, it can be concluded that each measurement technique has its advantages and drawbacks. The technique based on pressure gradient measurements should, however, provide reasonably accurate estimates of phase holdups over a wide range of gas flowrates, if suitable dampeners are used to minimize oscillations of liquid level in the manometers.

2.2.2.1.7 Impedance Probe Technique

This technique is based on the electrical impedance measurement which depends on the fraction and distribution of the phases. The basic technique has been reviewed by Hewitt (1978,1982). Depending on the system, the impedance will be governed by conductance or capacitance or both. It is, however, recommended to operate at conditions to ensure domination of capacitance, since the liquid conductivity can be easily affected by the presence of dissolved salts and/or temperature whereas the dielectric constant varies less (Hewitt, 1982). Hardy and Hylton (1984), however, modified the technique to measure relative capacitance in order to compensate for changes of media properties.

Impedance method offers very rapid response but there can be uncertainties in data interpretation making accuracy somewhat doubtful. The main problem with the technique is its potential sensitivity to flow patterns. Depending on the flow configuration a wide range of

impedance values might be expected for a given void fraction.

2.2.2.2 Effects of Operating Variables on Phase Holdups

2.2.2.2.1 Effects of Gas Velocity

Variation of gas holdup with gas velocity has been found to depend on the operating flow regime (Ohaki and Inoue, 1970; Deckwer et al., 1974; Deckwer et al., 1982). The relation between the gas holdup and the gas velocity is generally of the form:

$$\epsilon_g = C_1 V_g^{\,m} \qquad \text{.....(2.2.7)}$$

Where C_1 and m are empirical parameters obtained from the experimental data. The value of m depends on the flow regime (Shah et al., 1982). For the bubbly flow regime m varies from 0.7 to 1.2 (Reith et al., 1968; Bach and Pilhofer, 1978; Deckwer et al., 1980; Ozturk et al., 1987). In the churn turbulent regime the effect of V_g is less pronounced and the exponent m takes values from 0.4 to 0.7, while in the transition regime m may have negative values. The value of exponent 'm' could also be affected by the distributor type and coalescence behavior of liquid.

2.2.2.2.2 Effects of Liquid Velocity

The effects of liquid velocity on gas holdup in

cocurrent upflow bubble columns have not been studied extensively enough. The available data, however, shows that there is practically no effect of low liquid velocity (< 0.05 m/s) on gas holdup (Yoshida and Akita, 1965; Kumar et al., 1976; Botton et al., 1978). These observations could be explained by the large differences in bubble rise velocities (0.25 m/s to 0.4 m/s) and the liquid velocity used. Otake et al. (1981) investigated the effects of liquid velocities on gas holdup in cocurrent and countercurrent bubble columns. The gas holdup was found to decrease with increasing liquid velocity. The results of these researchers show that the effects of liquid velocity in cocurrent bubble column are generally more pronounced for liquid velocities higher than 0.05 m/s.

2.2.2.2.3 Effects of Column Diameter

The gas holdup has been found to be influenced by column diameters smaller than 0.1 m (Ohki and inoue, 1970; Akita and Yoshida, 1974; Kito et al., 1976; Botton et al., 1978). For higher diameters (D_C>0.1 m) a number of investigators have observed no significant effect of the column diameter on gas holdup (Akita and Yoshida, 1973; Botton and Cosserat, 1978; Hikita et al., 1980; Gopal and Sharma, 1983). These observations indicate the importance of wall effects for small diameter columns since the bubble size can then be of the same order of magnitude as the column diameter.

2.2.2.2.4 Effects of Gas Distribution

The gas phase holdup has been found to be strongly affected by the type of gas distributor specially for low gas velocities below 0.06 m/s (Ohki and Inoue, 1970; Yamashita and Inoue, 1975; Schügerl et al., 1977; Oels et al., 1978). Yamashita and Inoue (1975) used distributors with different hole diameters and found a maximum in the gas holdup as a function of hole size. Ohaki and Inoue (1970) and Yamashita and Inoue (1975) found that when the distributor holes were less than 1.0 mm in diameter two distinct types of regimes could be observed. At low gas velocities (below 0.06 m/s), the gas holdup increased linearly with gas velocity. This corresponds to the homogeneous or bubbly flow regime. At higher gas velocities there was a significant deviation from linearity. Yamashita and Inoue (1975) and McManamey et al. (1984) observed that the gas holdup depended on the fraction of the column base which was aerated and on the number, pitch and diameter of the orifices. The effect of orifice diameter on gas holdup was, however, found to become insignificant for diameters larger than 1.0 mm (Yamashita and Inoue, 1975; Gopal and Sharma, 1983,. This, however, may not apply for columns with low height to diameter ratio where the effects of distributor region are important (Haque et al., 1986). Rice et al. (1981) found that rubber sheet spargers can produce significant increases in gas holdup relative to rigid spargers.

Schuegerl et al. (1977) measured the gas holdup using different types of gas distributors in aqueous solutions of alcohols and electrolytes. The gas holdup was found to increase in the following order:

perforated plates < porous plates < injector nozzles < ejector nozzles

The distributor design affects the initial bubble size and consequently the gas holdup, however this influence on the gas holdup is observed mainly at low superficial gas velocities in the bubbly flow regime. At superficial gas velocities past the bubbly flow regime the effect of the distributor diminishes. For these conditions larger bubbles are seen leaving the distributor region (Prakash and Briens, 1988).

2.2.2.2.5 Effects of Physical Properties of Liquid

The gas holdup was found to decrease with increasing liquid viscosity by Akita and Yoshida (1973), Hikita et al. (1980) and Bach and Pilhofer (1978). Akita and Yoshida (1973) and Hikita et al. (1980) used a combination of pure liquids and aqueous solutions of glycol, surcose, alcohols and electrolytes. Bach and Pilhofer (1978) used pure organic compounds to study the effects of liquid viscosity while keeping the surface tension costant. Bach and Pilhofer (1978) also used different concentrations of glycerol in water (8 vol. % to 90.7 vol. %) to study the

effects of liquid viscosity on gas holdup, using liquid mixtures instead of pure liquids. For lower concentrations (less than 40 vol. %) the gas holdup increased with increasing concentration of glycerol, and consequently with increasing viscosity. The gas holdup started to decrease only at glycerol concentrations over 40 vol. %. And it was only above a concentration of 90.7 vol. % that the results obtained were similar to those of pure liquids for viscosity effects i.e a decrease in gas holdup with increasing viscosity. Bukur et al. (1987) measured gas holdup in three different waxes. The gas holdup was found to be greatly affected by the composition of the wax, even when the liquids had the same viscosity.

Based on the above studies, it can be concluded that the liquid mixtures should not generally be used to investigate the effects of liquid viscosity on gas holdup.

The effects of surface tension on gas holdup can be studied by either using pure liquids of different surface tension or by addition of surfactants to a given liquid. Using pure organic liquids Bach and Pilhofer (1978) found no significant effect of surface tension on gas holdup. The addition of a surfactant also generally changes the coalescing properties of the liquid phase. The effects on the gas holdup of the changes in surface tension and coalescence behavior cannnot therefore be observed separately with such a technique (Kelkar et al., 1983a). Kelkar et al. (1983a) used aqueous solutions of alcohols

(C_1 to C_4) at concentrations ranging from 0.5 to 2.4 wt. %. It was observed that for 0.5 wt. % alcohol solutions the gas holdup increased by more than 200 % over the values obtained with water while the change in surface tension was less than 10 %. However for alcohol concentrations higher than 0.5 wt. % , the gas holdup did not change significantly with increasing alcohol concentration, although the surface tension decreased significantly. The above observations suggest that the gas holdup was probably affected mainly by changes in liquid coalescing properties rather than by changes in surface tension. Aqueous solutions of surface active compounds should not therefore be used to establish a correlation between gas holdup and surface tension.

The gas holdup increased with increasing liquid density according to Akita and Yoshida (1973); Hikita et al. (1980) and Bach and Pilhofer (1978).

2.2.2.2.6 Effects of Coalescence Inhibitors

The effects of coalescence behavior of the liquid phase on gas holdup have been investigated with aqueous solutions of electrolytes and alcohols (Deckwer, 1974; Schügerl et al., 1977; Oels et al., 1978; Kelkar et al., 1983a; Koide et al., 1985). Hikita et al. (1980) studied the effects of various electrolytes on the gas holdup. Addition of an electrolyte to water resulted in a slight increase in gas holdup which depended on the nature and

concentration of the electrolyte. Oels et al. (1978) and Kelkar et al. (1983) observed significantly higher gas holdups in dilute aqueous solutions of alcohols. The gas holdup increased with increasing number of carbon atoms in the alcohol molecule. Posarac and Tekic (1987) confirmed the results obtained by Oels et al. (1978) and Kelkar et al. (1983a). As observed by Drogaris and Weiland (1983), the increase in gas holdup can be attributed to increases in bubbles coalescence times in aqueous solutions of surface active additives.

2.2.2.2.7 Effects of Solids on Gas Holdup

The gas holdup in slurry bubble columns has been found to be affected by solids concentration, density and size. A number of researchers have reported a decrease in gas holdup with increase in solids concentration (Kato et al., 1973; Kurten and Zehner, 1979; Kara et al., 1982; Koide et al., 1984; Sauer and Hempel, 1987). This effect has been more pronounced for gas velocities below 0.07 m/s. Hatate et al. (1986), however, found no effect of solid concentration on gas holdup. The small diameter columns (D_c < 0.05 m), used by these researchers suggest that they were operating in slug flow regime. Kato et al. (1973) found the gas holdup to decrease with an increase in particle size over the size range used for their study (i.e. 60-175 μm).

The gas holdup was also found to be affected by the

wettability of the solids (Kelkar et al., 1984). Kelkar et al. (1984) observed lower gas holdups with oil shale particles as compared to polystyrene beads. This could be attributed to higher apparent viscosity in presence of wettable particles.

Sauer and Hempel (1987) compared the gas holdup obtained in a slurry bubble column with the solid-free bubble column. It was observed that for low gas velocities (< 0.05 m/s), higher gas holdups were obtained in slurry bubble columns with low solids concentrations (< 10 vol. %) and density (ρ_p < 1300 kg/m^3). For higher gas velocities and higher solids concentrations and density , the gas holdup in slurry bubble columns was lower than in solid-free bubble columns. The decrease in gas holdups was attributed to increases in the apparent viscosity of the suspension. The higher gas holdups obtained at low solids concentrations and densities were explained by the qualitative turbulence model from Raebiger (1985).

2.2.2.2.8 Local Gas Holdup in Bubble Columns

Some researchers have also measured local gas holdups in bubble columns (Hills, 1974; Nottenkaemper et al., 1983; Wachi et al., 1987). Hills (1974) observed that for gas flow rates below 0.03 m/s, the radial profile of gas holdup were relatively flat, but at higher gas flowrates there was increasingly sharp maxima at centre. These observations were shared by Nottenkaemper et al., 1983 and

Wachi et al. (1987). Wachi et al. (1987) observed that the gas holdup at the column wall was 10 to 20 % of that at the centre.

These observations suggest that liquid circulation in bubble columns is developed by the buoyant force due to radial variations of gas holdup.

2.2.2.3 Correlations for Gas Holdup in Bubble Columns

The gas holdup in bubble column can be predicted with empirical correlations, the drift flux model or the force balance model.

A number of empirical correlations have been proposed in the literature for the prediction of gas holdup in bubble columns (see Table 2.2.1). However, no single correlation can account for the large dispersion of literature data. Schuegerl et al. (1977) and Bach and Pilhofer (1978) have attributed this dispersion to the sensitivity of holdup to the presence of impurities which affect the coalescence and bubble velocity.

The correlations proposed by Akita and Yoshida (1973) Hikita et al. (1980) are based on numerous experimental data. These correlations generally do not account for the effects of sparger characteristics. The correlation proposed by Bach and Pilhofer (1978) is based on the data obtained with pure organic compounds and cannot predict holdup in mixtures and electrolyte solutions. Quicker and

Table 2.2.1 Empirical correlations for gas holdup in bubble columns

Correlations	Systems	Range of Variables	Investigators	Remarks
$\epsilon_g = \frac{1}{2+(0.35/V_g)(\rho_l\sigma/72)1/3}$	Air/Water, Kerosene, Glycerol, Light oil Na_2SO_3, $ZnCl_2$	V_g=0.004 to 0.45 m/s; D_c>0.1 m ρ_l=780-1700 kg/m3. μ_l=0.0009 to 0.0152 Pa.s σ=0.025-0.076 N/m	Hughmark (1967)	Correlation based on data obtained in liquids with different coalescing behavior
$\epsilon_l = 1.02\ Fr_l^{-0.009}(\rho_g/\rho_l)^{-0.009} / Fr_g^{-0.036}$	Air/Water	V_g=0.0-0.26 m/s V_l=0.014-0.102 m/s	Kim et al. (1972)	Data obtained in two dimensional column
$\frac{\epsilon_g}{(1-\epsilon_g)^4} = C_2(Bo)1/8(Ga)1/12(Fr_g)$ f_1 = 0.2 for pure liquids and non-electrolytes f_2 = 0.25 for electrolytes	Air, Helium, CO_2, O_2/ Water, Methanol, CCl_4 Glycol, aq. soln. of methanol, glycol, NaCl and Na_2SO_3	V_g=0.003-0.4 m/s V_l=0-0.044 m/s D_c=0.152-0.6 m ρ_l=800-1600 kg/m3. μ_l=0.00058-0.021 Pa.s; σ=0.022-0.0742 N/m	Akita and Yoshida(1973)	Effects of distributor design not included
$\epsilon_g = 0.505V_g^{0.47}(0.072/\sigma)^{0.66}$ $(0.001/\mu_l)0.5$	Air/Water, aq. soln. of Methanol	V_g=0.042-0.38 m/s D_c=0.0756-0.61 m ρ_l=910-1200 kg/m3 μ_l=0.0007-0.0178 Pa.s; σ=0.0375-0.0748 N/m	Hikita and Kikukawa (1974)	Effects of distributor design cannot be accounted for
$\epsilon_g = 0.728U-0.485U^2+0.0975U^3$ $U=V_g/[\sigma(\rho_l-\rho_g)g/\rho_l^2]0.25$	Air/Water, Kerosene aq. soln. of Glycerol	V_g=0.0014-0.14 m/s D_c=0.05 and 0.1 m ρ_l=800-1100 kg/m3 μ_l=0.0009-0.0115 σ=0.0312-0.072 N/m	Kumar et al. (1976)	Correlation cannot account for distributor effects
$\frac{\epsilon_g}{1-\epsilon_g} = 0.115\{\frac{V_g^3}{\nu_l g(\rho_l-\rho_g)/\rho_l}\}0.23$	Air/pure organic liquids	V_g=0-0.1 m/s D_c=0.1 m ρ_l=824-2965 kg/m3 σ=0.0275-0.0495 N/m	Bach and Pilhofer (1978)	Recommended for pure organic liquids in the heterogeneous regime only
$\epsilon_g = 0.672f_2(V_g\mu_l/\sigma)^{0.578}$ $(\mu_l^4g/\rho_l^2\sigma^3)^{-0.131}(\rho_g/\rho_l)0.062$ $(\mu_g/\mu_l)0.107$ f_2 = 1.0 for nonelectrolyte Soln. f_2 = 100.0414I I<1.0 kg ion/m3 f_2 = 1.1 I > 1.0 kg ion/m3 I = Ionic strength of the solution	Air, N_2, CO_2, CH_4, C_3H_8 /Water, Organic liquids Electrolyte Solutions	V_g=0.042-0.38 m/s D_c=0.1 m ρ_l=790-1170 kg/m3. ρ_g=.84-1.84 kg/m3. μ_l=0.0009-0.0178 Pa.s; σ=0.0229-0.0796 N/m	Hikita et al. (1980)	Distributor effects are not accounted for

Table 2.2.1

Correlations	Systems	Range of Variables	Investigators	Remarks
$\epsilon_g = 3.96 V_g^{0.44} \rho_l^{-0.98} \sigma^{-0.16} \rho_g^{0.19} + 0.009$	Air, Helium, Argon/ Water, Trichlor-ethylene organic solvent (with and without solvent)	V_g=0.02-0.2 m/s D_c=0.3 m ρ_l=788-1450 kg/m3 ρ_g=0.168-1.34 kg/m3; μ_l=0.00055-0.00145 Pa.s; σ= 0.028-0.072 N/m	Reilly et al. (1986)	Purely espirical correlation, based on data obtained in liquids with different coalescence behavior
$\epsilon_g = f_3 NGa^{0.025} Fr_o^{0.84} (d_o/D_c)^{2.075}$	Air/Water, aq. soln. of glycerol, carboxy methylcellulose, poly-acrylamide	V_g=0.01-0.07 m/s Non-Newtonian slightly elastic and elastic liquids	Guy et al. (1986)	Correlation takes into account the distributor design effects
$\epsilon_g/(1-\epsilon_g) = 0.059 V_g^{0.8} \rho_g^{0.17} (\epsilon/72)^{-0.22} \exp(-P_1)$	Air, Hydrogen, Helium /Water, methanol, ethanol acetone and aq. soln. of alcohols	V_g=0.05-0.5 m/s D_c=0.05 m Pressure = atm. 5 MPa	Idogava et al. (1987)	

Deckwer (1981) measured gas holdup, using different types of spargers in various hydrocarbon liquids. These authors demonstrated that the correlations from the literature failed to predict their holdup data, although the physicochemical properties of the liquids were within the recommended range for these correlations. Hikita et al. (1980) partly attributed the difference between the various correlations to the differnces in the design of gas spargers. It was concluded that at low gas velocities a single gas sparger gave lower gas holdups than multinozzles or porous plate spargers.

Guy et al. (1986) measured gas holdups using perforated plates with various numbers and distributions of 1.0 mm orifices. The correlation proposed by Guy et al. (1986) takes into account the effects of the diameter (d_o) and number (N) of sparger orifices. The proposed correlation is, however, based on data obtained with a single orifice diameter and generally does not account for sparger design (i.e. orifice pitch) and coalescence behavior of liquid.

For coalescing liquids and coarse distributors, the correlations proposed by Akita and Yoshida (1973) and Hikita et al. (1980) should give reasonable estimates of gas holdup in batch bubble columns.

While, all the above correlations are based on the data obtained in batch bubble columns, the correlations proposed by Otake et al. (1981) are based on data obtained

in a continuous bubble column and account for the effect of liquid velocity on gas holdup. The proposed correlations, however, are based on limited data and fail to account for the effect of liquid coalescence behavior on gas holdup. The correlations for gas holdup in highly viscous Newtonian and non-Newtonian liquids have been proposed by Godbole et al. (1982). These correlations were obtained using aqueous solutions of glycerine and carboxy methyl cellulose which restricts their use for other solutions with different coalescing behavior.

The concept of drift flux was introduced in section 2.2.1.4. The drift flux concept can be combined with a correlation for the slip velocity to predict gas holdup in bubble columns. The slip velocity between the gas bubbles and the liquid in the ideal bubbly flow regime for cocurrent gas-liquid flow is defined as:

$$V_s = \frac{V_g}{\epsilon_g} - \frac{V_l}{1-\epsilon_g} \qquad \text{.....(2.2.8)}$$

Lapidus and Elgin (1957) have suggested that the slip velocity is independent of the phase velocities and is only a function of the rise velocity of an isolated bubble and of the gas holdup (which accounts for bubble-bubble interactions):

$$V_s = V_{bo}\phi(\epsilon_g) \qquad \text{.....(2.2.9)}$$

Combining Equations 2.2.2a, 2.2.8 and 2.2.9,

$$V_{gl} = V_s\epsilon_g(1-\epsilon_g) = V_{bo}\phi(\epsilon_g) \qquad \text{.....(2.2.10)}$$

Table 2.2.2 gives different forms of the function $\phi(\epsilon_g)$ suggested by different researchers. For given gas and liquid velocities, the gas holdup can be predicted, using Equations 2.2.2a and 2.2.10.

Table 2.2.2 Suggested forms of the function $\phi(\epsilon_g)$ for the description of drift flux by Equation 2.2.10

$\phi(\epsilon_g)$	Authors
$\epsilon_g(1-\epsilon_g)^{2.39}$	Richardson and Zaki (1954)
$\epsilon_g(1-\epsilon_g)^{n1}$ n1 = 2 (small bubbles) n1 = 0 (large bubbles)	Griffith and Wallis (1961)
$\epsilon_g\frac{(1-\epsilon_g)^2}{(1-\epsilon_g^{5/3})}$	Marrucci (1965)
$\epsilon_g(1-\epsilon_g)$	Turner (1966)
ϵ_g	Davidson and Harrison (1966)
$\epsilon_g(1-\epsilon_g)^{2.39}(1+2.55\epsilon_g^3)$	Lockett and Kirkpatrick (1975)
$\epsilon_g(1-\epsilon_g)^{n2}$ $n2 = f(D_c, \epsilon_s, \epsilon_l, \mu_{sl}, \rho_{sl}, V_t)$	Kara et al. (1981)

Lockett and Kirkpatrick (1975) reported that the Richardson and Zaki (1954) equation gave a good fit to their bubble swarm holdup data upto a holdup of 30 %. For higher holdups a correction factor was introduced to account for the effects of bubble deformations. For holdups in commercial paraffin, the expression by Marucci (1965) described the data well (Shah et al.,1982). For the churn turbulent regime, the concept of Zuber and Findlay (1963) has been found to work well for some cases (see section 2.2.1.4) The correlation proposed by Kara et al. (1981) is applicable to slurry bubble columns.

Wachi et al. (1987) derived an equation for mean gas holdup based on the force balance approach of Hills (1974) and Miyauchi and Shyu (1970). This correlation, however, requires knowledge of turbulent viscosity, slip velocity of bubbles relative to the liquid and shear stress at the column wall.

Based on the above review, it can be concluded that none of the available literature correlations can prove useful over the whole range of operating conditions in bubble columns. In order to develop more meaningful correlations, a more fundamental approach needs to be adopted. For example, the bubble size generated in the distributor region can account for the effect of gas distributor design on gas holdup. Also, separate correlations need to be developed for the different

operating regimes in bubble columns.

2.2.3 Bubble Size Distribution

The size distribution of bubbles affects the gas holdup, the interfacial area for mass transfer, the residence time distribution for gas phase and liquid circulation patterns in the column. All these factors influence the performance of a bubble column reactor.

2.2.3.1 Measurement of Bubble Size Distribution

Direct measurement of bubble size at the distributor is possible only for single orifice spargers for low gas flowrates. At high gas flowrates a jet of gas is formed which breaks into bubbles of different sizes above the distributor. For multiorifice spargers, there is bubble coalescence at the distributor and bubble coalescence and breakup just above the distributor.

As shown in Table 2.2.3, a number of techniques have been developed in the literature for the measurement of bubble size distribution. Following is a critical review of the various techniques.

2.2.3.1.1 Photographic Technique

As shown in Table 2.2.3, a number of investigators have used this technique for bubble size measurements. In order to avoid optical distortions caused by the column curvature, the measurements need to be made through plane-

Mashelkar, 1968; Mashelkar and Sharma, 1970).

For $1 < Re_{go} < 10$

$$d_{vs} = 1.56\ (Re_{go})^{0.058}\ (\sigma d_o^2/(\rho_l-\rho_g)g)^{0.25} \quad \text{.....(2.2.12)}$$

$10 < Re_{go} < 2100$

$$d_{vs} = 0.32\ (Re_{go})^{0.425}\ (\sigma d_o^2/(\rho_l-\rho_g)g)^{0.25} \quad \text{.....(2.2.13)}$$

$4000 < Re_{go} < 70,000$

$$d_{vs} = 100\ (Re_{go})^{-0.4}\ (\sigma d_o^2/(\rho_l-\rho_g)g)^{0.25} \quad \text{.....(2.2.14)}$$

It should be pointed out that these correlations are based on average bubble size measurements obtained with either the photography method or a chemical method. These correlations, therefore give only conservative estimates of bubble size.

The correlations proposed by Bhavaraju et al. (1978) are again based on measurements with the photography method. Moreover these researchers used only single nozzle spargers for their study which further limits the scope of their proposed correlations.

Idogawa et al. (1987) proposed a correlation to account for the effect of column pressure on average bubble size:

2.2.3.1.2 Conductivity Probe Technique

This method utilizes the difference in conductivity between the liquid and the gas phase. This technique can be used for measuring the diameter, velocity and frequency of bubbles.

Most of the researchers have used two electrode microprobes as the sensors for the measurement of bubble diameters (Yamashita et al., 1979; Koide et al., 1979; Buchholz et al., 1981; Lewis et al., 1984; Davis and Fungtamasan, 1984; Shah et al., 1985; Idogawa et al., 1986, 1987). For the spherical shape bubbles these probes would provide accurate measurements since in that case the measured piercing depth is equal to the diameter. However in case of ellipsoid bubbles or spherical caps the diameter determined by this method would be consistently small, since only the small axis of symmetry would be measured. In order to determine the volume of these bubbles, it would be necessary to use four or five electrode conductivity probes, where the outer probes are at different distance from the central probe. The bubble shape can then be inferred from the different signal lengths (Buchholz et al. 1981). In case of irregulary deformed bubbles however there can still be large errors in measurements because then the piercing depth has no relation to the volume.

Like other probe techniques, this technique too would interfer with bubble flow in the dispersion. Moreover, due

to limitations of probe design, it cannot detect small bubbles (d_b < 1 mm) in the dispersion. As shown by Wachi et al. (1[illegible], the probe technique failed to detect 30% of bubble volum[illegible]

2.2.3.1.3 Dynamic Gas Disengagement Technique

This technique involves fast filming of the drop in gas-liquid dispersion height after the gas has been shut-off. The rate at which the height drops would depend on the concentration and velocity of the gas bubbles in the dispersion. This technique has been used by a number of researchers to study the gas holdup structure and obtain the fractions of large and small bubbles (Sriram and Mann, 1977; Godbole et al., 1982, 1984; Schumpe and Deckwer, 1982; Schumpe and Grund, 1986).

Although relatively simple to use, this technique has a number of limitations. Schumpe and Grund (1986) have reviewed the major problems in the application of this technique. The inaccuracies in measurements can be caused by fluctuation in dispersion height and downward flow of liquid during the disengagement of large bubbles. There can also be an additional source of error caused by the residual flow of gas through the distributor after stopping the gas supply, due to pressure equilibration. This error can however be minimized by suitable sparger design. Since this technique provides information about bubble rise velocities, its use is limited to systems with

bubbles of wide range of velocities. In air/water systems, the bubble velocity is virtually unchanged for bubble sizes ranging from 3 to 8 mm (Clift et al., 1978). The disengagement technique would, therefore, generally be useful when there is a significant proportion of bubbles smaller than 3mm or larger than 8mm.

2.2.3.1.4 Other Techniques

Funnel Capture Technique

Weiland et al. (1980) used a technique whereby a small stream from the dispersion was sucked through a funnel into a transparent capillary tube in which the bubbles were transformed into slugs. The bubble size was obtained from the length of slug measured by a photoelectric probe. Although relatively simple to use, this technique suffers from a number of drawbacks which include: 1) There can be coalescence of bubbles when they are being sucked through the funnel 2) The funnel could also interfer with local hydrodynamics of the column.

Hot Wire Anemometer Technique

Hot wire anemometers have been widely used for turbulence measurement in liquids. Chuang and Goldschmidt, (1971) used this technique to detect and measure bubbles of air in water. The limitations of this technique are similar to those of other probe techniques (see section

2.2.3.1.2).

The measurement of bubble size in a gas-liquid dispersion is quite a challenging task. Depending on the operating flow regime, there can be quite a wide variation of bubble sizes and shapes. As reviewed above, none of the available techniques can prove useful for bubble size measurement over a wide range of operating conditions. Probe techniques can provide good estimate of bubble size in the intermediate range (2 to 8 mm). Small bubbles (< 1 mm) could be measured by a combination of photography and dynamic disengagement technique. New techniques need to be developed for the measurement of highly deformed large bubbles.

2.2.3.2 Effects of Operating Variables on Bubble Size

The average bubble size in a bubble column has been found to be affected by gas velocity, liquid phase properties, gas distribution, operating pressure and column diameter.

Some researchers have reported a gradual decrease in bubble size with increasing gas flowrates (Towell et al., 1965; Akita and Yoshida, 1974). Ueyama et al. (1980), however, observed that the average bubble size increased gradually with gas velocity. As pointed out by Ueyama et al. (1980), the results obtained by Akita and Yoshida (1974) were affected by the experimental technique

(photography) used by these researchers. Idogawa et al. (1987) obtained the cross-sectional average bubble diameter at different operating pressures in a column. These authors concluded that the average bubble diameter, for a given pressure, was almost independent of gas velocity. The discrepancies in the results of Ueyama et al. (1980) and Idogawa et al. (1987) could be explained by differences in distributor designs, column diameter and range of gas velocity studied.

The average bubble size has been observed to decrease with decreasing surface tension of liquid (Akita and Yoshida, 1974; Idogawa et al., 1987) and increase with increasing liquid viscosity (Bhavaraju et al., 1978). In electrolyte solutions, Marrucci and Nicodemo (1967) reported lower average bubble size as compared to pure water. For a given gas velocity, the average bubble size decreased with increasing electrolyte concentration and reached an asymptotic value.

At low operating pressures, the average bubble size was observed to depend on the distributor type (Idogawa et al., 1986). Lower average bubble size was obtained with a porous distributor as compared to a single nozzle sparger. This difference, however, disappeared with increasing operating pressure.

Koide et al. (1979) and Ueyama et al. (1980) measured average bubble size in columns of diameters 5.5 and 0.6 m

respectively. From these studies it can be concluded that a higher average bubble size is obtained in columns of larger diameters.

2.2.3.3 Correlations for Average Bubble Size

Correlations for average bubble size have been developed by a few researchers (Akita and Yoshida, 1974; Kumar et al., 1976; Bhavaraju et al., 1978; Idogawa et al., 1987). These correlations are reviewed below:

Akita and Yoshida (1974) proposed a correlation, using dimensionless numbers

$$\frac{d_{vs}}{D_c} = 26\ (Bo)^{-0.5}\ (Ga)^{-0.12}\ (Fr'_g)^{-0.12} \qquad ...(2.2.11)$$

This correlation is based on the results obtained in two dimensional columns, using a photography technique. Since the photography method gives information about bubbles close to the wall only, this correlation cannot provide true average values of bubble size. Moreover, the results obtained in two dimensional columns cannot generally be applied to circular columns due to differences in liquid circulation patterns.

Kumar et al. (1976) proposed the following correlations for average bubble size based on their data and four other literature studies (Van Krevelen and Hoftijzer, 1950; Leibson et al., 1956; Sharma and

Mashelkar, 1968; Mashelkar and Sharma, 1970).

For $1 < Re_{go} < 10$

$$d_{vs} = 1.56\ (Re_{go})^{0.058}\ (\sigma d_o^2/(\rho_l-\rho_g)g)^{0.25} \quad \text{.....(2.2.12)}$$

$10 < Re_{go} < 2100$

$$d_{vs} = 0.32\ (Re_{go})^{0.425}\ (\sigma d_o^2/(\rho_l-\rho_g)g)^{0.25} \quad \text{.....(2.2.13)}$$

$4000 < Re_{go} < 70,000$

$$d_{vs} = 100\ (Re_{go})^{-0.4}\ (\sigma d_o^2/(\rho_l-\rho_g)g)^{0.25} \quad \text{.....(2.2.14)}$$

It should be pointed out that these correlations are based on average bubble size measurements obtained with either the photography method or a chemical method. These correlations, therefore give only conservative estimates of bubble size.

The correlations proposed by Bhavaraju et al. (1978) are again based on measurements with the photography method. Moreover these researchers used only single nozzle spargers for their study which further limits the scope of their proposed correlations.

Idogawa et al. (1987) proposed a correlation to account for the effect of column pressure on average bubble size:

$$d_{vs} = 3.91\ \rho_g^{-0.07}\ (\sigma/72)^{0.228}\exp(-P_T) \quad \ldots(2.2.15)$$

This correlation is based on the results obtained with a single distributor only. It also does not account for the effects of column diameter on bubble size.

2.2.3.4 Bubble Formation at Single Orifice

The studies of bubble formation at single orifice nozzles are mainly of theoretical interest since the average bubble size in the bulk region is determined mainly by the turbulence in the dispersion. The bubble formation from an orifice has been assumed to take place in two stages namely the expansion stage and detachement stage (Ramakrishnan et al., 1969; Tsuge and Hibino, 1978). In the expansion stage, the bubble grows while its base remains attached to the tip of the orifice. This stage ends when the inertial force, surface tension and viscous drag force which act on the bubble are just balanced so that the bubble begins to rise. In the detachement stage the bubble continues to grow while it is still connected to the orifice by a small gas column or neck. This stage ends when the neck breaks off and the bubble separates. The mathematical formulation of the two-stage model has been well described by Ramakrishnan et al. (1969). The various bubble formation models were reviewed by Tsuge (1986).

2.2.4 Liquid Backmixing in Bubble Columns

The liquid backmixing in the bubble column is caused by the fast moving gas bubbles which accelerate the liquid in their wakes. This causes the liquid in other parts of the column to move downwards. Mixing of liquid phase reduces temperature and concentration gradients and thus strongly affects the heat and mass transfer processes.

2.2.4.1 Measurement Techniques

The liquid backmixing is evaluated from the residence time distribution of a tracer injected into the liquid phase. The various experimental techniques differ with respect to the type of tracer used and the mode of tracer injection. The proper choice of the tracer would ensure that the residence time distribution characteristic of the phase is not influenced by the tracer. Shah et al. (1978) have listed the basic requirements for a satisfactory tracer experiment. The different types of tracer and tracer inputs used in bubble columns are shown in Table 2.2.4. It can be seen that the most commonly used tracers are the solutions of sodium and potassium chloride which can be easily detected by means of an electrical conductivity cell. Another easily detectible tracer is the heat tracer (Aoyama et al., 1968), here care should be taken to ensure that the heat losses from the column wall are kept to a minimum.

Table 2.2.4 Techniques used in the Literature to Measure Liquid Backmixing in Bubble Columns

Techniques	References	Remarks
Pulse of salt or acid solution (KCl, $NaCl$, H_2SO_4)	Ohaki and Inoue(1970) Kato and Nishiwaki (1972); Hikita and Kikukawa (1974); Alexander and Shah (1976); Houzelot et al.(1985); Wachi et al.(1987)	This technique requires fast response probes
Steady state tracer injection		
Salt Solutions ($NaCl$, KCl)	Argo and Cova (1965) Eissa ans Schugerl (1975); Konig et al. (1978)	Dissolved salts can alter the coalescing behavior of liquid
Heat tracer	Cova (1974); Kelkar et al. (1983); Wendt et al. (1984)	Heat losses from column can affect. measurements
Color tracer (i.e. methylene blue dye)	Towell and Ackerman (1972); Konig et al. (1978)	This technique allows visual observations

2.2.4.2 Effects of Operating Variables on Liquid Backmixing

The liquid backmixing is usually characterized by the axial dispersion model which is a one-dimensional Fick's law type of diffusion equation. The constant of proportionality in this equation commonly known as axial

dispersion coefficient is a measure of the degree of backmixing.

2.2.4.2.1 Effects of Gas Velocity

The liquid backmixing has been found to increase with increasing gas velocity in bubble columns (Ohaki and Inoue,1970; Eissa et al., 1971; Deckwer et al., 1974; Hikita and Kikukawa, 1974; Wendt et al., 1984; Wachi et al., 1987). The higher backmixing could mainly be attributed to the higher liquid recirculation caused by the higher frequency of the formation of larger gas bubbles with increasing gas flow rates.

2.2.4.2.2 Effects of Liquid Velocity

A number of researchers found the axial dispersion in bubble columns to be insensitive to variation in liquid flow rate (Kato and Nishiwaki, 1972; Aoyama et al., 1968; Houzelot et al., 1985). Eissa et al. (1971) however reported liquid backmixing to decrease with increasing liquid velocity. These results have not been confirmed by other researchers. The effects of liquid velocity have been investigated over a narrow range only (V_l < 0.05 m/s). Further work is required to establish the effects of liquid velocity over a wide range of liquid velocity.

2.2.4.2.3 Effects of Column Diameter and Column Height

Liquid backmixing has been found to increase with

increasing column diameter by all the researchers (Aoyama et al., 1968; Kato and Nishiwaki, 1972; Deckwer et al., 1974; Hikita and Kikukawa, 1974; Wendt et al., 1984). The axial dispersion coefficient has been reported to increase with column diameter to the power 1.25 to 1.5. The increase in liquid backmixing with column diameter can mainly be attributed to decreasing wall effects.

Deckwer et al. (1973) observed two mixing zones with porous distributors with different axial dispersion coefficients. The axial dispersion coefficient was larger in the upper zone than in the lower zone close to distributor. The difference between the zones, however, disappeared at higher gas velocities and a constant backmixing coefficient was obtained. Deckwer et al. (1974) pointed out that this phenomenon was restricted to porous gas distributors only.

2.2.4.2.4 Effects of Gas Distribution

The axial dispersion coefficient in bubble columns has been found to be affected by the type of gas distributor used. Higher axial dispersion coefficients were obtained with distributors of small orifice size (d_o < 1.0 mm) and for gas velocities less than 0.15 m/s (Ohki and Inoue, 1970; Wendt et al., 1984). When the orifice size was larger than 1 mm, Wendt et al. (1984) observed no significant effects of distributor design on liquid backmixing.

The higher liquid backmixing observed with the distributors of small orifice size could be related to stronger convection currents established by the bubble swarm generated by these distributors.

2.2.4.2.5 Effects of Liquid Physical Properties

Liquid viscosity was found to have no effect on axial dispersion coefficient by a number of investigators (Cova, 1974; Alexander and Shah, 1976; Houzelot et al., 1985). Hikita and Kikukawa (1974) however found the dispersion coefficient to decrease with increasing liquid viscosity. It should be noted that except for Hikita and Kikukawa (1974) all other researchers used small diameter columns (D_C < 0.06m) for their study. The use of small diameter columns would have resulted in the formation of slug flow regime where the effects of liquid viscosity are not likely to be significant. More work in larger diameter column is, thus required to establish the effects of liquid viscosity on liquid backmixing.

No effect of surface tension has been observed on axial dispersion coefficient in bubble columns (Cova, 1974; Alexander and Shah, 1976)

2.2.4.2.6 Effect of Coalescence Inhibitors

The effect of coalescence inhibition has been studied mainly in the aqueous solutions of salts and alcohols (Deckwer et al., 1974; Schugerl et al., 1977; Koenig et

al., 1978; Kelkar et al., 1983a; Kelkar et al., 1983b). The results of these researchers suggest that there exists a complex relationship between liquid backmixing, gas distribution and the nature of coalescence inhibitor.

Kelkar et al. (1983a,1983b) found that axial dispersion was negligible in the aqueous solutions of propanol and butanol at low gas velocities (< 0.05 m/s). For higher gas velocities axial dispersion coefficient increased sharply with gas velocity. Kelkar et al. (1983b) however observed that electrolyte solutions behaved similar to air-water system i.e. axial dispersion coefficient increased over the whole range of gas velocity.

Schuegerl et al. (1977) and Koenig et al. (1978) also investigated the effects of gas distribution on axial dispersion coefficient. With perforated plate distributors the liquid backmixing was found to be lower for both salt solutions and alcohol solutions as compared to tap water. When porous plate distributors were used the liquid backmixing varied with the pore size and the type of alcohol.

2.2.4.2.7 Effects of Column Verticality

The axial dispersion coefficient in bubble columns has been found to be strongly influenced by even slight deviations from true verticality (Tinge and Drinkenburg, 1986; Rice and Littlefield, 1987). Tinge and Drinkenburg

(1986) showed that axial dispersion increased upto an order of magnitude even for very small angular deviations (<0.04 rad.) from true verticality. Similar results were also obtained by Rice and Littlefield (1987), who also observed that for tilted columns, large scale circulations arose very quickly with a length scale of the order of column height. There was, however, no significant effect of the column verticality once the angle of deviation was greater than one degree.

These results clearly demonstrate that column verticality should also be measured while investigating the effects of different operating variables on liquid backmixing.

2.2.4.3 Correlations for Axial Dispersion Coefficient

The various empirical correlations proposed for axial dispersion coefficient in the literature are summarized in Table 2.2.5. It can be seen that almost all the correlations take into account the important effects of gas velocity and column diameter on axial dispersion coefficient in bubble columns. However, the effects of other variables such as gas distribution, physical properties of liquid and coalescence inhibitors have not been covered adequately.

Baird and Rice (1975) derived an equation using the isotropic turbulence model of Hinze (1958). The proposed

Table 2.2.5 Empirical correlations for liquid backmixing in bubble columns

Correlations	Systems	Range of Variables	Investigators.	Remarks
Bubble Flow Regime $D_z=75.4D_c^{2}V_g^{1.2}+1700d_o$ Coalesced Bubble Flow Regime $D_z=0.14D_c/(1-\epsilon_g)^2$	Air/Water	V_g=0.0-0.25 m/s D_c=0.04,0.08,0.16 m Perforated plates (d_o=0.4,0.7,1.0,2.0, 3.0 mm)	Ohaki and Inoue(1970)	Effects of liquid phase properties not accounted for
$\frac{V_s D_c}{D_z}$ = 3.0 $V_s = \frac{V_g}{\epsilon_g} - \frac{V_l}{\epsilon_l}$	Air/Water	V_g=0.0088-0.022 m/s D_c=0.066,0.12,0.21 m Single nozzle (d_o=2 mm	Reith et al. (1968)	Effects of distributor design are not accounted for
$Pe = \frac{13Fr_g}{1+6.5Fr_g^{0.8}}$ (for D_c > 0.12 m and d_o > 2 mm	Air/Water	V_g=0.01-0.25 m/s D_c=0.066,0.12,0.21 m Perforated plates (d_o=1,1.4,2,3 mm)	Kato and Nishiwaki (1972)	Correction suggested for distributor effects
$D_z = 1.23\ D_c^{1.5}\ V_g^{0.5}$	Air/Water	V_g=0.0-0.152 m/s V_l=0.0024-0.014 m/s D_c=0.4-1.0 m Perforated plate (d_o = 6.35 mm)	Towell and Ackerman (1972)	Correlation cannot account for liquid phase properties and distributor effects
$D_z = (0.114+0.523V_g^{0.77})D_c^{1.25}(1/\mu_l)^{0.12}$	Air/Water, aq. solns of methanol and can Sugar	V_g=0.043-0.338 m/s D_c=0.1,0.19 m Single nozzles (d_o=13.1,20.6,36.2 mm)	Hikita and Kikukawa (1974)	Applicable to coarse distributor only
$D_z = 0.678\ D_c^{1.4}V_g^{0.3}$	Air/Water	V_g=0.01-0.15 m/s D_c=0.1,0.15 m Perforated plate (d_o=1 mm)	Deckwer et al (1974)	
$D_z = 1.7*10^{7}\ D_c^{1.4}(3.47V_g^{0.77}+1.93V_g^{0.1})$	Air/Water	V_g=0.01-0.85 m/s V_l=0.002-0.045 m/s D_c=0.04-1.0 m Porous diffusers (20-200 μm) Perforated plates (d_o=1-2 mm) Single nozzles (d_o=2-7.5 mm)	Wendt et al. (1984)	Correlation based on large amount of data

correlation provided a good fit to a large number of reported experimental data.

$$D_z = 0.35\ D_c^{4/3} (V_g g)^{1/3} \qquad \text{.....(2.2.16)}$$

A few researchers have also developed correlations for liquid axial dispersion based on liquid circulation models in bubble columns (Joshi and Sharma, 1979; Miyauchi et al., 1981; Viswanathan and Rao, 1984). Joshi and Sharma (1979) proposed a correlation for axial dispersion of liquid, based on their circulation cell model.

$$D_z = 0.31\ D_c^{1.5}\ V_c \qquad \text{.....(2.2.17)}$$

Here, V_c is the average velocity of circulation in a bubble column, given as:

$$V_c = 1.31[gD_c(V_g + \frac{\epsilon_g V_l}{1-\epsilon_g} - \epsilon_g V_{bo})]0.33 \qquad \text{.....(2.2.17a)}$$

The calculation of V_c requires the knowledge of gas holdup and bubble rise velocity (V_{bo}), the latter would vary with bubble size. As pointed out in section 2.2.3, the bubble size is usually not known accurately.

Starting with the basic equation of motion, Miyauchi et al. (1981) and Wachi et al. (1987) developed a correlations for axial dispersion with and without the liquid flow. The proposed correlations require information on the mean gas holdup and the turbulent viscosity in the

column. Miyauchi et al. (1981) derived the following equation, using empirical correlations for turbulent viscosity and average gas holdup.

$$D_z = \left[2.91\times10^{7} + \frac{3.41\times10^{7}}{(1 - 0.54V_g)^2} \right] V_g^{0.25} D_c^{1.5} \quad \text{.....(2.2.18)}$$

This correlation is applicable for coarse distributors only with no liquid flow.

Viswanathan and Rao (1984) developed a relation for the average liquid circulation velocity in bubble columns. The model was then used to drive an expression for liquid axial dispersion coefficient which compared well with the correlation of Deckwer et al. (1974). Zehner (1986) developed an equation for liquid blending in bubble columns based on his liquid eddies model. The dependence of liquid dispersion coefficient on column diameter and gas velocity predicted by this model are similar to those given by correlations of Deckwer et al. (1974) and Baird and Rice (1974).

2.2.5 Mass Transfer and Interfacial Area

2.2.5.1 Measurement Techniques for Volumetric Mass Transfer Coefficient ($k_l a$)

The various techniques used for the measurement of volumetric mass transfer coefficient can be divided into

two categories : 1) physical methods 2) chemical methods. Table 2.2.6 summarizes the list of literature studies based on these categories.

Table 2.2.6 Literature Techniques for Measurement of Volumetric Mass Transfer Coefficient in Bubble Columns

Techniques	References	Remarks
Physical Absorption/desorption of oxygen	Akita and Yoshida (1973); Nakanoh and Yoshida(1980); Hikita et al.(1981); Godbole et al.(1984); Ozturk et al.(1987)	Dynamic method Batch bubble Columns
Chemical absorption of oxygen in sodium sulfite solution	Godbole et al. (1983)	Dynamic method
Chemical absorption of CO_2 in sodium carbonate sodium bicarbonate buffer	Gopal and Sharma (1983)	Dynamic method
Chemical absorption of oxygen into alkaline solutions of sodium dithionite	Gopal and Sharma (1983)	Steady state method for continuous bubble column. k_1a values were affected by the presence of dissolved salts

A chemical method involves gas absorption accompanied by a chemical reaction which is sufficiently fast to maintain the dissolved gas concentration below its

equilibrium concentration with respect to the sparging gas stream; the reaction however should not be so rapid as to enhance mass transfer beyond physical absorption. The theory of mass transfer with chemical reaction was reviewed in section 2.1.5. The presence of a dissolved chemical and/or a catalyst used in chemical methods can alter the coalescing behavior of the liquid phase (Ruchti et al., 1985). This problem can be avoided by the physical methods which involve physical absorption or desorption of a gas into or from a liquid.

Both chemical and physical methods could be further divided into two classes, steady state and dynamic. While steady state methods are more commonly used for continuous bubble columns, dynamic methods find use in batch bubble columns (see Table 2.2.6). For the most commonly used dynamic method, the concentration of the oxygen in the gas phase undergoes a step change, and the concentration of the dissolved oxygen in the liquid phase is measured as a function of time. The dissolved oxygen concentration is usually measured with a polarographic oxygen electrode.

2.2.5.2 Effects of Operating Variables on Volumetric Mass Transfer Coefficient

The evaluation of volumetric mass transfer coefficient requires the knowledge of the residence time distribution of the phases. For the batch bubble columns,

liquid mixing has been assumed to be essentially instantaneous and perfect by various researchers (Akita and Yoshida, 1973; Nakanoh and Yoshida, 1980; Hikita et al., 1981; Koide et al., 1983). In continuous bubble columns, the assumption of complete mixing may be justifiable only in large diameter columns (D_c>1.0 m). It may, however, be necessary to take into account the effects of radial concentration profile on the measurements. In tall and small diameter bubble columns the k_1a should be evaluated by means of a model which accounts for the liquid mixing (e.g. the axial dispersion model, Deckwer et al., 1974; Mangartz and Pilhofer, 1981).

The parameters affecting the gas-liquid mass transfer rate in bubble columns have been found to be generally the same as those affecting the gas holdup.

2.2.5.2.1 Effects of Gas Velocity

The volumetric mass transfer coefficient has been found to increase with gas velocity (Akita and Yoshida, 1973; Deckwer et al., 1974; Hikita et al., 1981; Koide et al., 1983; Godbole et al., 1984). Deckwer et al. (1974) proposed an empirical correlation of the form:

$$k_1a = C_2 \, V_g^{n3} \qquad \text{.....(2.2.19)}$$

Based on the data from several researchers, Shah et al. (1982) have shown that the value of the constant C_2 is strongly affected by the sparger and the liquid medium.

For the same gas velocity, porous distributors like sintered plates, elastic rubber plates and nozzle spargers of injector and ejector type give higher k_1a values than single and multinozzle spargers.

Prakash and Briens (1988) have shown that the effect of distributor type becomes less significant in the churn turbulent regime.

The increase in k_1a with increasing gas velocity has been attributed mainly to increase in interfacial area per unit volume 'a' with gas velocity (Towell et al., 1965; Voyer and Miller, 1968; Mashelkar, 1970; Mangartz and Pilhofer, 1981).

2.2.5.2.2 Effects of Liquid Velocity

The liquid velocity was not found to have any effect on k_1a by a number of authors (Mashelkar, 1970; Deckwer et al., 1974; Burckhart and Deckwer, 1975; Schuegerl et al., 1977). Some researchers (Voyer and Miller, 1968; Alvarez-Cuenca et al., 1980) however, reported that k_1a depended on the liquid velocity. The observed increase in k_1a values by these authors could be due to assumption of plug flow model.

2.2.5.2.3 Effects of Physical Properties of Liquid

The effect of liquid viscosity on gas-liquid mass transfer rate has been studied mainly in aqueous solutions

of sodium carboxy methyl cellulose (CMC), sodium polyacrylate, glycerol, surcose and carbopol (Nakanoh and Yoshida, 1980; Schumpe and Deckwer, 1982; Deckwer et al., 1982; Koide et al., 1983; Kawase et al., 1987). The volumetric mass transfer coefficient has been found to decrease with increasing concentration of solutions and hence increasing viscosity of solutions.

Ozturk et al. (1987) used pure organic liquids to investigate the effect of liquid viscosity. The decrease in volumetric mass transfer coefficient which was observed when the viscosity was increased was attributed to the lower diffusion coefficient in the high viscosity liquids.

The effect of surface tension on the gas-liquid mass transfer rate has been studied using both pure liquids and mixtures of liquids (Akita and Yoshida, 1973; Koide et al., 1983 and Ozturk et al., 1987). Although there is a lack of systematic study, the available data suggest that volumetric mass transfer coefficient decreases with increasing surface tension.

No systematic work has been done to investigate the effects of liquid density on volumetric mass transfer coefficient.

2.2.5.2.4 Effects of Coalescence Inhibitors

The presence of coalescence inhibition additives such as electrolytes and surface active compounds in the liquid

phase has been found to affect the gas-liquid mass transfer rate (Zieminski et al., 1967; Jackson et al., 1975; Schuegerl et al., 1977; Hikita et al., 1980; Koide et al., 1985; Posarc and Tekic, 1987; Gurol and Nekovinaini, 1985).

The additive molecular weight has an important effect on the mass transfer. Posarac and Tekic (1987) studied the effects of the addition of n-alcohols with 1 to 4 carbon atoms at concentrations ranging from 0.5 to 1.0 %. Higher mass transfer rates were obtained in aqueous solutions of alcohols with higher molecular weight. Koide et al. (1985) on the other hand found that the volumetric mass transfer coefficient decreased with increasing alcohol molecular weights (for n-alcohols with 6 to 8 carbon atoms). Zieminski et al. (1967) found the volumetric mass transfer coefficient to increase with the additive molecular weight for n-alcohols with 3 to 7 carbon atoms. For monocarboxylic acids Zieminski et al. (1967) found that the volumetric mass transfer coefficient increased with the increasing molecular weight of the acids from propionic to heptanoic acids while the addition of decanoic acid reduced the mass transfer rate.

The nature of the additive polar group and the degree of substitution of its hydrocarbon chain also affected the effectiveness of an additive. Zieminski et al. (1967) found that the best additives were monocarboxylic acids followed by n-alcohols and dicarboxylic acids. Gurol and

Nekovinaini (1985) found that the addition of a methyl group on a phenol molecule increased its effectiveness while substitution of hydroxyl group decreased it.

Salts constitute another class of coalescence inhibitors. Hikita et al. (1981), for example observed higher mass transfer rates in aqueous electrolyte solutions than in pure water. Similar results with salt solutions were also obtained by Schügerl et al. (1977) and Oels et al. (1978).

2.2.5.2.5 Effects of Gas Distribution

Some researchers found no effect of the sparger type on volumetric mass transfer coefficient (Towell et al., 1965; Sharma and Mashelkar, 1968; Gopal and Sharma, 1983). The spargers used by these researchers had orifice diameter larger than or equal to 1 mm. Schuegerl et al. (1977) obtained higher volumetric mass transfer coefficient with porous distributor as compared with a perforated plate distributor. Oels et al. (1978) and Buchholz et al. (1983) studied the influence of gas distribution on interfacial area and mass transfer in both coalescing and noncoalescing media. They used gas distributors ranging from ejector and injector nozzles to porous and perforated plates in continuous bubble column. The distributor type did not have any effect on the interfacial area in coalescing media but a large effect in

noncoalescing media. Since the volumetric mass transfer coefficient is a product of the liquid phase mass transfer coefficient and the interfacial area, increases in interfacial area would lead to larger volumetric mass transfer coefficients.

2.2.5.2.6 Effects of Column Diameter and Column height

Gopal and Sharma (1983) found no effect of column diameter on volumetric mass transfer coefficient. These researchers used columns with inside diameter of 0.2 and 0.6 m. Gopal and Sharma (1983) also concluded that there was no significant effect of column height on volumetric mass transfer coefficient. Voigt and Schügerl (1979), however, observed that in coalescing media volumetric mass transfer coefficient decreased with increasing height to diameter ratio while in noncoalescing media the volumetric mass transfer coefficient was not affected by the column height to diameter ratio. The discrepencies between these results can be explained by the height upto which the effects of sparger design are significant (Voigt and Schugerl, 1979 and Heijnen and Vant Riet, 1984).

2.2.5.2.7 Effects of Solids on k_1a

The volumetric mass transfer coefficient in slurry bubble columns has been found to depend on the concentration, density, size and type of solids used. The volumetric mass transfer coefficient was found to decrease

with increasing solids concentration by most reseachers (Kato et al., 1973; Koide et al., 1983; Sauer and Hempel, 1987; Nigam and Schumpe, 1987; Schumpe et al., 1987). The decrease in volumetric mass transfer coefficient is attributable to decrease in interfacial area per unit volume. Sada et al. (1985) and (1986), however, observed an increase in interfacial area for low concentration slurries (< 2 wt %) of fine particles. The interfacial area, however, decreased at high solids concentrations. It was concluded that for low slurry concentration region the bubble size became smaller due to coalescence inhibition in the presence of small amount of fine particles. The enhancement of mass transfer in presence of solid particles was also reported by Godbole et al. (1983). As pointed out by Alper et al. (1980), the enhancement of mass transfer could be attributed to the type of solid particles used (i.e. oil shale particles). Alper et al. (1980) showed that the mass transfer rate enhanced in the presence of activated carbon particles and not in the presence of inert sand particles. Pal et al. (1982) showed that the specific rate of absorption was significantly enhanced in the presence of catalyst particles smaller than the diffusion film as compared to coarser particles. These results show that the gas-liquid mass transfer in slurry bubble columns is affected by particle size, concentration and the type of solid.

Schumpe et al. (1987) investigated the effects of

solid wettability on gas-liquid mass transfer in slurry bubble column. The lower values of volumetric mass transfer coefficients obtained in the suspension of Polypropylene particles as compared with the glass particles were attributed to the poor wettability of PP particles. It is suggested that the available mass transfer area is reduced by particle adsorption at the gas-liquid interface.

The effect of the presence of cells on oxygen mass transfer was investigated by Andrews et al. (1984). It was observed that the adsorbed cells were pushed around the bubbles by the drag force leading to higher capture efficiencies of the cells. The captured cells, however, accumulated in a packed mass near the rear stagnant point. It was argued that the demand for oxygen could exceed supply in this mass leading to local anoxic conditions.

2.2.5.3 Correlations for Volumetric Mass Transfer Coefficient

Various correlations proposed in the literature for the prediction of volumetric mass transfer coefficient in bubble columns are summarized in Table 2.2.7.

Shah et al. (1982) have shown that the correlation proposed by Akita and Yoshida (1973) well predicted the k_1a data obtained in bubble columns of various sizes. Ozturk et al. (1987), found that the correlations proposed

Table 2.2.7 Literature Correlations for Volumetric Mass Transfer Coefficient in Bubble Columns

Correlations	Systems		
$\frac{k_l a D_c^2}{D_l} = 0.6\left(\frac{\nu_l}{D_l}\right)^{0.5}\left(\frac{gD_c^2\rho_l}{\sigma}\right)^{0.62}\left(\frac{gD_c^3}{\nu_l^2}\right)^{0.31}\epsilon_g^{1.1}$	Air, O_2, CO_2, He/ Water, glycol and methanol (pure and aq. solns.)	Akita and Yoshida(1973)	Inclusion of gas holdup may account for distributor effects and changes in coalescing behavior
$\frac{k_l a D_c^2}{D_l} = 0.09\left(\frac{\nu_{l,eff}}{D_l}\right)^{0.5}\left(\frac{gD_c^2\rho_l}{\sigma}\right)^{0.75}\left(\frac{gD_c^3}{\mu_{l,eff}^2}\right)^{0.39}\left(\frac{V_g}{gD_c}\right)$	Air/Surcose aq. soln., CMC aq. soln.	Nakanoh and Yoshida(1980)	Purely empirical correlation
$k_l a = \frac{14.9g}{V_g} f_4\left(\frac{V_g\mu_l}{\sigma}\right)^{1.76}\left(\frac{\mu_l^4 g}{\rho_l\sigma^3}\right)^{-0.248}\left(\frac{\mu_g}{\mu_l}\right)^{0.243}\left(\frac{\mu_l}{\rho_l D_l}\right)^{-0.604}$ $f_4 = 1.0$ for nonelectrolytes $= 10^{0.068I}$ $I < 1.0$ $= 1.11410^{0.02I}$ $I > 1.0$	Air, O_2, CH_4, H_2/ Water, aq. solns. of surcose, methanol and 1-butanol	Hikita et al. (1981)	Accounts for changes in coalescing behavior due to presence of electrolytes
$k_l a = 0.00315\, V_g^{0.59}\, \mu_{l,eff}^{-0.84}$	Air/CMC aq. solns	Deckwer et al (1981)	Developed mainly for viscous liquids
$\frac{k_l a d_{vs}^2}{D_l} = 0.62\left(\frac{\nu_l}{D_l}\right)^{0.5}\left(\frac{g\rho_l d_{vs}^2}{\sigma}\right)^{0.33}\left(\frac{g\rho_l^2 d_{vs}^3}{\mu_l^2}\right)^{0.29}\left(\frac{V_G}{\sqrt{gd_{vs}}}\right)^{0.68}\left(\frac{\rho_g}{\rho_l}\right)^{0.04}$	Air, N_2, CO_2, He, H_2/ Pure organic liquids	Ozturk et al. (1987)	Mainly applicable to organic liquids. Requires knowledge of bubble diameter

by Akita and Yoshida (1973) and Hikita et al. (1981) could not satisfactorily predict the mass transfer coefficients obtained by them in organic liquids.

Ozturk et al. (1987) proposed a correlation modifying the correlation proposed by Nakanoh and Yoshida (1980). In this correlation the column diameter was replaced by surface-to-volume mean bubble diameter which cannot be easily estimated in most of the systems.

For highly viscous non-Newtonian solutions, the correlation proposed by Deckwer et al. (1982) has been found to give reliable predictions for volumetric mass transfer coefficients (Shah et al., 1982).

2.2.6 Gas-Liquid Interfacial Area

The gas-liquid interfacial area (a) is an important design variable in a number of gas-liquid and gas-liquid-solid systems. The volumetric mass transfer coefficient $k_l a$ is directly influenced by the factors affecting a. The interfacial area is related to the gas holdup and volume to surface mean bubble diameter as shown below:

$$a = 6\epsilon_g/d_{vs} \qquad \text{.....(2.2.20)}$$

It can be seen from Equation 2.2.20 that the parameters influencing gas holdup would also affect the interfacial area.

2.2.6.1 Measurement Techniques for Interfacial Area

The various techniques used for interfacial area measurements in gas-liquid dispersions can be divided into two classes namly; 1) chemical methods 2) optical methods. Following is a critical review of these techniques:

2.2.6.1.1 Chemical Methods

This is the most commonly used technique for the measurement of interfacial area in gas-liquid dispersion (see Table 2.2.8). This technique involves reaction between the two phases. The theory of mass transfer with chemical reaction was reviewed in section 2.1.5. The various systems useful for interfacial area measurements have been reviewed by Sharma and Danckwerts (1970). Table 2.2.8 summarizes various chemical systems which have been used by different researchers for interfacial area measurements in gas-liquid systems.

In order to select a suitable chemical method, it is important to take into consideraton the various factors which would affect the estimation of realistic values of interfacial area. The various factors which need to be considered include the selection of suitable reaction regime, the conversion of the gas and liquid phases and the dispersion characteristics of these phases. Schumpe and Deckwer (1980) have provided some conservative guidelines for the selection of a suitable chemical method

Table 2.2.8 Techniques used in the Literature to Measure Interfacial Area in Bubble Columns.

Techniques	References	Remarks
Chemical Methods CO_2/NaOH	Voyer and Miller (1968); Sharma and Mashelkar(1968);Kumar et al.(1976); Schumpe and Deckwer (1978)	Use of dissolved salts can alter the coalescing behavior of the liquid
CO_2/Na_2CO_3-Na_2CO_3 buffer	Mashelkar and Sharma (1970)	
O_2/Na_2SO_3	Carleton et al. (1967)	
Air/Na_2SO_3	Reith(1968); Schumpe and Deckwer(1978); Godbole et al.(1983)	
Photography method	Towell et al.(1965); Akita and Yoshida (1974)	This technique overestimates the interfacial area
Light Transmission	Calderbank(1958); Lee and Meyrick(1970); Sridhar and Potter (1980)	For good accuracy this technique requires special probe design

for the simultaneous measurement of interfacial area and volumetric mass transfer coefficient in gas-liquid dispersions. These authors have pointed out that the gas conversion should be kept low in the gas bubbles which of course would require knowledge of the distributions of bubble size and residence time in the dispersion.

The use of dissolved salts, required for chemical methods, can significantly alter the coalescing behavior of liquid. The results thus obtained are not generalizable. The chemical methods also require a thorough and often time-consuming investigation of the kinetics which makes these methods difficult to use for systematic investigation of the effect of liquid properties on interfacial area.

2.2.6.1.2 Photography Method

The photographic method does not directly yield interfacial areas. The mean bubble size is normally measured and when combined with the average gas holdup gives the average interfacial area using Equation 2.2.20. Although this is a relatively simple technique and can be applied to various kinds of dispersions without altering the coalescing behavior of the liquid, it suffers from a number of drawbacks.

The main drawback of the technique is that it provides information on bubble size distributions near the wall which may not be representative of the entire cross-section of the apparatus. Burgess and Calderbank (1975) have shown that photography technique can yield interfacial areas which are more than twice larger than those obtained by other methods.

Kewecki et al. (1967) measured the bubble size by

photographing the bubbles withdrawn from the gas-liquid dispersion into a translucent rectangular chamber. This procedure however can give rise to errors because of bubble coalescence at higher gas holdups during transfer from the apparatus to the chamber.

2.2.6.1.3 Light Transmission Method

The theory of light transmission through liquid-liquid and gas-liquid dispersions was first developed by Calderbank (1958), assuming monosize distribution. McLaughlin and Rushton (1973) extended the theory of monosize systems to polydisperse systems which was varified experimentally by Curl (1974). Calderbank (1958) deduced the following relationship between the fraction of incident light transmitted by the dispersion and the interfacial area per unit volume.

$$\ln (I_o/I') = K\, a l_o/4 \qquad \text{.....(2.2.21)}$$

Lockett and Safekourdi (1977) found the light transmission method to be useful for $al_o < 20$. For higher values of al_o, multiple scattering increasingly contributed to the overall error. Efforts made by different researchers to overcome this limitation of the light transmission technique can be divided into empirical modification of Equation 2.2.21 (Lockett and Safekourdi, 1977; Landau et al., 1977; Urua et al., 1987) and better probe design to reduce the path length l_o (Winstein and

Treybal, 1973; McLaughlin and Rushton, 1973; Sridhar and Potter, 1980; Taweel et al., 1984). Using laser beam as source of light, Taweel et al. (1984) modified the light attenuation technique to expand the range of applicability to al_o value of 460.

The probe used in light transmission technique need to be calibrated to check the applicability of Equation 2.2.21.

Although, the light transmission method hold good promise to measure interfacial areas in various gas-liquid dispersions, the cost of the equipment is usually prohibitive. A properly selected chemical method can provide a reasonable estimate of the interfacial area in most of the systems.

2.2.6.2 Effects of Operating Variables on Interfacial Area

It can be seen from Equation 2.2.20 that the parameters which affect the gas holdup would also affect the interfacial area, (a) and the volumetric mass transfer coefficient (k_1a). The effects of various parameters on gas holdup and volumetric mass transfer coefficient were reviewed in sections 2.2.2.2 and 2.2.5.2.

Following is a critical review of the influence of various parameters on interfacial area.

2.2.6.2.1 Effects of Gas Velocity

Gas-liquid interfacial area has been found to increase with increasing gas velocity (Towell et al., 1965; Mashelkar and Sharma, 1970; Sedelies et al., 1987). As observed with gas holdup, the rate of increase was higher for gas velocities in the bubble flow regime as compared to the churn turbulent regime. In the bubble flow regime, the interfacial area was generally found to vary with V_g to the power 0.9 to 1.2, while in the churn turbulent regime the dependence was in the range of 0.4 to 0.7.

2.2.6.2.2 Effects of Liquid Velocity

Most of the researchers have found only slight or no effect of superficial liquid velocity on interfacial area (Towell et al., 1965; Mashelkar and Sharma, 1970; Sedelies et al., 1987). Voyer and Miller (1968) however reported an increase in interfacial area with increase in liquid velocity. Their results were probably affected by the choice of flow model.

2.2.6.2.3 Effects of Gas Distribution

As observed with gas holdup, the gas distribution was found to have a strong influence on interfacial area at low superficial gas velocities by Schügerl et al. (1977) and Oels et al. (1978). The measurements were made in noncoalescing media using perforated plates, porous

plates, ejector and injector nozzles. The order in which the interfacial area increased was the same as for gas holdup (see section 2.2.2.2.4). The effect of gas distributor diminished at higher gas velocities (Towell et al., 1965; Mashelkar and Sharma, 1970; Sedelies et al., 1987).

2.2.6.2.4 Effects of Physical Properties of Liquid

The gas-liquid interfacial area was found to decrease with increasing liquid viscosity by Schumpe and Deckwer (1981) and Sedelies et al. (1987). Sedelies et al. (1987) however observed that the effect of viscosity became important only at viscosities higher than 5 mPa s.

The interfacial area was found to increase with decrease in interfacial tension of aqueous solutions of alcohols (Schügerl et al., 1977; Oels et al., 1978). These authors also observed however that the interfacial area not only depended on the surface tension but also on the type of alcohol used, which showed that the presence of alcohol molecules also affected the coalescence behavior of the liquid.

2.2.6.3 Correlations for Interfacial Area

Correlations for gas-liquid interfacial area in bubble columns have been proposed by Akita and Yoshida (1974), Nagel et al. (1979), Schumpe and Deckwer (1981)

and Sedelies et al. (1987).

Nagel et al. (1979) developed a correlation based on the Kolmogoroff's theory of isotropic turbulence. The proposed correlation applies when the conditions of isotropic turbulence and a spatially uniform energy dissipation are fulfilled. These conditions may not be fulfilled in the churn turbulent regime.

Akita and Yoshida (1974) proposed a correlation which takes into account the physical properties of liquid phase phase and the column diameter.

$$aD_c = 0.33(gD_c^2\rho_l/\sigma)^{0.5}\ (gD_c^3/\nu_l^2)^{0.1}\ \epsilon_g^{1.13} \quad ....(2.2.22)$$

This correlation is based on the data obtained in square cross-section columns and a narrow range of gas velocity.

The correlation proposed by Schumpe and Deckwer (1981) is based on the data obtained in carboxy methyl cellulose solutions (0.5 to 1.6 wt.%) and is valid for slug flow regime:

$$a = 48.7\ (V_g/\mu_{l,eff})^{0.51} \quad .....(2.2.23)$$

The effective viscosity $\mu_{l,eff}$ of the liquid phase in the aerated bubble column was obtained from the measured shear rate against shear stress curve by using the correlation of Nishikawa et al. (1977).

Sedelies et al. (1987) proposed different empirical correlations to account for the effects of distributor type, hydrodynamic regime and liquid viscosity on gas-

liquid interfacial area. These correlations apply only to noncoalescing systems (aqueous solutions of sodium sulfite and CMC) used by these researchers.

2.2.7 Liquid Side Mass Transfer Coefficient

The liquid side mass transfer coefficient (k_l) is obtained by dividing the volumetric mass transfer coefficient ($k_l a$) by the interfacial area per unit volume. Therefore, any errors in interfacial area measurement would also result in errors in mass transfer coefficient. As reviewed in section 2.2.6 there can be several sources of errors in interfacial area measurement. Therefore the literature values for the liquid side mass transfer coefficient should be used with caution.

The liquid side mass transfer coefficient has been found to depend on the liquid phase diffusivity, the bubble size, the physical properties of the liquid (Calderbank and Moo Young, 1961; Akita and Yoshida, 1974; Kawagoe et al., 1975; Nakao et al., 1983; Oosterhuis et al., 1985) and the presence of surface active compounds in the liquid phase (Raymond and Zieminski, 1971; Koide et al., 1976; Oosterhuis et al., 1985). The first comprehensive study of the mass transfer coefficient was presented by Calderbank and Moo-Young (1961). These researchers reported that large bubbles (d_b > 2.5 mm) gave larger mass transfer coefficient than small bubbles (d_b <

2.5 mm). It was argued that the large bubbles had a mobile surface and there was no significant effect of bubble size on k_l. The mass transfer coefficient was, however, decreased for bubbles smaller than 2.5 mm. This was attributed to the rigid surface of small bubbles where friction drag predominates causing boundary layer flow. In a subsequent study, Akita and Yoshida (1974) found that the mass transfer coefficient was proportional to the squre root of bubble diameter over a wide range of bubble size (1 mm < d_b < 15 mm). This was also confirmed by some other researchers (Kataoka et al., 1979; Nakao et al., 1983). The discrepancies between the results of Akita and Yshida (1974) and Calderbank and Moo-Young (1961) could be the consequence of different techniques used for the bubble size measurements and different gas-liquid contactors used for their studies.

The effect of change in viscosity, surface tension and coalescing behavior of the liquid would also significantly affect the bubble size which makes it difficult to quantify the effects of changes in physical properties of the liquid on the mass transfer coefficient. The mass transfer coefficient always increases with increasing liquid phase diffusivity.

The mass transfer coefficient could be significantly reduced in the presence of surface active compounds (Zieminski et al., 1967; Raymond and Zieminski, 1971; Koide et al., 1976). Raymond and Zieminski (1971) observed

large decreases in k_l values in dilute solutions of aliphatic alcohols with carbon numbers higher than six. Zieminski et al. (1967) made similar observations in the dilute solutions of aliphatic acids. The decrease in k_l values could be attributed to the retardation of surface flow by the adsorbed surfactant molecules. Raymond and Zieminski (1971) found a good correlation between mass transfer coefficient and the drag coefficient. In addition tne adsorbed molecules could also increase resistance to diffusion across the interface.

The k_l values for small bubbles (d_b < 2.5 mm) could be calculated assuming Froessling (1938) equation is applicable for their rigid surface.

$$k_l = 0.6(D_l/d_{vs})(Re_l)^{0.5}(Sc)^{0.33} \quad .....(2.2.24)$$

For larger bubbles the bubble surface is mobile, the k_l values can then be calculated using the Higbie model:

$$k_l = 1.13 \left(\frac{V_{bo}D_l}{d_{vs}}\right)^{0.5} \quad .....(2.2.25)$$

Empirical correlations for mass transfer coefficient have been proposed by Calderbank and Moo-Young (1961) and Akita and Yoshida (1974). Calderbank and Moo-Young (1961) proposed separate correlations for large bubbles and small bubbles:

for $d_{vs} > 2.5$ mm

$$k_l = 0.42\left(\frac{\Delta\rho\mu_l g}{\rho_l^2}\right)^{1/3} (Sc)^{-0.5} \quad \ldots\ldots\ldots (2.2.26)$$

for $d_{vs} < 0.6$ mm

$$k_l = 0.31\left(\frac{\Delta\rho\mu_l g}{\rho_l^2}\right)^{1/3} (Sc)^{-0.66} \quad \ldots\ldots\ldots (2.2.27)$$

No correlations were proposed for the intermediate bubble size (0.6 mm < d_{vs} < 2.5 mm).

Akita and Yoshida (1974) proposed a correlation based on large amount of experimental data (1974).

$$\frac{k_l d_{vs}}{D_l} = 0.5\left(\frac{\nu_l}{D_l}\right)^{1/2} \left(\frac{g d_{vs}^3}{\nu_l^3}\right)^{1/4} \left(\frac{g d_{vs}^2 \rho_l}{\sigma_l}\right)^{3/8} \quad \ldots\ldots\ldots (2.2.28)$$

This correlation is based on the data obtained with photographic method for bubble size measurements which limits its applicability (see section 2.2.3.1.1).

The correlation proposed by Akita and Yoshida (1974) is, however, recommended for conservative estimates of mass transfer coefficient in bubble columns.

2.3 Three-Phase Fluidized beds

First the limiting case when there is no gas flow is considered.

2.3.1 Liquid-Solid Fluidization

As the velocity of a liquid passing through a bed of solid particles from bottom to top is increased, different flow regimes are observed. At low flowrates the liquid moves through the interstices of a packed bed. As the flowrate is increased, some of the particles begin to move slowly. As the flowrate increases, the frictional forces acting on the particles increase until they balance exactly the buoyant weight of the particles. The particles then become suspended or "fluidized". The superficial liquid velocity required to reach this state is called minimum fluidization velocity. At higher velocities, expansion of the bed is observed until the free settling velocity of the smallest particles is reached and they are entrained out of the bed.

Liquid-solid fluidized beds are characterized by particulate fluidization. There are no large moving voids (or bubbles) as observed in gas-solid heterogeneous fluidization.

2.3.1.1 Minimum Fluidization Velocity

The minimum fluidization velocity can be obtained

from the pressure drop measurements across the bed. In the packed bed regime the pressure drop across the bed increases with increasing flowrates. However once the bed is fluidized the pressure drop across the bed increases very slowly, since the frictional pressure drop which supports the bed weight becomes constant. A plot of the logarithm of the pressure drop across the bed versus the superficial liquid velocity gives the minimum fluidization velocity at the point of change in the slope (Figure 3.2.3).

Ergun's equation (1956) has been the basis for a number of empirical correlations proposed in the literature for the minimum fluidization velocity. The prediction of the minimum fluidization, however, requires the knowledge of the shape factor and the porosity. Some authors have removed the need for experimental values of the shape factor and porosity by introducing suitable empirical constants obtained from experimental data. This however has resulted in getting different correlations based on different sets of data (e.g. Wen and Yu, 1966; Saxena and Vogel, 1977; Richardson and St. Jeronimo, 1979).

$$Re_{mf} = (C_4^2 + C_5 Ar)^{0.5} - C_4 \quad \text{.....(2.3.1)}$$

Where C_4 and C_5 are the empirical constants.

The application of these correlations is limited to beds of particles whose shape factor and porosity are

mostly present in the original data. In order to minimize the errors due to shape factors, Lucas et al. (1986) divided the particles into three groups (round,sharp,other) and developed a correlation for each group.

round particles ($0.8 < \Phi < 1$)

$$Re_{mf} = (29.5^2 + 0.0357Ar)^{0.5} - 29.5 \quad ....(2.3.2)$$

sharp particles ($0.5 < \Phi < 0.8$)

$$Re_{mf} = (32.1^2 + 0.0571Ar)^{0.5} - 32.1 \quad ....(2.3.3)$$

other ($0.1 < \Phi < 0.5$)

$$Re_{mf} = (25.2^2 + 0.0672Ar)^{0.5} - 25.2 \quad .....(2.3.4)$$

Chen (1987) proposed a single correlation for all shape groups.

$$Re_{mf} = [(33.67\Phi^{0.1})^2+(Ar/24.5\Phi^{0.45})]^{0.5} - 33.67\Phi^{0.1} \quad .....(2.3.5)$$

It is suggested that the same single equation can be used even if the shape factor is unknown by considering $\Phi = 1$ for near spherical particles, $\Phi = 0.5$ for sharp particles and $\Phi = 0.25$ for other shapes.

The correlations proposed by Lucas et al. (1986) and Chen (1987) attempt to minimize the errors due to particle shape factor, however, the effect of bed porosity has not been considered in detail. The bed porosity at minimum

fluidization depends on shape factor and width of particle size distribution.

2.3.2 Three-Phase Gas-Liquid-Solid Fluidization

Table 2.3.1 shows the different cases which can be encountered in gas-liquid-solid fluidization (Epstein 1981). Herein only cocurrent three-phase fluidization with a continuous liquid phase is discussed.

The simultaneous upward flow of a gas and a liquid through a bed of solid particles first results in a fixed bed regime at low flowrates. When one or both of the flowrates is increased past a critical value, a fluidized state is reached.

2.3.2.1 Minimum Fluidization Velocity

When the liquid velocity is above what the minimum fluidization velocity would be in the absence of gas, the bed of solids is said to be "liquid supported" (Epstein 1981, 1983). At liquid velocities below the liquid minimum fluidization velocity (V_{lmf}), the extra energy input provided by the upward flow of gas may be enough to reach fluidization; the bed is then said to be "bubble supported".

The minimum liquid velocity required to achieve fluidization in gas-liquid-solid fluidized beds decreased as the gas velocity was increased (Begovich and Watson, 1978a; Lee and Al-Dabbagh, 1978; Catros, 1986). Begovich

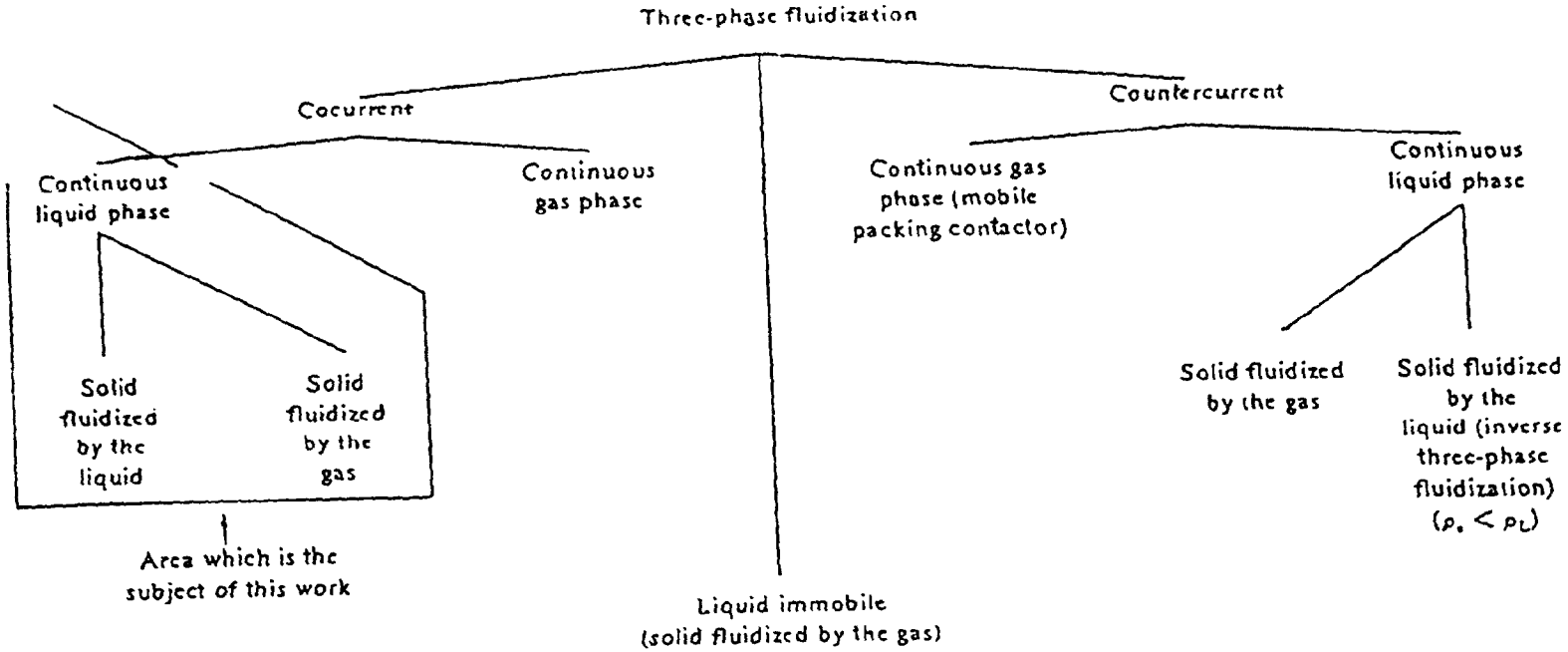

Table 2.3.1 Different cases of gas-liquid-solid fluidization (Epstein, 1981)

and Watson (1978a) proposed the following correlation for minimum liquid fluidization velocity in gas-liquid-solid systems:

$$(V_{lmf}/V_{lmfo}) = 1 - V_g^{0.436}\mu_l^{0.227}d_p^{0.598}(\rho_s-\rho_l)^{-0.305} \quad .....(2.3.6)$$

This correlation could be extrapolated to zero gas velocity, it does not however account for the effect of particle shape.

Recently Costa et al. (1986) proposed an empirical correlation to predict the minimum fluidization velocity for liquid for a given gas velocity;

$$V_{lmf} = 0.000697V_g^{-0.328}(\Phi d_p)^{1.086}(\rho_s-\rho_l)^{0.865} D_c^{0.042}\mu_l^{-0.355} \quad .....(2.3.7)$$

This correlation is based on a wide range of experimental data as compared with the correlation proposed by Begovich and Watson (1978a). It also takes into account the effects of column diameter and particle shape factor which increases the scope of its application.

Fan et al. (1985) found that in a bed containing a binary mixture of particles, the minimum fluidization velocity, V_{lmf}, depended on the incipient fluidization velocity of the flotsam particles $(V_{lmf})_1$, the incipient fluidization velocity of the jetsam particles $(V_{lmf})_2$ and the weight fraction of the jetsam particles (X_2). They correlated the minimum fluidization velocity (V_{lmf}) with

the equation:

$$(V_{lmf})/(V_{lmf})_1 = [(V_{lmf})_2/(V_{lmf})_1]^{X_2 \cdot 169} \quad ....(2.3.8)$$

$$(V_{lmf})_{1 \text{ or } 2} = 2.38\ V_g^{-0.5} V_t^{1.64} \quad .....(2.3.9)$$

Saberian et al. (1987) observed that the minimum liquid fluidization velocity in gas-liquid-solid fluidized beds was affected by the column diameter, due to formation of gas slugs. There was, however, practically no effect of bed height or gas properties. It may be pointed out that the minimum liquid fluidization velocity in gas-liquid-solid systems can also be affected by the gas distributor type and the coalescing behavior of the liquid. More work should be carried out to investigate these effects.

2.3.2.2 Bed Dynamics

The bed behavior in gas-liquid-solid fluidization is complicated by the interaction of solid particles and the gas bubbles. Following is a critical review of various phenomena observed in co-current three-phase fluidization.

2.3.2.2.1 Flow Regimes

Three types of flow regimes have been observed in co-current three-phase fluidization with liquid as the continuous phase.

- dispersed bubble flow regime: this regime is

characterized by relatively small and uniform bubble size, with a diameter of less than 6 mm (e.g. Michelsen and Ostergaard, 1970; Kim et al., 1972; Darton and Harrison, 1975; Epstein, 1983).

- coalesced bubble flow regime: in this regime large coalesced bubbles are seen rising through the suspension (Rigby et al., 1970a; Kim et al., 1972; Darton and Harrison, 1975; Epstein, 1983; Matsuura and Fan, 1984). Rigby et al. (1970a) measured the bubble size in three-phase fluidized beds of fine particles (120-775 microns). It was concluded that the bubbles coalesced as they moved up the bed. Matsuura and Fan (1984) reported that the coalesced bubble regime consisted of a mixture of large and small bubbles with diameters ranging from a few millimeter to a few centimeters.

- slug flow regime: as the gas velocity is increased in a co-current gas-liquid-solid fluidized bed in a small diameter column, the size of the large bubbles approaches the column diameter and slugs are formed. Matsuura and Fan (1984) also detected smaller bubbles in the slugging regime, intermixed with large bubbles.

Although the above are the most commonly observed flow regimes, Nacef et al. (1988) reported the presence of a solid piston flow regime as well in three-phase fluidized beds. This regime is likely to be observed in small diameter columns only.

Fan et al. (1986a) studied the relationship between the pressure fluctuations and the flow regime in three - phase fluidized beds. Although the pressure fluctuation signals looked very similar for all the three regimes, there was a distinct difference in the power spectral density functions of the different flow regimes. For each regime, a distinct peak existed between 0 to 2 Hz and a broad peak between 16 and 25 Hz, with a difference in the relative magnitude of the peaks for each regime.

2.3.2.2.2 Flow Regime Charts

Several flow regime charts have been presented in the literature to identify the boundaries of the various flow regimes (Fan et al., 1985; Muroyama and Fan, 1985; Wild et al., 1987). Figure 2.3.1 shows a flow regime chart developed from Fan et al. (1985). The transition from one regime to another is usually identified by visual observations which make the precise determination of the boundaries rather difficult and subjective.

The operating regime in three-phase cocurrent fluidization has been found to depend on particle size and density, gas and liquid flowrates, column diameter and liquid properties (Kim et al., 1972; Mukherjee et al., 1974; Darton and Harrison, 1975; Fan et al., 1985; Fan et al., 1986a; Wild et al., 1987).

The terminal velocity of the particles in the liquid phase has been found to affect the liquid velocity of

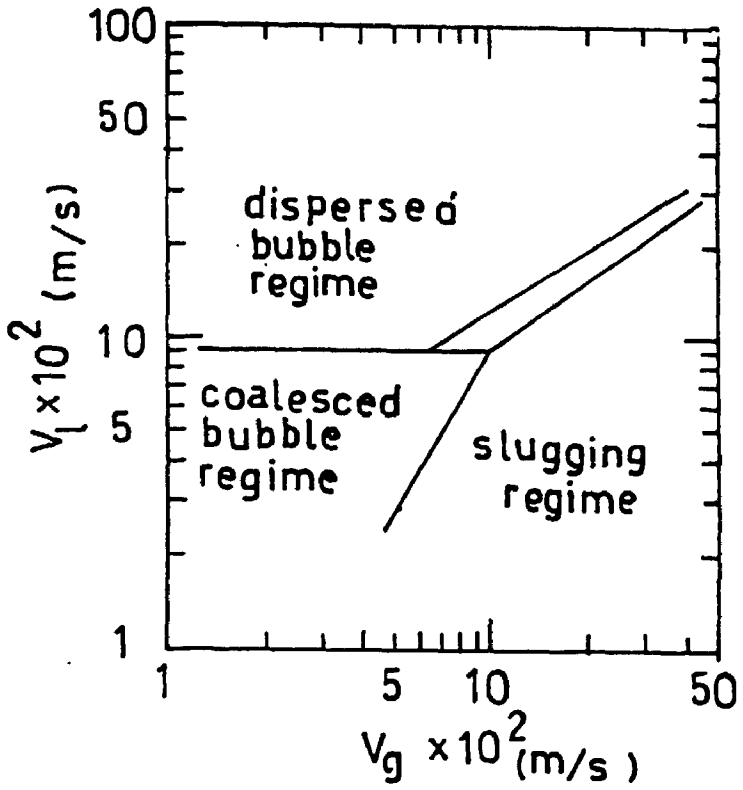

Figure 2.3.1

Flow regime chart for three-phase fluidized beds

(Fan et al., 1984)

transition from the coalesced to the dispersed bubble flow regime (Fan et al., 1985; Fan et al., 1986a). For small terminal velocities (< 0.034 m/s), an increase in particle size increased the transition liquid velocity but for higher terminal velocities opposite trends were observed. This behavior could be the result of two different phenomena, which need to be investigated further. The particle terminal velocity however had little effect on the transition velocities from dispersed to slugging and from coalesced to slugging regime (Fan et al., 1986a).

The flow regime chart presented by Muroyama and Fan (1985) also shows the strong effect of column diameter on the limits of flow regimes.

Wild et al. (1987) pointed out that the flow regime charts obtained with water as the liquid phase did not apply when liquids with different coalescing properties were used. It was observed, for example that the dispersed bubble flow appeared at much lower liquid velocities and slug flow at much lower gas velocities when weakly coalescing organic liquids (tetrachloro-ethylene and propylene carbonate) were used as the liquid phase. Using same particle size, Saberian (1984) found that different liquids exhibited different flow regime boundaries. Saberian et al. (1987) found that foaming liquids give a completely different behavior.

These observations clearly suggest that the flow regime charts obtained with a single liquid provide only a

qualitative picture. Further work is required to establish the effects of liquid physical properties and coalescing behavior on flow regime boundaries. It may also be pointed out that the important effect of gas distributor type in determining flow regime boundaries has not been investigated.

2.3.2.2.3 Bed Expansion/Contraction

Another phenomenon specific to three-phase fluidized bed is bed expansion or contraction (depending on particle size) which may result upon initial introduction of the gas into the liquid-solid fluidized bed (Massimilla et al.,1959; Turner, 1966; Ostergaard, 1964; Dakshinamurty et al., 1971; Epstein, 1981; Wild et al., 1982). Massimilla et al. (1959), who first reported the contraction phenomenon in a bed of fine particles, observed that bed contraction was larger when the liquid velocity was greater. An increasing gas flowrate caused further contraction up to a critical gas flowrate beyond which the bed expanded.

For low viscosity liquids, bed contraction is observed in suspensions of fine and light particles which promote bubble coalescence (Massimilla et al., 1961; Ostergaard, 1966; Rigby and Capes, 1970b; Dakshinamurty et al., 1971). Bed expansion and bubble disintegration is however observed in three-phase fluidized beds of large and heavy particles (Lee, 1965; Ostergaard, 1971; Kim et

al., 1975). For glass beads fluidized by air and water, the transition particle diameter is about 3 mm (Epstein, 1981).

In addition to particle size, the liquid viscosity could also play an important role in determining the bed behavior (Kim et al., 1975; Patwari et al., 1986). Kim et al. (1975) observed that when a bed of 6 mm glass beads was fluidized by air and high viscosity CMC solution, the porosity decreased slightly with increasing gas velocity. These authors combined their data with the literature data (Stewart and Davidson, 1964; Rigby and Capes, 1970b; Dakshinamurty et al., 1971) to conclude that bed contraction occurred in beds of solids having a V_{lmfo} less than around 0.0128 m/s in contrast beds of solids having a V_{lmfo} higher than 0.0128 m/s expanded upon gas introduction.

Stewart and Davidson (1964) pointed out that the bed contraction on the introduction of gas was related to the diversion of a part of the liquid flow to the bubble wakes. The liquid in bubble wake passes through the bed at a high velocity thus reducing the liquid flow for solids suspension. This effect may counteract the expansion due to the additional flow of gas. In the beds of small particles the formation of large coalesced bubbles (with large wakes) is attributed to the pseudohomogeneous medium of higher viscosity and density, as experienced by the bubbles rising in the suspension (Epstein, 1981).

Several theories have been proposed for the mechanism of bubble breakup in the beds of large and heavy particles (Epstein,1981). Lee et al.(1974) assumed that bubble breakup occurs when particles with high momentum penetrate into the bubble. These authors suggested a critical Weber number as a criterion:

$$We_{crit} = \frac{\rho_s V_{bo}^2 d_p}{\sigma} = 3 \qquad .....(2.3.10)$$

At $We < 3$ bed contraction occurs whereas at $W_e > 3$ bubble disintegration and bed expansion are observed. In this theory, the effect of liquid viscosity on bubble properties are neglected.

Bruck and Hammer (1986) modified the critical Weber number to include the effects of different wetting characteristics and shape factors of particles.

$$We_{crit} = \frac{(1+\sin\psi)\rho_e d_{vs} V_{br}^{\Phi}}{\sigma} = 2.5 \qquad 0^o<\psi<90^o$$

$$.....(2.3.11)$$

The bubble disintegrates when critical Weber number is larger than 2.5.

Henriksen and Ostergaard (1974), however, have shown that a large bubble does not necessarily disintegrate when its roof is penetrated by a single large particle. It was proposed that the bubble breakup occurred by Rayleigh-Taylor instability of the bubble roof. The proposed bubble

breakup theories need to be tested over wide range of operating conditions before making general conclusions.

2.3.3 Phase Holdups

The phase holdup in a multi-phase system is defined as the volume fraction occupied by the considered phase in the system.

In three-phase gas-liquid-solid fluidization, the individual holdups satisfy the following expression:

$$\epsilon_g + \epsilon_l + \epsilon_s = 1 \qquad \text{.....(2.3.12)}$$

The solids holdup and hence the bed porosity can be calculated directly from the mass of the particles and the bed height.

$$\epsilon_s = W_s/\rho_s A_c H_{bed} \qquad \text{.....(2.3.13)}$$

Where A_c is the cross-sectional area of the column and the static pressure gradient is given by:

$$(\Delta P/\Delta H) = g(\epsilon_g \rho_g + \epsilon_l \rho_l + \epsilon_s \rho_s) \qquad \text{.....(2.3.14)}$$

2.3.3.1 Measurement of the Phase Holdups

Various techniques used for the phase holdup measurements in three phase fluidized beds are summarized in Table 2.3.2. Following is a critical review of the various methods.

Table 2.3.2 Literature Techniques for Phase Holdup Measurement in Three-Phase Fluidized Beds

Techniques	Remarks	References
Simultaneous closure of the gas and liquid flow	Gas holdup in the bubble column above the bed needs to be known	Visvanathan(1965);Vail et al (1970);Bhatia and Epstein (1972);Razumov(1973); Ermakova(1976);Dhanuka and Stepanek(1978);Kusakabe et al.(1980);Hatate et al. (1986);Hwang and Fan(1986) Broudjenni et al.(1987)
Pressure profile measurements	Measurement acuracy can be reduced by level fluctuations in the manometers	Levsh et al.(1968);Efremov et al.(1970);Bhatia et al. (1972);Epstein and Nicks (1976);Begovich and Watson (1978a);Ostergaard(1978); Kato et al.(1981);Fan et al. (1985);Fan et al.(1986b); Fukuma et al.(1988);
Tracers	Difficult Technique; back mixing of phases a serious problem	Ostergaard and Michelsen (1968); Michelsen and Ostergaard(1970);El-Temtamy and Epstein(1979);Vasalos et al.(1980).
Electrical conductivity	Calibration by other method needed Limited to conducting liquids	Begovich and Watson(1978b) Dhanuka and Stepanek (1978) Kato et al.(1981a)
Resistance or Capacitance probes	Local measurements Bed hydrodynamics disturbed	Ostergaard(1966);Righby et al.(1970);Razumov et al. (1973); Linnweber and Blass (1983); Matsuura and Fan (1984); Hu et al.(1986); Morooka et al.(1986)
Light Transmission/Reflection using optical fibre probe	Can be used in non-aqueous liquids and at high temperatures Probes can interfere with bubbles	Ishida and Tanaka(1982); Lee et al.(1984);Hue et al. (1986); Lee et al. (1987)
Photography	Limited to low gas velocity	Page and Harrison(1972); Hassanien et al.(1981)
Laser Holography	Can provide bubble diameter shape and position Hard to setup.	Peterson et al.(1983)

2.3.3.1.1 Simultaneous Closure of the Gas and Liquid Feeds

This technique is based on simultaneous closure of the liquid and air flows and the subsequent recording of the liquid level (H_L) after gas escape. The difference between the initial dispersion height and the recorded liquid level corresponds to the volume of gas contained in the whole column during the run. In order to deduce the gas holdup in the bed from this gas volume the gas holdup in the bubble column above the fluidized bed ($\epsilon_{g,B}$) must have previously been determined. If H_C is the column height and H_{bed} the height of fluidized bed then the gas holdup in the fluidized bed can be obtained with:

$$H_L A_C = \epsilon_g H_{bed} A_C + \epsilon_{g,B}(H_C - H_{bed}) A_C \qquad .....(2.3.15)$$

$$\epsilon_g = \frac{H_C - H_L}{H_{bed}} - \frac{H_C - H_{bed}}{H_{bed}} \epsilon_{g,B} \qquad ... (2.3.15a)$$

The solids holdup can be obtained using Equation 2.3.13 if the entrainment of the solid particles in the freeboard region is negligible. The liquid holdup is then obtained using Equation 2.3.12.

As shown in Table 2.3.2, a number of researchers have used this technique in three-phase fluidized beds. Although relatively easy to use, this technique is not very accurate. The main sources of error are: 1) The

fluctuations of the dispersion height make it difficult to determine its value just before shut-off. Taking the column height as the dispersion height would be inaccurate due to the weir effects, 2) Because of the pressure drop through the gas distributor, the gas which is in the line between the shut off valve and the distributor will be at higher pressure than in the bed. The gas will therefore keep flowing into the bed until the pressures have equilibrated and might entrain some liquid out of the column. Bed liquid may also drain into the gas line . 3) The bed height cannot be measured with a precision for either small particles or high gas flowrates because it then fluctuates greatly with entrainment of particles in the freeboard region. 4) Some gas bubbles may remain trapped in-between the defluidized particles. Saberian (1985) recirculated the remaining liquid to refluidize the bed and eliminate these bubbles.

2.3.3.1.2 Holdup Measurements Based on Pressure Profile

This is the most commonly used technique to measure phase holdups in three-phase fluidized beds. This technique is based on the measurement of the pressure profile along the column, which when plotted as a function of the pressure tap heights will give two straight lines, the intercept of which corresponds to the bed height. The bed height could also be determined by visual observation in case of coarse or dense particles at low flowrates.

The solids holdup (for negligible entrainment) is then directly obtained from Equation 2.3.13 while the gas and liquid holdups could be calculated from the experimentally measured static pressure gradient data with Equations 2.3.12 and 2.3.14.

This technique is easy and accurate for low flowrates of gas, however the accuracy is expected to decline at high flowrates, due to fluctuations of the liquid level in the manometers. Catros (1986) used a freeze photography technique to minimize the measurement errors due to fluctuations of liquid level in the manometers. This is however a very time consuming technique. Lee (1986) employed a pressure transducer with a switch-wafer valve ("Scanivalve") which could be turned on by a solenoid. The wafer had 12 channels which could be connected to the pressure taps along the column. By connecting the transducer to a computer, accurate average values could be obtained. It should be noted that liquid pressure transducers are expensive and relatively inaccurate, giving a precision at best of 0.5 cm of water. It is also necessary to ensure that resonance in the line connecting the pressure tap to the transducer does not distort the signal and change its average value.

Dhanuka and Stepanek (1978b) and Begovich and Watson (1978) have shown that phase holdups obtained by the pressure profile technique are within 4 to 5 % of the values obtained by the electroconductivity methods.

2.3.3.1.3 Tracer Technique

This technique is based on the determination of the real velocity of the gas or the liquid from the mean time of passage of a tracer between two points separated by a vertical distance. The phase holdup can be obtained by dividing the average residence time of the phase between the two points by the vertical distance and multiplying by the phase superficial velocity (Wild et al., 1984).

The tracer used must be easily detectable at small concentrations and must not change the properties of the phase whose holdup is to be measured (e.g. it should not affect the coalescing behavior of the liquid).

Accurate measurements of phase holdups are difficult when using the tracer technique. Since it is difficult to sample the gas at the top of the bed itself, the gas is then sampled at the top of the column yielding only the total volume of gas contained in the column and not in the bed alone. Moreover, when the sample is collected from the gas space above the gas-liquid dispersion, it is impossible to avoid backmixing in that space. Backmixing is also a serious problem in the liquid while sampling the liquid at the boundary between the bed and the bubble column above the bed. At high gas flowrates, the large fluctuations of the bed surface would make it practically impossible to avoid this backmixing. This technique also

requires devices which measure the concentration with a very short response time.

2.3.3.1.4 Electrical conductivity Technique

The electroconductivity method is based on the measurement of the electrical conductivity of the bed. Begovich and Watson (1978b) reported the liquid holdup to be equal to the ratio of the conductivity of the bed to the conductivity of the liquid alone

$$\epsilon_l = \gamma/\gamma_o \qquad \text{.....(2.3.16)}$$

Where γ_o is the conductivity of the liquid alone.
The above relationship assumes that tortuosity factor remains approximately constant.

Kato et al. (1981a) introduced a correction factor to Equation 2.3.16 after calibrating the electrodes with known liquid holdup.

$$\epsilon_l^{n4} = \gamma/\gamma_o \qquad \text{......(2.3.16a)}$$

The value of n4 is given as 1.2

This technique gives only the liquid holdup and suffers from its limited application to conducting liquids. The addition of salt, which is required to make the liquid conductive, inhibits bubble coalescence and thus changes the holdups.

2.3.3.1.5 Electroconductivity (Resistance)/ Capacitance Probes.

Electroconductivity probes have been used by a number of researchers to measure local gas holdup (Ostergaard 1966; Righby et al., 1970; Linneweber and Blass 1981; Morooka et al., 1986; Hu et al., 1986; Wolff et al., 1990). The technique is based on the different conductivity responses given by the liquid and gas phases i.e. different values are obtained depending on whether the tip of the probe is in the liquid or in the gas.

Razumov et al. (1973) used a capacitance probe to measure the solid and liquid holdups in three-phase fluidized beds. It detected local changes in phase holdup from the changes in dielectric permeability.

Although it is possible to measure local holdups with these probes, the technique does not provide reliable results. The in-situ measuring probe disturbs the local hydrodynamics of the bed and the solid particles cannot be present at the same spot as the probe tip thus reducing the reliability of results. Rowe et al.(1965) have demonstrated that in gas-solid fluidized beds, gas bubbles tend to swerve to avoid the probes, thus giving inaccurate results. Similar errors are likely in three-phase fluidized beds.

2.3.3.1.6 Optical Probe Technique

Optical probe technique for phase holdup measurements

in bubble columns was reviewed in section 2.2.2.1.5. Recently several researchers have used this technique to measure phase holdup in three-phase fluidized beds. Ishida and Tanaka (1982) used a single quartz fiber probe with the dual function of projecting light and receiving its reflection. This probe could distinguish between gas bubbles, liquid and solid particles from the reflected light characteristics in a three-phase fluidized bed. De Lasa et al. (1984) and Lee et al. (1984, 1986,1987) used a silica optical fiber probe, with a U-shaped tip sensor whose operation is based on the difference of refraction indices between the gas and the liquid. The gas holdup was then obtained from the summation of all the gas bubbles contact time with the probe. Lee, (1986) noted that the base line of the probe signals increased with increasing solid holdup in liquid fluidized beds. Hu (1985) and Hu et al. (1986) used special calibration techniques to obtain solids holdup using optical fiber probes.

The main advantage of such probes is that they can be used in non-conducting liquids and at high temperatures (Lee S.L.P.,1986) e.g. in hydrogenation reactors. The limitation of the probes are 1) high equipment cost 2) interference of the probes with the motion of small bubbles and possible breakup of larger bubbles.

2.3.3.1.7 Laser Holography

A laser holography technique has been used only

recently for holdup measurement in a three-phase fluidized bed (Peterson, 1985). This technique can provide information about the diameter, shape and position of every gas bubble at a given time. It is the only non-intrusive technique which can provide such information. It is, however, very expensive, hard to setup and it cannot be applied at high gas velocities. This technique also requires that the liquid and the solid have the same refractive index.

2.3.3.1.8 Other Techniques

Vasalos et al. (1982) used γ-rays absorption technique to measure holdups in slurry fluidized beds. From the theoretical profile of the γ-rays absorption, they were able to estimate the bed height, and the liquid and gas holdups were obtained using Equations 2.3.14 and 2.3.12. The application of this technique is limited to the accurate determination of bed height. It should be used in conjunction with other techniques (i.e. pressure profile measurements) to obtain the phase holdups.

Kato et al. (1985) used a shutter plate technique to obtain the phase holdups in a gas-liquid(slurry)-solid system. The mean holdup of each phase was obtained by measuring the volume of trapped gas and solid particles between two shutter plates. The accuracy of this technique is however greatly limited by the requirement of

simultaneous and quick closure of shutter plates.

Based on the above review of various experimental techniques for phase holdup measurement, it may be stated that each technique has its own limitations. The technique based on pressure profile measurements should provide reasonably accurate estimates of mean phase holdups for negligible entrainment of particles in the freeboard. The accuracy of this technique can be further improved by using suitable dampeners to minimize errors due to fluctuations in manometers levels.

2.3.3.2 Effects of Operating Parameters on Phase Holdups

Based on the literature studies,the effect of various operating parameters such as gas velocity,liquid velocity, particle properties and liquid phase properties on phase holdups is systematically analysed below.

2.3.3.2.1 Effects of the Gas Velocity on the Holdups

As in bubble columns (see section 2.2.2.2.1) the gas holdup (ϵ_g) was found to increase with the gas velocity in three phase fluidized beds by many researchers (Michelsen and Ostergaard, 1970; Kim et al., 1972; Dhanuka and Stepanek, 1978; Saberian (1984,1985); Lee, S.L.P, 1986; Catros, 1986; Fan et al., 1986b; Saberian et al., 1987; Sun et al., 1988). The rate of increase of gas holdup with gas velocity has been found to vary with the particle size

(Michelsen and Ostergaard, 1970; Kim et al., 1972; Saberian et al., 1987) and the nature of the liquid (Kim et al., 1972; Blum and Toman, 1977; Fan et al., 1986b; Broudjenni et al., 1987; Sun et al., 1988). The gas holdup in three-phase fluidized beds of fine particles has been found to be lower than in the corresponding solid-free systems (Adlington and Thompson, 1965; Visvanathan et al., 1964). Michelsen and Ostergaard (1970), reported that for solid free systems and beds of 6 mm glass beads, the gas holdup is proportional to the superficial gas velocity raised to the power of 0.93 and 1.05 respectively while the exponents were found to be lower (0.88 and 0.78) for beds of smaller (0.25 and 1.0 mm) glass beads. These results indicate that the gas holdup behavior is dependent on the flow regime. Lower gas holdups are obtained in the beds of fine particles which are more likely to be in the coalesced bubble flow regime while higher gas holdups in beds of large particles which are more likely to be in the bubble breakup regime (see section 2.3.2.2).

Other studies have reported the effect of the gas flowrate on the other holdups i.e. the liquid and solid holdup:

Begovich and Watson (1978a) found that for a given liquid velocity , increasing the gas velocity increased the gas holdup but only slightly decreased the solid holdup. The liquid holdup has been found to decrease with increasing gas velocity by all researchers (Dhanuka and

Stepanek, 1978; Efremov and Vakrushev, 1970; Kato et al., 1981; Mukherjee et al., 1974). Dhanuka and Stepanek (1978) noted that the liquid holdup decreased with the gas velocity for all the particle sizes.

2.3.3.2.2 Effects of Liquid Velocity on the Holdups

Various studies have reported an increase in the liquid holdup with increasing liquid velocity (Michelsen and Ostergaard, 1970; Kim et al., 1972,1975; Mukherjee, 1974; Dhanuka and Stepanek, 1978; Begovich and Watson, 1978a; Catros,1986; Hu et al., 1986; Lee and de Lasa, 1987).

The effect of the liquid velocity on the gas holdup depends on the particle size. Dhanuka and Stapenak (1978) reported a decrease in the gas holdup for large particles (4.08 and 5.86 mm), but the gas holdup was independent of the liquid velocity for smaller particles (1.98 mm). Hu et al. (1986) reported the existence of a critical liquid velocity, beyond which the liquid velocity had no effect on the gas holdup. At higher liquid velocities, the bed was in "the developed fluidized region". For liquid velocities lower than the critical value, the gas holdup decreased when the liquid velocity was increased. They called this region 'undeveloped fluidized region'. The critical liquid velocity was found to depend on the column diameter and particle size. These observations could be explained on the basis of the slip velocity of the bubbles

i.e. the difference between interstitial liquid velocity and bubble rise velocity. When this difference is large there would be insignificant effect of the change in liquid superficial velocity on gas holdup (i.e. large coalesced bubbles in a bed of fine particles). Further work is required to verify this hypothesis. Some researchers also measured local gas holdups and radial gas holdup profiles in three-phase fluidized beds (Hu et al., 1986; Morooka et al., 1986; Lee and de Lasa ,1987). Highest gas holdups were found at the center of the bed and lowest at the column wall. Morooka et al. (1986) noted that the local gas holdup was proportional to the square of the distance from the wall. The effects of distributor design vis-a-vis column diameter on the radial gas holdup profiles need to be investigated to obtain further insights in local hydrodynamics of the bed.

2.3.3.2.3 Effects of the Liquid Properties

A number of researchers reported that the liquid viscosity did not affect the gas holdup in three-phase fluidized beds (Efremov and Vakushev, 1970; Bhatia and Epstein, 1972; Begovich and Watson, 1978a; Bruce and Revel-Chion, 1984). Patwari et al. (1986), however, observed that the gas holdup passed through a minimum with increasing liquid viscosity for both Newtonian and Pseudoplastic liquid solutions. These results, however could have been affected by the change in coalescing

behavior of the liquid solutions used (see Section 2.2.2.2.6).

Increasing the liquid viscosity increases the liquid holdup (Kim et al., 1972,1975; Begovich and Watson, 1978a Kato et al., 1981).

Saberian et al. (1987) used five different liquids; cyclohexane, tetrachloroethylene, kerosene, gas oil and water, to investigate the effects of liquid phase properties on gas holdup. From their data, it can be concluded that for pure compounds there is no correlation between surface tension and gas holdup.

Some researchers added surfactants to water to alter its surface tension (Kim et al., 1975; Fan et al., 1986b). As explained in section 4.1.3.3 , the addition of a surfactant can significantly alter the coalescing behavior of the liquid and consequently affect the phase holdups. Since, with pure liquids, the gas holdup could not be correlated with the surface tension, it seems that the gas holdup is primarily affected by the liquid coalescing properties which cannot be directly related to the surface tension.

2.3.3.2.4 Effects of Particle Size and Density

The gas holdup in three-phase fluidized beds is strongly influenced by the size and density of the solid particles (Viswanathan et al., 1964; Adlington and Thomson, 1965; Michelsen and Ostergaard, 1970; Dhanuka and

Stepanek, 1978; Sun et al., 1988). Viswanthan et al. (1965) observed that in the presence of particles smaller than 1.0 mm in diameter, the gas holdup was lower than that in the solid-free system, and in the case of particles larger than 4.0 mm, the gas holdup was higher than that in the solid-free system. The same observation was also shared by Michelsen and Ostergaard (1970). Sun et al. (1988), however, observed that for low density particles (ρ_p=10^3kg/m^3) there was no effect of particle size on gas holdup. These observations can be related to different flow regimes observed in three-phase fluidized beds (see Section 2.3.2.2). The formation of large coalesced bubbles in the beds of small and light particles (coalesced bubble flow regime) would result in low gas holdup while the formation of small bubbles in beds of large and heavy particles would result in high gas holdups (bubble breakup regime).

2.3.3.2.5 Effects of Solid Wettability

The effect of solids wettability on the hydrodynamics of three-phase fluidized beds was studied by Armstrong et al. (1976) and Bhatia et al. (1972). They both used glass beads and teflon coated glass beads as wettable and non-wettable solids. In the fluidized bed of 1 mm glass beads, Bhatia et al. (1972) found that the bed initially contracted before expanding, while with non-wettable 1 mm solids the bed expansion was continuous upon the

introduction of gas. Armstrong et al. (1976) observed that non-wettable solids (6 mm glass beads) gave lower gas holdups and higher liquid holdups than wettable solids. In their review article Muroyama and Fan (1985) explained that for 1 mm non-wettable particles the formation of liquid wake was probably inhibited while in beds of 6 mm non-wettable beads the bubble breakup was reduced due to adherence of the bubbles to the solids.

2.3.3.2.6 Effects of Gas and Liquid Distribution

Only a few researchers have investigated the effects of gas and liquid distribution on bed hydrodynamics and phase holdup in three-phase fluidized beds (Sisak and Ormos, 1985; Catros et al., 1985; Burru, 1988). Sisak and Ormos (1985) compared the efficiency of three different distributors (i.e. venturi-distributor, packed distributor and perforated-slotted distributor) in shallow beds of fine particles. The values of mean bubble diameter measured above the bed were lowest for venturi-distributor and highest for perforated-slotted distributor.

Catros et al.(1985) studied the influence of gas jets on the hydrodynamics of a three-phase fluidized bed of 3 mm glass beads. The following sequence could be observed when the liquid velocity was increased for a fixed gas velocity.

1) At very low liquid velocity, the liquid and the gas rose through a fixed bed without disturbing the particles.
2) At a certain liquid velocity the gas was able to form a

jet creating a bypass in the bed. A spouted bed was formed. The bed height increased as in a two-phase spouted bed with an annulus.

3) Further increase in liquid velocity fluidized the top of the bed and gas jets formed cavities within the bed.

4) When the liquid velocity was increased further the bed was fluidized by both gas and liquid. The gas jets, however, did not disappear even when then liquid velocity was greater than the minimum fluidization velocity.

Burru (1988) found that a more uniform distribution of both the liquid and the gas could be achieved by introducing a fluidized bed distributor between the gas jet distributors and the fluidized bed.

The above observations show that the distributor design plays an important role in determining the bed hydrodynamics in three-phase fluidized beds. The choice of a suitable distributor would however would vary from one application to other.

2.3.3.2.7 Effects of Column Diameter

The gas holdups have been found to decrease with increasing column diameter (Begovich and Watson, 1978a; Tsungting et al., 1985). Hu et al. (1985) showed that the gas holdup in their large diameter column were significantly lower than the smaller diameter column used by Ostergaard (1971). Tsungting et al. (1985), however,

did not account for the effect of gas distribution which could explain most of the difference observed by these authors.

Begovich and Watson (1978) found no significant effect of column diameter on liquid and solid holdups.

Further work is required to investigate the effects of column diameter vis-a-vis distributor design on gas holdups in three-phase fluidized beds.

2.3.3.2.8 Effects of Gas Properties

Saberian et al. (1987) found no measurable effect of gas properties on phase holdups when using helium, nitrogen or carbon dioxide gas.

2.3.3.3 Correlations for the Phase Holdups

2.3.3.3.1 Bed Porosity

The bed porosity (ϵ) is defined as the sum of gas holdup (ϵ_g) and liquid holdup (ϵ_l) in the bed.

$$\epsilon = \epsilon_g + \epsilon_l \qquad \text{.....(2.3.17)}$$

A number of correlations have been proposed in the literature for bed porosity in three-phase fluidized beds. Following is a critical review of the proposed correlations.

Soung (1978) proposed the following procedure to

evaluate expanded bed heights in three-phase fluidized beds:

$$F = 1.5 + 0.16\ln(V_l/V_g) - 0.065\ln(\Phi Re_t)$$

$$(0.06 < V_l/V_g < 5) \qquad .....(2.3.18)$$

$$F = 2.09 - 0.17\ln(\Phi Re_t) \quad \text{for } 0.6 < V_l/V_g < 5 \qquad .....(2.3.19)$$

$$F = \frac{(H_o/H_{bed})}{(H_o/H_{bed})\text{at } V_g=0} \qquad .....(2.3.19a)$$

$$(H_o/H_{bed})\text{at } V_g=0 = 1 - 4.5(V_l/V_t)^{2.15} \quad \text{for } V_l/V_t < 0.25 \qquad .....(2.3.19b)$$

$$(H_o/H)\text{at } V_g=0 = 1 - 1.22(V_l/V_t)^{1.2} \quad \text{for } V_l/V_t > 0.25 \qquad ....(2.3.19c)$$

These correlations are based on a narrow range of operating conditions and do not account for the bed contraction/expansion effects.

The correlations proposed by Dakshinamurty et al. (1971,1972) are based on data obtained in beds of various solids and liquid phases:

For $Re_t < 500$

$$\epsilon = 2.12\ (V_l/V_t)^{0.41}\ (V_g\mu/\sigma)^{0.08} \qquad .....(2.3.20)$$

For $Re_t > 500$

$$\epsilon = 2.85\ (V_l/V_t)^{0.6}\ (V_g\mu_l/\sigma)^{0.08} \qquad .....(2.3.21)$$

Here $Re_t = V_t\rho_l d_p/\mu_l$

These correlations however cannot account for bed contraction and column diameter effects.

Begovich and Watson (1978a) proposed correlations based on 2381 data points which were combined from ten other literature studies:

$$\epsilon_g + \epsilon_l = 3.93\ V_l^{0.271}\ V_g^{0.041}\ (\rho_s-\rho_l)^{-0.316}\ d_p^{-0.268}\ \mu_l^{0.055}\ D_c^{-0.033} \quad \text{.....(2.3.22)}$$

This correlation is not applicable at zero gas velocity and its application is limited to conditions similar to those tested. It does not take into account bed contraction or the effect of liquid viscosity and surface tension. Moreover, as pointed out by Wild et al. (1984) the dependence on the column diameter is based entirely on small diameter columns.

Correlations proposed by Kim et al. (1975) are expressed as:

$$\epsilon = 1.4\ (Fr_l)^{0.17}\ (We)^{0.078} \quad \text{.....(2.3.23)}$$

for beds with an initial expansion, and

$$\epsilon = 1.301\ (Fr_l)^{0.128}\ (We)^{0.073}\ \exp\ (0.031 V_l/V_g \cdot \epsilon_{12}) \quad \text{.....(2.3.24)}$$

for a bed with an initial contraction

ϵ_{12} is the liquid holdup in the corresponding liquid-solid fluidized bed which is given by

$$\epsilon_{12} = 1.353\ (Fr_1)^{0.205}\ (Re_1)^{-0.10} \qquad \text{..... (2.3.24a)}$$

This correlation is based on data obtained in two dimensional beds. The effects of solids density and column diameter are not accounted for in the correlation.

Saberian (1984) proposed a correlation which can also be used at zero gas velocity:

$$\epsilon = \epsilon_o\ (V_1/V_{1mfo})^{0.274}(1 + 0.07Re_{1g}^{0.334}) \qquad \text{.....(2.3.25)}$$

Here $\epsilon_o = (14\Phi)^{-1/3}$ .....(2.3.25a)

and $Re_g = \dfrac{V_g \rho_1 d_p}{\mu_1}$ .....(2.3.25b)

This correlation does not account for column diameter and liquid surface tension effects.

Lee and deLasa (1987) correlated bed porosity using two different correlations (power law and exponential)

Power Law correlation:

$$\epsilon = 0.659\ V_1^{0.205} V_g^{0.006} \ . \qquad \text{.....(2.3.26)}$$

This model cannot be extrapolated to zero gas velocity.

Exponential correlation:

$$\epsilon = 1 - 0.531\ \exp(-0.418V_1 - 0.004V_g) \qquad \text{.....(2.3.27)}$$

This correlation gave a better fit to their experimental data (+4%).

The correlations proposed by Lee and de Lasa(1987) do not account for liquid phase properties, solid particle size and density and column diameter.

Costa et al. (1986) developed a model for the evaluation of bed porosity based on drift flux approach. The gas and liquid mixture constituted the homogeneous fluid. This model however requires the use of an empirical correlation to estimate the void volume fraction occupied by the gas (ϵ_g/ϵ).

None of the proposed correlations/model account for the distributor effects on bed porosity. The empirical correlation proposed by Begovich and Watson (1978) and the model developed by Costa et al. (1986) should, however provide reasonable estimates of bed porosity for most practical systems.

2.3.3.3.2 Gas Holdup

The empirical correlations proposed for gas holdup in three-phase fluidized beds can be divided into two classes
1) correlations which take into account the particle size
2) correlations which do not take into account the particle size
First the correlations which account for particle size effects are considered.

Vail et al. (1970) proposed the following correlation

with adjustable parameters:

$$\epsilon_g = x_1(1-\epsilon_s)^{y_1}\ (V_g/V_l)^{z_1} \qquad \text{.....(2.3.28)}$$

Where x_1,y_1 and z_1 are empirical constants which varied with the types of solids, as shown below:

	x_1	y_1	z_1
0.73 mm glass beads	0.1026	0.708	2.09
0.77 mm Al-Si cat.	0.108	0.630	3.01
0.74 mm Co-Mo cat.	0.0525	0.670	1.69

This correlation does not account for the effects of column diameter and liquid physical properties. Moreover values of x_1, y_1 and z_1 must be determined experimentally for each particle type.

Begovich and Watson (1978a) proposed a correlation for gas holdup in three-phase fluidized beds based on 913 data points including five other literature studies:

$$\epsilon_g = 1.61\ V_g^{0.72}\ d_p^{0.168}\ D_c^{-0.125} \qquad \text{.....(2.3.29)}$$

This correlation does not account for the effects of particle density and liquid properties and velocity.

Kato et al. (1985) developed a correlation based on dimensionless groups.

$$\epsilon_g = 0.3W^{1.3}/((1+1.1W^{1.5})(1+0.01Re_t^{0.62})) \qquad \text{.....(2.3.30)}$$

$$W = (gD_c^2\rho_l/\sigma)^{0.198}(gD_c^3/\nu_l^2)^{0.035}(V_g/(gD_c)^{0.5}) \quad \text{.....(2.3.30a)}$$

This correlation is based on the assumption that a slurry of fine particles behaves as a homogeneous liquid of higher viscosity and density. The validity of this assumption has to be proven over a wider range of operating conditions.

Fan et al. (1986a) investigated the hydrodynamics of gas-liquid fluidization under conditions of high gas holdup (using aqueous solutions of alcohols). The gas holdup in three-phase fluidized beds was correlated using dimensionless numbers:

$$\epsilon_g = 13.1\ Re_g^{0.53}\ (1 + Re_l)^{-0.39}\ M^{0.10}\ C^{0.29} \quad \text{.....(2.3.31)}$$

where

M is the Morton number which incorporates the surface tension and other liquid properties.

C is the number of carbon atoms in the alcohol molecule

This correlation can be applied only to alcohol solutions. Moreover this correlation does not account for the effects of column diameter and particle density.

Following correlations do not account for particle size effcts

Khang et al. (1983) fitted their gas holdup data with a second-order polynomial. The proposed correlation is:

$$(1 - \epsilon_g)V_g + \epsilon_g V_l = \epsilon_g(0.2267\epsilon_g + 0.1044) \quad \text{.....(2.3.32)}$$

This correlation does not account for the effects of liquid phase properties, particle size and density and column diameter.

Hu et al.(1986) developed a correlation based on the gas holdup measurements in the beds of different column diameters. The bed was operated within what they called the 'developed fluidized region':

$$\epsilon_g = 0.0645\ V_g^{0.842} V_l^{0.096} D_c^{-0.419} \quad \text{..... (2.3.33)}$$

This correlation shows does not account for the effects of particle size and density and liquid phase properties on gas holdups.

Most of the proposed correlations are based on a limited set of data obtained over a narrow range of operating conditions. None of the proposed correlations account for the effects of gas distribution and coalescing behavior of the liquid. The correlation proposed by Begovich and Watson (1978a) is recommended for estimation of gas holdup in coalescing systems.

2.3.3.3.3 Liquid Holdup

A number of correlations have been reported in the literature for liquid phase holdup in three-phase fluidized beds (Razumov et al., 1973; Kim et al., 1975; Kato et al., 1981; Chiu and Ziegler, 1983; Lee, 1986).

Razumov et al. (1973) proposed a dimensional correlation:

$$\epsilon_l = 0.422 + 0.135V_l/d_p^{0.562} - 1.82V_g \qquad \text{.....(2.3.34)}$$

This correlation is based on the limited data which they obtained with air,water,sand and slag beads from a blast furnace. Its application needs to be tested over wider range of operating conditions (i.e. non-coalescing liquids, different distributor designs).

Kim et al. (1975) proposed a correlation using dimensionless numbers:

$$\epsilon_l = 1.504Fr_l^{0.234}\ Fr_g^{-0.086}\ Re_l^{-0.082}.We^{0.092} \qquad \text{.....(2.3.35)}$$

This correlation is based on the data obtained for a two dimensional bed. It should therefore be used with caution for cylindrical beds.

Kato et al. (1981) proposed a generalized correlation by modifying the formula of Garside and Al-Dibouni (1977). The liquid holdup is predicted using the following procedure:

$$(V_l/V_t) = (\epsilon_{l2} / \epsilon_{l3})^n \qquad \text{.....(2.3.36)}$$

where

$$\epsilon_{l3} = 1.0 - 9.7(350 + Re_t^{1.1})^{-0.5}k_o^{0.09} \qquad \text{.....(2.3.36a)}$$

and $$Re_t 0.9 = \frac{[5.1 + 86.2k_o^{0.285-n}]}{(n-2.7)[0.1+0.443k_o\ 0.165]} \quad \text{.....(2.3.36b)}$$

where

$$k_o = \rho_l V_g^4 / (g\sigma) \quad \text{.....(2.3.36c)}$$

The applicability of the correlation needs to be verified for non-aqueous liquids and larger bed particles (>2 mm).

Chiu and Ziegler (1983) proposed a correlation for the ratio of liquid holdup in liquid fluidized bed to that in three-phase fluidized bed.

$$\epsilon_{12}/\epsilon_{13} = 0.79 V_l^{-0.088} V_g^{0.059} (d_e \Phi)^{-0.058} \quad \text{.....(2.3.37)}$$

This correlation requires prior estimations of liquid holdup in liquid fluidized beds. Moreover the effects of liquid phase properties are not accounted for.

Lee (1986) used a power law and an exponential model to correlate the liquid phase holdup to gas and liquid velocities.

Power law model:

$$\epsilon_l = a_1 V_l^{b_1} V_g^{c_1} \quad \text{.....(2.3.38)}$$

where $a_1 = 0.659 + 0.004121$

$b_1 = 0.0248 + 0.01077$

$c_1 = 0.0060 + 0.01243$

Exponential model:

$$\epsilon_l = 1 - a_1 \exp(b_1 V_l + c_1 V_g) \qquad .....(2.3.39)$$

where $a_1 = 0.5305 + 0.1243$

$b_1 = -0.4176 + 0.01288$

$c_1 = -0.004038 + 0.01313$

These correlations do not account for the effects of particle size and liquid properties.

None of the proposed correlations for liquid phase holdup account for the effects of gas and liquid distribution and the coalescing behavior of the liquid.

2.3.3.3.4 Correlations Based on Drift Flux Models

The drift flux model for the bubble column was reviewed in section 2.2.1.4. Darton and Harrison (1975) extended the concept of drift flux to three-phase fluidized beds. For three-phase fluidized beds, the drift flux can be defined as:

$$\frac{V_{gl}}{\epsilon_g} = \frac{V_g}{\epsilon_g} - \frac{V_T}{\epsilon_g + \epsilon_l} \qquad .....(2.3.40)$$

or

$$V_{gl} = (V_g \epsilon_l - V_l \epsilon_g)/\epsilon \qquad .....(2.3.40a)$$

Saberian et al. (1987) found that the drift flux was practically independent of the nature of the particles and liquid velocity and surface tension. The proposed

correlation for coalescing liquids is shown:

$$v_{gl} = 0.017\ (\rho_l v_g^2)^{0.45} \qquad \text{.....(2.3.41)}$$

This correlation was developed based on the data obtained with one column diameter and one gas distributor. The applicability of this correlation needs to be tested over a wider range of operating conditions.

Nacef et al. (1988) have shown that the drift flux in three-phase fluidized beds can be predicted by a correlation of the form:

$$v_{gl} = a_2 v_g^{b_2} \qquad \text{.....(2.3.42)}$$

For a given type of distributor and a given column diameter the drift flux was found to be independent of the particle shape and size and the liquid viscosity. The values of constant a and exponent b generally varied with distributor type and column diameter.

Using the drift flux velocity and the bed porosity, the gas and liquid holdups can be calculated using the following equations:

$$\epsilon_g = \epsilon\frac{v_g - v_{gl}}{v_g + v_l} \qquad \text{.....(2.3.43)}$$

$$\epsilon_l = \epsilon\frac{v_{gl} + v_l}{v_g + v_l} \qquad \text{.....(2.3.44)}$$

Using the drift flux concept, Costa et al. (1986) developed an equation for bed porosity in three-phase

fluidized beds. The equations for frictional pressure gradient which are used in the model, assume the gas and the liquid form a pseudo homogeneous phase with suitable mean physical properties. This assumption, however, would not be valid in the heterogeneous flow regime where large bubbles create cavities in the bed.

Drift flux correlations in three-phase fluidized beds need to be developed over a wider range of operating conditions. It is likely that separate correlations will be required for different flow regimes.

2.3.3.3.5 Correlations Based on Wake Model

The wake models take into account the role of the wake behind the gas bubble in liquid flow as pointed out by Stewart and Davidson (1984). The wake concept

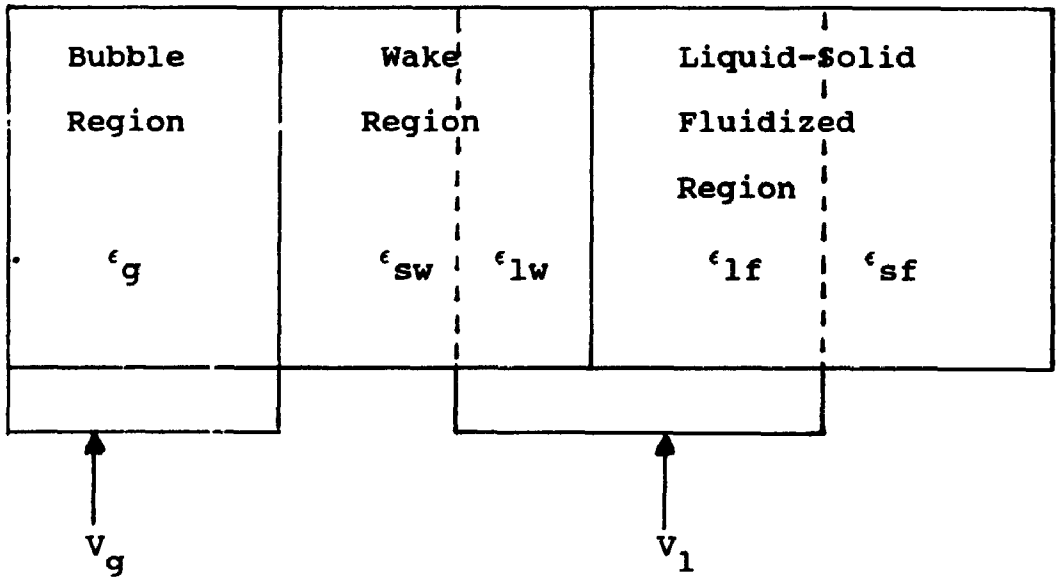

Figure 2.3.2
General description of a bubble wake model

considers the three-phase fluidized bed to be divided into 1) the gas bubble region 2) the wake region 3) the solid liquid fluidized region (Figure 2.3.2). The overall bed voidage (ϵ) consists of the total gas holdup (ϵ_g) and the total liquid holdup (ϵ_l) which is divided between the wake region (ϵ_{lw}) and the liquid-fluidized region (ϵ_{lf}).

The bubble wake models have been widely used to predict the bed expansion or contraction behaviors and the phase holdups. General descriptions of the models are given by Epstein (1981), Wild et al. (1984,1987), Muroyama and Fan (1985) and Fan et al. (1987). These models use two key parameters called k and x where k is defined as the ratio of wake volume to bubble volume and x is the ratio of solids holdup in the wake region to the solids holdup in the liquid fluidized region. The mathematical expressions for the two parameters are given below:

$$k = \epsilon_w/\epsilon_g \qquad \text{..... (2.3.45)}$$

$$x = \epsilon_{sw}/\epsilon_{sf} \qquad \text{.....(2.3.46)}$$

The correlations for k have been reviewed by Wild et al. (1987), Muroyama and Fan (1985) and Fan et al. (1987). The value of x in general lies between zero (solids-free wakes) and unity (wakes solids holdup same as in liquid-fluidized region).

Some researchers such as El-Temtamy and Epstein (1978), Dhanuka and Stepanek (1978), Khang et al. (1983)

assumed that the bubble wakes contained solids while others such as Efremov and Vakrushev (1970), Darton and Harrison (1975) and Baker et al. (1977) assumed solid-free wakes.

A generalized wake model was developed by Bhatia and Epstein (1974). The model assumes the relative velocity between the liquid and the solid in the liquid-solid fluidized region is related to the bed porosity by the Richardson and Zaki equation (1954). The resultant expression for the liquid holdup and bed porosity can be given as:

$$\epsilon_l = \left[\frac{V_l - V_g k(1-x)}{V_t(1-\epsilon_g - k\epsilon_g)}\right]^{1/n} [1-\epsilon_g(1+k-kx)] + \epsilon_g k(1-x) \quad \ldots\ldots\ldots (2.3.47)$$

$$1-\epsilon_s = \left[\frac{V_l - V_g k(1-x)}{V_t(1-\epsilon_g - k\epsilon_g)}\right]^{1/n} [1-\epsilon_g(1+k-kx)] + \epsilon_g(1+k-kx) \quad \ldots\ldots\ldots (2.3.48)$$

In order to be able to use Equation 2.3.47 to predict the solids holdup ,methods must be available to estimate V_t, n, k, ϵ_g, and x. For a given gas-liquid-solid system, the values of V_t (particle terminal velocity) and n (Richardson and Zaki exponent) are fixed. In the solid-free wake model, which assumes x=0, the values of k and ϵ_g need to be known to estimate the phase holdups or bed expansion.

The various empirical correlations proposed for k are reported in Table 2.3.3. The value of k should depend on

Table 2.3.3 Literature correlations for predicting 'k'

Correlations	Value for 'x'	References	Remarks
$k = 1.4\ \epsilon_g^{-0.5}(V_l - V_{lmfo})$	$x = 1.0$	Ostergaard (1965)	Low gas velocities (< 0.02 m/s). Assumption for x not justified.
$k = 5.1\ \epsilon_{12}^{4.85}\ (1 - \tanh\ \{\frac{40\ V_g(\epsilon_{12})^{10}}{V_l} - 3.32\epsilon_{12}^{5.45}\})$	$x = 0.0$	Efremov and Vakhrushev (1970)	Effects of liquid phase properties not accounted for. Assumption for x not justified.
$k = (0.61 + \frac{0.037}{\epsilon_g + 0.013})\epsilon^3$	$0.0 < x < 1.0$	Bhatia and Epstein (1974)	Both gas holdup and bed porosity required.
$k = 1.4\ (V_l/V_g)^{0.33} - 1$ for $V_l/V_g > 0.4$ $k = 0.0$ for $V_l/V_g < 0.4$	$x = 0.0$	Darton and Harrison (1975)	Effects of liquid phase properties not accounted for. Assumption for x not justified.
$k = 1.617\ (V_l/V_g)^{0.61}\ \sigma^{-0.654}$	$x = 0.0$	Baker et al. (1977)	Two dimensional bed data.
$k = k_b \exp(-5.08\ \epsilon_g)$ k_b = ratio of sphere completing volume to the bubble volume	$x = 1 - 0.07/x_1$ for $0 < x_1 \leq 1.14$ $x = 0.0$ for $x_1 > 1.14$ where $x_1 = \frac{V_t}{V_g/\epsilon_g - V_l/\epsilon_l}$	El-Temtamy and Epstein (1978)	Gas and liquid holdups required for evaluation of x.
$k = \epsilon_g^3[\exp(-1.2\epsilon_g + 2.5\exp(-32.2\epsilon_g))]$	$x = 0.1$	Khang et al. (1983)	No proper justification for the derived equation for x. Arbitary value for x.
$k = 0.31\ V_g^{-0.985}$	$x = 1.0 - 0.28\ V_l^{1.09}\ d_p^{-1.33}$ for $V_g < 0.2$ m/s and $d_p > 0.58$ mm	Morooka et al. (1986)	Correlation based on local liquid velocity measurements and mean gas holdups.

the average bubble size which in turn depends on the prevailing hydrodynamic regime. This has been taken into account only in the correlations proposed by Darton and Harrison (1975) and El-Temtamy and Epstein (1978). The correlation proposed by Darton and Harrison (1975) however assumes solid free wake which may not be justified in the beds of fine particles. Wild et al. (1984) have pointed out other limitations of the various correlations for k. Using literature correlations, Wild et al.(1984) have shown that there is a considerable scatter in the predictions of the coefficient k as a function of superficial gas velocity. The equations for k implicitly assume uniform bubble size distribution which is however not the case for large gas flowrates in the coalesced bubble flow regime when there are wide distributions of bubble diameters. In a subsequent publication Wild et al. (1987) have reported that there was practically no effect of the choice of a correlation for k on the prediction of phase holdups. The validity of these observations need to be tested over a wider range of experimental conditions.

Since the wake models provide only one equation between the three holdups, an extra equation such as a correlation for the prediction of the gas holdup (or its measurement) is required to solve for holdups. The available correlations for the prediction of the gas holdup have a limited range of applicability (see section 2.3.3.3.2 and 2.3.3.3.4). Bhatia and Epstein (1974) have

proposed gas holdup estimations based on bubble rise velocity. These velocities however depend on the bubble diameter for which no accurate correlation or model are available.

Other Problems with Wake Models:

1) In all the wake models, the Richardson and Zaki relationship is applied to the liquid-solid fluidized region which eliminates the use of these models for bubble-supported beds.

2) These models implicitly assume a constant bubble rise velocity (i.e. constant bubble diameter) which is not justified at high gas velocities in the coalesced bubble flow regime.

3) All the wake models developed so far have assumed the bubble wake to be rising at the same velocity as the bubble. In their review article, Fan et al. (1987) point out that due to vortex shedding, the net velocity of the wakes would be lower than that of the bubbles.

Fan et al. (1986c) proposed a structural wake model based on the physical description of the wake structure behind bubbles. According to this model, the wake structure can be considered to consist of a primary wake which moves in close association with the bubble and a secondary wake which includes a free shear layer and vortices shed from the primary wake. The primary wake is assumed to be responsible for hydrodynamic phenomena such as bed contraction and solids mixing (Fan and Tsuchiya,

1986). The primary wake is further divided into 1) the stagnant turbulent wake region and 2) the shedding vortical wake region. For the structural wake model, Fan and Tsuchiya (1986) assumed that the main mechanism of the solids exchange between the wake and the liquid-solid fluidized region was shedding of old vortex and formation of new vortex on the same side of the bubble. The proposed correlation for liquid phase holdup based on this model require quantitative information about several parameters which are not easy to measure in practice. At present this model is mainly an academic curiosity.

2.3.4 Liquid Backmixing in Three-phase Fluidized Beds

The information about liquid backmixing is important in order to select an appropriate flow model for the three-phase fluidized bed reactors.

2.3.4.1 Experimental Techniques

Various techniques available in the literature for the measurement of liquid backmixing were reviewed in section (2.2.4.1).

The following techniques have been used for the measurement of liquid backmixing in three-phase fluidized beds.

-Imperfect tracer pulse method, utilizing gamma ray emitting isotopes (bromine-82), (Ostergaard and

Michelsen, 1968; Ostergaard, 1969; Michelsen and Ostergaard, 1970)

-Continuous injection of colored tracer (Kim et al., 1972)

-Pulse of saline tracer (Kim and Kim, 1983; Kato et al., 1985; Hu, 1985; Morooka et al., 1986)

-Continuous injection of saline tracer (El-Temtamy et al.,1979; Hu, 1985)

The axial dispersion coefficient is obtained from the residence time distribution data as measured with these techniques.

All these techniques used a single probe at one radial location for the measurements of the residence time distribution. This approach however may not provide accurate information if radial mixing is poor and/or there are large variations in local liquid velocity.

2.3.4.2 Effects of Different Operating Variables

The liquid backmixing in three-phase fluidized beds is caused mainly by the motion of bubbles and particles. There is almost a continuous formation and separation of bubbles and particle wakes. The faster moving bubbles pick up and accelerate liquid and particles in their wakes which causes the downflow of the displaced liquid-fluidized phase in other parts of the bed. The extent to which such downflow or backmixing occurs depends upon the bubble relative velocity and on bubble and wake sizes.

In three-phase fluidized beds the bubble size depends on the flow regime (see section 2.3.2.2.1). Large bubbles are formed in the coalesced bubble flow and slug flow regimes while small bubbles are formed in the bubbly flow regime. In addition to the bubble motion, the particle motion is also expected to contribute to fluid mixing in three-phase fluidized beds. The extent of these effects depend on the operating conditions.

The effects of various operating parameters on liquid backmixing are discussed in the following sections.

2.3.4.2.1 Effects of Gas Velocity

Liquid backmixing was found to increase with increasing gas velocity by most researchers (Ostergaard and Michelsen, 1968; Ostergaard, 1969; Kim et al.,1972; El-Temtamy et al.,1979; Kim and Kim, 1983; Morooka, 1986). Muroyama et al. (1978), however, reported that the liquid backmixing in the dispersed bubble flow regime was not affected by the gas velocity while in the coalesced bubble flow regime it increased with increasing gas velocity. Similar observations were also reported by Hu et al. (1985).

From these observations, it may be concluded that the liquid backmixing increases with gas velocity in coalesced bubble flow regime as the frequency of formation of large bubbles increases with increasing gas velocity.

2.3.4.2.2 Effects of Liquid Velocity

The effect of liquid velocity on liquid dispersion has been found to vary with the bed particle size (Michelsen and Ostergaard, 1970; El-Temtamy et al.,1979; Kim and Kim, 1983). The axial dispersion coefficient was generally found to increase with increasing liquid velocity in beds of particles ranging from about 1.0 mm to 6.0 mm in diameter (El-Temtamy et al.,1979; Kim and Kim, 1983). Kim and Kim (1983) observed that in the bed of 1.7 mm particles, axial dispersion increased sharply with liquid velocity up to 0.6 m/s. At higher liquid velocities, however the rate of increase was not significant. The same trends were also exhibited in beds of 3 mm particles. These observations can be related to the change in flow regime from coalesced bubble flow to dispersed bubble flow as the liquid velocity is increased.

For beds of 0.45 mm particles, El-Temtamy et al.(1979), observed reverse trends i.e. the axial dispersion coefficient decreased with increasing liquid velocity. El-Temtamy et al. (1979) argue that the effect of increase in liquid velocity on liquid mixing is the net result of increased particle circulations and lower concentrations of particles and bubbles, although this interpretation may be questionable. While the last two effects should result in lower liquid mixing, the first effect would act to increase liquid mixing. Letan and

Elgin (1972) argue that the increased particle circulation in the bed of relatively large or high inertia particles adds to liquid mixing due to continuous formation and detachment of wakes on the roof of particles as the liquid flowrate is increased. Further work is required to establish the effects of solid circulation patterns on liquid backmixing in three-phase fluidized beds.

2.3.4.2.3 Effects of Particle Size

As mentioned in sections 2.3.4.2.1 and 2.3.4.2.2, the particle size was found to have important effect on axial mixing in three-phase fluidized beds. Ostergaard and Michelsen (1968) and Ostergaard (1969) found that the beds of 0.25 and 1.0 mm particles were characterized by a high degree of backmixing while beds of 6 mm glass beads were characterized by a very low degree of backmixing. Kato et al. (1985) found that the effect of particle size became less significant at higher gas flowrates. These results show that the effect of particle size is related to the flow regime. The low degree of liquid mixing observed in the beds of large particles could be related to the formation of the dispersed bubble flow regime at low gas flowrates while with increasing gas flowrates there is a transition to the coalesced bubble flow regime.

2.3.4.2.4 Effects of Column Diameter

The liquid axial dispersion has been found to

increase with column diameter (Ostergaard, 1978; Muroyama et al. 1978; Kim and Kim 1983; Kato et al.,1985; Hu et al., 1985; Morooka et al., 1986). Ostergaard (1978) observed that the liquid axial dispersion coefficient in a 0.228 m I.D. column was 50-100 % higher than in a 0.15 m I.D. column, depending on the particle size.

2.3.4.2.5 Effect of Liquid Viscosity and Surface Tension

The effect of liquid viscosity on liquid mixing was studied by Kim and Kim (1983). In a bed of 6 mm particles axial mixing generally increased with increasing liquid viscosity. In beds of 1.7 and 3.0 mm particles, while the axial mixing increased with liquid viscosity at low gas flowrates (< 0.01 m/s), but decreased at higher gas flow rates.

These observations could be related to the effect of liquid viscosity on flow regime boundaries (Saberian, 1985). The higher rate of bubble coalescence in high viscosity liquids would lead to increased axial mixing as the large coalesced bubbles with their large wakes rise in the bed. Kim and Kim (1983) observed only a slight increase in the axial dispersion coefficient with an increase in surface tension of the liquid. This observation could be related to the formation of slightly larger bubbles in the higher surface tension liquids.

From the above review, it can be concluded that the

effects of different operating variables on liquid backmixing in three-phase fluidized beds depends on the prevailing flow regime. In a given flow regime the average bubble size and particles circulation patterns can play important roles.

No systematic work has been done so far to investigate the effects of gas and liquid distributors and coalescence behavior of the liquid phase.

2.3.4.3 Correlations for Axial Dispersion

Correlations for the axial liquid mixing in three-phase fluidized beds have been proposed by Muroyama et al. (1978); El-Temtamy et al. (1979); Joshi (1980); Kim and Kim (1983) and Kato et al. (1985).

The correlation proposed by El-Temtamy et al. (1979) indirectly accounts for the effect of gas velocity, through the liquid holdup, as the axial dispersion was found to increase significantly with the gas velocity.

Joshi (1980) developed a unified model of the axial liquid mixing in gas-liquid two phase columns and three-phase fluidized beds. This correlation was developed based on an energy balance model for liquid mixing. Kim and Kim (1983) found a very poor agreement with their data when they tested the correlation proposed by Joshi (1980). They argued that the correlation proposed by Joshi (1980) was valid only for the ideal bubbly flow regime.

Muroyama et al. (1978) proposed separate correlations

for the dispersed bubble flow regime and for the coalesced bubble flow regime. The proposed correlations are:

Dispersed bubble flow regime;

$$\frac{V_l D_c}{D_z} = 26\,(d_p/D_c)0.5 \qquad \text{.....(2.3.49)}$$

valid in the range $0.02 < d_p/D_c < 0.12$

Coalesced bubble flow regime;

$$\frac{V_l D_c}{D_z} = 1.07(V_l)0.738(V_g)-0.167(D_c)-0.58 \qquad \text{.....(2.3.50)}$$

where V_l and V_g are in cm/s and D_c and d_p are in cm.

The correlations proposed by Muroyama et al. (1978) can be used only when the prevailing flow regime is known which in turn depends on a number of other operating variables (see section 2.3.2.2.1).

Kato et al. (1985) combined their data and the data of Michelsen and Ostergaard (1970) and Muroyama et al. (1978) to propose three correlations for three flow regions divided according to the gas velocity.

1) $V_g < 0.09$ m/s

It was found that in this region, the ratio of the Peclet number of the three-phase fluidized bed to that of

the bubble column could be considered independent of gas velocity and column diameter:

$$Pe(3PFB)/Pe(BC) = (1+V_t/V_l)^{n5} \quad \text{..... (2.3.51)}$$

where $n5 = 0.40Bo^{0.225}$

and $Pe(BC) = (\mu_l/\mu_w)^{0.07} \{13Fr_g/(1+6.5Fr_g^{0.8})\}$

.....(2.3.51a)

2) V_g>0.25 m/s

In this region the experimental data in three-phase fluidized beds were found to be close to the axial dispersion in bubble columns.

$$Pe(3PFB) = Pe(BC) \quad \text{.....(2.3.52)}$$

3) V_g = 0.09-0.25 m/s;

In this region the value of axial dispersion in three-phase fluidized beds approached the bubble column values with increasing gas velocity. The following correlation was proposed:

$$Pe(3PFB) = Pe_1(V_g/9)^{2.31\log_{10}(Pe_2/Pe_1)}$$

.....(2.3.53)

where Pe_1 and Pe_2 are the values of Pe(3PFB) given by Equation 2.3.51 at V_g=0.09 m/s and given by Equation 2.3.52 at V_g=0.25 m/s, respectively.

These correlations are based on the division of flow regions based on gas velocity alone which makes them less

generalizable since the three flow regime boundaries are also affected by particle properties, column diameter and liquid properties (see section 2.3.2.2.2).

Kim and Kim (1983), however proposed a single correlation based on their data and the data of other researchers (Michelsen and Ostergaard, 1970; El-Temtamy et al.,1979; Muroyama et al., 1978; Ostergaard, 1978):

$$Pe' = 20.19\ (d_p/D_c)^{1.66}\ [V_l/(V_l+V_g)]^{1.03} \qquad .....(2.3.54)$$

the Peclet number was based on the particle diameter. This correlation, however, does not take into account the effects of liquid physical properties.

Nguyen-Tien (1984) reported that while the correlation proposed by Kim and Kim (1983) gave a fair prediction of liquid axial dispersion coefficient in the beds particles larger than 3 mm the predicted values were much smaller in the beds of particles smaller than 1 mm. They showed that the coefficient 20.19 in Kim and Kim's (1983) correlation needs to be replaced by 61 to give a reasonable fit to their data in beds of particles having diameter less than 1 mm. These observations reflect a change of regime as affected by particle size.

Morooka et al. (1986) extended the momentum balance approach of Miyauchi et al. (1986) for bubble columns, to predict the axial dispersion coefficient in three-phase fluidized beds. They, however, pointed out that the model underpredicted the axial dispersion coefficient.

2.3.4.4 Radial Mixing

Radial temperature and concentration profiles have been shown to exist in three-phase fluidized beds (Chiu and Ziegler, 1983; Muroyama et al., 1985; Catros et al., 1985; Kang and Kim, 1986). A few researchers have also investigated the effects of different operating variables on radial mixing (El-Temtamy et al., 1979; Kang and Kim, 1986; Yasunishi et al., 1987).

Like axial mixing, radial mixing in three-phase fluidized beds is also expected to depend on the flow regime. In the dispersed bubble flow regime the bubbles move discretely upwards causing little mixing in the bed. However the fast moving large bubbles in the coalesced bubble flow regime would increase the level of turbulence in the bed, causing higher axial and radial mixings.

Radial mixing in three-phase fluidized beds has been found to increase with gas velocity (El-Temtamy et al., 1979; Kang and Kim, 1986; Yasunishi et al., 1986). Yasunishi et al. (1986) reported that the radial dispersion coefficient increased significantly with increasing gas velocity in coalesced bubble and slug flow regimes while in the dispersed bubble flow regime it increased only slightly with gas velocity. These observations can be related to bubble sizes and their wakes in different flow regimes.

Kang and Kim (1986) observed that the radial mixing

in three-phase fluidized beds exhibits a maximum with respect to the liquid velocity . These authors reported that the optimum bed porosities at the maximum radial dispersion coefficient were in the range of 0.57-0.7 which was similar to those of the maximum heat transfer coefficient in three-phase fluidized beds (Kang et al., 1985). These observations could again be related to a change in flow regime past the optimum range of bed porosities.

For the effects of particles size the reported results can again be related to the prevailing flow regime in the bed (Yasunishi et al., 1987; Kang and Kim, 1986).

The above observations point out that it is important to account for the radial mixing effects in a flow model for three-phase fluidized beds. The effects of gas and liquid distribution and liquid phase properties on radial mixing have not been investigated systematically.

2.3.5 Heat Transfer in Three-Phase Fluidized Beds

The heat transfer from wall-to-bed and from an immersed surface-to-bed in three-phase fluidized beds has been investigated by a number of researchers (Ostergaard, 1964; Viswanathan et al., 1965; Armstrong et al., 1976; Baker et al., 1978; Kato et al., 1981; Chiu and Ziegler, 1983; Muroyama et al., 1984 and 1986; Kang et al., 1985).

The heat transfer coefficient in three-phase fluidized beds was found to increase with increasing gas velocity by all the researchers. The rate of increase, however, depends on liquid velocity (Ostergaard, 1964; Chiu and Ziegler, 1983; Kang et al., 1985) and particle size (Chiu and Ziegler, 1983; Muroyama et al., 1984; Kang et al., 1985). The increase in heat transfer coefficient with the increase of gas flowrate is the result of increasing turbulence and mixing in the bed.

The wall to bed heat transfer coefficient passes through a maximum as the liquid velocity is increased, in both liquid-solid and gas-liquid-solid fluidized beds (Chiu and Ziegler, 1983; Muroyama et al., 1984; Kang et al., 1985). These observations can be related to the effects of liquid velocity on liquid axial axial in three-phase fluidized beds which also passes through a maximum as the liquid velocity is increased.

The heat transfer coefficient was found to increase significantly with particle size up to particle diameter of about 3 mm, the rate of increase was, however, gradual as the particle size was increased further. Chiu and Ziegler (1983) also observed that at higher gas velocities, the coefficient passed through a minimum value with progressive increase in particle size. Kang et al. (1985) reported a decrease in heat transfer coefficient with increasing liquid viscosity in beds of different particles. This decrease could mainly be attributed to the

increase of boundary layer thickness around the heater surface.

The above observations point to a complex interaction of gas, liquid and solid phases in determining the heat transfer rate in three-phase fluidized beds. However a clearer picture would have emerged if bed hydrodynamics (i.e. phase holdups and flow regime) had been investigated simultaneously with the heat transfer phenomena. For example, larger increases observed in heat transfer rate with light and small particles were probably the results of coalesced bubble flow regime. This regime is characterized by the formation of large coalesced bubbles which can provide a higher turbulence level in the bed as compared to small bubbles of the bubbly flow regime, observed with relatively large bubbles at low gas flow rates (see section 2.3.2.2.1).

Baker et al. (1978) and Chiu and Ziegler(1983) both reported that the heat transfer coefficient in three-phase fluidized beds is larger than that in two-phase beds. Muroyama et al.(1986) explained this effect by considering that the heat transfer mechanism near the wall region in three-phase fluidized beds may be almost the same as that in liquid-solid fluidized beds with the effect of the acceleration caused by the gas being accounted for by taking into account the effective hydraulic radius defined by $(\epsilon_l + \epsilon_g)\, d_p / (1 - \epsilon_g - \epsilon_l)$, and the interstitial velocity (V_l / ϵ_l).

Chiu and Ziegler (1983) and Muroyama et al. (1981, 1986a,b) studied the effect of gas and liquid velocities on the radial temperature distributions. Muroyama et al. (1986a,b) noted that the radial distribution is parabolic which indicates the existence of considerable thermal resistance in the core of the bed. These authors analyzed the wall-to-bed heat transfer phenomena on the basis of a series thermal resistance model which evaluated the effective radial and axial thermal conductivities in the bed interior and the apparent film coefficient in the near wall region. In the gas-liquid-solid fluidized beds, the variation of effective radial thermal conductivity with gas velocity was found to depend on the flow regime. In the beds of small particles where the coalesced bubble flow prevailed, the effective thermal conductivity of the bed increased significantly with increasing gas velocity. However, in the dispersed bubble flow regime the variation of effective thermal conductivity with gas velocity was small. In both liquid-solid and gas-liquid-solid fluidized beds, the effective radial thermal conductivity increased with increasing liquid velocity, reached a maximum and then decreased with further increase in liquid flowrate.

From these observations, it was concluded that the value of effective thermal conductivity was a measure of the intensity of the radial mixing of the liquid and solid phases which results from the action of large coalesced bubbles. The variation of effective thermal conductivity

with respect to liquid velocity indicated that maximum mixing occurred at a porosity of about 0.7.

The effective thermal conductivity decreased sharply with increasing particle diameter. This observation may be related to a decrease in bed porosity. For specified liquid and gas velocities, the increase in particle size leads to a decrease in bed porosity which reduces the bed mobility and hence the mixing.

The particle to liquid heat transfer in three-phase fluidized beds has been studied by only Grandjean et al. (1987). The results obtained by these authors are, however, inconclusive and further studies are required.

2.3.5.1 Correlations for Heat Transfer

Correlations for wall-to-bed heat transfer in three-phase fluidized beds have been proposed by Baker et al. (1978), Kato et al. (1981), Muroyama et al. (1984) Chiu and Ziegler (1983) and Kang et al. (1985).

Baker et al.(1978), correlated the wall to bed heat transfer with the superficial gas and liquid velocities and particle size :

$$h_3 = 1977\ V_l^{0.070}\ V_g^{0.059}\ d_p^{.106} \quad \text{.....(2.3.55)}$$

This empirical correlation is based on a limited set of

data and also does not account for the liquid phase properties.

Kato et al.(1981), modified their liquid-solid fluidized bed correlation by adding a gas Froude number (Fr_g) term to account for the effect of gas velocity in gas-liquid-solid fluidized beds.

$$Nu' = 0.044(Re''_1Pr)^{0.78} + 2.0\ Fr_g^{0.17} \quad ....(2.3.56)$$

where

$$Nu' = hd_p\ \epsilon_l\ /\ [l_l(1 - \epsilon_l)] \quad .....(2.3.56a)$$

$$Re''_1Pr = d_pV_l\ \rho_l\ C_{pl}/(l_l\ (1- \epsilon_l)) \quad .....(2.3.56b)$$

The applicability of this correlation need to tested over a wider range of operating variables. This correlation requires knowledge of liquid phase holdups for which there are no reliable correlations in three-phase fluidized beds.

Chiu and Ziegler (1983) noted that in both liquid-solid and gas-liquid-solid fluidized beds the relative in increase of heat transfer coefficient is equal to the corresponding relative decrease in liquid hold-up. These authors extended a correlation found in liquid-fluidized beds between the modified Stanton number and the modified Reynolds number (Chiu, 1982) to three-phase fluidized beds.

$$Pr^{2/3}St_{m3} = St_{m2}Pr^{2/3} = C_6Re_{m2}^{-0.305} \quad .....(2.3.57)$$

and

$$h_3 / h_2 = \epsilon_{12} / \epsilon_{13} \quad \text{.....(2.3.57a)}$$

This correlation requires knowledge of liquid phase holdup in both two and three-phase fluidized beds. However, as reviewed in section 2.3.3.3.3, there are no reliable correlations for liquid holdups in three-phase fluidized beds.

Muroyama et al. (1984) reported that the ratio of the wall-to-bed heat transfer in the gas-liquid-solid fluidized beds to that in the liquid-solid fluidized beds with an equivalent liquid velocity was correlated by the following equation:

$$h_3/h_2 = 1.0 + 0.0413(V_g/V_l)^{0.3} \times [(d_p/D_c)(\rho_s - \rho_l)/\rho_l]^{0.61} \quad \text{.....(2.3.58)}$$

Kang et al. (1985) developed a dimensionless correlation based on the combined data of their study and three other studies (Baker et al., 1978; Chiu and Ziegler, 1983; Kato et al., 1981) :

$$[h_3 d_p(1-\epsilon_s)/l_l\epsilon_s] = 0.036\,[C_p\mu_l/l_l]^{0.65}\,[d_p\rho_l(V_g+V_l)/(\mu_l\epsilon_s)]^{0.81} \quad \text{...(2.3.59)}$$

This correlation requires the knowledge of solids holdup in the bed which is not easily estimated.

Muroyama et al.,(1986b) reported that the behavior of

the apparent heat transfer coefficient (h) with respect to liquid velocity in three-phase fluidized beds is quite similar to that in the liquid-solid fluidized beds for the gradual increase with gas velocity. This similarity leads to the assumption that the heat transfer coefficient in three-phase fluidized beds may be correlated by a Colburn type equation in terms of a modified j-factor, j'_H, and a modified Reynolds number ($Re_{l,g}$) as follows:

$$j'_H = C_7 Re_{lg} \qquad \text{.....(2.3.60)}$$

$$Re_{lg} = Re_l \ (\epsilon_g + \epsilon_l) \ / \ \{\epsilon_l \ (1 - \epsilon_g - \epsilon_l)\} \qquad \text{.....(2.3.60a)}$$

The following equation was then given to correlate the whole range of data for three-phase fluidized beds with an error of 25 % on the heat transfer coefficient:

$$j'_H = \{ h_3/\rho_l \ C_{pl} \ V_l)\}\epsilon_l \ Pr^{2/3} = 0.137 Re_{lg}^{-0.271} \ldots \qquad \text{.....(2.3.60b)}$$

Equation 2.3.60a is identical with the correlation for liquid-solid fluidized bed system presented by Muroyama et al.,(1986a), in which case Re_{lg} reduces to Re_l for a gas flow rate equal to zero. These correlations too require knowledge of phase holdups which are not always easily estimated over a wide range of operating conditions.

The correlation proposed by Kang et al. (1985) should

provide reasonable estimates of heat transfer coefficient in three-phase fluidized beds, since it is based on a wide range of operating variables and includes the data obtained both from wall to bed and immersed surface to bed. The estimation of solids holdup, however, remains a potential problem.

2.3.6 Gas-Liquid Mass Transfer in Three-Phase Fluidized Beds

2.3.6.1 Measurement of Volumetric Mass Transfer Coefficient

The volumetric mass transfer coefficient (k_1a) is a measure of the mass transfer rate per unit of reactor volume. The following information is required to obtain k_1a 1) the transferred number of moles of an absorbing/desorbing solute 2) the flow patterns of liquid and gas which provide the local driving force. Usually the concentration change of the sparingly soluble solute in the gas phase is negligible. Therefore any changes in gas flow patterns would not affect the local driving force. In the liquid phase, however, the concentration of the solute can usually vary from zero to near saturation. It is, therefore, important to use a proper flow model for the liquid phase. The two most commonly used flow models are the plug flow and axial dispersion models. The axial and

radial mixing patterns of liquid in three-phase fluidized beds were reviewed in the previous section. Depending on the operating conditions, it may be important to account for the radial mixing in the bed. The general differential equation which accounts for both axial and radial dispersion is given in section 3.2.4 (Equation 3.2.4).

Two techniques have been used for the determination of the volumetric mass transfer coefficient in three-phase fluidized beds: 1) physical absorption (or desorption) of a gaseous solute, and 2) use of absorption with a chemical reaction which is sufficiently fast to maintain the dissolved gas concentration below its equilibrium concentration with respect to the sparging gas stream.

2.3.6.1.1 Physical Absorption

In the physical absorption technique, the column is fed with the gaseous feed and the liquid which are not at equilibrium with one another. The local mass transfer flux (N) in the reactor is given by the Equation 2.1.1.

The following systems have been used most commonly for the measurement of $k_l a$ using physical absorption:
- absorption of carbon dioxide in water (Massimilla et al., 1959; Ostergaard and Suchozebrski, 1969; Dakshinamurty et al., 1974; Lee and Worthington, 1974)
- absorption of oxygen in degassed water (Ostergaard and Fosbol, 1972; Alvarez-Cuenca and Nerenberg, 1981; Catros

et al., 1985; Nguyen-Tien et al., 1985a and b; Sun et al., 1988)

-desorption of dissolved oxygen in nitrogen containing a little CO_2 (simultaneous measurement of the interfacial area by the chemical absorption of CO_2) (Dhanuka and Stepanek, 1980; Chang et al., 1986)

The following limitations of this method should be taken into consideration :

- It is rapidly limited by the precision of the measurements as the equilibrium is approached between the gas and liquids flows.
- In a deep bed there is a risk of absorption at the bottom of the column where the static pressure is high, and of desorption higher up the column as a result of the decrease in the static pressure (Ostergaard, 1978).

However, for beds of moderate heights this method can be used; Alvarez-Cuenca (1979) has shown that for small bed heights the error involved in calculating k_1a by replacing the varying static pressure by a mean value is less than 10%.

2.3.6.1.2 Absorption with Chemical Reaction

The conditions required to determine k_1a by measuring an absorptive flux with a chemical reaction were detailed in section 2.1.5. A chemical system which meets the required conditions without changing the hydrodynamics of

the system need to be found. The following systems have been used in the the literature:

- Air/Sodium sulfite at low catalyst concentrations (Nishikawa et al., 1977)
- Air/Sodium sulfite with no catalyst (Fan et al., 1984; Fujie and Fan, 1986)
- CO_2/Carbonate-Bicarbonate buffer (Ostergaard, 1978)

The use of dissolved salts in these techniques can significantly alter the coalescing behavior of the liquid phase which make the results obtained with these methods less generalizable. Fujie and Fan (1986) however claimed that at low concentrations of sodium sulfite there was a negligible change in the coalescing behavior of the liquid (i.e. the bubble size was not affected).

As reviewed below, the estimation of the volumetric mass transfer coefficient in a three-phase fluidized bed can be subjected to several sources of errors:

In order to obtain representative liquid samples, many researchers have used only a single radial sampling location in the bed . As shown by Catros et al. (1985) and Nguyen-Tien (1985b) however, there exists a radial concentration profile in three-phase fluidized beds. The values of the mass transfer coefficient thus obtained would therefore vary, with the sampling location. Nguyen-Tien (1985b) pointed out that the radial concentration profile could be approximated by a parabolic shape which

allowed them to use a sampling location at r/R =0.7 to obtain an average value of the dissolved concentration at a given horizontal level. This assumes that the actual liquid velocity in the column is independent of the radial position. This, however, needs to be verified.

Most of the researchers have assumed a plug flow model flow models for the evaluation of volumetric mass transfer coefficient in three-phase fluidized beds. While the plug flow model may adequately represent the bed hydrodynamics for beds of large particles, the axial dispersion model would be more representative of the hydrodynamics in the beds of smaller particles (see section 2.3.4.2.3). Nguyen-Tien et al. (1985a), who tested three different flow models namely 1) plug flow model 2) axial dispersion model 3) backflow cell model with their data, reached a similar conclusion.

The effects of radial mixing and variations of actual liquid velocity on volumetric mass transfer coefficient have not been investigated.

2.3.6.2 Effects of System Variables on Volumetric Mass Transfer Coefficient

The volumetric mass transfer coefficient has been found to be strongly influenced by the various operating parameters in three-phase fluidized beds. Following is a

critical review of the observations of different researchers. Although the exact numerical values obtained in certain studies may be questionable due to the selection of an inappropriate flow model, the general trends are believed to hold.

2.3.6.2.1 Effects of Particle Size and Density

For a given solid density the gas-liquid mass transfer in three-phase fluidized beds has been generally found to increase with particle size (Ostergaard and Suchozebrski, 1969; Dakshinamurty et al., 1974; Dhanuka and Stepanek, 1980; Nguyen-Tien et al., 1985a; Chang et al., 1986; Sun et al., 1988).

The volumetric mass transfer coefficient in solid-free bubble columns has been used as the basis to compare the effects of particle size and density in three-phase fluidized beds. For glass beads, a particle diameter larger than 3 mm is required to achieve higher mass transfer rates than in the corresponding solid-free bubble column (Ostergaard and Suchozebrski, 1969; Dhanuka and Stepanek, 1980; Chang et al., 1986). In addition to the particle size, the particle density affected the volumetric mass transfer coefficient in three-phase fluidized beds (Dakshinamurty et al., 1974; Sun et al., 1988). Dakshinamurty et al. (1974) reported that higher mass transfer coefficients were obtained with iron and lead shot particles than with glass beads in the same size

range (2-3 mm) while Sun et al. (1988) reported lower mass transfer rates in beds of low density Ca-alginate particles (ρ_p=$10^3/m^3$).

The effects of particle size and density on volumetric mass transfer coefficient can be related to the different flow regimes observed in three-phase fluidized beds (see section 2.3.2.2.1). The lower mass transfer rate observed in the beds of small and light particles is related to the coalesced bubble flow regime characterized by large bubbles providing a smaller interfacial area for mass transfer. The higher mass transfer rate in the beds of large particles is provided by the smaller bubbles of dispersed bubble flow regime.

2.3.6.2.2 Effects of Gas and Liquid Velocities

All the investigators are in agreement that the volumetric mass transfer coefficient increases with the gas velocity (e.g. Ostergaard and Suchozebrski, 1969; Dakshinamurty et al., 1974; Dhanuka and Stepanek, 1980; Nguyen-Tien et al., 1985; Chang et al., 1986; Sun et al., 1988).

The effect of liquid velocity on the volumetric mass transfer coefficient has been found to be small when compared to the effects of particle size and gas velocity (Dakshinamurty et al., 1974; Dhanuka and Stepanek, 1980; Nguyen-Tien et al., 1985; Chang et al., 1986). Chang et al.(1986) compared the data of various researchers and

concluded that in beds of smaller particles (d_p<1 mm) the mass transfer coefficient increased slightly with the liquid velocity while in the beds of larger particles it passed through a maximum value. These authors argued that since the interfacial area also followed the same trends, the increase in liquid velocity in the lower range of liquid velocities helped promote bed turbulence resulting in bubble breakup. For higher range of liquid velocities, an increase in liquid velocity gave rise to higher bubble rise velocity which resulted in the decrease of gas holdup and interfacial area.

2.3.6.2.3 Effects of Column Diameter

Nguyen-Tien et al. (1985b) compared the volumetric mass transfer coefficients obtained in the columns of 0.14 and 0.3 m diameters. It was concluded that there was no effect of column diameter on $k_l a$. These observations, however need to be tested in the beds of smaller diameter columns where wall effects may be more predominant.

2.3.6.2.4 Effects of Liquid Physical Properties

The effects of liquid viscosity on the volumetric mass transfer coefficient have been investigated only by Patwari et al. (1986). The mass transfer coefficient decreased significantly with increasing viscosity in both the Newtonian glycerol solution and the pseudoplastic carboxymethyl cellulose solutions in beds of different

particle sizes. It was also observed that there was no correlation between mass transfer coefficient and gas holdup for these high viscosity solutions. The decrease in $k_l a$ values could, therefore be related to lower k_l values in high viscosity solutions.

No systematic study has been conducted to determine the effects of surface tension and density of the liquid and density and molecular diffusivity of the gas on the volumetric mass transfer coefficient.

2.3.6.2.5 Effects of Liquid Coalescing Properties

Higher volumetric mass transfer coefficients were obtained in noncoalescing liquids than in coalescing liquids (Chang et al., 1986; Sun et al., 1988). Chang et al. (1986), who used sodium chloride solutions as noncoalescing liquids reported an increase in $k_l a$ values with increasing ionic strength. The rate of increase was, however, higher in the beds of larger particles which promote bubble breakup. The smaller coalescence inhibition effect in the beds of smaller particles was attributed to the higher inertia of the larger bubbles which dominated the coalescence inhibition effects of the salt.

2.3.6.3 Correlations for Volumetric Mass Transfer Coefficient in Three-Phase Fluidized Bed

The correlations for mass transfer coefficient proposed by different researchers are listed in Table

2.3.4. Most of the researchers have assumed a plug flow model for the evaluation of volumetric mass transfer coefficient. As pointed out in section 2.3.4.2.3 this assumption cannot be justified in the beds of smaller particles. Nguyen-Tien et al. (1985a) developed a correlation using a proper hydrodynamic model to estimate the k_la values in the beds of smaller particles (d_p<1 mm). This correlation, however, does not account for the effects of particle density and liquid phase properties (except possibly through its use of solids holdup). Moreover, as pointed by Fan et al. (1986), the bed operated in the transport regime for these small size particles, which exhibits significant deviations compared to the expanded bed regime of large particles. For the beds of larger particles, the correlation proposed by Dakshinamurty et al. (1974, 1976) should give reasonable estimates of k_la values since it is based on a larger range of operating conditions. The applicability of this correlation has yet to be proved for the data obtained from other studies.

Further efforts are required to obtain a generalized expression for mass transfer coefficient to account for properties of solid particles and the liquid phase.

Table 2.3.4 Literature Correlations for Volumetric Mass Transfer Coefficient in Three-Phase Fluidized Beds

Correlations	Range of Variables	Investigators	Remarks
$\frac{k_l a d_p^2}{D_A} = k''\left(\frac{d_p V_t \rho_l}{\mu_l}\right)^{3.3}\left(\frac{\mu_l V_g}{\sigma}\right)^{.7}$ $k'' = 3.946 \times 10^{-7}$ for $Re_t > 2000$ $k'' = 2.3 \times 10^{-5}$ for $Re_t < 2000$	V_g = 0 to 0.1 m/s V_l = 0.05 to 0.17 m/s d_p = 1.0 to 6.84 mm ρ_s = 2400 to 11180 kg/m3	Dakshinamurty et al. (1976)	Correlation based on wide range variables. Plug flow model assumed for all particle sizes. Single probe location.
1.1 mm particles $k_l a = 4.7\ V_g^{0.76}$ 3.0 mm particles $k_l a = 7.0\ V_l V_g^{0.25}$ 6.0 mm particles $k_l a = 21.1\ V_g^{0.93}$ V_g, V_l in cm/s	V_g = 0.04 to 0.127 m/s V_l = 0.015 to 0.073 m/s d_p = 1.1, 3.0, 6.0 mm	Ostergaard (1978)	Effects of liquid phase properties are not accounted for.
$\frac{k_l a d_{pe}^2}{D_A \epsilon_g} = 1.4 \times 10^4\ Re_l^{.38}\ Re_g^{-.2}\ Sc_l^{0.5}(d_p/D_c)^{2.1}$	V_g =0.0003 to 0.012 m/s V_l =0.064 to 0.18 m/s d_p = 6.0 mm	Fukushima (1979)	Correlation based on limited data. Only single particle size used.
1.98 mm particles $k_l a = 3.23 \times 10^{-3}\ V_g^{10} V_l^{0.55}$ 4.08 mm particles $k_l a = 3.41 \times 10^{-2}\ V_g^{0.555}$ 5.86 mm particles $k_l a = 2.52 \times 10^{-2}\ V_g$	V_g = 0.02 to 0.08 m/s V_l = 0.061 to 0.138 m/s d_p = 1.98, 4.08, 5.86 mm glass beads	Dhanuka and Stepanek (1980)	Purely empirical correlations. Plug flow model assumed in beds of all particles.

Table 2.3.4

Correlations	Range of Variables	Investigators	Remarks
$k_l a = 0.39 \left(1 - \frac{\epsilon_s}{0.058}\right) V_g^{0.67}$	V_g =0.018 to 0.16 m/s d_p = 0.05 to 1.0 mm	Nguyen-Tien et al. (1985)	Applies to small particles only (< 1 mm). Effects of liquid phase properties not accounted for.
$k_l a = 956.6\ V_g^{0.37}\ V_l^{0.7}\ d_p$	V_g = 0.075 to 0.13 m/s V_l =0.0024 to 0.018 m/s d_p = 3.0 4.0 mm glass beads	Tosyali and Uysal (1985)	Only two particle sizes used. Assumed plug flow model.
$k_l a = 98.7\ V_g^{0.68} V_l^{0.63} d_p^{1.21}$	V_g = 0.005 to 0.07 m/s V_l = 0.0054 to 0.13 m/s d_p = 1.7, 4.0, 6.0 mm glass beads	Chang et al. (1986)	Effects of liquid phase properties not included.

2.3.6.4 The Mass Transfer Coefficient and Interfacial Area

In order to determine the mass transfer coefficient (k_l), it is necessary to obtain $k_l a$ and a simultaneously or under very similar conditions.

2.3.6.4.1 Chemical Absorption Method

Ostergaard (1978) used a technique based on CO_2 absorption. This technique provides only the interfacial area. The values of k_l were obtained from the volumetric mass transfer coefficients obtained by another technique. Since the volumetric mass transfer coefficient and the interfacial area are obtained in liquids of different compositions there can be a large error in k_l values if their coalescing behavior are very different.

2.3.6.4.2 Chemical Absorption coupled with a Physical Desorption

This technique is based on the method of Robinson and Wilke (1974). It involves simultaneous chemical absorption of carbon dioxide and desorption of oxygen (see section 2.2.6.1.1 for details). This technique allows evaluation of k_l and a under same hydrodynamic conditions.

In three-phase fluidized beds this technique was used by Dhanuka and Stepanek (1980), Tosyall and Uysal (1986) and Chang et al. (1986). The chemical system used by

Dhanuka and Stepanek (1980) and Chang et al. (1986) was sodium carbonate/bicarbonate solution with a buffer ratio of one, while Tosyali and Uysal (1986) used a 0.2 M NaOH solution for their measurements. The gas phase was a mixture of CO_2 and N_2 in both the studies.

The use of dissolved salts in this technique can significantly alter the coalescing behavior of the liquid which means the results obtained with this technique are not generalizable.

2.3.6.4.3 Effects of System Variables on a and k_l

Like the volumetric mass transfer coefficient the interfacial area has been found to increase with the bed particle size (Ostergaard, 1978; Dhanuka and Stepanek, 1980; Chang et al., 1986). The higher interfacial area in the beds of larger particles is a consequence of increased bubble breakup caused by the particles.

All the researchers have reported an increase in interfacial area with increasing gas velocity, irrespective of the bed particle size. These observations can be related to increases in gas holdup with increasing gas velocity.

The effects of liquid velocity on interfacial area are reported to be small and generally follow the trends observed with $k_l a$ (see section 2.3.6.2.2).

Only a few researchers have investigated the effects

of different operating variables on k_l (Ostergaard, 1978; Dhanuka and Stepanek, 1980; Chang et al., 1986). The liquid side mass transfer coefficient is reported to increase slightly with gas velocity in the beds of particles smaller than 2 mm (Dhanuka and Stepanek, 1980; Chang et al., 1986), while in the beds of larger particles, there is practically no effect of gas and liquid velocity on k_l (Chang et al., 1986).

The increase in k_l values in the bed of smaller particles can be related to the formation of larger coalesced bubbles. The large bubbles have a free motion of gas-liquid interface as compared to the rigid surface of smaller bubbles.

2.3.7 Liquid-Solid Mass Transfer

The local mass transfer flux (N) across the effective film surrounding a solid particle is given as:

$$N_s = k_s(C_s^* - C_s) \qquad \text{.....(2.3.61)}$$

Here k_s is the liquid-solid mass transfer coefficient and A is the interfacial area for mass transfer.

In order to account for the hydrodynamic effects (i.e. liquid mixing patterns) on the local driving force a suitable flow model must be used to obtain a true value of the mass transfer coefficient.

2.3.7.1 Measurement Techniques for Liquid-Solid Mass Transfer

The following methods have been used to measure the liquid-solid mass transfer coefficient in fluidized beds.

2.3.7.1.1 Dissolution of Sparingly Soluble Solids

This is the most commonly used technique for the measurement of liquid-solid mass transfer in two or three-phase systems. As shown in Table 2.3.5, a number of researchers have used this technique in two-phase systems. In three-phase systems, this technique l been used by Kirillov and Nasamanyan (1976), Prakash et al. (1984) and Arters and Fan (1986).

This technique is based on the measurement of the rate of dissolution of one or a few solid particles in a bed of inert solids (Prakash et al., 1984,1987) or the dissolution rate of a whole bed of soluble particles (Ballesteros et al., 1982; Arters and Fan, 1986).

The mass transfer rate can be calculated from the weight loss of the soluble solid particles during the course of the experiment (see section 3.2.5). The dissolution rate can also be measured by analyzing the liquid exit concentration using a spectrophotometer (Gato et al., 1975a; Specchia et al., 1978; Goto and Smith, 1975b; Arters, 1986) or by titration with sodium hydroxide Satterfield et al. (1978) and Shen et al. (1985). Another

Table 2.3.5 Techniques used for Liquid-Solid Mass Transfer Measurement

Technique	Rcmarks	References
Solids Dissolution	Solids surface can get roughned during experiments. Liquid phase dispersion can affect the results Time consuming	Two-phase beds: McCune and Wilhelm(1949); Evans and Gerald(1953); Fan et al.(1960); Rowe and Claxton(1965); Couderc et al.(1972); Upadhyay and Tripathi(1975); Laguerie and Angeln(1975); Vandrougwan et al.(1976); Tournie et al.(1977);Ballesteros et al.(1982); Shen et al.(1985) Three-Phase beds: Kirillov and Nasamanyan(1976); Prakash et al.(1984); Arters and Fan(1986)
Electrochemical Technique	Both instantaneous and average measurements possible. Deposits on electrode surface can interfer with measurements Effects of coalescing behavior cnnot studied due to presence of dissolved salts.	Fixed beds: Mochizuki and Matsui(1974); Colquhoun-Lee and Stepanek (1978); Delauney et al.(1980) Fluidized beds: Riba et al.(1978); Hassannien et al.(1984); Nikov and Delmas (1987); Fukuma et al.(1988); Burru(1988)
Ion Exchange method	Measurement depends on liquid mixing patterns	Koloni et al.(1977); Sanger and Deckwer(1981); Sano et al.(1974); Kikuchi et al. (1984)
Photographic Technique	Distortions caused by curvature of cylinderical columns can affect measurements.	Garner and Suckling(1958)

method of measuring the dissolution rate is by adding fluorescent dye to the dissolving solid and then measuring the dissolution rate by using a fluorometer (Lemay et al., 1975; Dudukovic, 1985). The solubility of the dye is much greater than that of the dissolving solid but the rate of release of the dye into the solution is controlled by the rate of the dissolution of the solid. Thus the actual steady state concentration of the dye measured by the fluorometer is converted to the corresponding dissolving solid concentration in the effluent water stream.

The solid dissolution technique for the study of liquid-solid mass transfer is relatively cheap, fairly accurate and simple to operate. But the preparation of test particles can be time-consuming and difficult. When using this technique care should be taken to minimize changes in particle size and the concentration built-up of solute in the bulk liquid. The use of a whole bed of benzoic acid particles (Arters and Fan, 1986) would result in large concentration levels of dissolved benzoic acid in the liquid and thus could significantly alter the bed hydrodynamics (dissolved benzoic acid acts as a bubble coalescence inhibitor). Also, the effects of liquid backmixing on the local driving force need to be taken into account by the use of a proper flow model. In addition the concentration measurements by methods such as titration may not be accurate due to the relatively low concentration of dissolved solute. The direct measurement

of the weight loss of only a few soluble particles is therefore more accurate. The other limitations of this technique are that the solid surface tends to get roughened during the course of the experiment which could lead to erroneous results. Also, no instantaneous measurement is possible with this technique.

2.3.7.1.2 Electrochemical Technique

The electrochemical technique is the other frequently applied method of measurement for liquid-solid mass transfer (see Table 2.3.5). This technique utilizes the principle of limiting current when the mass transfer to the electrode surface is diffusion-controlled. Selman and Tobias (1978) have presented a comprehensive review of the limiting current technique. Most of the studies which used this technique involved the redox reaction between potassium ferrocyanide and potassium ferricyanide. Particle-liquid mass transfer was thus studied in fixed beds (Mochizuki and Matsui, 1974; Colquhoun-Lee and Stepanek, 1978; Delauney et al., 1980) and in fluidized beds (Riba et al., 1978; Hassanien et al., 1984; Nikov and Delmas, 1987; Fukuma et al., 1988). King and Smith (1967) used this technique to measure the mass transfer coefficient between a wall and a liquid fluidized bed. Lin et al. (1951) and Reiss and Harnatty (1963) thus studied mass transfer in annular and open pipes respectively.

The electrochemical technique allows rapid and straightforward evaluation of the instantaneous mass flux on the particle (i.e. the measured current being proportional to the mass transfer rate), and avoids any changes in surface roughness or the particle size during the experiments. However, since the particle needs to be tethered, there can be interferences with the local bed hydrodynamics. In addition, the following problems need to be solved for accurate measurements of mass transfer, using this technique. The ferro and ferri-cyanide compounds used with the most commonly used electrochemical system decompose in the presence of light resulting in the formation of hydrogen cyanide and hydroxyl ions (Berger and Ziai, 1983):

$$Fe(CN)_6^{4-} \xrightarrow{\text{light}} [Fe(CN)_5]^{3-} + CN^- \quad ....(2.3.62)$$

$$CN^- + H_2O \xrightarrow{\text{light}} HCN + OH^- \quad .....(2.3.63)$$

Cyanide ions are thus generated and they poison the nickel and platinum electrodes which are commonly employed in ferrocyanide reduction. This necessitates a non-transparent column (apparatus) or dark light, which will exclude visual observation.

In the presence of oxygen, the ferrocyanide can be oxidized resulting in the formation of an oxide film on the electrode, which will reduce the effective area of the the electrode. Pure nitrogen is often used as a fluidizing gas instead of air but it is expensive and

makes the system unsuitable for large columns. Sutey and Knudsen (1967), however, reported that if the test solution was first saturated with nitrogen, further exposure to air for a short time did not greatly affect the mass transfer results. They noted that under certain flow conditions the technique could be applied with up to 70 % oxygen saturation (saturation with air) within an operating time of 275 min. with a maximum error of 5%. A large amount of nitrogen would still be required to saturate the solution with nitrogen and 99% saturation with oxygen would be reached in less than one minute in a three-phase bed fluidized by air.

An other electrochemical reaction is the reduction of dissolved oxygen in a supporting electrolyte solution. Goren and Mani (1968) used it to study the film thickness, the, the amplitude and frequency of the waves in a liquid film in a wavy motion. Tengjyh-Tong (1978) used the same reaction to study mass transfer in a pipe. He used a 4 wt% sodium chloride solution instead of an alkaline solution as a supporting electrolyte. Sedahmed (1986) also measured the rate of mass transfer at a cathode consisting of a fixed single layer of spheres stirred by oxygen evolved at a horizontal disc anode placed below. Economou et al. (1985) also applied the limiting current method to study the mass transfer to a solid electrode in cocurrent gas liquid flow through a vertical parallel plate. They used both the ferro / ferri cyanide and oxygen

reduction systems in a solution of 0.2 M potassium hydroxide (KOH). Recently Burru (1988) used the oxygen reduction method to study particle-liquid mass transfer in two-phase and three-phase fluidized beds. The supporting electrolyte solution was 5 wt.% sodium chloride solution.

Morooka et al. (1980) determined the mass transfer coefficient by measuring the limiting current for another reaction: reduction of copper.

Although the limiting current technique provides an elegant method to measure both instantaneous and average values of liquid-solid mass transfer coefficient without affecting the size and surface roughness of the particles, it suffers from following drawbacks. The use of electrolyte solutions precludes investigations of the effect of changes in liquid coalescing behavior on mass transfer. If there are any metal parts in the bed, the use of a salt or alkaline solution may also create corrosion problems and formation of oxide ions which would interfere with the measurements. Extra precautions are also required to ensure that the electrode surface remain free of any deposits. Dawson and Trass (1972) observed errors of up to 15% in the limiting current when two different methods of cleaning the electrode surface were used. Moreover, in order to ensure that tethering the particle did not affect the results experiments with another technique need to be conducted. For example, Burru (1988) had to use free-floating particles technique developed for the

present study (see section 3.2.5.1) to check the validity of his results.

2.3.7.1.3 Ion Exchange Method

The ion exchange technique for the measurement of liquid-solid mass transfer was used by Sano et al. (1974), Koloni et al.(1977), Saenger and Deckwer (1981), Kikuchi et al. (1984), and Marrone and Kirwan (1986). The technique is easy, and does not suffer from problems of changing shape and surface area of particles, except if swelling occurs. The bed can be regenerated over and over again by contacting it with a regenerating solution. This technique requires deionized water, which could be very expensive when used in large columns. Because of the large changes in solute concentration between the bottom and top of the bed, it is also dependent on liquid mixing patterns which would affect the local driving force. The ion exchange resin beads might swell or contract as the pH changes, requiring continuous monitoring of the pH necessary.

2.3.7.1.4 Other Methods

Snider and Perona (1974) and Morita and Smith (1978) both applied the hydrogenation of methyl styrene on a palladium catalyst to study the rate of liquid solid mass transfer. While Snider and Perona (1974) analyzed the α-methyl styrene and cumene in the feed by measuring the

refractive index by using a dipping refractometer, Morita and Smith (1978) determined the concentration of cumene used a chromatographic technique.

-Photographic technique: the change in diameter of a spherical soluble particle is detected by photographing it before and after dissolution (Garner and Suckling, 1958).

-Other measurement methods for liquid solid mass transfer include crystallization (Garside and Mulin, 1968; Laguerie and Angelino, 1975) and adsorption (Gahno, 1975; Tan and Smith, 1982).

2.3.7.2 Review of Literature Results obtained in Liquid-Solid Fluidized Beds

Liquid-solid mass transfer in two-phase fluidized beds has been widely studied. Most of the studies have been performed using the dissolution of benzoic acid and other solutes (Table 2.3.5).

The particle-liquid mass transfer coefficient was found to be practically independent of the superficial liquid velocity and the particle size by most authors (McCune and Wilhelm, 1949; Rowe and Claxton, 1965; Damronglerd et al., 1975; Upadhyay and Tripathi, 1975; Tournie et al., 1979; Ballesteros et al., 1982). Shen et al. (1985), however, reported an increase in mass transfer coefficient with liquid velocity. This deviation could be the result of channeling effects at the low liquid velocities used by these authors. Tournie et al.

(1979) and Ballesteros et al. (1982) found that the mass transfer was independent of particle shape. Ballesteros et al. (1982) studied the effect of particle shape using benzoic acid particles of different shapes. It was observed that for isometric particles (with equal height and diameter) the invariance of shape was perfect i.e. the ratio of height to the diameter remained almost constant during dissolution while there was some limited variation of the size ratios for non-isometric particles. Tournie et al. (1979) also pointed out that the liquid-solid mass transfer coefficient in liquid-solid fluidized beds is dependent mainly on the physico-chemical properties of the system. Burru (1988) observed that the particle-liquid mass transfer coefficient decreased with increasing liquid viscosity in non-newtonian solutions of carboxymethylcellulose and polyacrylamide.

Riba et al. (1978) observed that the local mass transfer coefficient was within 2% at different radial and axial positions in the bed. Kikuchi et al. (1984) used only a few active particles in a bed of inert particles to minimize the effects of liquid backmixing on the measurements. These authors demonstrated that the use of the plug flow model was not justified when a whole bed of active particles was used.

Liquid-solid mass transfer at the wall of liquid-solid fluidized beds has also been investigated (Jagannadharaju and Rao, 1965; King and Smith, 1967;

Morooka et al., 1980; Bohm, 1983; Tucker and Wragg, 1986). Tucker and Wragg (1986) pointed oud that the liquid-solid mass transfer rates in the fluidized beds were considerably enhanced over those for liquid flow alone. Morooka et al. (1980) observed that the mass transfer coefficient increased with increasing particle size. For the same size particles the mass transfer coefficient passed through a maximum value when plotted against liquid holdup (King and Smith, 1980 and Morooka et al.,1980; Tucker and Wragg, 1986).

2.3.7.3 Correlations for Particle-Liquid Mass Transfer in Liquid-Solid Fluidized Beds

A number of correlations have been proposed in the literature for liquid-solid mass transfer. In most of the cases, the particle-liquid mass transfer has been correlated in terms of dimensionless groups. The correlations usually express the Sherwood number (Sh) as a function of the Schmidt number (Sc) and the bed porosity (ϵ).

Table 2.3.6 shows some of the correlations. It can be seen that the bed porosity does not appear explicitly in all the correlations. Dwivedi and Upadhyay (1977) presented three different definitions of the Reynolds number as used by various researchers. In addition to the regular particle Reynolds number (Re_1), a modified Reynolds number (Re'_1) has also been used, it takes into

account the relative velocity between the solid particles and the liquid, the interstitial velocity, (usually the superficial liquid velocity divided by the liquid holdup). But Dwivedi and Upadhyay (1977) also indicate that, both fixed bed and fluidized bed data were successfully correlated with the Reynolds number ($Re"_l$) which uses $(1 - \epsilon)$ instead of the usual ϵ in the correlation. The use of porosity in these correlations indirectly takes into account the effects on mass transfer of liquid distribution, column size, bed height and particle shape and size. The bed porosity , however, needs to be measured or evaluated with another correlation. The other commonly used form of equation for liquid-solid mass transfer replaces the bed porosity by the Galileo number (Ga) and/or the density number (Mv). The general form of these correlations is:

$$Sh = f(Re,Ga,Mv,Sc) \qquad \ldots\ldots(2.3.64)$$

Some of the correlation developed by different researchers, based on the above form are also shown in Table 2.3.6. Tournie et al. (1979) concluded that the Sherwood number was practically independent of the Reynolds number which made the mass transfer coefficient independent of the liquid velocity. The correlation proposed by Dwivedi and Upadhyay (1977) is based on the data of a large number of researchers and hence covers a wide range of Reynolds number. The particle shape factor

has been taken into account only in the correlation proposed by Ballasteros et al. (1982).

Table 2.3.6 Correlations of Particle-Liquid Mass Transfer in Two-Phase Systems

Reference	Correlation
Evans & Gerald (1953)	$J_d(1-\epsilon)\, d_p^2 = 1.66 \times 10^{-3}\ Re"_l^{1.33}$ and $J_d(1-\epsilon) / f = Sh/Sc^{1/3}\ 2Re/Ga\ Mv$
Chu et al. (1953)	$J_d = 5.7\ Re"_l^{-0.78}$ for $1 < Re"_l < 30$ and $J_D = 1.77 Re"_l^{-0.44}$ for $0.01 < Re"_l < 100$
Fan et al. (1960)	$Sh = 2 + 0.46\ Re'_l{}^{0.543}\ Sc^{1/3}$ $Sh = 2 + 1.51\ (1-\epsilon)\ Re'_l{}^{1/2}\ Sc^{1/3}$
Rowe & Calxton (1965)	$Sh = 2/(1-\epsilon)^{1/3} + 0.7/e\ Re^n\ Sc^{1/3}$ with $(2-3n)/(3n-1) = 4.56\ Re^{-0.28}$
Garside & Mulin (1968)	$Sh = 0.37\ Re_l^{0.62}\ Sc^{0.33}$
Couderc et al. (1972)	$Sh = 5.4 \times 10^{-2} / \epsilon\ Sc^{1/3}$
Ganho et al. (1974)	$J_d = 2.55\ Re"_l^{-0.537}$
Upadhyay & Tripathi (1975)	$J_d = 3.8155\ Re"_l^{-0.7313}$ for $Re"_l < 20$ $J_d = 1.86\ Re"_l^{-0.451}$ for $Re"_l > 20$
Damronglerd et al. (1975)	$Sh = 0.01\ Re_l^{0.305}\ Sc^{1/3}$ for $\epsilon < 0.815$ $Sh = 0.138\ Re_l^{-0.086}\ Ga^{0.412}\ Sc^{1/3}$ for $\epsilon > 0.815$

Table 2.3.6 Cont,d

Laguerie & Angelino (1975)	$Sh = 0.124\ Re_l^{0.18}\ Ga^{0.31}$ or $\epsilon^{-1.8}\ Sh = 0.36\ Re_l^{0.5}\ Sc^{1/3}$
Vanadurongwan et al. (1976)	$Sh = 0.215\ Re_l^{0.011}\ Ga^{0.309}\ Sc^{0.436} Mv^{0.303}$ for $\epsilon < .81$ $Sh = 0.125\ Re_l^{-0.076}\ Ga^{0.390}\ Sc^{0.436}\ Mv^{0.33}$ for $\epsilon > 0.815$
Dwivedi & Upadhyay (1977)	$\epsilon J_d = (0.765 / Re_l^{0.82}) + 0.365 / Re^{0.386}$ for $0.01 < Re_l < 1500$
Riba et al. (1978)	$Sh = 0.264\ Re_l^{-.011}\ Ga^{0.36}\ Sc^{0.33}$
Tournie et al. (1979)	$Sh = 0.253\ Re_l^{0.004}\ Ga^{0.319}\ Mv^{0.299}\ Sc^{0.400}$ or $Sh = 0.245\ Ga^{0.323}\ Mv^{0.300}\ Sc^{0.400}$
Rahman and Streat (1981)	$J_d\epsilon = 0.86 Re_l^{-0.5}$ $2 < Re_l < 25$
Ballesteros et al. (1982)	$Sh = 0.245\Phi^{1.35} Ga^{0.323}\ Mv^{0.3}\ Sc^{0.4}$ valid in the range factor value $0.7 < \Phi < 1$
Shen et al. (1985)	$J_d = 0.506\ Re"_l^{-0.453}\ \epsilon^{-1.416}$ $0.644 < Re"_l < 7.3$

The various literature correlations for wall to bed mass transfer have been reviewed by Tucker and Wragg (1986). These correlations usually express the mass transfer J-factor as a function of Re_l" and ϵ.

2.3.7.4 Liquid-solid mass transfer in three-phase fluidized beds

Compared to two phase fluidized beds, liquid-solid mass transfer in three-phase fluidized beds has been studied by only a limited number of researchers so far (Hassannien et al.,1984; Arters and Fan, 1986, 1987; Prakash et al., 1984, 1987; Fan et al.,1987; Nikov and Delmas, 1987; Ermakova et al., 1988; Burru et al., 1988; Fukuma et al., 1988).

2.3.7.4.1 Effects of liquid velocity.

As was observed in two-phase liquid-solid fluidized beds (please see section 2.3.7.2), the liquid-solid mass transfer in three-phase fluidized beds too is practically independent of liquid velocity (Hassannien et al., 1984; Nikov and Delmas, 1987; Arters and Fan, 1986; Fukuma et al., 1988).

2.3.7.4.2 Effects of the gas velocity

The mass transfer coefficient for particle-liquid mass transfer in three-phase fluidized beds increases with the superficial gas velocity (Hassannien et al, 1984; Arters and Fan, 1986 and Prakash et al., 1984; Nikov and Delmas, 1987; Ermakova et al., 1988; Fukuma et al., 1988). Arters and Fan (1986) reported that introduction of gas into a liquid-solid fluidized bed resulted in a large

increase in the mass transfer coefficient, at almost all liquid flowrates. They observed an increase of up to 150 % for their highest gas velocity (0.26 m/s). Prakash et al. (1984), however, reported that the gas introduction resulted in a maximum increase of only 30 % in the mass transfer coefficient. The large differences in the results of these two studies could be attributed to differences in bed hydrodynamics resulting from different liquid coalescing behavior. The mass tranfer mechanisms may also be different with the lighter particles used by Arters and Fan (1986).

Ermakova et al. (1988) used the electrochemical technique to investigate the local instantaneous mass transfer rate from a particle to a liquid in three-phase fixed and fluidized beds. It was observed that both the average value and the standard deviation of the mass transfer coefficient increased with increasing gas velocity. The standard deviation was found to be 13 to 21 % of the average value. The fluctuations in the mass transfer coefficient were less intense (3-5%) in the absence of gas.

2.3.7.4.3 Effects of particle size and density

Hassanien et al.(1984) studied the effects of particle diameter (ranging from 5 to 10 mm) and reported that the particle size has almost no influence on the mass transfer coefficient which was in agreement with

observations in the two-phase systems (Section 2.3.7.2). They also noted that the mass transfer rate from a fixed particle was nearly the same as the mass transfer rate from a mobile particle which could move freely as the rest of the bed particles. Arters and Fan (1986) reported that at zero or low gas velocities (< 0.066 m/s) the mass transfer coefficient was independent of the particle size, while at higher gas velocities (> 0.066 m/s), it was dependent on the particle size.

Nikov and Delmas (1987) used particles with densities ranging from 1.34 to 8.15 X10^3 kg/m^3. The rate of increase of the mass transfer coefficient with the gas velocity was large for light particles near the minimum fluidization velocity, but became smaller with increasing solid densities and liquid velocities. Hassannien et al. (1984) and Arters and Fan (1986) confirmed these results.

2.3.7.4.4 Effects of Gas Distribution

The effects of gas distribution on liquid-solid mass transfer rate was investigated by Prakash et al., 1987 and Burru (1988). Prakash et al. (1987) reported an increase in mass transfer rate when the gas distribution was improved. Burru (1988), however, observed that a worse distributor gave slightly higher mass transfer coefficients. This discrepancy could be explained by the non-uniformities in bed structure which can result from poor liquid distribution.

2.3.7.4.5 Effects of Radial Position

Fukuma et al. (1988) measured the variation of particle-liquid mass transfer with radial position in a three-phase fluidized bed. It was observed that the variation of mass transfer coefficient was generally small except in the region near the wall where it was 20% lower than in the core region at high gas velocities.

These results could be related to lower local liquid velocities close to the wall region as reported by Morooka et al. (1985).

The particle-liquid mass transfer in batch slurry bubble columns has been investigated by Kabayashi and Saito (1965), Sano et al. (1974) and Sänger and Deckwer (1981). The mass transfer rate was found to increase with increasing gas flowrate. Sano et al. (1974) studied the effect of particle shape, using spherical ion exchange beads and granular particles of benzoic acid, $KMnO_4$ and β-naphthol. They included a shape factor in their correlations to account for the effect of particle shape on liquid-solid mass transfer.

The liquid-solid mass transfer from the wall of a gas-liquid-solid fluidized bed was studied by Morooka et al. (1980). They noted that when gas was introduced into a liquid fluidized bed, the mass transfer rate increased for beds of 0.42 and 1.0 mm particles while it decreased

slightly in the bed of 2.12 mm particles.

The effects of gas and liquid distributions and liquid coalescing properties on particle-liquid mass transfer in gas-liquid-solid fluidized beds have not been investigated systematically.

2.3.7.5 Correlations for Particle-Liquid Mass Transfer in Three-Phase Fluidized Beds

The correlations for particle-liquid mass transfer in three-phase fluidized beds have generally been developed by including the data from liquid-solid fluidized beds (Arters and Fan, 1986; Nikov and Delmas, 1987; Ermakov et al., 1988).

Hassanien et al. (1984) were the first to propose a correlation for liquid-solid mass transfer in three-phase fluidized beds. These authors used particles of two different densities. The exponents for the proposed correlations depended on the particle density. Correlation for glass beads (ρ_p=2524 kg/m^3):

$$Sh = 0.264\ Fr_g^{0.056}\ Ga^{0.41}\ Re^{-0.51}\ Sc^{0.34} \quad ...(2.3.65)$$

Correlation for plastic beads (ρ_p=1350 kg/m^3):

$$Sh = 0.151 Fr_g^{0.11}\ Ga^{0.44}\ Re^{-0.11}\ Sc^{0.34} \quad ...(2.3.66)$$

These correlations show that the effect of the physico-chemical properties of the liquid, as characterized by the Schmidt number, is essentially the same in three-phase and two-phase fluidized beds. The correlations proposed by Hassanien et al. are not general specially with respect to the effect of particle density. Moreover these correlations cannot be applied to the limiting case of liquid-solid fluidization since the predicted value of mass transfer coefficient will be zero for a zero gas velocity.

Nikov and Delmas (1987), using the same electrochemical technique, extended the work of Hassanien et al. (1984) to include a wider range of particle densities and diameters. They recommended the following correlation based on their experimental results and those of Hassanien et al. (1984):

$$Sh = 0.33(Ga\ Mv\ Sc)^{1/3}\ [1+0.22Mv^{-0.57}\ (V_g/V_l)^{0.77}] \quad \ldots\ldots(2.3.67)$$

The mean deviation between their experimental values and the predictions from the correlation was found to be 5.7 %. This correlation is also applicable to liquid-solid fluidized beds. The applicability of this correlation, however, need to be tested with liquids of different coalescing properties.

Arters and Fan (1986) proposed a generalized correlation for both two and three-phase fluidized beds.

They used the correlation developed by Ballesteros et al. (1982) for two-phase fluidized beds by modifying it by a "gas effect" term which represents the gas Reynolds number:

$$Sh = (1 + \alpha Q^{\beta})\ Sh_2 \quad \text{.....(2.3.68)}$$

where

$$Sh_2 = 0.245\ \phi_s^{1.35}\ Ga^{0.323}\ MV^{0.300}\ Sc^{0.400} \quad \text{....(2.3.68a)}$$

and

$$Sh = 0.228\ (1 + 0.0828\ Re_g^{0.623})\phi_s^{1.35}\ Ga^{0.323}\ Mv^{0.300}\ Sc^{0.4} \quad \text{.....(2.3.68b)}$$

According to the authors this correlation predicted the experimental data with a standard deviation of 7.5%. This purely empirical correlation is based on the data obtained with light particles and a limited range of liquid properties. Its applicability in the beds of denser particles need to tested.

Arters and Fan (1987) also presented another correlation combining a term representing the effects of gas and liquid velocities as well as particle and fluid properties, with the equation proposed by Calderbank (1967) for liquid-solid fluidized beds :

$$Sh = 0.31 \phi_{ss}^{0.6} Ar^{1/3} Sc^{1/3} \left[1 + \frac{32 (Re_g Fr_g)^{0.28}}{410 + (Re_g Fr_g)^{0.28}} Mv^{-1.0} \right] \quad \text{.....(2.3.69)}$$

The correlation is valid over the ranges :

$$6.4 < Re_l < 2500$$

$$0 < Re_g < 120$$

$$0.0 < Fr_g < 2.4$$

$$8500 < Ar < 23.4 \times 10^6$$

$$1.3 < Mv < 2.5$$

$$0.87 < \phi_s < 1$$

This correlation can be used for both two and three-phase fluidized beds. As pointed out by the authors, this correlation is not applicable to either dense particles or particles smaller than 1.0 mm in diameter, and systems with different coalescing properties.

Ermakova et al. (1988) developed a dimensionless correlation of the form Sh = f(Re,Sc), which is claimed to be valid for two and three-phase fixed and fluidized beds. The proposed correlation is:

$$Sh = 0.68 \, Re_e^{1/2} \, Sc^{1/3} \quad \text{.....(2.3.70)}$$

The Reynolds number in this equation is obtained by using a "characteristic" velocity, expressed in terms of the overall rate of dissipation of energy for the gaseous and liquid phases:

$$V_e = 2^{0.5}\ ((E_g+E_l)\lambda)^{1/3},\quad \lambda=d_p\epsilon_s^{-1/3} \qquad .....(2.3.70a)$$

where E_g and E_l are the rates of energy dissipation in the liquid and gaseous streams and λ characterizes the dimension of the elementary cell of the bed for energy dissipation. The total rate of energy dissipation (E_l+E_g) can be obtained from the following equation:

$$E_l+E_g = [((\Delta P/L)_l U_l/\epsilon_l\rho_l)+((\Delta P/L)_g V_g/\epsilon_l\rho_l)] \qquad .....(2.3.70b)$$

The calculation of energy dissipation term requires information on the liquid phase holdup. The applicability of this correlation needs to be proven in liquids of various coalescing behaviors.

More recently Fukuma et al. (1988) also presented a correlation based on energy dissipation in the bed. The proposed correlation is given below:

$$Sh = 2 + 0.51(E^{1/3}d_p^{4/3}/V_l)^{0.61}\ Sc^{1/3} \qquad .....(2.3.71)$$

$$E = (\Delta P_d/d_p)V_l/(\epsilon_l\rho_l) + V_g g + (\Delta P_w/H_{bed})V_l/(\epsilon_l\rho_l) \qquad .....(2.3.71a)$$

Where ΔP_d is the pressure drop across a particle of diameter d_p and ΔP_w the pressure drop due to wall friction across the bed height (H_{bed}). However the pressure drop due to wall friction is usually negligible in three-phase fluidized beds, therefore the last term in Equation

2.3.71a can be neglected.

Fukuma et al. (1988) concluded that the values of particle-liquid mass transfer coefficient observed by Arters and Fan (1986), Prakash et al. (1987) and Nikov and Delmas (1987) were well correlated by this correlation.

It should be noted that calculation of energy dissipation terms require the knowledge of phase holdups. Moreover the correlation has not been tested in systems with different coalescing properties.

The correlation proposed by Nikov and Delmas (1987) is expected to provide a good estimate of particle-liquid mass transfer, for coalescing systems, in three-phase fluidized beds.

2.3.8 Entrainment

The particles from a three-phase fluidized beds can be carried over into the freeboard region when relatively large gas bubbles are rising through the bed. Wild et al. (1984) have proposed three mechanisms by which the particles can be entrained into the freeboard region.

1) bubbles breaking through the surface eject the particles from the bed into the freeboard (i.e. impart momentum)
2) particles are carried in the wakes of the bubbles.
3) the bubbles passing through the bed can displace

the particles into the disengagement section.

Page and Harrison (1974) noted that the second mechanism appeared to predominate. They observed that the particles were pulled from the upper surface of the fluidized bed and carried into the freeboard where particles were shed from the wake by vortices. The last mechanism is expected to contribute to entrainment only in the immediate vicinity of the bed. From the freeboard region the particles re-enter the bed by wake shedding from the bubbles and sedimentation.

Particle entrainment in three-phase fluidized beds has been investigated by only a limited number of researchers (Kafarov et al., 1973; Page and Harrison, 1974; El-Temtamy and Epstein, 1980; Razumov et al., 1980; Muir et al., 1987). Most of these studies have been limited to particle sizes less than 1 mm and low gas and liquid velocities (Kafarov et al., 1973; Page and Harrison, 1974 and El-Temtamy and Epstein, 1980). Muir et al. (1987) measured the entrainment of 3 mm glass beads from a three-phase fluidized bed using a slide valve. They determined the bed height by recording the pressure profile and changing the position of the slide valve. Page and Harrison (1974) used cine-photography to obtain the maximum height to which the particles were carried in the freeboard of a liquid- fluidized bed into which a single bubble was injected. They measured the solids concentration at a given height in the freeboard was

measured by a sampling technique. Muir et al. (1987) developed a downflux-probe to measure the particle flux in the freeboard.

Page and Harrison (1974) reported that entrainment decreased with decreasing bubble size, and frequency and with increasing liquid velocity, particle size and height above the bed surface. Muir et al.(1987) noted that entrainment of particles into the freeboard decreased exponentially with increasing height above the bed. They also observed that the entrainment of particles increased with increasing gas or liquid velocities.

Dayan and Zalmovich (1982) and El-Temtamy and Epstein (1980) based their models on gas bubble wakes and both reported a good agreement between their respective experimental and predicted values. El-Temtamy and Epstein (1980) proposed a stagewise model, based on the bubble-wake model of Bhatia and Epstein (1974), to represent solids entrainment and de-entrainment in the freeboard of a three-phase fluidized bed.

The axial dispersion of solids holdup was studied by Kato et al. (1985) and Ueyama et al. (1985). The solids holdup decreased gradually with increasing height. The holdup distribution was explained by a sedimentation and diffusion model.

The work done so far on particle entrainment in three-phase fluidized beds is scattered and the effects of important variables such as gas and liquid velocities vis-

a-vis particle size and density have not been investigated extensively enough to obtain general trends and models.

The work done by Page and Harrison (1974) is mainly of theoretical importance since particle entrainment was studied by injecting a single bubble into a liquid-fluidized bed which excluded the effects of bubble to bubble interactions. The models developed by El-Temtamy and Epstein (1980) and Dayan and Zalmanovich (1982) reed to be tested over wider range of operating conditions.

3. Experimental

3.1 Bubble Columns

3.1.1 Experimental Setup

Experiments for mass transfer studies in bubble columns were conducted in a column of 0.08 m inside diameter and 1.0 m height. Figure 3.1.1 shows the experimental setup used for batch bubble column studies. The clear liquid height was maintained at about 0.7 m. The liquid used were tap water and aqueous solutions of various surface active chemicals (see Table 3.1.1 for details). The temperature was maintained at 20 ± 1°C.

The gases used were air, oxygen-free nitrogen and a mixture of carbon dioxide and nitrogen (9.5 vol. % CO_2). The gas entered the column through a sonic nozzle which provided the advantage of instant flow which was not affected by the back pressure fluctuations. The flow rate was varied by adjusting the pressure upstream of the sonic nozzle with a pressure regulator (see Appendix-1 for nozzle calibration).

Five gas distributors were used to study the effects of sparger orifice diameter and the effective distributor area (see Table 3.1.2 for distributors details). A combination of a porous distributor (PR2) and a four arm sparger (SP1) was also used.

Five pressure taps, installed along the column wall

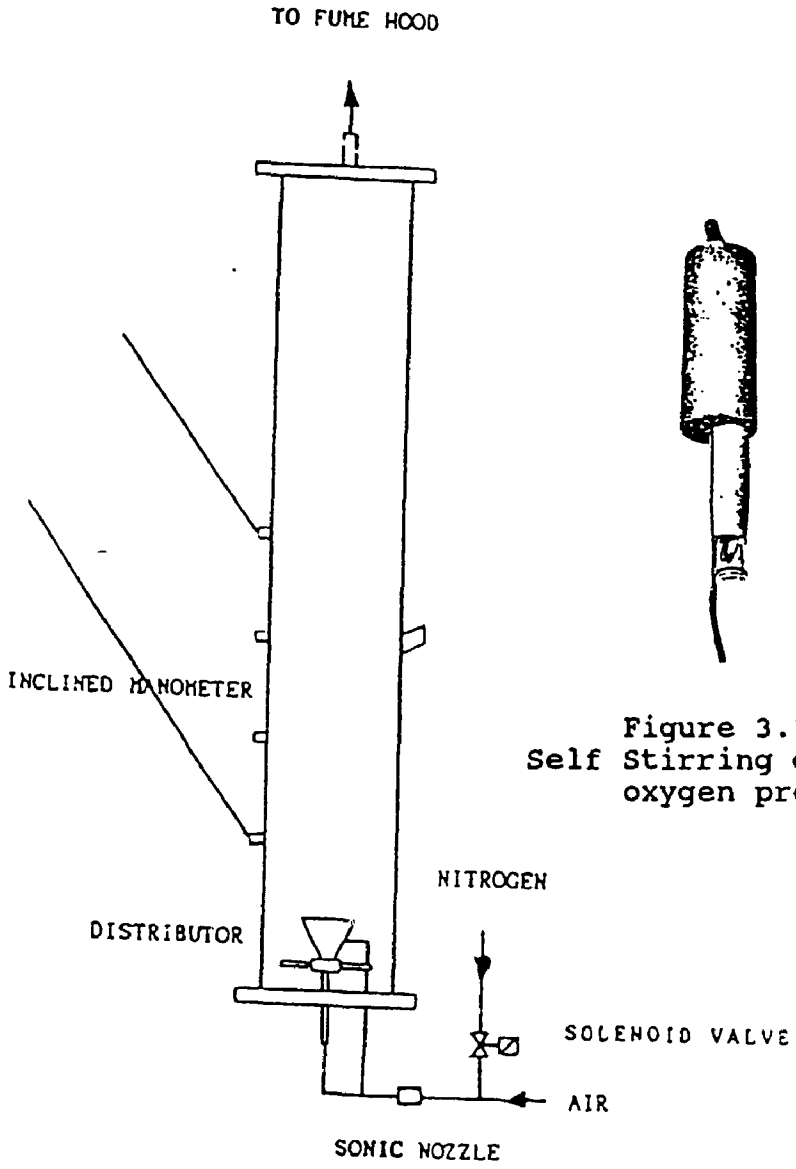

Figure 3.1.1A
Self Stirring dissolved oxygen probe

Figure 3.1.1
Schematic of batch bubble column

Table 3.1.1 List of Additives used for Mass Transfer Study in Batch Bubble Column

Sr. No.	Additive Name	Molecular Formula
1	Methanol	CH_3OH
2	Ethanol	CH_3CH_2OH
3	n-Propanol	$CH_3CH_2CH_2OH$
4	Acetone	$CH_3-\overset{\overset{O}{\|}}{C}-CH_3$
5	n-Butanol	$CH_3CH_2CH_2CH_2OH$
6	Iso-Butyl Alcohol	$CH_3-\overset{\overset{CH_3}{\|}}{CH}-CH_2OH$
7	Methyl Ethyl Ketone	$CH_3\overset{\overset{O}{\|}}{C}-CH_2CH_3$
8	n-Pentanol	$CH_3CH_2CH_2CH_2CH_2OH$
9	Iso-Amyl-Alcohol	$CH_3-\overset{\overset{CH_3}{\|}}{CH}-CH_2CH_2OH$
10	Ter-Amyl-Alcohol	$CH_3CH_2-\overset{\overset{CH_3}{\|}}{\underset{\underset{OH}{\|}}{C}}-CH_3$
11	Methyl Iso-Butyl ketone	$CH_3-\overset{\overset{CH_3}{\|}}{CH}-CH_2-\overset{\overset{O}{\|}}{C}-CH_3$
12	Hexanal	$CH_3CH_2CH_2CH_2CH_2CH_2CHO$
13	Hexanol	$CH_3CH_2CH_2CH_2CH_2CH_2OH$
14	2-Hexanone	$CH_3CH_2CH_2CH_2-\overset{\overset{O}{\|}}{C}-CH_3$
15	3-Hexanone	$CH_3CH_2CH_2-\overset{\overset{O}{\|}}{C}-CH_2CH_3$
16	Tri-Ethyl Amine	$(CH_3CH_2)_3N$
17	Di-iso-propyl ether	$CH_3\overset{\overset{CH_3}{\|}}{CH}-O-\overset{\overset{CH_3}{\|}}{CH}CH_3$

Table 3.1.1 Cont'd

18	Cyclohexanone	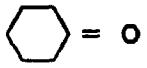
19	Butyl Acetate	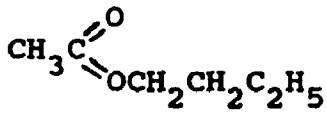
20	Hexanoic Acid	$CH_3CH_2CH_2CH_2CH_2COOH$
21	Citric Acid	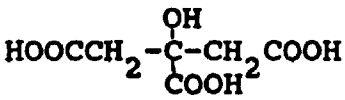
22	Adipic Acid	$HOOCCH_2CH_2CH_2CH_2COOH$
23	Heptanol	$CH_3CH_2CH_2CH_2CH_2CH_2CH_2OH$
24	Benzaldehyde	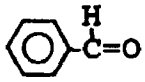
25	Octanol	$CH_3(CH_2)_7OH$
26	Acetaphenone	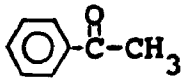
27	2-Octanone	$CH_3CH_2CH_2CH_2CH_2CH_2COCH_3$
28	Decanol	$CH_3(CH_2)_9OH$
29	2-Decanone	$CH_3(CH_2)_7COCH_3$

Table 3.1.2 Details of Gas Distributors Used in the Study

Distributor	Distributor type	Distributor diameter(m)	Distributor tube diameter (mm)	Orifice Diameter (mm)	Number of Orifices	Materials of Construction	Symbols Coalescing	Symbols Non Coalescing
PR1	Porous plate	0.08	-	0.035	-	Polyethylene	◇	◆
PR2	Porous plate	0.05	-	0.035	-	Polyethylene	○	●
PR3	Porous plate	0.03	-	0.035	-	Polyethylene	□	■
SP1	Four Arm sparger	0.06	12.5	1.0	28	Copper	△	▲
SP2	Ring sparger	0.06	6.0	3.0	4	Copper	▽	▼
PR SP	Porous plate (PR2) cum Four arm sparger	0.06	-	-	-	Copper	⬡	⬢

were connected to inclined water manometers (for improved accuracy) to measure static pressure along column height. At high gas flow rates, there were large fluctuations of the liquid levels in the manometers which would have reduced the accuracy of measurements. In order to dampen the oscillations capillary restrictions (0.55 mm ID and 25 mm long) were used in the tubes connecting the pressure taps to the manometers. Extensive testing showed that the measured average pressures were not affected by the restrictions (Appendix-2).

Figure 3.1.2 shows the experimental setup used for the continuous bubble column study. The column diameter was 0.08 m and its height was 1.0 m. The liquid was continuously pumped into the column bottom from a recirculating tank (400 L). Its flow rate was monitored with the help of an elbowmeter (see Appendix-3 for calibrations). The liquid entered the column through two 12.5 mm ID nozzles which were fitted with tees at the top in order to minimize liquid jetting effects. The liquid outlet from the column could be diverted to the recirculation tank or to the drain. For each run a fresh batch of liquid was taken in the tank. The temperature of liquid was maintained at 20 $\pm$ 1^{o}C during the runs.

For the runs conducted with the continuous bubble column, tap water was the coalescing liquid phase, while dilute aqueous solutions of iso-amyl alcohol (5 and 30 vppm) were the noncoalescing liquid phases. The gas phase

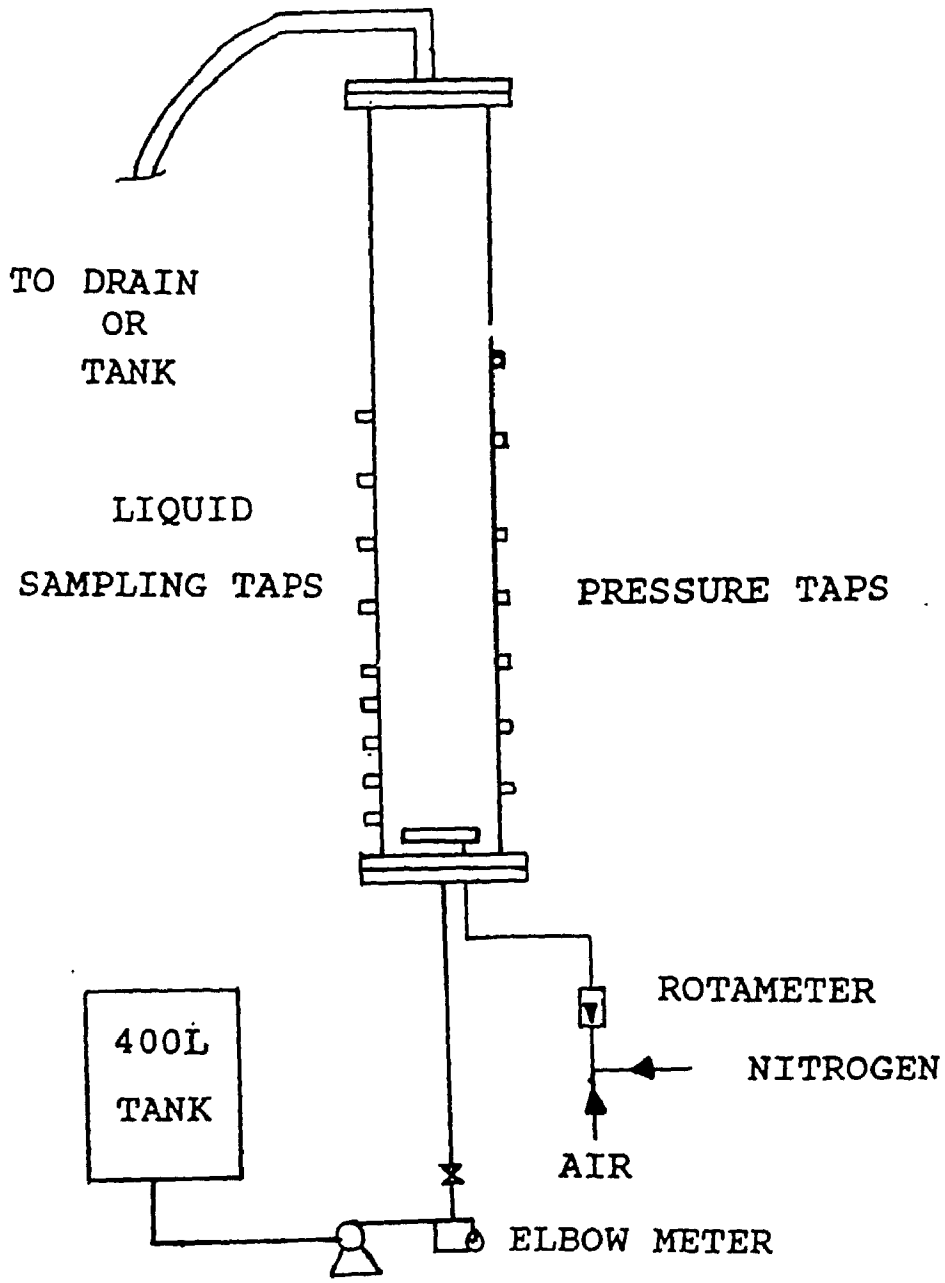

Figure 3.1.2
Schematic of continuous bubble column

was either air or oxygen free nitrogen. The gas flow was monitored with a rotameter (see Appendix-4 for calibrations). Two types of gas distributors, namely, sparger SP1 and porous distributor PR2 were used for the continuous bubble column study.

Nine sampling probes were available along the column height to collect liquid samples. The first five probes were 0.06 m apart and the last four probes were 0.09 m apart. The sampling probes were designed so as to avoid entrainment of gas bubbles in the liquid sampling lines. Figure 3.1.3 shows details of one such sampling probe. The liquid samples for mass transfer measurements were obtained from the fifth sampling probe (height from column bottom : 0.31 m). The sampling location was selected to minimize the effects of distributor region on mass transfer measurements.

3.1.2 Phase Holdup Measurements

The gas holdups in the bubble column were obtained from static pressure profile measurements along the column height. For the batch bubble column five pressure taps were available along the column height with a spacing of 0.1 m. For the continuous bubble column a sixth pressure tap was also available, 0.12 m above the fifth probe.

Equations 2.2.4 and 2.2.5 can be solved simultaneously to obtain an expression for gas holdup:

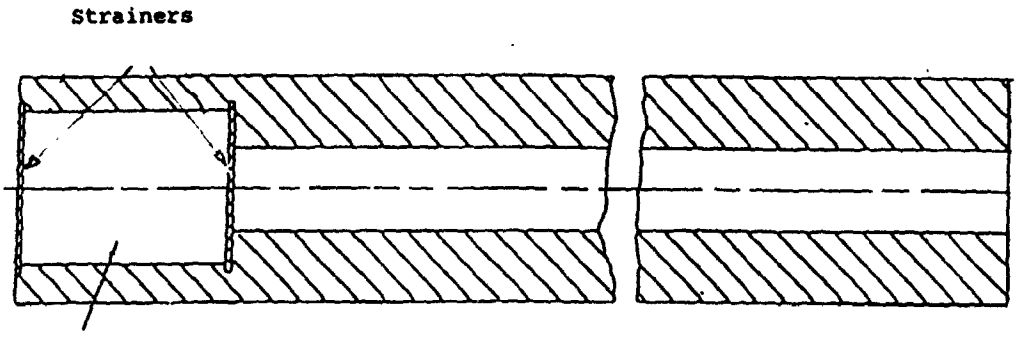

Figure 3.1.3
Details of sampling probe used to collect liquid samples from columns

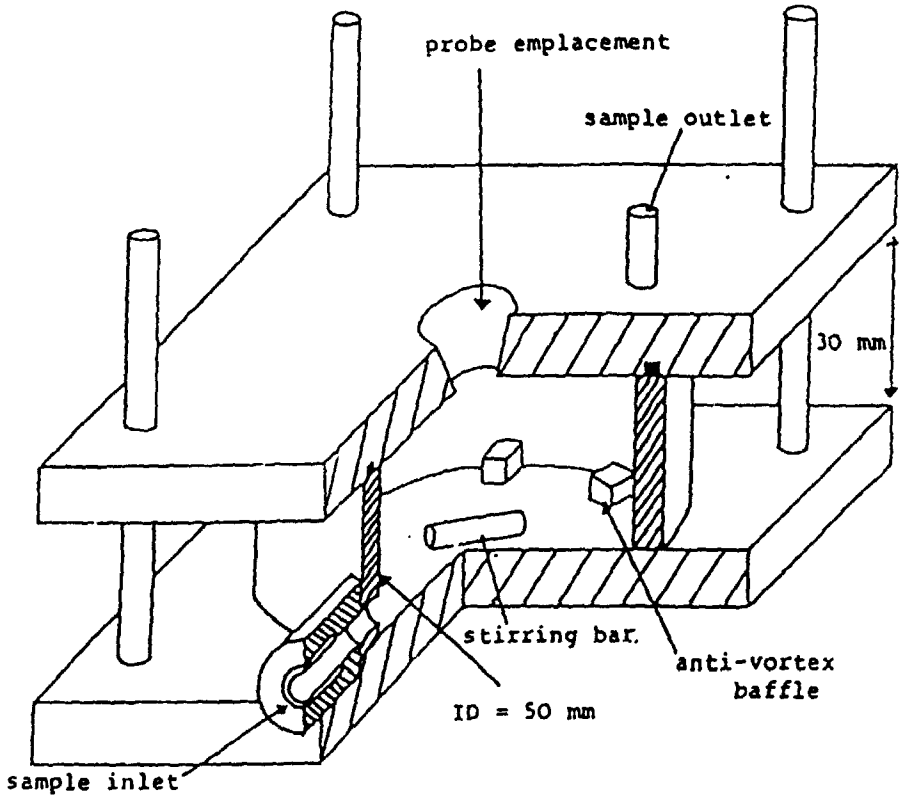

Figure 3.1.3A
Details of stirred cell used to measure oxygen concentration in liquid samples

$$\epsilon_g = 1.0 - \frac{(\Delta P/\Delta z)}{g \cdot \rho_l} \qquad \text{.....(3.1.1)}$$

The pressure gradient can be obtained from manometer readings (see Appendix-5 for details):

$$\frac{\Delta P}{\Delta z} = \rho_l g \left(\frac{\Delta h}{\Delta z} + 1\right) \qquad \text{.....(3.1.2)}$$

Most of the measurements for mean gas holdup in the batch bubble column were made using the second and fifth pressure taps to get a mean value of the gas holdup inside the column. A few measurements were also made, using other and fifth pressure taps to obtain the gas holdup as a function of column height.

3.1.3 Liquid Mixing Measurements

The liquid mixing in the batch bubble column was investigated by measuring oxygen concentration at different heights in the liquid at the end of a run. The liquid samples were collected starting from top to bottom using the available sampling probes. The oxygen concentration in the liquid samples was always within 1% (see Appendix-6). These results indicated that the liquid in the batch bubble column could be assumed to be completely mixed.

The measurements for liquid backmixing in the continuous bubble column were made using continuous injection of a colored tracer. The tracer was a dilute solution of methylene blue (0.05 kg/m^3) in water. The tracer solution was continuously injected through the seventh sampling port with the help of a precalibrated dosing pump. The injection rate of tracer solution was maintained at about 1% of the liquid flow rate through the column. The use of methylene blue tracer provided the advantage of visual observations of the liquid mixing patterns in the column. The steady state was assumed to be attained when the concentration of the tracer in consecutive liquid samples was constant. The liquid samples were then collected from five sampling ports upstream of the tracer injection point, one at a time. The sampling ports were close to the column wall.

For most of the measurements, the tracer solution was injected at a distance of 0.01 m from the wall. For one case (PR2, V_l=0.037 m/s, V_g=0.078 m/s) tracer injections were made at different radial positions starting from the column centre to the wall (0.01 m apart).

The tracer concentration in the liquid samples was measured with the help of a UV/VIS spectrophotometer (Phillips Model PU 8600) at a wavelength of 655 nm. The spectrophotometer was initially calibrated, using tracer solutions of known concentrations (see Appendix-7 for calibrations).

The axial mixing effects in the bubble column were analyzed, assuming that the liquid phase flow could be described by an axially dispersed plug flow model. When the system has reached steady state and there is no reaction taking place, the model can be represented by the following diffusion type equation:

$$\frac{d^2C_t}{dz^2} = \frac{V_l}{D_z\epsilon_l}\frac{dC_t}{dz} \qquad \text{.....(3.1.3)}$$

The boundary conditions are:

$$C_t = C_{to} \qquad \text{at } z = 0 \qquad \text{.....(3.1.3a)}$$

$$C_t = 0.0 \qquad \text{at } z = \infty \qquad \text{.....(3.1.3b)}$$

The standard solution of equation 3.1.3 upstream of the tracer injection source is given as:

$$\frac{C_t}{C_{to}} = \exp\left(-\frac{V_l}{D_z\epsilon_l} z\right) \qquad \text{.....(3.1.4)}$$

If the system can be represented by the model then a plot of $\ln(C_t/C_{to})$ versus the axial distance should produce a straight line of slope $V_l/D_z\epsilon_l$. Figure 3.1.4 is one such plot for two sets of conditions. Since the plots are straight lines, the system could be represented by the above model.

The axial dispersion coefficient was found to be slightly dependent on the radial position of the tracer injection (Appendix-7A). Higher values of axial dispersion

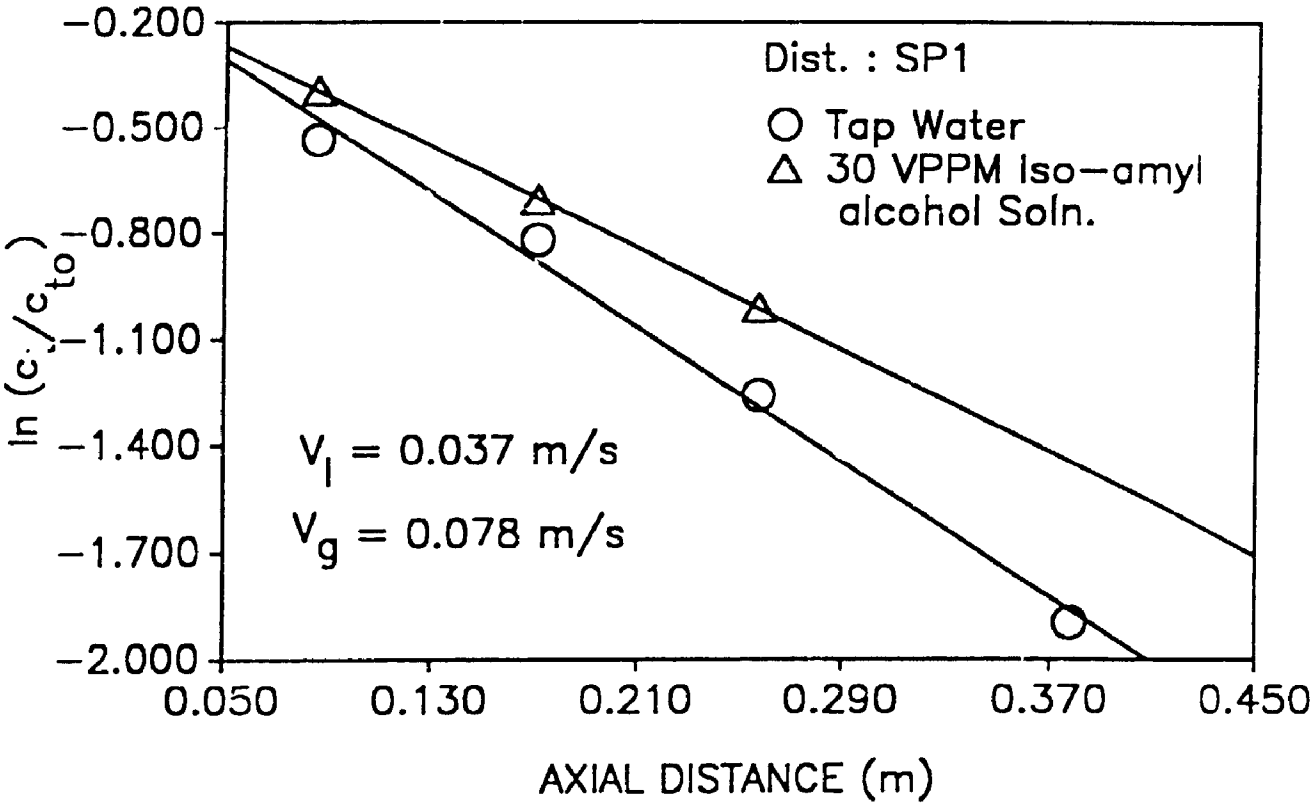

Figure 3.1.4
Verification of the model used to calculate the axial dispersion coefficient (Equation 3.1.4).

coefficient were obtained when the tracer was injected close to the column wall; the variation, however, was within 12% only. These results indicated that there was good radial mixing in the bubble column. In order to minimize the wall region effects, the tracer was injected about 0.01 m from the wall for most of the runs.

The axial dispersion coefficients were measured at a few selected conditions only. These conditions were a combinaions of minimum and maximum flows of gas and liquid. Table 3.1.3 gives the values of axial dispersion coefficients obtained for these conditions. It can be seen that the axial dispersion coefficient was lowest in the additive solution with distributor PR2, for low gas flow rate. At high gas flow rate there was practically no effect of the distributor type or the liquid medium used. Similar observations were made by Kelkar et al. (1983), who reported that compared to air/water system, axial dispersion coefficients were significantly lower in aqueous solutions of alcohols for gas velocities below 0.15 m/s. These researchers, however, used significantly higher concentrations of alcohols (5000 -24000 wppm) for their measurements.

Literature correlations were tested to predict the axial dispersion coefficients measured in this study. The correlation proposed by Baird and Rice (1975) generally gave a good prediction (within 10 %) of the measured values, except when additive solution was used with

distributor PR2, in bubbly flow regime (Table 3.1.3).

Table 3.1.3 Comparison of Measured and Predicted Values of Axial Dispersion Coefficient in Continuous Bubble Column (Predictions by Baird and Rice (1975) correlation)

Dist. Type	Liquid Phase	V_g (m/s)	V_l (m/s)	D_z (m²/s)	
				Measured	Predicted
SP1	Tap water	0.03	0.057	0.0085	0.008
SP1	Tap water	0.078	0.037	0.01	0.011
SP1	30 vppm iso-amyl alcohol solution	0.03	0.057	0.0084	0.008
SP1	30 vppm iso-amyl alcohol solution	0.078	0.037	0.011	0.011
PR2	Tap water	0.03	0.057	0.0082	0.008
PR2	Tap water	0.078	0.037	0.011	0.011
PR2	30 vppm iso-amyl alcohol solution	0.03	0.057	0.0055	0.008
PR2	30 vppm iso-amyl alcohol solution	0.078	0.037	0.012	0.011

3.1.4 Gas-Liquid Mass Transfer Measurements

3.1.4.1 Batch Bubble Column

The volumetric mass transfer coefficient in bubble columns can be determined either by physical or chemical methods. As pointed out in section 2.2.5.1, the chemical methods require the presence of a dissolved chemical which can alter the coalescing behavior of the liquid. One of the objectives of this study was to investigate the effects of various coalescence inhibitors on gas liquid mass transfer rate. It was therefore decided to use a technique which provided an accurate estimate of these effects on mass transfer rate. The selected technique involved dynamic desorption of dissolved oxygen into oxygen-free nitrogen. This technique also ensured that the mass transfer measurements were not affected by any changes in the solubility of oxygen in the presence of additives. The following procedure was used to determine the volumetric mass transfer coefficient in the batch bubble column.

A batch of known volume (appx. 4L) of water was taken into column at the desired temperature. In order to prepare an additive solution of a desired concentration the required amount of the additive was then injected in the middle of the column. Air flowrate was then started at the desired level to prepare a homogeneous solution of the additive and also to achieve a high dissolved oxygen

concentration in the liquid. The manometer readings were taken after four minutes to ensure steady state conditions. The air flowrate was then stopped and the gas bubbles were allowed to escape. The initial dissolved oxygen concentration (C_{01}) was then measured by a self stirring polarographic probe (YSI 5720A) mounted on the column (Figure 3.1.1A). Nitrogen was then sparged for a preset duration (15 to 25 s), which was controlled by a timer operated solenoid valve, mounted on the gas inlet line (see Figure 3.1.1). The final dissolved concentration (C_{02}) was measured after the nitrogen was stopped.

When the liquid is assumed to be perfectly mixed (CSTR) then the instantaneous change of the dissolved oxygen concentration is described by the following differential equation, for either absorption or desorption:

$$V_R (1-\epsilon_g) dC_o = k_l A (C_0^* - C_0) dt \quad .....(3.1.5)$$

Equation 3.1.5 assumes that the batch bubble column can be modelled as a CSTR. For the liquid this assumption was verified experimentally by analyzing oxygen concentration in liquid samples collected from different column heights at the end of a run (see Appendix-6 for details). The oxygen concentration was found to be the same in all the samples collected. The dissolved oxygen

concentration at the gas-liquid interface (C_o^*) would depend on the oxygen concentration in the gas phase. For the gas phase the plug flow model should apply in the bubbly flow regime where isolated bubbles move up the dispersion, while perfect mixing would be more appropriate in the churn turbulent regime. In the following analysis equations for volumetric mass transfer coefficient are derived assuming both plug flow and perfect mixing for the gas phase.

Plug Flow in the Gas Phase:

If Henry's law holds, then the dissolved oxygen concentration in equilibrium with the average partial pressure ($p_{o,av}$) of oxygen in the column is given by:

$$C_o^* = H_{eo} p_{o,av} \qquad \text{.....(3.1.6)}$$

An oxygen balance for a differential column volume at a given height is given as:

$$\frac{V_g}{RT} \frac{dp_o}{dz} = k_l a \, (C_o - H_{eo} p_o) \qquad \text{.....(3.1.7)}$$

Equation 3.1.7 assumes that change in molar flow rate of gas due to increase in oxygen concentration is negligible (see Appendix-8). Since the liquid phase is perfectly mixed C_o is the same at all column heights. Equation 3.1.7 can be integrated to give:

$$p_o = \frac{C_o}{H_{eo}} \left[1 - \exp\left(- \frac{k_l a H_{eo} RT}{V_g} z\right) \right] \quad \ldots\ldots(3.1.8)$$

Since the oxygen partial pressure would change along the column height an average partial pressure is required to be calculated at any given time:

$$p_{o,av} = (1/H_d) \int_0^{H_d} p_o dz \quad \ldots\ldots\ldots(3.1.9)$$

From Equations 3.1.8 and 3.1.9

$$p_{o,av} = \frac{C_o}{H_{eo}} \left(1 - \frac{1-e^{-j}}{j}\right) \quad \ldots\ldots\ldots(3.1.10)$$

where $j = k_l a H_{eo} RTA_c H_L/(1-\epsilon_g)Q_g$ $\ldots\ldots\ldots(3.1.10a)$

Substituting Equation 3.1.10 into Equation 3.1.5 and integrating with the conditions:

$t = 0 \qquad C_o = C_{01}$ $\ldots\ldots\ldots\ldots(3.1.11)$

$t = t \qquad C_o = C_{02}$ $\ldots\ldots\ldots\ldots(3.1.12)$

$$k_l a = - \frac{1-\epsilon_g}{t} \left[\frac{j}{1-e-j}\right] \ln \frac{C_{o2}}{C_{o1}} \quad \ldots\ldots\ldots(3.1.13)$$

Perfect Mixing in Gas Phase:

An oxygen balance for the entire column is given by:

$$(p_{o,out}/P_{T,out})N_{g,out} - (p_{o,in}/P_{T,in})N_{g,in} = -A_c H_d (1-\epsilon_g)(dC_o/dt) \quad \ldots\ldots\ldots(3.1.14)$$

The oxygen content in the inlet gas was negligible (oxygen < 5 vppm). Moreover the change in molar flowrate of the gas during a run was negligible (Appendix-8). Thus $N_{g,out} = N_{g,in} = N_g$. From Equation 3.1.14

$$p_{o,out} = -(1-\epsilon_g)\frac{RTH_d}{V_g}\frac{dC_o}{dt} \qquad \text{.....(3.1.15)}$$

The average oxygen partial pressure $p_{o,av}$ in the column is given by:

$$p_{o,av} = P_{T,av}(p_{o,out}/P_{T,out}) \qquad \text{.....(3.1.16)}$$

Substituting Equations 3.1.6, 3.1.15 and 3.1.16 into Equation 3.1.5 and integrating with the conditions:

$$t = 0 \qquad C_o = C_{01} \qquad \text{.....(3.1.17)}$$

$$t = t \qquad C_o = C_{02} \qquad \text{.....(3.1.18)}$$

$$k_l a = -\frac{1-\epsilon_g}{t}\left[1+j\frac{P_{T,av}}{P_{T,out}}\right]\ln\frac{C_{o2}}{C_{o1}} \qquad \text{....(3.1.19)}$$

In Equations 3.1.13 and 3.1.19, the terms in the brackets account for the effects of gas phase mixing pattern on volumetric mass transfer coefficient. In order to quantify the effects of gas phase mixing, the terms in the brackets were estimated for a case of high mass transfer rate (Appendix-8). As pointed out in Appendix-8, the contribution from the terms in the brackets was less

than 3%. Therefore, the volumetric mass transfer coefficient could be obtained by the following equation:

$$k_l a = - \frac{1-\epsilon_g}{t} \ln \frac{C_{02}}{C_{01}} \qquad \text{.....(3.1.20)}$$

The technique used in the present study also ensured that the mass transfer measurements were not affected by any changes in the solubility of oxygen in the additive solutions. The above procedure avoided to a large extent the errors associated with the probe response lag and the start-up period which were shown to be significant by Linek and Vacek (1977). The probe response characteristics did not have to be determined since the dissolved oxygen concentration was measured by a self-stirring probe (Figure 3.1.1A), after sparging had been stopped. It should be pointed out that this procedure could be followed since the liquid phase in the column was completely mixed (see Appendix-6). The use of sonic nozzles to control the gas flow ensured reproducible start-up periods. In order to quantify any errors due to the unsteady state behaviour of the column during start-up and shutdown, measurements were made for different sparging times for two sets of conditions. As shown in Appendix-9, the measurement errors could be reduced to less than 5 % by a proper selection of the sparging time.

In most of the industrial processes oxygen is

transferred to the liquid phase (absorption), while in the above technique oxygen was transferred to the gas phase (stripping). In order to ensure that the results obtained with the present technique could be applied to the absorption processes, a few measurements were also made with the oxygen absorption technique. For this technique, oxygen was first desorbed from the liquid using nitrogen stripping. The initial dissolved oxygen concentration was then measured. Air was sparged through the liquid for a preset duration. The final dissolved oxygen concentration was then measured. The volumetric mass transfer coefficient was obtained from the following equation:

$$k_l a = - \frac{1-\epsilon_g}{t} \ln \frac{C_o^* - C_{o2}}{C_o^* - C_{o1}} \quad \text{.....(3.1.21)}$$

There was practically no difference between the results obtained with the two techniques (see Appendix-10). Measurements were also carried out to study the effects of other sources of error such as day to day variations in the quality of tap water and air on the mass transfer coefficient (Appendix-11).

3.1.4.2 Mass Transfer in Continuous Bubble Column

The gas-liquid mass transfer rate in the cocurrent continuous bubble column was also measured, using the same technique i.e. desorption of dissolved oxygen in nitrogen stream. Here, a large holding tank (400 L) was used to

prepare the liquid solution at the desired temperature and additive concentration. Initially liquid was recirculated through the column with air sparging at preset liquid and gas flowrates. After about five minutes of air sparging, the manometer readings were taken. The air flow was then stopped but liquid circulation continued. The dissolved oxygen concentration at column inlet was then measured. The liquid from the sampling port flowed into a stirred cell where the dissolved oxygen concentration was measured with the help of the polarographic probe (YSI 5750) mounted on the cell (Figure 3.1.3A).

Nitrogen flow was then started at the desired flowrate and the liquid from the column outlet was diverted to the drain. Once steady state was reached, the dissolved oxygen concentration in the liquid from the sixth sampling port (0.26 m from column bottom) was measured. The liquid from the sampling port flowed into the stirred cell. The liquid flowrate into the sampling cell was adjusted so as to avoid any entrainment of gas bubbles with the liquid. It was also ensured that no gas bubbles were entrapped inside the cell. The dissolved oxygen concentration was displayed on a digital meter.

An accurate estimate of volumetric mass transfer coefficient from the concentration measurements requires the use of a proper hydrodynamic flow model. Three flow models namely, plug flow, CSTR and plug flow with axial dispersion were reviewed for this purpose. The liquid

backmixing measurements showed that there was large backmixing of liquid in the continuous bubble column (see section 3.1.3) which excluded the plug flow conditions for the liquid phase. Since the dissolved oxygen concentration in the liquid samples was found to vary along the column height, the CSTR model too could not represent the hydrodynamics of continuous bubble column. The axial dispersion model was then assumed to represent the flow behavior of the continuous bubble column, since this model can account for different levels of liquid backmixing observed at different flow conditions. For axial dispersion model the mass balance for the liquid phase over a differential element is given by:

$$\epsilon_l D_z \frac{d^2 C_o}{dz2} - V_l \frac{dC_o}{dz} + (k_l a)_d (C_o^* - C_o) = 0.0 \qquad \text{.....(3.1.22)}$$

Since oxygen-free nitrogen was used as the desorbing gas there was no significant effect of oxygen concentration buildup on the mass transfer rate (Appendix-12). Therefore in Equation 3.1.22 the interfacial concentration C_o^* could be neglected as compared to bulk concentration of oxygen. The jump boundary conditions proposed by Danckwerts (1953) which assume no mixing across the zone boundaries were selected.

$$V_l\ C_o^- = V_l\ C_o^+ - D_z \epsilon_l \frac{dC_o^+}{dz} \qquad \text{.....(3.1.23)}$$

$$\frac{dC_o\ (L)}{dz} = 0.0 \qquad \text{.....(3.1.23a)}$$

Equation 3.1.23 describes the boundary conditions for the column inlet zone. It states that a liquid element just above the column inlet receives oxygen concentration carried by water flowing from below the boundary (where the concentration is C_o^-) as well as oxygen transferred from the column above the zone boundary by axial dispersion. This boundary condition is justified here because the liquid enters the column through small diameter pipes at high velocity which precludes any liquid backmixing below the column inlet. Equation 3.1.23a gives the boundary condition for upper end of the zone considered (i.e. column top). This condition states that the oxygen concentration gradient becomes zero at the upper zone boundary. This condition is justified because the oxygen concentration profile tends to flatten at the column top.

Assuming that both volumetric mass transfer coefficient ($k_l a$) and the axial dispersion coefficient (D_z) are constant over the whole zone, the solution of this second order differential equation is given as:

$$C_o = A_1 e^{m_1 z} + A_2 e^{m_2 z} \qquad \text{.....(3.1.24)}$$

Here

$$m_1 = \frac{-V_l + (V_l^2 + 4D_z\epsilon_l(k_la)_d)^{0.5}}{2D_z\epsilon_l} \quad \ldots\ldots(3.1.24a)$$

$$m_2 = \frac{V_l - (V_l^2 + 4D_z\epsilon_l(k_la)_d)^{0.5}}{2D_z\epsilon_l} \quad \ldots\ldots(3.1.24b)$$

$$A_1 = \frac{V_lC_{01}(m_2/m_1)\exp(m_2-m_1)L}{V_l[1-(m_2/m_1)\exp(m_2-m_1)L]-m_2D_z(1-\exp(m_2-m_1)L)} \quad \ldots\ldots(3.1.24c)$$

$$A_2 = \frac{V_lC_{01}}{V_l[1-(m_2/m_1)\exp(m_2-m_1)L]-m_2D_z(1-\exp(m_2-m_1)L)} \quad \ldots\ldots(3.1.24d)$$

Using above equations, volumetric mass transfer coefficient can be calculated knowing oxygen concentrations at inlet and outlet, liquid holdup, liquid velocity and axial dispersion coefficient. Except for axial dispersion coefficient, values of all other variables were measured for each run. It was,however, pointed out in section 3.1.3 that axial dispersion coefficient could be predicted by the correlation of Baird and Rice (1975) for most of the conditions. The predictions were, however, high (about 40%) when additive solution was used with distributor PR2 in the bubbly flow regime. The predicted axial dispersion coefficients were,

therefore, reduced by about 40 % for these conditions. It may, however, be pointed out that the calculation of volumetric mass transfer coefficient was not very sensitive to values of axial dispersion coefficients. For example, a 40 % decrease in axial dispersion coefficient resulted in about 2.5 % decrease in volumetric mass transfer coefficient.

3.1.5 Interfacial Area Measurement

The experimental technique used for interfacial area measurements involved simultaneous physical desorption of dissolved oxygen and absorption with chemical reaction of carbon dioxide with [OH^-] in the liquid phase. The rate of desorption of oxygen was used to evaluate the overall volumetric mass transfer coefficient (k_1a). The interfacial area was then obtained from absorption rate of of carbon dioxide and volumetric mass transfer coefficient measurements. This method offers the advantage that both k_1a and a (and therefore k_1) are determined under truly identical physico-chemical and hydrodynamic conditions. A preliminary study, based on gas holdup measurements showed that the chemical system selected for the interfacial area measurements did not significantly alter the coalescing behavior of the liquid (Appendix-13).

For the present study, a 9.5 mole % CO_2 in nitrogen mixture was sparged for a preset duration (15 to 30 s)

through an aqueous solution of KOH (starting PH > 12) containing a desired concentration of an additive. The dissolved oxygen concentration in the solution was measured before and after gas sparging using the self stirring dissolved oxygen probe mounted on the column (Figure 3.1.1). The volumetric mass transfer coefficient was then calculated using Equation 3.1.20.

The CO_2 absorption rate was determined by titration (see Appendix-14). Whenever gas absorption is accompanied by chemical reaction, the presence of chemical reaction may affect the overall absorption rate capability of the system in several ways the exact effect being dependent upon the relative magnitudes of the reaction rate and the physical mass transfer rate capability of the system. The theory of mass transfer with chemical reaction was briefly reviewed in section 2.1.5. The absorption rate of a gas which undergoes a fast pseudo first order irrerversible reaction is given by equation 2.1.10.

The overall reaction between dissolved carbon dioxide and hydroxyl ions in aqueous solutions, containing sufficiently high concentration of the hydroxyl ions, is essentially irreversible and may be given as:

$$CO_2 + 2OH^- \rightarrow CO_3^{2-} + H_2O \qquad \text{.....(3.1.25)}$$

This is a second order reaction, being first order with respect to dissolved $[CO_2]$ and $[OH^-]$ concentrations.

Robinson and Wilke (1974) used a similar technique for interfacial area measurements in well mixed agitated contactor. For their study, Robinson and Wilke (1974) treated the above reaction as pseudo-first order, assuming that the concentration of [OH^-] ions in the surface elements and the bulk liquid was nearly constant over the gas-liquid contact period. These investigators tried to maintain a constant hydroxyl ions concentration by a continuous injection of concentrated KOH solution, the injection rate being based on PH control. The liquid analysis, however, showed that the concentration of hydroxyl ions decreased with time in all runs. Moreover, since most of the reaction occurs in the liquid film near the interface, the hydroxyl concentration in the surface elements would drop at a faster rate. Therefore the assumption of a pseudo first order reaction, based on constant hydroxyl concentration in the surface elements is not fully justified.

In the present study, the following modifications were made to improve the accuracy of the technique.

1) The concentration of hydroxyl ion in the bulk liquid was allowed to vary with time as the reaction proceeded and the concentration of hydroxyl ions at the interface was determined, following the analysis by DeCoursey (1974).

2) The depletion of CO_2 in the gas bubbles, as they rose through the gas-liquid dispersion was taken into

account by modelling the bubble flow.

The assumption of segregated bubble classes can, however, give rise to errors in the estimation of the interfacial areas of the various bubble classes (Schumpe and Deckwer, 1980). In order to estimate the errors caused by the assumption of a single bubble class (assuming frequent bubble coalescence resulting in essentially the same CO_2 content of all bubbles at a given height), the absorption process was also modelled assuming two segregated classes of bubbles. The run conditions (i.e. liquid height, sparging time, initial OH ion concentration) were then selected so as to minimize the errors for interfacial area measurements (see Appendix-15 for details).

In the following analysis, the absorption process was modelled, assuming single bubble class with uniform composition. Similar equations for two classes of bubbles are given in Appendix-15.

Mass balance for single bubble class:

$$-d(N_g y_c) = E_n k_l (adV)(C_c^* - C_{cb}) \quad \text{.....(3.1.26)}$$

Here

$$N_g = P_T Q_g / RT \quad \text{.....(3.1.26a)}$$

$$C_c^* = p_c / H_{ec} \quad \text{.....(3.1.26b)}$$

$$p_c = P_T y_c \quad \text{.....(3.1.26c)}$$

$$C_c^* = P_T y_c / H_{ec} \quad \text{.....(3.1.26d)}$$

The changes in volumetric flowrate of gas (Q_g) and the total pressure (P_T) along the column height were small due to dilute mixture of gas used for absorption and the small column height. These values were, therefore assumed to be constant and were taken equal to their average values. For fast reaction of carbon dioxide in the presence of high concentration of hydroxyl ions, the bulk concentration of dissolved carbon dioxide would be negligible (Danckwerts, 1971). Equation 3.1.26 can now be written as:

$$-dy_c = \frac{P_T A_c}{H_{ec} N_g} E_n (k_l a)_c y_c dz \qquad \text{.....(3.1.27)}$$

The volumetric mass transfer coefficient for CO_2 $(k_l a)_c$ can be obtained, assuming the penetration model describes the absorption and desorption process:

$$(k_l a)_c = (k_l a)_o (D_{co}/D_o)^{0.5} \qquad \text{.....(3.1.28)}$$

The enhancement factor (E_n) for the reaction is a function of liquid phase mass transfer coefficient (k_l), the reaction rate constant (k_r), the diffusivity of carbon dioxide (D_{co}) and the bulk concentration of hydroxyl ions (C_{hb}). The enhancement factor could be assumed to be constant if the bulk concentration of hydroxyl ions remained constant. In practice, it is difficult to maintain a constant hydroxyl ion concentration during short absorption periods. In the present analysis, the

hydroxyl ion concentration was assumed to vary with time.

The following equation gives a unsteady state balance on a gas being absorbed in a liquid in the zone between the interface at x=0 and the location of the reaction plane.

$$\frac{\partial^2 C_c}{\partial x^2} - \frac{1}{D_{co}} \frac{\partial C_c}{\partial t} - \frac{k_r C_{hi} C_c}{D_{co}} = 0 \qquad \text{.....(3.1.29)}$$

with the boundary conditions:

$$\text{at } t = 0 \text{ and } x > 0,\ C_c = 0 \qquad \text{.....(3.1.29a)}$$

$$\text{at } t > 0 \text{ and } x = \infty,\ C_c = 0 \qquad \text{.....(3.1.29b)}$$

$$\text{at } t > 0 \text{ and } x = 0,\ C_c = C_c^* \qquad \text{.....(3.1.29c)}$$

Following the analysis by DeCoursey (1974), the time-mean ratio for the interfacial concentration of the reactive component in the liquid to its bulk concentration for the surface renewal model can be approximated as:

$$\frac{C_{hi}}{C_{ho}} = \frac{E_a - E_n}{E_a - 1} \qquad \text{.....(3.1.30)}$$

Where E_a is the asymptotic value of the enhancement factor at infinite reaction rate (Danckwerts, 1970), given as:

$$E_a = 1/\mathrm{erf}(\zeta/\sqrt{D_{co}}) \qquad \text{.....(3.1.30a)}$$

and ζ is given by:

$$e^{\zeta^2/D_{ho}}\mathrm{erfc}(\zeta/\sqrt{D_{ho}}) = \frac{C_{ho}}{zC_c^*}\left(\frac{D_{ho}}{D_{co}}\right) e^{\zeta^2/D_{co}} \mathrm{erf}(\zeta/\sqrt{D_{co}}) \qquad \text{.....(3.1.30b)}$$

In Equation 3.1.29, the interfacial concentration of hydroxyl ion (C_{hi}) can be replaced by its time-mean ratio (C_{hi}/C_{ho}) multiplied by its bulk concentration (C_{ho}). For a fast irreversible reaction, the concentration of the absorbing gas in the bulk of liquid is negligible (Danckwerts 1970). Since (C_{hi}/C_{ho}) is independent of time, Equation 3.1.29 can now be solved to give the time-mean absorption rate.

$$F_c = k_l C_c^* [1 + M_2(C_{hi}/C_{ho})]^{0.5} \quad \text{.....(3.1.31)}$$

where

$$M_2 = \frac{D_{co} k_r C_{ho}}{(k_l)^2} \quad \text{.....(3.1.31a)}$$

Then the enhancement factor is

$$E_n = [1 + M_2(C_{hi}/C_{ho})]^{0.5} \quad \text{.....(3.1.32)}$$

Using Equation 3.1.30

$$E_n = [1 + M_2(E_a - E_n)/(E_a - 1)]^{0.5} \quad \text{....(3.1.32a)}$$

Equation 3.1.32a can be rearranged to obtain an explicit expression for E_n

$$E_n = -\frac{M_2}{2(E_a - 1)} + \left[\frac{M_2^2}{4(E_a - 1)^2} + \frac{E_a M_2}{(E_a - 1)} + 1\right]0.5$$

.....(3.1.33)

Global mass balance on CO_2:

The total numbers of CO_2 moles absorbed per unit of liquid volume during a time Δt is given as:

$$F_c \Delta t = \frac{V_g P_T (y_{c,in} - y_{c,out})}{RTH_L} \Delta t \qquad .....(3.1.34)$$

The values of diffusivities, reaction rate constant and solubilities were obtained from the literature (Appendix-16). The rate constant for CO_2 absorption in KOH solutions can be affected by the presence of ionic impurities. For the interfacial area measurements, the KOH solutions were therefore prepared in deionized water. The following procedure was used to obtain the interfacial area:

- The volumetric mass transfer coefficient for carbon dioxide was calculated using Equation 3.1.28.

- A value for interfacial area was assumed and the liquid side mass transfer coefficient was calculated from the volumetric mass transfer coefficient obtained in the first step.

- Equations 3.1.33 and 3.1.27 were then used to calculate enhancement factor and conversion, respectively along the column height. Equation 3.1.27 was integrated numerically over the column height for the given sparging

time. Hydroxyl ion concentration, enhancement factor and conversion were estimated for each interval of length and time.

- The change in carbonate ion concentration in the liquid was obtained from Equation 3.1.34.

For a given run, the above procedure was repeated for 4 to 5 assumed values of interfacial area. An approximate range for interfacial area was estimated from the bubble population study data (section 3.1.6). A curve was then generated, using the assumed values of interfacial area and the calculated values of carbonate ion concentrations (Appendix-15). The actual interfacial area was obtained, using the curve and the experimental value of carbonate ion concentration.

3.1.6 Bubble Population Study

The experimental technique used for the bubble population study involved fast filming of the drop in the gas-liquid dispersion height after the gas was shut off. This technique is based on the principle that different bubble classes in a gas liquid dispersion can be distinguished if there are significant differences between their rise velocities. The rate at which the height drops would depend on the concentration and rise velocities of the gas bubbles. Initially, when the fast rising large

bubbles are escaping, the drop in interface height would be fast. The rate of drop would, however, slow down when only small bubbles are escaping the gas-liquid dispersion. Due to its limited accuracy this technique cannot distinguish between bubbles of narrow size distribution. The technique, however, can provide reasonably approximate information if there are two distinct classes of bubbles. The various assumptions and sources of errors associated with the technique have been reviewed by Schumpe and Grund (1986). The main assumptions for the applicability of the technique are; 1) the holdup structure is not affected by the bubble interactions after the gas supply is cut off. 2) the holdup structure is axially uniform. The holdup structure can, however, be affected during the initial period of disengagement of large bubbles, which can accelerate the smaller bubbles in their wake. Moreover, the assumption of uniform axial holdup may not be applicable in every case. The other sources of errors are discussed below:

1) In the heterogeneous regime, the large bubbles cause wild fluctuations of dispersion height which makes it difficult to measure the dispersion height accurately. The error for initial height can, however, be reduced by multiple observations.

2) After the gas supply is shut off, the flow through the sparger orifices reduces to zero only gradually due to pressure equilibration. This source of error can be

reduced by keeping the sparger volume sufficiently small (Schumpe and Grund, 1986).

The fractional holdups and the rise velocities of two classes of bubbles were obtained from the plots of interface height as a function of time. Two such plots are shown in Figure 3.1.5. The equations for the two lines were obtained by regression analysis. The two straight lines were considered separately only when their slopes were statistically different. The initial dispersion height at time t=0 is denoted by H_{do}. After stopping the gas the dispersion height drops fast, if the large bubbles are present. At time t_1 the rear end of the large bubble swarm reaches the dispersion level then at H_{d1}. In the second period only small bubbles disengage and the slope is much smaller. Then at time t_2 the rear of the small bubble reaches the clear liquid height H_L. The slope of the line in the first period corresponds to superficial gas velocity.

$$(dH_d/dt)_1 = V_g \qquad \text{.....(3.1.35)}$$

The individual holdups, the superficial gas velocities and the rise velocities for the two bubble classes can be obtained using the following relations:

$$\epsilon_{g,1} = (H_{do} - H_{d3})/H_{do} \qquad \text{.....(3.1.36)}$$

$$\epsilon_{g,s} = (H_{d3} - H_L)/H_{do} \qquad \text{.....(3.1.37)}$$

$$V_{gl} = V_g - V_{g,s} \qquad \text{.....(3.1.38)}$$

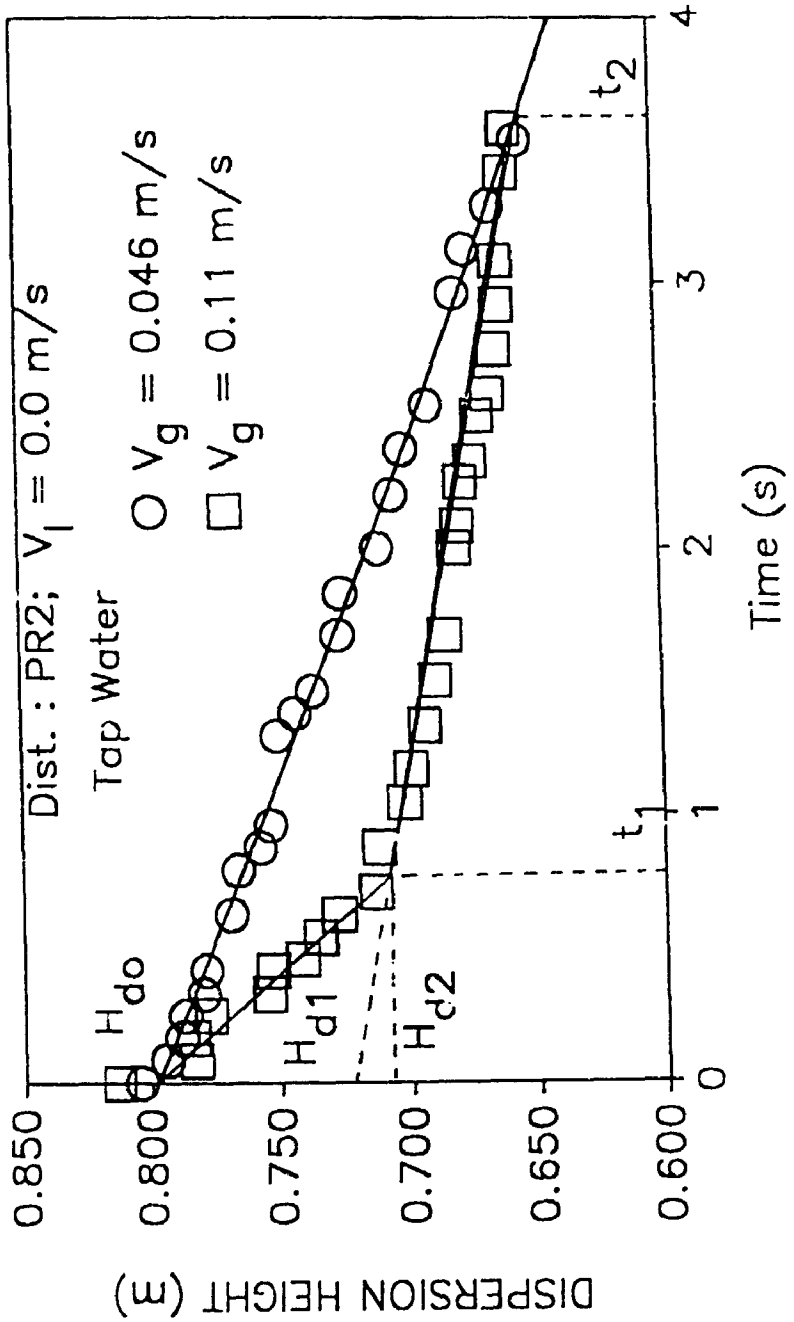

Figure 3.1.5
Plots of gas-liquid dispersion height as a function of time

$$V_{b,l} = V_{gl}/\epsilon_{g,l} \qquad \text{.....(3.1.39)}$$

$$V_{b,s} = V_{g,s}/\epsilon_{g,s} \qquad \text{.....(3.1.40)}$$

Here H_{d3} is the height which accounts for the disengagement of small bubbles during both periods. If the small bubbles disengage at the same rate in both periods then $H_{d3} = H_{d1}$; if there is no disengagement of small bubbles during the first period then $H_{d3} = H_{d2}$. The true value may, however, lie between these two extremes. The disengagement rate of the small bubbles can be accelerated by the wakes of large bubbles, while the liquid backflow due to bubble disengagement can slow their disengagement rate. These two effects can, however, compensate for each other. Schumpe amd Grund (1986) accounted for the effects of liquid backflow on the disengagement rate of the small bubbles, during the first period and proposed the following procedure to obtain H_{d3}.

$$(dH_d/dt)_{1,s} = (dH_d/dt)_2 \frac{(H_{do}-H_{d3})(H_{d1}-H_L t_1/t_2)}{H_{do}\,(H_{d1}-H_L)} \qquad \text{.....(3.1.41)}$$

$$H_{d3} = H_{d1} - t_1(dH_d/dt)_{1,s} \qquad \text{.....(3.1.42)}$$

The value of H_{d3} was obtained by an iterative procedure, using Equations 3.1.41 and 3.1.42. A value for H_{d3} was assumed and the slope calculated from Equation 3.1.41 was used to obtain next estimate of H_{d3} from Equation 3.1.42.

The values of H_{d3} were always found to be close to H_{d1} (within 2 to 4 %).

Table 3.1.4 gives the values of bubble rise velocities and fractions of large and small bubble classes obtained in tap water and solutions of an effective additive.

3.2 Three-Phase Fluidized Beds

3.2.1 Experimental Setup

Two columns of 0.08 and 0.171 m inside diameters were used for the mass transfer and phase holdup studies in three-phase fluidized beds. While most of the experiments for gas-liquid mass transfer were conducted in the smaller diameter column, all the measurements for particle-liquid mass transfer were made in the larger diameter column.

The experimental setup used for the gas-liquid mass transfer measurements in the small diameter column consisted of the same column and accessories used for the continuous bubble column study (see Figure 3.1.2).

The bed solid particles were 3.2 and 5.2 mm glass spheres with densities of 2490 and 2510 kg/m^3, respectively. The bed mass was 2.2 kg for the 3 mm particles and 2.15 kg for the 5 mm particles.

Table 3.1.4 Bubble Population Study Data

Distributor Type	Liquid Phase	Superficial Gas Velocity (m/s)	Small Bubbles Rise Velocity (m/s)	Large Bubbles Rise Velocity (m/s)	Percentage of small bubbles	Percentage of large bubbles
PR2	Tap water	0.0465	0.22	0.22		100.0
PR2	5 VPPM solution of of iso-amyl alcohol	0.0465	0.18	0.23	57.0	43.0
PR2	30 VPPM solution of iso-amyl alcohol	0.0465	0.15	0.29	86.0	14.0
SP1	Tap water	0.0465	0.26	0.42	49.0	51.0
SP1	5 VPPM solution of iso-amyl alcohol	0.0465	0.20	0.45	49.0	51.0
SP1	30 VPPM solution of iso-amyl alcohol	0.0465	0.22	0.47	62.5	37.5

The liquid entered the column through two 12.5 mm I.D. nozzles which were each fitted with a tee at the top in order to minimize any jetting effects. The liquid outlet from the column went to the drain during mass transfer measurements. For each run a fresh batch of liquid was taken in the tank. It was then recirculated through the column with air sparging maintained to increase the dissolved oxygen concentration. The temperature of the liquid was maintained at 20.0±1 degrees Celsius during the runs.

Two types of gas distributors were used namely: sparger (SP1) and a porous (PR2) distributor (see Table 3.1.2 for details). Tap water was used as the coalescing liquid phase and low concentrations of iso-amyl alcohol (5 and 30 vppm) were used to inhibit coalescence. The liquid flow rate was measured with an elbow meter.

The gas phase for mass transfer measurements was alternatively oil-free compressed air and oxygen-free nitrogen (Oxygen < 5 ppm) from cylinders supplied by Cannox. The nitrogen flowrate was measured with a rotameter (for calibration see Appendix-4).

Nine probes were available to sample liquid from the column (see section 3.1.2 for the details). The probes could be moved back and forth to facilitate sampling from different radial positions. All these probes could be moved along diameters which were located in the same vertical plane. In most cases, the fourth sampling probe

was used to collect the liquid sample from the bed (height from the top of bottom flange: 0.26 m). The location of the sampling probe was selected to minimize the distributor effects and to avoid the oxygen concentration in the liquid to drop below the detection limit of the oxygen meter. A sampling port was also available to collect liquid sample from a different angular position (90^{o} from the probe vertical plane). Its distance from the top of the bottom flange was around 0.3 m.

Of the nine pressure taps installed along the column wall, five were usually in the fluidized bed region. The pressure taps were connected to water manometers to measure the static pressures in the bed and in the disengaging height above the bed. There were large fluctuations of the manometers level at high gas throughputs. For improved accuracy, the capillary restrictions (0.55 mm ID and 25 mm long) were again in the tubes connecting the pressure taps to the manometers.

The liquid-solid mass transfer in co-current three-phase fluidization was investigated in a 1.76 m high column with a 0.171 m internal diameter (Figure 3.2.1). The column was made of plexiglas, to enable visual observations of the bed height and hydrodynamics. It consisted of three sections, namely: the distributor section, the study section and the solid disengagement section.

The bed solids were 5.2 mm glass spheres with a

A	WATER TANK
B	PUMP
C	WATER ROTAMETER
D	CALMING CHAMBER
E	GRID
F	COLUMN
G	WATER OVERFLOW
H	AIR ROTAMETER
I	PRESSURE TAPS
P_1/P_2	PULLEY
Q_1/Q_2	COUNTERWEIGHTS
R	PLEXIGLASS TUBE
S	MONOFILAMENT TUBE
T	PARTICLE
S_1/S_2	STOPPERS
F_1/F_2	FOAM
R	ROD
T	PIPE

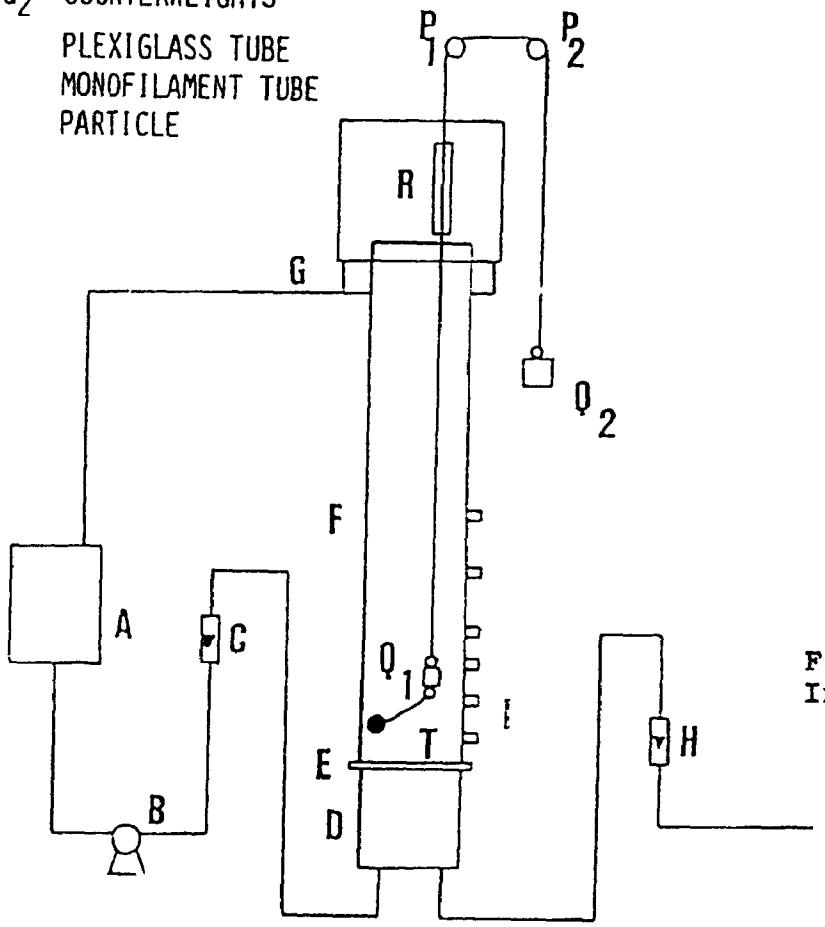

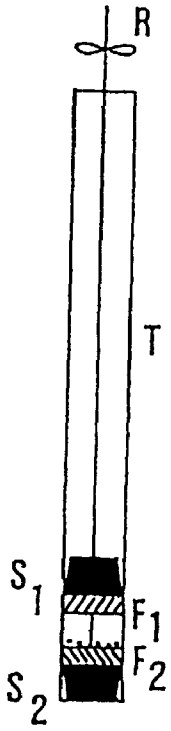

Figure 3.2.1A
Injector Tube

Figure 3.2.1
Schematic of large diameter three-phase fluidized bed column.

density of 2520 kg/m^3 and a constant mass of solids of 13.6 kg was maintained for all experiments. The settled bed height was about 0.4 m.

The liquid was an aqueous solution made with tap water which was continuously recirculated through the column via a 250 L tank. The liquid from the column flowed over a weir into a 0.3 m square box which was 0.7 m high and exited through two 32 mm inside diameter ABS pipes. The temperature of the liquid was regulated to 23.0±0.1 degrees Celsius by running an appropriate flowrate of cold water through a coil immersed in the recirculation tank ("A" on Fig. 3.2.1). The water in the column and the tank was regularly renewed (every 2 to 3 runs) to prevent any build-up of contaminants from either the active solid particles or the gas.

The oil-free compressed air from the house line was used as the gas phase and its inlet pressure was kept constant with the help of a pressure regulator.

Two types of gas and liquid distributors were used. Water entered the column at the bottom of the calming chamber through three 19 mm pipes and then passed through a 2 mm thick aluminium perforated plate which had 54 holes, 5.0 mm in diameter evenly spaced on a triangular 25 mm pitch. The perforated plate was covered with 60 mesh screen. For the first distributor, air was introduced into the liquid fluidized bed at the grid level through four 20.0 mm I.D. nozzles (see Figure 3.2.2). Introduction of

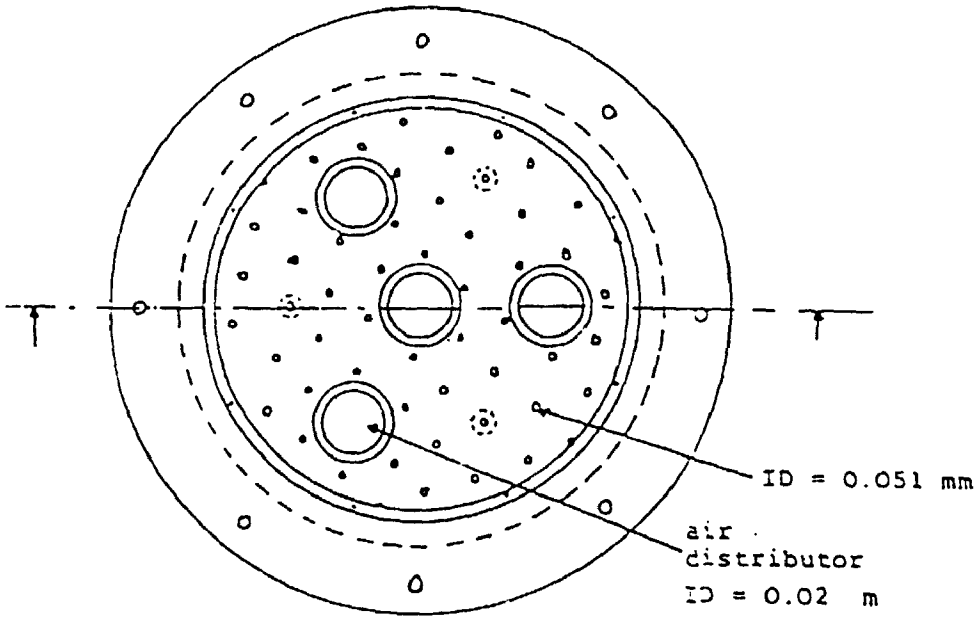

top view

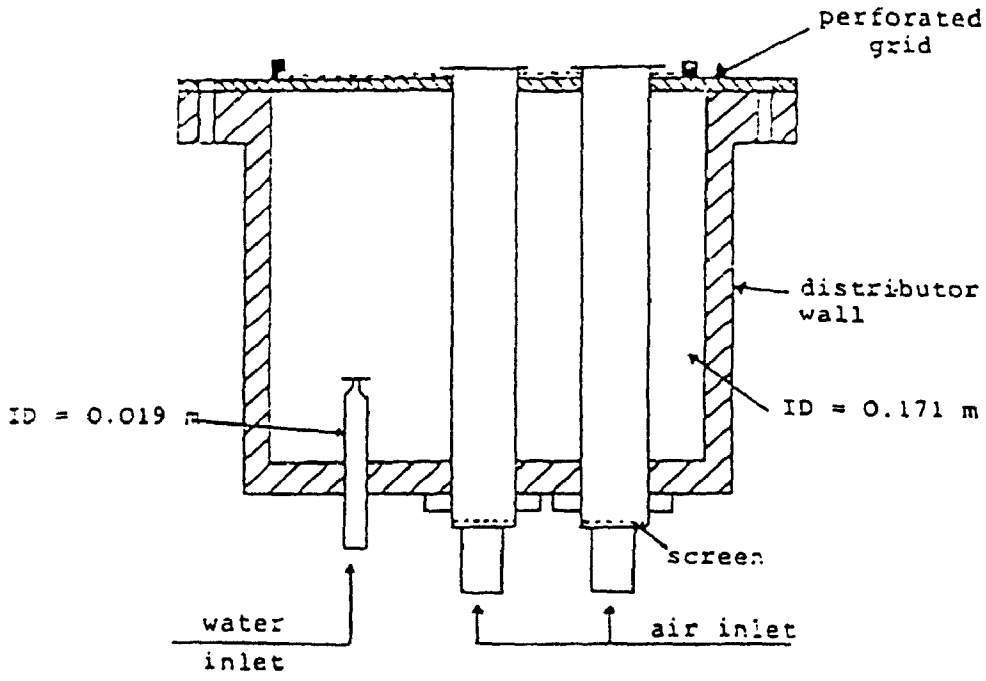

Side View Gas-Liquid Distributor

Figure 3.2.2
Gas-Liquid distributor for large diameter column

the gas through these large nozzles created jetting in the fluidized bed. In order to prevent jetting and thus improve gas and liquid distribution inside the fluidized bed, a packed bed was introduced between the grid and the bed. The packed bed was about 0.12 m high and the packings consisted of 80 Berl saddles (50 mm X 30 mm). The bed particles were then supported by a plexiglas perforated plate (fifty, 5.0 mm holes) which was covered with a 60 mesh screen.

The liquid flow rate was measured with the help of a rotameter (calibration in Appendix 17). The gas flowrate was monitored with the help of four rotameters, one each for the four inlet nozzles (see Appendix-18 for calibrations).

Tap water was used as the coalescing liquid and dilute solutions of benzoic acid (50 to 1100 wppm) and methyl iso-butyl ketone (100 to 200 wppm) were the noncoalescing liquids. Carboxy methyl cellulose (CMC) was used to change the viscosity of the liquid from 0.97 to 1.7 cp.

Twelve pressure taps were installed along the wall of the column. The distance between the lower eight consecutive pressure taps was 0.08 m and 0.016 m for the next four taps. The pressure taps were connected to water manometers with 5 mm I.D. plastic tubing to measure the static pressure in the bed and the disengaging section above the bed. The level fluctuations in the manometers

were minimized by pinching the plastic tubing with suitable clamps, ensuring, however, that there was no blockage of flow. The temperature inside the bed was measured by means of a thermocouple inserted through a port. The thermocouple was connected to a digital display meter which was capable of reading the temperature to the first decimal.

A few gas-liquid mass transfer measurements were also made in the large diameter column, using the packed bed distributor. For these experiments, tap water was used as the coalescing liquid and a dilute solution of methyl-iso-butyl-ketone (100 wppm) was the noncoalescing liquid. The gas phase was oil-free compressed air from in-house line.

The measurements for liquid mixing were conducted only in the small diameter column (0.08 m ID). The experimental technique was similar to the one used for the continuous bubble column (see section 3.1.3). A solution of methylene blue (tracer) was continuously injected through a sampling port immediately below the bed surface (fifth from bottom) at a radial location midway between column wall and centre. The liquid samples were collected from the second, third and fourth sampling ports at the midway radial location. A run was also conducted to observe qualitatively, the liquid flow patterns in the bed of 5 mm particles. The tracer solution was continuously injected close to the distributor (using lowest sampling

probe). The liquid samples were collected from near the wall, centre and midway between centre and wall using third, fourth and fifth sampling probes respectively.

3.2.2 Minimum Fluidization Velocity Measurements

The minimum fluidization velocity was determined by plotting the pressure drop across the bed as a function of superficial liquid velocity (Davidson and Harrison, 1971). The pressure drop across a fixed bed of particles increases with the superficial liquid velocity until the bed becomes fluidized. Once the bed is fluidized the pressure drop becomes equal to the bed weight per unit cross-sectional area of the column. Further increases in liquid flowrate will bring about an increase in the bed height and a decrease in the solids holdup and the bed density.

The minimum fluidization velocity can thus, be determined by plotting the measured pressure gradient as a function of the liquid flowrate: it corresponds to the superficial liquid velocity at which the change in the slope occurs (Figure 3.2.3).

Figure 3.2.3 is a plot of pressure drop in the bed as a function of superficial liquid velocity, as measured in a bed of 5 mm glass beads in 0.171 m diameter column. In order to minimize any hysteresis effects the bed was initially fluidized vigorously and the pressure drop was

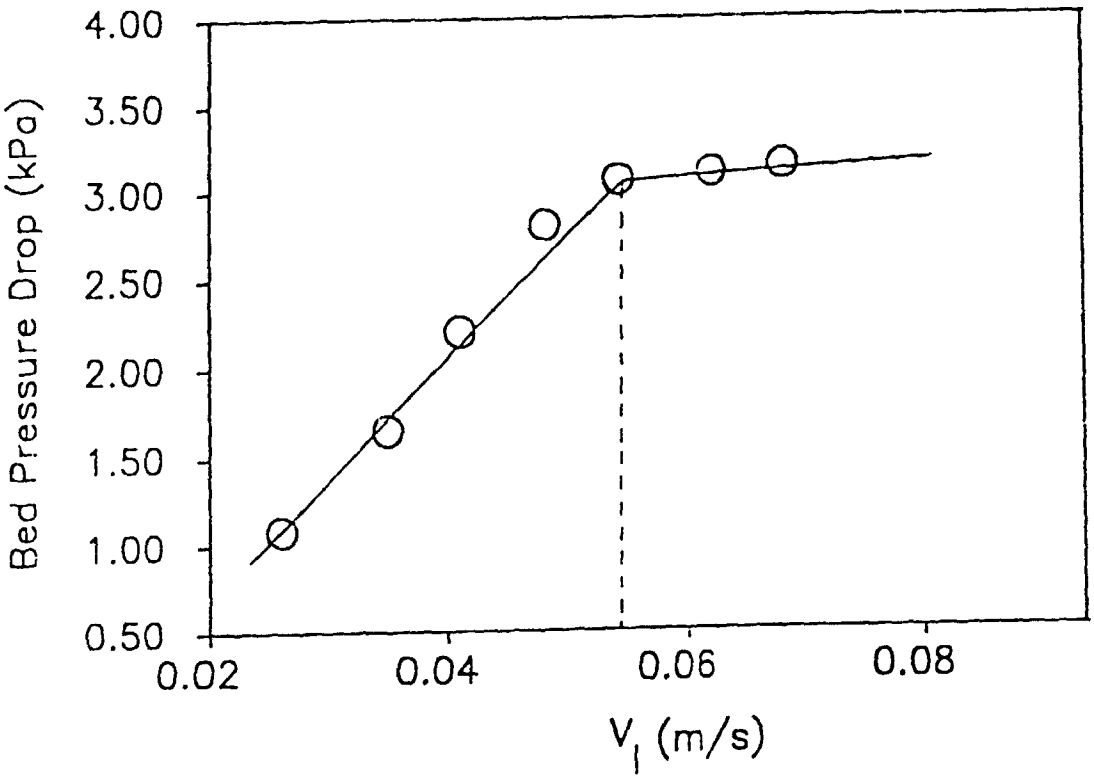

Figure 3.2.3
Determination of minimum fluidization velocity in liquid-solid fluidized bed (D_c = 0.17 m; d_p = 5 mm; Tap water)

then, measured as the liquid flowrate was gradually increased, after the bed had been defluidized.

The intersection point was determined by linear regression of the pressure drop with the flow rate for both straight lines. The minimum fluidization velocity for the 5 mm glass beads was found to be 0.051 m/s (Figure 3.2.3) while for 3 mm glass beads, it was 0.035 m/s (Figure 3.2.4). The measured values of the minimum fluidization velocity were within 6 % of the values predicted by the correlations of Wen and Yu (1966) and Lucas et al. (1986).

3.2.3 Phase Holdups and Liquid Mixing Measurements

The phase holdups in the three-phase fluidized beds were obtained from the pressure profile measurements along the column heights. The bed heights were given by the intercept of the two regression lines based on the pressure profile measurements for each run. The bed heights were also determined by visual observations, whenever possible. The solids holdups were then obtained using Equation 2.3.13. The slope of the pressure profile line in the fluidized bed region provided the pressure gradient in the bed. The liquid holdups were then determined using Equation 2.3.14, neglecting the first term on the right hand side compared to the other two. The gas holdups were then given by Equation 2.3.12.

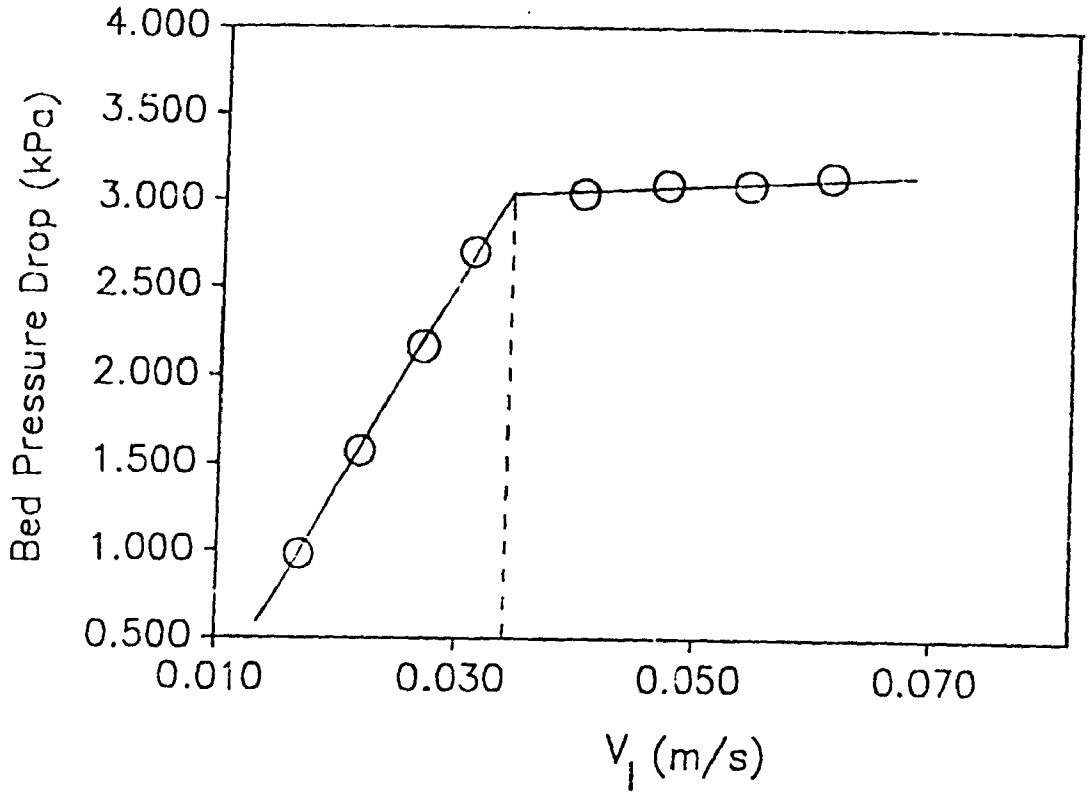

Figure 3.2.4
Determination of minimum fluidization velocity in liquid-solid fluidized bed (D_c = 0.17 m; d_p = 3 mm; Tap water)

Based on the above procedure, a computer programme (TPFBP) was written to provide the bed heights and phase holdups in the fluidized bed region and the phase holdups in the free-board region. The estimated errors for phase holdups were about 6% at low gas velocities (V_g<0.1 m/s) and around 15% at higher gas velocities. The two main sources of error were fluctuation of bed height and entrainment of particles into free-board region at high gas velocities.

The axial dispersion coefficients in the beds were obtained from the tracer concentration profiles measured upstream of the tracer injection point. The details of the procedure are similar to the one used for continuous bubble column (see section 3.1.3 for details).

3.2.4 Gas-Liquid Mass Transfer Measurement

A few gas-liquid mass transfer measurements were made in the large diameter column, using packed bed distributor. The measurement technique was based on the absorption of oxygen from air into the deoxygenated liquid (Catros, 1986). For the gas-liquid mass transfer study in the smaller column, an improved technique was used.

The experimental technique used for the measurement of gas-liquid mass transfer in the smaller diameter fluidized bed column involved desorption of oxygen from

the liquid by oxygen-free nitrogen. The oxygen concentration in the liquid was measured at the column inlet and in the three-phase fluidized bed, just below the bed surface. The liquid sample from the probe flowed into a stirred cell where the dissolved oxygen concentration was measured with the help of a polarographic probe mounted on the cell (see Figure 3.1.3A). The liquid flowrate was adjusted so as to avoid any entrainment of the gas bubbles with the liquid into the cell. It was also ensured that no gas bubbles were entrapped inside the cell. The steady-state reading of the dissolved oxygen probe was attained within 240 to 300 s and it was displayed on a digital meter.

In order to select a proper sampling location, the concentration of dissolved oxygen was measured at several radial positions in the same horizontal plane. Figure 3.2.5 shows plots of dimensionless radial concentration (c_{or}/c_{ol}) as a function of dimensionless radial position. It can be seen from Figure 3.2.5 that for different conditions the oxygen concentration was always lowest at the centre (i.e. high mass transfer rate) and highest near the wall of the column. For the data of this study the following equation was found to correlate the dimensionless radial concentration (c_{or}/c_{oc}) to the dimensionless radial position (ϕ).

$$c_{or}/c_{oc} = 1 + 0.202\ \phi^{0.5} \qquad \text{.....(3.2.1)}$$

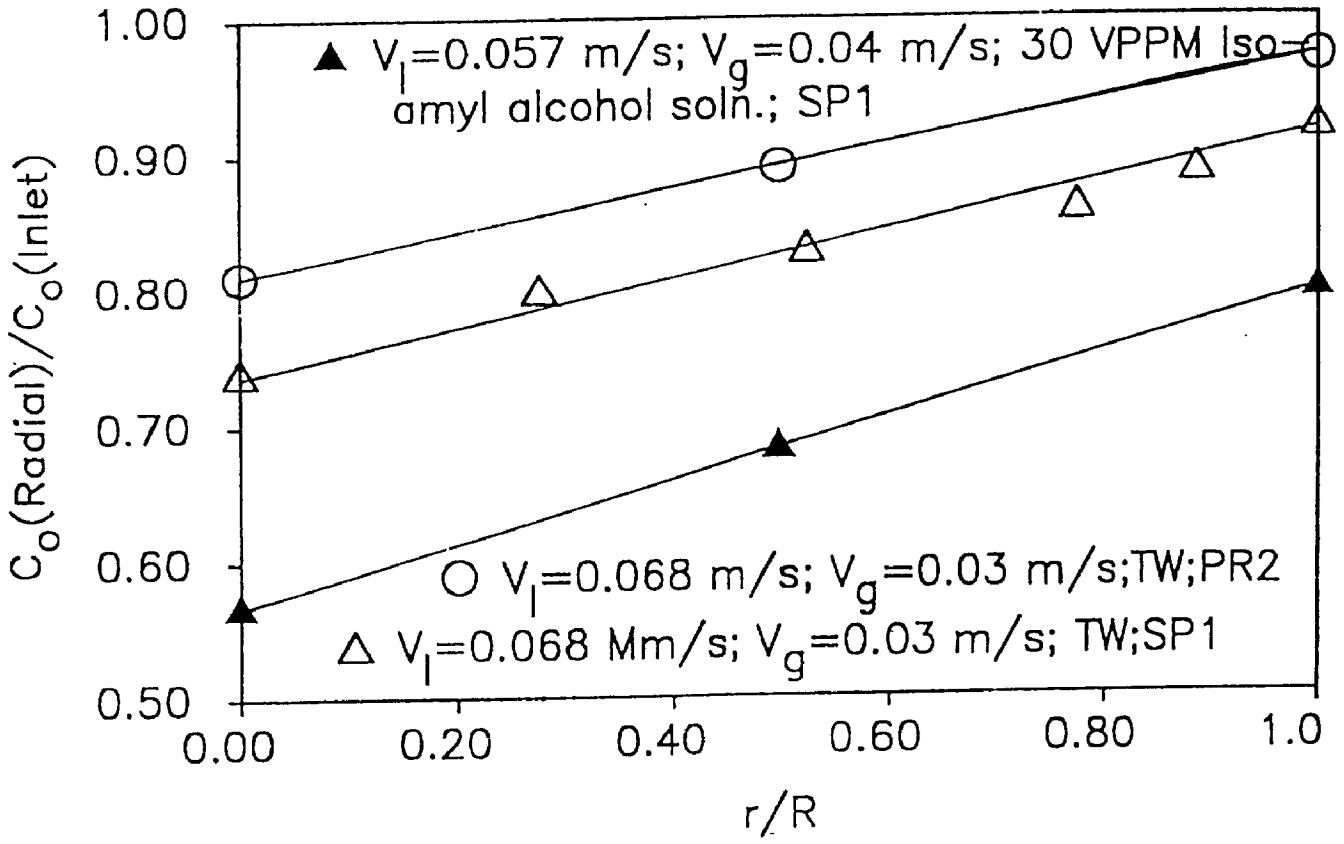

Figure 3.2.5
Dimensionless radial concentration profile as a function of dimensionless radial position (3-phase fluidized bed).

Figure 3.2.6 shows a plot of the calculated values using Equation 3.2.1 and the experimental data points. The relatively large scatter in the wall region could be due to wall effects.

The average dimensionless concentration (C_{or}/C_{oc}) in a given horizontal plane assuming there were no angular concentration profiles could be evaluated using the following procedure:

$$\left(\frac{C_{or}}{C_{oc}}\right) = \frac{1}{A_c}\int_0^R \left(\frac{C_{or}}{C_{oc}}\right) 2\pi r dr \qquad \ldots\ldots\ldots (3.2.2)$$

Equation 3.2.2 also assumed that the liquid velocity was independent of the radial position. Substituting for C_{or}/C_{oc} from Equation 3.2.1 and integrating we get:

$$(C_{or}/C_{oc}) = 1.162 \qquad \ldots\ldots\ldots (3.2.2a)$$

The radial sampling position which should provide the average concentration can be obtained from Equations 3.2.1 and 3.2.2a.

$$r_{avg.} = 0.65R \qquad \ldots\ldots\ldots (3.2.3)$$

Most of the concentration measurements for this study were made at midway between centre and wall (r=0.5R). The error due to this selection was found to be less than 2%.

Nguyen-Tien et al. (1985) measured radial concentration profiles in a bed of larger diameter (0.3 m ID). These authors approximated the radial concentration

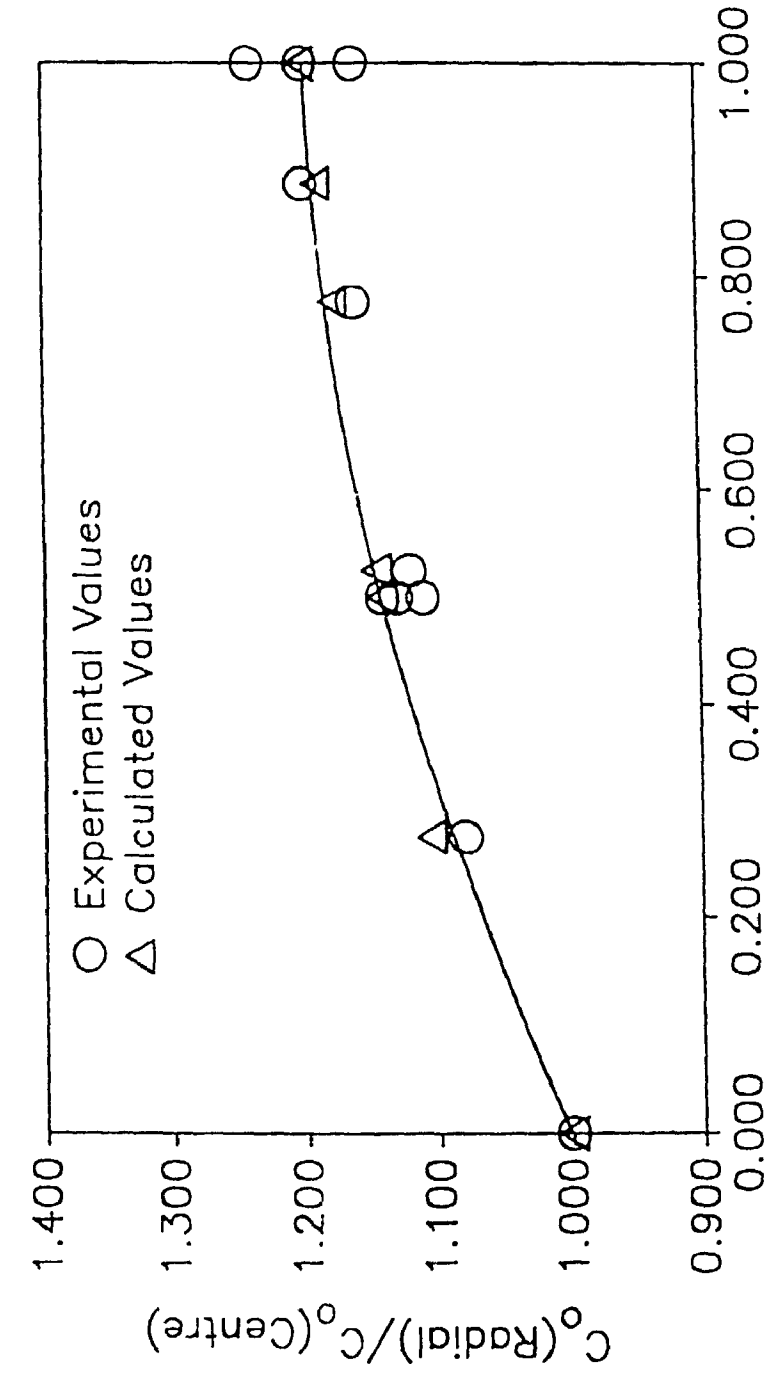

Figure 3.2.6
Comparison of experimental and calculated values of dimensionless radial concentration profile (Equation 3.2.1).

profile by a parabolic shape and the oxygen concentrations were thus measured at r/R = 0.7, since this corresponds to the average value for a parabolic profile.

In addition to radial variations, the oxygen concentration was also found to vary with the angular sampling position in the three-phase fluidized bed. The radial concentration profiles were measured for two angular positions, ninety degrees apart. The probe in the usual vertical plane was about 0.02 m higher than the probe at ninety degree orientation. Figure 3.2.7 shows dimensionless radial concentration profiles for two angular positions for tap water and a 5 vppm iso-amyl alcohol solution. It can be seen that the concentrations at ninety degree orientation are significantly lower even though the probe was at a lower vertical position.

These observations show that the situation is quite complex and could be a result of distributor effects, wall effect, bubble motion and local liquid velocity variations. The general equation of change for a differential element with physical mass transfer in cylindrical co-ordinates is given as (Ray, 1983):

$$V_{lr}\frac{\partial C_o}{\partial r} + V_{l\theta}\frac{\partial C_o}{\partial \theta} + V_{lz}\frac{\partial C_o}{\partial z} = D_r\frac{\partial(r(\partial C_o/\partial r))}{r\partial r} + D_\theta\frac{\partial^2 C_o}{r2\partial\theta 2}$$

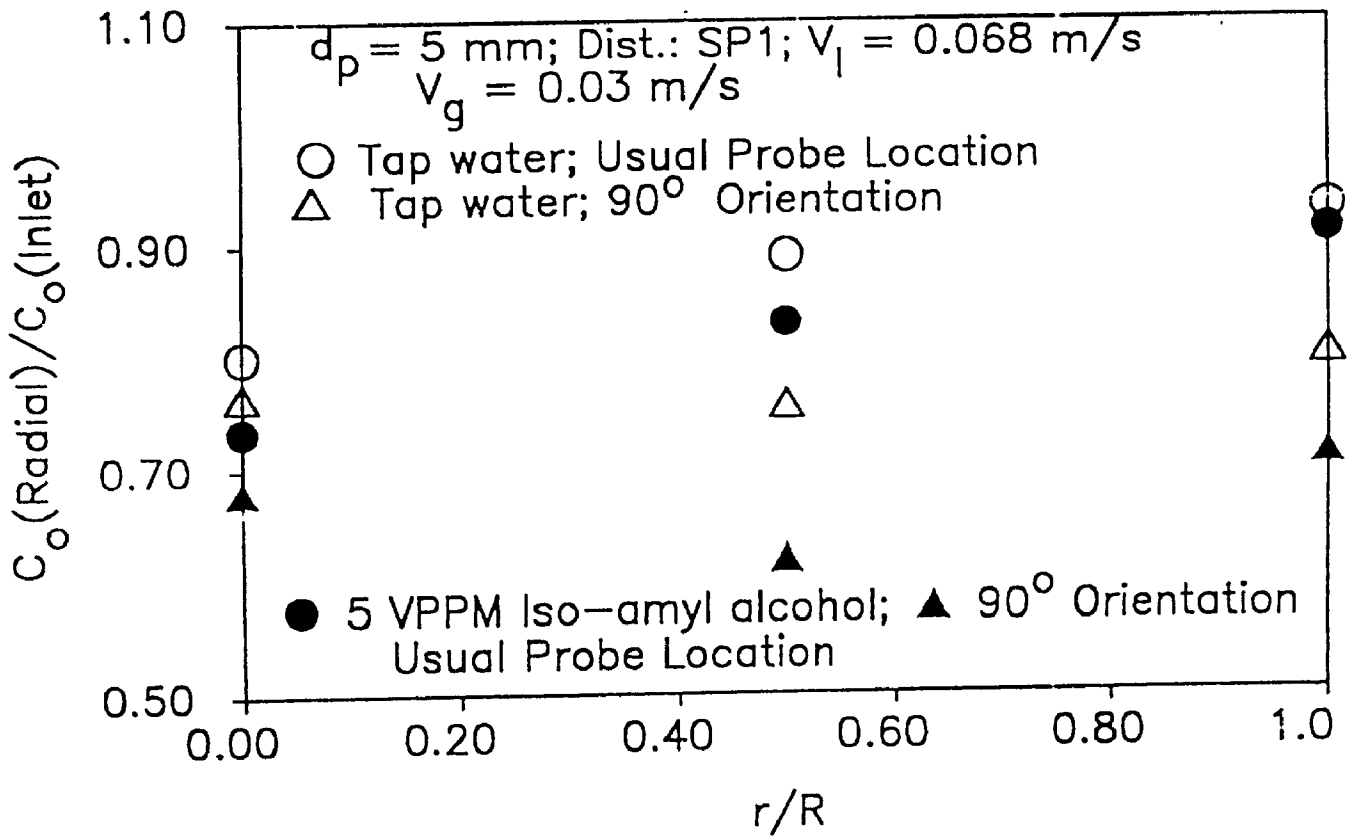

Figure 3.2.7
Plots of dimensionless radial concentration profiles for two angular positions.

$$+ D_z \frac{\partial^2 C_o}{\partial z^2} + K_l a(C_o^* - C_o)$$

.....(3.2.4)

Here V_{lr}, $V_{l\theta}$ and V_{lz} are the radial, angular and axial components of liquid velocity and D_r, D_θ and D_z are the radial, angular and axial dispersion coefficients.

There are a number of unknowns in this equation (i.e. V_{lr}, $V_{l\theta}$, D_θ, D_r), following simplifying assumptions were made to obtain the values of mass transfer coefficients which should more appropriately be called "pseudo mass transfer coefficients" from concentration measurements.

1) Axial, radial and angular mixing in the liquid could be neglected therefore plug flow conditions could be assumed. The assumption of low axial mixing in the liquid phase was justified by the measurements of this study (see section 4.2.2) and other literature studies (Dhanuka and Stepanek, 1980; Catros et al., 1985; Nguyen-Tien et al., 1985a). Dhanuka and Stepanek (1980) observed no significant differences in the estimations of volumetric mass transfer coefficient with and without the allowance for low liquid mixing in a bed of 2 mm particles. Nguyen-Tien et al. (1985a) concluded that the mass transfer coefficients obtained with their back flow cell model were in agreement with the plug flow model in the beds of large particles of this study.

Radial and angular mixing effects were also

neglected. In three-phase fluidized beds, radial mixing has been reported to be low as compared to axial mixing (El-Temtamy et al., 1979) Also, angular mixing is unlikely to be important in three-phase fluidized beds of large particles used for this study.

2) The effects of radial concentration profile were accounted for by the selection of a suitable sampling location for the concentration measurements (Equation 3.2.3). However, the angular variations in the concentration profile could not be accounted for due to lack of sufficient measurements at different angular positions.

The above assumptions reduce Equations 3.2.4 to well known plug flow model. Replacing V_{lz} by superficial liquid velocity (V_l) we get:

$$V_l \frac{dC_o}{dz} = k_l a \ (C_o^* - C_o) \qquad \text{.....(3.2.5)}$$

Since there was no significant effect of the oxygen concentration buildup on the mass transfer rate (see Appendix-12), the value of C_o^* could be neglected. If C_{o1} and C_{o2} are the inlet and outlet concentrations respectively then Equation 3.2.5 can be integrated to give $k_l a$:

$$k_l a = \ln \frac{C_{o1}}{C_{o2}} \frac{V_l}{z} \qquad \ldots\ldots\ldots\ldots (3.2.6)$$

3.2.5 Liquid-Solid Mass Transfer Measurement

The various experimental techniques available for the measurement of liquid-solid mass transfer in two-phase and three-phase fluidized beds were reviewed in section 2.3.7.1 One objective of this study was to develop a technique which could be used to study liquid-solid mass transfer without altering the coalescence behavior of the liquid phase. This technique could then be used to investigate the effects of changes in coalescence behavior of the liquid on liquid-solid mass transfer.

Two experimental techniques were developed for the study of liquid-solid mass transfer, based on the dissolution rate of benzoic acid, which is controlled by particle-liquid mass transfer. Both the techniques used only a few particles coated with benzoic acid (typically less than 15) in a bed of inert glass beads. The presence of such a small fraction (< 0.05 wt. %) of active particles had a negligible effect on the concentration buildup of dissolved benzoic acid in the liquid (even after several runs the concentration of dissolved benzoic acid in the recirculated water remained less than 1 wppm). It also ensured that there was no significant effect of

the liquid flow patterns profiles in the bed on the mass transfer rate from the particles. For the present case Equation 3.2.4 reduces to:

$$V_l \frac{dC_s}{dz} = k_s a_s (C_s^* - C_s) \qquad \text{.....(3.2.7)}$$

Here, the bulk concentration of the solute (C_s) can be neglected compared to its saturation concentration (C_s^*). Integrating Equation 3.2.7 over the bed height (H_{bed}) :

$$V_l (C_{s1} - C_{s2}) = k_s a_s H_{bed} C_s^* \qquad \text{.....(3.2.8)}$$

Multiplying both sides of Equation 3.2.8 by the column cross-sectional area (A_c) :

$$Q_l (C_{s1} - C_{s2}) = k_s A_s C_s^* \qquad \text{.....(3.2.9)}$$

Since the concentrations of the dissolved solute in the liquid could not be measured accurately, the actual weight loss measurements of the active particles were used to obtain the mass transfer rate. By mass balance, the weight of the dissolved solute carried is equal to the weight loss of active solid particles in the bed. Therefore:

$$Q_l (C_{s1} - C_{s2}) = \frac{\Delta W}{\Delta t \; M_s} \qquad \text{.....(3.2.10)}$$

Then

$$k_s = \frac{\Delta w}{\Delta t A_s M_s C_s^*} \qquad \text{.....(3.2.11)}$$

The particle-liquid mass transfer coefficient (k_s) can now be calculated if the weight loss per unit area per unit time ($\Delta w/(\Delta t.A_s)$ for the particles and the solubility of benzoic acid in water are available.

In order to obtain a true average value of the mass transfer coefficient in the bed, it was ensured that there was no segregation of the particles in the bed and the active particles moved freely inside the bed. Segregation of the active particles was observed during preliminary runs when coated particles were prepared using glass cores. The density of the active particles was then lower than the density of the rest of the bed particles. In order to match the size and density of the inert bed particles and thus avoid segregation, the coated particles were prepared with an appropriate core (see Appendix-19 for details on preparation of the coated particles). Several active particles were used for each run to obtain a good average value for the weight loss per unit time. Two experimental techniques used to obtain the dissolution rate of the active particles in the bed are described in sections 3.2.5.1 and 3.2.5.2.

The literature data on the solubility of benzoic acid in water have been compared by Irandoust and Andersson (1986) and Burru (1988). Although there is some scatter,

most of the reported values are within 5% of each other. While most of the researchers have reported the solubility data at 25°C, Stephen and Stephen (1963) provide the solubility of benzoic acid at different temperatures. The solubility of benzoic acid reported by Stephen and Stephen (1963) at 25°C were within 5% of the experimental values of Kumar et al. (1978) and Burru (1988). Therefore the solubility of benzoic acid for the temperature of this study (23°C) was obtained from Stephen and Stephen (1963). Its value was 26.3 mole/m^3.

3.2.5.1 Free Floating Particles Technique

The first measurement technique used free-floating particles. Two batches of pre-weighed coated particles (6 to 8 particles per batch) were injected into the bed at preset time intervals. The injector tube is shown in Figure 3.2.1A. The stoppers (S_1 and S_2) prevented water from reaching the particles when the tube was being inserted into the bed. Foam layers (F_1 and F_2) provided a cushioning effect for the particles. The particles were injected from the top of the column and the injection tube was long enough to reach the middle of the fluidized bed. The first batch of particles remained in the bed for 240 to 300 seconds and the second batch for 60 to 120 seconds. At the end of each run, the water and air flows were stopped simultaneously and the water was drained from the

column in less than 35 s. The bed was then dumped into a container lined with foam. All the active particles were then hand picked and kept in a desiccator for at least 10 hours before they were weighed again in a microgram balance. Before weighing each particle was examined under a microscope for possible chipping of the coating during the run. Only those particles which had perfectly smooth surface were used for the weight loss calculations. Each particle was identified by a mark etched on the core of the particle. The actual weight loss per unit time in the fluidized bed was obtained by regression analysis of the two sets of weight loss data corresponding to the two batches of the particles. Figure 3.2.8 demonstrates the validity of the method, since the slope of the line from which the mass transfer was obtained is constant.

3.2.5.2 Suspended Probe Technique

For the suspended probe technique, the coated particle was suspended inside the bed with the help of a monofilament. The coated particle was tied to a weight (a cylindrical piece of brass weighing about 0.1 kg) with the help of a monofilament which was longer than the bed height. The weight was, in turn, suspended inside the bed with the help of a monofilament tied to the hook at the other end of the weight. The weight and the particle were pulled out of the bed by a counterweight attached to the other end of the monofilament. The introduction of the

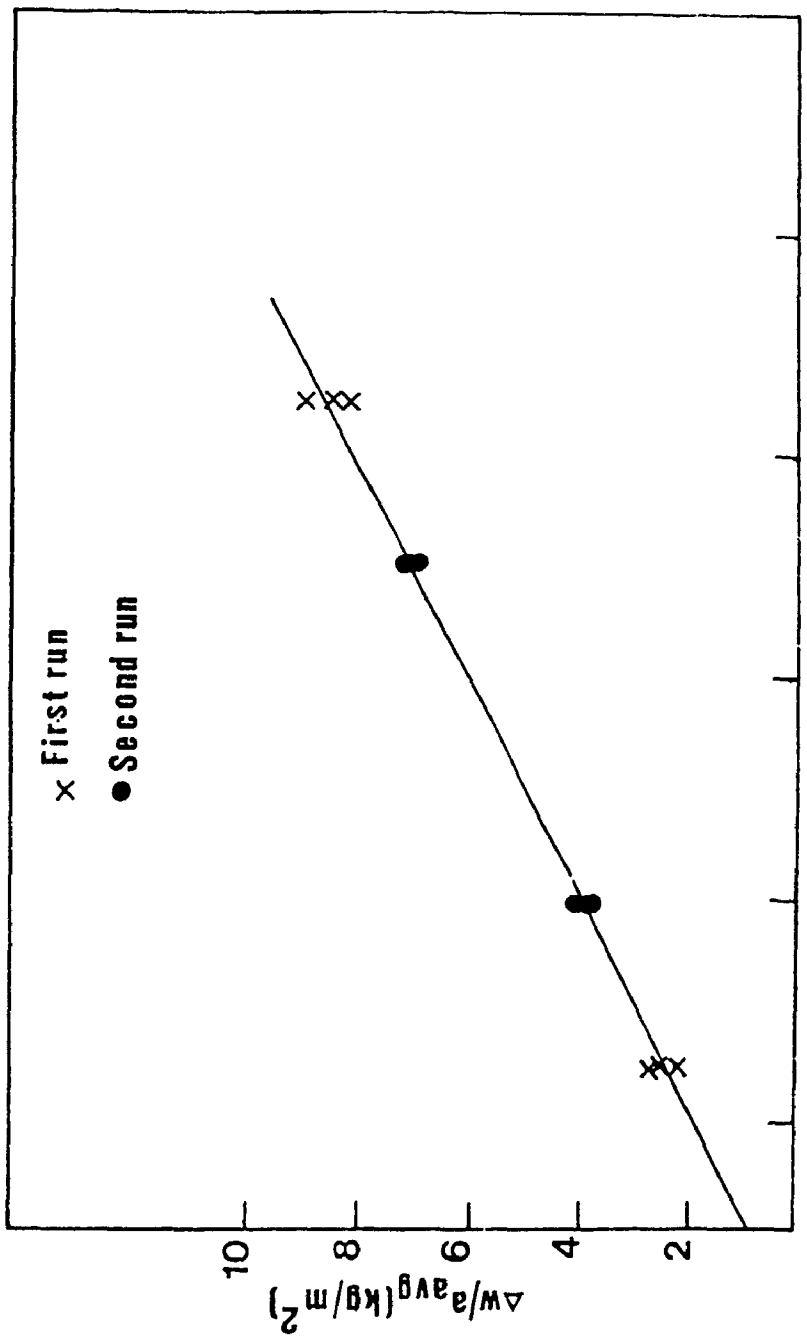

Figure 3.2.8
Plot of weight loss per unit area of particles as a function of residence time in the bed.
(Tap water; V_l = 0.06 m/s; V_g = 0.1 m/s)

particle and the weight into the bed and its removal from the bed were guided by an arrangement of pulleys and a plexiglas tube (Figure 3.2.1). For every measurement a fresh particle was introduced into the bed by dropping the weight to which it was attached into the column from a given height. It remained inside the bed for 40 to 100 s. It was then removed from the column by the counter-weight attached to the other end of the filament. The weight loss experienced by the particle while traveling in and out of the column was, thus, kept constant. For each condition, measurements were taken with four to six particles which remained in the bed for different durations.

The actual weight loss per unit time inside the bed was again obtained by regression analysis of the weight loss data obtained with individual particles for various residence times in the bed.

The diameter of each particle was calculated from its total volume which was obtained by adding the volumes of the core and the benzoic acid coating (obtained from the weight of the coating). The particle diameter thus obtained was within 2% of the value measured with a micrometer. Micrometer measurements also demonstrated that the particles had sphericities of about 0.988. The surface area of the particles decreased by less than 4% during a run and was, therefore, assumed to remain constant and equal to its mean value. The weight loss per unit of particle surface area could, thus, be calculated

for each particle. The mass transfer rate (or weight loss per unit area per unit time) could then be obtained with the techniques described earlier and the mass transfer coefficient k_s was computed using Equation 3.2.11.

3.2.5.3 Comparison of the Two Measurement Techniques.

Figure 3.2.9 compares the values of the mass transfer coefficient obtained with the two experimental techniques for various gas flow rates. It can be seen that under conditions for which there was segregation of the low density particles, the mass transfer coefficient obtained with the low density free-floating particles technique was about 15 % lower than with the suspended probe technique. It can also be seen that for gas velocities higher than 0.05 m/s, when no particle segregation occurred, the values of mass transfer coefficient obtained with the two techniques and low density particles differed by less than 5 %.

The values of mass transfer coefficients obtained with the two techniques differed by less than 5%, when the density of the coated particles was kept close (within 5%) to the density of the inert glass beads. The coated particles with the desired density were obtained by using 3 mm steel spheres as the core. Initially some coated particles were prepared by using 3 and 5 mm glass spheres as the core, and the density of these particles was 25 to 30% lower than the density of the inert glass beads. When

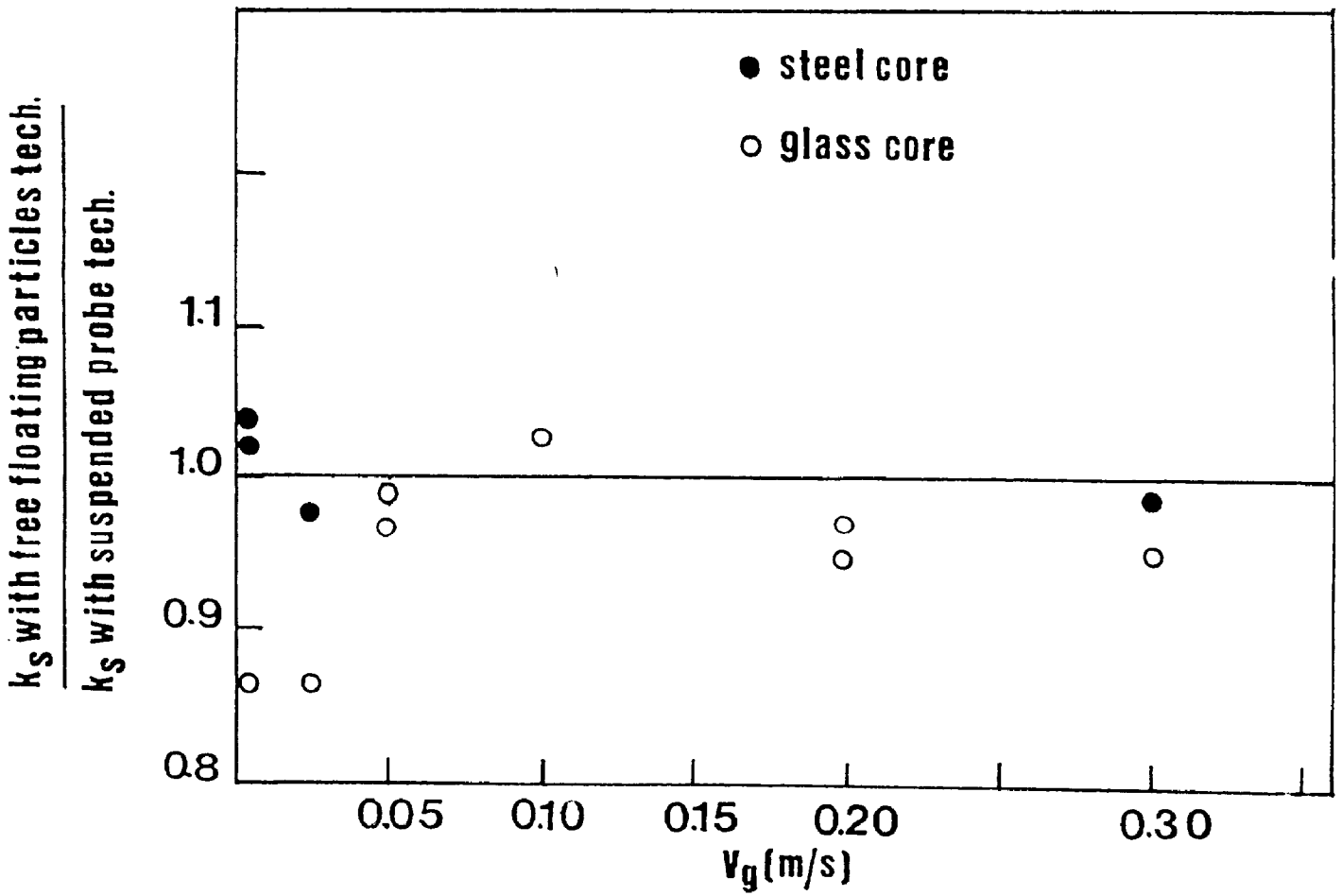

Figure 3.2.9
Ratios of particle-liquid mass transfer coefficients obtained with two techniques as a function of gas velocity. (Tap water; V_l = 0.06 m/s)

these lower density active particles were injected into the bed, they were found to segregate at the top of the bed for low gas flow rates (< 0.05 m/s). At higher gas flow rates, however, these particles were seen moving all over the bed. With the suspended probe technique, it was possible to keep even the low density particles inside the bed.

The mass transfer measurements could be affected by the day-to-day variations in the quality of tap water. In order to study these effects a few measurements of particle-liquid mass transfer were made over several weeks for a given set of conditions. As shown in Appendix-20, no significant change in the values of mass transfer coefficient was observed.

ENHANCEMENT OF GAS-LIQUID AND PARTICLE-LIQUID MASS TRANSFER IN BUBBLE COLUMNS AND THREE-PHASE FLUIDIZED BEDS

Volume-2

by

Anand Prakash

Faculty of Engineering Science

Department of Chemical and Biochemical Engineering

A thesis submitted in partial fulfilment of
the requirements for the degree of
Doctor of Philosophy

Faculty of Graduate Studies
The University of Western Ontario
London, Ontario
March 1991

TABLE OF CONTENTS

TABLE OF CONTENTS (Cont'd)

TABLE OF CONTENTS (Cont'd)

TABLE OF CONTENTS (Cont'd)

TABLE OF CONTENTS (Cont'd)

TABLE OF CONTENTS (Cont'd)

4. Results and Discussions

4.1 Bubble Columns

4.1.1 Flow Regimes

The flow regimes were studied in the batch bubble column only. From visual observations, the bubble flow regime could be easily identified with large area porous distributors (PR1,PR2). In this regime the gas holdup increased rapidly with gas velocity (Figure 4.1.1 and 4.1.9). The bubble size appeared uniform which was also confirmed by the bubble population study (see section 3.1.6). The end of bubble flow regime was marked by a sudden drop in the gas holdup, onset of transition regime (Figure 4.1.1 and 4.1.9). In the transition regime the gas holdup decreased with increasing gas flowrate. Here large bubbles could be seen moving up the column in the swarm of smaller bubbles. The heterogeneous regime was identified by violent and turbulent motion caused by the formation of fast moving large bubbles in the distributor region. The gas holdup again increased with increasing gas velocity in this regime (curve for PR2, Figure 4.1.1 and 4.1.9). The bubble population study clearly indicated that there were two classes of bubbles in this regime (see section 3.1.6). The boundaries for the flow regimes, observed with distributors PR1 and PR2 with the coalescing medium are marked on Figure 4.1.1. Due to equipment limitations, the

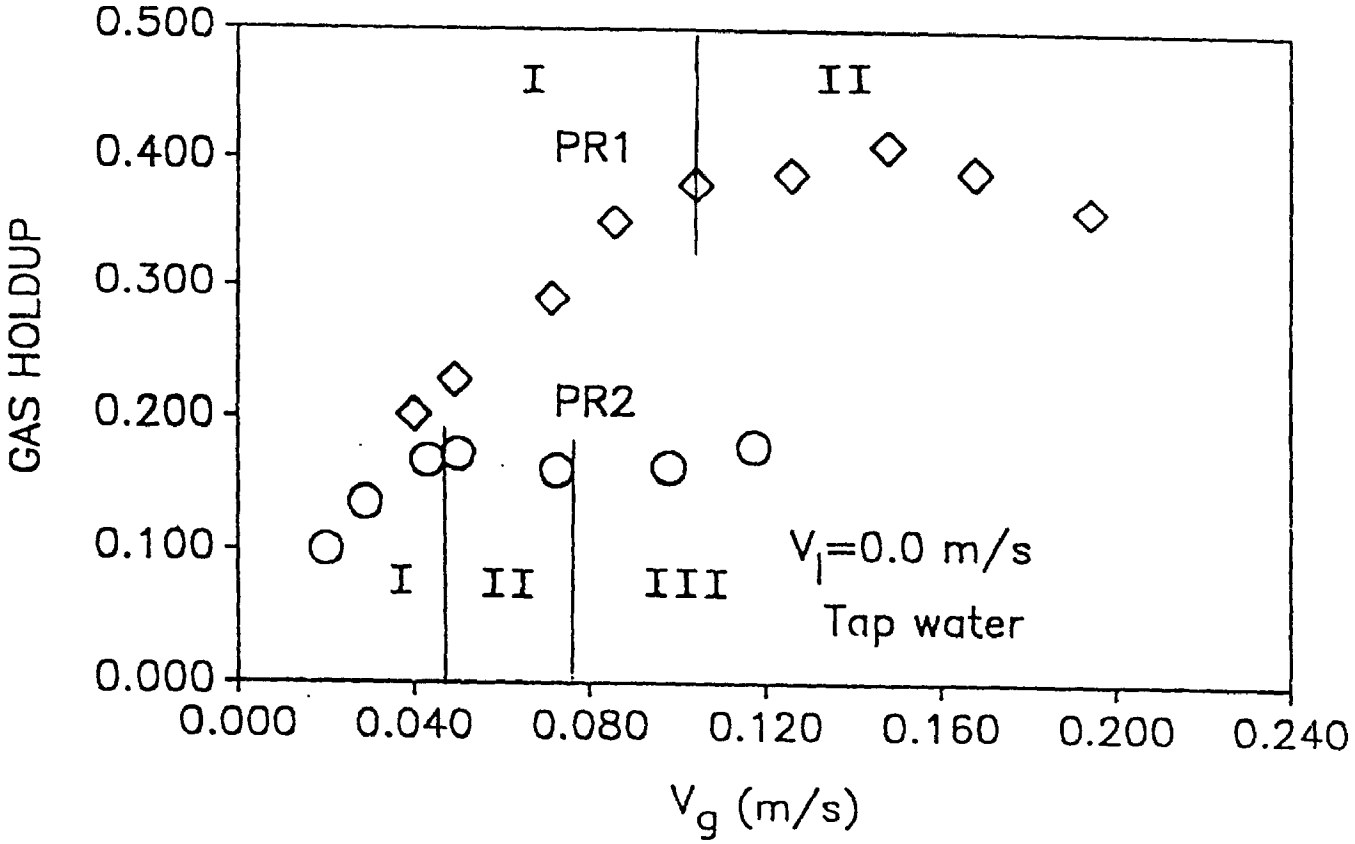

Figure 4.1.1
Flow regime mapping based on gas holdup data obtained with porous distributors

I Bubbly Flow Regime II Intermediate Regime
III Churn Turbulent Regime

fully developed heterogeneous regime could not be observed with porous distributor PR1. There was practically no effect of change in the coalescing behavior of the liquid on flow regime transition (see Figures 4.1.4 and 4.1.5).

Figure 4.1.2 and 4.1.3 are plots of drift flux versus gas holdup for different distributors in coalescing and noncoalescing liquids respectively. It can be seen that for porous distributors PR1 and PR2, the change of slope approximately corresponds to the end of bubble flow regime. Sparger SP1 and SP2 always operated in the heterogeneous flow regime.

The main difference between porous distributors and spargers is the orifice size. The small orifices of porous distributors generate small initial bubbles which grow in the distributor region due to coalescence. Bowonder and Kumar (1970) developed a model to predict the bubble size in the distributor region of porous plate distributors (see Appendix 21). This model was used in the present study to predict the bubble size coming from the distributor regions of the porous distributors at different gas flowrates. The main assumptions of the model are: 1) The effective bubbling sites are equal to the number of bubbles found simultaneously on the porous plate; 2) Constant flow conditions are assumed through active pores due to large resistance through the plate; 3) The effective sites decrease with increasing flowrate.

In the present study , the transition from bubbly

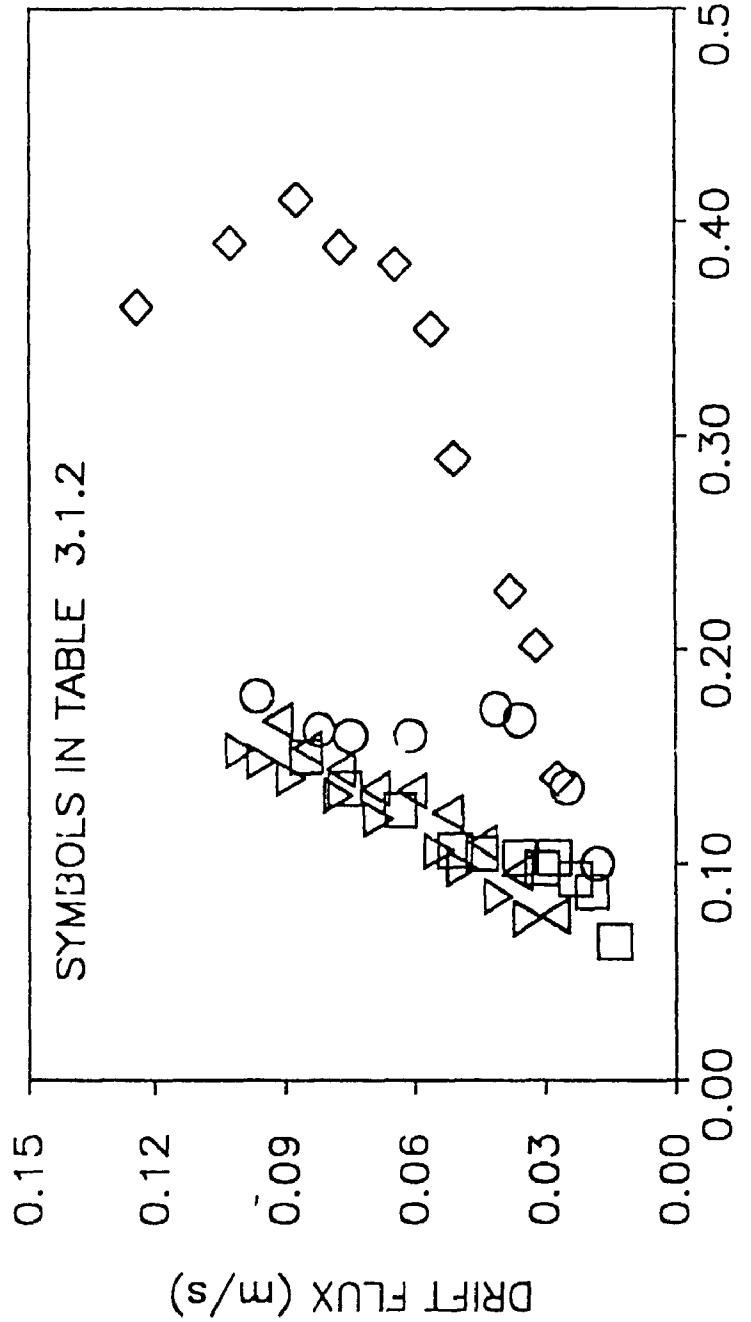

Figure 4.1.2
Plot of drift flux as a function of gas holdups
(Coalescing medium)

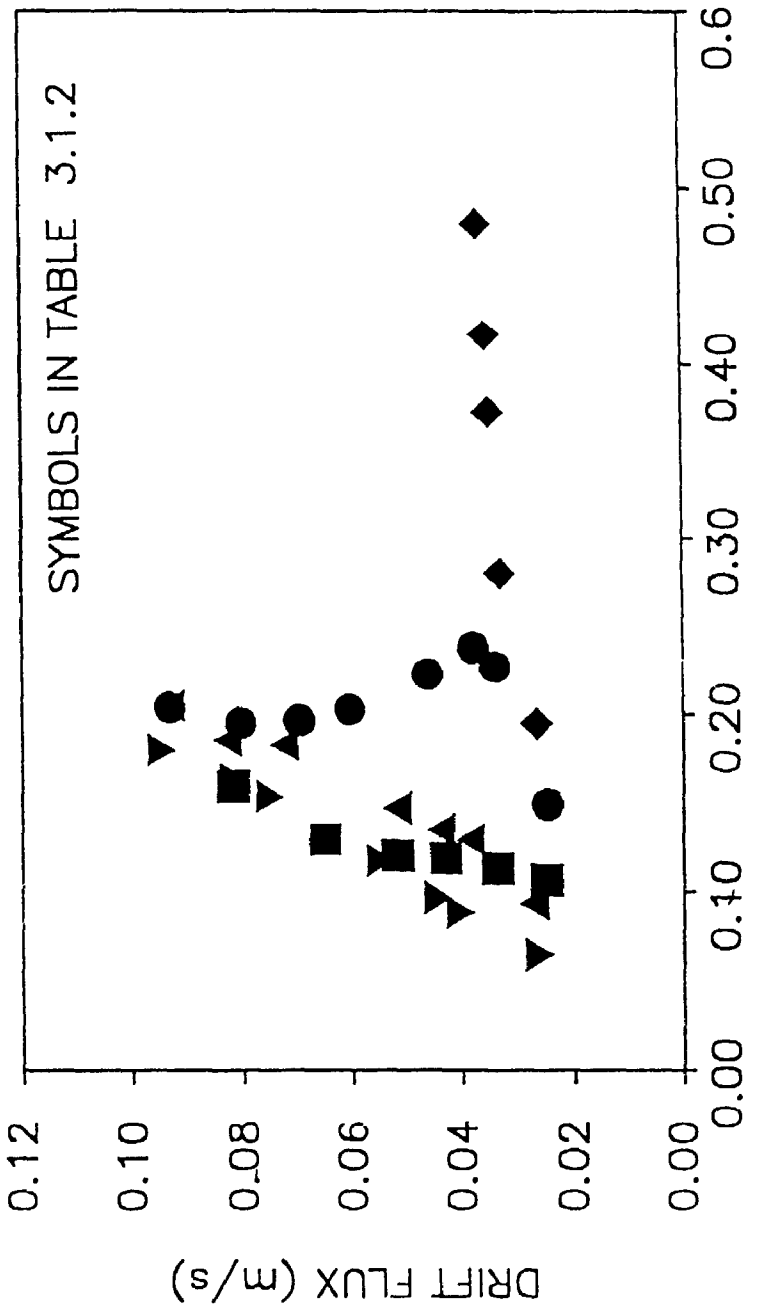

Figure 4.1.3
Plot of drift flux as a function of gas holdup
(Noncoalescing medium)

flow to the onset of heterogeneous flow in coalescing liquid was found to correspond to an initial bubble size of 6 mm. The model of Bowonder and Kumar (1970) predicted that an initial bubble size of 6 mm would be obtained for a gas velocity of 0.14 m/s for distributor PR1, 0.05 m/s for PR2 and 0.02 m/s for PR3. These values are in good agreement with the experimental transition velocities which correspond to the local maximum in gas holdup (see Figure 4.1.1). Bowonder and Kumar (1970) model does not, however, account for coalescence inhibition effects on the bubble size.

For spargers SP1 and SP2, the bubble size in the distributor region was obtained from the correlation proposed by Bhavaraju et al. (1978). The bubbly flow regime was not observed with the spargers and the size of the bubbles formed at the spargers was always larger than 6 mm. This confirms that the heterogeneous regime starts when bubbles larger than 6 mm are formed in the distributor region. This criterion holds for all distributors of this study with coalescing liquid but might not be verified for larger columns.

4.1.2 Phase Holdups

4.1.2.1 Effects of Gas and Liquid Velocities

The gas holdups were found to increase with gas velocity in bubble flow regime and heterogeneous flow

regime, while in the transition regime there was a slight decrease in gas holdup with increasing gas velocity (Figure 4.1.1). Figure 4.1.4 shows the gas holdups obtained with three distributors (SP1,SP2,PR2) in the coalescing liquid. It can be seen that with spargers (SP1,SP2), the gas holdup always increased with gas velocity. Similar effects of gas velocity on gas holdups were also observed in noncoalescing liquid (Figure 4.1.5). Figure 4.1.7 shows, how the gas holdups varied with gas velocity in the contiuous bubble column. It can be seen that the gas holdup increased continuously with gas velocity with sparger SP1, while a plateau was reached with distributor PR2 at higher gas flowrates (V_g > 0.05 m/s). Figure 4.1.7 shows the gas holdups obtained in continuous bubble column. It can be seen that with SP1 gas holdup increased continuously with gas velocity while with PR2 it slightly decreased at higher gas velocities.

The effect of liquid velocity on gas holdup is shown in Figure 4.1.6. It can be seen that initially the gas holdup decreased as the liquid flow rate was started. There was, however, very little effect of increasing liquid velocity on gas holdup.

4.1.2.2 Effects of Gas Distribution

Figure 4.1.4 compares the gas holdups obtained with the porous distributor PR2 and two spargers (SP1 and SP2) and Figure 4.1.8 compares the gas holdups obtained with

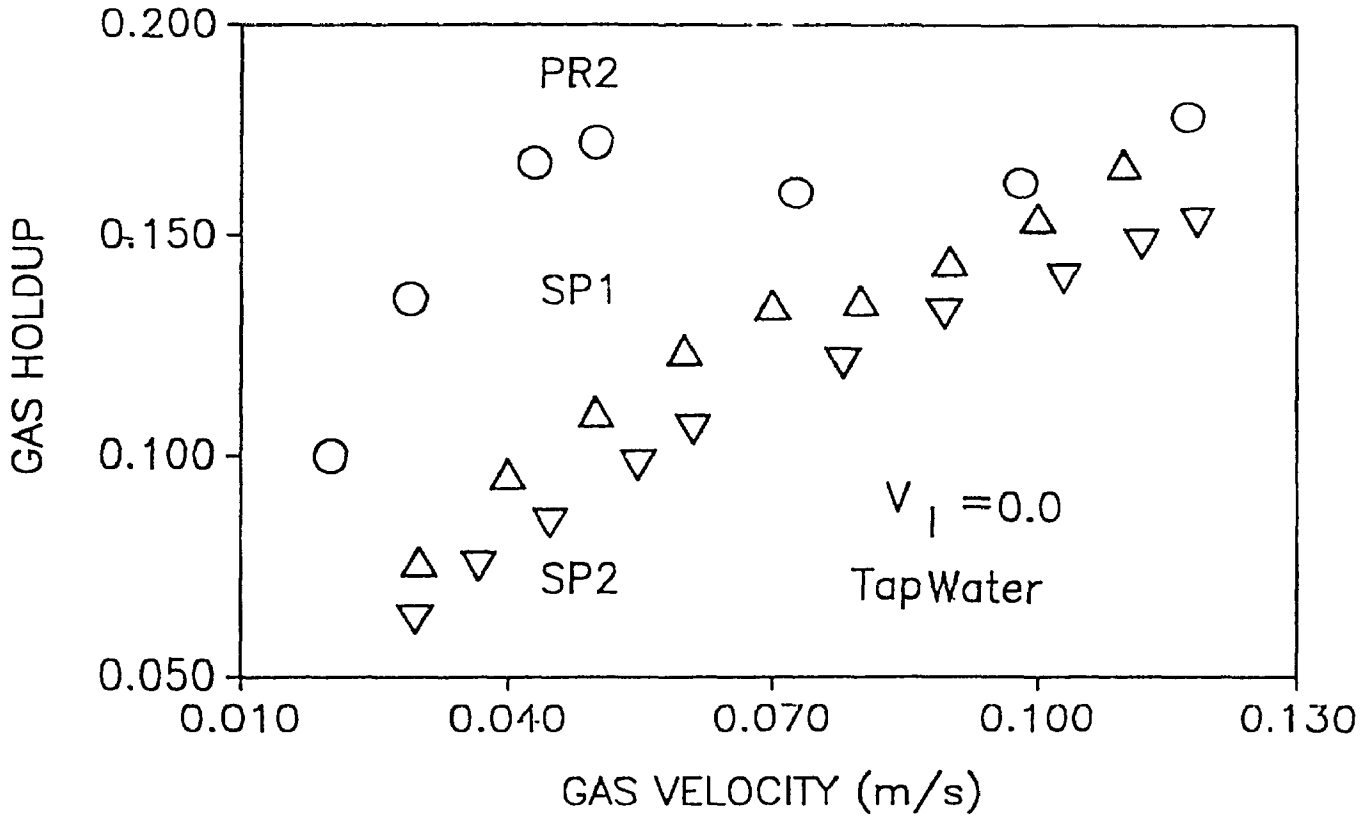

Figure 4.1.4
Comparison of gas holdups obtained with different distributors (Coalescing medium)

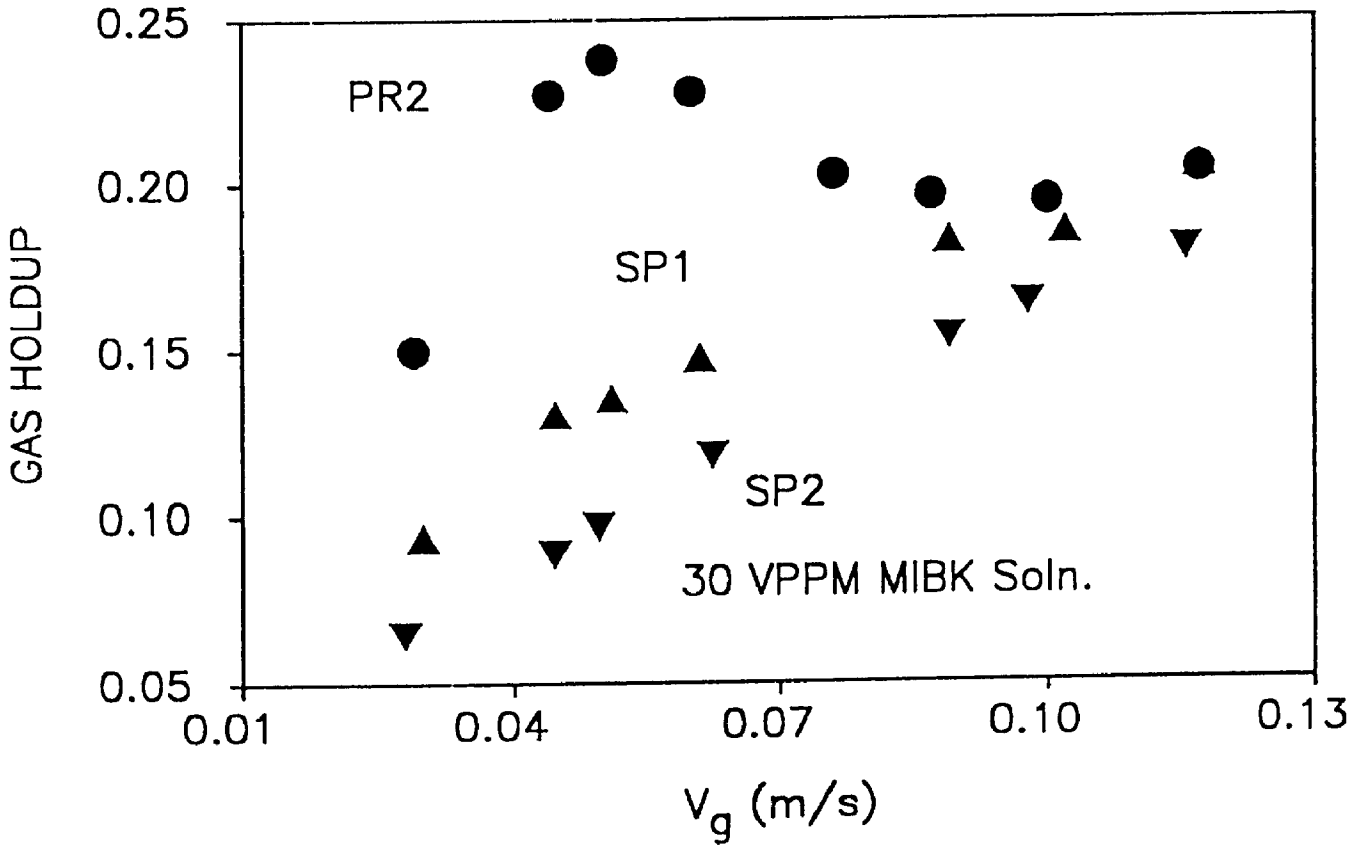

Figure 4.1.5
Comparison of gas holdup obtained with different gas distributors (Noncoalescing medium)

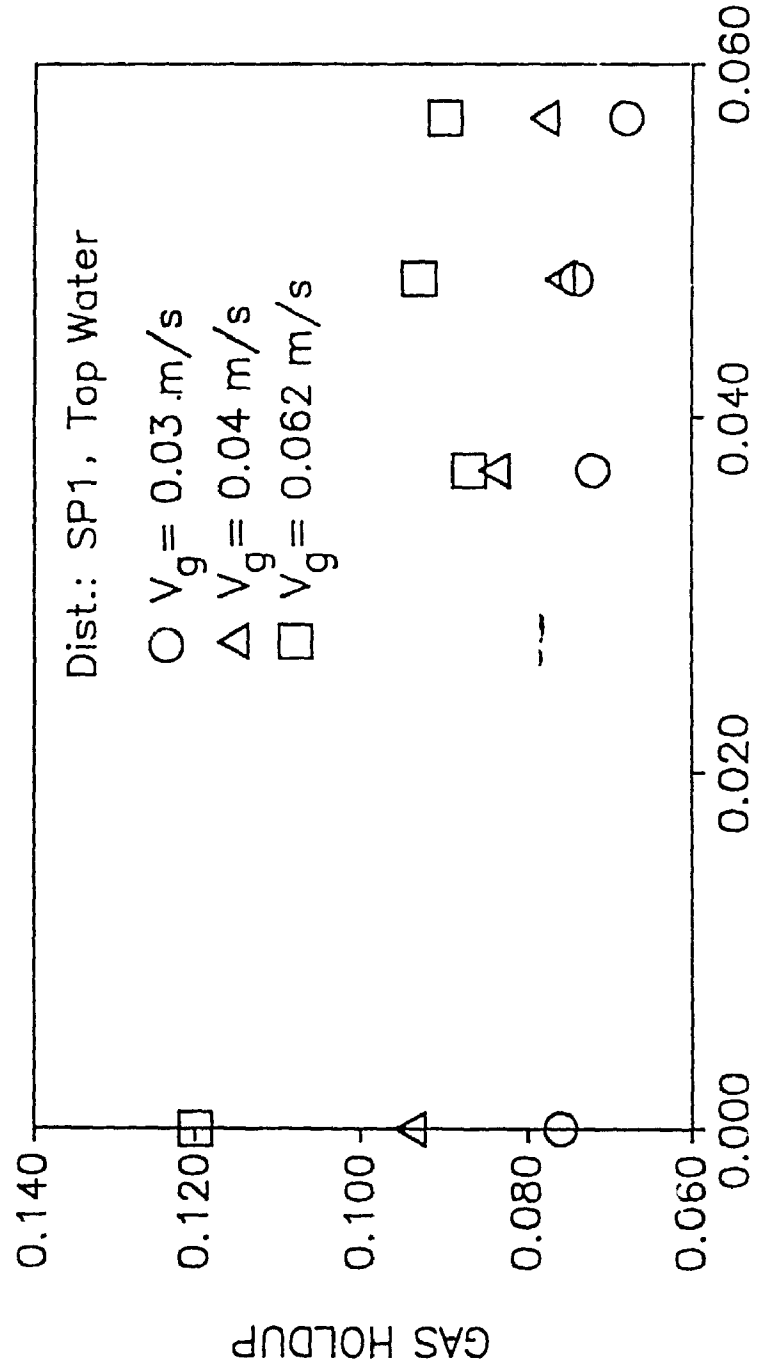

Figure 4.1.6
Effect of liquid velocity on gas holdup in bubble column

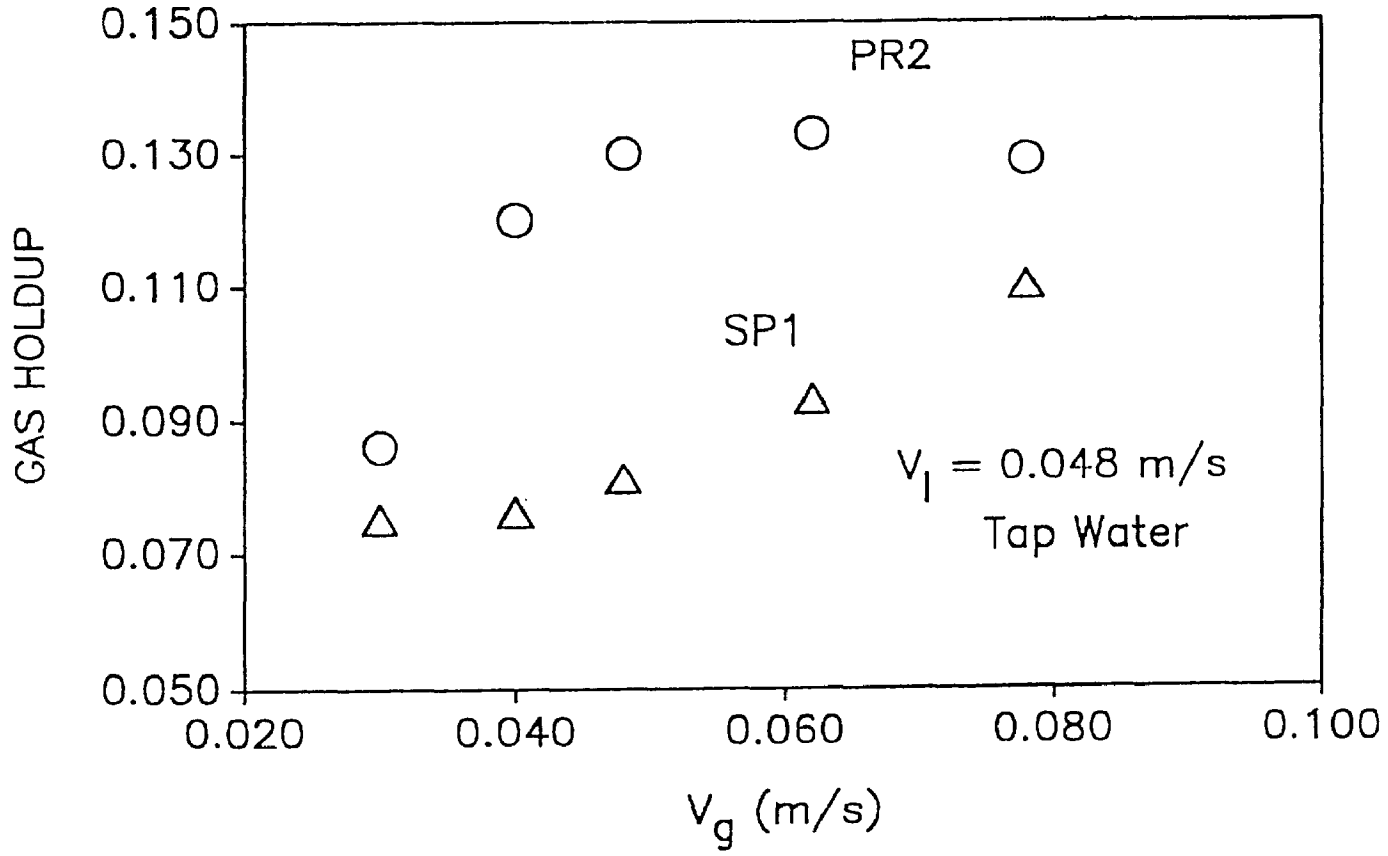

Figure 4.1.7
Effect of gas distribution on gas holdup in continuous bubble column

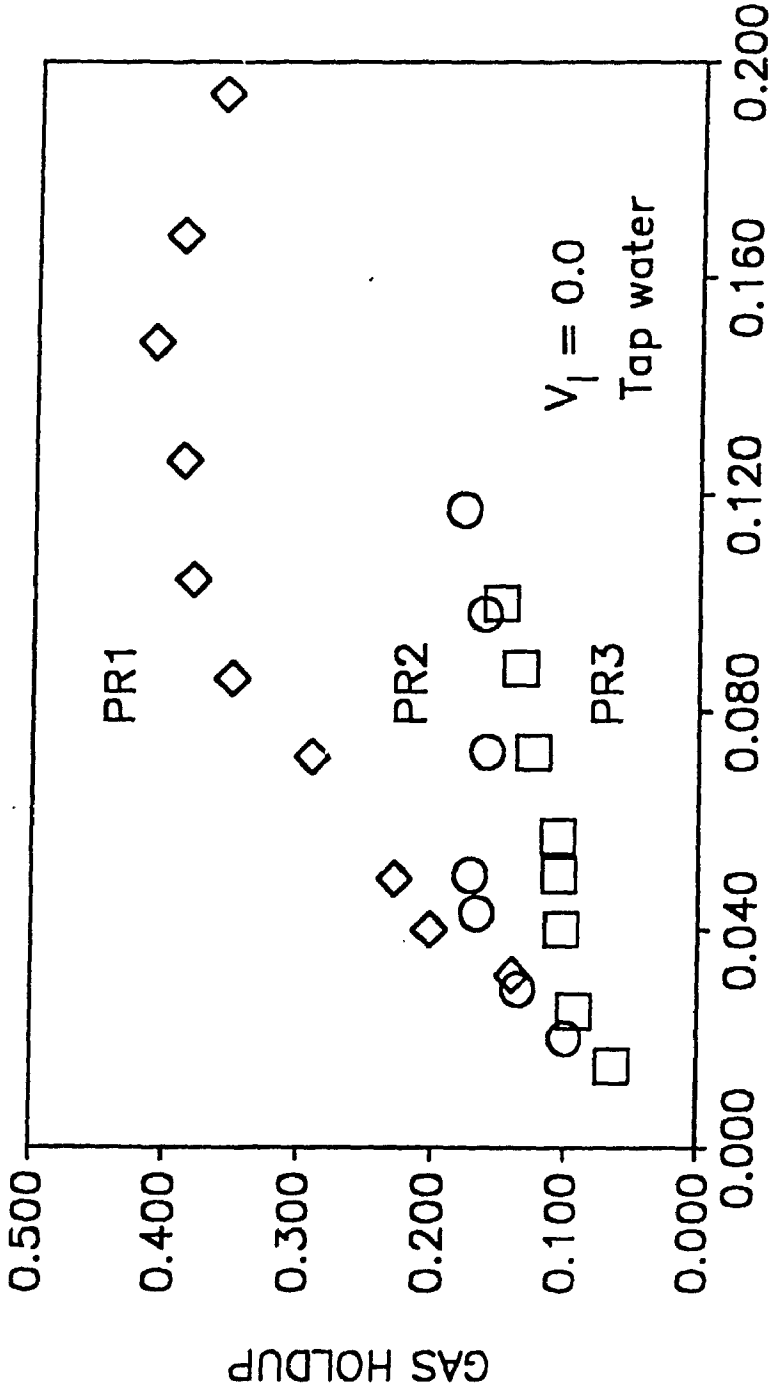

Figure 4.1.8
Effect of porous plate area on gas holdup

three porous distributors in coalescing liquid. The porous distributor PR1 gave the largest holdups. Figure 4.1.4 shows that in the bubbly flow regime and the transition flow regime the porous distributor PR2 gave significantly higher gas holdups than the four arm sparger SP1 and the ring sparger SP2. In the heterogeneous flow regime, however, all the distributors tend to come together. The porous distributor PR1 could not, however, be operated in the heterogeneous flow regime due to equipment limitations (i.e. excessive column vibrations, column overflow). Figure 4.1.4 also shows that the gas holdups obtained with the four arm sparger (SP1) were generally 10 to 15 % higher than those obtained with the ring sparger (SP2). This difference in gas holdup can mainly be attributed to the smaller bubbles issuing from the smaller holes of sparger SP1. The higher gas holdups obtained with porous distributors could also be attributed to the small size bubbles generated by these distributors in the homogeneous flow regime. Figure 4.1.7 compares the gas holdups obtained with sparger SP1 and porous distributor PR2 in a continuous bubble column. It can be seen that the gas holdups obtained with porous distributor PR2 were again significantly higher.

Figure 4.1.8 shows the effects of porous plate area on gas holdup, measurements were made with a full cross-section porous distributor (PR1) and two reduced area porous distributors (PR2 and PR3). The highest gas phase

holdups were obtained with the full cross-section porous distributor (PR1) followed by the intermediate distributor (PR2) and the distributor with the smallest area (PR3). It was observed that as the porous plate area was reduced the bubble concentration increased in the centre of the column. The higher bubble concentration enhanced the rate of bubble coalescence just above the distributor, resulting in larger bubbles and lower gas holdups. The end of the homogeneous flow regime, which corresponds to the maximum gas holdup was therefore reached at a lower gas velocity when the distributor area was reduced (Figure 4.1.8).

4.1.2.3 Effects of Coalescence Inhibitors

The gas holdups were found to depend on the type of additive present in the liquid phase. The gas holdups obtained in the dilute solutions of methyl-iso-butyl ketone and iso-amyl alcohol were significantly higher (20 to 60 %) than in the coalescing liquid phase (see Figures 4.1.9 and 4.1.10). In the dilute solutions of 2-decanone, the gas holdups were generally close to the tap water values (± 10 %). These results clearly show that gas holdups in bubble columns are strongly affected by the type of the additive present in the liquid phase. The higher gas holdups obtained in the solutions of MIBK and iso-amyl alcohol could be attributed to the strong coalescence inhibition effects of these additives (see

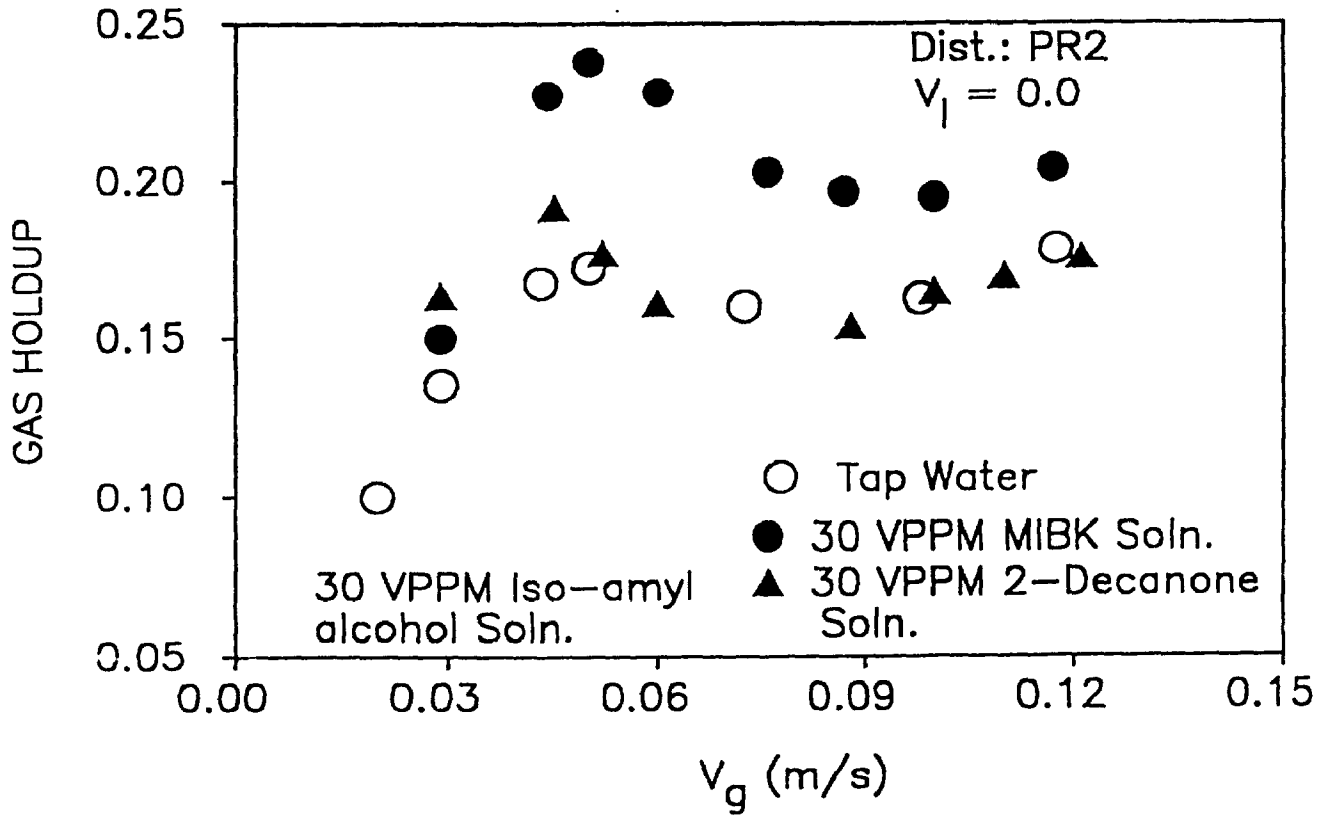

Figure 4.1.9
Comparison of gas holdups obtained with distributor PR2 in dilute solutions of MIBK and 2-Decanone

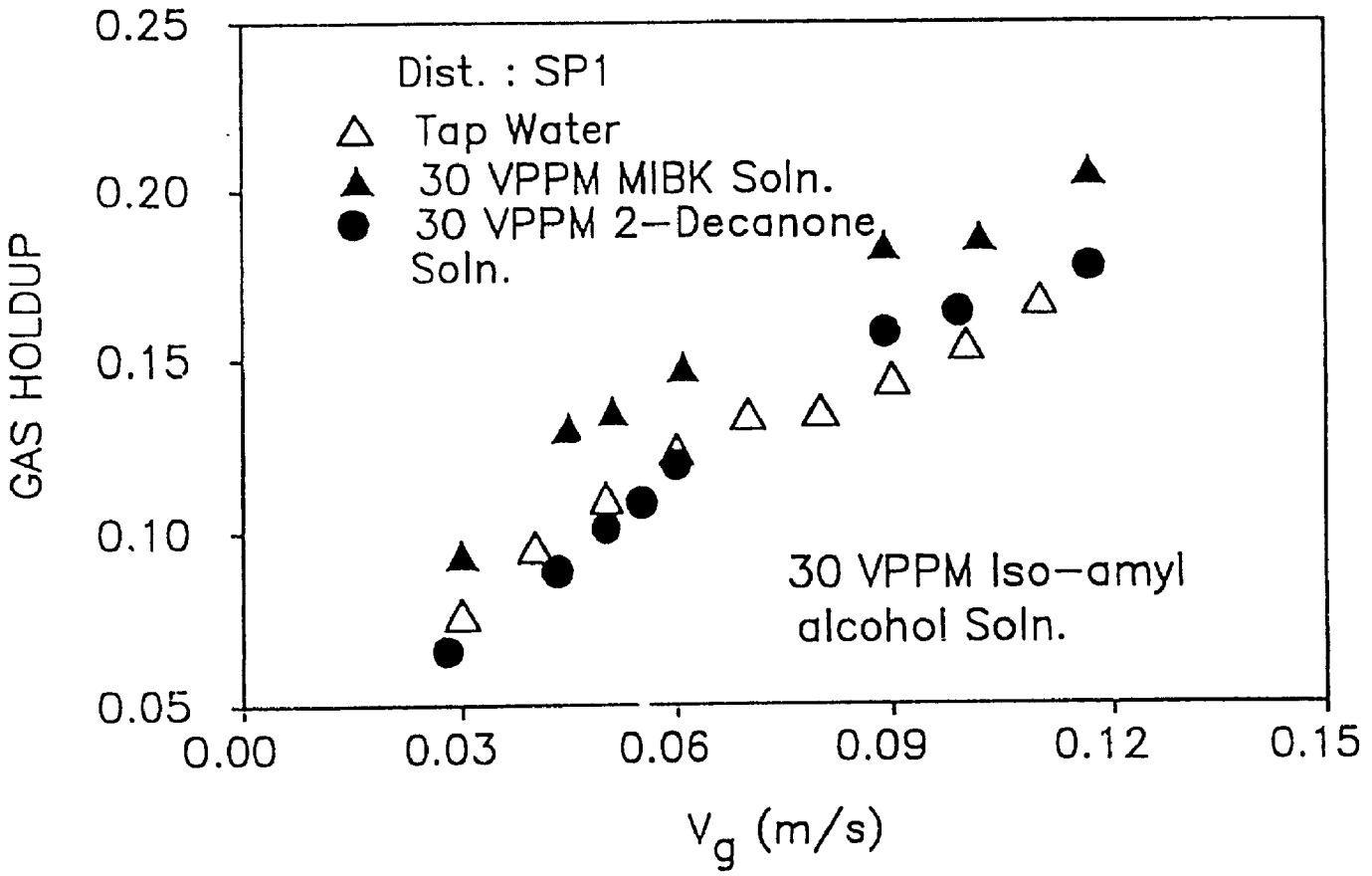

Figure 4.1.10
Comparison of gas holdups obtained with distributor SP1 in dilute solutions of MIBK and 2-Decanone

section 5.1). The solution of 2-decanone on the other hand showed either mild coalescence inhibition effects at low gas veloities (V_g < 0.05 m/s) and some coalescence promotion effects at higher gas flowrates. The gas holdups in the additive solutions varied with gas velocity in the same manner as in the coalescing medium. In particular, a maximum in the gas holdup with distributor PR2 was obtained at a gas velocity of 0.05 m/s in all cases (Figure 4.1.9). This again confirms that the flow regime transition was not affected by the presence of coalescence inhibitors in liquid.

Figure 4.1.11 shows how the gas holdups varied with additive concentrations. It can be seen that the gas holdup in MIBK solutions increased with the additive concentration. The rate of increase, however, was very sharp up to a concentration of about 30 vppm and decreased at higher concentrations. In the solutions of 2-decanone, there was no significant change in gas holdups with increase in additive concentration.

The gas holdups were also measured in the solutions of the additives tested for the gas-liquid mass transfer. These additives were selected to investigate the effects of functional group, hydrocarbon backbone structure and hydrocarbon chain length on gas holdup and mass transfer rate. Table 4.1.1 shows how the effectiveness based on the gas holdup varied in the aqueous solutions of different additives. It can be seen that C_5 and C_6 aliphatic

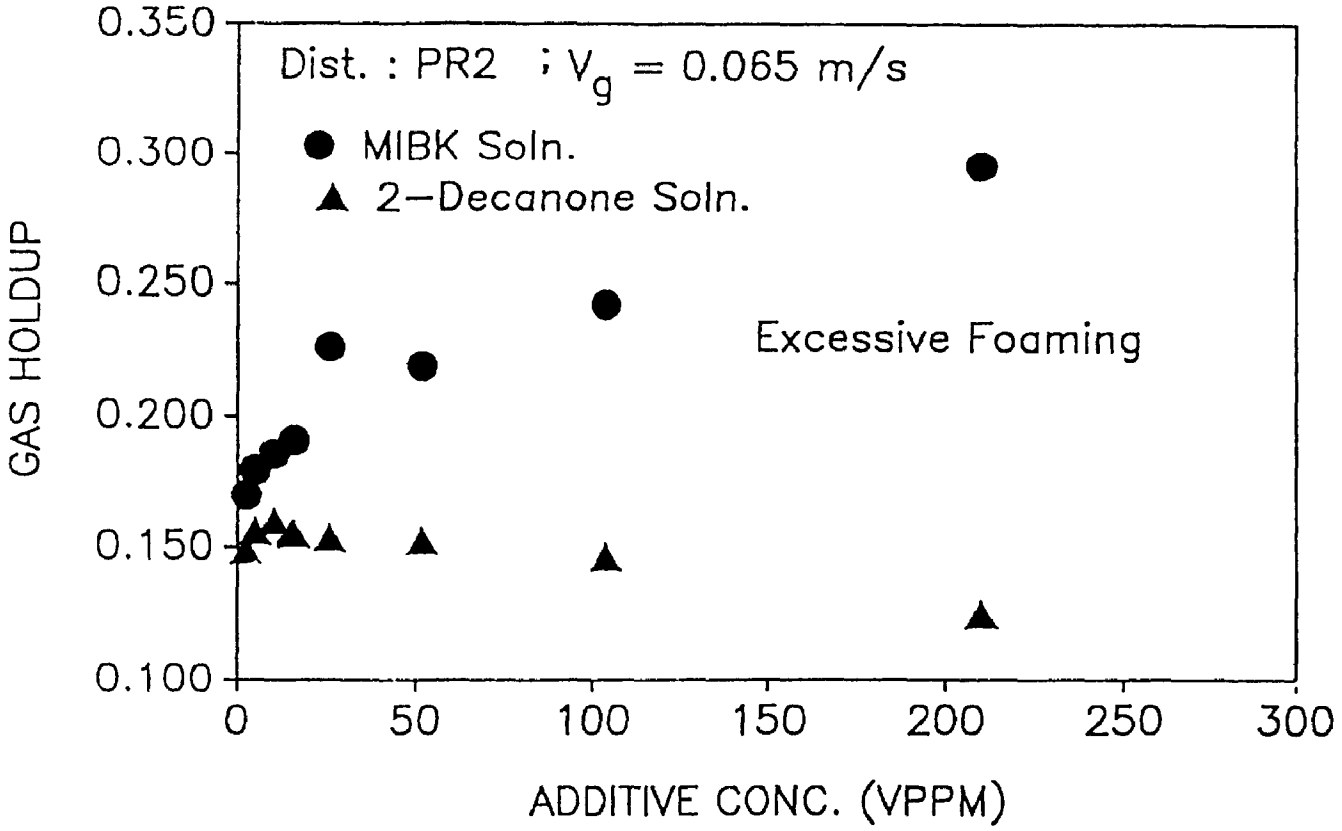

Figure 4.1.11
Effects of additive concentration on gas holdups

alcohols and ketones were very effective in increasing the gas holdup.

Table 4.1.1 Ratio of Gas Holdup in Additive Solutions to that in Tap Water (additive conc.: 50 vppm)

Additives	ϵ_g(additive soln.)/ϵ_g(tap water)			
	PR2		SP1	
	V_g=0.065 m/s	V_g=0.125 m/s	V_g=0.065 m/s	V_g=0.125 m/s
Pentanol	1.43	1.17	1.42	1.14
Iso-amyl alcohol	1.4	1.21	1.46	1.16
Ter-amyl alcohol	1.4	1.17	1.45	1.25
Hexanol	1.35	1.16	1.32	1.12
MIBK	1.46	1.17	1.56	1.24
Cyclohexanone	1.47	1.17	1.38	1.15
2-Hexanone	1.35	1.18	1.47	1.25
3-Hexanone	1.27	1.13	1.57	1.16
Butyl Acetate	1.17	1.12	1.6	1.16
Hexanoic Acid	1.12	1.11	1.11	1.11
Benzaldehyde	1.0	1.0	1.16	0.98
Acetophenone	1.02	1.03	1.27	1.03
Di-isopropyl ether	0.91	0.93	1.06	0.93
Tri-ethyl amine	0.85	0.96	1.2	0.96
Hexanal	0.74	0.92	1.05	0.92
Benzoic Acid	0.70	0.90	0.90	0.90

4.1.2.4 Correlations for Gas Holdup

The dependence of gas holdup on gas velocity in a given flow regime is generally of the form given by the equation below.

$$\epsilon_g = C_1 V_g^m \qquad \text{.....(2.2.7)}$$

The present study showed that for a given sparger and liquid medium the gas holdup could be well correlated by an equation of this type. For the porous distributor a different correlation was required for each regime. In all cases, the values of C_1 and m were affected by the distributor type and the liquid coalescing behaviour (Table 4.1.2).

The various other correlations proposed in the literature for the prediction of gas holdup in bubble columns were reviewed in section 2.2.2.3. It was pointed out that these correlations generally do not account for the effects of gas distributor type and liquid coalescence behavior on gas holdup. The correlations proposed by Akita and Yoshida (1973) and Hikita et al. (1980) are based on numerous experimental data. They could not, however, be applied to the experimental data of this study since they do not account for the effects of sparger characteristics. Guy et al. (1986) proposed a correlation which takes into account the effects of the orifice diameter and number of sparger orifices. The gas holdups obtained in the coalescing medium with the spargers of the

Table 4.1.2 Values of Constant C_1 and Exponent m for Different Distributors

Distributor Type	Flow Regime	C_1 Coalescing medium	C_1 Noncoalescing Medium	m Coalescing Medium	m Noncoalescing Medium
PR1	Homogeneous Regime	1.94	11.94	0.73	1.2
	Intermediate Regime	0.165	-	-0.48	-
	Heterogeneous Regime	-	-	-	-
PR2	Homogeneous Regime	1.39	3.45	0.67	0.88
	Intermediate Regime	0.114	0.072	-0.136	-0.41
	Heterogeneous Regime	0.42	0.40	0.40	0.31
PR3	Homogeneous Regime	1.55	-	0.756	-
	Heterogeneous Regime	0.34	0.41	0.38	0.42
SP1	Heterogeneous Regime	0.57	0.66	0.56	0.54
SP2	Heterogeneous Regime	0.6	0.9	0.62	0.74

present study (SP1 and SP2) could be predicted within 20% of their experimental values. None of the above correlations account for the effect of distributor area on gas holdup. McManamey et al.(1984) studied the effects of gas distributor area on gas holdups in a loop type air-lift fermenter . Most of the data were obtained in the bubbly flow regime at low gas flow rates; the liquid was pure water. McManamey et al. found that for a given gas flowrate the gas holdup was proportional to the distributor area to the 0.366 power. This relationship did not however, fit the data of this study.

Since various physical properties of the liquid phase were not varied for the measurements of this study, no attempt was made to obtain general correlations. The available data for the batch bubble column were used to investigate the effects of coalescing properties of the liquid and distributor region bubble size on gas holdup in different flow regimes. The gas holdup in the bulk region should in general depend on the bubble size coming from the distributor region the coalescence rate and the break-up rate. The bubbles rising from the distributor region can either coalesce or breakup. The coalescence rate should depend on the coalescing properties of the liquid, bubble concentration and bubble size, while the break-up rate for a given liquid medium should mainly be controlled by the turbulence level. The bubble concentration and turbulence level increase with increasing gas flowrates.

The gas holdup should therefore depend on the distributor region bubble size, the gas velocity and the liquid coalescing properties. The bubble size in the distributor region of different distributors can be calculated using a proper model (see section 4.1.1). The coalescing properties of the liquid depend on the type and concentration of the additive in the liquid (see section 5.1).

The following correlations were obtained to describe the gas holdup in the bubbly and heterogeneous regime in the coalescing media.

Homogeneous (or bubbly flow) regime :

$$\epsilon_g = 0.033\ V_g^{0.87}\ d_{bo}^{-0.83} \qquad \text{.....(4.1.1)}$$

$$R^2=0.99$$

Heterogeneous regime :

$$\epsilon_g = 0.364\ V_g^{0.64}\ d_{bo}^{-0.145} \qquad \text{.....(4.1.2)}$$

$$R^2=0.99$$

These correlations show that as observed earlier, the initial bubble size, which accounts for the effect of the gas distributor, had a much stronger effect on the gas holdup in the homogeneous regime than in the heterogeneous regime.

The heterogeneous regime correlations were developed with the data obtained with the spargers only. The experimental values of the gas holdups which were obtained with the porous distributors in the fully developed

heterogeneous regime were within 15% of the values predicted with these correlations. No correlations were developed for the transition regime since it is of little practical significance.

As shown in section 4.1.2.3, the gas holdups in various additive solutions depend on the type and concentration of the additive used. Table 4.1.1 gives the effectiveness factors which could be used to predict the gas holdups in various additive solutions, at given conditions knowing the gas holdup in tap water. More data would, however, be required at different additives concentrations and gas velocities to present a more general approach for the prediction of gas holdup in additive solutions.

4.1.3 Volumetric Mass Transfer Coefficient

4.1.3.1 Effects of Gas and Liquid Velocities

As the gas phase holdup, the volumetric mass transfer coefficient in the coalescing liquid increased with gas velocity in homogeneous and heterogeneous regimes, while in the transition regime there was a slight decrease with increasing gas velocity (Figure 4.1.12 and 4.1.13). Figure 4.1.14 shows that there was a slight effect of liquid velocity on the volumetric mass transfer coefficient. This could mainly be attributed to the higher turbulence level

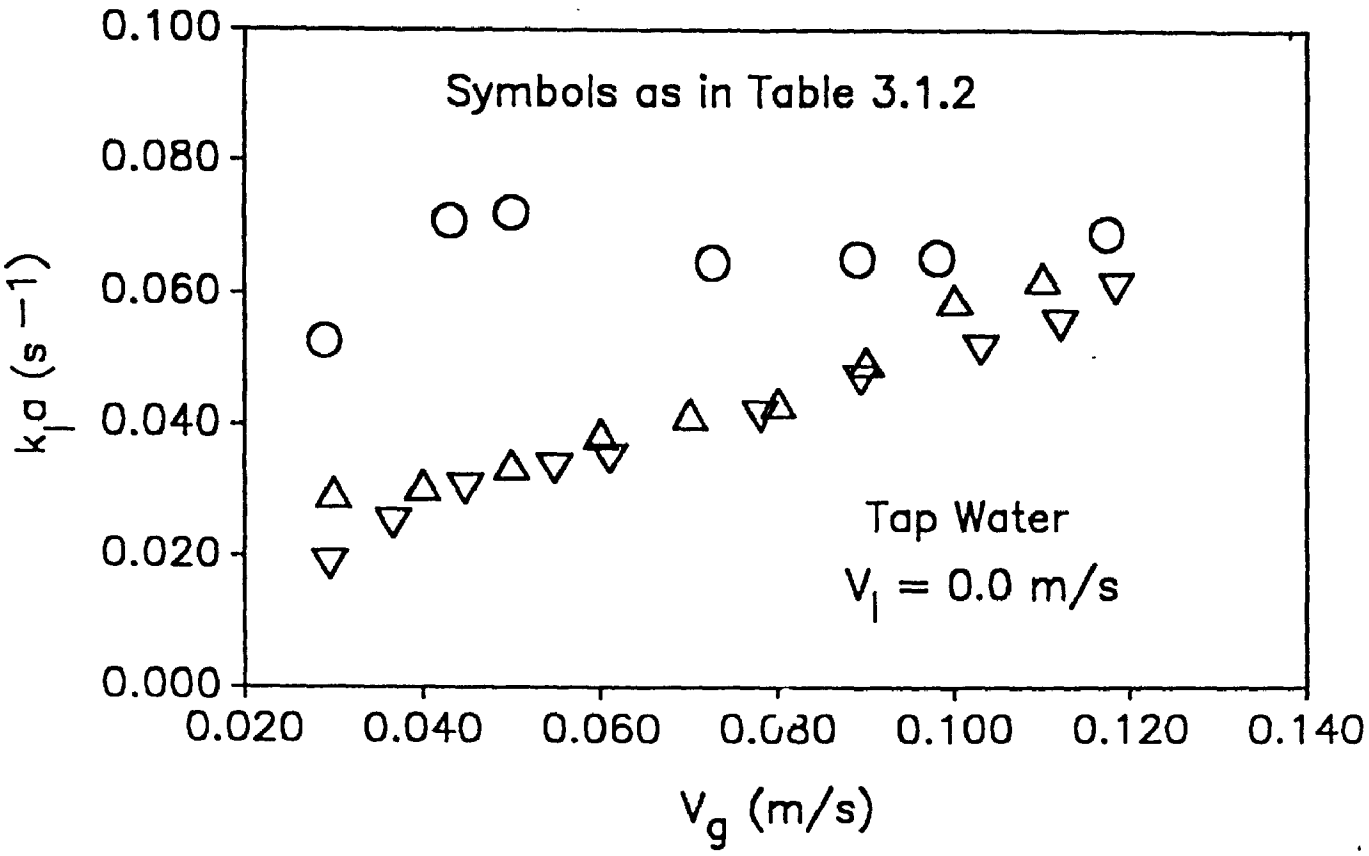

Figure 4.1.12
Effect of gas distribution on volumetric mass transfer coefficient in batch bubble column

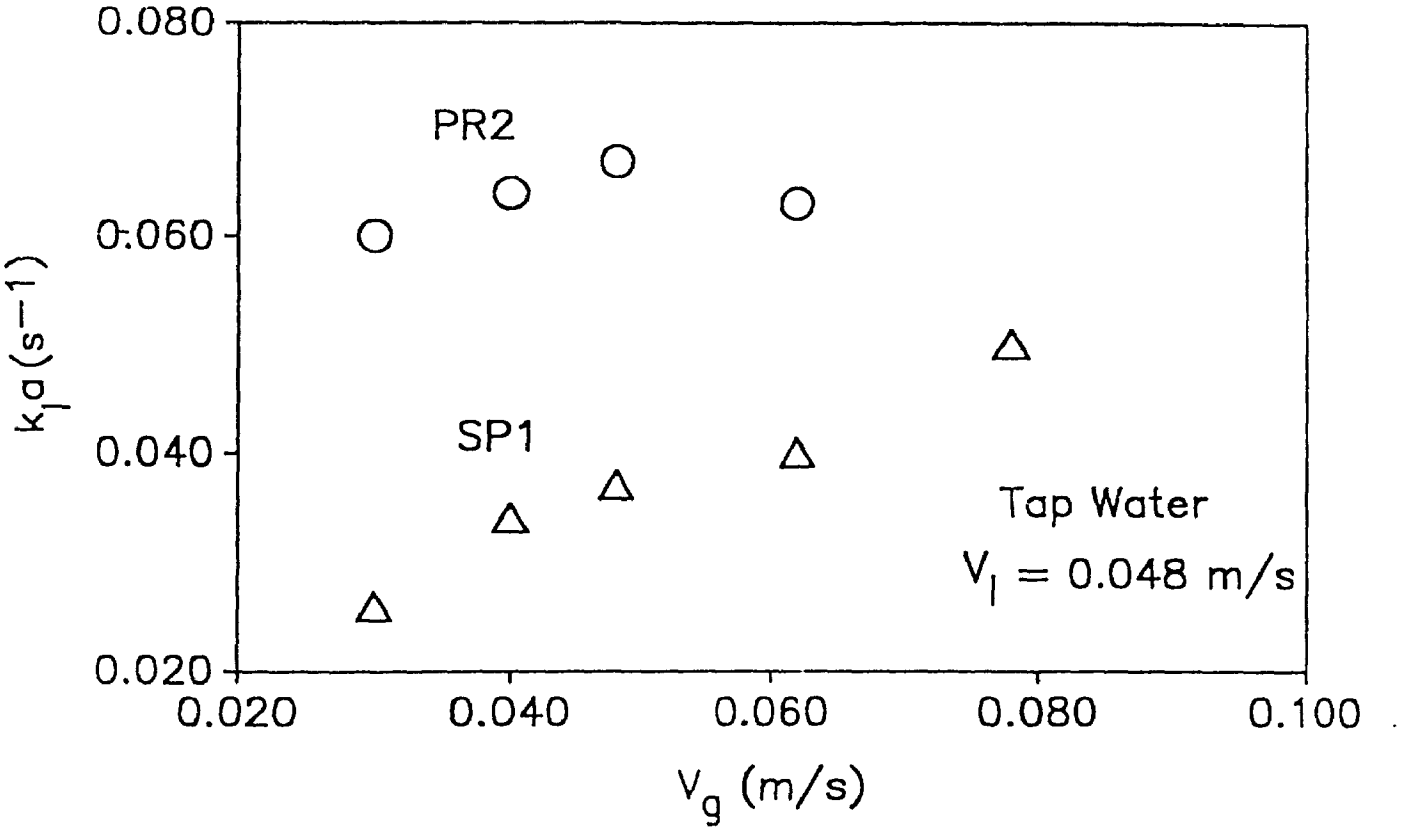

Figure 4.1.13
Effect of gas distribution on volumetric mass transfer coefficient in continuous bubble column

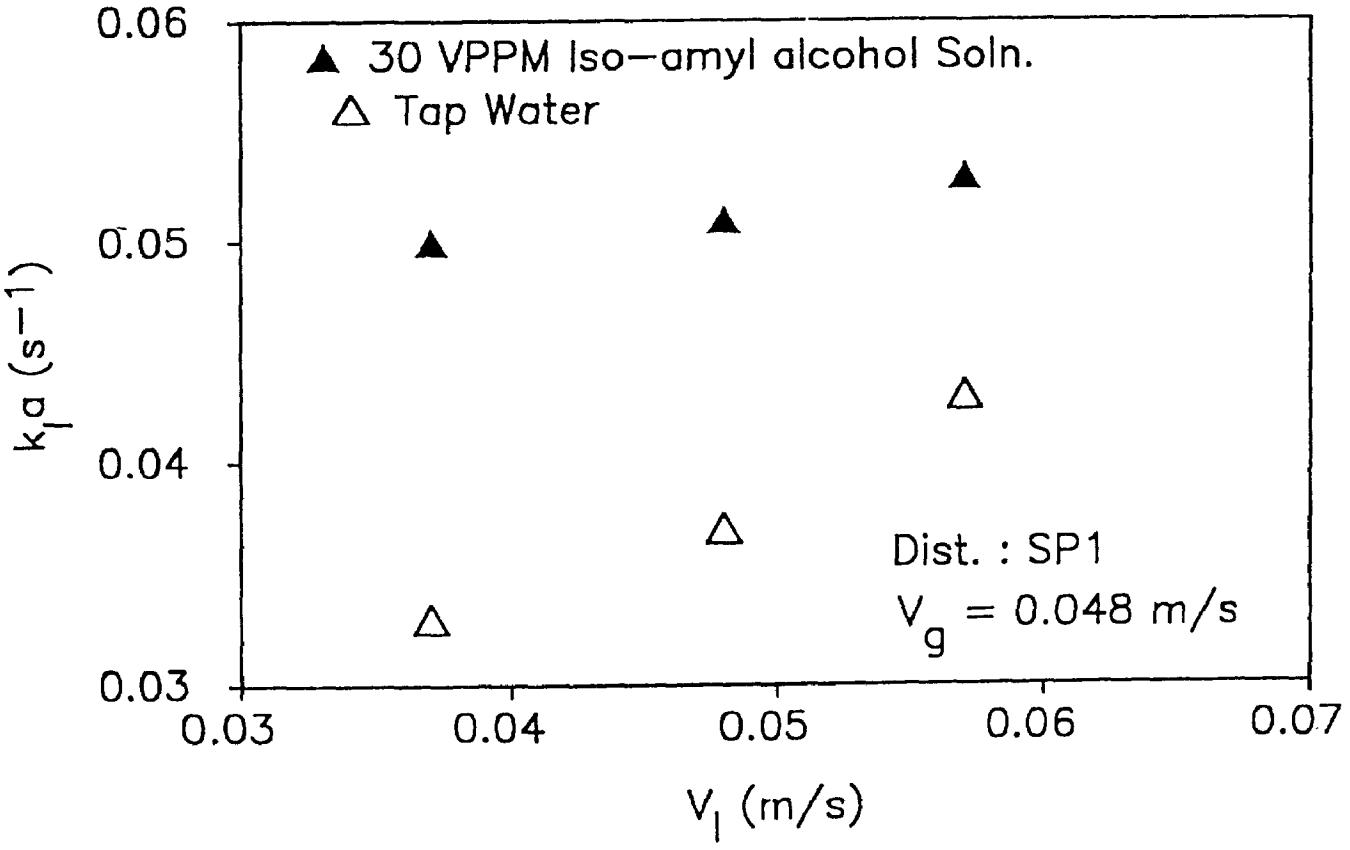

Figure 4.1.14
Effects of liquid velocity on volumetric mass transfer coefficient in bubble column

generated in the distributor region due to liquid flow. Higher turbulence level would result in bubble break-up in the distributor region. It should be pointed out that the effect of liquid flow would also depend on the design of gas and liquid distributors and the mixing patterns in the distributor region.

4.1.3.2 Effects of Gas Distribution

The volumetric mass transfer coefficient was found to be affected by the choice of the gas distributor. Significantly higher mass transfer coefficients were obtained with porous distributors operating in homogeneous and transition flow regimes while in the heterogeneous flow regime different distributors tend to come together (Figure 4.1.12, 4.1.13 and 4.1.15). It may also be pointed out that as observed with gas holdup, distributors PR1 and PR2 tend to come together at high gas velocities only.

Figure 4.1.16 shows that the mass transfer rate in the coalescing medium could be significantly increased by increasing the porous plate area. As observed with the gas holdup (Figure 4.1.8), distributors PR1 and PR2 do not converge over the range of gas velocities studied.

4.1.3.3 Effects of Additives

One of the objectives of the present study was to investigate how the gas-liquid mass transfer was affected by the additives, which alter the coalescing behavior of

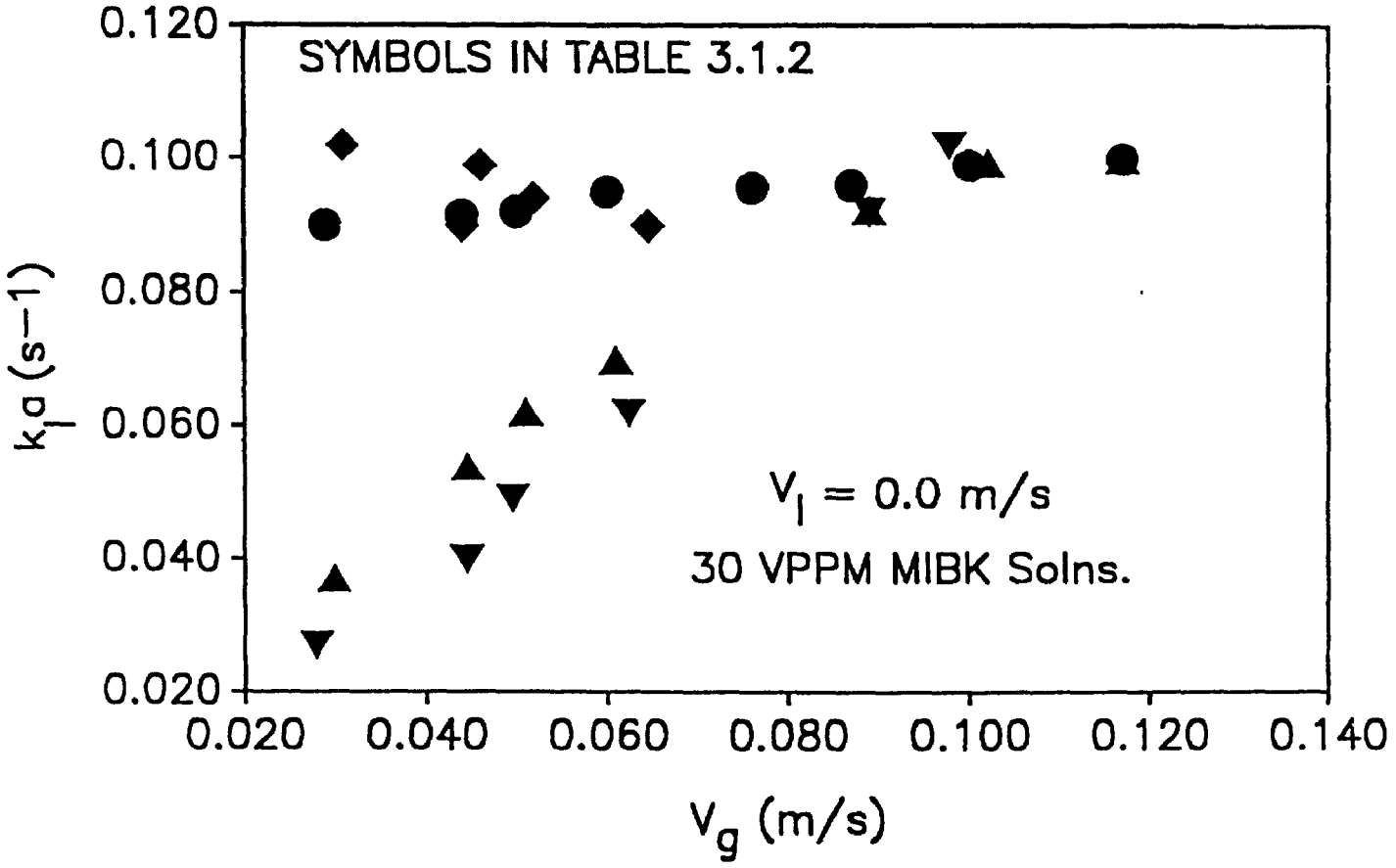

Figure 4.1.15
Comparison of volumetric mass transfer coefficients obtained with different distributors in a noncoalescing medium

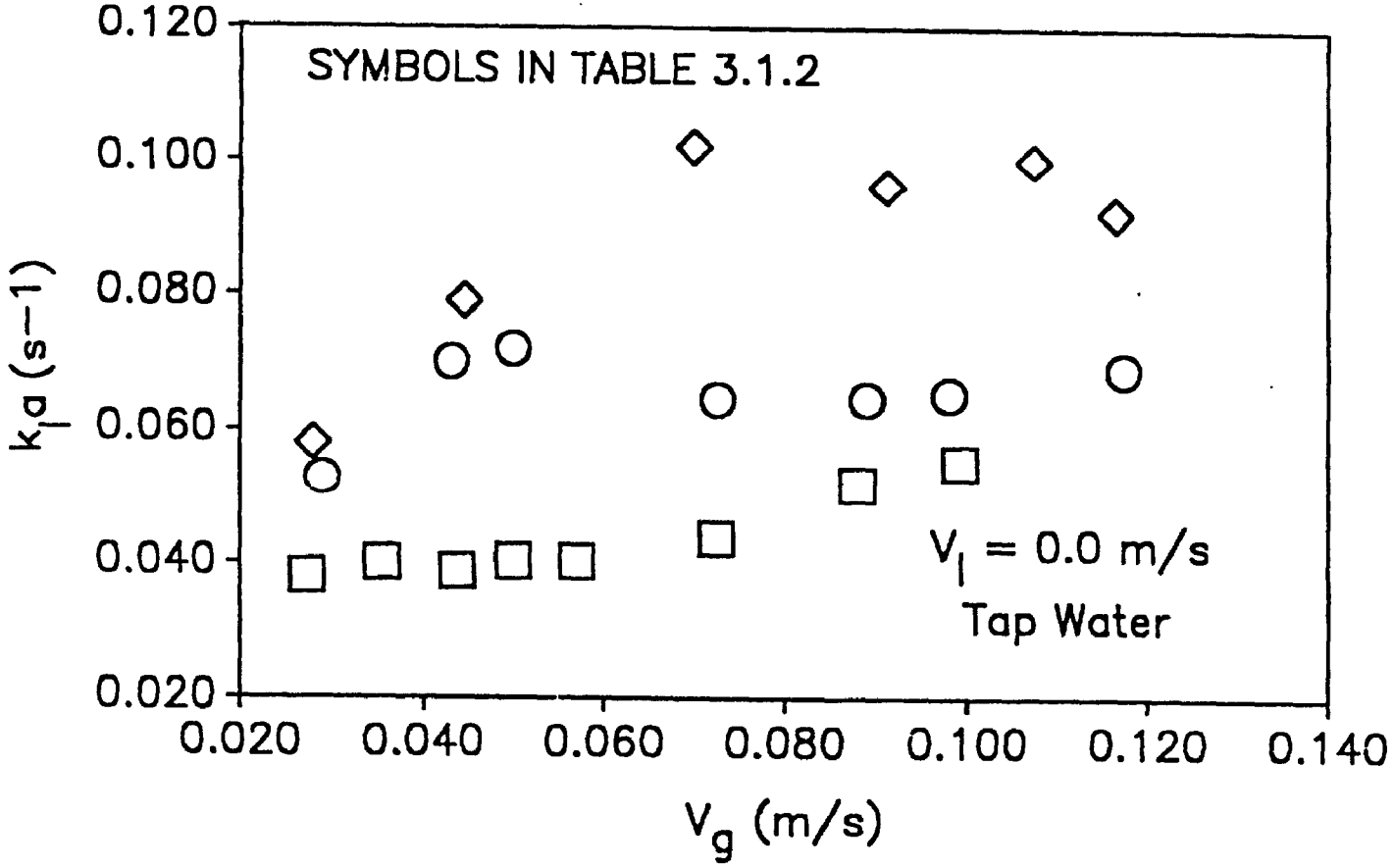

Figure 4.1.16
Effect of porous plate area on volumetric mass transfer coefficient (Batch Bubble Column)

the liquid. A systematic study was conducted to find an optimum molecular structure of the additive (i.e. functional group and hydrocarbon backbone) for mass transfer enhancement. A total of sixteen additives were selected to represent various functional groups and hydrocarbon backbones. The number of carbon atoms in the backbone of these additives were six.

The results of gas-liquid mass transfer for 50 vppm additive solutions are shown in Figure 4.1.17 as mass transfer effectiveness factor (k_1a additive solution/k_1a tapwater) for two types of distributors (PR2,SP1) and two gas velocities (i.e. 0.065 m/s and 0.125 m/s). Figure 4.1.17 shows that ketones and alcohols were the most effective additives in all four cases. Some additives however, had a detrimental effect: they reduced the volumetric mass transfer coefficient.

The degree of branching of the hydrocarbon backbone did not significantly affect the additive effectiveness (Table 4.1.3). It was, however, found that for the same functional group (i.e aldehyde), aromatic backbone gave results which were quite different from results obtained with an aliphatic backbone. The mass transfer effectiveness of the aromatic aldehyde (benzaldehyde) was about 1.32 at a 50 vppm concentration and increased when additive concentration was increased in the solution. Aliphatic aldehyde (hexanal), however, proved detrimental (effectiveness factor less than 1.0) at both the

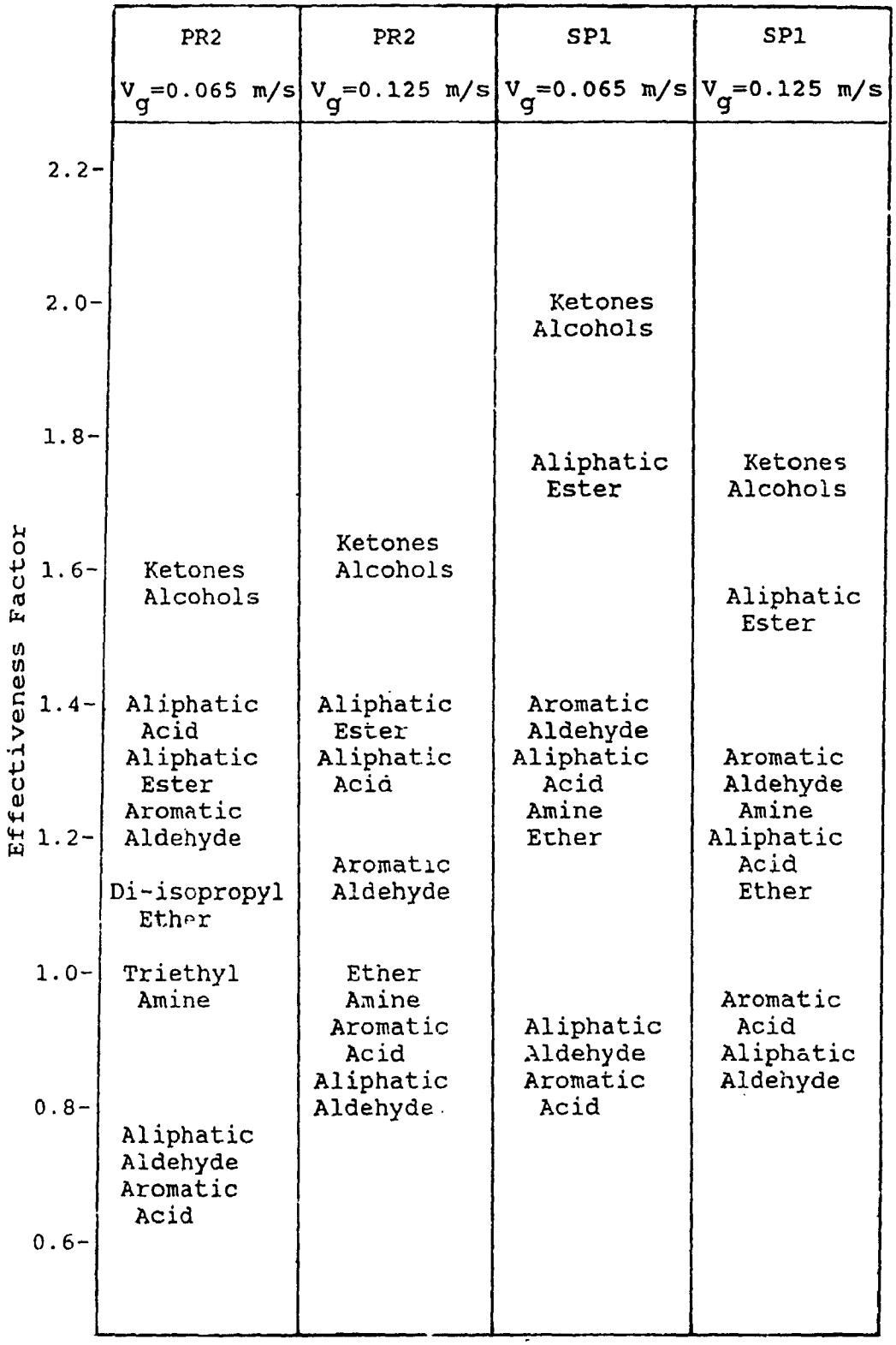

Figure 4.1.17
Effectiveness factors for different types of additives

concentrations used (Figure 4.1.18). The additives can affect volumetric mass transfer coefficient by either changing the liquid side mass transfer coefficient (k_l) and/or the interfacial area (a). The liquid side film coefficient has been generally found to decrease with increasing concentration and/or increasing hydrocarbon chain length of surface active additives (Raymond and Zieminski, 1971; Koide et al., 1976). An increase in the volumetric mass transfer coefficient observed in aqueous solutions of effective additives can be attributed to an increase in the interfacial area, which is a result of coalescence inhibition property of these additives. Benzaldehyde is therefore a better coalescence inhibitor compared to haxanal. Various bubble coalescence theories are discussed in section 5.1. It is pointed out that during the bubble coalescence process, dynamic surface tension effects can become important in determining the effectiveness of the additive. Because of the finite rate of diffusion of the surface active agents, a freshly formed surface will not generally have the same surface tension as that obtained after sufficient time has elapsed to establish equilibrium. When two bubbles come in contact in a gas-liquid dispersion, a thin liquid film has to drain and rupture before the bubbles coalesce. This draining and rupture of the liquid film is resisted by the surface active molecules which can diffuse to the interface quickly. Analysis of dynamic surface tension

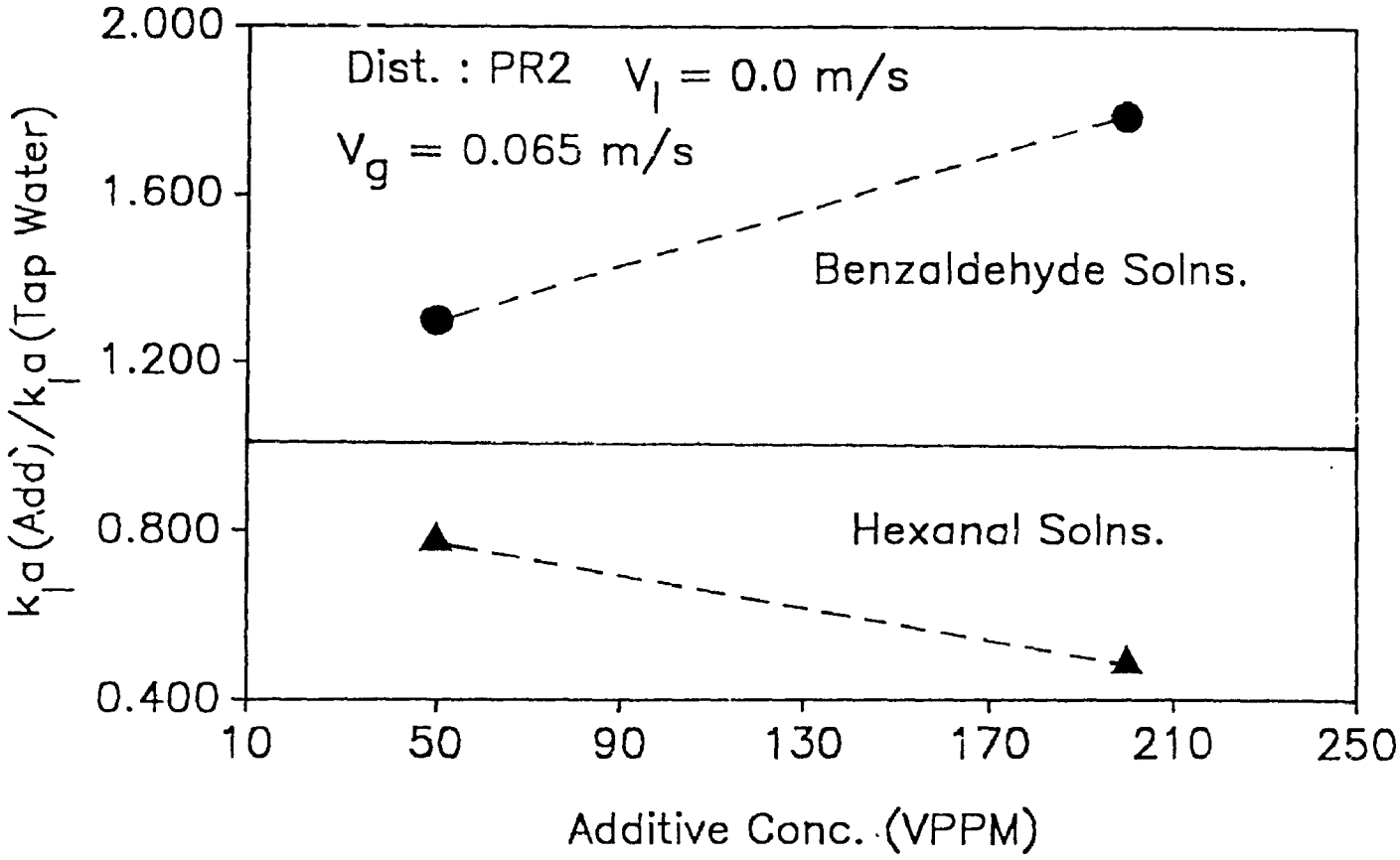

Figure 4.1.18
Comparison of mass transfer effectivenesses of aromatic and aliphatic aldehydes

data for different additives can therefore provide information about their effectiveness as coalescence inhibitors. Such data could not be found in the literature for hexanal and benzaldehyde. The dynamic surface tension effects are expected to become more significant with increasing hydrocarbon chain length, since these larger molecules will take longer to diffuse to the interface. A systematic study was therefore conducted to investigate the effects of hydrocarbon chain length on additive effectiveness.

Table 4.1.3 Effects of Degree of Branching of Hydrocarbon Backbone on Additive Effectiveness (PR2, V_g = 0.065 m/s)

Additive	k_1a(Additive)/k_1a(Tap water)	
	50 vppm additive solutions	5 vppm additive solutions
n-Pentanol	1.54	-
Iso-amyl alcohol	1.60	1.48
Tert-amyl alcohol	1.58	1.42
2-Hexanone	1.55	1.42
3-Hexanone	1.50	1.38

The effect of hydrocarbon chain length (i.e. number of carbon atoms in the hydrocarbon backbone) on additive effectiveness was investigated for straight chain alcohols and ketones. As shown in Figure 4.1.19, the mass transfer enhancement increased with increasing carbon number up to carbon number of five and then decreased for higher carbon numbers. Similar results were also obtained with ketones (Figure 4.1.20). Figure 4.1.19 also shows that the optimum chain length of five carbon atoms was independent of the additive concentration. It was also independent of the gas distributor and the gas velocity (Figure 4.1.21 and 4.1.22).

Figure 4.1.23 shows that the maxima for gas holdup was also obtained for alcohols with five carbon atoms. These results indicate that the effective additives acted primarily by reducing the average bubble size and thus increasing the interfacial area. This was confirmed by interfacial area measurement for a C_5 alcohol (iso-amyl alcohol) solution. Table 4.1.4 shows that while the interfacial area in a 50 vppm iso-amyl alcohol solution increased by about 30% there was no significant change in the mass transfer coefficient. The increase in volumetric mass transfer coefficient could be accounted for by the increase in the interfacial area. The effective additives therefore acted primarily by reducing the average bubble size which resulted in higher gas holdups and interfacial areas for mass transfer.

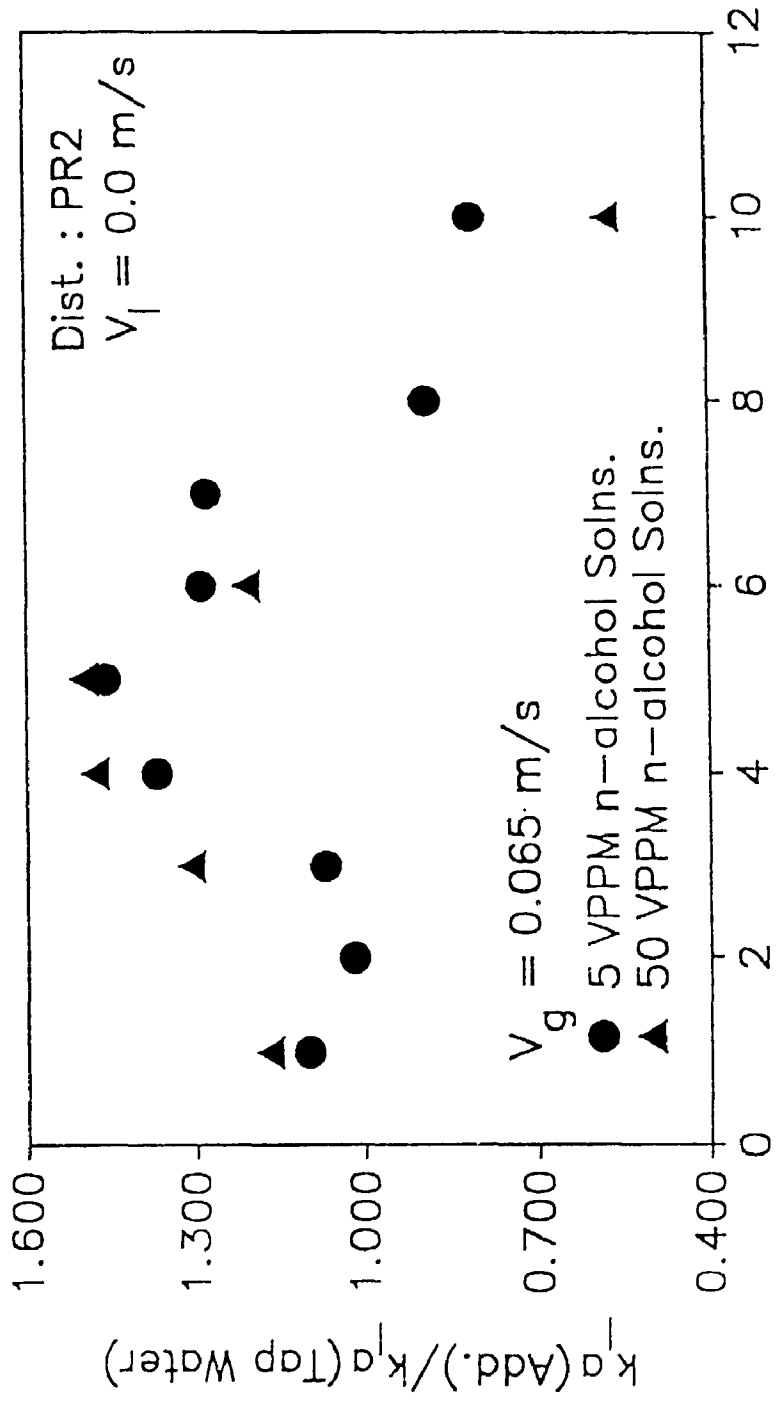

Figure 4.1.19
Effect of hydrocarbon chain length on mass transfer effectiveness of n-alcohols

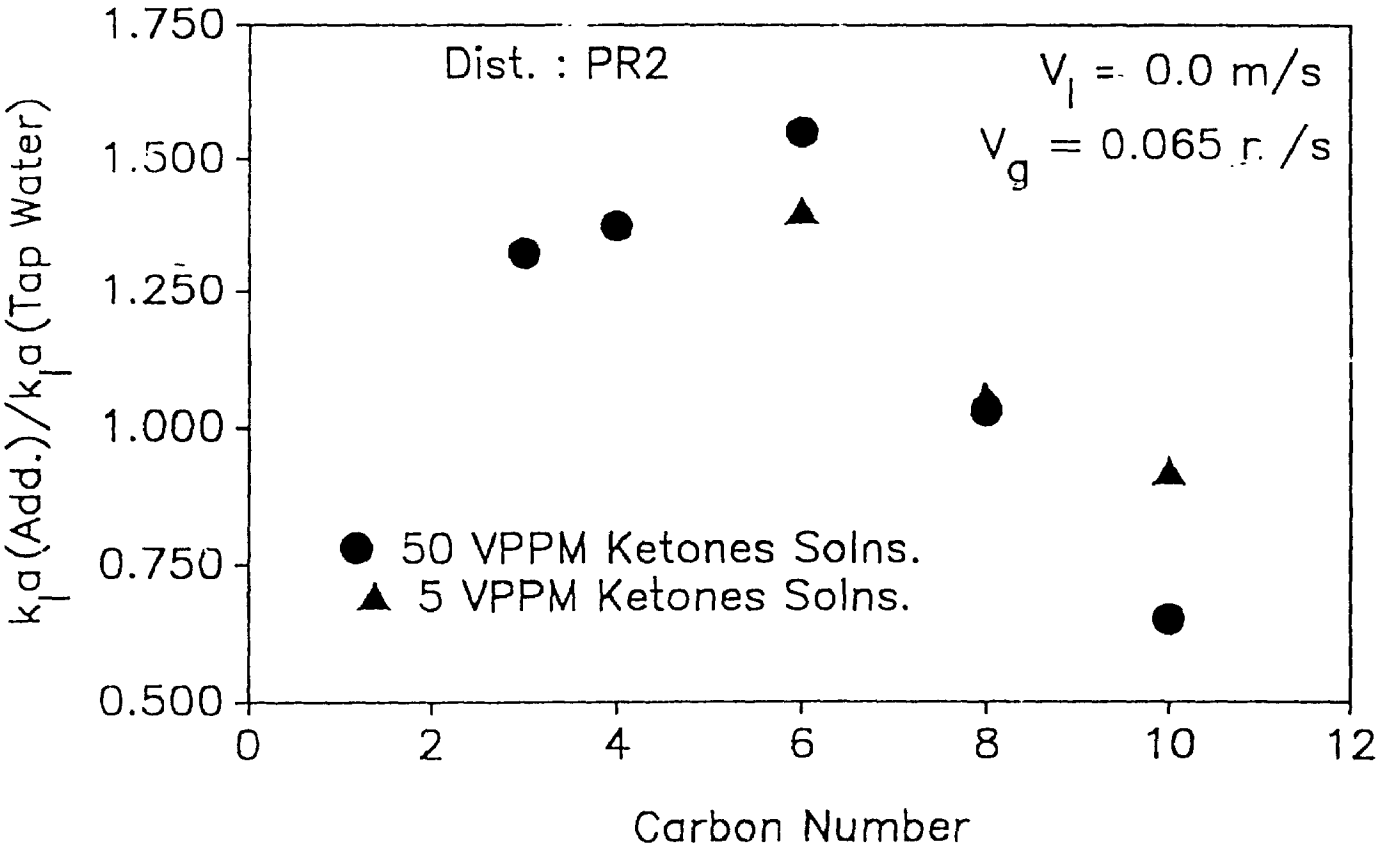

Figure 4.1.20
Effect of hydrocarbon chain length on mass transfer effectiveness of ketones

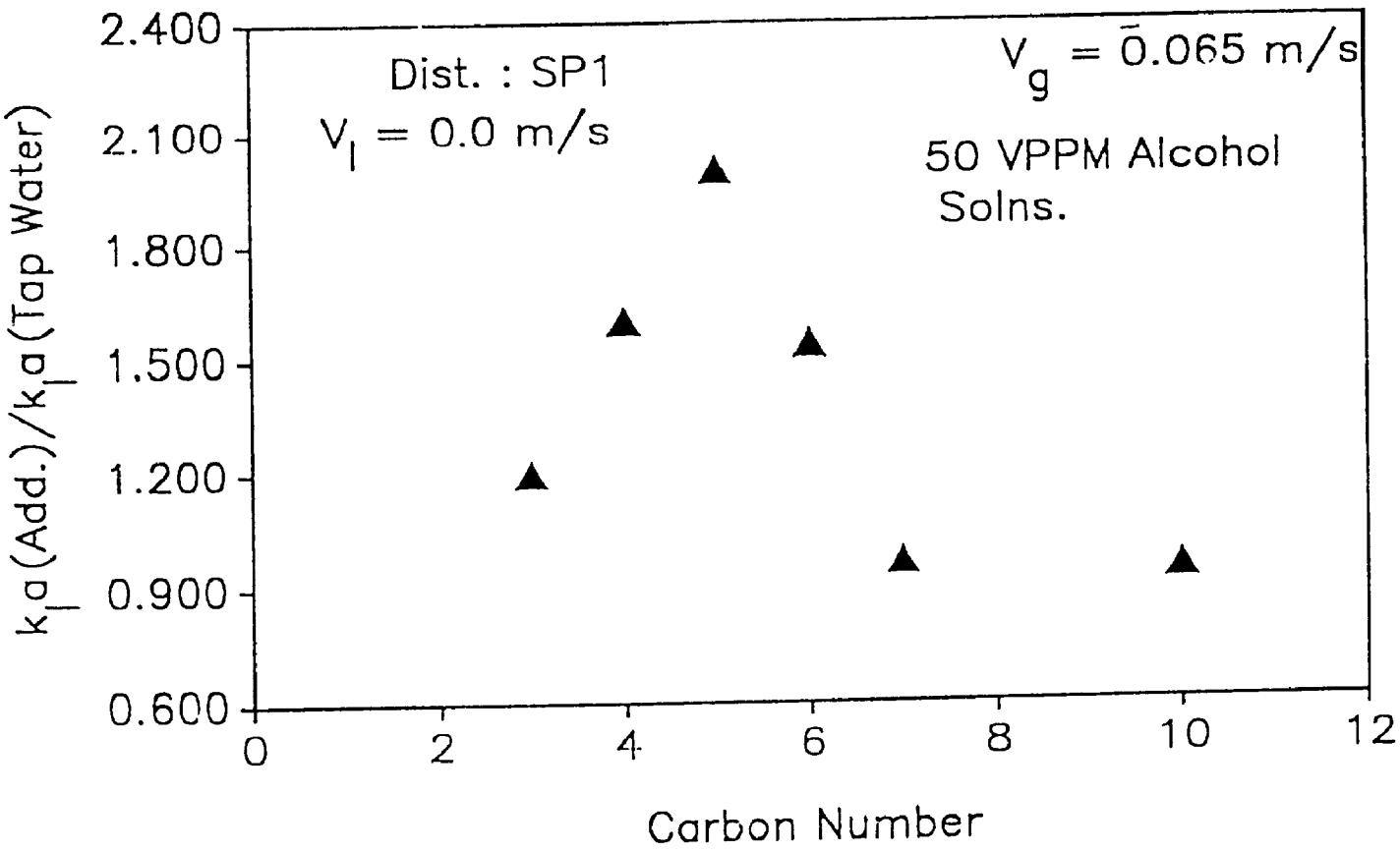

Figure 4.1.21
Mass transfer effectiveness as a function of hydrocarbon chain length; Effects of gas distribution

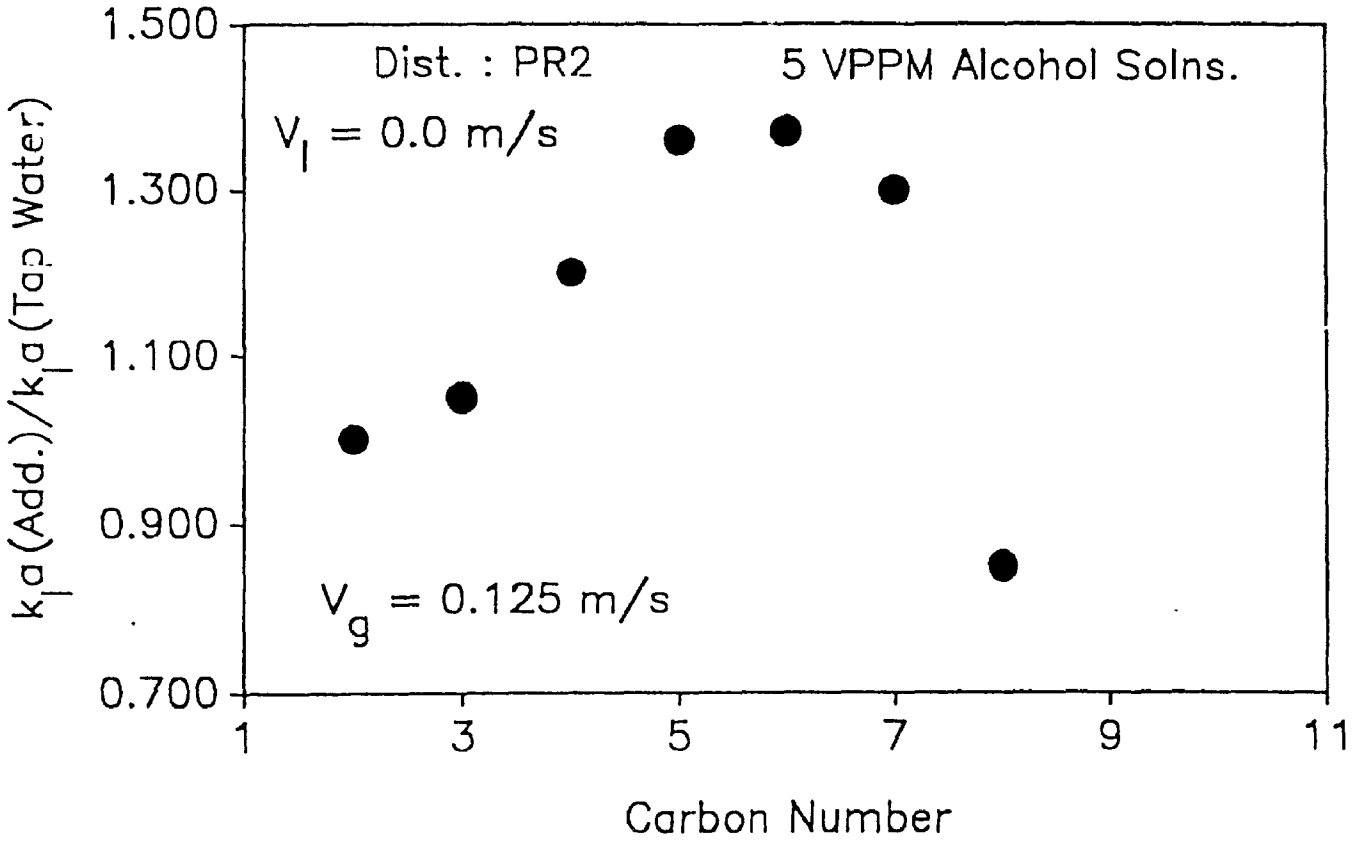

Figure 4.1.22
Mass transfer effectiveness as a function of hydrocarbon chain length; Effect of gas velocity

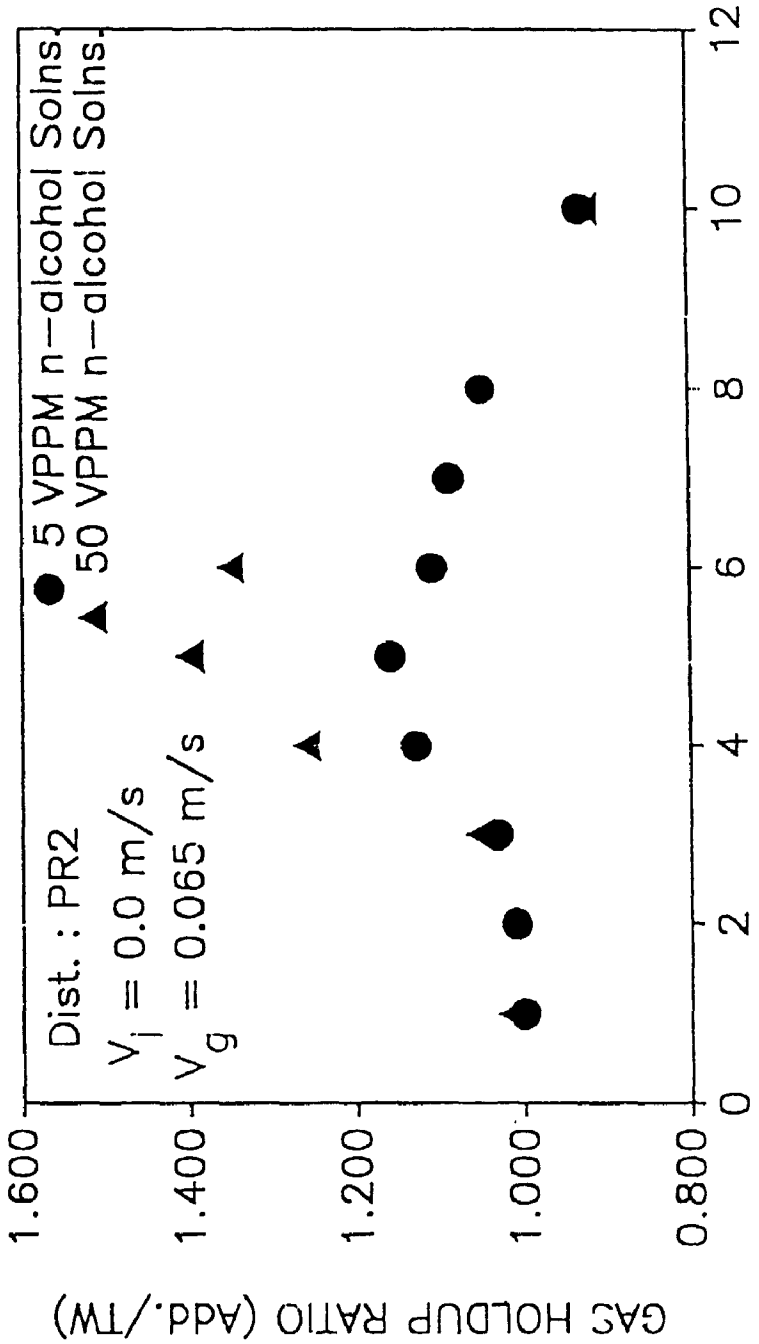

Figure 4.1.23
Gas holdup effectiveness as a function of hydrocarbon chain length

Table 4.1.4 Values of Interfacial Areas and Liquid Side Mass Transfer Coefficients (V_l=0.0;V_g=0.062 m/s)

Liquid phase	Distributor type	Interfacial area (a) m^{-1}	Liquid side film coeff. (k_l) m/s
Tap water	SP1	125.0	0.00028
50 vppm iso-amyl alcohol solution	SP1	177.0	0.00029
50 vppm 2-Decanone solution	SP1	132.0	0.00015

The bubble size can be reduced by either a reduction in surface tension (Walter and Blanch, 1986) or by inhibition of bubble coalescence. The additives selected for the study had a hydrophobic and a hydrophilic group. These additives could thus alter the surface tension of water. However, for the dilute additive solutions used for this study there were no detectable changes in surface tension (Table 4.1.5).

The effective additives therefore reduced the average bubble size by inhibiting bubble coalescence. The various theories of bubble coalescence are reviewed in section 5.1. The bubble coalescence time was found to increase rapidly with the solute concentration in dilute aqueous solutions of alcohols (Sagert and Quinn, 1978; Kim and

Table 4.1.5 Static Surface Tension in the Dilute Solutions of Additives (50 vppm)
(Dist.: PR2; V_g = 0.065 m/s)

Additive Name	σ (N/m)	$\frac{k_1a(add.)}{k_1a(TW)}$	Remarks
Methyl Isobutyl Ketone	0.0736	1.52	No correlation between additive effectiveness and static surface tension
Butyl Alcohol	0.0738	1.48	
Butyl Acetate	0.0733	1.37	
Cyclohexanone	0.0738	1.53	
Tap Water	0.074	1.0	

Lee, 1987). The dynamic disengagement technique used for bubble population measurement in this study clearly showed that the population of small bubbles increased in the solution of an effective coalescence inhibitor both for porous distributor, PR2 and sparger, SP1 (see Table 3.1.3).

A sparger distributor generates large bubbles which split above the distributor. The average bubble size results from a dynamic equilibrium between coalescence and splitting. For a given power input rate the splitting rate is affected by surface tension and liquid viscosity (Walter and Blanch, 1986). Since both these properties were unaffected in the dilute solutions of the additives used, the observed increase in the population of small

bubbles with the sparger can again be attributed to coalescence inhibition effects.

Higher gas holdup in an additive solution did not always result in higher mass transfer rate. As shown in Table 4.1.6, while the gas holdup increased in the hexanol and heptanol solutions the mass transfer rate was reduced. The additive effectiveness data for long chain alcohols suggest that these additives reduced the k_l values. This was confirmed by the measurements of k_l and a. As shown in Table 4.1.4 the liquid side film coefficient (k_l) was significantly reduced in the solution of 2-decanone.

Table 4.1.6 Comparison of Mass Transfer and Gas Holdup Effectiveness for Long Chain Alcohols (Sparger: SP1 ; V_g=0.065 m/s)

Additive	5 vppm Additive solution		50 vppm Additive solution	
	$\frac{k_l a(Add.)}{k_l a(TW)}$	$\frac{\epsilon_g(Add.)}{\epsilon_g(TW)}$	$\frac{k_l a(Add.)}{k_l a(TW)}$	$\frac{\epsilon_g(Add.)}{\epsilon_g(TW)}$
n-Hexanol	1.74	1.17	1.54	1.32
Heptanol	1.70	1.20	0.97	1.24

The reduction of k_l in the solutions of long chain additives could be attributed to either interface immobilization or the "barrier effect". Interface

immobilization results from the surface tension gradient created by the concentration of additive molecules at the rear end of the bubble (Griffith, 1962). The immobilization of the interface reduces internal circulation inside the bubble. The individual gas film mass transfer coefficient may then no longer be negligible. Raymond and Zieminski (1971) found that the coefficient k_l decreased linearly with increasing drag coefficients of bubbles in the solutions of alcohols. They concluded that the decrease of k_l in the aqueous solutions of surface active materials was primarily due to the changes in the hydrodynamic characteristics of the system.

The other possible explanation for lowering of k_l in additive solutions is that the additive molecules get packed so closely at the interface that they interfere with the diffusion of the oxygen molecules (molecular diameter 10 -15 A^o). The calculated centre to centre distance between adsorbed molecules decreased sharply for higher chain alcohol molecules (Table 4.1.7), and became of the same order as the size of oxygen molecule. Interference with the diffusion of oxygen molecule was thus very likely.

The interface concentration of the adsorbed molecules was obtained using the ideal adsorption isotherm given below (Davies and Radeal, 1963):

$$n_c = d_m \, c_{nb} \, (N_{Ao}/1000) \exp(y_e/R_g T) \quad \ldots\ldots\ldots (4.1.3)$$

Table 4.1.7 Centre to Centre Distance Between Adsorbed Alcohol Molecules

Alcohol Molecule Carbon Number	Centre to Centre Distance Between Adsorbed Molecules	
	5 vppm Soln. (A^o)	50 vppm Soln. (A^o)
C_1	1156.0	366.0
C_2	530.0	167.0
C_3	267.0	84.0
C_4	140 .0	44.0
C_5	75.0	24.0
C_6	41.0	13.0
C_7	23.0	7.3
C_8	12.3	4.0
C_9	6.6	2.1
C_{10}	3.0	1.13

The centre to centre distance between the molecules was calculated assuming hexagonal packing. These distances could, however, be higher since equation (4.1.3) assumes no interaction between adsorbed molecules which would not be valid for high concentration of adsorbed molecules. The trend however shows that the barrier effect could become important for higher chain alcohols.

4.1.3.4 Effects of additive concentration

Figure 4.1.24 shows how the effectiveness for mass transfer varied with additive concentration for an effective additive (MIBK) and a long chain detrimental one (2-Decanone). The mass transfer coefficient increased with increasing additive concentration of the effective additive and decreased with increasing concentration of the detrimental one and reached a plateau. As the concentration of a surface active solute is increased in the liquid phase, the concentration at the interface also increases. The relacionship between the bulk concentration (C_{nb}) and the surface excess concentration is provided by the Gibbs equation:

$$\Gamma = - \frac{1}{R_g T} \frac{\Delta\sigma}{\Delta \ln C_{nb}} \qquad \text{.....(4.1.4)}$$

The value of surface excess concentration reaches a limiting value as the additive concentration is increased. This corresponds to the formation of complete monolayer of the surface active molecules at the interface (Adamson, 1964). The surface excess concentration reaches a constant value when the slope of the surface tension vs the curve becomes constant. The additive concentration required to reach a constant slope for this curve, decreases with increasing molecular weight (Hommelen, 1959). Calculations for decanone solution show that the

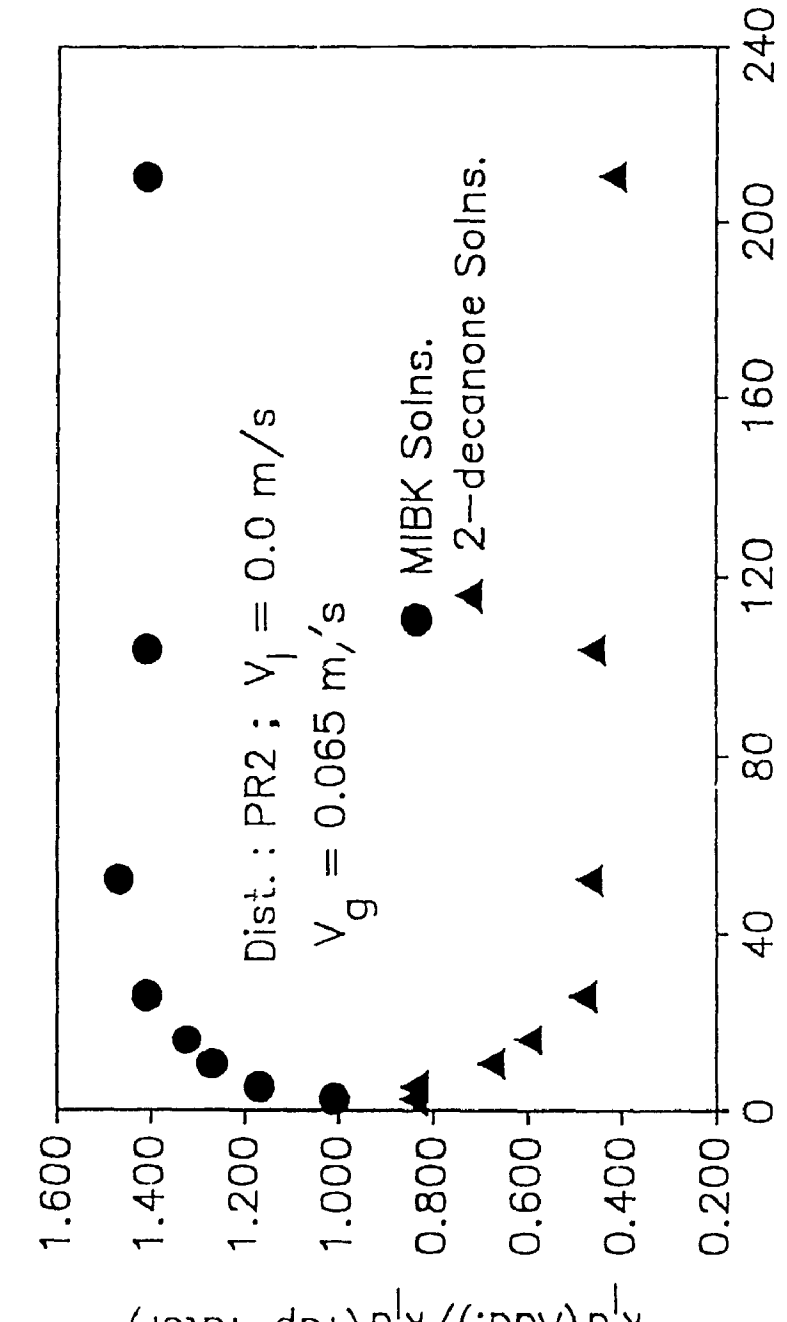

Figure 4.1.24
Mass transfer effectiveness as a function of additive concentration

bubble interface could have reached saturation at the concentration at which plateau was reached for k_1a. However for the MIBK solution the concentration at which the plateau is reached, would be several orders of magnitude lower than the concentration required for saturation at interface. For the solution of effective additive, it was observed that a foam layer was formed above the gas-liquid dispersion at concentrations above 50 vppm. The height of the foam layer increased with increase in the additive concentration. With the decanone solutions no significant foam layer could be observed. The formation of the foam layer with effective additive suggests that the additive molecules were stripped from the solution by small bubbles which stay long enough in the solution to reach high concentration at the interface. Therefore there was little advantage of increasing the additive concentration in the solution beyond 50 vppm. The highest rate of increase in the mass transfer with the additive concentration were obtained in the concentration range of zero to 20 vppm. Therefore this should be the most cost effective range of concentration to be studied, when an effective additive is to be used to enhance the gas-liquid mass transfer rate.

4.1.3.5 Correlations for Volumetric Mass Transfer Coefficient

Figure 4.1.25 shows plots of volumetric mass transfer

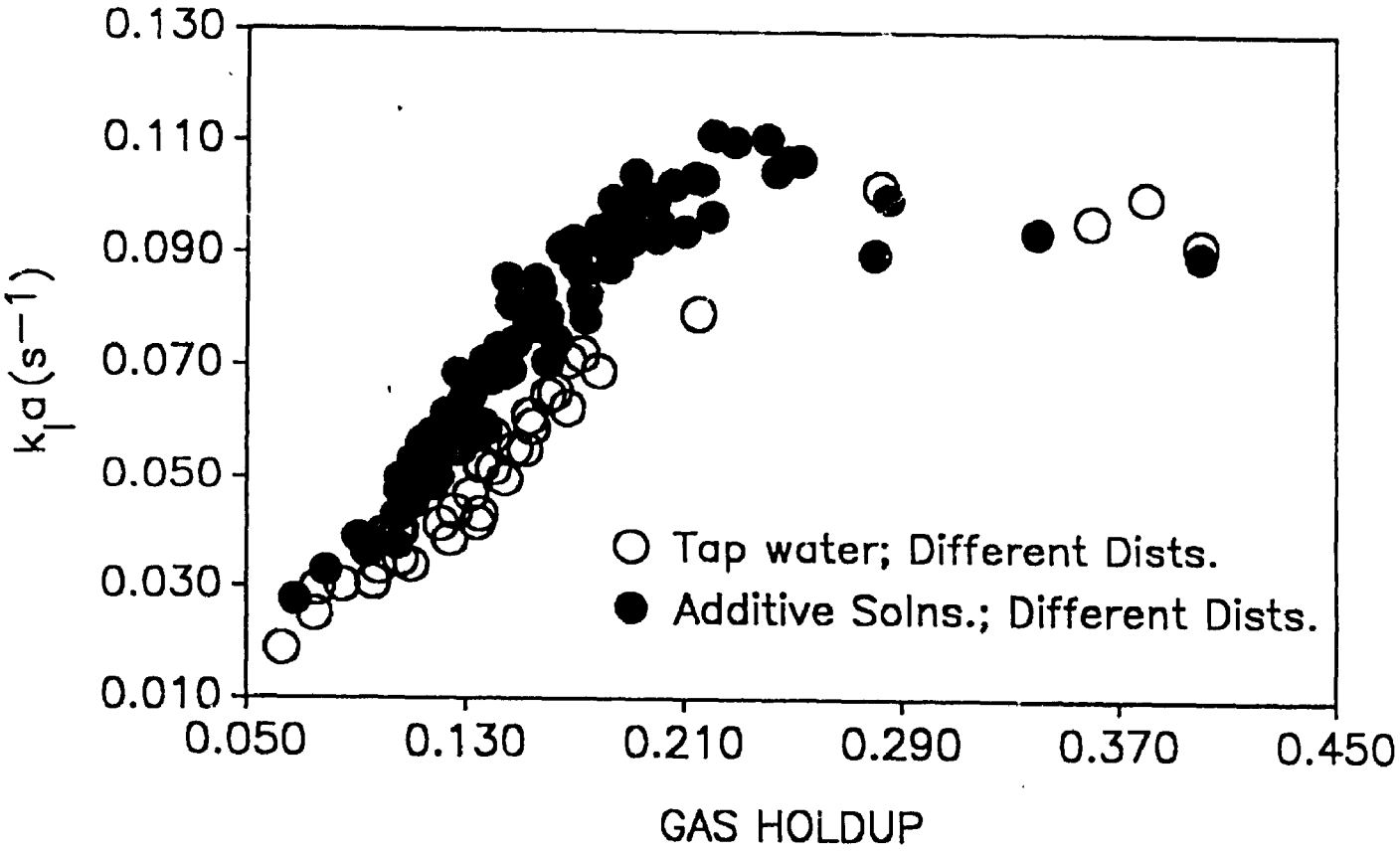

Figure 4.1.25
Volumetric mass transfer coefficient as a function of gas holdup; Batch bubble column data (effective additives)

coefficient as a function of gas holdup for the data obtained in the coalescing liquid and in the dilute solutions (50 vppm or less) of effective additives (carbon number less than six). The data obtained in continuous bubble column and with detrimental additives was not included since no correlation between volumetric mass transfer coefficient and gas holdup could be observed.

It can be seen from Figure 4.1.25 that there is generally a good correlation between the volumetric mass transfer coefficient and the gas holdup for gas holdups of less than about 0.22. At higher gas holdups, the volumetric mass transfer coefficient slightly decreased with increasing gas holdups. This could be attributed to increase in the concentration of smaller bubbles with increasing gas holdup in the column. As discussed in section 2.2.7, the liquid side mass transfer coefficient (k_l) has been found to decrease for smaller bubbles (d_{avg} < 2.5 mm). In this study, high gas holdups (> 0.22) were obtained with distributors PR2 (solutions of effective additives) and PR1 (both tap water and solutions of effective additive) which indicated the presence of small bubbles in the dispersion. Bubble population study data (Table 3.1.4) showed that the concentration of small bubbles (d_{avg} < 2.5 mm) increased as the gas holdup increased with increasing concentration of an effective additive in the solution. Although interfacial area increased with decreased bubble size, the liquid side mass

transfer coefficient decreased. These two opposite effects seem to compensate for each other at high gas holdups.

It can also be seen from Figure 4.1.25 that two separate correlations one each for the coalescing medium and the noncoalescing media were required to give good fit of the data. For a given gas holdup, the volumetric mass transfer coefficient was higher in the additive solutions. The relationship between gas holdup, interfacial area and average bubble size is given by the following equation:

$$a = 6\epsilon_g/d_{vs} \qquad \text{.....(2.2.20)}$$

In additive solutions, the average bubble size is reduced by coalescence inhibition which results in higher interfacial area for mass transfer for a given gas holdup.

Suggested correlations:

- Coalescing medium ($\epsilon_g < 0.25$)

$$k_l a = 0.5\ \epsilon_g^{1.156} \quad (R^2 = 0.94) \qquad \text{.....(4.1.5)}$$

- Noncoalescing media ($\epsilon_g < 0.25$)

$$k_l a = 0.6\ \epsilon_g^{1.3} \quad (R^2 = 0.93) \qquad \text{.....(4.1.6)}$$

The various literature correlations for volumetric mass transfer coefficient in bubble columns were reviewed

in section 2.2.5.3. These correlations generally failed to take into account the effects of gas distribution and the coalescence behavior of liquid on volumetric mass transfer coefficient. Akita and Yoshida (1973) developed a general correlation for the volumetric mass transfer coefficient using dimensionless groups and the gas phase holdup. When applied to the data of this study, this correlation predicted values of the volumetric mass transfer coefficient which were 40 to 50% lower than the experimental values.

4.1.3.6 Volumetric Mass Transfer Coefficient as a Function of Energy Input per Unit of Reactor Volume for the Batch Bubble Column

From a practical point of view, it is important to know how the mass transfer rate varies with the energy input per unit of reactor volume. This information can help select the best gas distribution system for a given application.

The energy input rate was calculated with the following equation:

$$E_i = \Delta P_{dh} \times Q_g = [\rho_L g(1-\epsilon_g)H_d + \Delta P_f]\, Q_g \quad \ldots.(4.1.7)$$

The total pressure drop (ΔP_{dh}) includes the frictional pressure drop across the distributor and the hydrostatic liquid head (to get the actual energy consumption, the pressure drop ΔP_f, through the distributor was corrected to account for the change in the kinetic energy of the gas between the pressure measurement locations). Figure 4.1.26 shows that at low energy inputs, the largest porous distributor (PR1) gave the highest volumetric mass transfer coefficients followed by the reduced area porous distributor (PR2) and the spargers (SP1, SP2).

Figure 4.1.27 compares the variations of the volumetric mass transfer coefficient with the energy input rate for the three porous distributors. It can be seen that for a given energy input rate the large porous distributor gave significantly larger mass transfer rates, although at high energy input rates the difference became smaller. The smallest porous distributor (PR3) did not give higher mass transfer rates than the spargers for a given energy input rate (Figure 4.1.26). Due to the higher maintenance costs associated with porous distributors, spargers would be more attractive than small area porous distributors in practical applications.

The intermediate porous distributor (PR2) on the other hand, gave a much better performance than the spargers (Figure 4.1.26). For a given energy consumption,

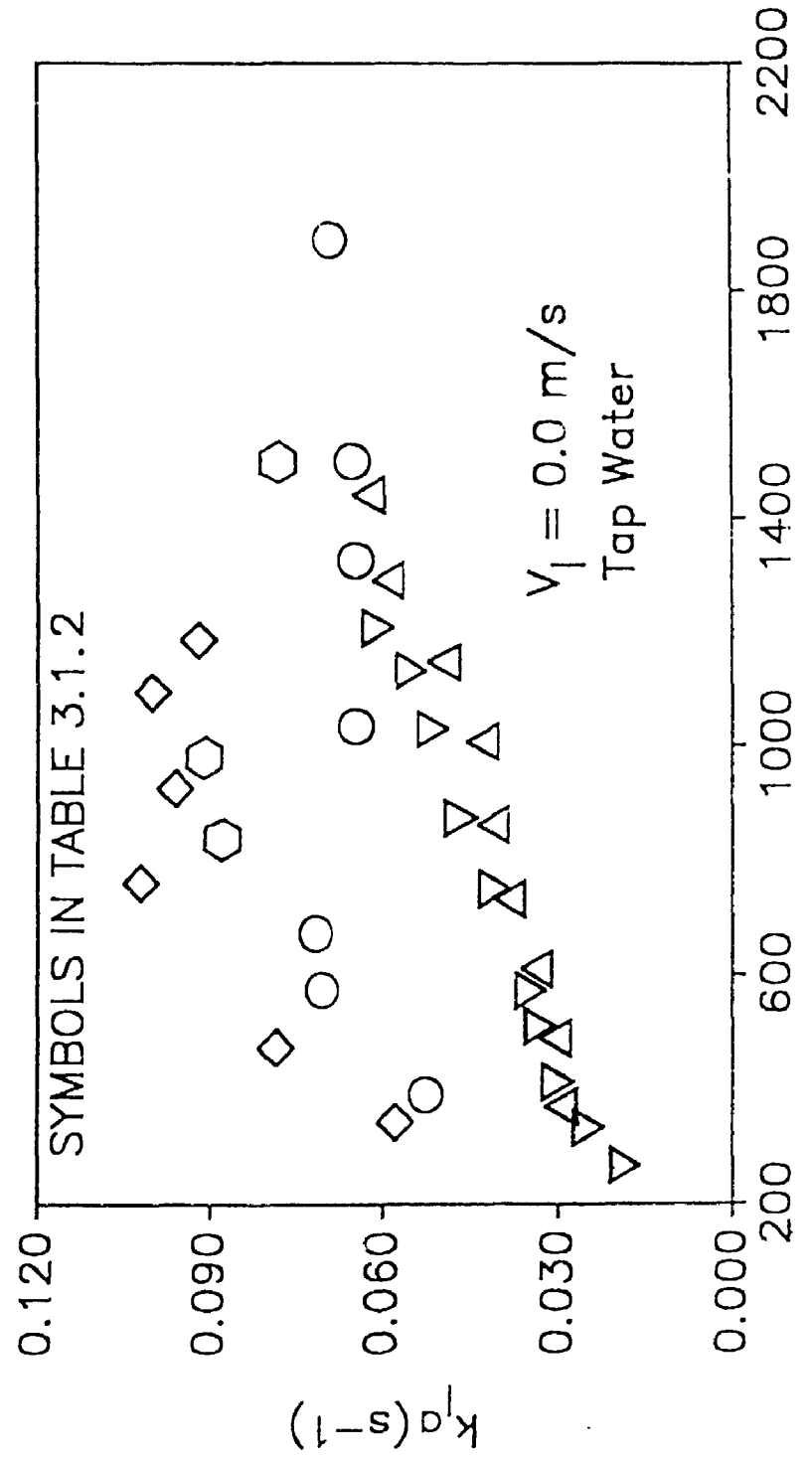

Figure 4.1.26
Volumetric mass transfer coefficient as a function of energy input per unit reactor volume (various distributors)

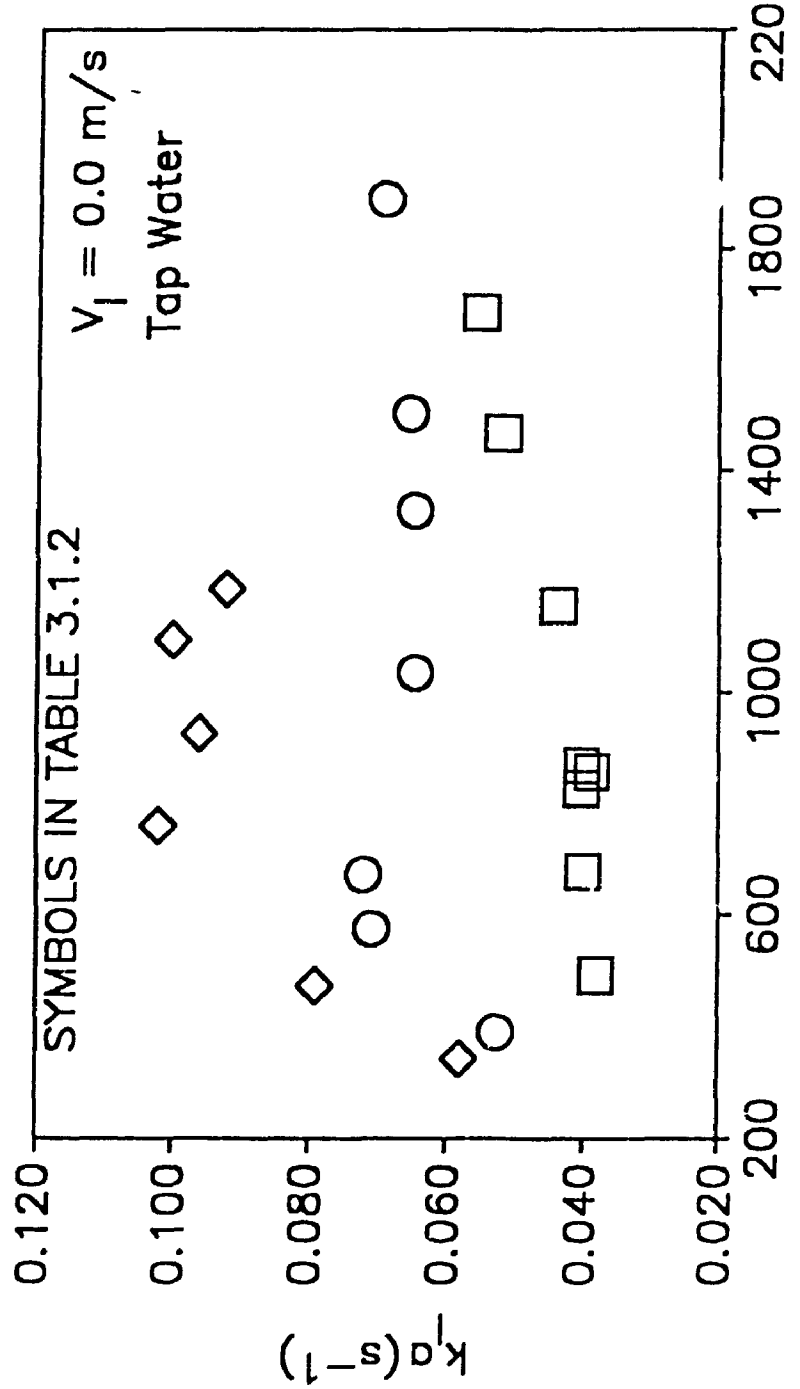

Figure 4.1.27
Comparison of volumetric mass transfer coefficient as a function of energy input per unit reactor volume; Effect of porous plate area.

this porous distributor gave mass transfer rates which were almost 100% higher than those obtained with the spargers. Figure 4.1.27 shows that with the coalescing medium and porous distributor PR2, the mass transfer rate dropped when the energy input was increased past a critical value. This critical value corresponds to the gas velocity which gave the maximum gas holdup (Figure 4.1.4) and the maximum mass transfer coefficient (Figure 4.1.12). This gas velocity corresponds to the onset of transition regime and can be predicted since it corresponds to an initial bubble size of 6 mm which can be calculated with a porous distributor model.

With the large porous distributor (PR1) , however, the maximum mass transfer rate was reached at an energy input rate (Figure 4.1.26) and a gas velocity (Figure 4.1.15) which was much smaller than the gas velocity at which the transition to heterogeneous flow occured (Figure 4.1.1). This could be explained by Figure 4.1.25 which shows that the volumetric mass transfer coefficient cannot be increased past about 0.11 s^{-1} and that increasing the gas holdup past 20 to 25% does not result in higher mass transfer rates. Figure 4.1.15 shows that with the noncoalescing system the maximum volumetric mass transfer coefficient was reached at lower gas velocities and hence, lower energy input rates.

In practical applications, energy costs have to be balanced against maintenance costs and capital

expenditures. Although spargers require higher energy consumption rates, their capital and maintenance costs are lower than for the porous distributors which plug easily. If a decision is made to use a porous distributor, the same considerations will enter into the selection of the appropriate distributor area. Distributors with a very small area do not perform better than spargers and should not be used. With larger porous distributors, the performance improves as the distributor area is increased. There is, however, a limit to which the mass transfer rate can be increased by improving the gas distribution.

4.1.3.7 Combination of a Porous Distributor with a Sparger

Figure 4.1.28 compares the values of volumetric mass transfer coefficient obtained in the coalescing medium with the porous distributor (PR2) and with its combination with sparger SP1. It can be seen that significantly larger mass transfer rates were obtained by combining the porous distributor PR2 with sparger SP1.

In order to maximize the mass transfer coefficient obtained with the combination of the two distributors, different splits of the flowrate between the distributors were tried. The largest mass transfer coefficients were obtained when the gas flowrate through the porous distributor was close to its optimum value for the porous

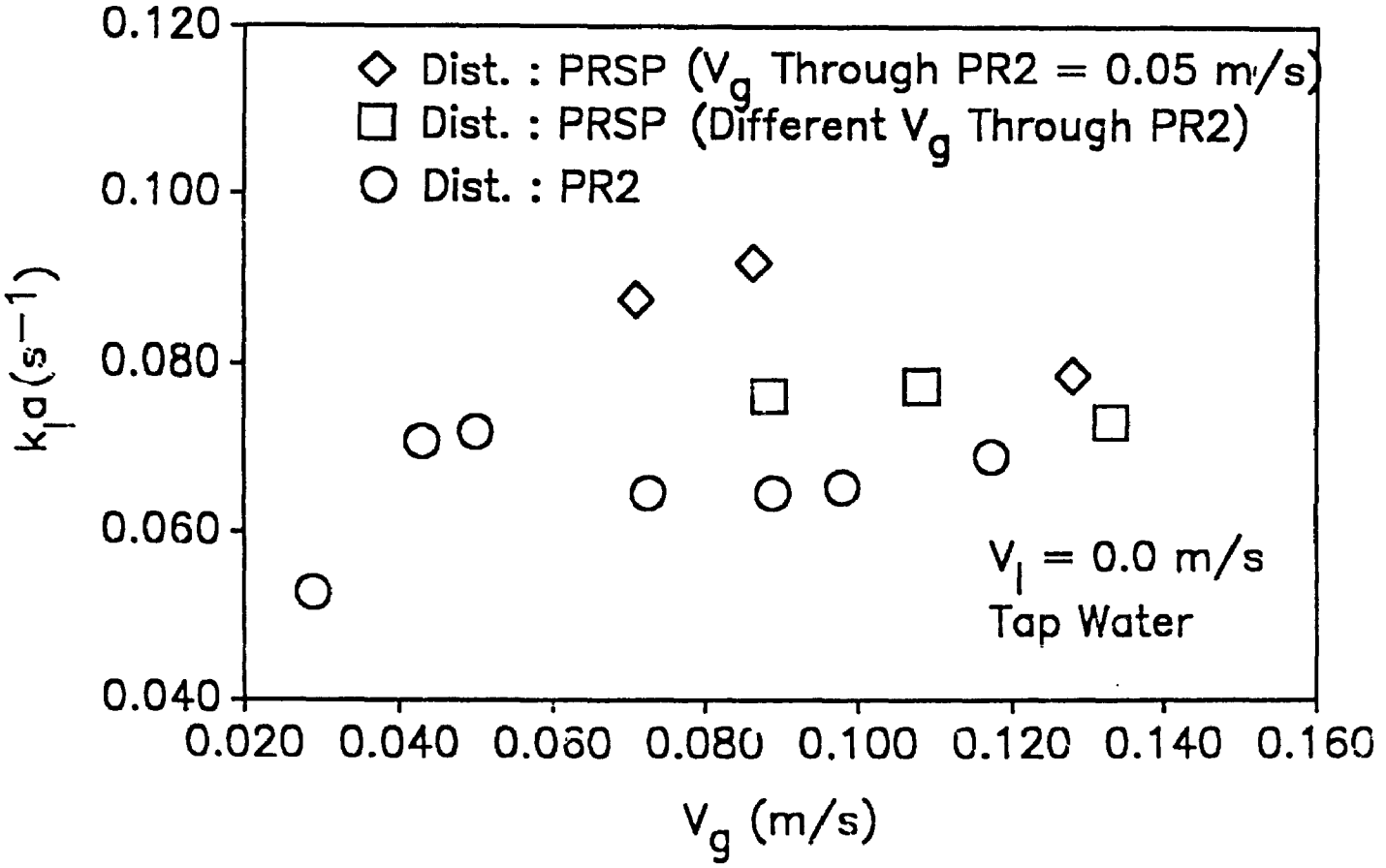

Figure 4.1.28
Comparison of volumetric mass transfer coefficient obtained with porous distributor PR2 and combination of porous distributor PR2 and sparger SP1

distributor alone, (i.e. corresponding to V_g = 0.05 m/s, see Figure 4.1.12). As shown by Figure 4.1.28, the mass transfer coefficient obtained with the sparger/porous combination dropped significantly when the gas flowrate through the porous distributor was less than its optimum value.

The combination out-performed the porous distributor (PR2) over the whole range of gas flowrates larger than the optimum gas flowrate for this porous distributor (Figure 4.1.28).

The improvements in mass transfer rates obtained with the combination resulted from the higher gas holdups and hence the interfacial area for mass transfer (Figure 4.1.29). From visual observations, it was seen that there was a high concentration of bubbles in the bubble swarm as it was moving upwards from the distributor PR2. The larger bubbles generated at the sparger (SP1) created the turbulence which broke up the swarm and dispersed the bubbles over the entire cross-sectional area of the column.

Figure 4.1.26 compares the variations of the mass transfer coefficient with the energy input rate per unit of reactor volume obtained with various distributors. It can be seen that at low energy input rates the large area porous distributor (PR1) was more energy efficient than

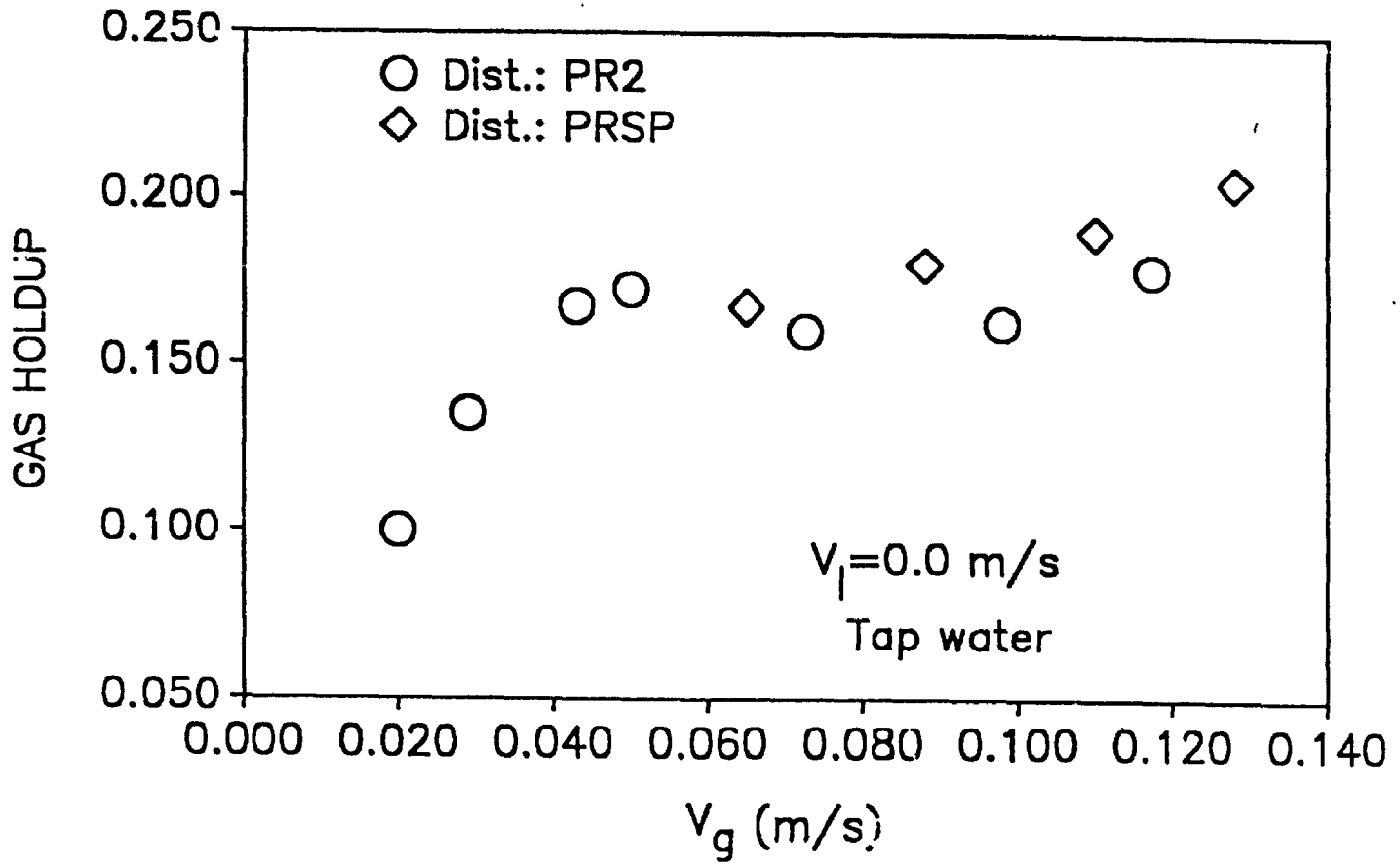

Figure 4.1.29
Comparison of gas holdups obtained with porous distributor PR2 and combination of PR2 and SP1

other distributors. However, at higher energy input rates the difference between the large area porous distributor and the porous sparger combination (PRSP) was reduced.

4.2 Three-Phase Fluidized beds

4.2.1 Phase Holdups

The measurements of gas and liquid holdups provide information about the effect of operating variables on bed hydrodynamics The variations of the phase holdups can often be related to the variations of the mass transfer rates. The effects of various operating variables on the gas and liquid holdups are discussed in the following sections.

4.2.1.1 Effects of Gas and Liquid Velocities

Gas holdup in three-phase fluidized beds increased with increasing gas velocities in all systems (Figures 4.2.1, 4.2.2, 4.2.3). The gas holdup values, however, depended on the particle size and the liquid coalescing behavior. Since, particle sizes were large and liquid viscosities were low, no bed contraction could be observed.

The liquid holdup was found to decrease with

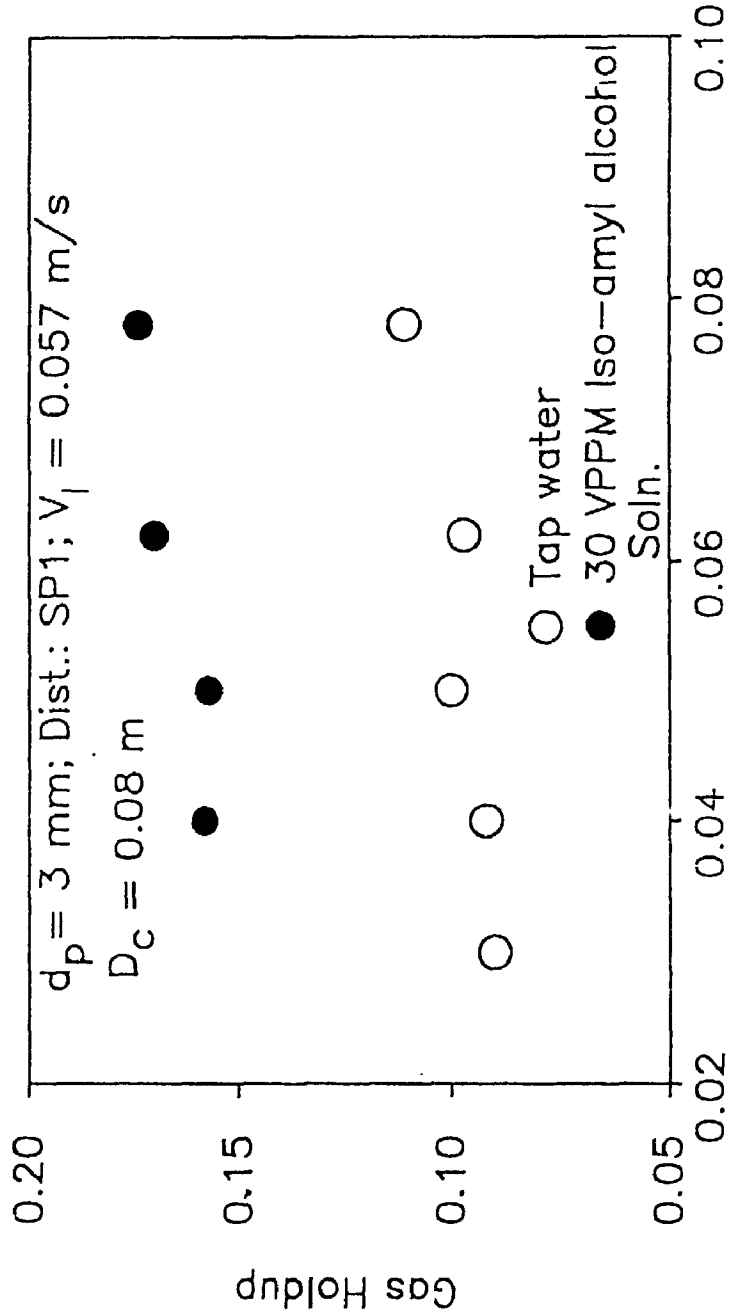

Figure 4.2.1
Effects of gas velocity on gas holdups in coalescing and noncoalescing liquids (3-phase fluidized bed; d_p = 3 mm).

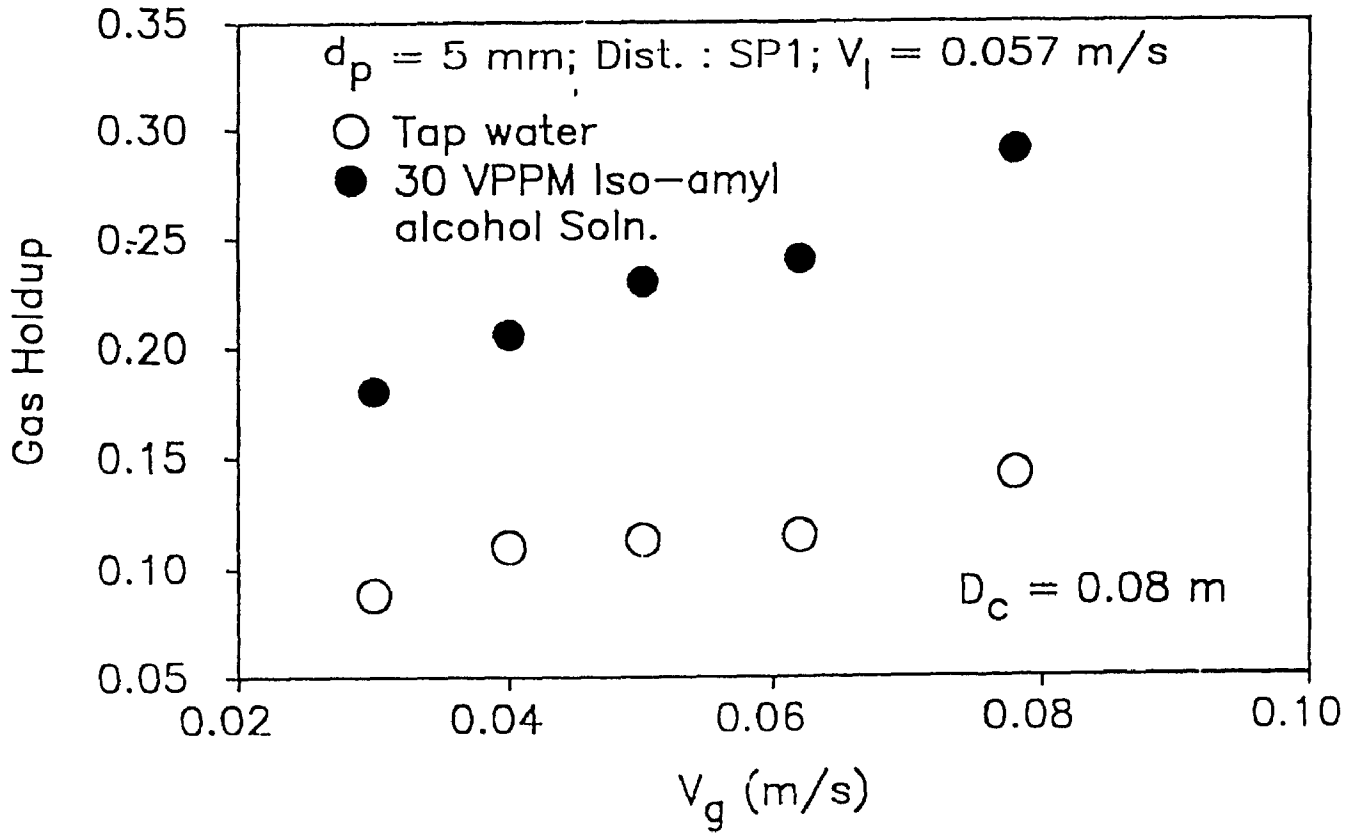

Figure 4.2.2
Effects of gas velocity on gas holdups in coalescing and noncoalescing liquids (3-phase fluidized bed; d_p = 5 mm).

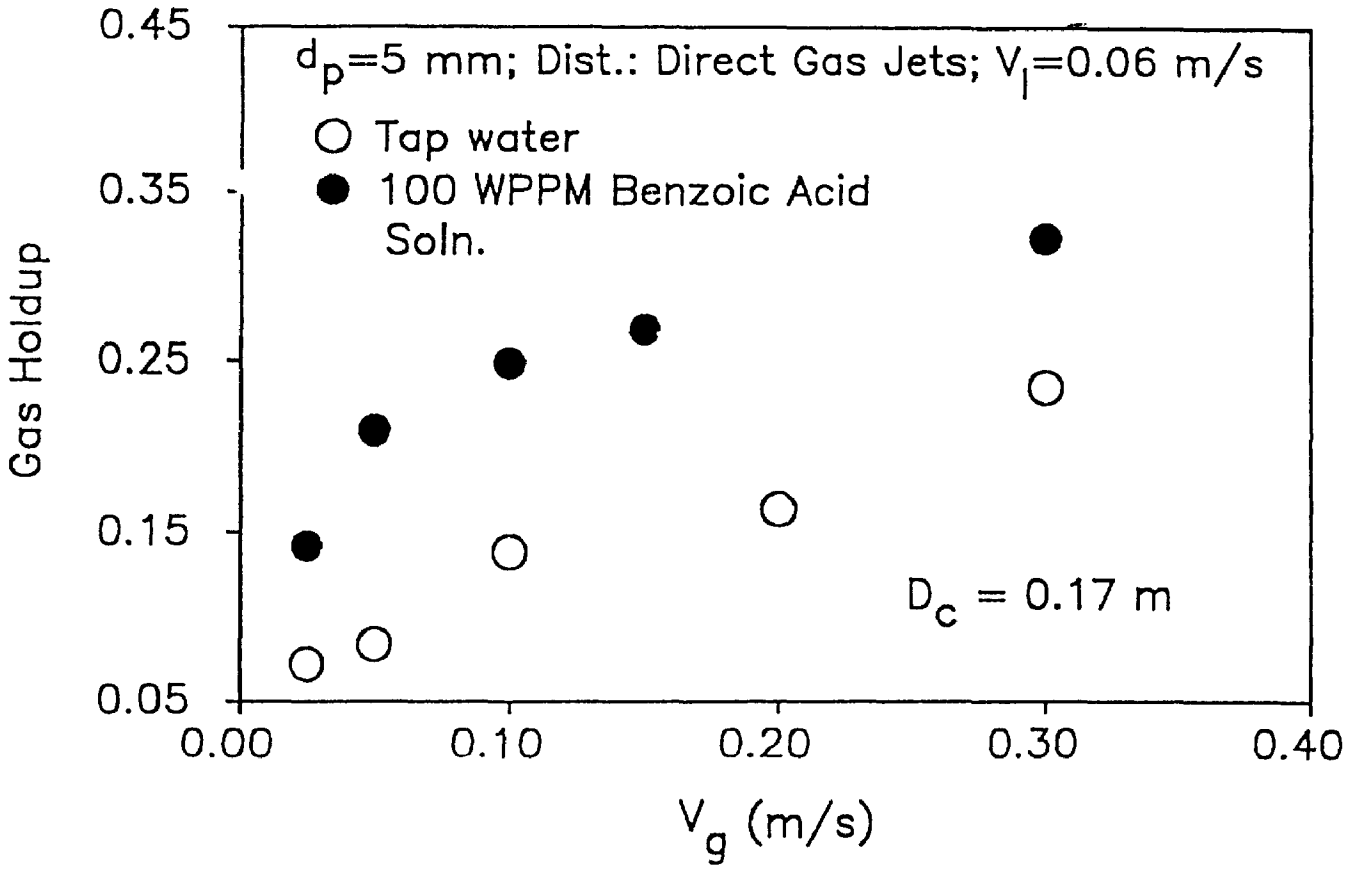

Figure 4.2.3
Comparison of gas holdups obtained in coalescing and noncoalescing liquids; Large diameter column (d_p = 5 mm)

increasing gas velocities (Figures 4.2.4 and 4.2.5).

These results are generally in agreement with the literature studies (see section 2.3.4.2.1).

Although no systematic study was conducted to investigate the effects of liquid velocity on phase holdup, the data of this study showed that there was no significant effect of liquid velocity on gas holdup over the range of operating conditions studied (Figure 4.2.6).

4.2.1.2 Effect of Coalescence Properties of Liquid

The gas holdups in noncoalescing liquid solutions were significantly higher than in the coalescing liquid for various systems (Figures 4.2.1, 4.2.2, 4.2.3). The gas holdup was increased by 40 to 80% when the liquids became non-coalescing. The small concentrations of coalescence inhibitors used for the study did not affect other physical properties of the liquid such as surface tension and viscosity. The higher gas holdups were the results of the coalescence inhibition effects of the additive molecules (see section 4.1.3.3).

4.2.1.3 Effects of Particle Size

Higher gas holdups were obtained in the beds of 5 mm glass beads as compared with the beds of 3 mm beads, in both coalescing and noncoalescing system. Figure 4.2.7 compares the gas holdups obtained in a noncoalescing

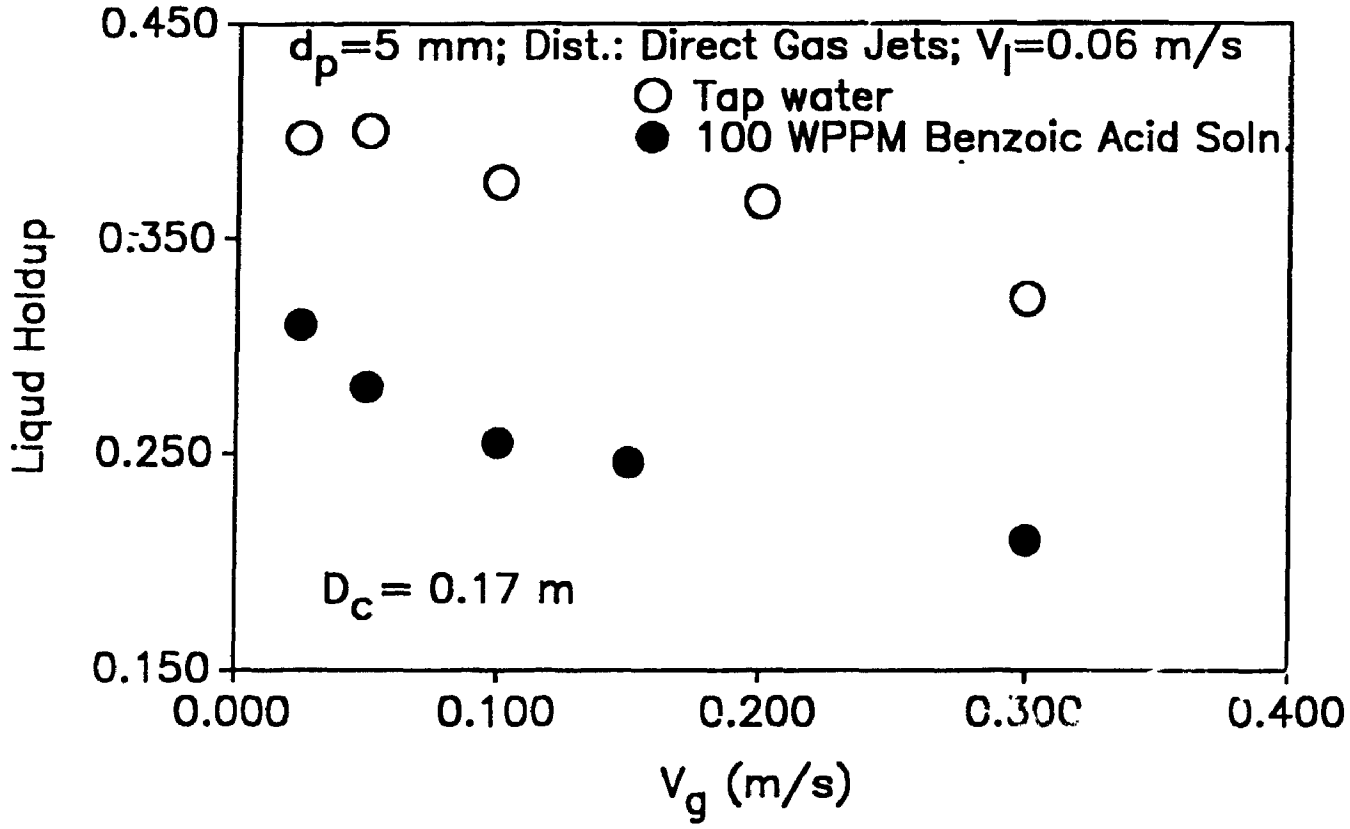

Figure 4.2.4
Effects of gas velocity on liquid holdups; Large diameter column

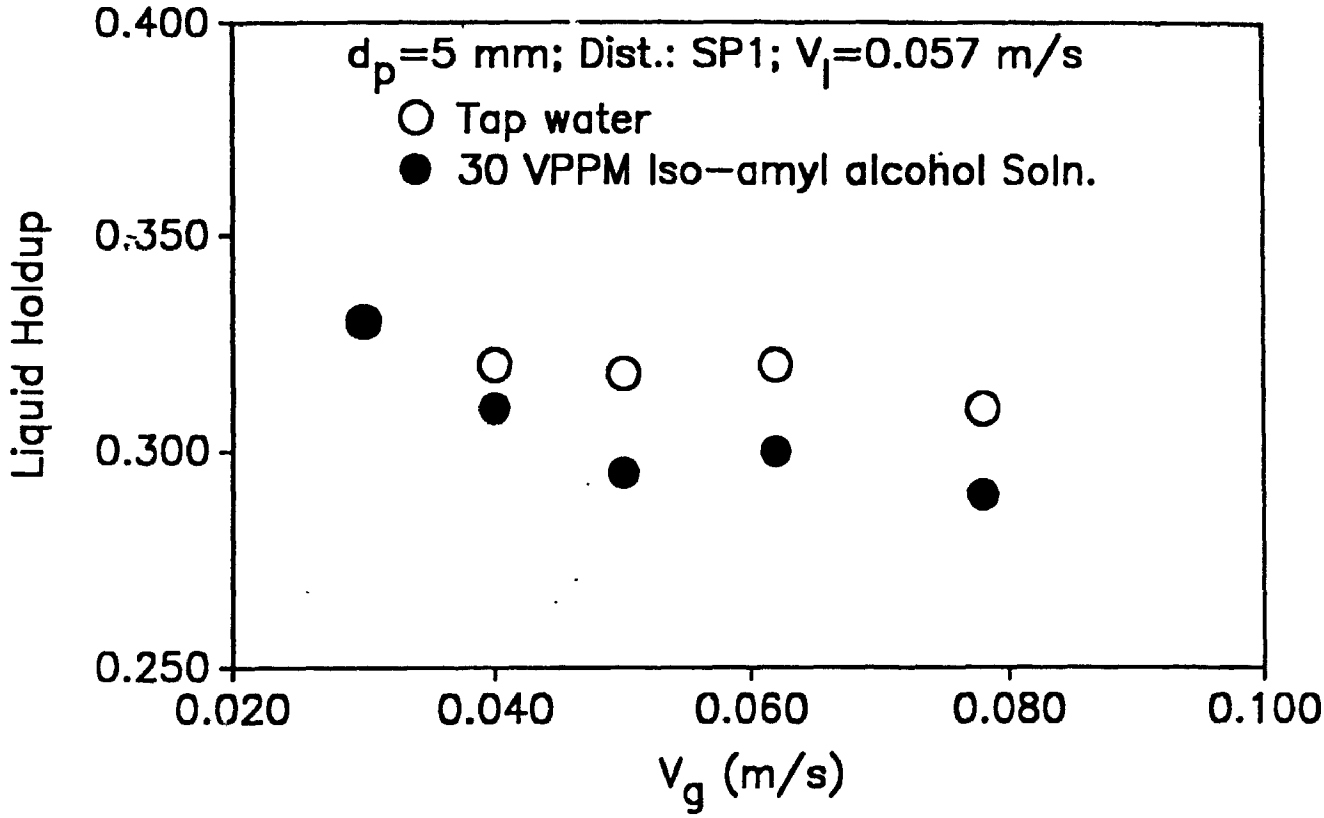

Figure 4.2.5
Effects of gas velocity on liquid holdups; Small diameter column

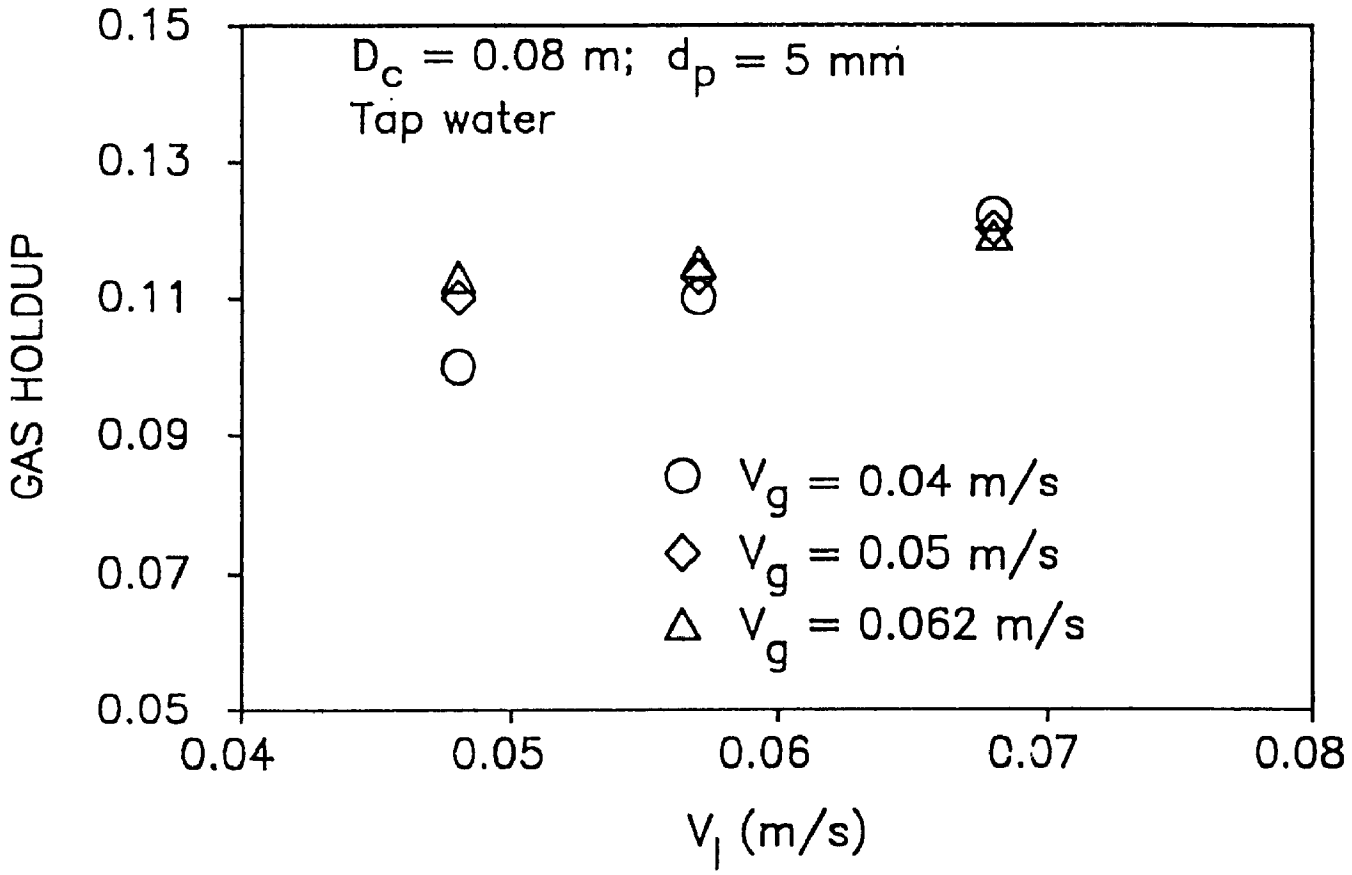

Figure 4.2.6
Effect of liquid velocity on gas holdup; Three-phase fluidized bed

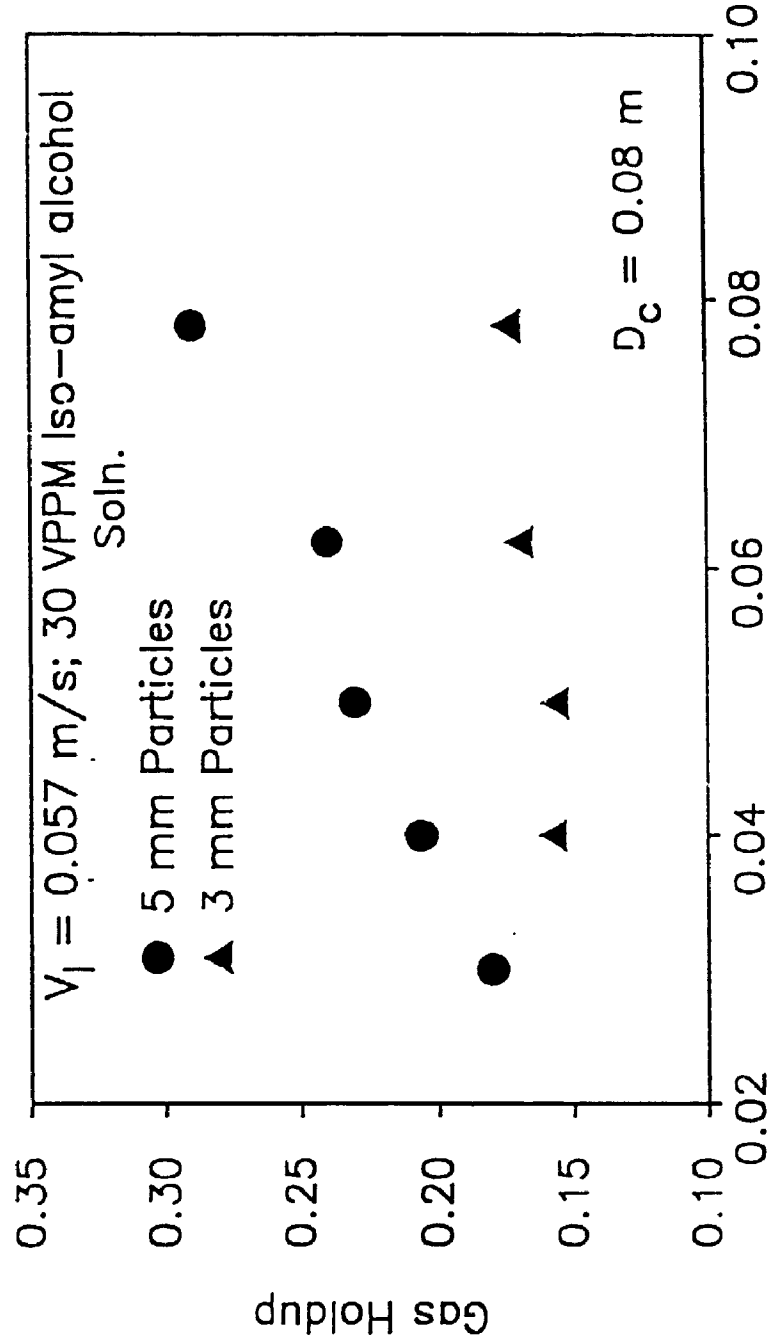

Figure 4.2.7
Comparison of gas holdups obtained in 3 mm and 5 mm particles beds.

liquid phase in the small diameter column. These observations are in agreement with other literature studies (see section 2.3.3.2.4).

4.2.1.4 Effects of Gas Distribution

The phase holdups were found to depend on the type of gas distributor used in the bed. Figure 4.2.8 compares the gas holdups obtained with two different types of distributors used in the small diameter column. The lower gas holdups obtained with the porous distributor (PR2: see Table 3.1.2). could be attributed to the formation of defluidized zones in the vicinity of the distributor.

Figure 4.2.9 compares the liquid holdups obtained in the large diameter column with direct gas jets and packed bed distributors. The lower liquid holdups obtained with the packed bed distributor could mainly be attributed to improved gas distribution which leads to smaller gas bubbles hence, larger gas holdups.

4.2.1.5 Test of Literature Correlations/Models

The various literature correlations and models developed for the prediction of phase holdups in three-phase fluidized beds were reviewed in section 2.3.3.3. These correlations and models are tested here, using the following data of this study.

Column ID: 0.171 m

Distributors: Direct jets, Packed bed

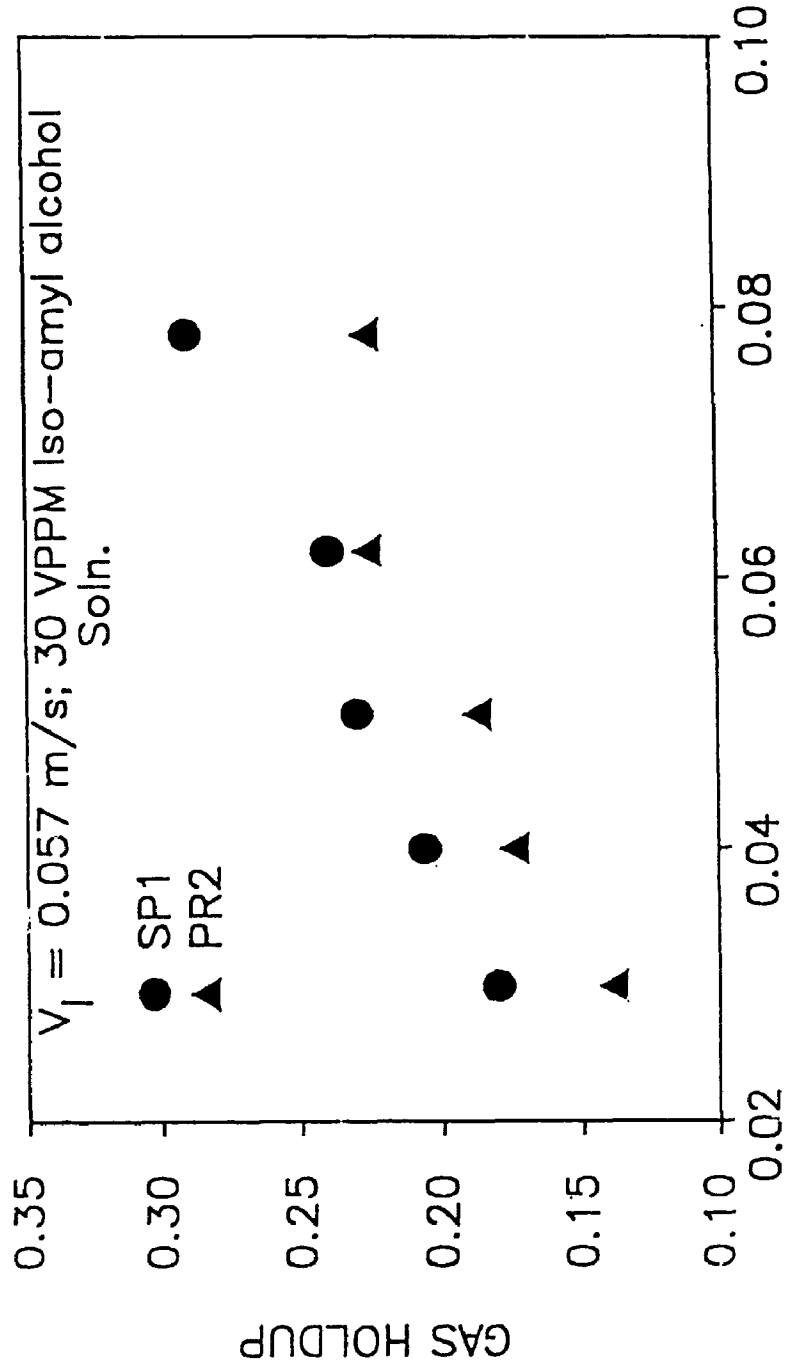

Figure 4.2.8
Comparison of gas holdups obtained with distributors SP1 and PR2 (d_p = 5 mm).

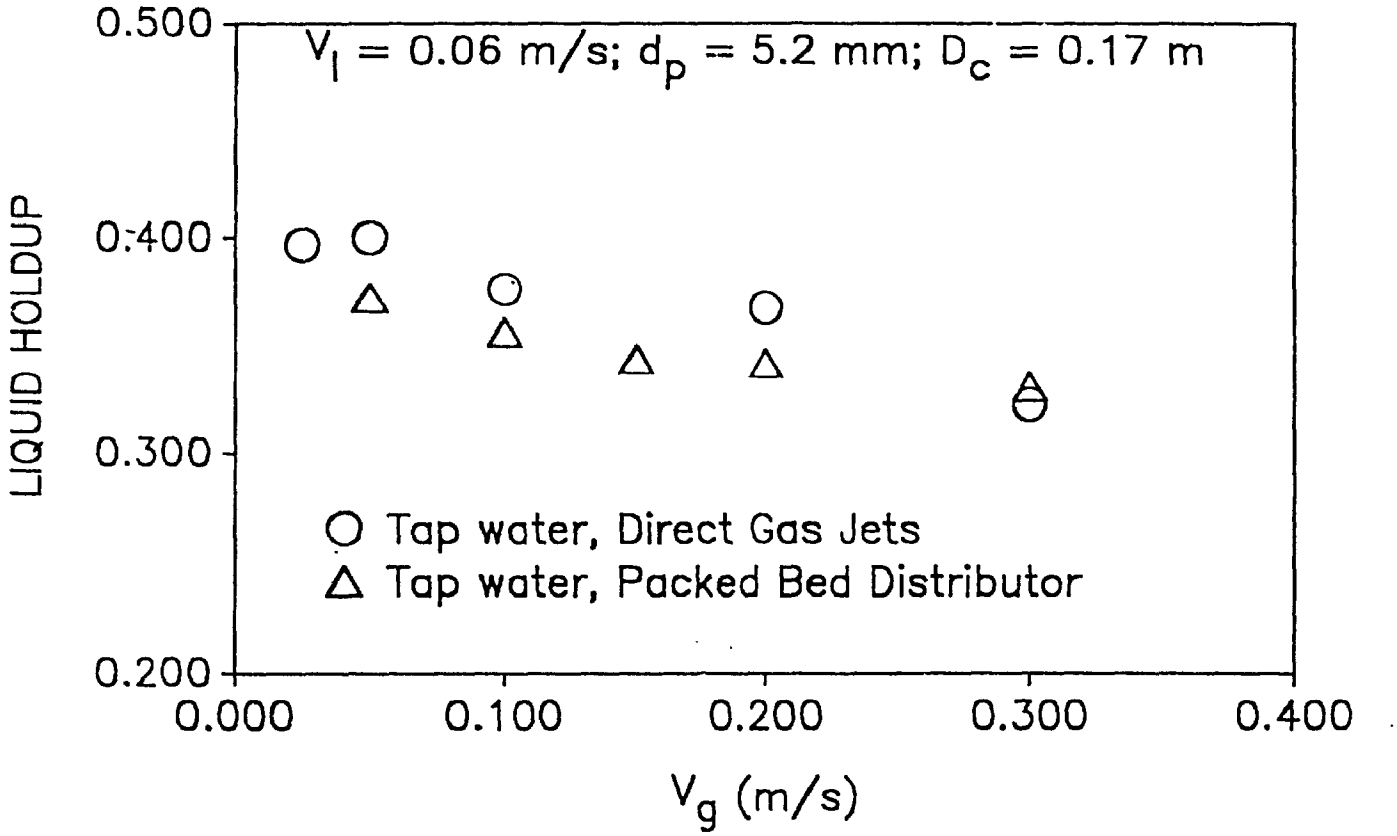

Figure 4.2.9
Effect of gas distribution on liquid holdups (3-Phase fluidized bed).

Particle size: 5 mm; Liquids: Tap water, Benzoic acid Solutions

Column ID: 0.08 m

Distributor: SP1

Particle sizes: 3 and 5 mm; Liquids: Tap water, 30 vppm amyl alcohol solutions.

Table 4.2.1 shows the absolute average relative errors when the various empirical correlations from the literature were used to predict the gas holdup for the coalescing liquid phases of this study.

Table 4.2.1: Test of Literature Empirical Correlations for Gas Holdups in Coalescing System (see section 2.3.3.3.2 for correlations)

Investigators	Average Absolute Relative Error	Remarks
Begovich and Watson (1978)	15 %	Although gives minimum error there is large scatter in predicted values (-35 to 60 %)
Kato et al. (1985)	66 %	Predicted values always lower (50 to 80 %)
Khang et al. (1983)	156 %	Predictions always high (50 to 250 %)
Hu et al. (1986)	62 %	Predictions always low (25 to 80 %)

$$\text{Average Absolute Relative Error} = \frac{\Sigma \left| \frac{\text{Calc. Value} - \text{Exptl. Value}}{\text{Exptl. Value}} \right| X100}{n_T}$$

It can be seen that the correlation proposed by Begovich and Watson (1978) gives the best predictions with a relative average error of about 15 %. The correlations proposed by Hu et al. (1986) and Kato et al. (1985) predict significantly lower values while the predictions from the correlation proposed by Khang et al. (1983) are much higher than the experimental values of this study.

None of the literature correlations could, however, give a good prediction of the gas holdups in the noncoalescing liquids. The predicted values were generally significantly lower (40 % or more) than the experimental values.

The tests of various empirical correlations for the prediction of liquid phase holdups are summarized in Table 4.2.2. It can be seen that the correlations proposed by Kim et al. (1975) and Chiu and Ziegler (1983) provide the best predictions for the liquid holdups for coalescing liquid phase.

The liquid phase holdups for the noncoalescing liquids could not, however, be predicted by the literature correlations.

The literature correlations for bed porosity were

also tested for both the coalescing and noncoalescing systems of this study. Table 4.2.3 shows absolute average relative errors for the two systems. It can be seen that the correlation proposed by Dakshinamurty et al. (1972) gave good predictions of the bed porosity for both coalescing and noncoalescing systems. Apparently, the coalescing properties of the liquid did not significantly affect the bed porosity.

Table 4.2.2: Test of Literature Correlations for Liquid Holdups in Coalescing Systems (see section 2.3.3.3.3 for correlations)

Investigators	Average Absolute Relative Error	Remarks
Razumov et al. (1973)	43 %	Large scatter in predicted values (-42 to 66 %)
Kim et al. (1975)	8 %	Lowest relative error and lowest scatter(-18 to 15%)
Kato et al. (1981)	29 %	Predicted values always high (8 to 53 %)
Chiu and Ziegler (1983)	11.7 %	Low scatter for predicted values (-13 to 23 %)
Lee (1986)		
Power law model	79 %	Predicted values always high
Exponential	43 %	

Table 4.2.3: Test of Literature Correlations for Bed Porosity (see section 2.3.3.3.1 for correlations)

Investigators	Average Absolute Relative Error		Remarks
	Coales.	Noncoal.	
Dakshinamurty et al. (1972)	5 %	6 %	Lowest average relative error and low scatter of predicted values (-15 to 7 %)
Soung (1978)	8 %	8.8 %	
Begovich and Watson (1978a)	39 %	30 %	Predictions always higher (18 to 50 %).
Saberian et al. (1987)	36 %	34 %	Predictions always high (17 to 50 %)

The various correlations based on the wake model were reviewed in section 2.3.3.3.5. It was mentioned that these correlations differ with respect to the assumptions for 'x' and correlation for 'k'. The liquid phase holdups and bed porosities were obtained, using various correlations for k and x and experimental values of gas holdups. It can be seen from Table 4.2.4 that except for the correlation of Morooka et al. (1986) the various correlations predicted the liquid holdup and the bed porosity within 15% of the experimental values for both coalescing and noncoalescing liquids. The best predictions

Table 4.2.4 Test of Literature Correlations based on Wake Model (using experimental gas holdup)

Investigators	Average Absolute Relative Error		Remarks
	Liquid Holdup	Bed Porosity	
Ostergaard (1965)	13 %	10 %	Scatter for predicted values (0 to 26 %)
Efremov and Vakhrushev (1970)	11.6 %	9 %	Scatter for predicted values (-5 to 25 %)
Bhatia and Epstein (1974)	11 %	8.5 %	Scatter for predicted values (-6 to 25 %)
Darton and Harrison (1975)	8 %	6 %	Lowest relative error
Baker et al. (1977)	12 %	9 %	Scatter for predicted values (-2 to 20 %)
El-Temtamy and Epstein (1978)	9 %	7 %	Scatter for predicted values (-20 to 26 %)
Khang et al. (1983)	15 %	11 %	Low scatter for predicted values (1 to 25 %)
Morooka et al. (1986)	68 %	51 %	Predicted values always high (2 to 140 %)

were, however, given by the correlations of Darton and Harrison (1975) and El-Temtamy and Epstein (1978).

Prediction of phase holdups, using the wake model, requires knowledge of gas holdup. However, no correlations are available for the prediction of gas holdup in noncoalescing systems.

The drift flux model for three-phase fluidized beds was discussed in section 2.3.3.3.4. Using the drift flux concept the gas and liquid phase holdups can be calculated if the correlations for drift flux velocity and bed porosity are available. Saberian et al. (1987) proposed a correlation for drift flux for coalescing liquids. This correlation however gave a poor prediction of drift flux for the data of this study (average relative error was more than 50%).

Since none of the proposed correlations could predict the gas and liquid phase holdups in noncoalescing system, it was decided to explore ways to develop suitable correlations for such systems. The drift flux concept makes more physical sense for the noncoalescing systems, where the average bubble size is very small, and the gas-liquid mixture can be treated as a pseudo homogeneous phase. It was, therefore decided to develop new correlations for the drift flux based on the data of this study for both systems.

4.2.1.6 New Correlations Based on Drift Flux Model

The following correlations were developed for drift flux velocity for the two systems using data obtained with the two columns (section 4.2.1.5)

Coalescing System:

$$V_{gl} = 0.85\ V_g^{1.2} \qquad \text{.....(4.2.1)}$$

$$R^2 = 0.85$$

Noncoalescing System:

$$V_{gl} = 0.063\ V_g^{1.76}\ D_c^{-1.4} \qquad \text{.....(4.2.2)}$$

$$R^2 = .93$$

Based on the data of this study, the drift flux was not found to depend on the particle size for both systems.

Figures 4.2.10 and 4.2.11 show the plots of drift flux velocity as a function of gas velocity, based on the above correlations. It can be seen that the proposed correlations predict the drift flux velocity fairly well. A unified correlation based on the combined data of the two systems could not, however, be developed. It may also be noted that based on the data of this study, the drift flux was found to be independent of the column diameter for coalescing system while it depended on the column diameter for noncoalescing systems.

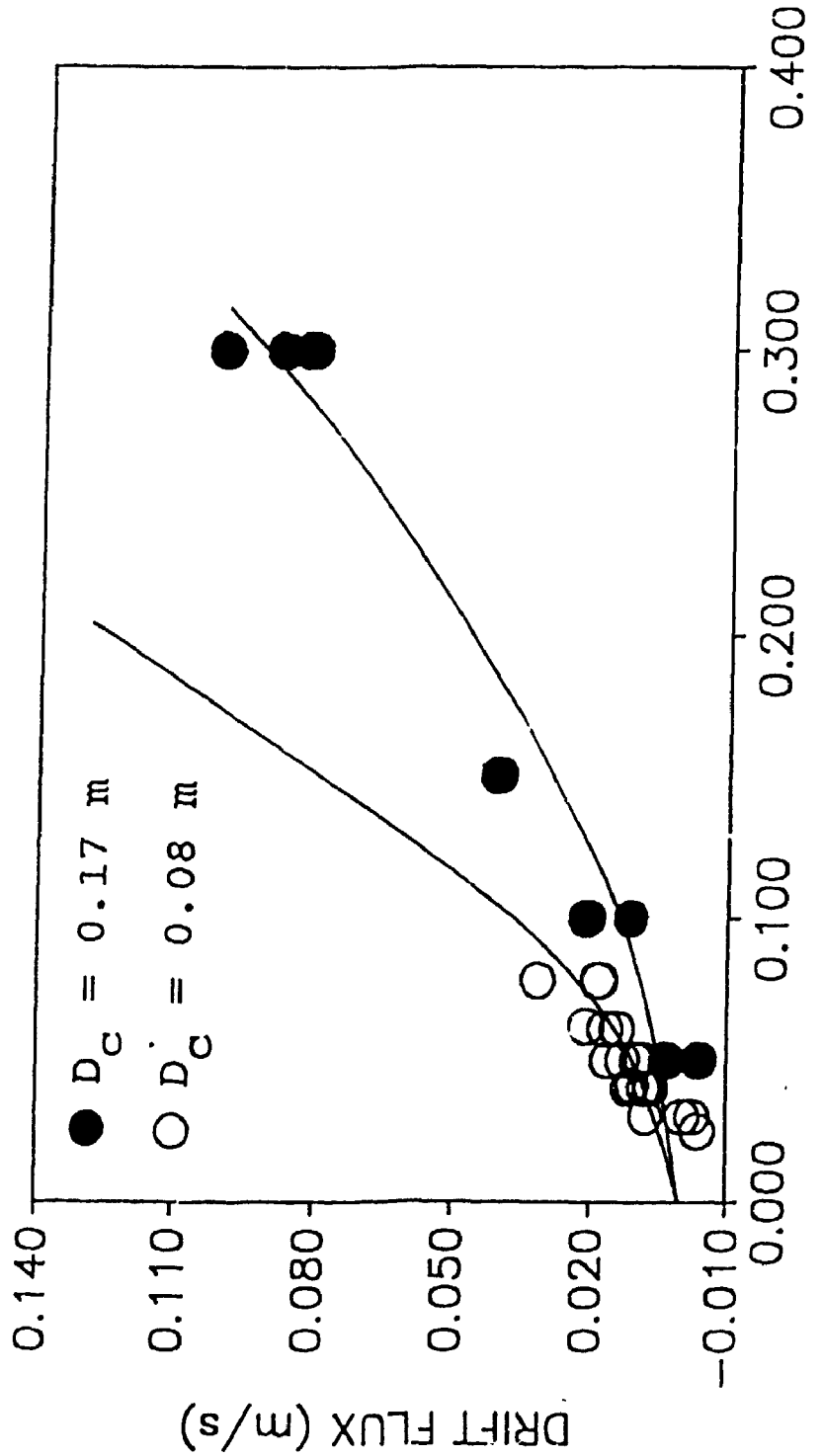

Figure 4.2.10
Plot of drift flux velocity as a function of gas velocity
(3-phase fluidized beds; noncoalescing medium).

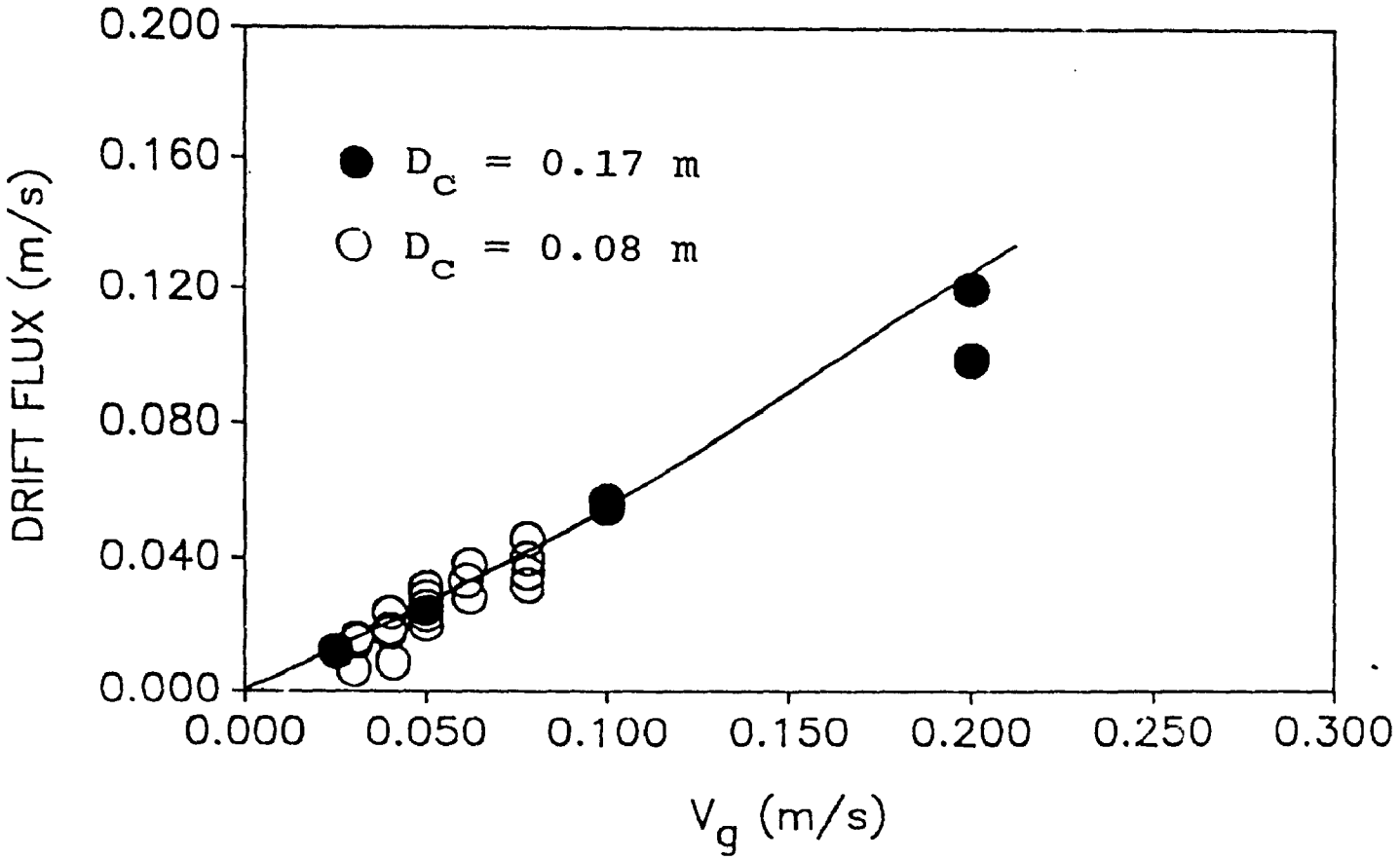

Figure 4.2.11
Plot of drift flux velocity as a function of gas velocity (3-phase fluidized beds; coalescing medium).

Using the proposed correlations for the drift flux, the gas and liquid phase holdups could be determined if bed porosity was known (see section 2.3.3.3.4 for details). It was shown in section 4.2.1.5 that the correlation proposed by Dakshinamurty et al. (1972) provided good predictions of bed porosity for both coalescing and noncoalescing systems. The correlation of bed porosity proposed by Dakshinamurty et al. (1972) was therefore combined with Equations 4.2.1 and 4.2.2 to predict the gas and liquid phase holdups for the two systems. Table 4.2.5 shows the absolute relative average errors for the predicted values of phase holdups.

Although, there is a reasonable prediction of the phase holdups in both systems, better fit is obtained for the noncoalescing system. This is confirmed by the plots of calculated values against the experimental values (Figures 4.2.12, 4.2.13, 4.2.14 and 4.2.15).

As reviewed in section 4.2.1.5, the literature correlations can provide a good prediction of phase holdups in the coalescing system, while there is no correlation for noncoalescing system. The proposed correlations for the noncoalescing system can provide a good estimate of the phase holdups for such systems.

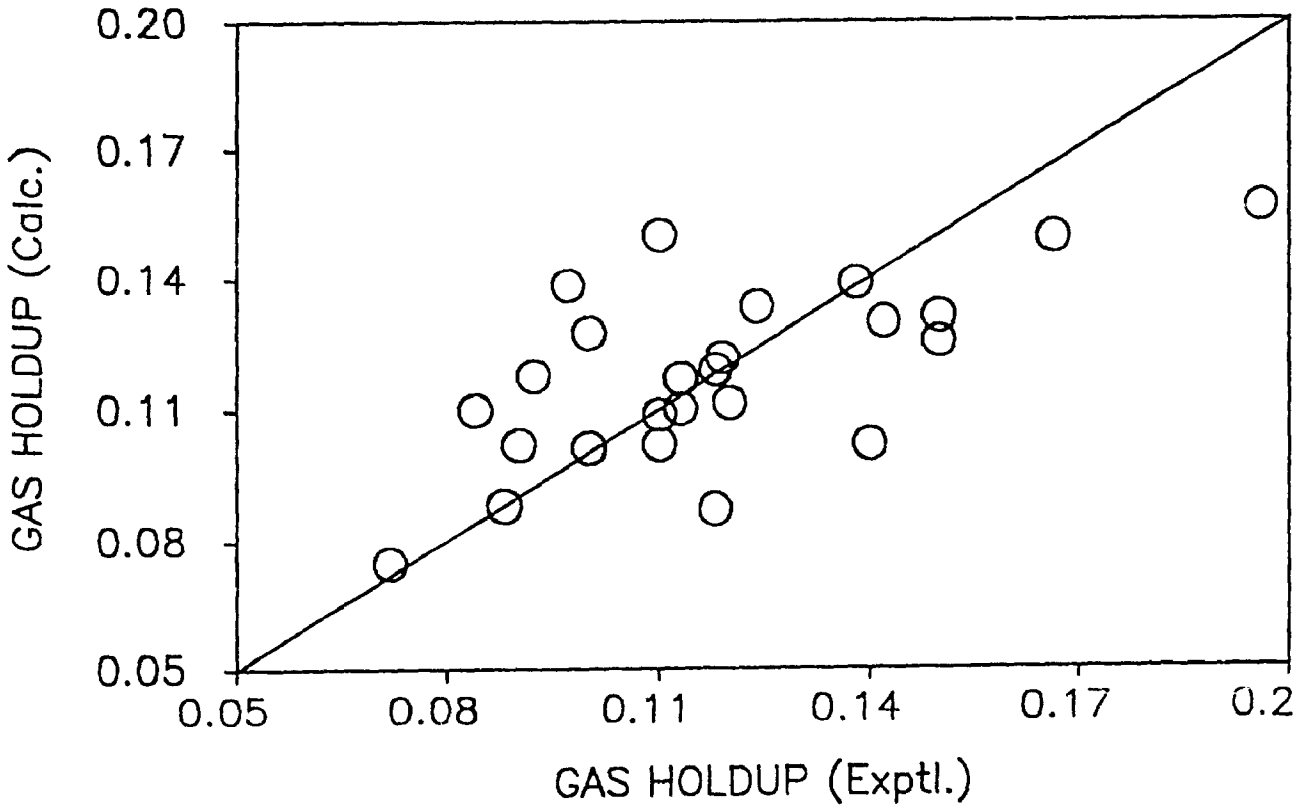

Figure 4.2.12
Calculated versus experimental values of gas holdups;
Drift flux model (3-phase fluidized beds;
Coalescing medium)

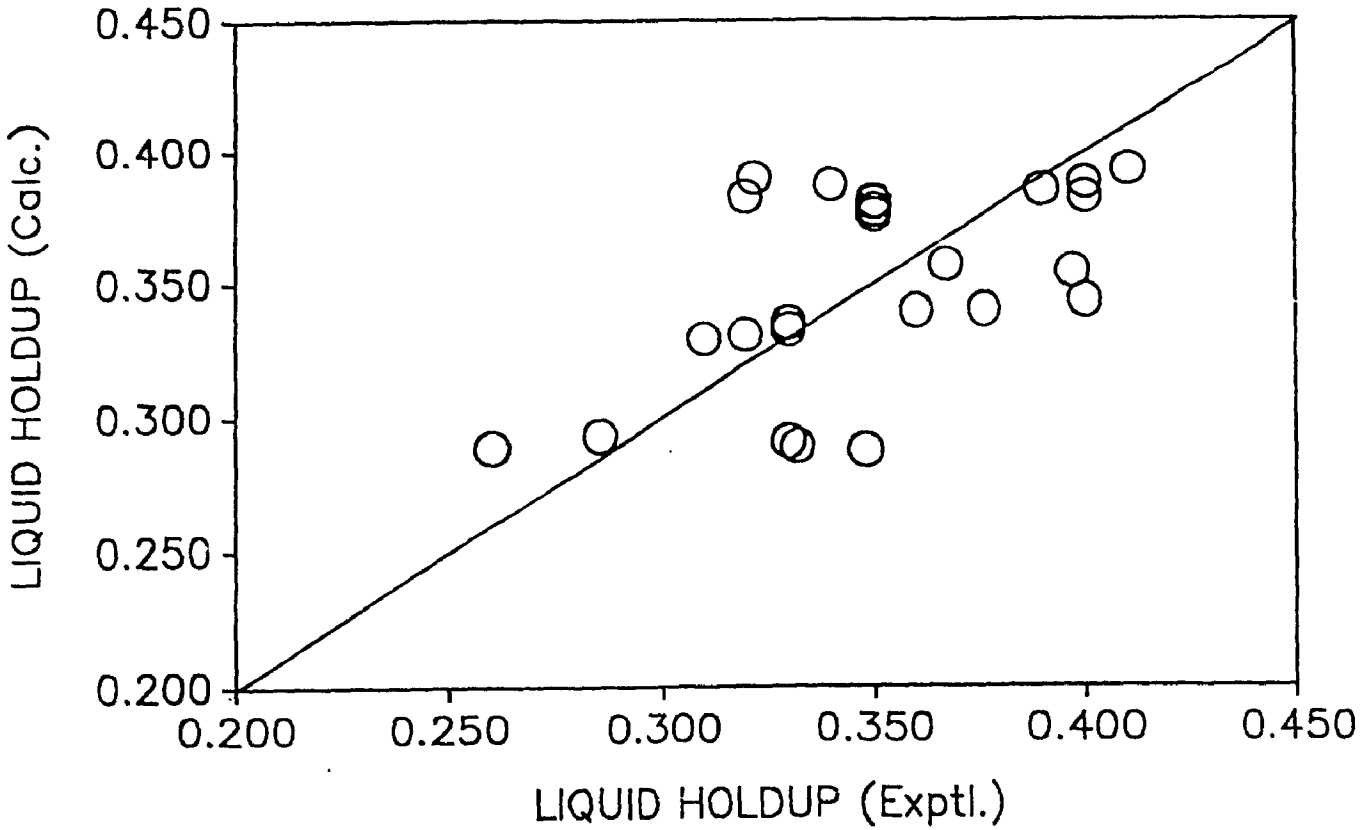

Figure 4.2.13
Calculated versus experimental values of liquid holdups
Drift flux model (3-phase fluidized beds;
Coalescing medium)

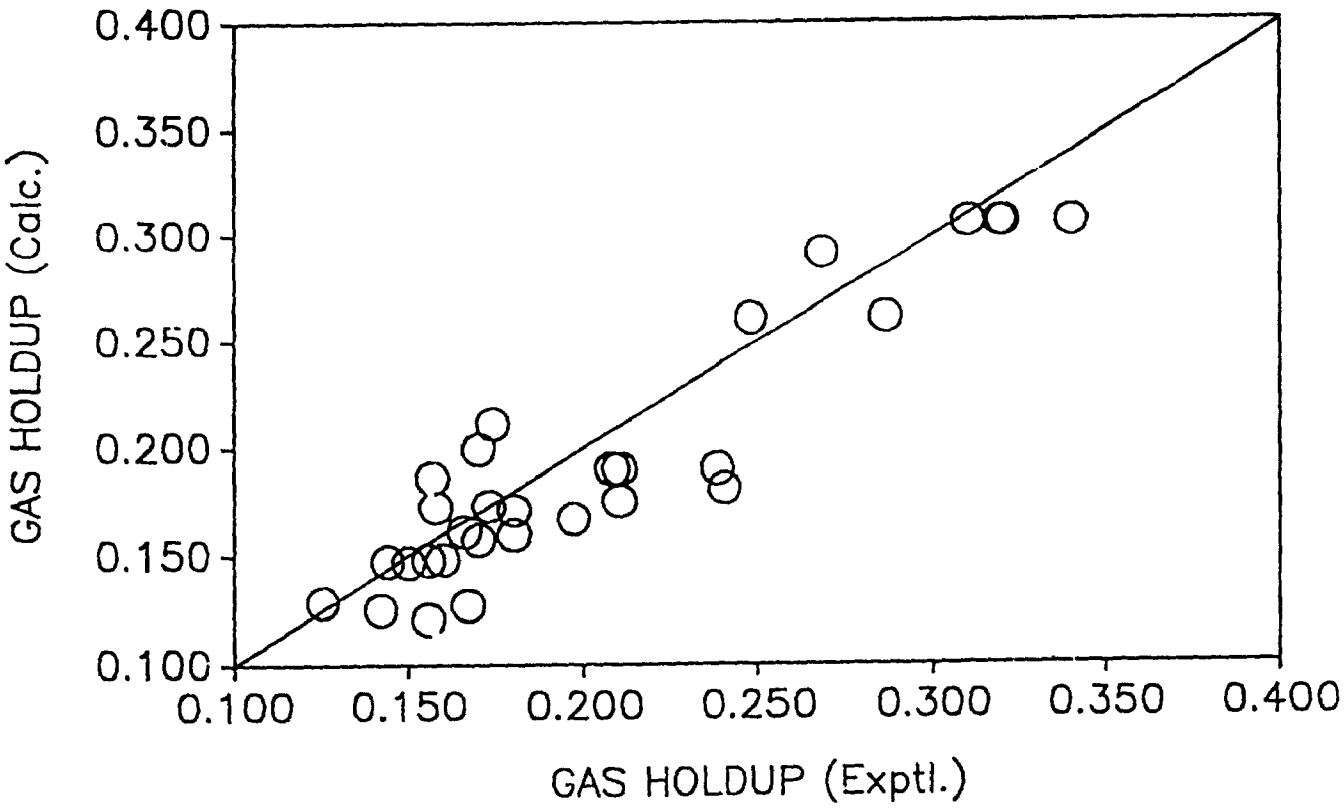

Figure 4.2.14
Calculated versus experimental values of gas holdups;
Drift flux model (3-phase fluidized beds;
Noncoalescing medium)

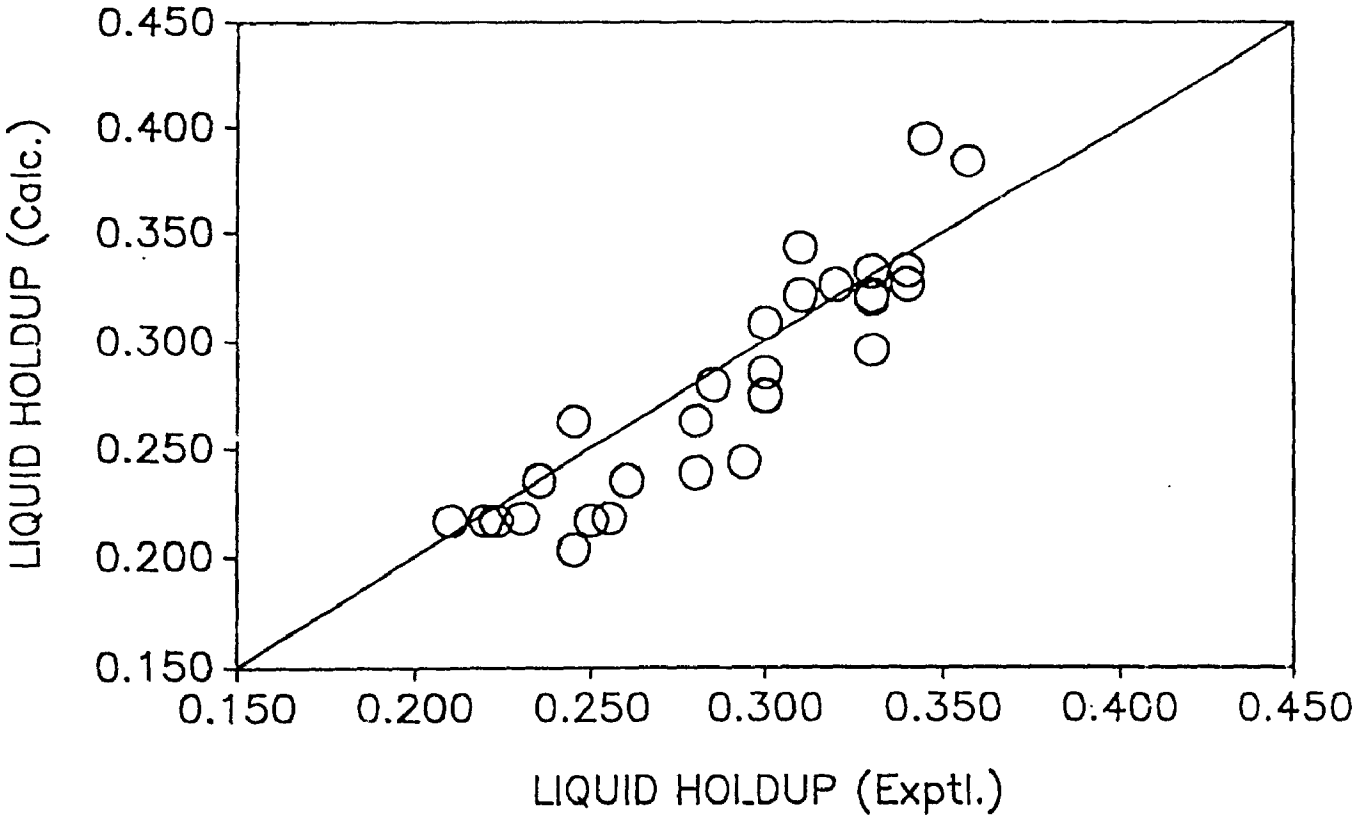

Figure 4.2.15
Calculated versus experimental values of liquid holdups;
Drift flux model (3-phase fluidized beds;
Noncoalescing medium)

Table 4.2.5: Test of Proposed Drift Flux Correlations for Predictions of Phase Holdups: Three-Phase Fluidized Beds

Phase	System	Mean Absolute Relative Error.
Gas	Coalescing Liquid	13.4 %
Liquid	Coalescing Liquid	8.4 %
Gas	Noncoalescing Liquid	10.2 %
Liquid	Noncoalescing Liquid	7.0 %

4.2.2 Liquid Mixing

As reviewed in section 2.3.4, the liquid backmixing in three-phase fluidized beds has been extensively studied. The beds of larger particles are generally characterized by a low degree of backmixing. For the present study, the axial dispersion coefficients were measured only for one set of gas and liquid flowrates, selected for each particle size. The tracer was injected at 0.01 m from the column wall and about 0.04 m below the bed surface. The objective of these measurements was to obtain information for the selection of a proper flow model for the estimation of mass transfer coefficient. It can be seen from Table 4.2.6 that the values of axial

dispersion coefficients obtained were quite low and in agreement with the predictions by correlations of Kim and Kim (1983).

Table 4.2.6: Axial Dispersion Coefficient: Three Phase Fluidized Beds

Operating Conditions	Axial Dispersion Coefficient	
	Measured(m^2/s)	Predicted(m^2/s)
V_g = 0.078 m/s V_l = 0.057 m/s d_p = 5 mm	0.0036	0.0034
V_g = 0.068 m/s V_l = 0.057 m/s d_p = 3 mm	0.0057	0.005

Some qualitative observations of liquid flow patterns were also made in the bed of 5 mm particles for one set of conditions (V_l = 0.068 m/s; V_g = 0.062 m/s). The tracer solution was continuously injected close to the distributor (using lowest sampling probe), about half way between centre and wall. The liquid samples were collected from near the wall, centre and midway between centre and wall using third, fourth and fifth sampling probes respectively (see Figure 3.1.2). The tracer concentration was found to be highest at the centre and lowest at the wall. These observations suggest that in three-phase

fluidized beds, the liquid preferentially moves to the column centre (i.e the liquid flow has a radial component). This could be caused by the motion of bubbles which tend to concentrate at the centre of the bed (Lee and De Lasa, 1987).

The liquid flow patterns could also be affected by the choice of the gas and liquid distributors, specially in the region close to the distributors where the flows are not fully established. Further work is, however, required to establish the effects of liquid and gas distribution on liquid flow patterns in three-phase fluidized beds.

4.2.3 Gas-Liquid Mass Transfer

As reviewed in section 2.3.6, a number of researchers have studied gas-liquid mass transfer in three-phase fluidized beds. While the effect of various operating variables such as gas and liquid velocity, particle size and density has been investigated extensively, no work has been done so far to investigate the effect of the liquid coalescence behavior. The main objective of this study was thus, to investigate how gas-liquid mass transfer was affected by the liquid coalescence behavior. To change the liquid coalescing behavior without affecting any of its other properties such as viscosity and surface tension, low concentrations (30 vppm and less) of an effective

coalescence inhibitor were used. Measurements were also made in the coalescing liquid (tap water) for the purpose of comparison.

The procedure used for the estimation of mass transfer coefficient was discussed in section 3.2.4 and various assumptions were clearly stated. It was pointed out that given the complex nature of liquid flow patterns in the bed, the simplified flow model provides only approximate estimates of the volumetric mass transfer coefficients in three-phase fluidized beds.

The effects of different operating variables, on mass transfer rate is discussed in the following sections.

4.2.3.1 Effects of Gas and Liquid Velocities

The mass transfer coefficient was found to increase with gas velocity for both particle sizes and different liquid solutions (see Figure 4.2.16, 4.2.17). These observations are generally in agreement with other researchers (see section 2.3.6.2.2).

Figure 4.2.18 is a plot of volumetric mass transfer coefficient as a function of liquid velocity. It can be seen that the mass transfer coefficient passed through a maximum with increasing liquid velocity. These observations are again in agreement with the results of literature studies (see section 2.3.6.2.2).

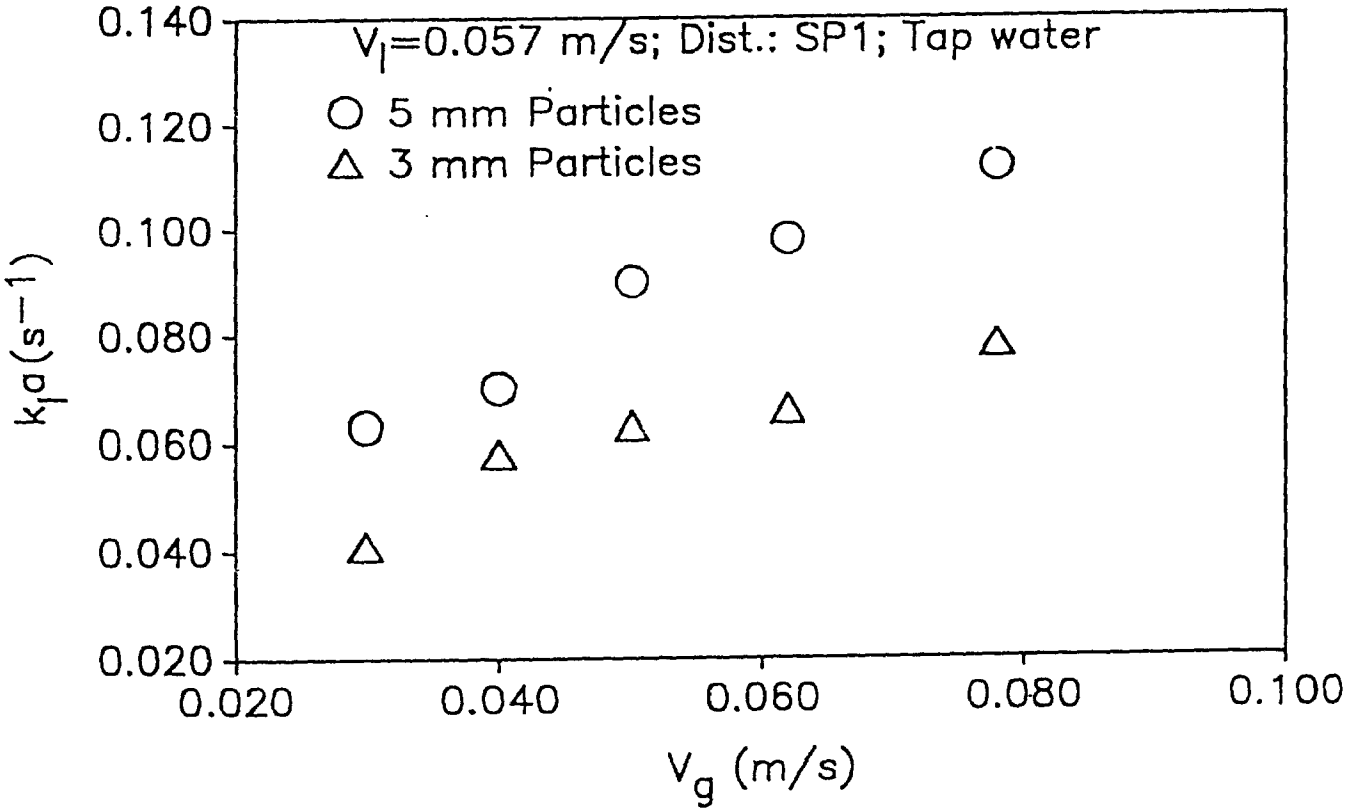

Figure 4.2.16
Comparison of volumetric mass transfer coefficients obtained in 3 and 5 mm particles beds

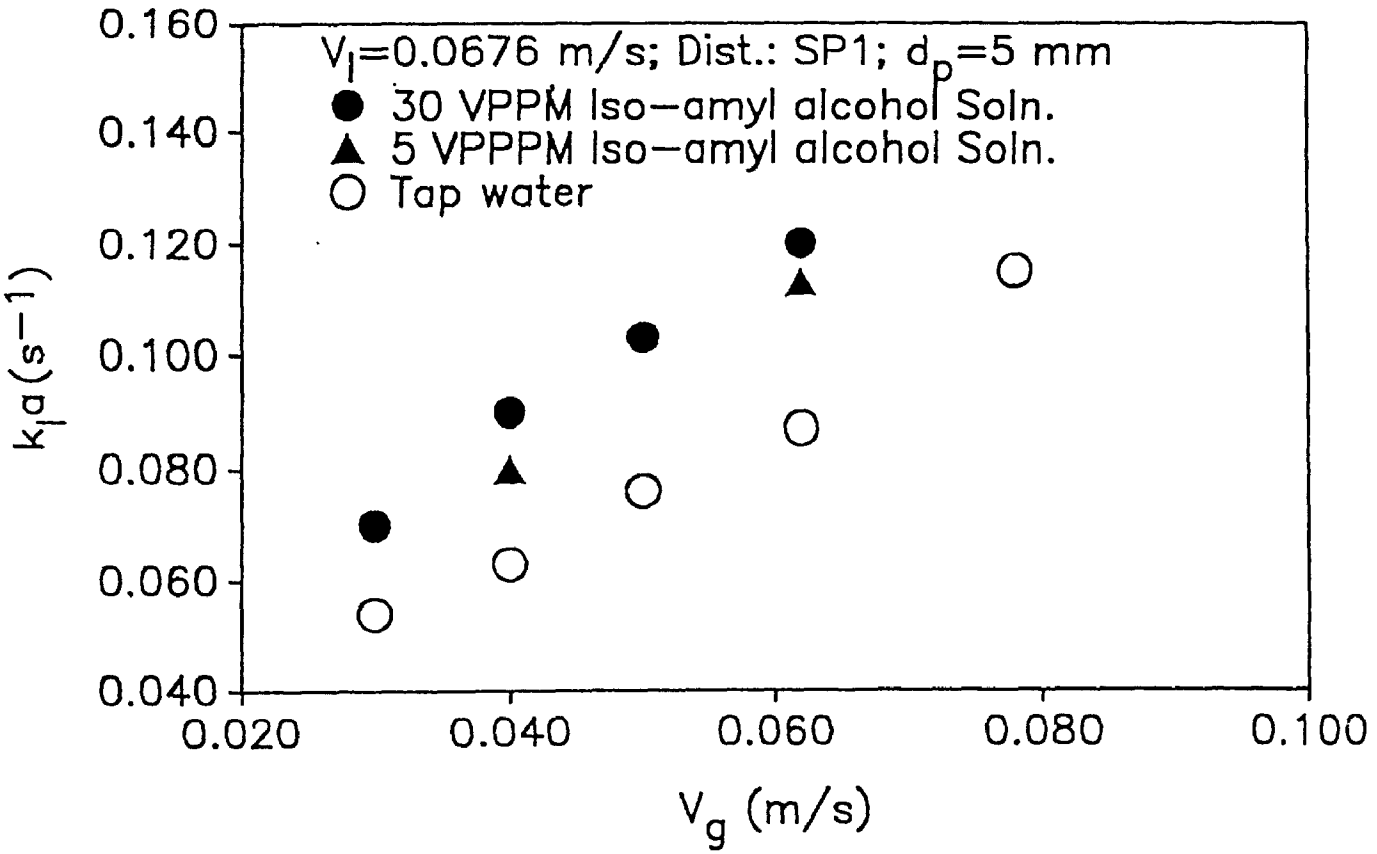

Figure 4.2.17
Comparison of volumetric mass transfer coefficients obtained in coalescing and noncoalescing media (3-phase fluidized beds)

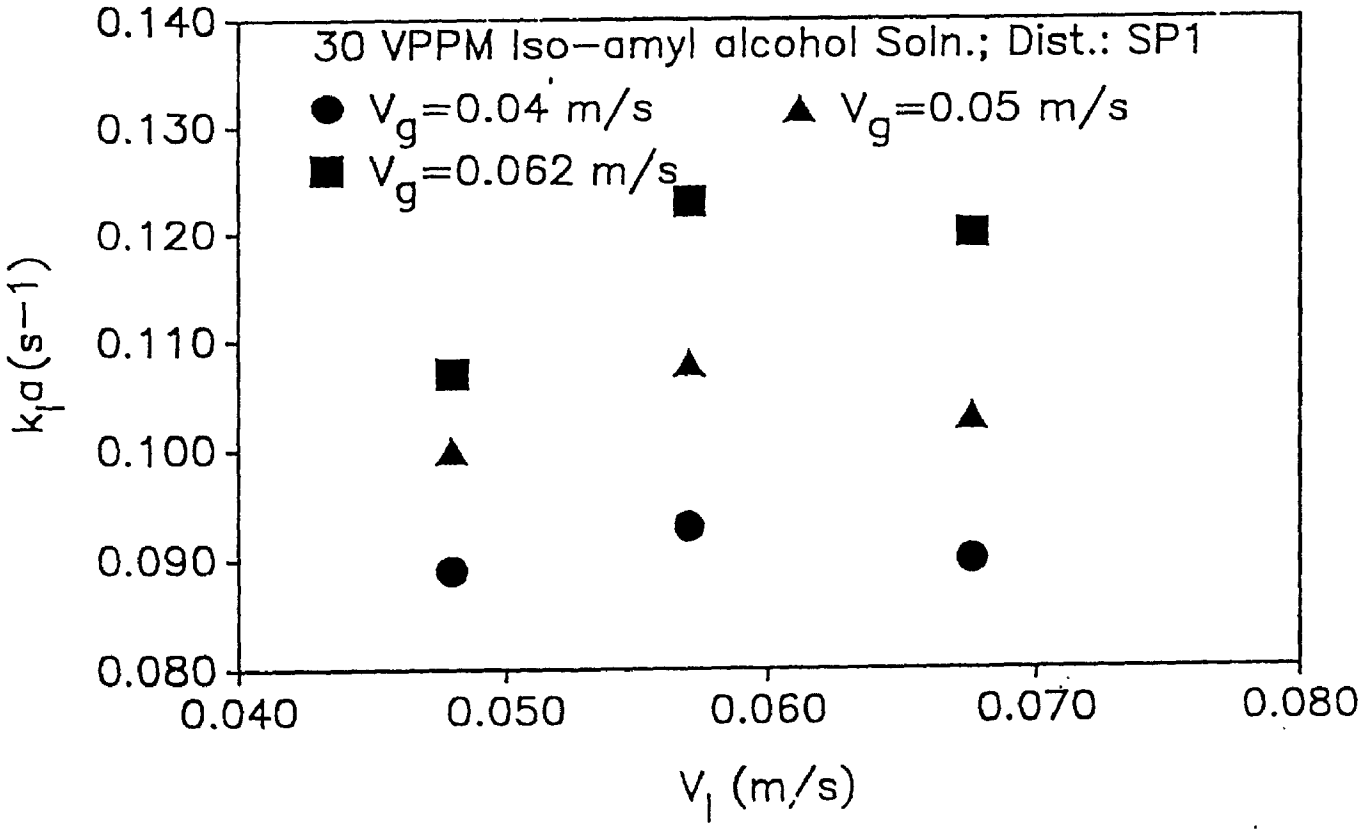

Figure 4.2.18
Effects of liquid velocity on volumetric mass transfer coefficient; 3-phase fluidized bed (D_c = 0.08 m; d_p = 5 mm)

4.2.3.2 Effects of Coalescence Inhibitor

It can be seen from Figure 4.2.17 that higher mass transfer coefficients were obtained when dilute solutions of iso-amyl alcohol were used as the liquid phase. As shown in section 4.2.1.2, the corresponding values of the gas phase holdups were also higher (Figure 4.2.2).

The effect of additive concentration was studied by using two different concentrations (5 and 30 vppm) of iso-amyl alcohol solutions. Figure 4.2.17 compares the values of mass transfer coefficient obtained with these two solutions to those obtained with tap water. Although the $k_l a$ values in the 5 vppm solution are slightly lower than in the 30 vppm solution, they are still significantly higher than the tap water values. These results demonstrate that iso-amyl alcohol is an effective coalescence inhibitor in three-phase fluidized beds even at very low concentrations.

The various theories for bubble coalescence were reviewed in section 5.1. These theories provide some insights in the coalescence inhibition effects of surface active solutes. The significant increases in the gas phase holdups in three-phase fluidized beds in the presence of iso-amyl alcohol (Figure 4.2.2) is a direct consequence of its coalescence inhibition effects.

The higher gas-phase holdups generally result in higher interfacial area per unit volume and hence higher values of volumetric mass transfer coefficient.

4.2.3.3 Effects of Particle Size

Higher values of mass transfer coefficients were obtained with 5 mm particles compared to 3 mm particles (Figure 4.2.16). These observations are shared by all the researchers who studied the effects of particle size on gas-liquid mass transfer in three-phase fluidized beds (see section 2.3.6.2.1). The higher values of mass transfer rates in in beds of larger particles are obtained due to the formation of smaller average bubble size hence larger interfacial area (Dhanuka and Stepanek, 1981).

4.2.3.4 Effects of Gas Distribution

The gas-liquid mass transfer rate was found to depend on the type of the gas distributor used. Two type of gas distributors namely the sparger (SP1) and porous distributor (PR2) were used for this study.

Lower values of mass transfer coefficients were obtained with porous distributor as compared to the sparger (Figure 4.2.19). This is the opposite of what was observed in bubble columns (see section 4.1.3.2), where the porous distributor provided higher mass transfer rates.

Figure 4.2.8 shows that the gas holdups were also generally lower with the porous distributor as compared to the sparger. With the porous distributor in the three-phase fluidized bed, it was observed that the particles in the vicinity of the porous plate remained defluidized; the

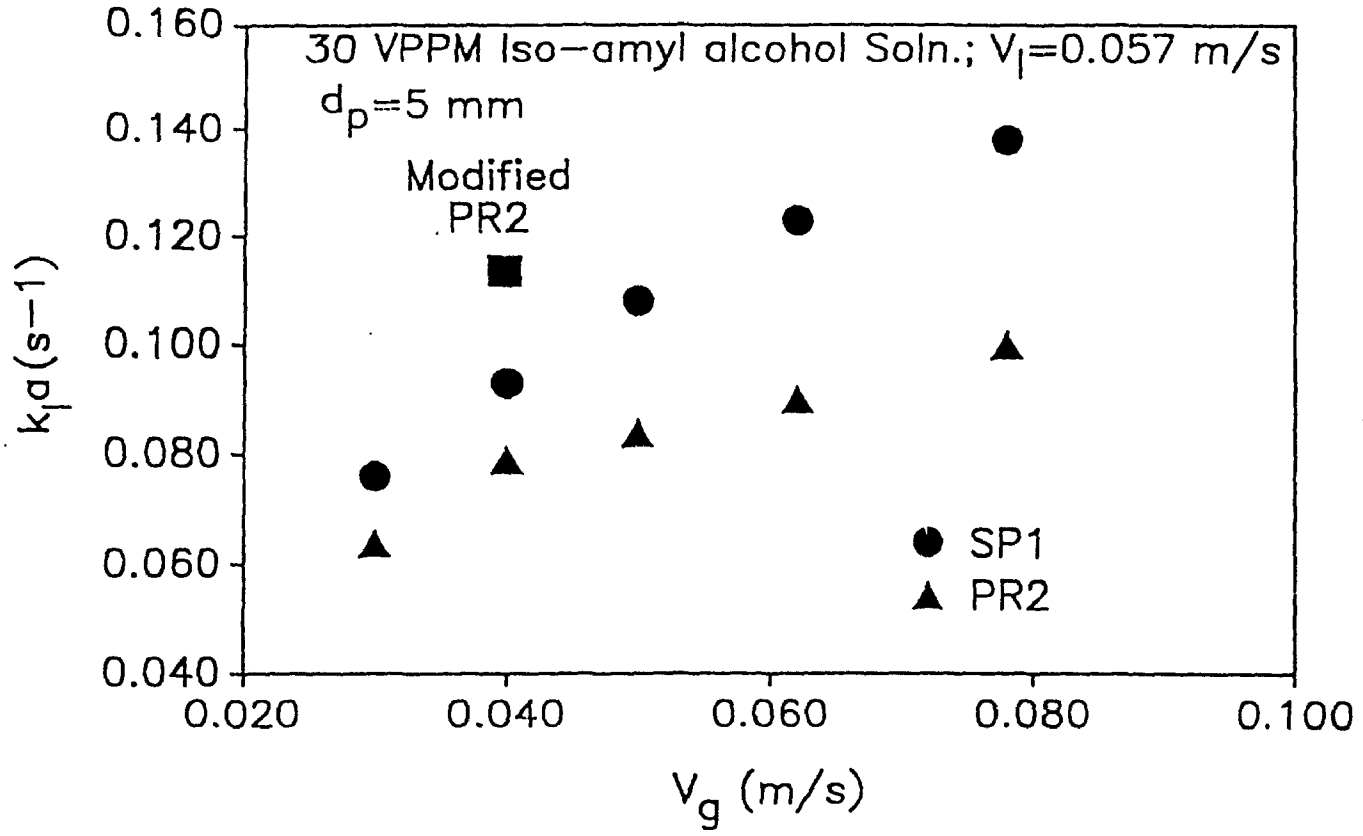

Figure 4.2.19
Comparison of volumetric mass transfer coefficients obtained with distributors SP1 and PR2 (3-phase fluidized beds)

liquid entered the column below the porous distributor as a result it bypassed the bed particles just above the porous plate. The gas bubbles generated at the porous plate were therefore rising up a through fixed bed, rather than a fluidized bed.

In order to avoid the formation of the defluidized bed region above the porous distributor, a piece of wire mesh formed into the shape of a cone was clamped over the porous plate. This arrangement avoided the formation of the defluidized zone; the value of mass transfer coefficient then obtained with the porous distributor was higher than the sparger (see Figure 4.2.19).

It could therefore be concluded that the presence of a defluidized zone just above the distributor could lead to lower gas-liquid mass transfer rate in three-phase fluidized beds. This was probably a consequence of higher rate of bubble coalescence in the defluidized bed region just above the distributor. The lower values of gas holdups obtained under these conditions lend support to this hypothesis.

4.2.3.5 Effects of column Diameter

Two runs for gas-liquid mass transfer were also conducted in the large diameter column, using a coalescing (tap water) and a noncoalescing liquid (100 ppm MIBK). The objective of these measurements was to show that an effective coalescence inhibitor can enhance the mass

transfer rate irrespective of column diameter.

The measurements were made in beds of 5 mm particles, for a given set of gas and liquid flow rates (V_l = 0.055 m/s; V_g = 0.1 m/s). The volumetric mass transfer coefficients in the noncoalescing liquid were about 70% higher than the coalescing liquid.

4.2.3.6 New Correlations for Gas-Liquid Mass Transfer

The literature correlations for volumetric mass transfer coefficient in three-phase fluidized beds were reviewed in section 2.3.6.3. Most of the proposed correlations are based on relatively narrow range of operating conditions. Moreover, it should be pointed out that the estimations of mass transfer coefficient in the literature studies have been obtained without proper consideration for sampling location which creates doubt about the validity of these correlations.

Using the gas-liquid mass transfer data obtained with distributor SP1, the following empirical correlations were obtained by least square analysis.

Coalescing System:

$$k_l a = 5.4\ V_g^{0.72}\ V_l^{-0.61}\ d_p^{0.71} \quad \text{.....(4.2.3)}$$

$$R^2 = 0.93$$

Noncoalescing System:

$$k_l a = 32.5\ V_g^{0.61}\ d_p^{0.74} \qquad \text{.....(4.2.4)}$$

$$R^2 = 0.95$$

The data obtained with distributor PR2 was not used, since this distributor created a defluidized zone inside the bed (section 4.2.3.4).

Equation 4.2.4 demonstrates that, the volumetric mass transfer coefficient is not affected by liquid velocity in the noncoalescing liquid, while there is only a small effect in the coalescing liquid (Equation 4.2.3).

A single correlation for the combined data of coalescing and noncoalescing system could be obtained when the gas holdup was also included as a variable for the correlation. This unified correlation is given below:

$$k_l a = 8.4\ V_g^{0.54}\ V_l^{-0.6}\ d_p^{0.69}\ \epsilon_g^{0.46} \qquad \text{....(4.2.5)}$$

$$R^2 = 0.92$$

Figure 4.2.20 shows that the proposed correlation predicts the experimental values fairly well.

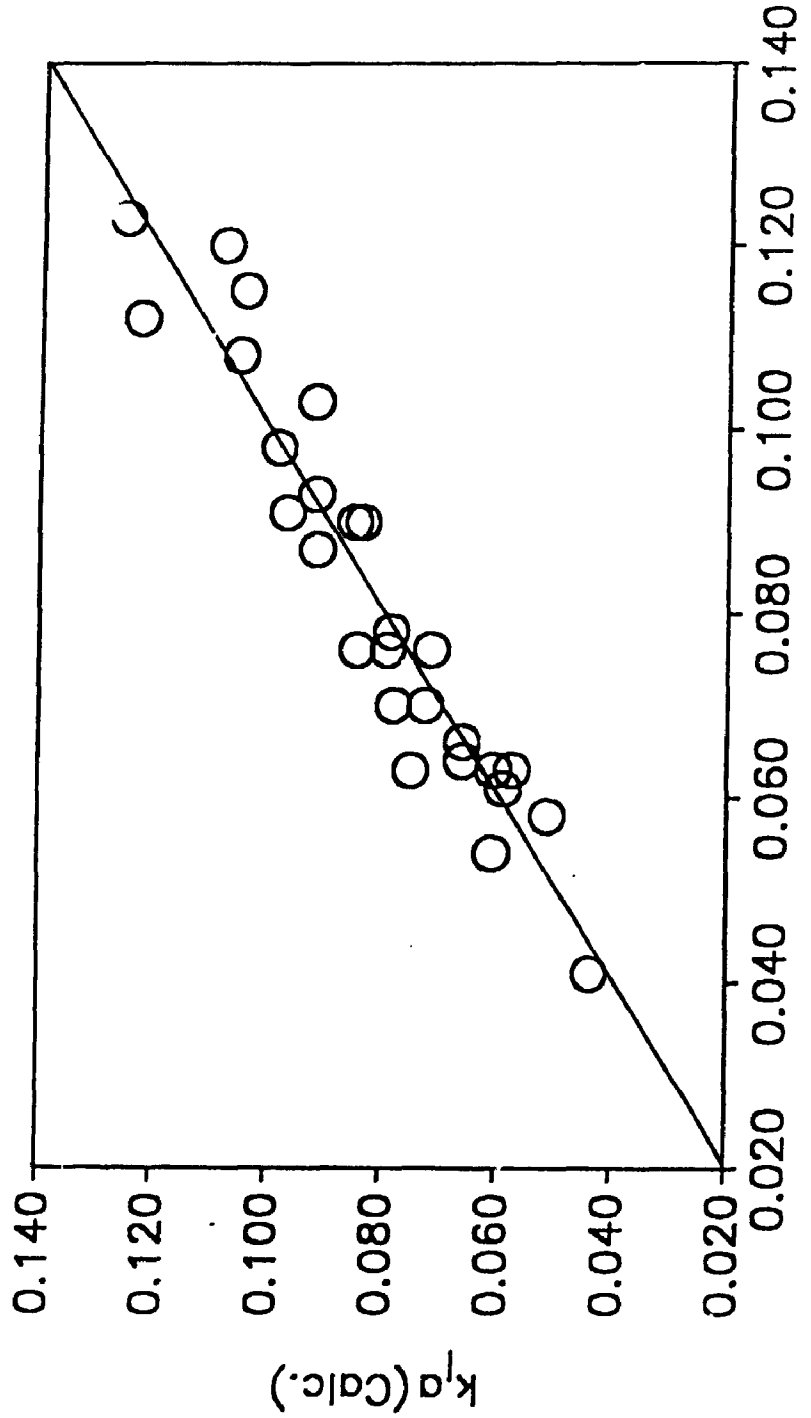

Figure 4.2.20
Calculated versus experimental values of volumetric mass transfer coefficients (Equation 4.2.5)

4.2.4 Particle-Liquid Mass Transfer

4.2.4.1 Effects of Gas and Liquid Velocities

The liquid velocity was found to have no significant effect on particle-liquid mass transfer rate for velocities above the minimum fluidization velocity. However, at liquid velocities which were below the minimum fluidization velocity (0.051 m/s), the bed was in the bubble-supported fluidized bed regime and the particle - liquid mass transfer coefficient was higher than when the bed was in the standard fluidized bed regime (see Figure 4.2.21).

The variation of the mass transfer coefficient with the superficial gas velocity is shown in Figure 4.2.22 for the two distributors and various liquid solutions. It can be seen that, the mass transfer coefficient increased with gas velocity and reached an asymptotic value at gas velocities above 0.1 m/s. One exception, however, was observed when direct gas jets and tap water were used: for gas velocities between 0.05 m/s and 0.15 m/s, the mass transfer coefficient decreased slowly when the gas velocity was increased.

The curve obtained with gas jets and tap water can be divided into three zones, depending on the gas velocity. In the first zone, for gas velocities below 0.05 m/s, the mass transfer coefficient increased with the gas velocity. The gas went through the bed as gas bubbles which appeared

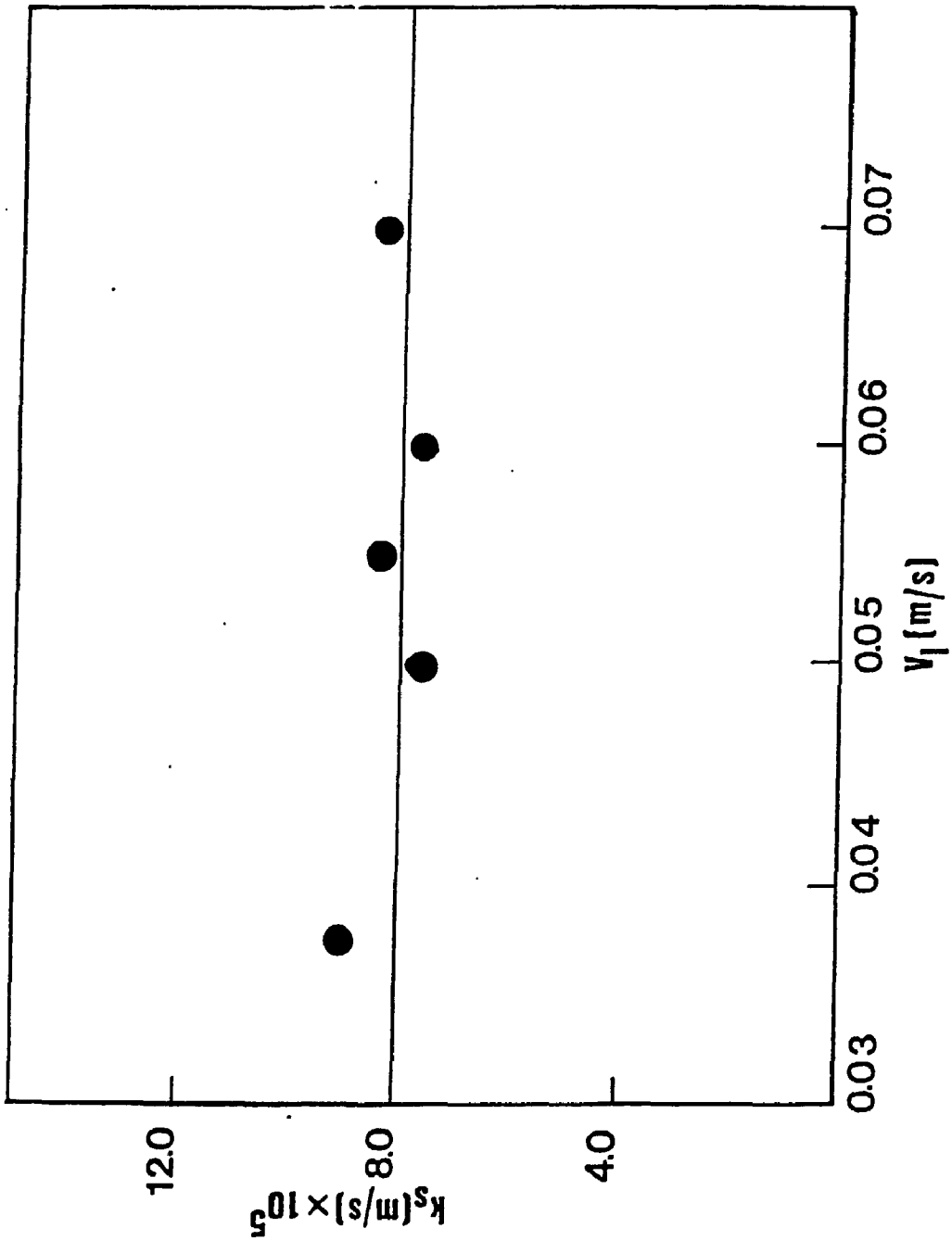

Figure 4.2.21
Effect of superficial liquid velocity on particle-liquid mass transfer coefficient (D_c = 0.17 m; d_p = 5 mm; V_g = 0.1 m)

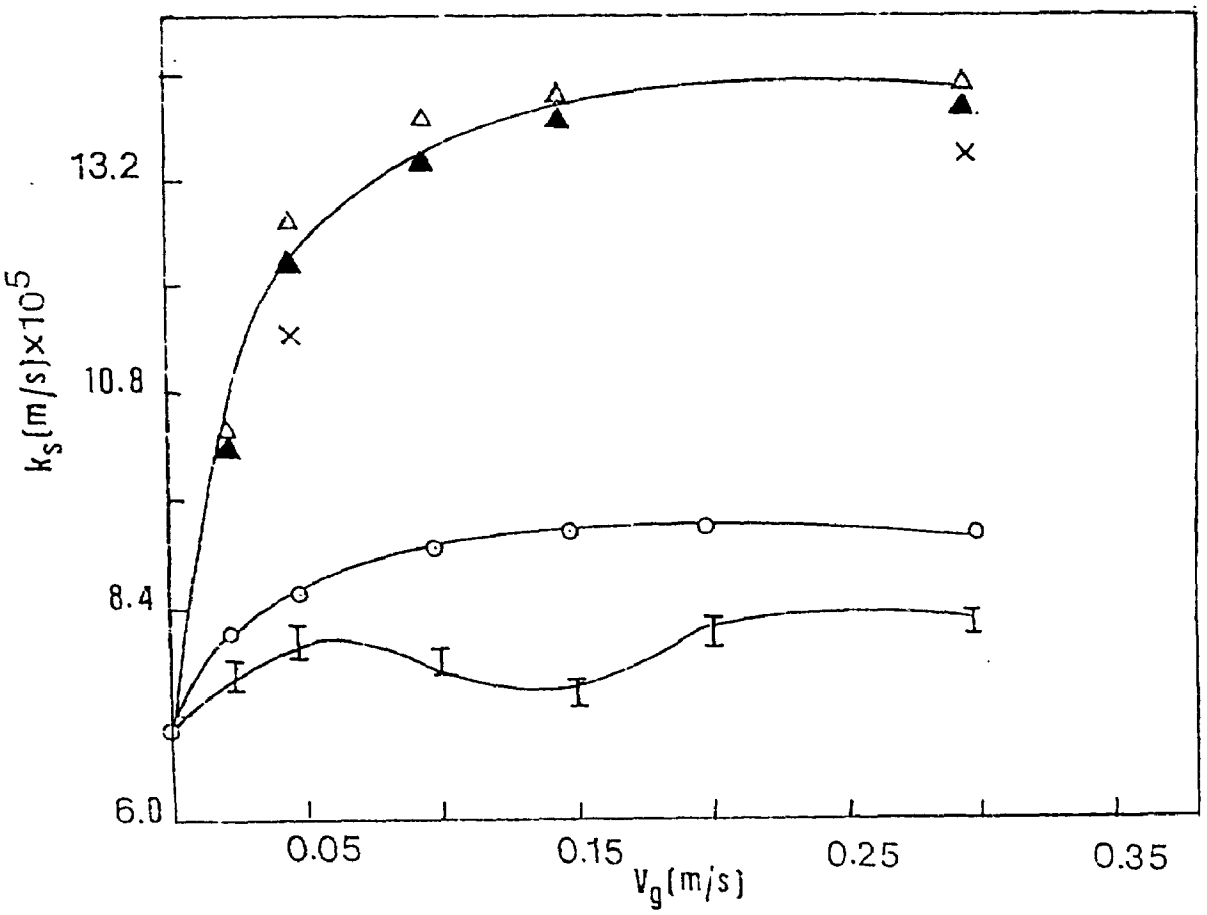

Figure 4.2.22
Effect of gas velocity on particle-liquid mass transfer coeff.

I 90% confidence interval;Tap water;Direct gas jets ○ Tap water;Packed bed distributor

▲ 200 wppm benzoic acid soln.;Direct gas jets △ 200 wppm benzoic acid soln.;packed bed dist.

X 150 wppm MIBK soln.;Direct gas jets

to be uniformly distributed over the whole cross-section of the bed. In the second zone, for gas velocities between 0.05 m/s and 0.15 m/s, the mass transfer coefficient decreased gradually when the gas velocity was increased. This zone was characterized by the formation of large gas jets which bypassed most of the bed. The bed was then divided into a gas jet region where there were fewer particles and a region where there were few gas bubbles (Catros et al., 1985). The energy provided by the gas was therefore not utilized efficiently to promote particle-liquid mass transfer. As the gas velocity was increased above 0.15 m/s, the gas jets were broken by the churn turbulence at the top of the bed and their length was reduced to about 50 % of the bed height. The mass transfer coefficient increased and reached an asymptotic value at high gas velocities (third zone).

Nishikawa et al. (1976) studied particle-liquid mass transfer in a three-phase spouted bed. They observed that for low gas flow rates, the mass transfer coefficient increased with increasing gas velocity and reached a maximum value at a gas velocity of around 0.005 m/s. Further increases in gas velocity resulted in a decrease of the mass transfer coefficient. These observations correspond to the first and second zones observed in the present study. Nishikawa et al. did not, however, observe a subsequent increase in the mass transfer coefficient. They were probably limited by the significant carry-over

of their small size bed particles at high gas velocities.

As can be seen from Figure 4.2.22 the particle - liquid mass transfer rate in three-phase fluidized bed, with tap water as the liquid phase increased by up to 30 % over the corresponding two-phase liquid-solid fluidized bed. Arters and Fan (1984), however, reported that particle-liquid mass transfer rates in three-phase fluidized beds were up to 100 % higher than in liquid-solid fluidized beds. These authors used a bed of benzoic acid particles which would have resulted in a high dissolved concentration of benzoic acid. The dissolved benzoic acid then acted as a coalescence inhibitor giving smaller gas bubbles, higher gas holdup and lower liquid holdup thus significantly altering the bed hydrodynamics.

4.2.4.2 Effects of Coalescence Inhibitors

As discussed in sections 4.2.1.2 and 4.2.3.2, the phase holdups and gas-liquid mass transfer in three-phase fluidized beds were affected in the presence of coalescence inhibitors in the liquid phase. The effect of a change in liquid coalescence behavior on particle-liquid mass transfer in three-phase fluidized beds has not been investigated. The technique developed in this study for the measurement of particle-liquid mass transfer offered the advantage of investigating the particle-liquid mass transfer without altering the coalescence behavior of the liquid. The effects of changes in liquid coalescence

behavior was investigated by using dilute aqueous solutions of benzoic acid (150-450 wppm) and methyl isobutyl ketone (100-200 wppm).

When these aqueous solutions were used as the liquid phase, the particle-liquid mass transfer rate in the three-phase fluidized bed was magnified by up to 100 % over its value in the liquid fluidized bed (see Figure 4.2.22). The aqueous solutions of both benzoic acid and MIBK resulted in the formation of very small gas bubbles in the fluidized bed. There were significant increases in gas holdup (Figure 4.2.3) which led to corresponding reductions in the liquid holdups (Figure 4.2.4). The addition of surfactants thus increased the interstitial liquid velocity (V_l/ϵ_l) inside the bed which resulted in a lower hydrodynamic film thickness for mass transfer.

These results also demonstrate the importance of selecting a proper experimental technique for the measurement of liquid-solid mass transfer in three-phase fluidized beds. For example the experimental technique used by Arters and Fan (1984) could result in a high concentration of dissolved benzoic acid in the liquid and hence alter the coalescing behavior of the liquid. The electrochemical technique used by a number of researchers (see section 2.3.7.1.2) requires the use of dissolved salts which can again alter the coalescing behavior of the liquid and hence influence the mass transfer measurements.

4.2.4.3 Effects of Liquid Viscosity

The effect of liquid viscosity on particle-liquid mass transfer rate was studied by using solutions of Carboxy methyl cellulose (CMC) in tap water. The viscosity of the liquid was thus, varied from 0.97 to 1.7 cp.

The particle-liquid mass transfer rate decreased with increasing viscosity, but the rate of decrease was very gradual. An increase of about 75 % in liquid viscosity resulted in a decrease of about 10 % in the mass transfer rate.

The effects of CMC concentrations on the solubility and diffusivity of benzoic acid in aqueous solutions have been investigated by Kumar et al. (1978) and Hansfor and Litt (1968) respectively. For the low concentrations of CMC in the solutions (< 0.06 wt. %) used for this study, the increased solubility was estimated to be less than 3 %, while the diffusivity would have decreased by less than 2 %. Since these two effects approximately cancelled each other, the decrease in mass transfer coefficient observed in CMC solutions could mainly be attributed to the increase in the film thickness for mass tranfer.

4.2.4.4 Effects of Gas Distribution

The two types of distributors used in this study were discussed in section 3.2.1. As can be seen from Figure

4.2.22, in the absence of coalescence inhibitors, the particle-liquid mass transfer was by about 10 % higher when the packed bed distributor was used. Although the turbulence intensity was increased to some extent, direct introduction of gas jets resulted in poor gas distribution, since the jets bypassed most of the bed. At gas velocities larger than 0.1 m/s, the entrainment rate, which was measured by collecting the entrained particles at various heights above the bed surface, was found to be more than doubled when the jet distributor was used instead of the packed bed distributor. The particles were collected in a conical container (0.04 m I.D.), hanging from a steel rod. Although, this technique provided only crude estimates of the entrainment rates, the trends were quite clear.

The high particle entrainment rates would result in a lower estimated value of the liquid holdup since the actual weight of solids in the bed would be less than the initial bed weight. This could explain the lower value of liquid holdup which was estimated with the direct gas jets as compared to the packed bed distributor when the gas velocity was above 0.2 m/s (Figure 4.2.9).

However, in the presence of coalescence inhibitors in the liquid, there was little effect of gas distribution on particle-liquid mass transfer rate. The average bubble size, as observed visually near the bed surface, was reduced from about 5 mm to about 1.5 mm. This effect could

also be detected by the increased gas holdup (see Figure 4.2.3). Here the coalescence inhibitors could be viewed to act as fine gas distributors which resulted in a more efficient utilization of the gas energy input for particle-liquid mass transfer.

4.2.4.5 Selection of Diffusivity of Benzoic Acid for Test of Literature Correlations

The various correlations proposed in the literature for particle-liquid mass transfer correlate the mass transfer coefficient, with the dimensionless Sherwood number (see section 2.3.7.5). This requires the knowledge of the solute diffusivity at the operating conditions. A number of researchers have measured the diffusivity of benzoic acid in water (Chang, 1949; Pradhan and Heideger, 1971; Lozar et al., 1975; Kumar et al., 1977; Irandoust and Anderson, 1986). There is, however, a wide scatter in the reported data of the diffusivity of benzoic acid (Irandoust and Anderson, 1986; Burru, 1988).

For a given temperature, the diffusivity of benzoic acid has been observed to depend on the bulk concentration of the dissolved solute (Chang, 1949; Pradhan and Heideger, 1971; Irandoust and Anderson, 1986). Table 4.2.7 gives the formulas proposed by these researchers for the concentration dependent diffusivity of benzoic acid.

Assuming that the film theory applies, the

concentration of the dissolving solute would vary from sauration concentration at the surface of the solid particle to bulk concentration at the end of the film. The average diffusivity can be obtained by the following procedure which assumes that the film theory is verified.

Table 4.2.7: Formulas for Concentration Dependent Diffusivity of Benzoic Acid

Investigators	Formula ($T = 298^{o}C$)	Remarks
Chang (1949)	$D'_1 = 1.21*10^{-9} - 0.028*10^{-9} \sqrt{C_s} - 0.0022 C_s$	Purely empirical
Pradhan and Heideger(1971)	$D'_1 = 1.283*10^{-9} - 0.714*$ 10-9 C_s/C_s*	Purely empirical
Irandoust and Andersson (1986)	$D'_1 = (0.41*10^{-9} + 1.156*10^{-9}) / k_1 - 1.779*10\text{-}11 C_s$	Accounts for dissociation of solute species

The mass transfer flux across a spherical particle for dilute solutions is given as:

$$N_s = -D_1' \frac{dC_s}{dr_p} \qquad \text{.....(4.2.6)}$$

For steady state: $N_s 4\pi r_p^2 = \text{constant}$

Integrating Equation 4.2.6 over the film of thickness δ

$$(N_s R_p 2)\int_{R_p}^{R_p+\delta} \frac{dr_p}{r_p^2} = -\int_{C_s}^{C_s^*} D_1' \, dC_s \qquad \text{.....(4.2.7)}$$

or

$$N_s = \frac{(R_p+\delta)\int_{C_s}^{C_s^*} D_1' dC_s}{R_p \, \delta} \qquad \text{.....(4.2.8)}$$

From Equations 3.3.61 and 4.2.8

$$k_s(C_s^* - C_s) = \frac{(R_p+\delta)}{R_p \delta}\int_{C_s}^{C_s^*} D_1' dC_s \qquad \text{.....(4.2.9)}$$

According to film theory $k_s = D_1/\delta$

Since $\delta << R_p$, Equation 4.2.9 can be written as below to give average diffusivity :

$$D_1 = \frac{\int_{C_s}^{C_s'} D_1' dC_s}{(C_s^* - C_s)} \qquad \text{.....(4.2.10)}$$

Equation 4.2.10 was used to obtain the formulas for average diffusivities for the three literature studies. These formulas were then used to obtain the numerical

values of average diffusivities of benzoic acid at different bulk concentrations (see Table 4.2.8).

Table 4.2.8: Average Diffusivities of Benzoic Acid at Different Bulk Concentrations (Temp. = 23°C)

Investigators	Average Diffusivity $m^2/s * 10^9$ $C_s=0.0$	$C_s=0.045C_s^*$	$C_s=0.35C_s^*$	Remarks
Chang (1949)	1.086	1.08	1.07	Values used for this study
Pradhan and Heideger(1971)	0.925	0.9	0.8	
Irandoust and Andersson (1986)	0.942	0.929	0.853	

In the present study the bulk concentration of benzoic acid was varied from nearly zero to about 35 % of saturation concentration. For most of the measurements, however, the bulk concentration was either nearly zero or 4.5% of saturation concentration. When the bulk concentration was at 35% of saturation, the particle-liquid mass transfer was found to be about 12% lower. The correlations of Pradhan and Heideger (1971) and Irandoust and Anderson (1986) predicted that the diffusivity of

benzoic acid decreased by about 13 and 10% respectively at 35% saturation concentration (Table 4.2.8). These correlations therefore account for decrease in benzoic acid diffusivity at higher concentration of solutions.

Most of the literature studies have used the benzoic acid diffusivity from Chang (1949). In order to compare the results of this study with literature data the experimental values of Sherwood numbers were obtained, using the average diffusivities given by Chang's correlation (Table 4.2.8). The diffusivity of benzoic acid at the operating temperature of this study (23^{o}C) was obtained, using the formula from Chang (see Appendix 22 for details).

4.2.4.6 Test of Literature Correlations for Liquid-Solid Fluidized Beds

A number of correlations for liquid-solid mass transfer in two-phase fluidized beds are available in the literature. These correlations were reviewed in section 2.3.7.3. A generalized correlation for particle-liquid mass transfer in fixed and fluidized beds in the absence of gas was proposed by Dwivedi and Upadhyay (1977). They concluded that the mass transfer factor J_d was inversely proportional to the bed voidage (ϵ). These authors verified this conclusion by plotting experimental data for all types of beds as ϵJ_d vs. Re_1. From these plots it was

observed that the inclusion of bed voidage along with the Chilton-Colburn J_d factor reduced the scatter of the points considerably when plotted against Re_l. The proposed correlation gave a good fit (within 10% of the two-phase fluidized bed mass transfer data of this study.

4.2.4.7 Test of Literature Correlations for Three-Phase Fluidized Beds

The available correlations for liquid-solid mass transfer in three-phase fluidized beds were reviewed in section 2.3.7.5. These correlations were tested, using the data of this study. Table 4.2.9 gives the average relative errors and absolute average relative errors, for various correlations.

It can be seen that the correlation proposed by Arters and Fan (1987) gives the best estimates of mass transfer coefficients in the coalescing system. None of the literature correlations provides good estimates of the particle-liquid mass transfer coefficients in the noncoalescing liquids.

The correlations for particle-liquid mass transfer in slurry bubble columns and agitated vessels which have been proposed by Sano et al. (1974) and Sanger and Deckwer (1981) use a Reynolds number based on Kolmogoroff's theory of isotropic turbulence. The general forms of these

correlations is given by Equation 4.2.11.

Table 4.2.9: Test of Literature Correlations for Particle-Liquid Mass Transfer in Three-Phase Fluidized Beds

Investigators	Average Absolute Relative Error (Average Relative Error) Coalescing system	Noncoalescing system	Remarks
Arters and Fan (1986)	680 % (680 %)	490 % (490 %)	Predicted values way too high
Arters and Fan (1987)	5.8 % (-5.8 %)	35 % (-35 %)	Good predictions for coalescing system
Nikov and Delmas (1987)	21 % (21 %)	19 % (-19 %)	
Ermakova et al. (1988)	45 % (-45 %)	62 % (-62 %)	Low predictions for both systems
Fukuma et al. (1988)	22 % (-22 %)	48 % (-48 %)	Low predictions for both systems .

$$Sh = 2 + C_8 \, (E \, d_p^{\,4}/\nu^3)^{m3} \, Sc^{m4} \qquad .....(4.2.11)$$

E is the local energy dissipation per unit mass.

The energy input rate for the three-phase system is

given by Joshi (1980):

$$E_i = (Q_g + Q_l)\ \Delta P_{bed}$$

$$= A_c\ H_{bed}\ (V_g + V_l)\ (\epsilon_s \rho_s + \epsilon_l \rho_l)\ g \quad ....(4.2.12)$$

In order to obtain the energy dissipation in the bed, the potential energy gained by the liquid ($Q_l \rho_l g H_{bed}$) as it is pumped above the bed height is subtracted from Equation 4.2.11. For jet distributors, the kinetic energy from the jets ($1/2\ \rho_g\ V_j^2\ Q_g$) can be added to Equation 4.2.12. The energy dissipation can be based on the bed liquid mass, the solids mass in the bed or the total particle-liquid interfacial area in the bed.

Figure 4.2.23 is a plot of the particle-liquid mass transfer coefficient (k_s) as a function of the energy dissipation term per unit liquid mass (the energy balance included the potential energy recovery at the top of the bed). The plot gives three different curves for the three systems. Similar plots were obtained when k_s was plotted against other types of energy dissipation.

It can be seen from Figure 4.2.23 that for a given energy input rate, the particle-liquid mass transfer rate is strongly influenced by the gas distributor and the coalescence behavior of the liquid. Any attempts at correlating the data of this study with an energy dissipation term would thus require different coefficients and exponents to account for variations in the efficiency

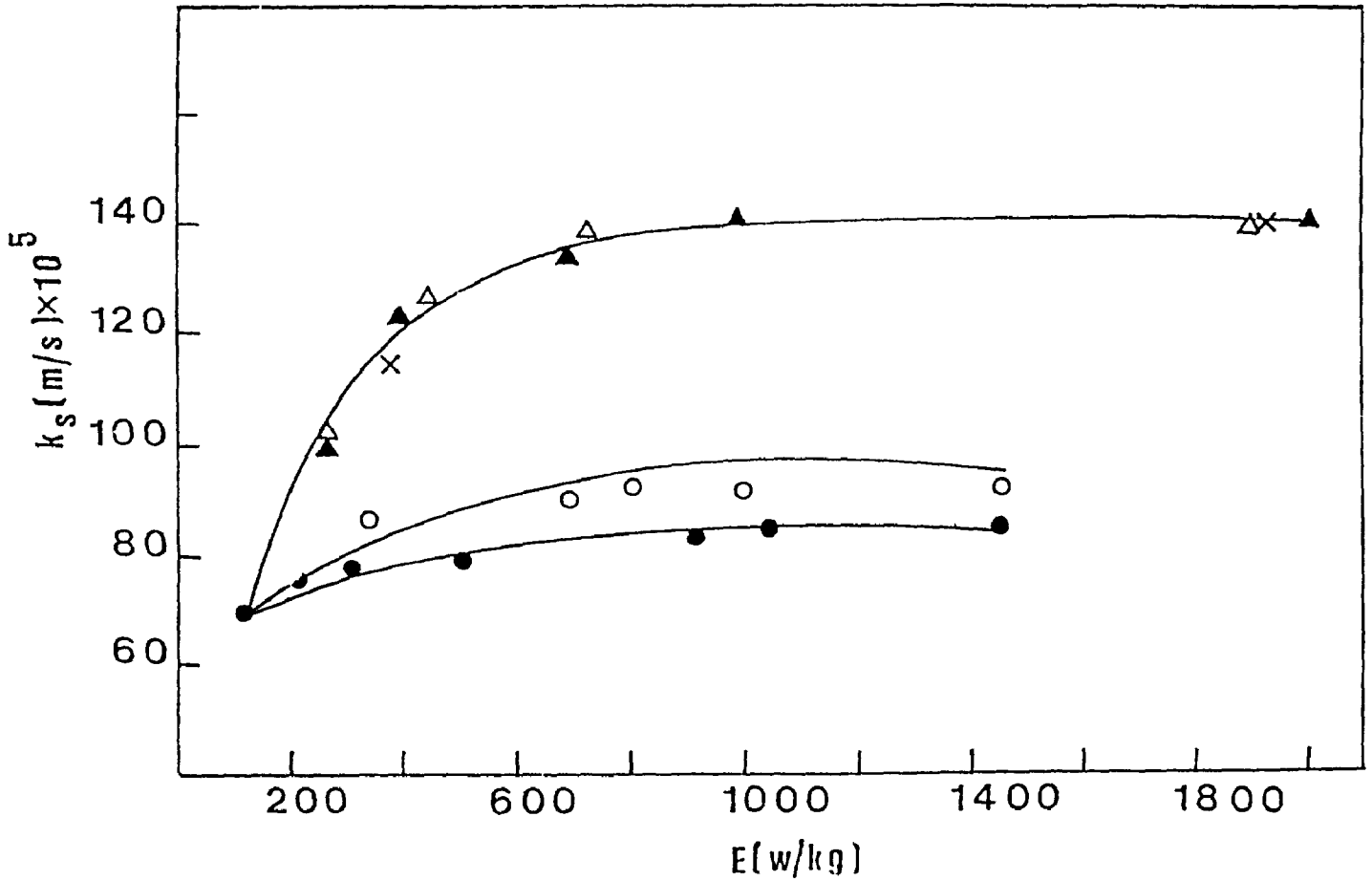

Figure 4.2.23
Particle-liquid mass transfer coefficient versus energy dissipation in the bed. Symbols as in Figure 4.2.22

of energy utilization with the gas distribution and the coalescing properties of the liquid.

4.2.4.8 Analogy with Heat Transfer in Three-Phase Fluidized beds

As reviewed in section 2.3.5, heat transfer in three-phase fluidized beds has been investigated by a number of workers. Chiu and Ziegler (1983) studied wall-to-bed heat transfer and found that the relative increase in heat transfer coefficient was equal to the relative decrease in liquid holdup when the gas velocity was increased. The experimental data of the present study demonstrated that mass transfer in three-phase fluidized beds was similarly related to liquid holdup.

Chiu and Ziegler (1983) extended to three-phase beds the relationship between the modified Stanton number and the modified Reynolds number which had been derived from liquid fluidized beds (Chiu, 1982):

$$Pr^{2/3}\ St_{m3} = St_{m2}\ Pr^{2/3} = C_6\ R_{m2}^{-0.305} \qquad .....(2.3.57)$$

which simplifies to:

$$h_3/h_2 = (\epsilon_{13}/\epsilon_{12})^{-1} \qquad .....(2.3.57a)$$

where ϵ_{13} and ϵ_{12} are the liquid holdup in three-phase and two-phase fluidized beds respectively. Using the J-factor

analogy, Equation (2.3.57) and (2.3.57a) can be rewritten for mass transfer in two-phase and three-phase fluidized beds:

$$Sc^{2/3}\ St_{m3} = St_{m2}\ Sc^{2/3} = C_6\ Re_{m2}^{-0.305} \quad \text{.....(4.2.13)}$$

and

$$k_{s3}/k_{s2} = (\epsilon_{13}/\epsilon_{12})^{-1} \quad \text{.....(4.2.13a)}$$

There was poor agreement between the experimental values of the mass transfer coefficient and the values predicted by Equation (4.2.13), using the value for 'C_6' as suggested by Chiu and Ziegler (1983). Since Chiu and Ziegler (1983) measured heat transfer from a wall to the bed, the above disagreement could partly be explained by the different mechanisms governing transport processes from wall to bed and from particle to liquid.

Using Equation (4.2.13a) and experimental values for k_{s2}, the three-phase particle-liquid mass transfer coefficient of this study could be predicted with an average relative error of less than 10 %. This demonstrates that in three-phase fluidized beds, the liquid holdup is the most important factor for both particle-liquid mass transfer and wall-to-bed heat transfer.

4.2.4.9 New Correlation for Particle-Liquid Mass Tranfer

A plot of the mass transfer coefficient against the

interstitial liquid velocity (V_l/ϵ_l) indicated that a correlation which included the liquid holdup should give a good fit of the mass transfer data in three-phase fluidized beds (Figure 4.2.24).

A generalized correlation developed by Dwivedi and Upadhyay (1977) for two-phase systems was adapted to three-phase systems by replacing bed porosity (ϵ) with liquid holdup (ϵ_l). A generally good fit between predicted and experimental values of the particle-liquid mass transfer coefficient was then obtained (the average relative error was 9%). The correlation from Dwivedi and Upadhyay (1977) is a good correlation for two-phase systems which was developed from a large number of data points from the literature. It is thus likely that it can be used with the suggested modification in many three-phase systems.

A new correlation giving a better fit over the entire range of the mass transfer data of this study was also developed. This correlation is given below:

$$\epsilon_l \, J_d = 0.35 \, (Re_l)^{-1/3} \qquad \text{.....(4.2.14)}$$

Range of variables:

Re_l	180 to 360
Sc	916 to 1600
ϵ_l	0.20 to 0.42

Figure 4.2.25 is a plot of the calculated values of the

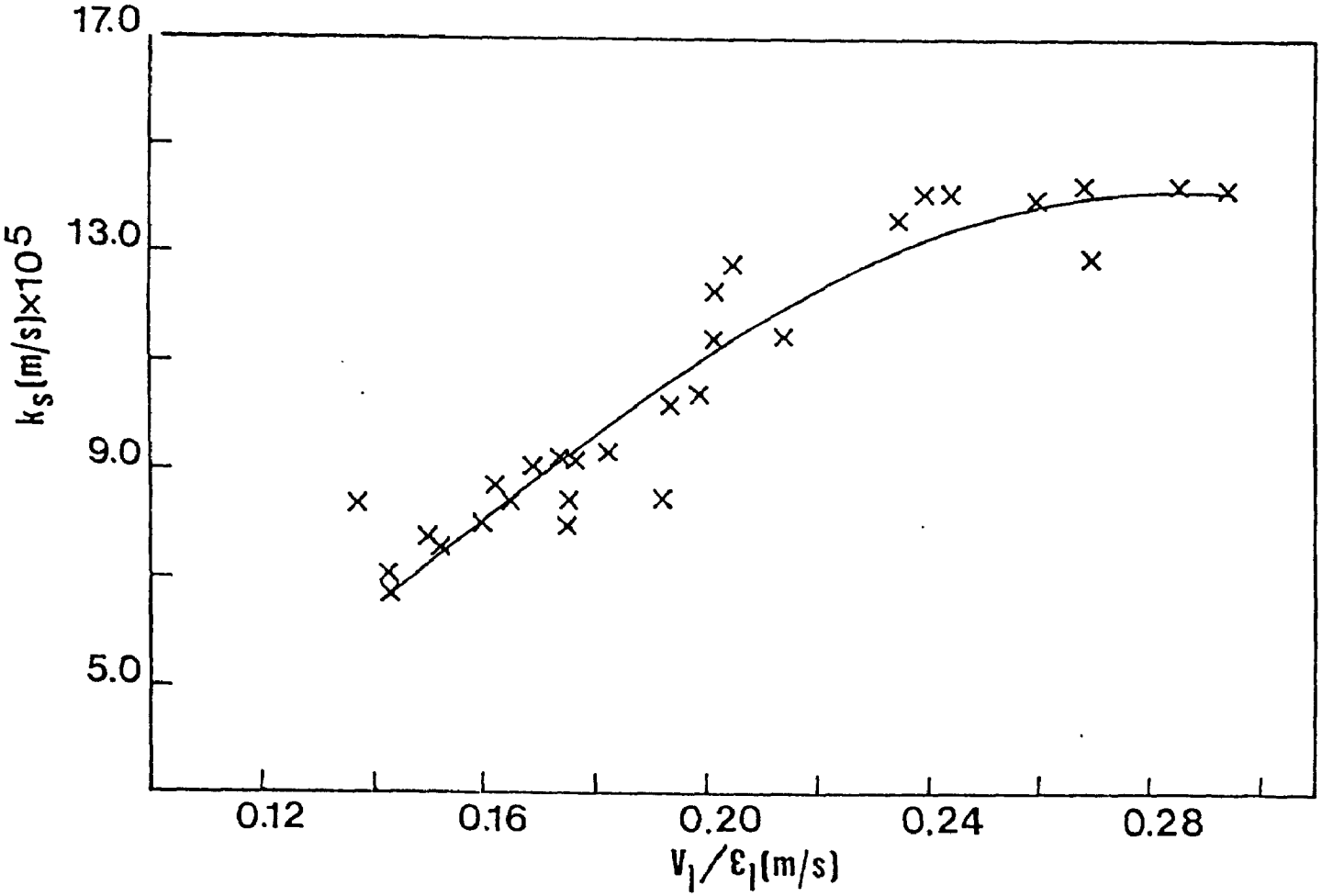

Figure 4.2.24
Particle-liquid mass transfer coefficient versus interstitial liquid velocity (V_l/e_l)

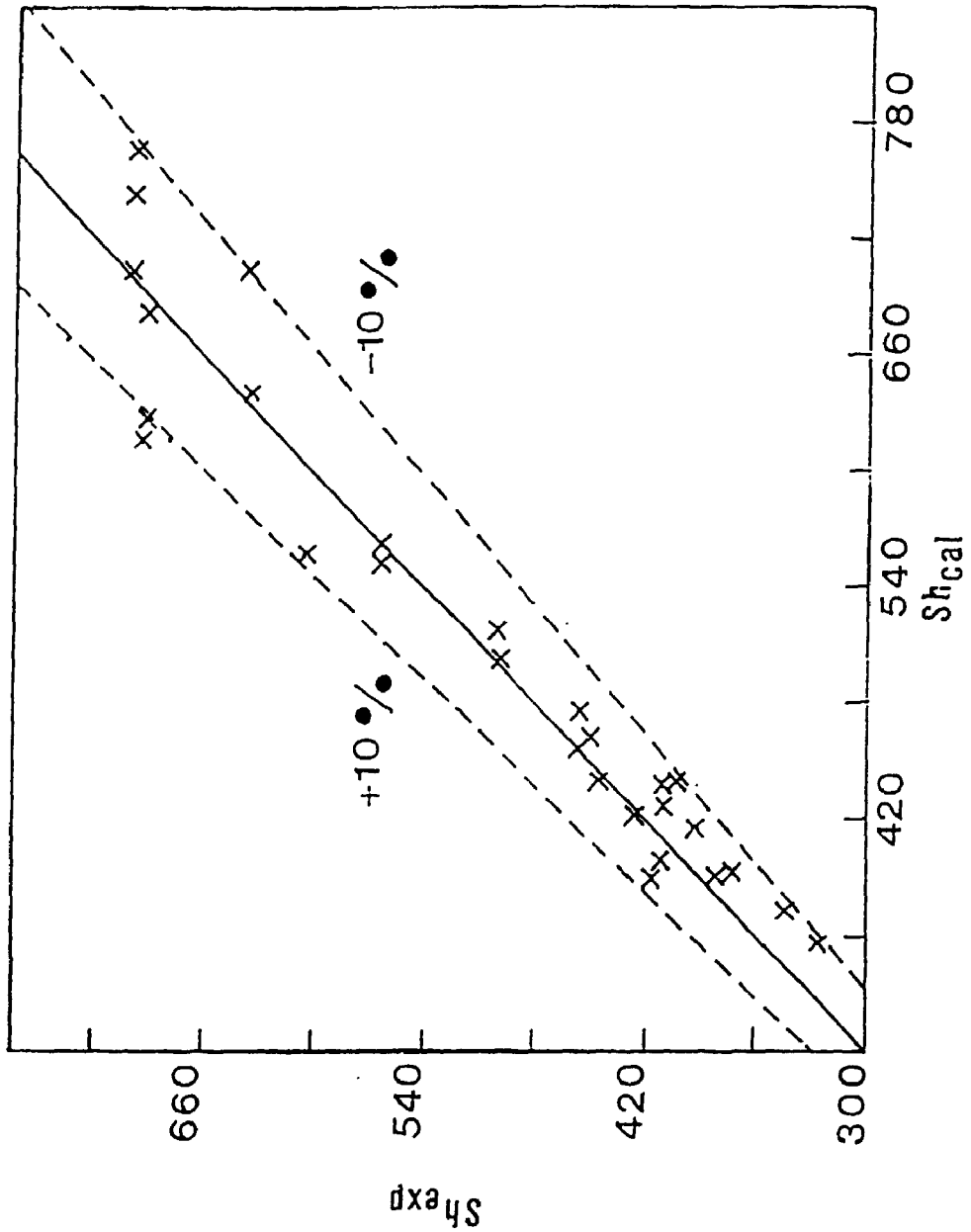

Figure 4.2.25
Experimental versus predicted values of particle-liquid mass transfer coefficient (Equation 4.2.15)

Sherwood number (using experimental values of ϵ_l) against the experimental values. The average relative error for the thirty data points is less than 6%.

Although both this correlation and the modified Dwivedi and Upadhyay correlations gave a good prediction of the particle-liquid mass transfer coefficient, they require the knowledge of the liquid holdup in three-phase fluidized beds. Empirical correlations proposed by various researchers for liquid holdups in three-phase fluidized beds were tested in section 4.2.1.5. The correlations proposed by Kim et al. (1975) and Chiu and Ziegler (1983) gave good estimates of the liquid holdups for coalescing liquid. None of the literature correlations could, however, give good predictions of liquid holdup for noncoalescing liquids. Therefore a new correlation, based on the drift flux model was proposed for noncoalescing liquids (see section 4.2.1.6). The resulting error for particle-liquid mass transfer could be about +10%.

If experimental values for liquid holdups are available then the proposed correlation or the modified correlation of Dwivedi and Upadhayay (1977) should give a good estimate of the particle-liquid mass transfer in three-phase fluidized beds. When the liquid holdup is not known then the correlation proposed by Arters and Fan (1987) should provide a good estimate of the mass transfer coefficient in the coalescing systems. For the noncoalescing systems, a good estimate of the liquid

holdup can be obtained using the drift flux model of this study. Then the mass transfer coefficient can again be obtained using the correlation proposed in this study. The resulting error could, however, be as high as 20%.

4.2.4.10 Theoretical Interpretation

Liquid-solid mass transfer in a three-phase fluidized bed can be modeled with Kolmogoroff's theory or with the slip velocity approach. The correlations based on Kolmogoroff's theory require the use of an energy dissipation term. As shown in this study any energy dissipation term will require variable coefficients and exponents in order to account for variations in energy utilization with the gas distribution and the presence of coalescence inhibitors in the liquid. The slip velocity between the solid particles and the liquid can be approximated as V_l/ϵ_l for three-phase and two-phase fluidized beds (this approximation may not be valid when there is significant entrainment in the freeboard). From the correlation developed in this study, it can be shown that:

$$k_s \propto (V_l/\epsilon_l)^{2/3} (\epsilon_l)^{-1/3} \qquad .....(4.2.15)$$

for constant liquid and solid physical properties.

Equation 4.2.15 shows the significance of the slip velocity for particle-liquid mass transfer in two-phase

and three-phase fluidized beds. The possible dependence of the particle-liquid mass transfer coefficient on ϵ_g, ϵ_s and bed porosity ($\epsilon_g + \epsilon_l$) was also explored; however no suitable correlation could be derived based on the above parameters.

For the limiting case of mass transfer from a single sphere ($\epsilon_l = 1$), the correlation developed in this study (Equation 4.2.14) agrees closely with the correlation developed by Steinberger and Treybal (1960) for mass transfer from a single particle to a liquid.

For the case of two-phase liquid-solid, fixed and fluidized beds, ϵ_l in Equation (4.2.14) is equal to the bed porosity and this equation is in good agreement with the correlations proposed by other authors (e.g. Wilson and Geankoplis, 1966; Dwivedi and Upadhyay, 1977).

The increase in slip velocity of the liquid in the bed would reduce the thickness of the hydrodynamic boundary layer around the particles, hence reducing the resistance to mass transfer. However, there can also be secondary effects due to changes in concentration of particles and bubbles in the bed. These effects may be accounted for by the $\epsilon^{-1/3}$ term. As the gas holdup increases, the liquid holdup is reduced and the concentration of gas bubbles in the bed is increased. The gas bubbles can then act as local turbulence promoters in the bed and thus aid in mass transfer enhancement.

5. Theoretical Analysis and Modeling

In the previous sections, models were developed for the following:

1) Calculation of interfacial area in a batch bubble column using simultaneous absorption of carbon dioxide and desorption of oxygen for changing concentration of reactant (hydroxyl ion) in the liquid (section 3.1.5).

2) Calculation of molecular diffusivity of benzoic acid for different solution concentrations (section 4.2.4.5).

In this chapter, theories of bubble coalescence have been critically reviewed in view of the data of this study. Moreover, models have been developed for porous distributor to predict bubble size from the distributor.

5.1 Theories of Bubble Coalescence

The mechanism of bubble coalescence is considered to be a three step process (Marrucci, 1969).

1) The gas bubbles come in contact with each other within the liquid phase. There is a flattening of the bubble surfaces against each other leaving a thin liquid film separating them. The initial thickness of this film is typically 10 to 1 μm. This step is controlled by the

hydrodynamics of the bulk liquid phase.

2) The intervening liquid film must thin to a dimension of about .01 μm before it will rupture. If this thinning mechanism takes longer than the bubble contact time coalescence will not occur. This step is controlled by the hydrodynamics of the liquid film.

3) Once the film is sufficiently thin it will rupture via an instability mechanism. This step is very rapid in comparison to the first two.

The hydrodynamics of the bulk of the liquid phase which control the first step in bubble coalescence would depend on the distributor design and the gas velocity. Fine distributors generate a large population of small bubbles which result in high concentration of bubbles in the distributor region. Coarse gas distributors on the other hand generate a smaller number of large gas bubbles which would usually split above the distributor depending on the turbulence level in the liquid. The turbulence level would be determined by the superficial gas velocity. Higher turbulence level in the bulk of liquid would increase the frequency of interaction between gas bubbles, however, the contact time between bubbles would also be reduced which would lower the rate of coalescence.

The second step in the bubble coalescence process i.e. thinning of the intervening liquid film is very fast in pure liquids. However, in presence of surface active

impurities quasi-equilibrium films are maintained after contact (Kim and Lee, 1987).

When two bubbles come in contact in a liquid the intervening liquid film will be flattened as a result the pressure inside the film will be equal to the pressure inside the bubble. The pressure inside the bubble is higher than the pressure in the bulk liquid outside the film due to curvature of the bubble surface. Therefore the pressure inside the film is higher than the pressure in the bulk liquid outside the film by an amount shown below:

$$\Delta P_s = 2\sigma/r_b \qquad \text{.....(5.1.1)}$$

Where σ is the bulk surface tension on the bubble surface. Here the curvature of the bubbles (r_b) is assumed equal for both bubbles (Figure 5.1.1).

In absence of any forces opposing the pressure gradient, the liquid film will continue thinning and at very small film thickness, the Vander Waals forces of attraction become significant. The higher density region in the bulk of the film would more strongly attract the molecules on the surface compared to low density gas phase of the bubbles, resulting in a higher pressure in the film than in the gas phase. This force of intermolecular attraction for the thin liquid film surrounded by gas can be quantified as below (Hamaker,1937):

$$\Delta P_m = H_m/6\pi h_f^3 \qquad \text{..... (5.1.2)}$$

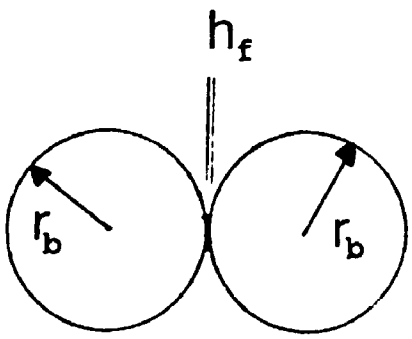

Figure 5.1.1
Intervening liquid film between two bubbles in contact in the liquid

Where H_m is the Hamakar constant for the liquid and h_f is the intervening liquid film thickness. This force will become insignificant at the outside edge of the film where the gas-liquid interface rapidly diverge. Thus the net pressure gradient along the radial direction of the film is:

$$\Delta P_{ft} = 2\sigma/r_b + H_m/6\pi h_f^3 \qquad \text{.....(5.1.3)}$$

For single component liquids this is the only force causing the film thi ng. When a gas distributor with a large number of closely spaced small orifices (i.e. porous plate) is used, the small bubbles generated will be in contact at the distributor. The small radius of the bubbles would also increase the pressure inside the liquid film and thus would accelerate the bubble coalescence rate. Therefore, bubble coalescence is expected to be high in the distributor region of porous distributors.

In a gas-liquid dispersion, the average bubble size is determined by contributions from both bubble break-up and coalescence rates. Changes in bubble size may result from the effects of additives on either bubble break-up or bubble coalescence rate. For a given gas velocity, the bubble break-up rate can be increased by lowering the interfacial tension. Since the interfacial tension was not altered for the dilute solutions of additives used in this study, the change in bubble size (hence gas holdup) can be attributed to change in coalescence rate. Bubble sizes

have been measured in aqueous solutions of electrolytes and organic additives (Marrucci and Nicodemo, 1967; Keitel and Onken, 1982). With a porous distributor Keitel and Onken (1982) found the bubble Sauter mean diameter to be 4.1 mm with pure water. However, the bubble diameter decreased rapidly with increasing concentrations of electrolyte or organic solute. Keitel and Onken (1982) used very low gas velocity (0.004 m/s) for their measurements which would preclude any bubble splitting, hence the decrease in bubble diameter was the result of coalescence inhibition. Marrucci and Nicodemo (1967) found that in pure water, the bubble diameter increased with increasing gas velocity. The bubble diameter, however, decreased with increasing concentration of coalescence inhibitors and reached an asymptotic value of 400 μm for 8 and 20 μm pore sizes for all gas velocities. The asymptotic value of the bubble diameter would represent the bubble size at the distributor.

The above observations point out that in the presence of electrolytes and surface active organic solutes, a force resisting the thinning of liquid film between the bubbles is developed, which deaccelerates the process of colescence.

Marrucci (1969) developed a coalescence theory taking into account the surface tension gradient across the liquid film which is induced due to the presence of surface active molecules. He defined a dimensionless

parameter ($C_m r_b k_m^2/\sigma$) where:

$$C_m = \frac{2a_{m1}}{RT}\,\frac{d\sigma}{da_{m1}}\,\frac{d\sigma}{dC_{nb}}\,\frac{1}{1+(x_{m1}/x_{m2})(V_{m1}/V_{m2})}$$

and

$$k_m = (12\pi\sigma/H_m r_b)^{1/3}$$

a_{m1} and a_{m2} are activities of components 1 and 2

It was specified that coalescence would be inhibited whenever this parameter was larger than 1.89. Under these conditions a quasi-equilibrium thickness is reached when the overall balance of forces can be written as:

$$h_f \Delta P_{ft} = 2\Delta\sigma \qquad \text{.....(5.1.4)}$$

The surface tension difference ($\Delta\sigma$) is caused by a difference in additive concentration between the film and the bulk liquid outside the film. The coalescence time is determined by the further thinning of the liquid film from the quasi-equilibrium thickness to rupture.

According to Marrucci (1969), further thinning of the quasi-equilibrium film occurs by a diffusion controlled mechanism. The concentration of the additive molecules in the film liquid is lower than in the bulk liquid outside the film and, as a result, the additive molecules diffuse into the film liquid. This diffusion process would destroy the built up difference in surface tension. For

additives molecules with similar diffusivities, higher values of the Marrucci parameter should result in a more effective coalescence inhibition. However, the data of the present study showed that this was not always the case.

In the additive solutions used for this study, the values of the Marrucci parameter were always much higher than the specified minimum value for coalescence inhibition. Table 5.1.1 shows the values of Marrucci parameter for some of the additives used in this study for a concentration of 250 vppm and a bubble diameter of 2.0 mm. It can be seen that cyclohexanone is a very effective coalescence inhibitor while the data for hexanal solution suggests some coalescence promotion. The

Table 5.1.1 Values of Marrucci Parameter for some of the Additives used for the Study

Additive	Marrucci Parameter	Dipole moment	ϵ_g(add.)/ϵ_g(TW)
Hexanol	$30X10^5$	1.67	1.44
Hexanal	$4.14X10^5$	1.68	0.74
Cyclo-hexanone	$3.85X10^5$	3.02	1.47
Benzal-dehyde	$4.35X10^5$	2.79	1.08
Hexanoic Acid	$25X10^5$	1.31	1.12
2-hexanone	$9.2X10^5$	2.7	1.35

Marrucci parameter, however were practically the same for cyclohexanone and hexanal solutions and much higher than the critical value of 1.89. Marrucci's theory, thus, completely fails to predict the behaviour of hexanal. Moreover, although cyclohexanone and hexanol are almost equally effective additives, the value of the Marrucci parameter for hexanol is about an order of magnitude higher.

For the development of his theory Marrucci (1969) assumed that there was always equilibrium between film surface and the film liquid. This assumption, however, may not be valid for additive molecules which migrate slowly to the surface of the thinning film. Marrucci also assumed the absence of any electric forces inside the thinning film.

Sagert and Quinn (1978) included electrostatic double layer repulsion in their model to account for the effect of surface charge on coalescence inhibition. They showed that electric double layer repulsion should be considered for values of the Marrucci parameters higher than 25. The dipole moments of additive molecules can be used to compare the surface charge associated with different types of additives. The dipole moment of the cyclohexane molecule is about twice that of hexanol (Table 5.1.1). The higher surface charge associated with cyclohexanone molecules might compensate for its lower Marrucci parameter. The behaviour of hexanal might be explained by

dynamic surface tension effect. If the hexanal molecules are slow to adsorb at one interface, their net effect on coalescence inhibition will be greatly reduced. However no data for dynamic surface tension of hexanal solution was available for further analysis.

Marrucci's theory was again tested for the results obtained with straight chain alcohols solutions. It was shown in section 4.1.3.3. that the effectiveness for gas holdup and mass transfer coefficient peaked at pentanol. The Marrucci number is proportional to the square of the slope of surface tension versus concentration curve. The value of this slope keeps increasing with hydrocarbon chain length of the alcohol molecules (Hommelen, 1959). For decanol solutions, slight coalescence promotion effects could be observed (the gas holdup effectiveness were less than one; section 4.1.3.3). Marrucci's theory therefore fails to predict the behaviour of alcohols higher than pentanol.

For his model, Marrucci assumed instant equilibrium of the additive molecules at the interface, this, however, may not be true for long chain molecules. The rate of adsorption of the molecules at the interface can be determined from the dynamic surface tension data. The difference between the dynamic and static tension indicate how far the additive concentration at the interface is from its equilibrium value. The dynamic surface tension of a solution is a function of time as well as composition

(Defay and Hommelen, 1958). The dynamic surface tension effects could play an important role in determining the coalescence inhibition effects of long chain alcohol molecules. For 0.116 kg/m^3 n-octyl alcohol solution, Defay and Mommelen (1958) found no drop in surface tension up to 15 milliseconds. The concentration of the additive solution used for the measurement of dynamic surface tension was three orders of magnitude higher than the concentration used in this study. Therefore, the dynamic surface tension effect would be more pronounced in the dilute solutions of this study. It may be pointed out, however, that the decrease in gas-liquid mass transfer rate in the solutions of long chain alcohols indicated that these molecules had reached the interface where they created barrier to mass transfer. The effects of dynamic surface tension during bubble coalescence can be explained as below.

When two bubbles come into contact with each other and the intervening liquid film starts to flatten the molecules of long chain alcohols adsorb slowly at the interface. These molecules, therefore, fail to create the surface tension difference between the film and the bulk of liquid outside the film which resists the further thinning of the liquid film (Equation 5.1.4). Therefore, dynamic surface tension effects come into play only during bubble coalescence.

5.2 Porous Distributor Pressure Drop Model

The distributor pressure drop was obtained from the difference between the pressure below the distributor plate and the pressure in the freeboard region above the liquid. The liquid hydrostatic head was then subtracted. Figures 5.2.1 and 5.2.2 show the pressure drops obtained with porous distributors PR1 and PR2 in the absence of liquid in the empty column and in the presence of liquid. It can be seen that the pressure drops obtained in the presence of liquid were much higher than the pressure drops obtained in absence of liquid. Figure 5.2.2 also shows that with "wet" PR2 distributor, which was thoroughly wetted prior to the measurements, the pressure drops were 15 to 30% higher than with the "dry" PR2 distributor. The "intermediate" startup procedure resulted in pressure drops which were between the values obtained with the "dry" and "wet" startup procedures (Figure 5.2.2). These results show that the startup procedure significantly affected the distributor pressure drop.

For "dry" porous plate distributors, the pressure drops obtained in the empty column could be accurately described with a power law:

$$\Delta P_{f,1} = 5872\ v_g^{1.06} \qquad \text{.....(5.2.1)}$$

$$\Delta P_{f,2} = 32300\ v_g^{1.3} \qquad \text{.....(5.2.2)}$$

The exponent was closer to 1.00 for distributor PR1 than for distributor PR2. This indicates that the gas

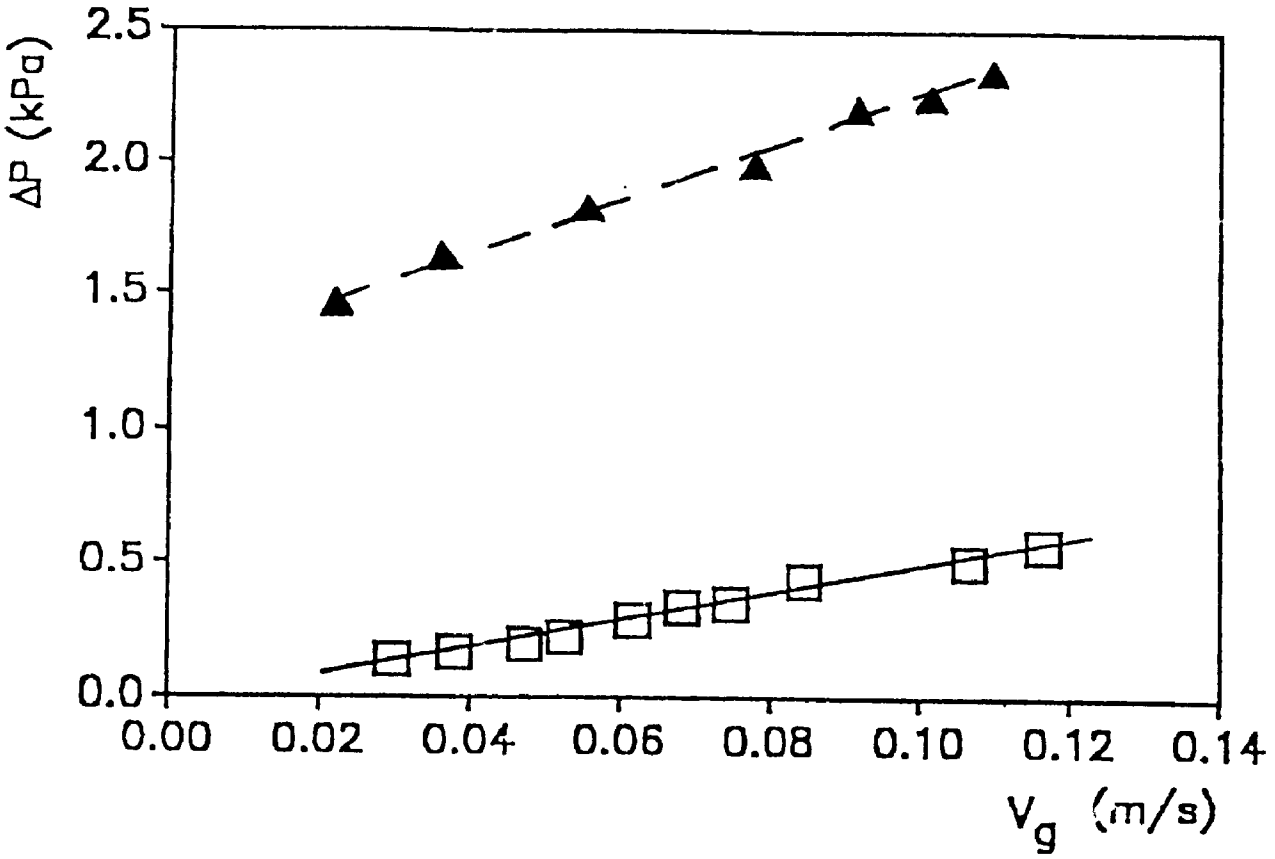

Figure 5.2.1
Distributor pressure drop versus superficial gas velocity; Distributor PR1

□ in the absence of water; solid line represents Equation 5.2.1
▲ in the presence of water, "dry" startup procedure

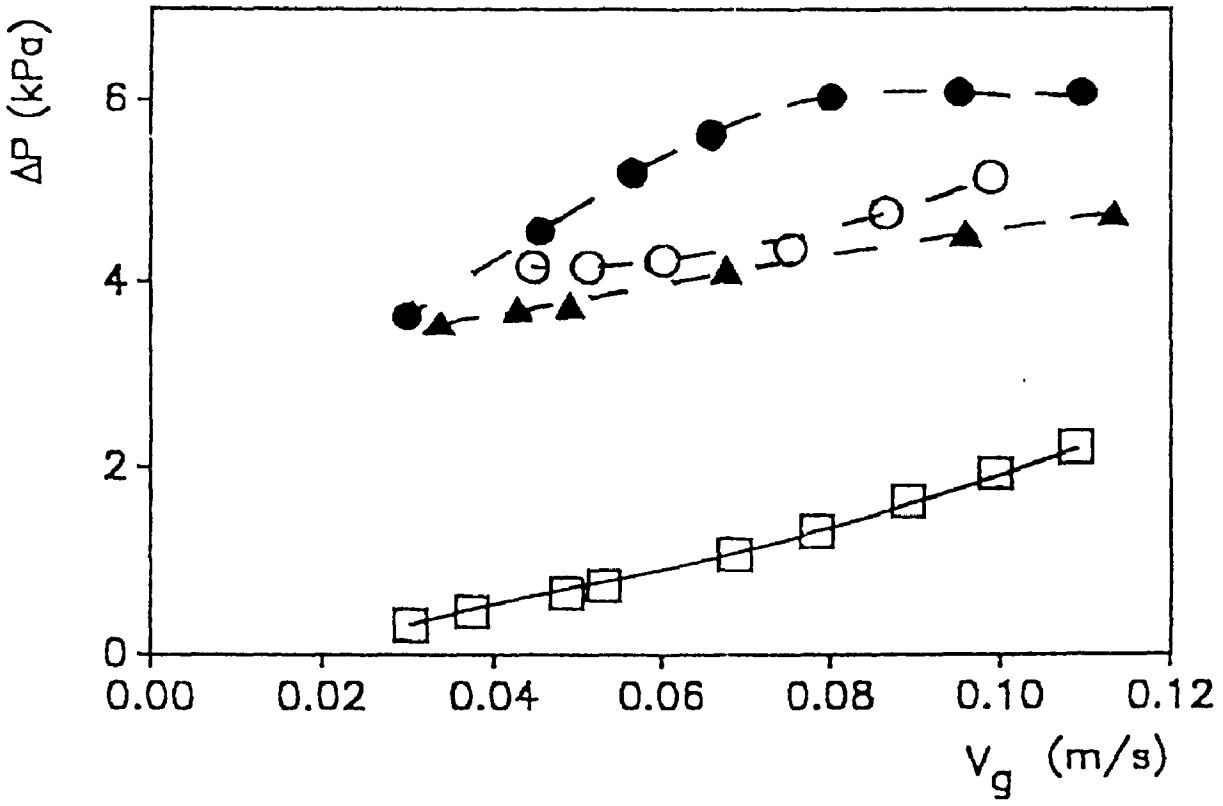

Figure 5.2.2
Distributor pressure drop versus superficial gas velocity; Distributor PR2

□ in the absence of water; solid line represents Equation 5.2.2
▲ in the presence of water; "dry" startup procedure
○ in the presence of water, "intermediate" startup procedure
● in the presence of water, "wet" startup procedure

velocity through the pores of distributor PR2 was too high for streamline flow. The pressure drop should depend primarily on the thickness of the porous plate, the size of its pores and the gas velocity through each of its pores. In streamline flow, at low gas velocities, the distributor pressure drop is proportional to the gas velocity through the pores. If the thickness, pore size and pore concentration per unit of plate area had been the same in both distributors, the pressure drop through distributor PR2 should have been about 160 % higher than the pressure drop measured through distributor PR1 at the same gas flowrate (this is strictly valid for streamline flow only, i.e. at low gas velocities). For gas velocities ranging from 0.03 to 0.06 m/s, the pressure drop through distributor PR2 was about 140% to 180% larger than the pressure drop through distributor PR1. This confirms that distributors PR1 and PR2 were made of the same material.

The presence of liquid increased the pressure drop by an amount which was almost independent of the gas flowrate: 1300 to 1700 Pa for distributor PR1 (see Figure 5.2.1) and 2400 to 2700 Pa for distributor PR2 (see Figure 5.2.2). The following section analyses the effect of the presence of liquid on the distributor pressure drop for the case of the "dry" startup procedure.

According to Davidson and Schuler (1959), the instantaneous pressure drop through a distributor in a

bubble column is given by the sum of 3 terms:

$$\Delta P_{dl} = \Delta P_f + \Delta P_s + \Delta P_h \quad \text{.....(5.2.3)}$$

The frictional pressure drop ΔP_f is due to friction between the flowing gas and the walls of the distributor pores. It is obtained from the data obtained in the empty column, i.e. Equations (5.2.1) or (5.2.2), depending on the distributor. ΔP_s is caused by the surface tension forces acting on the bubble of radius r_b:

$$\Delta P_s = 2\ \sigma\ /\ r_b \quad \text{.....(5.2.4)}$$

ΔP_h, which comes from the local reduction of the hydrostatic head above the developing bubble, is given by:

$$\Delta P_h = \rho_L\ g\ r_b \quad \text{.....(5.2.5)}$$

Researchers have usually considered two extreme conditions: constant pressure in the chamber below the distributor and constant flow through the distributor orifices (Tsuge, 1986). From Equations (5.2.3) and (5.2.4) and the experimental data presented in Figures 5.2.1 and 5.2.2, it appears that the surface tension term ΔP_s is so large for a small bubble at the beginning of its growth that flow would be impossible under constant pressure conditions. It was, therefore, assumed that bubbling at all the pores was synchronized and that the gas flowrate through the distributor was constant. Synchronization is required to ensure that the pressure

under the chamber builds up to a level sufficient to compensate for the large surface tension pressure ΔP_s acting on a bubble at the beginning of its cycle.

Under these conditions, the frictional pressure drop ΔP_f is constant but the surface tension and hydrostatic terms vary with the size of the growing bubbles. Bubbles are assumed to grow from a radius r_{bi} and detach from the pores when they reach a radius r_{bf}. The average pressure due to surface tension forces can be given as:

$$\Delta P_s = \frac{1}{t}\int_0^t \Delta P_s(t)\,dt \qquad \text{.....(5.2.6)}$$

$$= \frac{1}{t}\int_0^t \frac{2\sigma}{r_b}\,dt \qquad \text{.....(5.2.7)}$$

For constant gas flow conditions, the following equation gives the change in bubble volume during time Δt.

$$Q_g \Delta t = \Delta V_b = 4\pi r_b^2 dr_b \qquad \text{.....(5.2.8)}$$

Substituting for dt in Equation 5.2.7, we get

$$\Delta P_s = \frac{8\pi\sigma}{Q_g t}\int_{r_{bi}}^{r_{bf}} r_b\,dr_b \qquad \text{.....(5.2.9)}$$

$$= \frac{8\pi\sigma}{Q_g t}\left(r_{bf}^2 - r_{bi}^2\right) \qquad \text{.....(5.2.10)}$$

Moreover

$$Q_g t = V_{bf} - V_{bi} = \frac{4\pi}{3} (r_{bf}^3 - r_{bi}^3) \quad .....(5.2.11)$$

Substituting for t in Equation 5.2.10, we get

$$\Delta P_s = 3\sigma (r_{bf}^2 - r_{bi}^2)/(r_{bf}^3 - r_{bi}^3) \quad .....(5.2.12)$$

A similar analysis also provides the average value of the local reduction of the hydrostatic head, given as:

$$\Delta P_h = 0.75\rho_l g(r_{bf}^4 - r_{bi}^4)/(r_{bf}^3 - r_{bi}^3) \quad ..(5.2.13)$$

Knowledge of initial and final bubble radii is thus required to calculate the average distributor pressure drop. Most researchers have taken the orifice radius as initial radius r_{bi} (Tsuge, 1986) and the average pore radius was therefore used in this study. The only model for the prediction of the final size r_{bf} of bubbles formed at a porous distributor was proposed by Bowonder and Kumar (1970). Their two-stage model, as well as a simpler one-stage model developed for this study, gave final bubble radii which were well into the millimeter range for the conditions of this study. Such final bubble radii gave distributor pressure drops which were much lower than the measured pressure drops.

5.3 Model for Bubble Size at Detachement from a Porous Distributor

A new model has been developed to predict the bubble size at detachment from a porous distributor. S ıce bubble growth is synchronized, the bubbles growing at neighboring pores are identical (Figure 5.2.3a). When two bubbles growing on adjacent pores touch, their probability of coalescence is very high since they are attached to their pores and cannot bounce off each other. Moreover, when two growing bubbles touch each other, the momentum force helps drain the intervening liquid film. This would further accelerate the coalescence of bubbles at the distributor plate. Figure 5.2.3b shows a coalesced bubble which is still connected to the two pores. This bubble is unstable and instantaneously assumes the most stable shape for small bubbles: the spherical shape (Grace and Wairegi, 1986). Severing of the bubbles from the pores results (see Figure 5.2.3c). The final bubble radius just before coalescence and detachment is thus equal to half the average center-to-center distance between neighboring pores. Although the coalescence of more than two adjacent bubbles is possible, this will not change the bubble radius just before coalescence and the pressure drop will not be affected.

All the distributor pores are not, however, active. This results from the relatively large contribution of the surface tension pressure drop to the distributor pressure

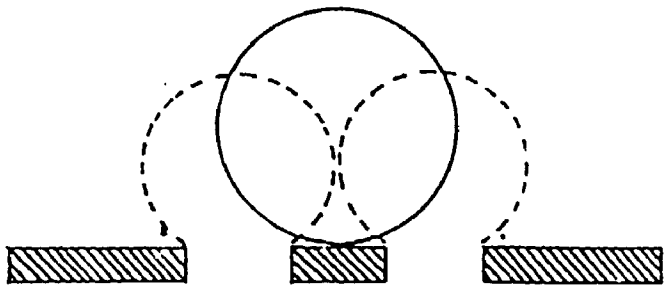

Figure 5.2.3c -the new coalesced bubble shape

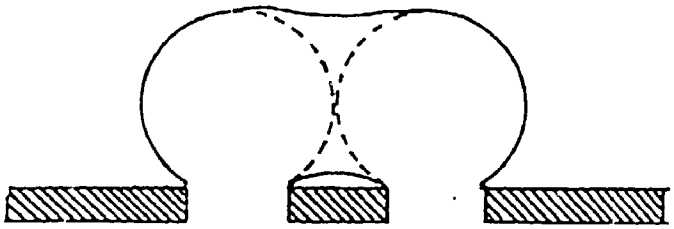

Figure 5.2.3b -bubbles coalesce: unstable intermediate stage

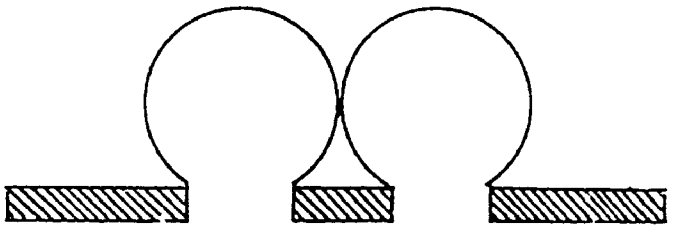

Figure 5.2.3a -just before coalescence

Figure 5.2.3
Bubble formation at the distributor according to the proposed model

drop. If only a few pores are active, the gas velocity through the active pores and hence the frictional pressure drop will be high. The surface tension term ΔP_s, however, will be smaller since the average distance between active holes will be larger, resulting in a larger final bubble radius (see Equation 5.2.12). On the other hand, if all the pores are active, the frictional pressure drop will be small but the smaller bubbles will result in a large surface tension pressure drop. It was therefore assumed that the fraction f_o of the distributor pores which were active was such that the average overall distributor pressure was minimized. This would correspond to the minimum energy consumption. The average center-to-center distance between neighboring holes is given by (assuming an equilateral pitch):

$$\Delta l = 0.537\ D_d\ [\pi / (N_o f_o)]^{0.5} \qquad \text{.....(5.2.14)}$$

where D_d is the diameter of the porous plate and N_o is the total number of pores in the plate. The final bubble radius r_{bf} just before coalescence and detachment is then set to half this distance Δl. The surface tension and hydrodynamic contributions ΔP_s and ΔP_h are then given by Equations 5.2.12 and 5.2.13. The frictional pressure drop is calculated with:

$$\Delta P_f = K_f\ (V_g/f_o)^{m'} \qquad \text{.....(5.2.15)}$$

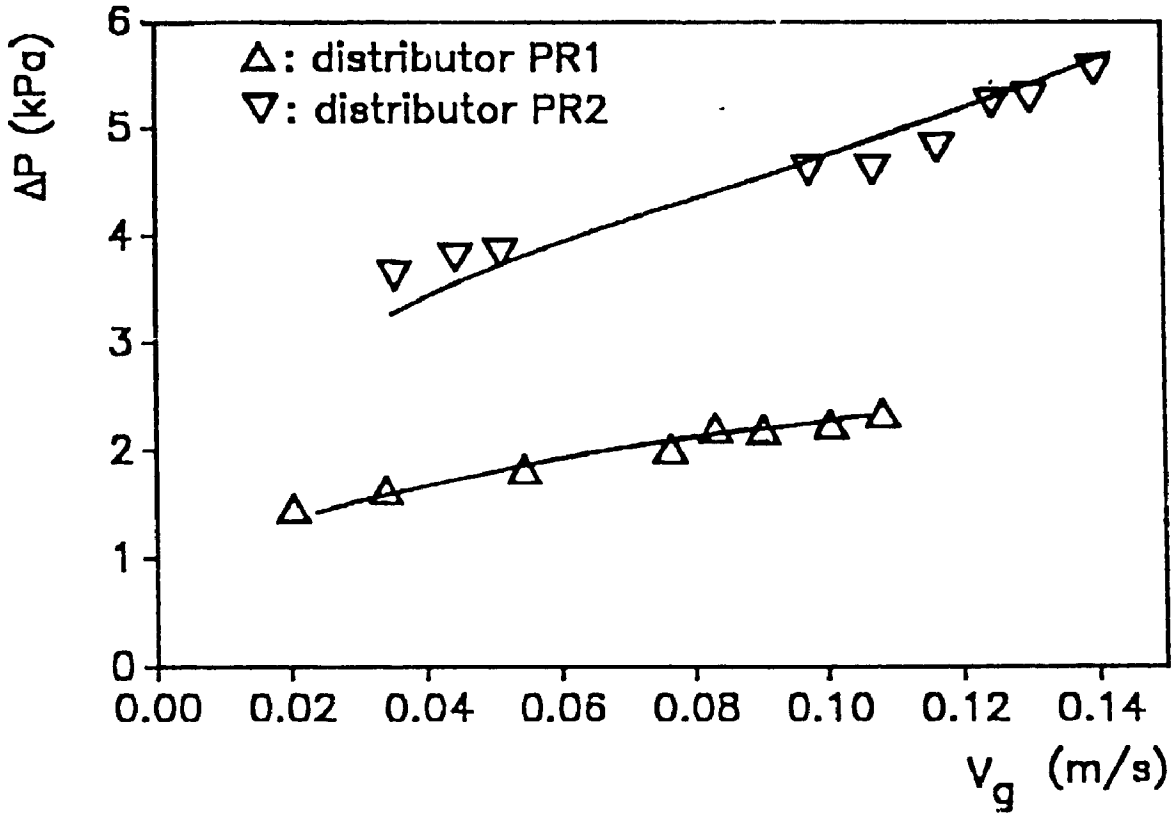

Figure 5.2.4
Distributor pressure drop predictions by the models; Distributors PR1, PR2

Where the constants K_f and m' are obtained from the pressure drop data in the absence of liquid (Equations 5.2.1 and 5.2.2). The total number of pores N_o could not be obtained from the porous plate manufacturer and was thus calculated from pressure drop data obtained with distributor PR2 at high gas velocities for which all pores were active. For distributor PR2, this procedure yielded N_p = 131 000 pores.

Figures 5.2.4 shows that the new model gave accurate predictions of the distributor pressure drops obtained with distributors PR1 and PR2 respectively. It should be noted that the approximation which resulted from the assumption of a constant distance between neighboring holes which would change with the proportion of active pores (see Equation 5.2.14) did not seem to adversely affect the accuracy of the predictions.

With distributor PR2, full operation of all the pores was reached at a superficial velocity of 0.10 m/s. With distributor PR1, full operation of all the pores was never reached, even at a superficial gas velocity of 0.14 m/s where less than 40% of all the pores were active. For a given gas flowrate, distributor PR2, in spite of its smaller area, always had more active pores than distributor PR1. Distributor PR1, however, gave a better mass transfer performance because it distributed the bubbles more uniformly over the whole column cross-section and thus reduced the rate of bubble coalescence in the

distributor region.

For a given gas flowrate, the smallest bubble size will be obtained when the largest number of pores are active. The model indicates that smaller initial bubbles would not be obtained by increasing the total number of distributor pores since, at practical gas flowrates, the number of active pores is less than the total number of pores. Smaller gas bubbles could be obtained by increasing the number of active pores, i.e. by shifting the balance between the surface tension pressure drop ΔP_s and the frictional pressure drop ΔP_f. The frictional pressure drop should, thus, be increased. This could be achieved by either reducing the pore size or increasing the distributor thickness. In most applications, the bubbles which are formed at the distributor should be as small as possible to achieve high mass transfer rates.

5.4 Effects of Startup Procedures on the Performance of Porous Distributors

5.4.1 Effects on gas holdup

Figure 5.2.5 shows that the distributor startup procedure had a significant effect on the gas holdup obtained in the bubble column. The variation of the gas holdup with the superficial gas velocity was as expected for a bubble column with a porous distributor . As the

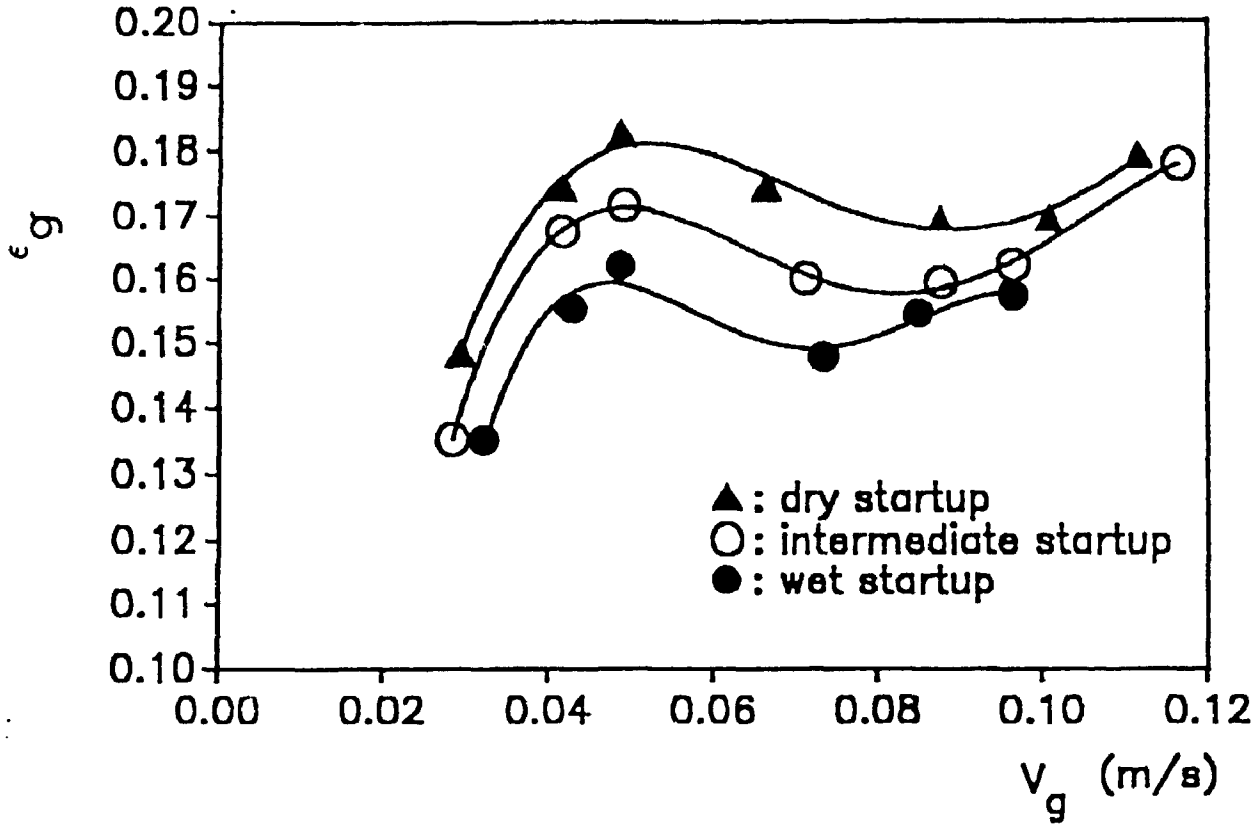

Figure 5.2.5
Gas holdup as a function of gas velocity (Distributor PR2); Different startup procedures

gas velocity was increased, the gas holdup first increased, reached a maximum corresponding to the transition from the bubbly flow regime to the heterogeneous flow regime, decreased when the velocity was further increased and then increased again when the churn turbulent regime became fully establisned (see section 4.1.2.1). The startup procedure did not affect the gas velocity at which the transition from bubbly flow occurred but it affected the velocity at which the the churn turbulent flow became fully established (see Figure 5.2.5). The "dry" startup procedure, however, always resulted in larger gas holdups For example, the maximum gas holdup which was obtained with the "dry" startup procedure was about 10% higher than the holdup obtained with the "wet" startup procedure. Since larger gas holdups are generally obtained when smaller gas bubbles are formed at the distributor the bubbles formed at the "dry" distributor must therefore have been smaller than the bubbles formed at the "wet" distributor.

5.4.2 Effects on the volumetric mass transfer coefficient

Figure 5.2.6 shows that the mass transfer results confirmed the gas holdup results although the transition to the heterogeneous regime and to the fully established churn turbulent regime appeared to occur at slightly lower gas velocities with the "wet" distributor. Significantly

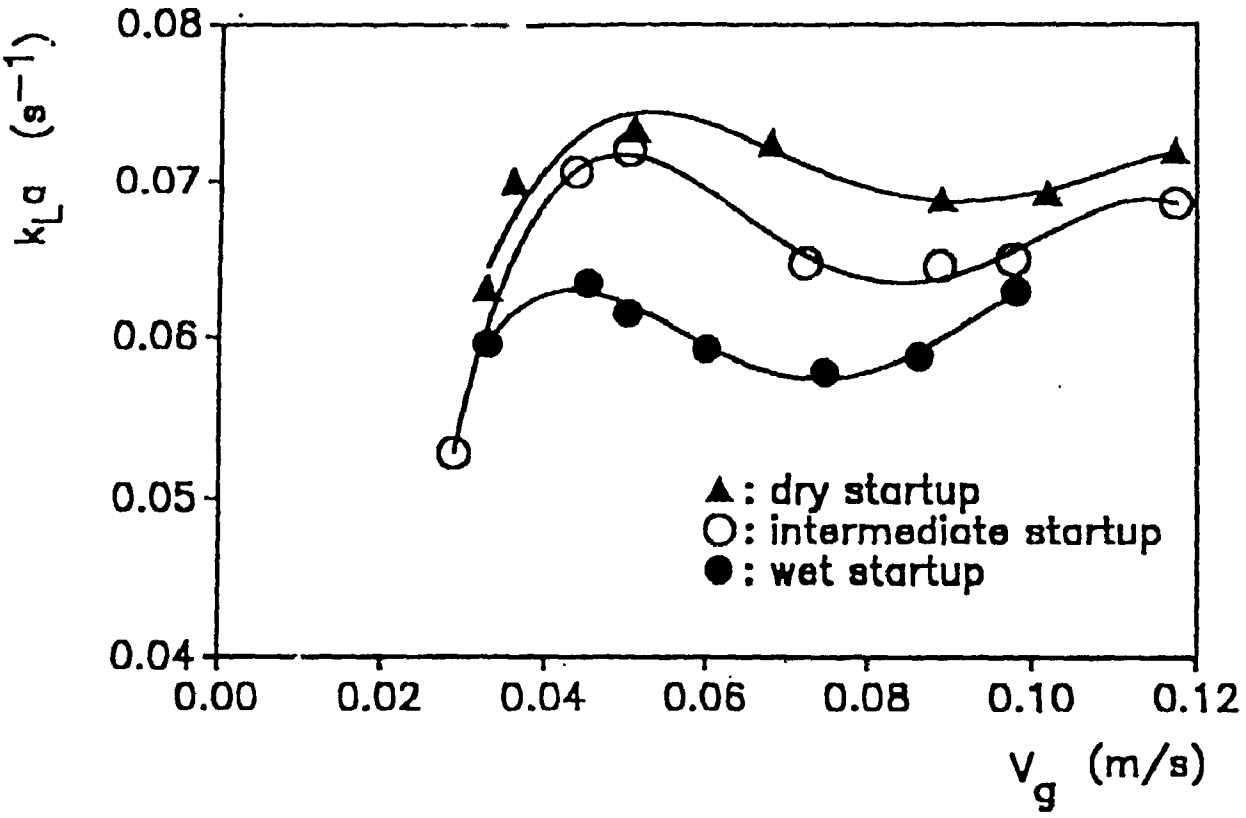

Figure 5.2.6
Volumetric mass transfer coefficient as a function of gas velocity (Distributor PR2); Different startup procedures

higher volumetric mass transfer coefficients were obtained with the "dry" startup procedure than with the other startup procedures. For example, the maximum volumetric mass transfer coefficient which was obtained with the "dry" startup procedure was about 15 % higher than the maximum coefficient obtained with the "wet" procedure. The "dry" startup procedure should therefore be used to achieve top mass transfer performance.

5.4.3 Effects on performance of sparging time since "wet" startup

Experiments were conducted with distributor PR2 to establish whether the detrimental effects of the "wet" startup procedure would disappear after a few days of operation. A constant gas velocity of 0.05 m/s was used since it corresponded to the maximum volumetric mass transfer coefficient which could be achieved with all startup procedures. The distributor pressure drop did not decrease to the value obtained with the "dry" startup procedure, even after 4 days of continuous operation. The mass transfer performance, however, improved steadily and practically matched the performance obtained with the "dry" startup procedure after only two days of continuous operation. Although the "dry" startup procedure should always be used in laboratory studies, it is not essential in industrial practice.

5.4.4 Effect of distributor startup procedure

When the "wet" startup procedure was used, some of the pores were plugged by liquid and were therefore inactive. The fraction of the distributor pores which were thus plugged was calculated by fitting the distributor pressure drops calculated by the above model to the experimental values. Figure 5.2.7 shows that the pores which were plugged by liquid were gradually freed of liquid as the gas flowrate was increased. The number of plugged pores was always much larger than the number of pores which became inactive with the "dry" distributor to minimize the overall pressure drop (see Figure 5.2.7). The process which set the number of active pores with the "wet" distributor was therefore different from the process which set this number for the "dry" distributor.

Clearing of the liquid from the distributor pores is resisted by the hydrostatic pressure of the liquid inside the pores and the capillary pressure. In practice, the plate was not thick enough for the hydrostatic pressure to be significant. The capillary pressure is given by:

$$\Delta P_p = - 2 \sigma \cos\theta / r_c \qquad \text{.....(5.2.16)}$$

Where r_c is the pore radius and θ is angle of wetting of the distributor material by water.

The pressure drop ΔP_{dl} through the active distributor holes, which is given by Equation (5.2.3), was such that

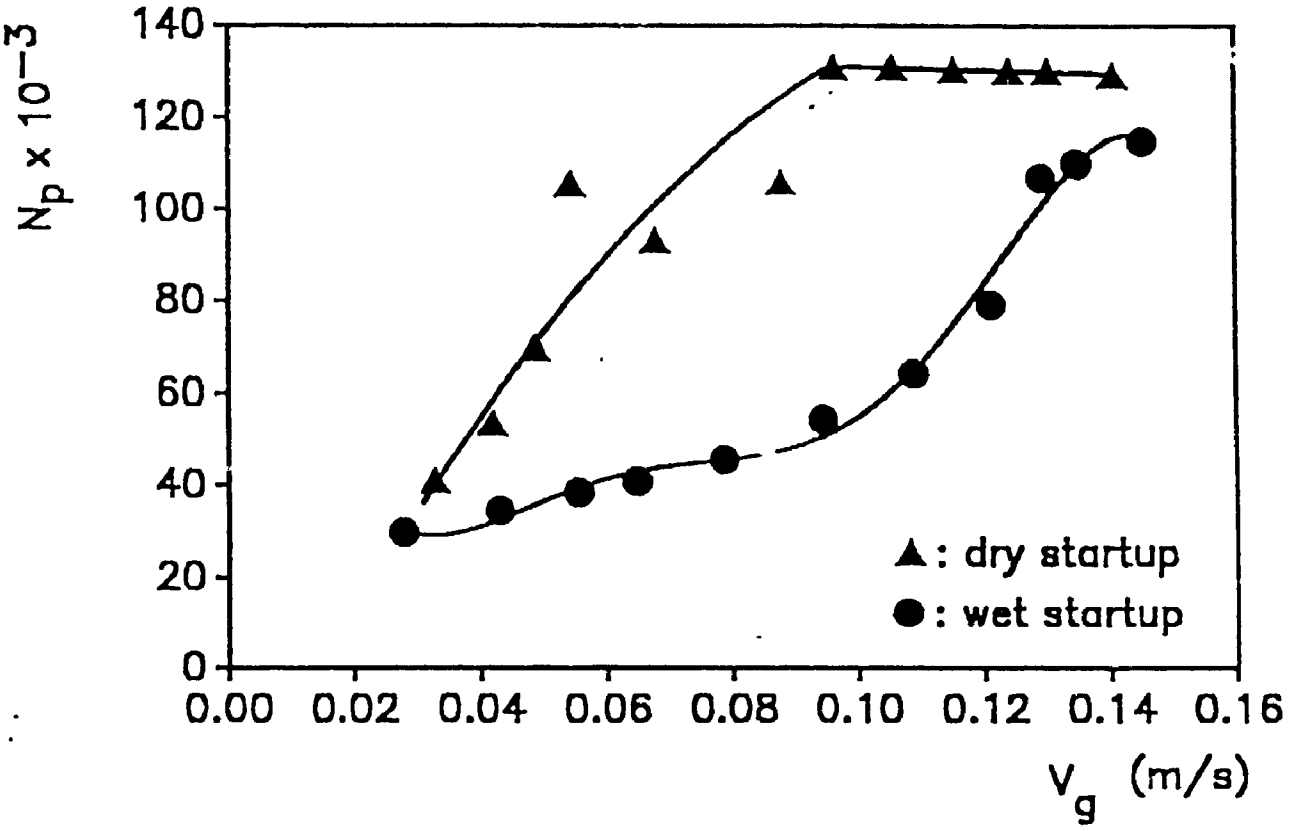

Figure 5.2.7
Number of active pores versus superficial gas velocity for distributor PR2

the pressure at the bottom of the pores was larger than at the top. This pressure drop therefore tended to clear the liquid from the plugged pores. As shown earlier, bubbling at all the active pores was synchronized and the gas flowrate through the distributor was constant. The distributor pressure drop thus fluctuated with a period of below one millisecond. It reached its largest value at the beginning of the bubbling cycle and gradually decreased until bubble detachment. The distributor pressure drop was therefore larger than the capillary pressure at the beginning of the cycle and liquid was then pushed out of the plugged pores. At the end of the bubbling cycle, the distributor pressure drop became smaller than the capillary pressure drop and liquid flowed back into the plugged pores. The liquid level inside the plugged pores thus fluctuated with the same period as the bubbling cycle. Due to the very short bubbling period and the large friction forces which slowed liquid motion through the pores, unsteady-state effects may be neglected. Clearing of a pore, thus, occurred only when the average distributor pressure drop becomes larger than the capillary pressure in that pore.

Larger pores were cleared first, at low gas velocities, because the capillary pressure was smaller for large pores, as shown by Equation (5.2.16). If the average distributor pressure drop is ΔP_{dl}, the diameter of the smallest active pore will be given by:

$$d_c = - 4 \sigma \cos\theta / \Delta P_{dl} \qquad \text{.....(5.2.17)}$$

The pore diameter distribution of a distributor can, thus, be evaluated by comparing the measured distributor pressure drop to the number of active holes as calculated by the model presented earlier. Figure 5.2.8 shows the results of this evaluation for distributor PR2; about 70% of the pores had a diameter near 35 μm.

The results presented in Figure 5.2.8 required the knowledge of the angle of wetting of the distributor material by water. An angle of - 42^{o} was obtained by assuming that the average pore diameter was exactly 35 μm, as specified by the manufacturer. The distributor material, which was polyethylene, was therefore hydrophilic. Although one would expected polyethylene to be hydrophobic, it is known that polyethylene will eventually become hydrophilic when exposed to aqueous solutions (this has been observed in absorption columns which use polyethylene packings). If the "wet" startup procedure is to be used, the distributor should therefore be "aged" to obtain reliable results (the distributor PR2 was "aged" for more than one year).

The models presented in this paper can explain the smaller volumetric mass transfer coefficients which were obtained with the "wet" startup procedure. The capillary pressure of the water in the pores of the "wet" distributor prevented gas flow through an optimum number of pores. Gas was, thus, bubbling through a smaller

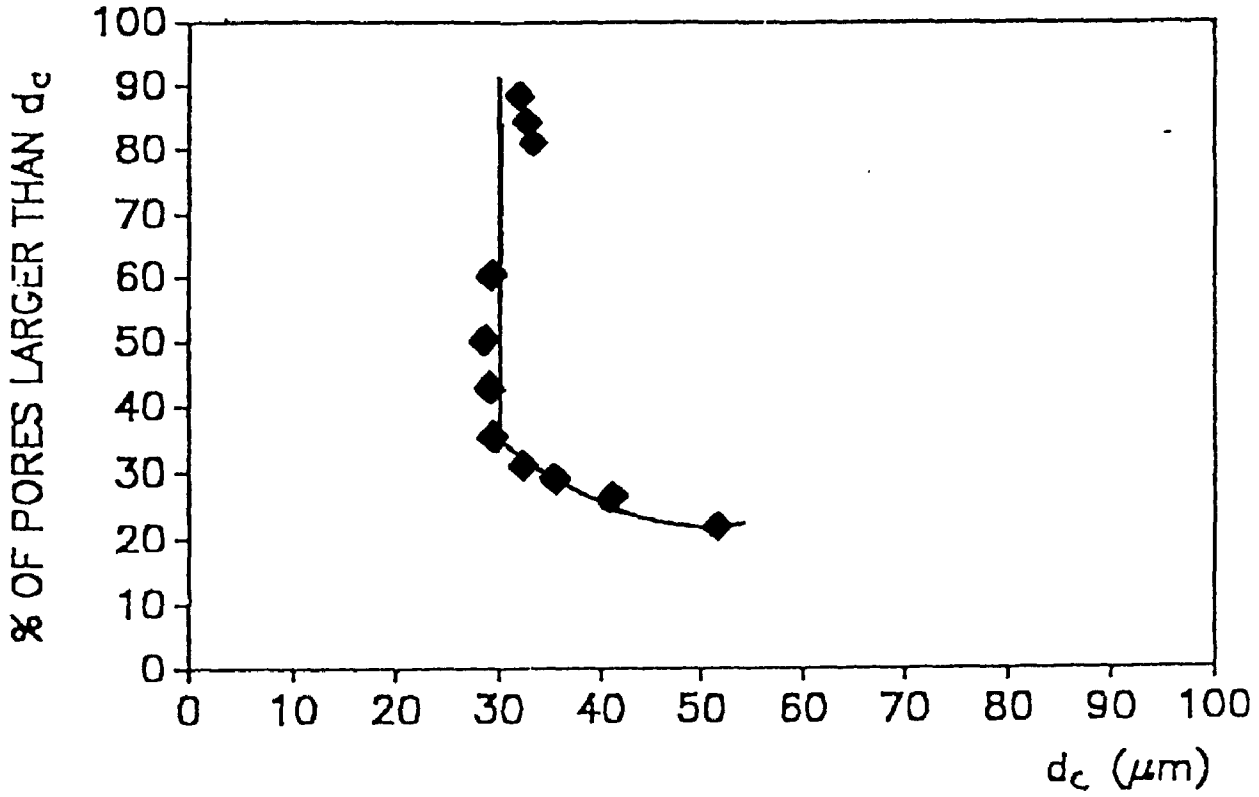

Figure 5.2.8
Percentage of pores with a diameter larger than d_c (Distributor PR2)

number of pores than when the "dry" startup procedure was used. This explains why the distributor pressure drop was larger. Moreover, the larger distance between neighboring active pores meant then a bubble growing at the distributor was able to grow further before it coalesced with a neighboring bubble and detached itself from the distributor. Everything else being equal, a larger initial bubble size resulted in a larger average bubble size throughout the whole column. Since larger bubbles have a smaller surface-to-volume ratio and rise more quickly, they gave a smaller gas holdup, a smaller interfacial area a per unit of column volume and, hence, a smaller volumetric mass transfer coefficient k_1a.

6.0 Conclusions and Recommendations

6.1 Conclusions

Gas-liquid mass transfer in a bubble column was enhanced by using a fine gas distributor and/or by addition of small amount of an effective coalescence inhibitor in the liquid. This study identified suitable and effective additives which enhanced the gas-liquid mass transfer rate by about 40% at a concentration of less than 20 vppm. The effectiveness of coalescence inhibitors was found to depend on their functional group and hydrocarbon chain length. The most effective additives were alcohols and ketones with five or six carbon atoms. The gas-liquid mass transfer enhancement in presence of effective additives can mainly be attributed to the higher interfacial area resulting from an increase in the population of small bubbles in the gas-liquid dispersion.

Porous distributors generate fine gas bubbles as compared to spargers and thus provide high interfacial area for mass transfer. The performance of the porous plate distributor was found to increase with increasing porous plate area. It could also be improved further by adding coalescence inhibitors.

Gas-liquid mass transfer in three-phase fluidized beds was enhanced by about 30% by the addition of only about 5 vppm of the effective additive in the liquid. The increase in the mass transfer rate was always accompanied

by an increase in gas holdup.

This study identified additives which alter the coalescence properties of a liquid without changing any other properties. This makes it possible now to study effects of coalescing properties in multiphase reactors.

Introduction of gas in a liquid-solid fluidized bed enhanced the particle-liquid mass transfer rate by about 20 % in the absence of coalescence inhibitors. However, particle-liquid mass transfer in three-phase fluidized bed was enhanced by more than 80% (over the liquid fluidized bed value) by addition of coalescence inhibitors in the liquid.

The volumetric mass transfer in a batch bubble column can be correlated to gas holdup. Separate correlations, however, are required to correlate the data obtained in coalescing and noncoalescing liquid phases. A generalized correlation for gas holdup in a coalescing medium was developed, based on the bubble size in the distributor region. For noncoalescing media, no generalized correlation could be developed to account for the effects of different coalescence inhibitors on gas holdups.

The volumetric mass transfer coefficient in three-phase fluidized beds was correlated by a single correlation for bot. coalescing and noncoalescing medium by the inclusion of gas holdup in the correlation. Generalized correlations for gas and liquid holdups in three-phase fluidized beds were developed based on drift

flux model.

Particle-liquid mass transfer in three-phase fluidized beds was found to increase with increasing interstitial liquid velocity. A generalized correlation was developed for the prediction of particle-liquid mass transfer in two-phase and three-phase fluidized beds.

6.2 Recommendations

This study investigated gas-liquid mass transfer and hydrodynamics in bubble columns and three-phase fluidized beds. These two systems constitute the two extremes, while in between lies the slurry bubble columns with particle size less than 500 microns. Slurry bubble columns have good potential for industrial applications such as Fischer Tropsch synthesis and coal liquefaction. It would therefore, be useful to investigate the effects of additives and gas distribution on mass transfer rate and hydrodynamics in slurry bubble columns. Such a study can be based on the information generated in this study.

There is also a lack of data on mass transfer and hydrodynamics using organic liquids. Since a number of industrial processes use organic liquid streams, it would be useful to study the effects of additives using different organic liquids.

From a practical point of view, it would also be important to investigate the effects of various additive mixtures on mass transfer rates. Such a study may point out additives which have synergistic effects.

Although porous distributors provide higher mass transfer rate as compared to spargers, their performance can be easily affected by different startup procedures and/or due to plugging of pores. It would, therefore, be advantageous to explore alternative distributor designs to

overcome the limitations of porous distributors.

More fundamental studies, aimed at developing theories of bubble coalescence should take into account the effects of dynamic surface tension and electrostatic double layer effects.

There exists a radial concentration profile in a three-phase fluidized bed. In this study, the average concentration across the column cross-section was obtained assuming uniform liquid velocity across the cross-section. A more detailed model should take into account the radial dispersion and radial distribution of liquid velocity.

Appendix-1

Calibration of flow nozzles used with batch bubble column.

Notations

A_2 cross-sectional area of throat (m^2)

C coefficient of discharge

C_1 dimensional constant; 0.0405 SI units

k ratio of specific heats

p_1 pressure upstream of nozzle (Pa)

p_2 pressure downstream of nozzle (Pa)

r_c critical pressure ratio

R gas law constant

T_1 temperature upstream of flow nozzle (^oK)

w_{max} maximum weight flow rate (kg/s)

The flow nozzles were designed to operate as critical flow meters over a wide range of flowrate. For very low flowrates, however, these nozzles operated in subcritical region. For a given set of upstream conditions the rate of discharge of a gas from a nozzle increases with a decrease in the absolute pressure ratio p_2/p_1 until the linear velocity in the throat reaches that of the sound at that location. After which any further decrease of the outlet pressure does not produce any further increase in the rate of flow. The ratio of the outlet to the inlet pressure at which this maximum rate of flow is obtained is termed the critical pressure ratio r_c. The condition for maximum throat velocity is also the condition for maximum

weight rate of flow.

The critical pressure ratio r_c can be obtained from the following theoretical equation which assumes perfect gas and a frictionless nozzle (Fluid meters, 1959).

$$r_c^{(1-k)/k} + [(k-1)/2]\beta^4 r_c^{2/k} = (k+1)/2 \quad .....(1)$$

for $\beta < 0.2$ this reduces to

$$r_c = [2/(k+1)]^{k/(k-1)} \quad .....(2)$$

For $k = 1.4$ $r_c = 0.528$

Under critical flow conditions, only the upstream conditions p_1, v_1 and T_1 need be known to determine the flow rate, which for $\beta < 0.2$ is given by

$$w_{max} = CA_2 [g_c k(p_1/v_1)(2/(k+1)^{(k+1)/(k-1)}]^{0.5} \quad .....(3)$$

For air Equation 3 reduces to

$$w_{max} = C_1 CA_2 p_1/T_1^{0.5} \quad .....(4)$$

The flow nozzles were calibrated by measuring the volumetric flowrate at the column outlet with the help of a wet testmeter. Since the gas at the column outlet was always saturated, no correction for humidity was required. The corresponding superficial velocity of gas in the column was obtained by dividing the volumetric flowrate by the column cross-sectional area. The calibration curves are shown in Figure 1.1 and 1.2.

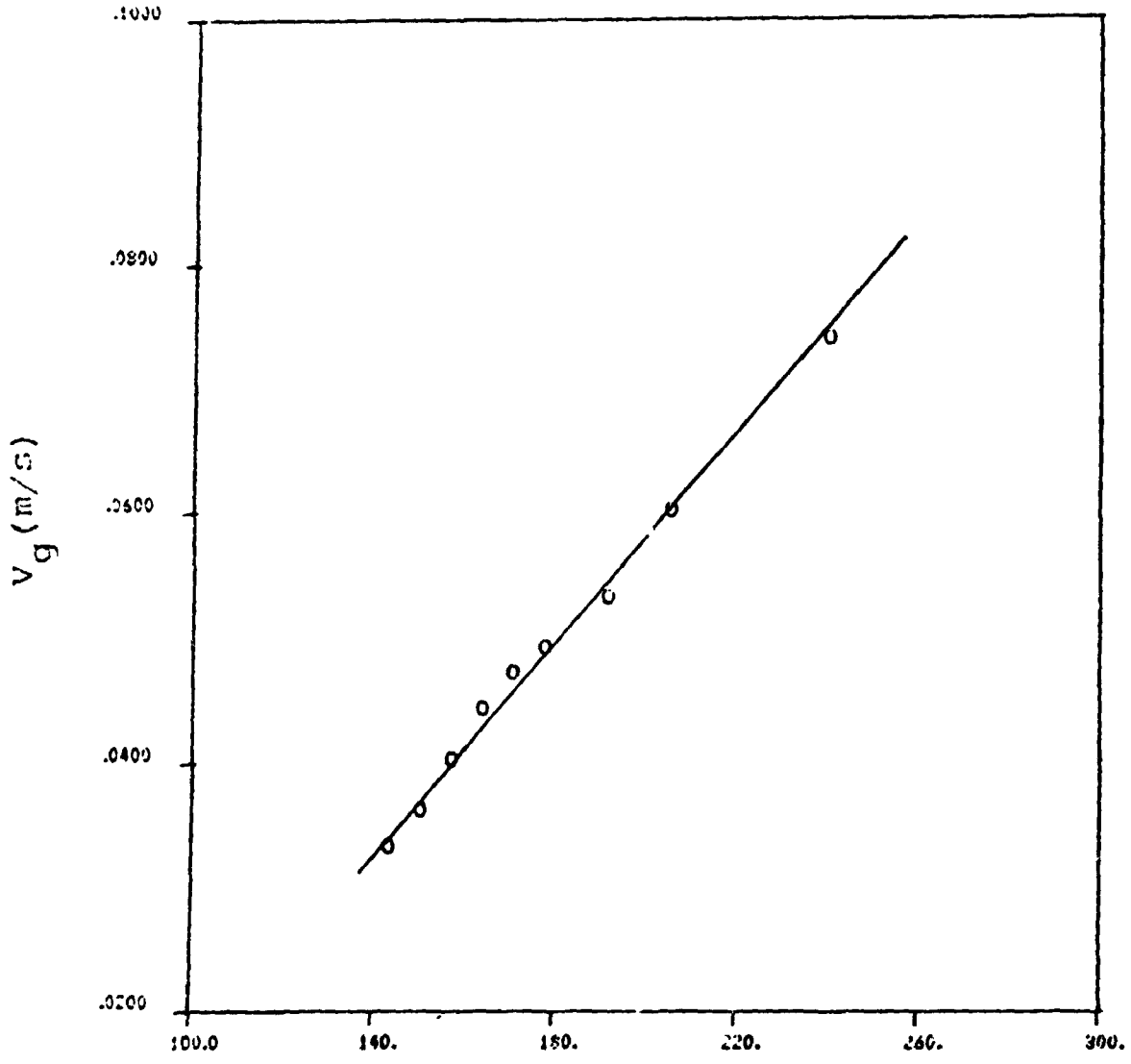

Figure 1.1 Calibration curve for nozzle # 1

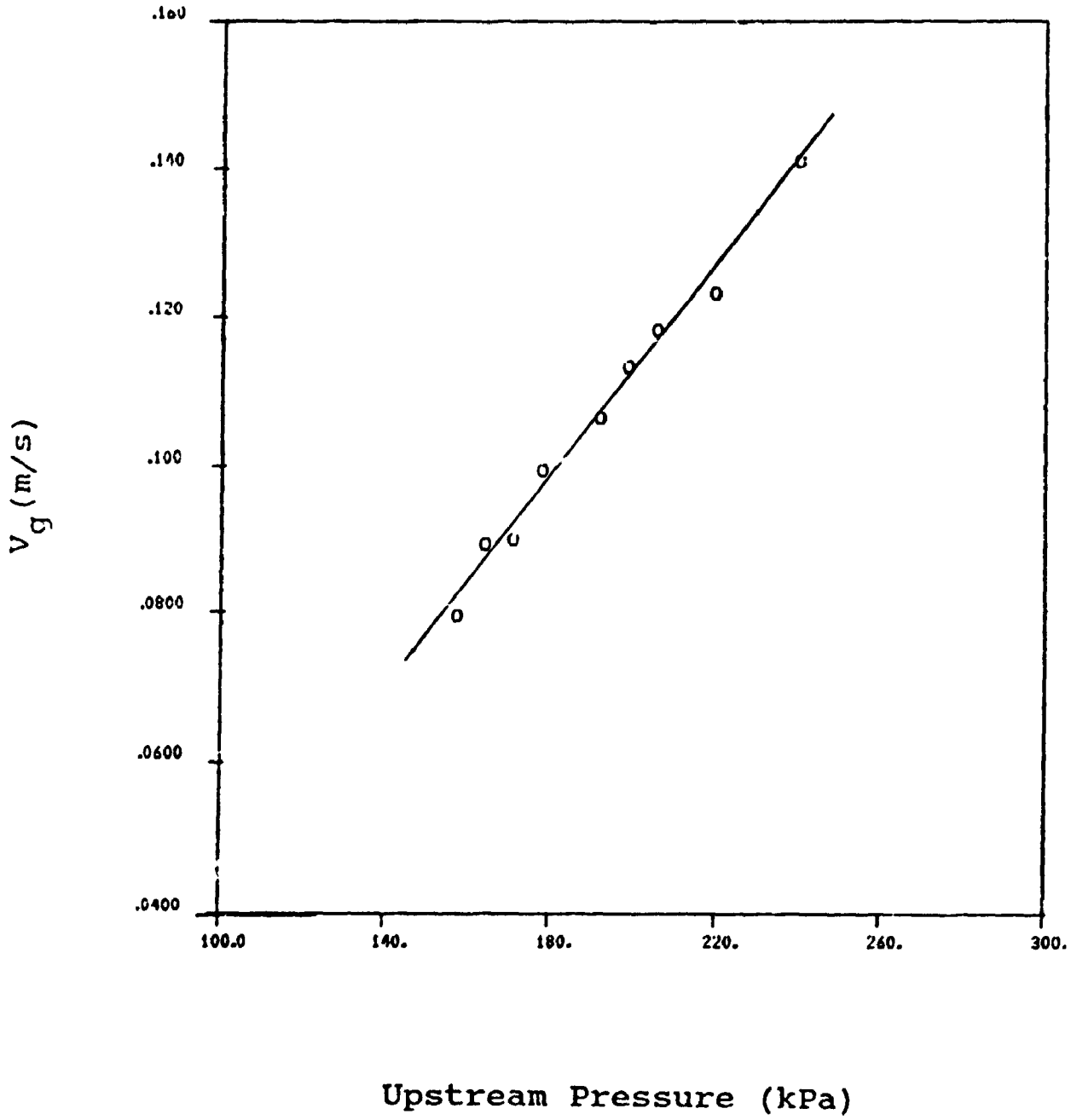

Figure 1.2 Calibration curve for nozzle # 2

Appendix-2

Tests conducted to investigate, the effects of capillary restrictions on pressure measurements along the column.

Gas holdups were obtained from pressure measurements made along the column with and without capillary restrictions. Without restrictions a total of seventeen photographs of manometers were taken in the batch bubble column at a superficial gas velocity of 0.09 m/s. These results were then compared with the gas holdup obtained from average dispersion height. In order to obtain a good average value for the dispersion height, the interface level was fast filmed for about three minutes. The average dispersion height was obtained from sixteen values.

Distributor: SP1; Gas velocity: 0.091 m/s

1) Gas holdup obtained with capillary restrictions:

$\epsilon_g = 0.145$

Standard deviation = 0.0012

2) Gas holdup based on interface level measurements:

$\epsilon_g = 0.144$

Standard deviation = 0.00147

3) Gas holdup obtained without capillary restrictions:

$\epsilon_g = 0.155$

Standard deviation = 0.0053

Appendix-3

Calibration of elbowmeter used for liquid flow measurements in continuous bubble column and small diameter three-phase fluidized bed.

When a fluid flows along a curved channel, it is subjected to angular acceleration and the basic relation between acceleration, force and mass applies. The force in this case is evidenced by the difference between the pressures observed at the outside and inside of the curve. An elbowmeter is a simple form of centrifugal meter with pressure taps in the outer and inner surfaces in the plane determined by the curved centre line of the elbow. An elbow flowmeter was used to measure the flow of liquid for continuous bubble column and small diameter three-phase fluidized bed.

This flowmeter was calibrated by measuring the volume of water collected in a given period of time. The corresponding superficial velocity in the column was obtained by dividing the volumetric flowrate by the cross-sectional area of the column. The calibration curve is shown in Figure 3.1.

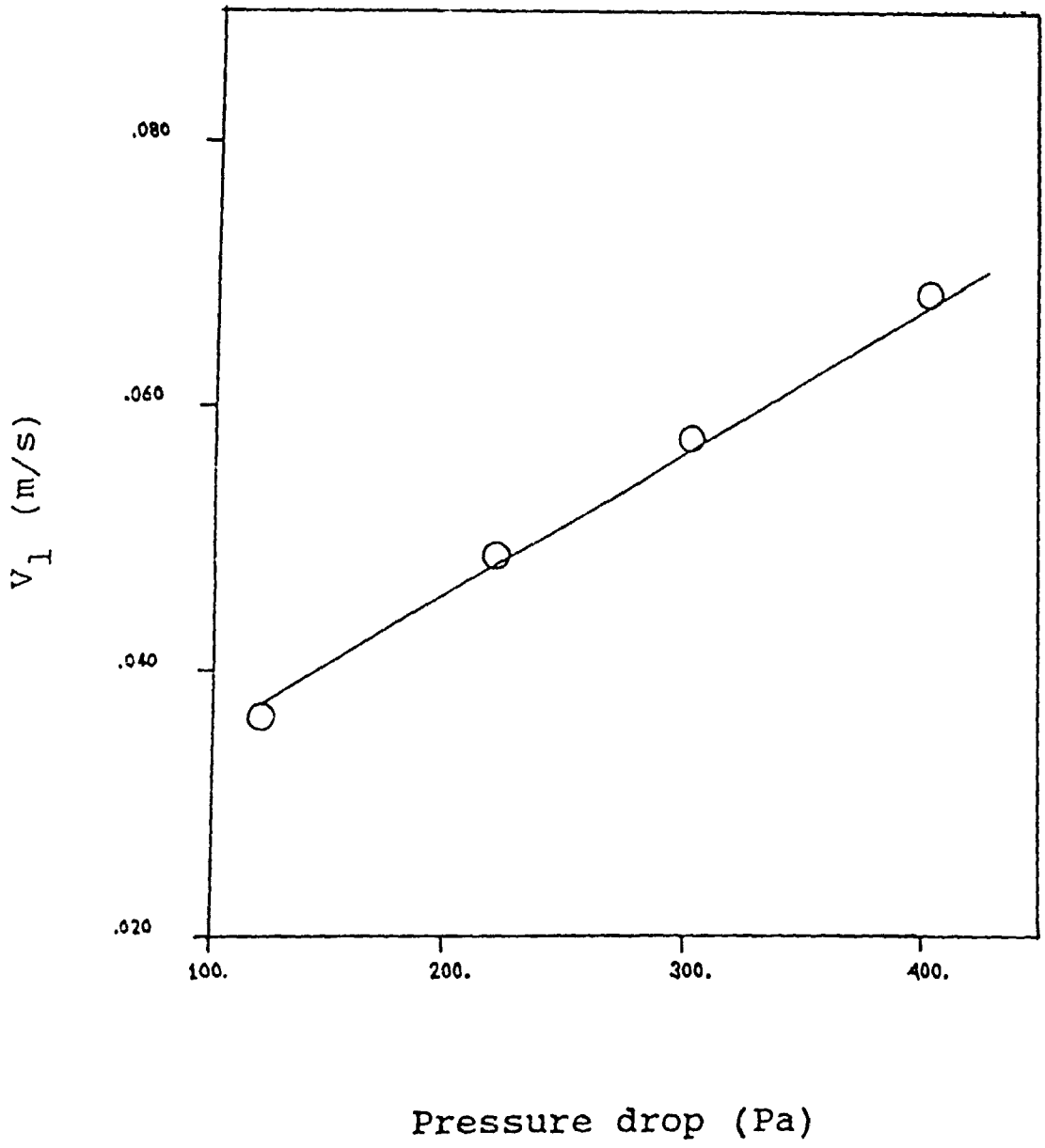

Figure 3.1 Calibration curve for liquid flow elbowmeter

Appendix-4

Calibration of the rotameter used to monitor gas flowrate for continuous bubble column and small diameter three-phase fluidized bed.

This rotameter was calibrated using a wet test meter connected at column outlet. The volumetric flowrate measured by the wet test meter was divided by the column cross-sectional area to obtain the superficial gas velocity through the column. The back pressure at rotameter outlet was maintained at 135.79 kPa for all flowrates. The calibration curve is given in Figure 4.1.

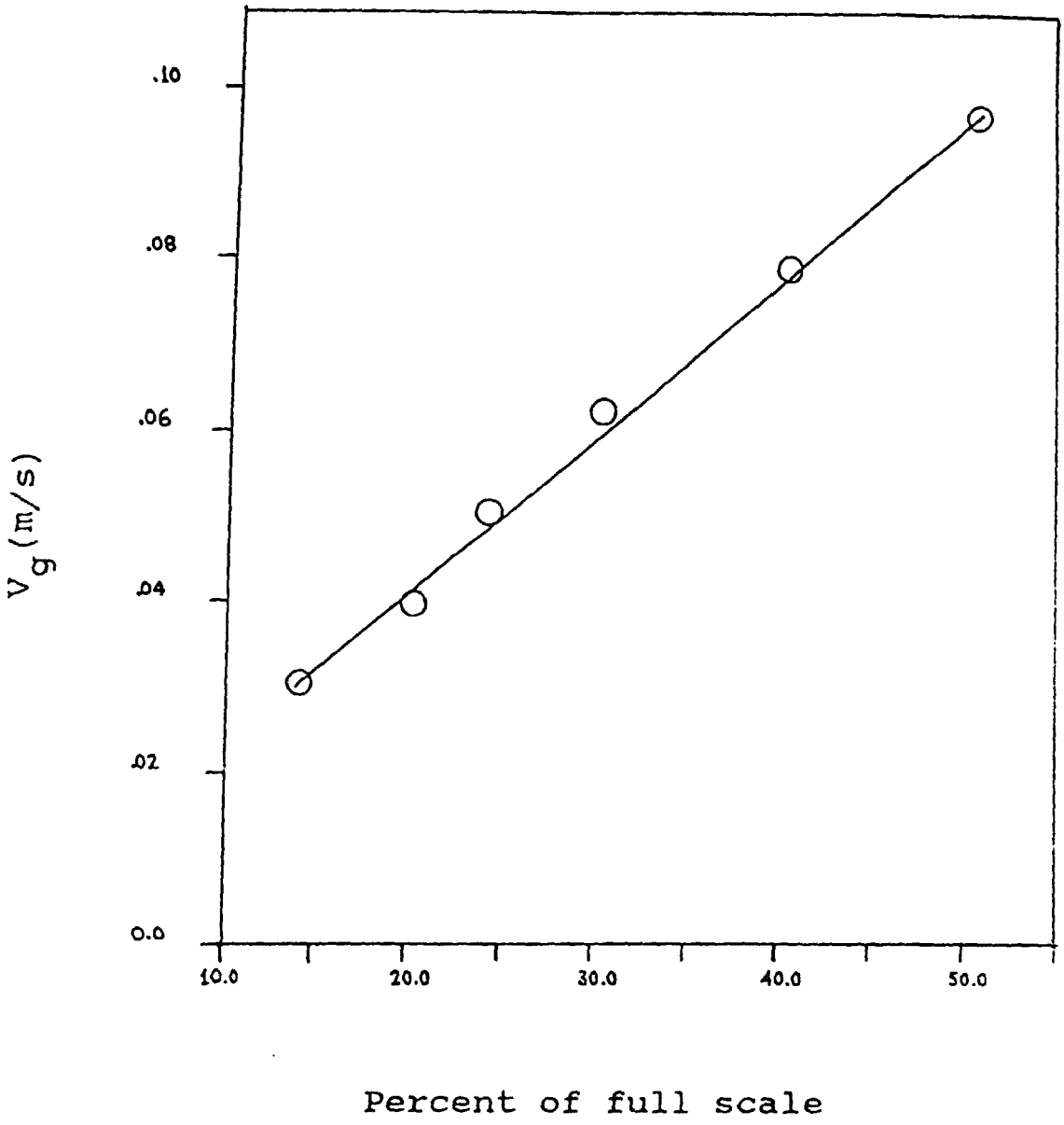

Figure 4.1 Calibration curve for the gas rotameter used with small diameter column

Appendix-5

Pressure gradient along the column as obtained from inclined manometers readings.

Notations:

h_1, h_2	vertical distance from liquid level in the manometer to the column bottom when there was no gas flow (m)
h'_1, h'_2	vertical distance from liquid level in manometers to the column bottom with gas bubbling through the liquid (m).
H_1, H_2	liquid heights in the column (m)
P_1, P_2	pressures in column at levels z_1 and z_2 from column bottom (Pa)
$\Delta P/\Delta z$	pressure gradient along column height (Pa/m)
y_1, y_2	inclined manometers readings with liquid alone (m)
y'_1, y'_2	inclined manometers readings with gas bubbling through liquid (m)
y_{z1}, y_{z2}	distances from column bottom to the inclined manometers scale (m)
z_1, z_2	vertical distances from column bottom to pressure taps of the two manometers (m)

Greek Letters

α	angle of inclination of the manometers (degrees)

ρ_1 liquid density (kg/m^3)

Angle of Inclination (α)

The angle of inclination (α) of the manometers was obtained by the following procedure:

Water was filled in column upto a height h_1. If y_1 is the manometer reading and y_{z1} is the distance from the horizontal line (through column bottom) to the zero of the manometers scale (Figure 5.1) then

$$\text{Sin } \alpha = \frac{h_1}{y_1+y_{z1}} \qquad \text{.....(1)}$$

or

$$h_1 = (y_1+y_{z1})\text{Sin}\alpha \qquad \text{.....(2)}$$

Next the water level in the column was raised to a height h_2. The level in the manometer tube rises to y_{12}, then:

$$h_2 = (y_{12}+y_{z1})\text{Sin}\alpha \qquad \text{.....(3)}$$

From Equations 2 and 3

$$h_2-h_1 = (y_{12}-y_1)\text{Sin}\alpha \qquad \text{.....(4)}$$

Calculation of pressure gradient using inclined manometers:

Figure 5.3 shows the water level in two inclined manometers with gas bubbling through the liquid in the column.

$$h'_1 = (y_{z1}+y'_1)\text{Sin}\alpha \qquad \text{.....(5)}$$

$$h'_2 = (y_{z2}+y'_2)\sin\alpha \quad \text{.....(6)}$$

From Equations 5 and 6

$$h'_1-h'_2 = (y_{z1}-y_{z2}+y'_1-y'_2)\sin\alpha \quad \text{.....(7)}$$

Since the values of y_{z1} and y_{z2} are not known accurately enough, the two manometers were first calibrated with water alone (see Figure 5.2). For liquid level h_1 in the column:

$$\frac{h_1}{y_1+y_{z1}} = \sin\alpha \quad \text{.....(7)}$$

$$\frac{h_1}{y_2+y_{z2}} = \sin\alpha \quad \text{.....(8)}$$

From Equations 7 and 8

$$y_1 - y_2 = y_{z2}-y_{z1} \quad \text{.....(9)}$$

From Equations 6 and 9

$$h'_1-h'_2 = (y_2-y_1+y'_1-y'_2)\sin\alpha \quad \text{.....(10)}$$

Converting manometer readings to pressure at levels z_1 and z_2 (Figure 5.3):

$$P_1 = \rho_1 g(h'_1-z_1) \quad \text{.....(11)}$$

$$P_2 = \rho_1 g(h'_2-z_2) \quad \text{.....(12)}$$

From Equations 11 and 12

$$p_1-p_2 = \rho_1 g(h'_1-h'_2-z_1+z_2) \quad \text{.....(13)}$$

or

$$\frac{p_1-p_2}{z_2-z_1} = \rho_1\left(\frac{h'_1-h'_2}{z_2-z_1} + 1\right) \quad \text{.....(14)}$$

or

$$\frac{\Delta p}{\Delta z} = \rho_1 g\left(\frac{\Delta h}{\Delta z} + 1\right) \qquad \text{.....(15)}$$

From Equations 14 and 15

$$\frac{\Delta h}{\Delta z} = \frac{1}{z_2 - z_1}(y'_1 - y_1 + y_2 - y'_2)\sin\alpha \qquad \text{.....(16)}$$

For vertical manometers

$$\frac{\Delta h}{\Delta z} = \frac{(y'_1 - y'_2)}{(z_2 - z_1)} \qquad \text{.....(17)}$$

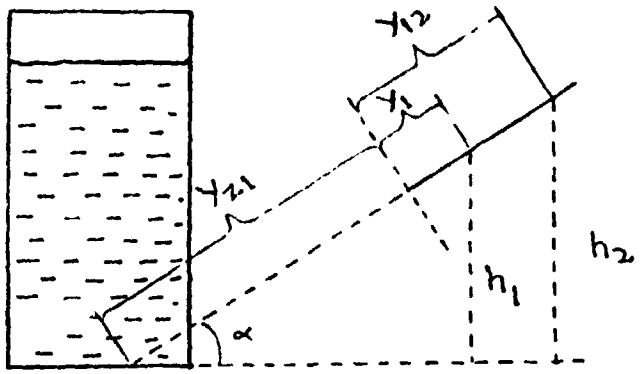

Figure 5.1

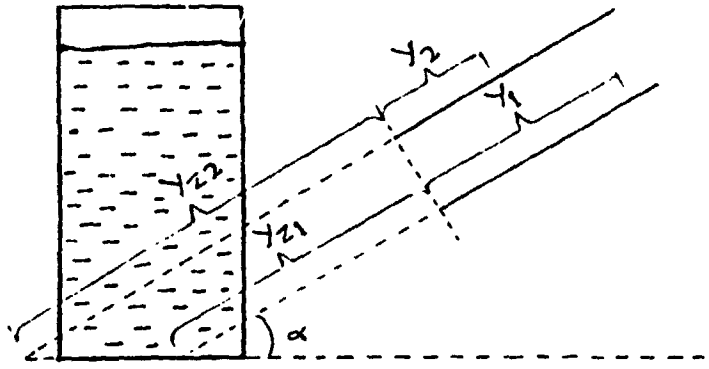

Figure 5.2

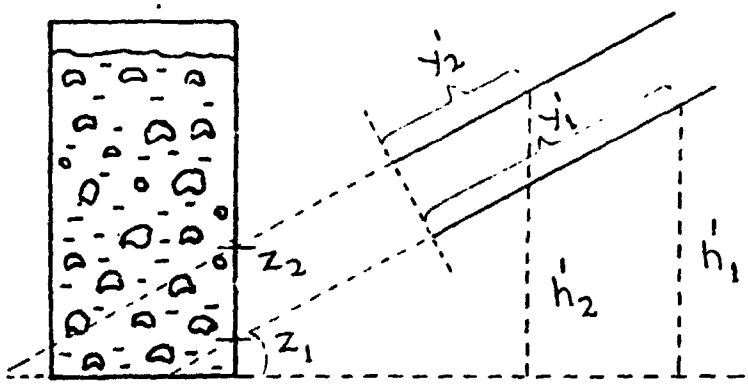

Figure 5.3

Appendix-6

Oxygen concentration in liquid samples collected from different heights of batch bubble column

The liquid backmixing effects in the batch bubble column were investigated by measuring the oxygen concentration in the liquid collected from three different levels in the column at the end of gas sparging. The liquid samples were collected using the pressure taps (0.15 m, 0.35m and 0.55m from top of liquid). In order to minimize liquid mixing during sampling, the samples were collected top down. As shown below there was no significant difference in the concentration of oxygen between different samples.

Distributor: PR2; Gas velocity: 0.045 m/s

Range of oxygen concentration: 2.98 to 3.0 ppm

Average oxygen concentration: 2.99

Percent variation: less than 0.5%

Distributor: SP1; Gas velocity: 0.064 m/s

Oxygen concentration at all levels: 3.8 ppm

Appendix-7

Calibration of spectrophotometer (UV/VIS) used to measure tracer (methylene blue) concentration in liquid phase.

Spectrophotometer model: PU 8600

Wave length used: 655 nm

The spectrophotometer was calibrated using dilute solutions (1 to 5 ppm) of methylene blue in water. The dilute solutions of methylene blue in water were prepared by serial dilutions.The calibration curve was obtained by plotting sample concentration (ppm) against the absorption (Figure 7.1).

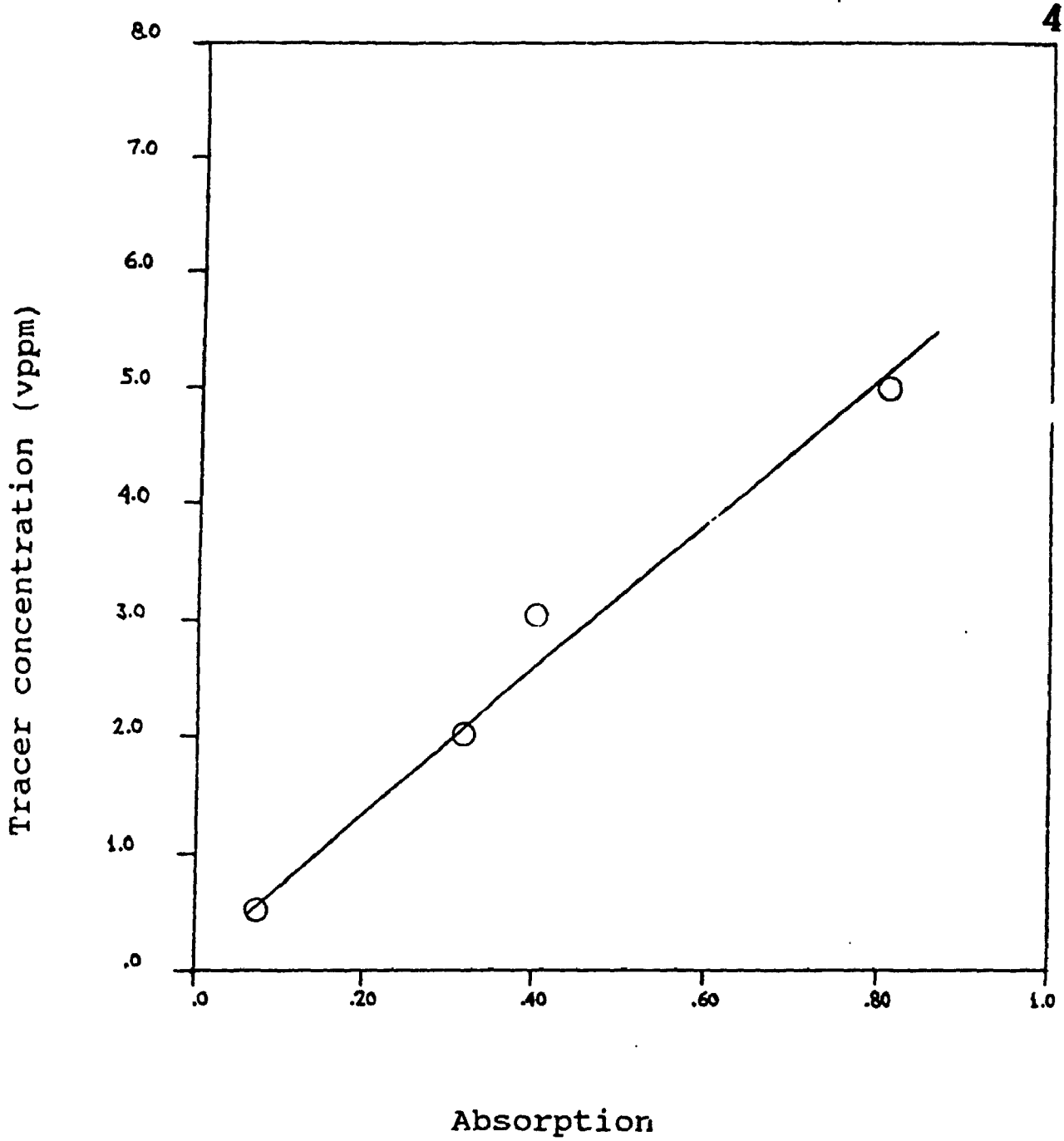

Figure 7.1 Calibration of UV/VIS spectrophotometer

Appendix-7A

Effects of radial position of tracer injection on axial dispersion coefficient.

The mixing patterns in a bubble column can vary along the column cross-section due to wall effects and/or changes in bubble concentrations. If a tracer is injected at different radial positions along the column cross-section then the measured values of axial dispersion coefficient would vary depending on the local mixing patterns. For one set of conditions, axial dispersion measurements were made by injecting tracer at five different radial positions. As shown below, there was about 11 % variation among measured values which indicated that there was good radial mixing in the column.

Liquid: Tap water

Dist.: PR2; V_l = 0.037 m/s; V_g = 0.078 m/s

Average axial dispersion coefficient= 0.0116 m^2/s

Standard deviation = 0.00126 or 11.0 %

Table 7.1 Measured Values of Axial Dispersion Coefficient for Different Radial Positions

Radial Position (r/R)	D_z (m^2/s)
0.0	0.01
0.25	0.012
0.5	0.0138
0.87	0.0114
1.0	0.11

Appendix-8

Effects of oxygen pressure buildup on gas flowrate and mass transfer rate in the batch bubble column.

Notations : As defined in main text

Effect on molar flowrate of gas:

The change in molar flowrate of the gas during a mass transfer run was calculated for the case of high mass transfer conditions:

Dist.: PR2; Liquid: 100 ppm MIBK solution

V_g = 0.065 m/s; C_{o1} = 0.00898 kg/m^3;

k_1a = 0.11 s^{-1}

Volumetric flowrate of gas = 0.0003216 m^3/s

Molar flowrate of gas = 0.01338 mole/s

The dissolved oxygen concentration at any time can be calculated using the following formula:

$$C_{o2} = C_{o1} \exp[-(tk_1a)/(1-\epsilon_g)] \quad .....(1)$$

Amount of oxygen desorbed from 0.004 m^3 liquid solution during one second:

= 0.004(0.00898 - 0.00773)

= 0.000005 kg or 0.000156 mole

Change in molar flowrate of gas = 1.17 %

Calculations for the 'j' variable

The variable 'j' was defined as:

$$j = \frac{k_l a H_{eo} R T H_L}{(1-\epsilon_g) V_g} \qquad \text{.....(2)}$$

Here the calculations were performed for the following run conditions of highest mass transfer:

Distributor: PR2

Gas velocity : 0.065 m/s (at column top)

Liquid Phase: 50 vppm solution of MIBK

Following values were used for the different variables in Equation 2:

H_{eo} = 7.3X10^4 Pa.m^3/mol

H_L = 0.65 m

$k_l a$ = 0.11 s^{-1}

R = 8.31 Pa.m^3/mol^{o}K

T = 293^{o}K

ϵ_g = 0.23

Substituting the values in Equation 2

j = 0.048

Calculations of value in the bracket of equation 3.1.13 and 3.1.19

Gas plug flow:

$$\left(\frac{j}{1-\exp(-j)}\right) = 1.03$$

Perfect mixing in gas phase:

$$\left(1 + J\frac{P_{T,avg}}{P_{T,out}}\right) = 1.049$$

It can be seen that for the gas plug flow case, the maximum contribution from the term in bracket was less than 3 % while for the case of perfect mixing in the gas phase, the maximum contribution could be about 5 %.

It may be pointed out that the assumption of perfect mixing in the gas phase is not fully justifiable for the conditions of high mass transfer rates. High mass transfer rates were obtained when there was little bubble coalescence in the bulk region (i.e. homogeneous flow regime with porous distributors and/or in solutions of effective additives) and gas plug flow conditions prevailed. It may, therefore, be concluded that the effect of neglecting gas phase mixing on volumetric mass transfer coefficient was less than 3 %.

Appendix-9

Effects of startup and shutoff of gas sparging on gas-liquid mass transfer measurements in batch bubble column.

The procedure used for the gas-liquid mass transfer measurements in the batch bubble column involved starting the gas flowrate and switching off at the end of the run. When the gas was switched on the gas bubbles did not get distributed over the entire liquid height immediately. Also when the gas was switched off, the bubbles continued to disengage from the gas-liquid dispersion until all the bubbles escaped. These two end effects largely cancelled each other; the time required for the bubbles to get distributed over the entire height was approximately equal to the time taken by the bubbles to disengage at the end of the run. Any residual errors due to these end effects could be minimized by optimizing the sparging time. The lower limit for the sparging time was set by the time required by the gas bubbles to get well distributed into the liquid. This varied from 3 to 5 seconds. The upper limit for sparging time was set by the final dissolved oxygen concentration; dissolved oxygen concentration lower than about 0.3 ppm could not be read accurately by the meter. Based on these limits the sparging time was always maintained between 10 and 35 seconds.

Error estimation on k_1a:

Linear regression analysis was carried out for two sets of data (from two runs) to estimate errors on measured values of k_1a for different sparging times.

Run 'A'

Liquid: 200 ppm MIBK solution

Dist.: PR2; V_g = 0.065 m/s

Run 'B'

Liquid: Tap water

Dist.: SP1; V_g = 0.065 m/s

Figure 9.1 is a plot of $\ln(C_{01}/C_{02})$ vs. sparging time for run 'A'. The errors due to end effects are expected to be high in such a system due to the formation of large number of bubbles which take longer to disengage.

Linear regression equation for the data of run A (Figure 9.1)

$$y = 0.122\ x + 0.08$$

Table 9.1 shows the errors estimated by comparing experimental values of $\ln(C_{02}/C_{01})/t$ with the regression value.

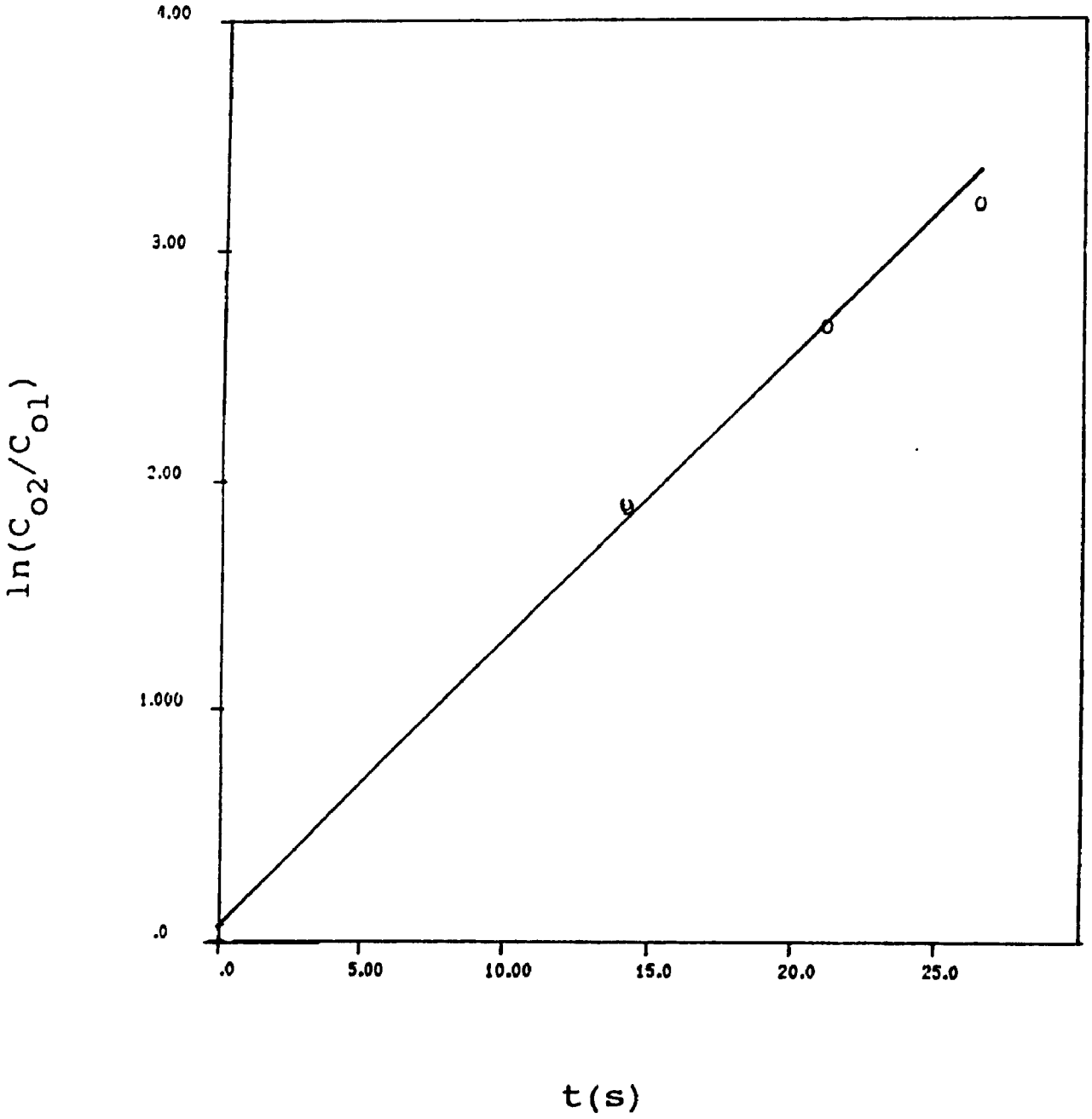

Figure 9.1 Effects of different sparging times on k_1a (200 vppm MIBK soln.; V_1 =0.0; V_g = 0.067 m/s; Dist.: PR2)

Table 9.1 Estimated errors for different sparging times (run A)

t (s)	Error (%)
14.0	9.6
14.1	8.3
21.0	3.2
26.3	-0.62

It can be seen from Table 9.1 that the estimated error due to end effects, in additive solutions, is expected to be less than 3 % for sparging times between 21.0 to 26.0 seconds.

Regression equation for the data of run B:

$$y = 0.049\ x - 0.05$$

Table 9.2 shows the errors estimated by comparing experimental values of $\ln (C_{02}/C_{01})/t$ wit the regression value.

Table 9.2 Estimated errors for different sparging times for run B

t (s)	Error (%)
14.1	-3.1
20.14	-2.0
20.14	-4.2
31.9	-2.0
31.9	1.0

It can be seen from Table 9.2 that experimental errors due to end effects are about 3 % for sparging times between 14.0 to 20.0 seconds.

Appendix-10

Comparison of $k_l a$ values obtained with absorption of oxygen in the liquid with the one obtained with desorption of oxygen in the liquid.

Notations:

C_{o1} initial concentration of oxygen in the liquid (mole/m3)

C_{o2} final concentration of oxygen in the liquid (mole/m3)

$k_l a$ volumetric mass transfer coefficient (s^{-1})

t sparging time (s)

ϵ_g gas phase holdup

Batch Bubble Column:

Column ID: 0.08 m; Sparger: SP1; V_g = 0.06 m/s

Run with absorption of oxygen:

$$k_l a = -\frac{1-\epsilon_g}{t} \ln \frac{C_o^* - C_{o1}}{C_o^* - C_{o2}}$$

$$= -\frac{0.89}{15} \ln \frac{8.81-5.85}{8.81-2.36}$$

$$= -\frac{0.89}{15} \ln \frac{2.96}{6.45}$$

$$= 0.046\ s^{-1}$$

Run with desorption of oxygen:

$$k_l a = - \frac{1-\epsilon_g}{t} \ln \frac{C_{o2}}{C_{o1}}$$

$$= - \frac{0.89}{14.1} \ln \frac{4.2}{8.9}$$

$$= 0.047 \ s^{-1}$$

Appendix-11

Effects of day to day variations in the quality of tap water and air on gas-liquid mass transfer measurements.

Measurements were made in the batch bubble column to study the effects of day to day variations in experimental conditions such as quality of tap water and air, and possible contaminants from plastic tubings and column material. These measurements were made over a period of several weeks. Fresh water was taken into the column for every run. The measurements were made after air had been sparged for about 4 to 5 minutes. As shown below, the variation of volumetric mass transfer coefficient was witin 5 %.

Number of measurements: 10

Conditions of measurement:

Liquid: Tap water

Sparger: SP1; Gas Velocity: 0.065 m/s

Average value of $k_l a = 0.042\ s^{-1}$

Standard deviation = 0.002 Or 4.7 %

Table 11.1 Values of volumetric mass transfer coefficient measured over a period of several months (Batch bubble column; tap water; V_g = 0.065 m/s)

No.	$k_l a$ (s^{-1})
1	0.04
2	0.042
3	0.045
4	0.042
5	0.0415
6	0.042
7	0.045
8	0.041
9	0.040
10	0.046

Appendix-12

Effect of oxygen pressure buildup on gas-liquid mass transfer rate

In the following analysis the gas-liquid mass transfer equations were derived taking into account the oxygen pressure buildup in the nitrogen gas stream. The mass transfer coefficients obtained with this procedure were then compared with the values obtained by neglecting the effect of oxygen pressure buildup. The plug flow model was assumed for both gas and liquid phases. This assumption is expected to show the maximum effect of the oxygen pressure buildup on the mass transfer rate.

Notations : As in the main text

Oxygen mass balance for the liquid phase:

$$A_c V_l dC_o = k_l a(C_o^* - C_o)dzA_c \qquad \text{.....(1)}$$

Oxygen balance for gas phase:

$$\frac{V_g}{RT}\frac{dp}{dz} = k_l a(C_o - H_{eo}p_o) \qquad \text{.....(2)}$$

or

$$p_o = \frac{C_o}{H_{eo}}[1 - \exp(-Kz)] \qquad \text{.....(3)}$$

where $K = k_l a H_{eo} RT/V_g$

From Henery's law $C_o^* = H_{eo}p_o$ .....(4)

Substituting Equations 3 and 4 in Equation 1

$$V_l dC_o = k_l a[C_o \exp(-Kz)]dz \qquad \ldots\ldots\ldots\ldots(5)$$

Integrating Equation 5 between inlet (C_{o1}) and outlet (C_{o2}) concentrations and rearranging gives:

$$k_l a = \frac{V_g}{H_{eo} RTz} \ln\left[1 - \ln\frac{C_{o2}}{C_{o1}} \frac{V_l H_{eo} RT}{V_g}\right] \qquad \ldots.(6)$$

If oxygen pressure buildup is neglected then Equation 6 reduces to;

$$k_l a = \ln\frac{C_{o1}}{C_{o2}} \frac{V_l}{z} \qquad \ldots\ldots\ldots\ldots(7)$$

Continuous bubble column:

$k_l a$ values were calculated using Equations 6 and 7

Dist.: SP1; Liquid : 30 vppm iso-amyl alcohol solution.

$V_l = 0.048$ m/s $\qquad V_g = 0.062$ m/s

$C_{o1} = 0.00938$ kg/m^3 $\qquad C_{o2} = 0.0049$ kg/m^3

$k_l a$ (Equation 6) = 0.057 s^{-1}

$k_l a$ (Equation 7) = 0.056 s^{-1}

It can be seen that the two values are within 2% of each other.

Three-phase fluidized bed:

Dist.: SP1; Liquid: 30 vppm iso-amyl alcohol soln.

V_l = 0.057 m/s; V_g = 0.062 m/s

C_{o1} = 0.00963 kg/m^3; C_{o2} = 0.00582 kg/m^3

$k_l a$ (Equation 6) = 0.12 s^{-1}

$k_l a$ (Equation 7) = 0.123 s^{-1}

The two values are within 3%.

Appendix-13

Selection of a suitable chemical system for interfacial area measurements.

The chemical methods used for the interfacial area measurement require the presence of dissolved salts in the liquid phase. These salts can significantly alter the coalescence behavior of the liquid. Since the objective of this study was to investigate the effects of coalescence inhibitors on the mass transfer coefficient and the interfacial area for mass transfer, it was important to use a method which allowed these measurements to be made without significantly altering the coalescence behavior of the liquid.

One simple way to detect a change in the coalescence behavior of the liquid is by gas holdup measurements. As pointed out in section 2.2.6.1.1, the sulfite oxidation method is a commonly used chemical method for interfacial area measurements. The gas holdups in the sodium sulfite solutions were, however, found to be about 20% higher than that of tap water. It showed the strong coalescence inhibition effects of these solutions. Another chemical method uses absorption of Carbon dioxide in aqueous KOH or NaOH solutions. As shown below, the gas holdups in KOH solutions were not significantly different from those of tap water. This method was therefore selected for the interfacial area measurements in this study.

Distributor : SP1 ; V_g = 0.06 m/s

Liquid Phase	ϵ_g(salt solution)/ϵ_g(tap water)
Na_2SO_3 solution (30 moles/m3)	1.2
KOH solution (25 moles/m^3)	1.02

Appendix-14

Titration procedure used to determine carbonate ion concentration in the liquid.

The moles of carbon dioxide absorbed during an interfacial area measurement run were obtained from the concentrations of cabonate ions in the liquid before and after gas sparging. The carbonate ion concentration in the liquid samples was determined by titrating a 20 cc sample of the solution with 0.01 N HCl solution. A titration curve for the reaction of carbonate ion with acid is characterized by two end points. As the PH of the solution drops, the following reaction occurs first:

$$CO_3^{2-} + H^+ - HCO_3^- \quad \text{.....(1)}$$

This reaction essentially goes to completion at PH of about 8.5. This end point can be determined with the help of phenolphathalein indicator. As the PH of the solution drops further the following reaction essentially goes to completion below PH of about 4.

$$HCO_3^- + H^+ - H_2CO_3 \quad \text{.....(2)}$$

Figure 14.1 shows two titration curves obtained for a run with MIBK solution. The carbonate ion concentration was determined using the first end point.

Calculations for change in carbonate ion concentration due to gas (CO_2/N_2 mixture) sparging (Figure 14.1):

Volume of HCl solution required before sparging = 30.0 cc

Volume of HCl solution required after sparging = 24.0 cc

Change in carbonate ion concentration = 3 mol/m^3

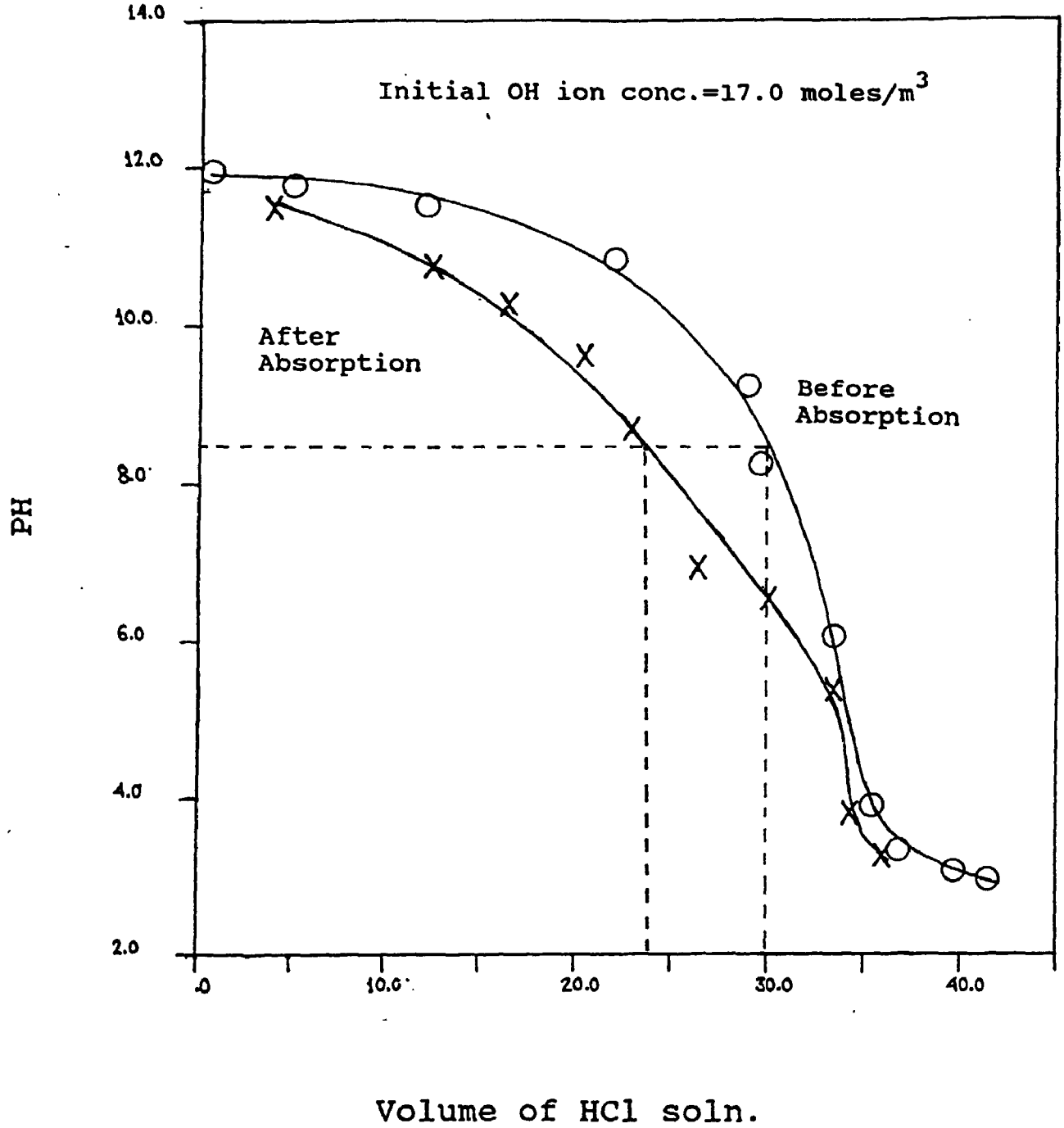

Figure 14.1 Plot of PH vs volume of HCl solution (0.01N) added (30 vppm MIBK soln.; V_g=0.06 m/s; Dist.: SP1)

Appendix-15

Selection of run conditions to minimize errors for interfacial area measurements.

Notations:

E_1 percent error in interfacial area measurement due to assumption of single bubble class

E_2 percent error in interfacial area measurement attributable to carbonate ion concentration measurement

E_{n1} enhancement factor for mass transfer with chemical reaction for bubbles in class 1

E_{n2} enhancement factor for mass transfer with chemical reaction for bubbles in class 2

F_{c1} absorption rate for carbon dioxide from bubbles in class 1 (moles/m3.s)

E_T total error in interfacial area measurement; sum of errors E_1 and E_2

F_{c2} absorption rate for carbon dioxide from bubbles in class 2 (moles/m3.s)

$(k_1a_1)_c$ volumetric mass transfer coefficient for carbon dioxide; bubbles in class 1 (s-1)

$(k_1a_2)_c$ volumetric mass transfer coefficient for carbon dioxide ; bubbles in class 2 (s-1)

N_{g1} molar flow rate of gas through class 1 bubbles (moles/s)

N_{g2} molar flow rate of gas through class 2 bubbles (moles/s)

V_{g1} gas velocity through class 1 bubbles (m/s)

V_{g2} gas velocity through class 2 bubbles (m/s)

y_{c1} mole fraction of carbon dioxide in class 1 bubbles

y_{c2} mole fraction of carbon dioxide in class 2 bubbles

$y_{c1,in}$ mole fraction of carbon dioxide in the inlet gas in class 1 bubbles

$y_{c1,out}$ mole fraction of carbon dioxide in the outlet gas

in class 1 bubbles

$y_{c2,in}$ mole fraction of carbon dioxide in the inlet gas in class 2 bubbles

$y_{c2,out}$ mole fraction of carbon dioxide in the outlet gas in class 2 bubbles

Rest of notations, as in the main text

The chemical method used for the measurement of interfacial area could result in significant errors if run conditions were not selected properly. The main sources of errors are::

1) Lower values of interfacial area can be estimated due to assumption of single bubble class. The bubbles of different sizes undergo different extents of conversions in the dispersion. At higher conversions there is highly nonlinear relationship between extent of conversion and interfacial area. This can lead to significantly lower estimates of interfacial areas (Schumpe and Deckwer, 1980).

2) The measurement errors for carbonate ions (CO_3^{2-}) concentration could become significant for only small changes in carbonate ion concentration.

Following steps were taken to minimize these sources of errors:

- the extent of conversion in the bubbles could be reduced by reducing the residence time of bubbles in the dispersion. This was achieved by minimizing the liquid

height . The lower limit for the dispersion height, however, is controlled by the distributor effects. At lower dispersion heights the distributor effects become important and the results are then no more representative of the phenomena in the bulk phase. The distributor effects are significant upto heights of about three times the column diameter. Accordingly the liquid height was selected to be about 0.4 m.

- The extent of conversion in the bubbles could be further reduced by lowering the initial hydroxyl concentration in the liquid. However, for lower hydroxyl concentrations the carbonate ions concentration would also be low in the solution. This would then lead to higher measurement errors for carbonate ion concentrations.

In section 3.1.5, the absorption process was modelled assuming single bubble class with uniform composition. In the following analysis, two classes of bubbles have been assumed.

Following equations can be written to evaluate the absorption of carbon dioxide, based on two bubble classes

$$dy_{c1} = \frac{P_T A_c}{H_{ec} N_{g1}} E_{n1} (k_1 a_1)_c y_{c1} dz \qquad \text{.....(15.1)}$$

$$dy_{c2} = \frac{P_T A_c}{H_{ec} N_{g2}} E_{n2} (k_1 a_2)_c y_{c2} dz \qquad \text{.....(15.2)}$$

Here the liquid side mass transfer coefficient (k_1)

is assumed to be same for the two classes of bubbles.

The number of moles of carbon dioxide absorbed per unit liquid volume, for each bubble class, during a time Δt is given as:

$$F_{c1}\Delta t = \frac{V_{g1}P_T(y_{c1,in}-y_{c1,out})}{R_g T H_L}\Delta t \quad \ldots\ldots\ldots(15.3)$$

$$F_{c2}\Delta t = \frac{V_{g2}P_T(y_{c2,in}-y_{c2,out})}{R_g T H_L}\Delta t \quad \ldots\ldots\ldots(15.4)$$

The total number of moles of carbon dioxide absorbed per unit liquid volume can be obtained by adding Equations 15.3 and 15.4. The gas velocities corresponding to the two classes of bubbles (V_{g1}, V_{g2}) were approximately determined from bubble population study (see section 3.1.6).

Two separate subroutines, based on the procedures of single bubble class and two classes of bubbles were developed to calculate the carbonate ion concentration for an assumed value of interfacial atea. For a given set of conditions (i.e. gas velocity, starting hydroxyl ions concentration, sparging time etc.) the carbonate ions concentration was obtained for an assumed value of interfacial area. For the two classes of bubbles, the interfacial area for each class of bubbles was approximately determined from bubble population study data. A curve was then generated by assuming different starting values for interfacial areas (Figure 15.1).

Initially, the above procedure was used to determine an optimum hydroxyl ion concentration to minimize errors due to assumption of single class of bubbles in the dispersion. The results of this error analysis are shown in Table 15.1

Table 15.1 Error analysis to determine optimum hydroxyl ion concentration

Hydroxyl ion conc. ($moles/m^3$)	E_1* (%)	E_2** (%)	E_T# (%)
25.0	19.6	4	23.6
20.0	12.5	4.2	16.7
15.0	3.4	4.7	8.1
12.0	4.6	5.0	9.6

* error due to assumption of single bubble class

** measurement error for carbonate ions concentration

\# total error (E_1+E_2)

Based on the results of the above analysis, an initial hydroxyl ion concentration of about 17 moles/m^3 was selected for the interfacial area measurement experiments. The error in interfacial area measurements due to the assumption of single bubble class is expected to be less than 10%.

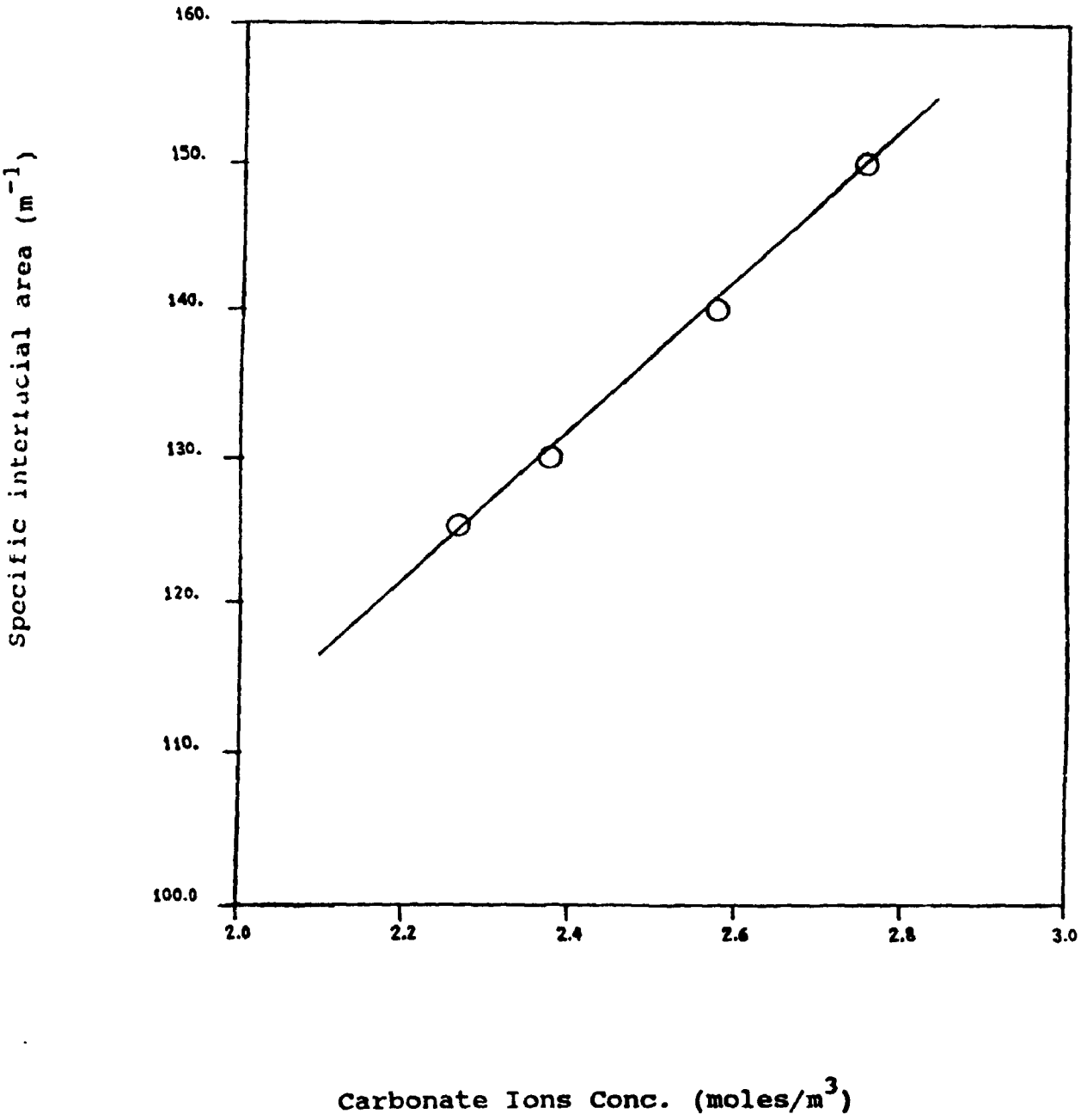

Figure 15.1 Calculated values of carbonate ions concentrations for different starting values of interfacial areas

Appendix-16

Selection of diffusivity, solubility and reaction rate constant for interfacial area measurement technique based on CO_2 absorption in KOH solutions.

Notations:

C_c^*	solubility of CO_2 in KOH solution (mol/m^3)
$C^*_{c,water}$	solubility of CO_2 in water (mol/m^3)
D_c	diffusivity of oxygen in the liquid phase (m^2/s)
D_o	diffusivity of oxygen in the liquid phase (m^2/s)
D_{oh}	diffusivity of hydroxyl ions (m^2/s)
h	a solubility factor of salt which is the sum of contribution of the species of +ve and -ve ions and the species of gas (m^3/mol)
I	ionic strength of the electrolyte solution
k_r	second order reaction rate constant ($m^3/mol.s$)
T	temperature (K)

The reaction rate constant (k_r):

The second order reaction rate constant for the dissolved carbon dioxide and the hydroxyl ions was estimated using the following formula, derived from the experimental data of Pinsent et al. (1956).

$$\log k_r = 13.635 - 2895/T \qquad \text{.....(1)}$$

Solubility of Carbon Dioxide:

The solubility of carbon dioxide in the solutions of electrolytes can estimated using the following procedure (Danckwerts, 1970).

$$\log\left(\frac{C_c^*}{C_{c,water}^*}\right) = -hI \qquad \text{.....(2)}$$

Here, h is the solubility factor of the salt which can be determined as:

$$h = h_+ + h_- + h_G \qquad \text{.....(3)}$$

$C^*_{c,water}$, the saturation concentration of carbon dioxide in water can be calculated from the following formula (Danckwerts and Sharma, 1966):

$$\text{og } C_{c,water}^* = 1140/T - 2.3 \qquad \text{....(4)}$$

Diffusivity of Oxygen:

The diffusivity of oxygen was obtained from literature (Vivian and King, 1964)

Diffusivity of hydrxyl ions:

The diffusivity of hydroxyl ion was estimated from the Nerst and Haskell equation (Reid et al., 1977)

D_{oh} at $20^oC = 2.5X10^{-9}$ m^2/s

at $25^oC = 2.9X10^{-9}$ m^2/s

Diffusivity of Carbon Dioxide:

The liquid phase diffusivity of carbon dioxide was estimated from the following formula which is based on the experimental data of Thomas and Adams (1965):

$$D_C = 2.22X10^{-9} + 0.0555X10^{-9}(T-303)$$

Appendix-17

Liquid Flowmeter Calibration

Large Column (D_C = 0.171 m)

A rotameter was used to monitor the liquid flowrate to the large column. This rotameter was calibrated by measuring the volume of water collected in a given period of time. The corresponding superficial velocity in the column was obtained by dividing the volumetric flowrate by the cross-sectional area of the column. The calibration curve is given in Figure 17.1.

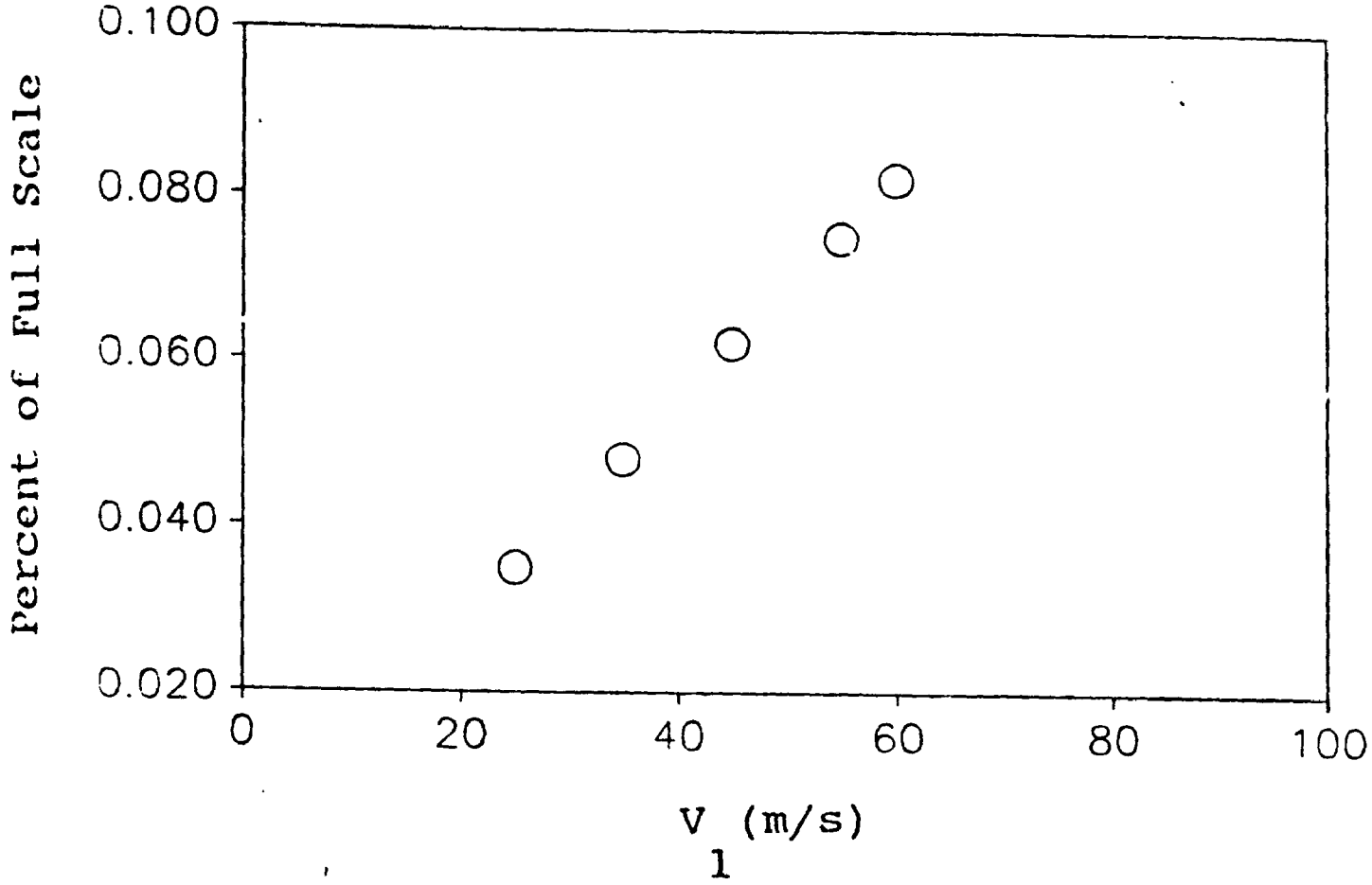

Figure 17.1 Calibration curve for liquid flowmeter used with the large diameter column

Appendix-18

Calibration of gas rotameters used with large diameter column.

Notations:

A_2 crossectional area of the orifice (m^2)

C_D orifice coefficient

F mass flowrate of gas (kg/s)

k specific heat ratio C_p/C_v

P_1 pressure upstream of orifice (Pa)

P_2 pressure downstream of orifice (Pa)

r pressure ratio P_2/P_1

Y expansion factor $= r^{2/k}\left(\frac{k}{k-1}\right)\left(\frac{1-r\left(\beta-1/k\right)}{1-r}\right)\left(\frac{1-\beta^4}{1-\beta^4 r^{2/k}}\right)$

β ratio of orifice diameter to pipe diameter

ρ_g density of air at upstream.

In the large diameter column the gas flowing through each of the four nozzles was regulated by a rotameter. These rotameters were calibrated with a sharp edged orifice plate. The calibration equipment consisted of a 1.5 m long pipe with inside diameter of 0.0381 m, used to stabilize the flow at the inlet of the orifice. The diameter of the orifice was 0.00754 m and it was followed by a 0.5 m long pipe. The pressure taps were mounted on the flange. The flowrate was computed by the following

equation.

$$F = \frac{C_D Y A_2}{1-\beta 4} 2(P_1 - P_2)\rho_g \qquad \text{.....(1)}$$

All the four rotameters were calibrated with a working pressure of 156.4 kPa at the upstream of the flowmeters. The calibration curves is shown in Figure 18.1. The superficial gas velocity was taken at the conditions at the top of the column i.e. ambient conditions.

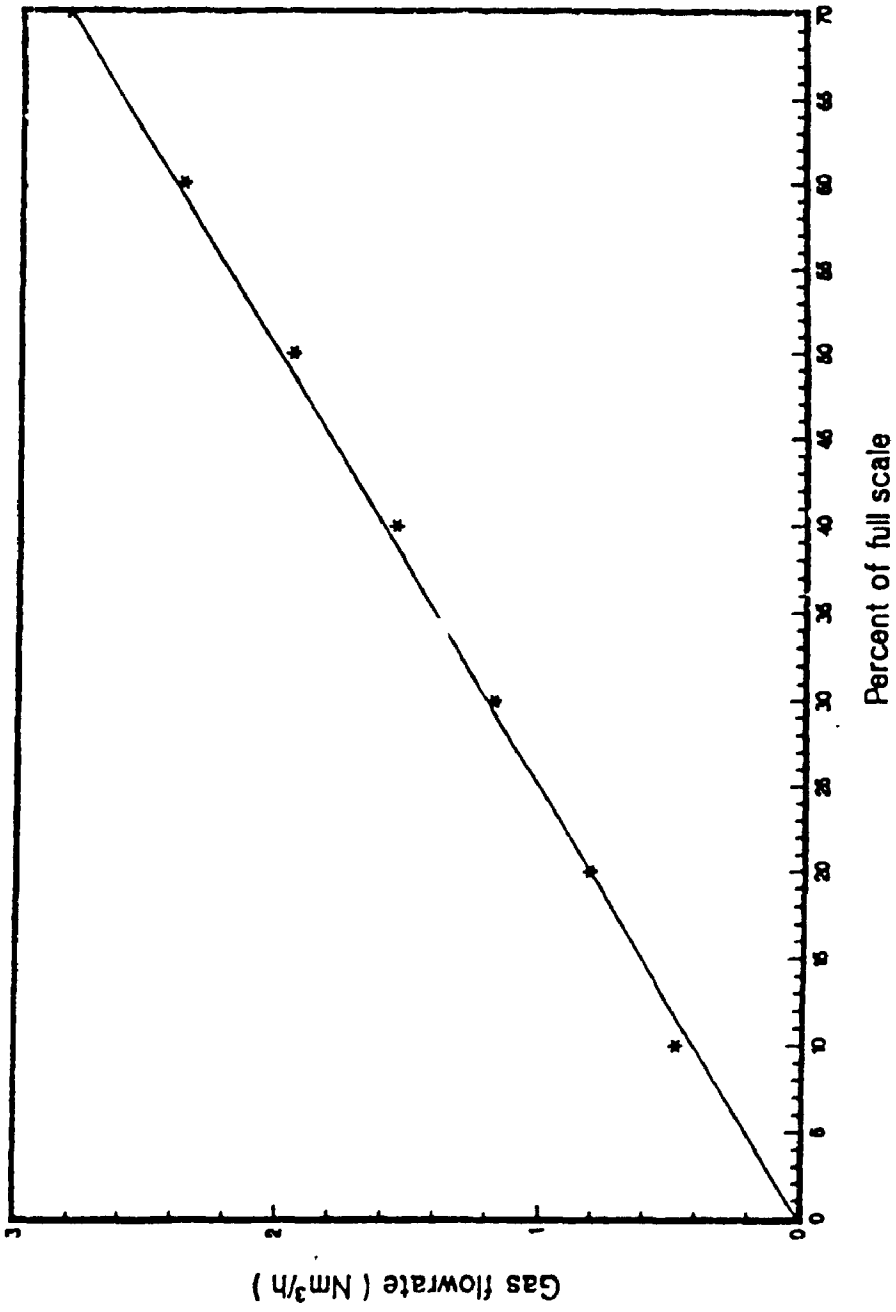

Figure 18 J Calibration curve for gas flowmeters used with the large diameter column

Preparation of coated benzoic acid particles used for particle-liquid mass transfer study in three-phase fluidized bed.

Notations:

W_p total weight of the coated particle (kg)

W_s weight of the steel/glass core (kg)

W_b weight of the benzoic acid coating (kg)

d_p diameter of the coated particle (m)

ρ_p density of the particles (kg/m^3)

Benzoic acid has a much lower density (ρ_p=1260 kg/m^3) than that of the glass particles (ρ_p=2520 kg/m^3) used in the three-phase fluidized bed. In order to avoid segregation of the active particles at the top of the fluidized bed, it was found necessary to use active particles with density close to those of the bed particles. This was achieved by coating benzoic acid on 3 mm steel spheres. The steel core was weighed first and its surface was etched for identification.

The coated particles were prepared by dipping the steel spheres in molten benzoic acid. In order to obtain uniform thickness for the coating and a proper particle diameter, it was found necessary to dip the particles three to four times. The coating was allowed to cool down and solidify between dips. The temperature of molten benzoic acid was maintained about 8 to 10°C above its

melting point (126°C). When the desired coating thickness was reached, the particle surface was polished with a very fine emery paper to smmoth out rough edges. The particle surface was then inspected through a microscope (X64) for any cracks. The particle was weighed again.

The diameter of the particle was determined by direct measurement with a micrometer (several measurements were made to obtain a good average value) and also from the volume of the particle obtained by adding the volume of the core and volume of the coating. The volume of the coating was obtained from its weight and the density of benzoic acid. The particle diameters obtained from the two procedures were always within 4% of each other.

The figure below shows a cut section of a coated particle. The string attached to the particle was a monofilament glued to the steel core. The attached string facilitated the dipping of the particle in molten benzoic acid.

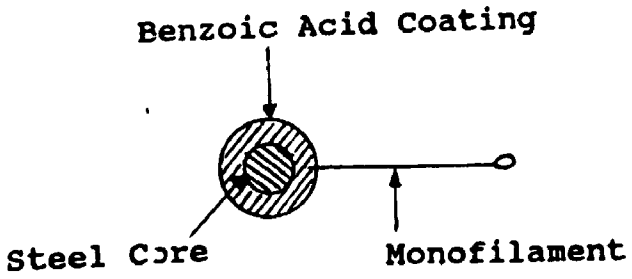

The density of the particle was estimated as below:

$$W_p = W_s + W_b$$

$$\rho_p = \frac{W_s + W_b}{\pi/6 d P V p_p^3}$$

The coated particle density thus obtained was compared with the density of the inert bed particles. Only those coated particles with a density of within 4 % of the inert particles were used for the mass transfer measurements. The string attached to the particle was cut off, after coating, for the 'Free Floating Particles' technique.

Appendix-20

Effects of variations in tap water quality on particle-liquid mass transfer.

Some measurements of particle-liquid mass transfer in three-phase fluidized beds were made to observe any effects of day-to-day variations in tap water quality. One measurement was made every month for a period of four months. As shown below, there was practically no effect of any variations of the tap water quality on the particle-liquid mass transfer rate.

Column ID : 0.17 m d_p = 5.2 mm

Liquid Phase : Tap water

V_g = 0.05 m/s ; V_l = 0.06 m/s

Total number of runs: 4

Measured values of k_{ls} (m/s):

1) 0.0078; 2) 0.0082; 3) 0.0081; 4) 0.0076

Average value = 0.00792 m/s

Maximum variation = 3.5 %

Details of the model proposed by Bowender and Kumar (1970) for the bubble formation from a porous distributor.

Assumptions of the model:

Notations:

A_1 as defined by equation 5

A_p area of the porous plate (cm^2)

B_1 as defined by equation 6

C_1 as defined by equation 7

d_o diameter of the orifice (cm)

G_1 as defined by equation 8

n_s number of effective sites

q_g flowrate through each effective site (cm^3/s)

Q_g flowrate through column (cm^3/s)

r_e radius of bubble at the end of expansion stage (cm)

V_E bubble volume at the end of expansion stage (cm3)

V_F final bubble volume (cm^3)

Greek Letters

ρ_l density of liquid (g/cm^3)

μ_l viscosity of liquid (g.cm/s)

σ surface tension of liquid (dynes/cm)

1) The porous disc was made up of an extremely large numbers of pores of uniform diameter and length having same resistance.

2) The operative sites were assumed to be equal to

the number of bubbles found simultaneously on the disc. These sites were only a fraction of the total number of potential sites. This was based on visual observations.

3) The gas flowed through effective sites only. Each effective site was considered to be a single pore with equal flow of gas.

4) Due to large resistance through the disc constant flow conditions were assumed during bubble formation.

5) The effective sites decreased with increasing flowrate.

6) The bubbles arranged themselves in close hexagonal packing so that the whole of the porous disc was covered.

7) The flow through each effective site is given as:

$$q_g = Q_g/n_s \qquad \ldots\ldots\ldots(1)$$

Since the bubbles were assumed to arrange in close hexagonal packing:

$$n_s = \frac{A_p[2.356V_F]^{-2/3}}{3.464} \qquad \ldots\ldots(2)$$

The bubbles were assumed to form under constant flow conditions on the basis of a two step mechanism (Kumar and Kuloor, 1969). According to this mechanism the final bubble volume is the sum of the volumes of the two stages of bubble formation i.e. 1) the expansion stage 2) detachement stage. During the first stage the bubble expands while its base remains attached to the tip of the orifice whereas in the detachement stage the bubble base moves away from the tip, the bubble itself being in

contact with the orifice through the neck. The equations for the two stages are given below:

First stage:

$$V_E^{5/3} = \frac{11\,Q_g^2}{192\pi(3/4\pi)2/3g} + \frac{3\mu_l Q_g V_F^{1/3}}{2(3/4\pi)1/3g\rho_l} + \frac{\pi d_o \sigma V_E^{2/3}}{\rho g} \quad \ldots\ldots\ldots(3)$$

Second Stage:

$$r_e = \frac{B_1}{2Q_g(A_1+1)}(V_F 2 - V_E 2) - \frac{C_1}{A_1 Q_g}(V_F - V_E) - \frac{3G_1}{2Q_g(A_1 - 1/3)}(V_F 2/3 - V_E 2/3) \quad \ldots\ldots\ldots(4)$$

where

$$A_1 = 1 + \frac{96\pi(1.25)r_e\mu_l}{11\,\rho_l Q_g} \quad \ldots\ldots\ldots(5)$$

$$B_1 = 16g/11Q_g \quad \ldots\ldots\ldots(6)$$

$$C_1 = \frac{16\pi d_o \sigma}{11\rho_l Q_g} \quad \ldots\ldots\ldots(7)$$

$$G_1 = \frac{24\ \ l}{11(3/4\pi)1/3\rho_l} \quad \ldots\ldots\ldots(8)$$

An iterative method was used to estimate the number of effective sites and cosequently the bubble diameter.

Appendix-22

Estimation of benzoic acid diffusivity at different temperatures.

The diffusivity of benzoic acid at different temperatures can be estimated using an equation of the form given below:

$$D_l = D_o\, e^{(-E/RT)} \qquad \text{.....(1)}$$

From Chang (1951)

$$E = 1.615 \text{ Kcal/mol}$$

For $C_b = 0.0$

$D_l = 1.24X10^{-9}$ at 298^oK

From Equation (1)

$D_o = 1.9X10^{-9}\ m^2/s$

For $T = 296^oK$

$D_l = 1.21X10^{-9}\ m^2/s$

Therefore

$D_l(\text{at } 23^oC) = 0.98D_l(\text{at } 25^oC)$

Appendix 23

Listings of computer programs

```
$USES UIO IN IO.CODE
      PROGRAM KLAC
C*****************************************************************************
*****
C  This program calculates the volumetric mass transfer coefficient in
C  batch bubble column taking into account the reduction in driving
C  force due to build-up of oxygen concentration in the nitrogen
C  bubbles
c*****************************************************************************
c  VALUES OF CONSTANTS

         HE =13.6E-6
         R = 8.31
         T1 = 293.0
         X1=HE*R*T1
       CALL IO('I',VG,'SUPF. GAS VELOCITY                    ')
       CALL IO('I',EG,'GAS HOLDUP                            ')
       CALL IO('I',C1,'INITIAL OXYGEN CONC.                  ')
       CALL IO('I',C2,'FINAL OXYGEN CONC.                    ')
       CALL IO('I',TS,'SPARGING TIME                         ')
       CALL IO('I',HL,'CLEAR LIQ. HEIGHT                     ')

            START=.01
            STEP=.001
            EPS=.1E-5
            NMAX= 200
       CALL EONOR2(START,STEP,EPS,NMAX,XKL,X1,VG,EG,C1,C2,TS,HL,FMIN)

       CALL IO('O',XKL,'VOL. MASS TRANSFER COEFF.             ')
        STOP
        END


      SUBROUTINE EONOR2 (START,STEP,EPS,NMAX,X,X1,VG,EG,C1,C2,TS,
     * HL,FMIN)
c*****************************************************************************
c   finds the x value xmin which minimizes the function funct(x)
c*****************************************************************************
c   uses a success-failure linear search with parabolic inverse
c      interpolation ( see nash j.c., "compact numerical methods for
c      computers: linear algebra and function minimisation", adam hilger
c      ltd., bristol, 1979, 126-130)
c*****************************************************************************
c INPUT:
c       start:  starting value for x
c       step:   initial step length (for x) (can be negative to start
c                 search in other direction)
c       eps:    required precision on x, i.e. required minimum value of
c                 the x step.
c       nmax:   maximum number of function evaluations
c*****************************************************************************
c OUTPUT:
c       xmin: x value which minimizes the function funct(x)
c       fmin:   funct (xmin)
c*****************************************************************************
c NOTE:  apple fortran does not allow names of subprograms to be as
c          parameters to another subprogram.
c        before eonor2 can be used either the name of the function to be
c          minimized must be changed to 'funct' or "funct" in eonor2 must
c          be replaced by the appropriate function name
c*****************************************************************************
c  WARNING: this method will usually find one of the local minima close
```

```
C              to the starting point
C*************************************************************
      NFUNEV = 0
      A1 = 1.5
      A2 = -0.25
      BIG = 1.E25
      X = START

1     CONTINUE
      NFUNEV = NFUNEV + 1
      F = FUNCT (X,X1,VG,EG,C1,C2,TS,HL)

2     CONTINUE
      F1 = F
      F0 = - BIG
      STEP1 = 0.
      XMIN = X

3     CONTINUE
      STEP2 = STEP1 + STEP
      X = XMIN + STEP2

4     CONTINUE
      IF  ( ABS(STEP) .LE. EPS ) THEN
         FMIN = FUNCT(XMIN,X1,VG,EG,C1,C2,TS,HL)
         RETURN
      ENDIF
      IF ( NFUNEV .GT. NMAX ) THEN
         WRITE(*,121) 'MAXIMUM NUMBER OF FUNCTION EVALUATIONS REACHED'
121      FORMAT(A8)
         RETURN
      ENDIF

5     CONTINUE
      NFUNEV = NFUNEV + 1
      F = FUNCT(X,X1,VG,EG,C1,C2,TS,HL)

6     CONTINUE
      IF ( F .LT. F1) GO TO 10

7     CONTINUE
      IF ( F0 .GE. F1 ) GO TO 11

8     CONTINUE
      F0 = F
      STEP0 = STEP2

9     CONTINUE
      STEP = A2 * STEP
      GO TO 3

10    CONTINUE
      STEP0 = STEP1
      F0 = F1
      STEP1 = STEP2
      F1 = F
      STEP = A1 * STEP
      GO TO 3

11    CONTINUE
      STEP0 = STEP0 - STEP1
      F0 = (F0 - F1) * STEP
      F = (F - F1) * STEP0

12    CONTINUE
```

```
13    CONTINUE
      STEP = 0.5 * ( F*STEP0 - F0*STEP ) / (F - F0 )

14    CONTINUE
      STEP2 = STEP1 + STEP
      X = XMIN + STEP2

15    CONTINUE
      IF ( ABS(XMIN + STEP1 - X) .LT. 1.E-25 ) GO TO 20

16    CONTINUE
      NFUNEV = NFUNEV + 1
      F = FUNCT(X,X1,VG,EG,C1,C2,TS,HL)

17    CONTINUE
      IF ( F .LT. F1 ) GO TO 19

18    CONTINUE
      X = XMIN + STEP1
      F = F1
      GO TO 20

19    CONTINUE
      STEP1 = STEP2

20    CONTINUE
      STEP = STEP * A2
      GO TO 2

      RETURN
      END



      FUNCTION FUNCT(X,X1,VG,EG,C1,C2,TS,HL)


      XK=X
      Z1= XK*X1*HL
      Z2= Z1/(1.0-EG)
      Z3= Z2/VG
      Z4= 1.0 - EXP(-Z3)
      Z5= ALOG(C2/C1)
      FUNCT = XK+ (1.0-EG)*(Z5/TS)*(Z3/Z4)
       FUNCT = FUNCT * FUNCT
      CALL IO('o',FUNCT,'funct                                    ')

      RETURN
      END
```

```
C*************************************************************************
C   This program calculates the volumetric mass transfer coefficient in
C   a bubble column based on axial dispersion model
C*************************************************************************

      REAL*4 VL(20),VG(20),DZ(20),EL(20),CO(20),C1(20)
      REAL*4  L
     OPEN (UNIT=10,FILE='VL.DAT',STATUS = 'OLD')
     OPEN (UNIT =11,FILE='KL.DAT',STATUS ='NEW')



C       Height of column

        L = .98
                WRITE (6,*) L
C       Height of sampling probe

         Z = .55

      WRITE(11,4)
   4  FORMAT(5X,'LIQUID: TAP WATER',5X,'DIST.: SP1')

      WRITE(11,5)
  5   FORMAT(5X,'VL',14X,'VG',14X,'KLA',/)

        XKL=.02

C      WRITE(11,21)
C   21  FORMAT(/,5X,'VOL. MASS TRANSFER COEFF')

         N=14
      DO 2 I=1,N
      READ (10,*) VL(I),VG(I),DZ(I),EL(I),CO(I),C1(I)

      CALL  INTH(I,L,XKL,VL,DZ,EL,CO,C1,Z,AKL)

        WRITE (11,6) VL(I),VG(I),AKL
    6   FORMAT(5X,E12.5,2X,E12.5,2X,E12.5)

        XKL =.02
    2   CONTINUE
        STOP
        END

      SUBROUTINE INTH(I,L,XKL,VL,DZ,EL,CO,C1,Z,AKL)

c *************************************************************************
c  This subroutine uses interval halving technique for the solution
c  of algebraic equations.
c  *************************************************************************


      REAL*4 VL(20),DZ(20),EL(20),CO(20),C1(20)
      REAL*4 L

C       INTERVAL HALVING

        DXKL =.01
```

```
      FLAGM=-1.
      FLAGP=-1.
      LOOP=0

       WRITE (6,*) I,CO(I)
100    XM = (VL(I)**2 + 4.*EL(I)*DZ(I)*XKL)**.5
       XM1 = (VL(I)+XM)/2./DZ(I)/EL(I)
       XM2 = (VL(I)-XM)/2./DZ(I)/EL(I)
       X1 = (1.- (XM2/XM1)*EXP(L*XM2-L*XM1))
       X2 = (1.-EXP(L*XM2-L*XM1))
       X3 = -VL(I)*(XM2/XM1)*EXP(XM2*L-XM1*L)
       XA1 = X3/(VL(I)*X1-XM2*DZ(I)*EL(I)*X2)
       XA2 = VL(I)/(VL(I)*X1-XM2*DZ(I)*EL(I)*X2)

       F1 = (XA1*EXP(XM1*Z)+XA2*EXP(XM2*Z))-C1(I)/CO(I)

       LOOP=LOOP+1
       IF(LOOP.GT.100) STOP
       IF(ABS(F1).LT. .001) GO TO 50
       IF(F1) 10,10,1
 1     IF(FLAGP.LT. 0.) GO TO 2
        DXKL=DXKL/2.
 2      XKL=XKL+DXKL

        FLAGM=1.
        GO TO 100
 10     IF(FLAGM .LT. 0.) GO TO 11
        DXKL=DXKL/2.
 11     XKL=XKL-DXKL

        FLAGP=1.
        GO TO 100

 50     AKL=XKL
        RETURN
        END
```

```
      SUBROUTINE TPFBP ( H, HMAN, N, XMBED, DC, ROP, ROL,
     1HBED, ESB, EGB, ELB, EGF, ELF)
C*****************************************************************************
C calculates bed height and holdups for three-phase fluidized bed with
C  negligible entrainment of solids into the freeboard
C*****************************************************************************
C INPUT
C h      table of pressure tap heights above the grid (ranked in increasing
C          order)
C hman   table of height of liquid in manometers connected to pressure taps
C          (heights taken from bottom of manometers not top)
C          (origin of heights unimportant provided it is the same for all
C                                                              manometers)
C n      number of pressure taps
C mbed mass of solids introduced into the column
C dc     inside column diameter
C rop    particle density
C rol    liquid density
C*****************************************************************************
C hbed   bed height
C esb    solid holdup in the bed
C egb    gas holdup in the bed
C elb    liquid holdup in the bed
C egf    gas holdup in the freeboard
C elf    liquid holdup in the freeboard
C*****************************************************************************
C note: density of gas assumed to be negligible when compared to liquid density
C*****************************************************************************

      DIMENSION H(16), HMAN(16), X(100), Y(100)

      DATA PI /3.14159/

C     general procedure to find the bed height:  try various bed heights
C      (or, rather separation between pressure taps in bed and in freeboard)
C      height which gives the best overall fit of the experimental pressure
C      data is the actual bed height.

21                    FORMAT(A8)
22                    FORMAT(6E15.6)
24                    FORMAT(I6)
      N4 = N - 4
      SM = 1.E15
      DO 1 K = 4, N4
C       fit pressure data in assumed bed with a straight line
C       (do not use 2 points directly on each side of transition)
        KB = K - 1
        NB = KB
        DO 2 I = 1, NB
          Y(I) = HMAN(I)
          X(I) = H(I)
2       CONTINUE
        CALL LINREG( NB, X, Y, AB, BB, R, DA95, DB95 )
C       compute sum of square of difference between estimated and experimental
```

```
          S = 0.
          DO 3 I = 1, NB
            XINT = Y(I) - AB * X(I) - BB
            S = S + XINT * XINT
 3        CONTINUE

 *        same procedure for freeboard
          KF = K + 1
          NF = N - KF
          J = KF
          DO 4 I = 1, NF
            Y(I) = HMAN(J)
            X(I) = H(J)
            J = J + 1
 4        CONTINUE
          CALL LINREG( NF, X, Y, AF, BF, R, DA95, DB95 )
          DO 5 I = 1, NF
            XINT = Y(I) - AF * X(I) - BF
            S = S + XINT * XINT
 5        CONTINUE

 *        test to see if best fit obtained and save corresponding data
          IF ( S .LT. SM ) THEN
            SM = S
            ABM = AB
            BBM = BB
            AFM = AF
            BFM = BF
            KM = K
          ENDIF

 1      CONTINUE

 *      bed height from intersection between 2 straight lines
        HBED = (BBM - BFM) / (AFM - ABM)

 *      compute holdups in bed and freeboard
        ACOL = 0.25 * PI * DC * DC
        ESB = XMBED / ACOL / ROP / HBED
 *      real pressure slopes (in m of liquid) from slope of manometer height
        SLOPB = ABM - 1.
        SLOFF = AFM - 1.
        ELB = - SLOPB - ESB * ROP / ROL
        ELF = - SLOFF
        EGB = 1. - ELB - ESB
        EGF = 1. - ELF

        RETURN
        END


      SUBROUTINE LINREG ( N, X, Y, A, B, R, DA95, DB95 )
C*************************************************************************
C     computes the least square line y = ax + b which fits the
C       data x, y
C*************************************************************************
C INPUT
C       n       : number of experimental points (x,y)
C       x       : table of experimental x values
C       y       : table of experimental y values
C*************************************************************************
C OUTPUT
C       a       : slope of fitted straight line
C       b       : y-intercept of fitted straight line
C       r       : correlation coefficient
```

```
C*************************************************************************

      DIMENSION X(100), Y(100)

      SX = 0.
      SYX = 0.
      SY = 0.
      SYY = 0.
      SXY = 0.
      SX2 = 0.
      XN = FLOAT(N)
72                                FORMAT(5E15.6)
74                                FORMAT(I6)

      DO 1 I = 1, N
        SX2 = SX2 + X(I) * X(I)
        SX = SX + X(I)
        SY = SY + Y(I)
      CONTINUE

      XM = SX / XN
      YM = SY / XN

      DO 2 I = 1, N
        DXM = X(I) - XM
        DYM = Y(I) - YM
        SXX = SXX + DXM * DXM
        SYY = SYY + DYM * DYM
        SXY = SXY + DXM * DYM
      CONTINUE

      A = SXY / SXX
      B = YM - A * XM
      R =  SXY / ABS(SXX*SYY)**.5

     calculation of confidence intervals on estimates
     see Benjamin j.r., Cornell c.a., "probability, statistics and decision
       for civil engineers", mc. graw hill, 1970, p. 432-435

      DY2 = 0.
      DO 3 I = 1, N
        RR = Y(I) - B - A*X(I)
        DY2 = DY2 + RR * RR
      CONTINUE

      DY2 = DY2 / (XN - 2.)
      SA2 = DY2 / SXX
      SB2 = DY2 / XN * (1. + XM*XM / SXX * XN)
      NU = N - 2
      CALL T975 (NU, T)
      DB95 = 100. / B * T * (ABS(SB2))**.5
      DA95 = 100. / A * T * (ABS(SA2))**.5

     RETURN
     END


     SUBROUTINE T975 ( NU, T )
C*************************************************************************
     computes the t factor from student's t distribution
       for a probability of 97.5 % and
       for nu degrees of freedom
     interpolation formula from the "Handbook of Mathematical Functions"
       (see in file 'student - t - distribution')
C*************************************************************************
```

```
C     NU     : nb of degrees of freedom
C*************************************************************************
C OUTPUT
C     T      : t factor
C*************************************************************************

      Z = FLOAT(NU)
      Z2 = Z * Z
      Z3 = Z2 * Z
      Z4 = Z3 * Z

      T = 1.96 + 2.3724 / Z + 2.8227 / Z2 + 2.5561 / Z3 + 1.5897 / Z4

      RETURN
      END
```

```
$USES UIO IN IO.CODE
      PROGRAM WKCOR

*************************************************************************
* computes gas holdup using various literature correlations
* compares with exptl. values to give min, max and avg errors

*************************************************************************

      CHARACTER IN, OUT, SPC, TXT
      REAL  K,KO

      DIMENSION  EG(40), KO(40),R1(40),K(8,30), TAN(40)
      DIMENSION  VG(40), VL(40), DC(40), DP(40), ES(40), ELO(40)
      DIMENSION  E1(40), E2(40), E3(40), EL1(40), EP1(40)
      DIMENSION  EPF1(40), ELF1(40),X1(40)

      DATA  G,DL,SL/9.81,997.,73./

      EK = 1.
      CALL IOINIT(IN,OUT,TXT,SPC)
      PRT = 1.
      CALL RDF(IN,N,EG,'Exptl. values for gas holdup          ')
      CALL RDF(IN,N,ELF1,'Exptl. values for liquid holdup     ')
      CALL RDF(IN,N,EPF1,'Exptl. values for bed porosity      ')
      CALL RDF(IN,N,ELO,'File name for liquid holdup at vg=0. ')
      CALL RDF (IN,N,ES,'File for solids holdup               ')

      CALL RDF(IN,N,VG,'file for gas velocity data             ')
      CALL RDF(IN,N,VL,'file for liquid velocity data          ')
      CALL RDF(IN,N,DC,'file for column dia.                   ')
      CALL RDF(IN,N,DP,'file for particle dia.                 ')

      N1=20

      DO 1 I = 1,N1
      C = DP(I) - 0.0052
      IF(C) 3,4,4

3     VLM = 0.3764
      GO TO 30

4     VLM = 0.487

30    CONTINUE

      K(1,I)= 0.14*(EG(I)**(-.5))*(VL(I)-VLM)

      KO(I) = .61+ .037*(EG(I)+.013)**(-1.)

      K(2,I) = KO(I)*(1.-EG(I)-ELF1(I))**3.

      R1(I) = VL(I)/VG(I)
      R2 = R1(I) -.4
      IF(R2) 6,7,7

6     K(3,I) = 0.
      GO TO 24
7     K(3,I) = 1.4*(R1(I))**.33-1.

24    K(4,I) = 1.617*(R1(I)**.61)*(SL**(-.634))
```

```
      K(5,I) = EK*EXP(-5.08*EG(I))

      K(6,I) = EG(I)*((1.-ES(I))**3.)*(EXP(-1.2*EG(I)))+
     *  2.5*EXP(-32.8*EG(I))

      TAN(I) = (40.*VG(I)*ELO(I)**10.)/VL(I) -3.32*ELO(I)**5.45
      K(7,I)=(5.1*(ELO(I))**4.85)*(1.-TANH(TAN(I)))

      K(8,I) = .31*VG(I)**(-.985)
    1 CONTINUE

      DO 21 J=1,7

      GO TO(8,9,10,11,12,13,14),J

    8 X=1.

      CALL IO(TXT,DUM,'Correlation of k by Ostergaard (1965)     ')
      GO TO 15

    9 X=0.
      CALL IO(TXT,DUM,'Correl. of k by Bhatia and Epstein(1974) ')
      GO TO 15

   10 X=0.
      CALL IO(TXT,DUM,'Correl. of k by Darton and Harrison (1975)')
      GO TO 15

   11 X=0.
      CALL IO(TXT,DUM,'Correl. of k by Baker et al. (1977)      ')
      GO TO 15

   12  X=0.1
      CALL IO(TXT,DUM,'Correl. of k by El-Temtamy and Epstein   ')
      GO TO 15

   13 X=1.
      CALL IO(TXT,DUM,'Correl. of k by Khang et al.(1987)       ')
      GO TO 15

   14 X=0.
      CALL IO(TXT,DUM,'Cor. of k by Efermov and Vakhrushev(1970) ')


   15 DO 22 I = 1,N1

      E = DP(I)-0.00520

      IF(E) 17,18,18

   17  VT = .3764
       RN = 2.5
       GO TO 20
   18  VT = .487
       RN= 2.14

   20  E1(I)=ABS((VL(I)-VG(I)*K(J,I)*(1.-X)))

       E2(I) =ABS( VT*(1.-EG(I)-K(J,I)*EG(I)))

       E3(I)=(1. - EG(I)*(1.+K(J,I)-K(J,I)*X))
       EL1(I)=((E1(I)/E2(I))**(1./RN))*(E3(I))+EG(I)*K(J,I)*(1.-X)

       EP1(I) = ((E1(I)/E2(I))**(1./RN))*(E3(I))+EG(I)*(1.+K(J,I)
     *  -K(J,I)*X)
```

```
 22          CONTINUE

             CALL ERROR (N,ELF1,EL1,PRT,EMIN,EMAX,EAVG,EAVGA,RMS,IN,
     *        OUT,TXT,SPC)

             CALL ERROR (N,EPF1,EP1,PRT,EMIN,EMAX,EAVG,EAVGA,RMS,IN,
     *        OUT,TXT,SPC)


 21          CONTINUE

             DO 35 I=1,N1

             X1(I) = 1. - .278*(VL(I)**1.09)*DP(I)**(-.33)

 35          CONTINUE

             J=8

           CALL IO(TXT,DUM,'Corr. of k & x by Moruoka et al.          ')


           DO 25 I = 1,N1

            E = DP(I)-0.00520

            IF(E) 26,27,27

 26          VT = .3764
             RN = 2.5
             GO TO 28
 27          VT = .487
             RN= 2.44

 28          E1(I)=ABS((VL(I)-VG(I)*K(J,I)*(1.-X1(I))))

             E2(I) =ABS( VT*(1.-EG(I)-K(J,I)*EG(I)))

             E3(I)=(1. - EG(I)*(1.+K(J,I)-K(J,I)*X1(I)))
             EL1(I)=((E1(I)/E2(I))**(1./RN))*(E3(I)+EG(I)*K(J,I)*
     *       (1.- X1(I))

            EP1(I) = ((E1(I)/E2(I))**(1./RN))*(E3(I)+EG(I)*(1.+K(J,I)
     *     -K(J,I)*X1(I))

 25          CONTINUE
              CALL ERROR (N,ELF1,EL1,PRT,EMIN,EMAX,EAVG,EAVGA,RMS,IN,
     *        OUT,TXT,SPC)

             CALL ERROR (N,EPF1,EP1,PRT,EMIN,EMAX,EAVG,EAVGA,RMS,IN,
     *        OUT,TXT,SPC)
              STOP
              END


         SUBROUTINE ERROR(N,EXP,CALC,PRT,EMIN,EMAX,EAVG,EAVGA,RMS,
     *   IN,OUT,TXT,SPC)

*************************************************************************
* computes various errors between two files (calc. and exptl. values)
*************************************************************************
* INPUT
* n     number of points to compare
* exp   table of experimental values
* calc  table of calc values
```

```
* ='0') in,out,txt,spc standard io parameters
*************************************************************************
* OUTPUT
* emin  minimum relative error (%)
* emax  maximum relative error (%)
* eavg  average relative error (%)
* eavga average of abs (relative errors), %
* rms  square root of (relative errors) **2, %
*************************************************************************

      CHARACTER IN, OUT, SPC, TXT

      DIMENSION EXP(50), CALC(50)

      S = 0.
      SA = 0.
      S2 = 0.
      XN = FLOAT (N)
      EMAX = -1.E30
      EMIN = 1.E30

      DO 1 I = 1, N
      ER = (CALC(I)/EXP(I) - 1.)*100.
      EMIN = AMIN1(EMIN,ER)
      EMAX = AMAX1(EMAX,ER)
      S=S+ER
      SA=SA+ABS(ER)
      S2=S2+ER*ER

1     CONTINUE

      EAVG = S/XN
      EAVGA = SA/XN
      RMS = SQRT(S2)/XN

      IF (PRT .EQ. 1.) THEN
       CALL IO(OUT,EAVG,'average relative error, %                ')
       CALL IO(OUT,EAVGA,'average abs (relative error), %         ')
       CALL IO(OUT,RMS,'root mean square of errors,%              ')
       CALL IO(OUT,EMIN,'minimum relative error, %                ')
       CALL IO(OUT,EMAX,'maximum relative error,%                 ')
       CALL IO(SPC,1.,'  ')
      END IF
      RETURN
      END
```

```
*USES UIO IN IO.CODE
      PROGRAM EPCOR

C*********************************************************************
C * computes bed porosity using various literature correlations
C * compares with expti. values to give min, max and avg errors
C*********************************************************************

      CHARACTER IN, OUT, SPC, TXT

      DIMENSION  EP1(40), E1(40), E2(40), E3(40), E4(40)
      DIMENSION  VG(40), VL(40), DC(40), DP(40)
      DIMENSION  RT(40),RLG(40), DS(40)
      DIMENSION  EG5(40), EG6(40)

      DATA  G,DL,SL,UL/9.81,997.,.073,.984E-3/
      CALL IOINIT(IN,OUT,TXT,SPC)
      PRT = 1.
      CALL RDF(IN,N,EP1,'Expt. values of bed porosity          ')
      CALL RDF(IN,N,DS,'values for particle density           ')
      CALL RDF(IN,N,VG,'file for gas velocity data            ')
      CALL RDF(IN,N,VL,'file for liquid velocity data         ')
      CALL RDF(IN,N,DC,'file for column dia.                  ')
      CALL RDF(IN,N,DP,'file for particle dia.                ')

      CALL IO(TXT,DUM,'Test of lit. corr. for bed porosity    ')

      CALL IO (TXT,DUM,'Corr. by Dakshinamurty                ')

      DO 11 I= 1,N
      C = DP(I) - 0.005
      IF(C) 2,3,4

    2 VT = 0.3764
      GO TO 12

    3 VT = 0.479
      GO TO 12

    4 VT = 0.486

   12   E1(I) = 2.65*((VL(I)/VT)**0.6)*(VG(I)*UL/SL)**0.08

   11   CONTINUE

      CALL ERROR (N,EP1,E1,PRT,EMIN,EMAX,EAVG,EAVGA,RMS,IN,
     *            OUT,TXT,SPC)

      CALL IO(TXT,DUM,'Corr. by Begovich and Watson           ')

      DO 5  I = 1,N

      E2(I) =5.06*(VL(I)**0.271)*(VG(I)**0.041)*(DP(I)**(-0.268
     *))*(UL**0.055)*(DC(I)**(-0.033))*(DS(I)-DL)**(-0.316)

    5   CONTINUE

      CALL ERROR(N,EP1,E2,PRT,EMIN,EMAX,EAVG,EAVGA,RMS,IN,OUT,
     *           TXT,SPC)

      CALL IO(TXT,DUM,'Corr. by Broudjenni et al. (1984)      ')
```

```
      DO 10 I=1,N

      C1 = DP(I) - .005

      IF(C1) 6,7,8

 6    VMF = 0.035
 7    VMF = 0.05
 8    VMF = 0.051

      RLG(I) = DL*VG(I)*DP(I)/UL

      E3(I) = 0.415*((VL(I)/VMF)**0.27)*(1. + 0.07*RLG(I)**0.34)

10    CONTINUE
      CALL ERROR (N,EP1,E3,PRT,EMIN,EMAX,EAVG,EAVGA,RMS,IN,
     *            OUT,TXT,SPC)


      STOP
      END


      SUBROUTINE ERROR(N,EXP,CALC,PRT,EMIN,EMAX,EAVG,EAVGA,RMS,
     *  IN,OUT,TXT,SPC)

C*********************************************************************
C* computes various errors between two files (calc. and expti. values)
C*********************************************************************
C* INPUT
C* n    number of points to compare
C* exp  table of experimental values
C* calc table of calc values
C* prt  if 1.0 ,then values are displayed by subroutine (printed if out
C* ='0') in,out,txt,spc standard io parameters
C*********************************************************************
C* OUTPUT
C* emin  minimum relative error (%)
C* emax  maximum relative error (%)
C* eavg  average relative error (%)
C* eavga average of abs (relative errors), %
C* rms  square root of (relative errors) **2, %
C*********************************************************************

      CHARACTER IN, OUT, SPC, TXT

      DIMENSION EXP(50), CALC(50)

      S = 0.
      SA = 0.
      S2 = 0.
      XN = FLOAT (N)
      EMAX = -1.E30
      EMIN = 1.E30

      DO 1 I = 1, N
      ER = (CALC(I)/EXP(I) - 1.)*100.
      EMIN = AMIN1(EMIN,ER)
      EMAX = AMAX1(EMAX,ER)
      S=S+ER
      SA=SA+ABS(ER)
      S2=S2+ER*ER

1     CONTINUE
```

```
EAVG = S/XN
EAVGA = SA/XN
RMS = SQRT(S2)/XN

IF (PRT .EQ. 1.) THEN
 CALL IO(OUT,EAVG,'average relative error, %              ')
 CALL IO(OUT,EAVGA,'average abs (relative error), %       ')
 CALL IO(OUT,RMS,'root mean square of errors,%            ')
 CALL IO(OUT,EMIN,'minimum relative error, %              ')
 CALL IO(OUT,EMAX,'maximum relative error,%               ')
 CALL IO(SPC,1.,'  ')
END IF

RETURN
END
```

```
$USES UIO IN IO.CODE
      PROGRAM EGCOR

C*********************************************************************
C* computes gas holdup using various literature correlations
C* compares with expti. values to give min, max and avg errors
C*********************************************************************

      CHARACTER IN, OUT, SPC, TXT

      DIMENSION  EGF1(40), EG1(40), EG2(40), EG3(40), EG4(40)
      DIMENSION  VG(40), VL(40), DC(40), DP(40), W1(40), W2(40)
      DIMENSION  W3(40), W4(40), W(40), RT(40), B(40), R1(40)
      DIMENSION  EG5(40), EG6(40)

      DATA  G,DL,SL,UL/9.81,997.,.073,.984/
      CALL IOINIT(IN,OUT,TXT,SPC)
      PRT = 1.
      CALL RDF(IN,N,EGF1,'Expti. values for gas holdup          ')
      CALL RDF(IN,N,VG,'file for gas velocity data             ')
      CALL RDF(IN,N,VL,'file for liquid velocity data          ')
      CALL RDF(IN,N,DC,'file for column dia.                   ')
      CALL RDF(IN,N,DP,'file for particle dia.                 ')

      CALL IO(TXT,DUM,'TEST OF LITERATURE CORRELATIONS FOR GAS
     *     HOLDUP')
      CALL IO(TXT,DUM, 'Correlation by Bagovich and Watson     ')

      DO 1 I= 1,N

      EG1(I)=1.61*(VG(I)**0.72)*(DP(I)**.168)*(DC(I)**(-.125))

1     CONTINUE

      CALL ERROR (N,EGF1,EG1,PRT,EMIN,EMAX,EAVG,EAVGA,RMS,IN,
     *            OUT,TXT,SPC)

      CALL IO(TXT,DUM,'Correlation by Hu et al.                ')

      DO 2  I = 1,N

      EG2(I)=0.29*(VG(I)**.842)*(VL(I)**(-.096))*(DC(I)**(-.125))

2     CONTINUE

      CALL ERROR(N,EGF1,EG2,PRT,EMIN,EMAX,EAVG,EAVGA,RMS,IN,OUT,
     *           TXT,SPC)

      CALL IO(TXT,DUM,'Correlation by Kato et al.              ')

      DO 3 I=1,N

      W1(I) = (G*DC(I)**2.*DL/SL)**.198
      W2(I) = (G*DC(I)**3./UL**2.)**.035
      W3(I) = VG(I)/(G*DC(I))**.5
      W(I) = W1(I)*W2(I)*W3(I)

      C = DP(I) - .005
```

```
      IF(C) 4,5,6
 4    VT=0.3664
      GO TO 7
 5    VT=.471
      GO TO 7
 6    VT=.482

 7    RT(I) = UP(I)*VT/UL

      ELS(I) = 1.-9.7*((350.+RT(I)**1.1)**(-.5))*AK(I)**.092

      A1(I)= 5.1*(1.+16.9*AK(I)**.285)

      A2(I) = .1*(1.+4.43*AK(I)**.165)*RT(I)**.9

      AN(I) = (A1(I)+2.7*A2(I))/(A2(I)+1.)
      AP(I) = 1./AN(I)
      EL3(I) = ELS(I)*(VL(I)/VT)**AP(I)
 3     CONTINUE

      CALL ERROR (N,ELF1,EL3,PRT,EMIN,EMAX,EAVG,EAVGA,RMS,IN,
     *            OUT,TXT,SPC)


      CALL IO(TXT,DUM,'Correlation by S.L.P Lee (1984)        ')

      DO 8 I=1,N

      EL4(I) = .659*(VL(I)**.025)*(VG(I)**.006)

      EL5(I) = 1. - .53*(EXP(-.42*VL(I)-.004*VG(I)))
 8    CONTINUE

      CALL ERROR (N,ELF1,EL4,PRT,EMIN,EMAX,EAVG,EAVGA,RMS,IN
     *  ,OUT,TXT,SPC)
      CALL ERROR (N,ELF1,EL5,PRT,EMIN,EMAX,EAVG,EAVGA,RMS,IN
     *  ,OUT,TXT,SPC)

      CALL IO(TXT,DUM,'Correlation by Chiu and Ziegler(1983)     ')

      DO 10 I=1,N

      C1=DP(I) -.005

      IF(C1) 11,12,13
11    VT = .376
      RN =2.5
      GO TO 14

12    VT = .471
      RN= 2.4
      GO TO 14

13    VT=.486
      RN = 2.33


14    EL6(I)=1.26*((VL(I)/VT)**(1./RN))*(VL(I)**.088)
     *    *(VG(I)**(-.059))*(DP(I)**.058)

10     CONTINUE
      CALL ERROR (N,ELF1,EL6,PRT,EMIN,EMAX,EAVG,EAVGA,RMS,IN
     *  ,OUT,TXT,SPC)
      STOP
      END
```

```
      SUBROUTINE ERROR(N,EXP,CALC,PRT,EMIN,EMAX,EAVG,EAVGA,RMS,
     *    IN,OUT,TXT,SPC)

*************************************************************************
* computes various errors between two files (calc. and expti. values)
*************************************************************************
* INPUT
* n     number of points to compare
* exp   table of experimental values
* calc  table of calc values
* prt   if 1.0 ,then values are displayed by subroutine (printed if out
* ='0') in,out,txt,spc standard io parameters
*************************************************************************
* OUTPUT
* emin  minimum relative error (%)
* emax  maximum relative error (%)
* eavg  average relative error (%)
* eavga average of abs (relative errors), %
* rms   square root of (relative errors) **2, %
*************************************************************************

      CHARACTER IN, OUT, SPC, TXT

      DIMENSION EXP(50), CALC(50)

      S = 0.
      SA = 0.
      S2 = 0.
      XN = FLOAT (N)
      EMAX = -1.E30
      EMIN = 1.E30

      DO 1 I = 1, N
      ER = (CALC(I)/EXP(I) - 1.)*100.
      EMIN = AMIN1(EMIN,ER)
      EMAX = AMAX1(EMAX,ER)
      S=S+ER
      SA=SA+ABS(ER)
      S2=S2+ER*ER

1     CONTINUE

      EAVG = S/XN
      EAVGA = SA/XN
      RMS = SQRT(S2)/XN

      IF (PRT .EQ. 1.) THEN
       CALL IO(OUT,EAVG,'average relative error, %              ')
       CALL IO(OUT,EAVGA,'average abs (relative error), %       ')
       CALL IO(OUT,RMS,'root mean square of errors,%            ')
       CALL IO(OUT,EMIN,'minimum relative error, %              ')
       CALL IO(OUT,EMAX,'maximum relative error,%               ')
       CALL IO(SPC,1.,'  ')
      END IF

      RETURN
      END
```

```
$USES UIO IN IO.CODE
$USES ULINREG IN LINREG.CODE

      PROGRAM DDH
*************************************************************************
* computes intersection point of two bubble population using
* dynamic disengagement technique
*************************************************************************

        DIMENSION  HD(100),TM(100),HL(100),HS(100)

       CALL IO('I',RNB,'RUN NUMBER                                    ')
*      NUMBER OF DATA POINTS OF RUN
       CALL IO('S',2.,'   ')
       CALL IO('I',XNL,'data points for large bubbles(appx.)          ')
       NL=NINT(XNL)
       CALL RDF(NP,HD,'interface height                          ')
       XNP = FLOAT(NP)
       CALL IO('O',XNP,'TOTAL DATA POINTS                        ')
       CALL RDF(NP,TM,'time (sec.)                               ')
       XNP = FLOAT(NP)
       CALL IO('O',XNP,'TOTAL DATA POINTS                        ')

       CALL LINFT(HD,TM,NP,NL,AL,BL,CS,DS,KM,DAL95,DBL95,DCS95,DDS95)
       CALL IO('O',AL,'slope for large bubbles                   ')
       CALL IO('O',BL,'intersection for large bubbles            ')
       CALL IO('O',CS,'slope for small bubbles line              ')
       CALL IO('O',DS,'intersection for small bubbles line       ')
       CALL IO('O',DAL95,'95% conf.int.for slope of large bubb.line   ')
       CALL IO('O',DBL95,'95% conf.int.for ints. of large bubb.line   ')
       CALL IO('O',DCS95,'95% conf.int.for slope of small bubb.line   ')
       CALL IO('O',DDS95,'95% conf.int.for intr. of small bubb.line   ')
       DO 21 I = 1,KM
         HL(I) = AL * TM(I) + BL
21     CONTINUE
         CALL IO('O',HI,'height of int. of two lines               ')
       CALL WTF(KM,HL,'calc. int. level for large bubbles          ')

       J=KM+1
       NK=NP-KM
       DO 22 K=1,NK
       HS(K)=CS*TM(J)+DS
       J=J+1
22     CONTINUE

       CALL WTF(NK,HS,'calc. int level small bubbles               ')

       STOP
       END


      SUBROUTINE LINFT(H,T,N,N1,AL,BL,CS,DS,KM,DAL95,DBL95,DCS95,DDS95)
      DIMENSION H(100),T(100),X(100),Y(100)

*************************************************************************
*  genera. procedure to find the least square lines y=ax+b and y=cx+d
*  which fit the data points for large and small bubbles population
*************************************************************************

                              WRITE(*,123)N, N1
123                           FORMAT(3I6)
       NL=N1
       N2=N-NL
```

```
      XN2=FLOAT(N2)
      CALL IO ('o',XN2,'value of N2                                    ')
      SM= 1.E10

      DO 11  K=N1,N
*     fit interface height data points with straight lines

      DO 4  I=1,N1
      Y(I)=H(I)

      X(I)=T(I)


4     CONTINUE

      CALL LINREG(NL,X,Y,A,B,R,DA95,DB95)

*     compute sum of the square of differences between estimated and
*     experimental values

      S=0.
      DO 5 I=1,N1
      XRT=Y(I)-A*X(I)-B
      S=S+ XRT*XRT
5     CONTINUE

*     same procedure for small bubbles population

      J=N1+1
      NF=N-N1

      DO 6 I=1,NF

      X(I)=T(J)
      Y(I)=H(J)

      J=J+1

6     CONTINUE

      CALL LINREG(NF,X,Y,C,D,R,DC95,DD95)
      DO 7 I=1,NF
      XRT=Y(I)-C*X(I)-D
      S=S+XRT*XRT

7     CONTINUE

* test to see if best fit obtained and save the data

      IF (S.LT.SM) THEN
        SM=S
        AL=A
        BL=B
        CS=C
        DS=D
        KM=N1
        DAL95=DA95
        DBL95=DB95
        DCS95=DC95
        DDS95=DD95
        ENDIF
11      CONTINUE

* interface height at the intersection of two straight lines
```

```
      SUBROUTINE LINREG ( N, X, Y, A, B, R, DA95, DB95 )
C*****************************************************************
C     computes the least square line y = ax + b which fits the
C       data x, y
C*****************************************************************
C INPUT
C       n       : number of experimental points (x,y)
C       x       : table of experimental x values
C       y       : table of experimental y values
C*****************************************************************
C OUTPUT
C       a       : slope of fitted straight line
C       b       : y-intercept of fitted straight line
C       r       : correlation coefficient
C       da95    : 95 % confidence interval on a (in %)
C       db95    : 95 % confidence interval on b (in %)
C*****************************************************************

      DIMENSION X(100), Y(100)

      SX = 0.
      SXX = 0.
      SY = 0.
      SYY = 0.
      SXY = 0.
      SX2 = 0.
      XN = FLOAT(N)

      DO 1 I = 1, N
        SX2 = SX2 + X(I) * X(I)
        SX = SX + X(I)
        SY = SY + Y(I)
1     CONTINUE

      XM = SX / XN
      YM = SY / XN

      DO 2 I = 1, N
        DXM = X(I) - XM
        DYM = Y(I) - YM
        SXX = SXX + DXM * DXM
        SYY = SYY + DYM * DYM
        SXY = SXY + DXM * DYM
2     CONTINUE

      A = SXY / SXX
      B = YM - A * XM
      R =  SXY / ABS(SXX*SYY)**.5

*     calculation of confidence intervals on estimates
*     see Benjamin J.r., Cornell c.a., "probability, statistics and decision
*       for civil engineers", mc. graw hill, 1970, p. 432-435

      DY2 = 0.
      DO 3 I = 1, N
        RR = Y(I) - B - A*X(I)
        DY2 = DY2 + RR * RR
3     CONTINUE

      DY2 = DY2 / (XN - 2.)
      SA2 = DY2 / SXX
      SB2 = DY2 / XN * (1.  + XM*XM / SXX * XN)
```

```
      NU = N - 2
      IF (NU .LE. 1) THEN
        DA95 = 0.
        DB95 = 0.
        RETURN
      ENDIF
      CALL T975 (NU, T)
      DB95 = 100. / B * T * (ABS(SB2))**.5
      DA95 = 100. / A * T * (ABS(SA2))**.5

      RETURN
      END


      SUBROUTINE T975 ( NU, T )
*************************************************************************
*     computes the t factor from student's t distribution
*       for a probability of 97.5 % and
*       for nu degrees of freedom
*     interpolation formula from the "Handbook of Mathematical Functions"
*       (see in file 'student - t - distribution')
*************************************************************************
* INPUT
*     nu     : nb of degrees of freedom
*************************************************************************
* OUTPUT
*     t      : t factor
*************************************************************************

      Z = FLOAT(NU)
      Z2 = Z * Z
      Z3 = Z2 * Z
      Z4 = Z3 * Z

      T = 1.96 + 2.3724 / Z + 2.8227 / Z2 + 2.5561 / Z3 + 1.5897 / Z4

      RETURN
      END
```

```
$USES UIO IN IO.CODE
      PROGRAM KSLT

*************************************************************************
* computes particle-liquid mass transfer using literature correlations
* compares with exptl. values to give min, max and avg errors

*************************************************************************

      CHARACTER IN, OUT, SPC, TXT

      DIMENSION  AKV(40),DP(40),UL(40),GA(40),SC(40)
      DIMENSION  VG(40), VL(40), DC(40),AKS(40)
      DIMENSION  SH1(40),SH2(40),SH3(40),SH4(40),REG(40)
      DIMENSION  REP1(40),REP2(40),REP3(40),EG(40),EL(40)
      DIMENSION  EP(40),DPL(40),DPG(40),ET(40),ALM(40),WL(40)
      DIMENSION  RL1(40),DPD(40),ET1(40),SHO(40)
      DIMENSION  AR(40),FRG(40),AFR(40),SH5(40)

      DATA  G,DL,SL/9.81,997.,.073/
      DATA  DG,UG/1.21,1.8E-5/

       DF = 1.06E-9

       DS = 2520.

      CALL IOINIT(IN,OUT,TXT,SPC)
      PRT = 1.
      CALL RDF(IN,N,AKS,'expt. val. of mass transfer coeff.      ')
      CALL RDF(IN,N,EG,'file for gas holdup                      ')
      CALL RDF(IN,N,EL,'file for liq. holdup                     ')
      CALL RDF(IN,N,EP,'Expt. values of bed porosity             ')
      CALL RDF(IN,N,VG,'file for gas velocity data               ')
      CALL RDF(IN,N,VL,'file for liquid velocity data            ')
      CALL RDF(IN,N,DP,'file for particle dia.                   ')
      CALL RDF(IN,N,UL,'file for liq. vis.                       ')


      CALL IO(TXT,DUM,'Test of lit. corr. for L/S mass transfer  ')

       N=30
       DO 1 I= 1,N

       AKV(I) = UL(I)/DL
       GA(I) = (DP(I)**3)*(DL**2)*G/(UL(I)**2)

       AMV = (DS-DL)/DL
       SC(I) = AKV(I)/DF
       REG(I) = VG(I)*DP(I)*DG/UG
       C = REG(I)
       IF(C) 4,4,5
 4     SH1(I)=.228*(GA(I)**.323)*(AMV**.3)*(SC(I)**.4)
        GO TO 6

 5     SH1(I)=.228*(1.+.826*(C**.623))*(GA(I)**.323)*(AMV**.3)
     *  *(SC(I)**.4)


 6      IF(VG(I))  7,7,8

 7     SH2(I) =.33*(1.+ .22*(AMV**(-.57)))*(GA(I)*AMV*SC(I))**.33
        GO TO 9
 8     SH2(I) = .33*(1.+ .22*(AMV**(-.57))*(VG(I)/VL(I))**.77)*(GA
```

```
     *      (I)*AMV*SC(I))**.33

  9          REP1(I) = ((1.-EP(I))**2)/EP(I)**3.
             REP2(I) = 6.*(1.-EP(I))/EP(I)*DP(I)
             DPL(I) = 4.5*DL*AKV(I) 5.*REP1(I)*VL(I)/DP(I)**2. + .3*DL*
     *      REP2(I)*VL(I)**2.
             DPG(I) = G*EL(I)*DL

             ET(I) = DPL(I)*VL(I)/(EL(I)*DL) + DPG(I)*VG(I)/(EL(I)*DL)
             ALM(I) = DP(I)*(1.-EP(I))**(-.33)
             WL(I) = 1.41*(ET(I)*ALM(I))**.333

             RL1(I) = WL(I)*DP(I)/AKV(I)

             SH3(I) = .66*(RL1(I)**.5)*SC(I)**.33

             VT = .486
             CO = .4

             DPD(I) = .5*EL(I)*CD*DL*VT**2.
             ET1(I) = (DPD(I)/DP(I))*VL(I)/(EL(I)*DL)+VG(I)*G
             REP3(I) = (ET1(I)**.33)*(DP(I)**1.33)/AKV(I)

             SH4(I) = 2.+.51*(REP3(I)**.6)*(SC(I)**.33)

             AR(I) = (DP(I)**3)*DL*(DS-DL)*G/UL(I)**2

             IF (VG(I)) 11,11,12

 11          SH5(I) = .31*(AR(I)**.33)*(SC(I)**.33)
              GO TO 13

 12          REG(I) = VG(I)*DP(I)*DG/UG
               FRG(I) = VG(I)**2/(DP(I)*G)


             AFR(I) = REG(I)*FRG(I)

             SH5(I) = .31*(AR(I)**.33)*(SC(I)**.33)*(1.+((32.*AFR(I)**
     *      .28)/(410.+ AFR(I)**.28))*AMV**(-1))

 13          SHO(I) = AKS(I)*DP(I)/DF

  1          CONTINUE

             CALL IO(TXT,DUM,'Corr. by Artes and Fan (1986)            ')

            CALL ERROR (N,SHO,SH1,PRT,EMIN,EMAX,EAVG,EAVGA,RMS,IN,
     *                 OUT,TXT,SPC)

            CALL IO(TXT,DUM,'Corr.by Nikov and Delmas (1987)           ')

            CALL ERROR(N,SHO,SH2,PRT,EMIN,EMAX,EAVG,EAVGA,RMS,IN,OUT,
     *                 TXT,SPC)

            CALL IO(TXT,DUM,'Corr. by Ermakova et al. (1988)           ')

            CALL ERROR (N,SHO,SH3,PRT,EMIN,EMAX,EAVG,EAVGA,RMS,IN,
     *                 OUT,TXT,SPC)

            CALL IO(TXT,DUM,'Corr. by Fukuma et al. (1988)             ')


            CALL ERROR (N,SHO,SH4,PRT,EMIN,EMAX,EAVG,EAVGA,RMS,IN,
     *                 OUT,TXT,SPC)
```

```
      CALL IO(TXT,DUM,'2ND Corr. by Arters and Fan (1987)          ')

      CALL ERROR (N,SH0,SH5,PRT,EMIN,EMAX,EAVG,EAVGA,RMS,IN,
     *            OUT,TXT,SPC)

      STOP
      END


      SUBROUTINE ERROR(N,EXP,CALC,PRT,EMIN,EMAX,EAVG,EAVGA,RMS,
     *  IN,OUT,TXT,SPC)
C**********************************************************************
C* computes various errors between two files (calc. and exptl. values)
C**********************************************************************
C* INPUT
C* n     number of points to compare
C* exp   table of experimental values
C* calc  table of calc values
C* prt   if 1.0 ,then values are displayed by subroutine (printed if out
C* ='0') in,out,txt,spc standard io parameters
C**********************************************************************
C* OUTPUT
C* emin  minimum relative error (%)
C* emax  maximum relative error (%)
C* eavg  average relative error (%)
C* eavga average of abs (relative errors), %
C* rms   square root of (relative errors) **2, %
C**********************************************************************

      CHARACTER IN, OUT, SPC, TXT

      DIMENSION EXP(50), CALC(50)

      S = 0.
      SA = 0.
      S2 = 0.
      XN = FLOAT (N)
      EMAX = -1.E30
      EMIN = 1.E30

      DO 1 I = 1, N
      ER = (CALC(I)/EXP(I) - 1.)*100.
      EMIN = AMIN1(EMIN,ER)
      EMAX = AMAX1(EMAX,ER)
      S=S+ER
      SA=SA+ABS(ER)
      S2=S2+ER*ER

1     CONTINUE

      EAVG = S/XN
      EAVGA = SA/XN
      RMS = SQRT(S2)/XN

      IF (PRT .EQ. 1.) THEN
       CALL IO(OUT,EAVG,'average relative error, %                 ')
       CALL IO(OUT,EAVGA,'average abs (relative error), %          ')
       CALL IO(OUT,RMS,'root mean square of errors,%               ')
       CALL IO(OUT,EMIN,'minimum relative error, %                 ')
       CALL IO(OUT,EMAX,'maximum relative error,%                  ')
       CALL IO(SPC,1.,'  ')
      END IF

      RETURN
```

```
$USES UIO IN IO.CODE
      PROGRAM PORBUB
C*****************************************************************
C   This  program calculates bubble diameter formed  at  the
C   porous dist. using model of Bowonder and Kumar in Chem.
C   Eng. Sci., 1970 vol. 25, p. 25-32
C   Warning: CGS Units
C*****************************************************************

C  VALUES OF CONSTANTS
             G=981.0
             PI=3.1416
             DL=1.045
             VL=0.0098
             D=0.0035

     CALL IO('I',DC, 'COLUMN ID (CM)                          ')
     CALL IO('I',DP,'POROUS PLATE DIAMETER (CM)               ')
     CALL IO('S',1.,' ')

6    CONTINUE
     CALL IO('I',VG,'SUPF. GAS VELOCITY (CM/S)                ')
            NMAX = 200

* WARNING: Next line valid only if porous occupies the whole
* column section
             Q1=PI*DC*DC*VG/4.
             RN1=100.
5            Q=Q1/RN1
             IFLAG=-1
             START=.04
             STEP=.001
             EPS=.1E-5
  CALL EONOR2(START,STEP,EPS,NMAX,VE,RE,Q,A,C,G,VE,FMIN,IFLAG)

  RE=(VE*3./(4.*PI))**.33
  A=.321*RE/Q+1.
  B=1426.9/Q
  C=1.1*D/Q
  G=0.0338
  IFLAG=1
  START=1.5
  STEP=.15
 CALL EONOR2(START,STEP,EPS,NMAX,VF,RE,Q,A,B,C,G,VE,FMIN,IFLAG)
  A1=PI*DP**2/4.
  RN2=(A1/(.75*VF/PI)**.67)/3.464
  DN=ABS(RN1-RN2)
    IF(DN.LT.1.)THEN
    CALL IO('O',VF,'FINAL BUBBLE VOL.,CM3                    ')
    DB=(6./PI*VF)**.33333
    CALL IO('O',DB,'FINAL BUBBLE DIA, CM                     ')
    CALL IO('O',RN2,'NUMBER OF ACTIVE SITES,                 ')
    ELSE
    RN1=RN2
```

```
          GO TO 5
          END IF
          GO TO 6
          STOP
          END


        SUBROUTINE EONOR2 (START,STEP,EPS,NMAX,XMIN,RE,Q,A,B,C,G,
      * VE,FMIN,IFLAG)

C*********************************************************************
C  finds the x value xmin which minimizes the function funct(x)
C*********************************************************************
C  uses a success-failure linear search with parabolic inverse
C  interpolation (see Nash J.C.,"compact numerical methods for
C  computers: linear algebra and function minimization", Adam
C  Hilger Ltd., Bristol, 1979, 126-30
C*********************************************************************
C  INPUT:
C         start:  starting value of x
C         step:   initial step length (for x) (can be negative to
C                 start search in othe rdirection)
C         eps:    required precision on x, i.e. required minimum
C                  value of the x step
C         nmax:   maximum number of function evaluations
C*********************************************************************

        NFUNEV=0
        A1 = 1.5
        A2 = -0.25
        BIG = 1.E25
        X = START

1       CONTINUE
        NFUNEV = NFUNEV + 1
        F = FUNCT (X,VE,VF,RE,Q,A,B,C,G,IFLAG)

2       CONTINUE
        STEP2 = STEP1 + STEP
        X = XMIN + STEP2

4       CONTINUE
        IF (ABS(STEP) .LE. EPS) THEN
        FMIN = FUNCT(XMIN,VE,VF,RE,Q,A,B,C,G,IFLAG)
        RETURN
        END IF

        IF (NFUNEV .GT. NMAX) THEN
        WRITE(*,121) 'MAX NUMBER OF FUNCTION EVALUATIONS REACHED'
121       FORMAT(A$)
          RETURN
         END IF

5        CONTINUE
```

```
      NFUNEV = NFUNEV + 1
      F = FUNCT(X,VE,VF,RE,Q,A,B,C,IFLAG)

 6    CONTINUE
      IF (F.LT.F1) GO TO 10

 7    CONTINUE
      IF (FO .GE. F1) GO TO 11
 8    CONTINUE
      FO = F
      STEPO = STEP2

 9    CONTINUE
      STEP = A2 * STEP
      GO TO 3

 10   CONTINUE
      STEPO = STEP1
      FO = F1
      STEP1 = STEP2
      F1 = F
      STEP = A1*STEP
      GO TO 3

 11   CONTINUE
      STEPO = STEPO - STEP1
      FO = (FO - F1)*STEP
      F = (F-F1)*STEPO

 12   CONTINUE
      IF (ABS(F-FO) .LT. 1.E-20) GO TO 18

 13   CONTINUE
      STEP = 0.5*(F*STEPO - FO*STEP)/(F - FO)

 14   CONTINUE
      STEP2 = STEP1 + STEP
      X = XMIN + STEP2

 15   CONTINUE
      IF (ABS(XMIN + STEP1 - X) .LT. 1. E-25) GO TO 20

 16   CONTINUE
      NFUNEV = NFUNEV + 1
      F = FUNCT(X,VE,VF,RE,Q,A,B,C,G,IFLAG)

 17   CONTINUE
      IF (F .LT. F1) GO TO 19

 18   CONTINUE
      X = XMIN + STEP1
      F = F1
      GO TO 20
```

```
10      CONTINUE
        STEP1 = STEP2

20      CONTINUE
        STEP = STEP*A2
        GO TO 2

        RETURN
        END

        FUNCTION FUNCT(X,VE,VF,RE,Q,A,B,C,G,IFLAG)
        IF(IFLAG.LT.0.)THEN
        VE = X
           CALL IO('o',VE,'ve                                          ')
        IF (VE .LE. 1.E-10) THEN
        FUNCT = (10. - VE)*1.E10
        RETURN
        ENDIF
        FUNCT = VE**1.67-.485E-4*Q*Q+.245E-4*Q*VE**.33+.78E-3*VE
     # **.67
        FLSE
        VF=X

        IF (VF .LE. 1.E-10) THEN
           FUNCT = (10. - VF)*1.E10
           RETURN
           ENDIF

          FUNCT=RE-B*(VF**2-VE**2)/(2.*Q*(A+1))-C*(VF-VE)/(A*Q)
     *    -3.*G*(VF**.67-VE**.67)/(2*Q*(A-.33))
          ENDIF
          FUNCT = FUNCT*FUNCT
          RETURN
          END
```

```
$DEBUG
      SUBROUTINE AMEAT( DCO2, DO2, DOH, XK2, CO2SOL, VG, EPSG, HLPURE,
     1OHBEG, PHEND, TEND, XKLAO2, YCO2IN, CO3END, A, AROUGH, EMIN,
     2DBS, UBS, DBL, UBL, STS, XS, STL, XL, EAVG, CO2MAX, OHRMIN,
     3COR, CINST, TLIM)
C*************************************************************************
C for testing the sensitivity of the experimental technique
C determines the final dissolved carbonate concentration
C  for carbon dioxide absorption in a caustic solution, from an assumed
C  interfacial area.
C uses special method which does not have to meet usual requirements
C  (see clb memos 87 12 17 and 89 03 16)
C*************************************************************************
C INPUT
C dco2   molecular diffusivity of carbon dioxide in the liquid
C do2    molecular diffusivity of oxygen in the liquid
C doh    molecular diffusivity of oh- ions in the liquid
C xk2    true second order kinetic rate constant for reaction
C             co2 + 2 oh- = co3-- + h2o
C             WARNING: this assumes that the ph is high enough to preven
C                      the formation of hco3-
C co2sol solubility of carbon dioxide in the solution (warning: si units
C           mole/m3 for a partial pressure of carbon dioxide of 1 atm)
C vg    superficial gas velocity
C epsg  gas holdup
C hlpure  height of pure liquid in the column, i.e. height of liquid in
C                absence of gas
C ohbeg concentration of oh- ions at the beginning of the experiment, mo
C tend  experiment duration
C xklao2   volumetric mass transfer coefficient for oxygen (as determine
C            by desorption experiments)
C yco2in    mole fraction of co2 in inlet gas
C a     interfacial area per unit of column volume
C dbs   diameter of smallest bubbles
C ubs   velocity of smallest bubbles
C dbl   diameter of largest bubbles
C ubl   velocity of largest bubbles
C cor   correction for concentration of carbon dioxide in bulk liquid
C          (if cor = 'YES   ', then this correction will be made)
C cinst selection of method for calculation of enhancement factor
C         'FILM  ': film theory (but surface renewal theory is still use
C                   get the actual enhancement factor from the enhanceme
C                   factor for an instantaneous reaction
C         'SURREN': surface renewal theory
C*************************************************************************
C OUTPUT
C phend ph of solution at the end of experiment
C emin   minimum value of enhancement factor
C co3end   final concentration of dissolved carbonate
C sts    stanton number for smallest bubbles (at start)
C xs     conversion at start of experiment for smallest bubbles
C stl    stanton number for largest bubbles (at start)
C xl     conversion at start of experiment for largest bubbles
C eavg   average enhancement factor
C co2max maximum concentration of dissolved co2 in the bulk liquid
C ohrmin minimum value of the ratio of the concentration of oh-
C         at the gas-liquid interface to its concentration in the bulk l
C tlim   time for which ph drops below 11 (then, hco3 formation
C                                                      becomes signif
C*************************************************************************
```

```
*  WARNING: assumes no carbonate in the initial solution
*************************************************************************
      CHARACTER*6 COR, CINST
*     assuming a total pressure of 1 atm and a temperature of 20 celsius
      CTOTAL = 1.013E5 / (8.32 * 293)
      CO2IN = YCO2IN * CTOTAL
*     kla for co2, assuming surface renewal theory
      XKLACO = XKLAO2 * SQRT(DCO2/DO2)
*     height of liquid-gas dispersion
      HDIS = HLPURE / (1. - EPSG)
*     concentration of dissolved co2 in bulk liquid
      CO2B = 0.

*     integrate over time
      TLIM = 1.E30
      EMIN = 1.E30
      OHRMIN = 1.E30
      CO2MX = 0.
      T = 0.
      NT = 100
      DT = TEND / FLOAT(NT)
      OH = OHBEG
      CO3 = 0.
      EAVG = 0.
      NEAVG = 0
      DO 1 I = 1, NT
        T = T + DT

*       initialize beta
        BETA = 1000.
*       integrate over height
        X = 0.
        NZ = 20
        DZ = HDIS / FLOAT(NZ)
        DZL = DZ * HL / HDIS
        ZL = 0.5 * DZL
        XINT3 = CO2SOL * 8.32 * 293 / 1.013E5
        XINT = DZ * XINT3 * XKLACO / VG
        XINT4 = YCO2IN * CO2SOL
        DO 2 J = 1, NZ
*         local saturated concentration of co2
          CO2STR = (1. -X) * XINT4
*         correction for pressure using the height of pure liquid
          CO2STR = CO2STR * (10.326 + ZL) / 10.326
          ZL = ZL + DZL
*         get enhancement factor
          CALL ENHANC( DCO2, DOH, XK2, XKLACO, A, OH, CO2STR, E,
     1BETA, EA, CINST)
          EAVG = EAVG + E
          NEAVG = NEAVG + 1
*         ratio of concentration of oh- at interface to concentration in
*          from Coursey et al.
          XINTT = EA - 1.
          OHRAT = (EA - E)
          OHRAT = OHRAT / XINTT
          OHRMIN = AMIN1(OHRMIN,OHRAT)
          EMIN = AMIN1(EMIN,E)
          DX = XINT * E * (1. - X)

          IF (COR .EQ. 'YES   ') THEN
```

```
*           correction for the effect of co2 dissolved in bulk on driving
            DX = DX * (CO2STR - CO2B) / CO2STR
          ENDIF

          X = X + DX
2       CONTINUE
        DCO3 = DT * VG * X * CO2IN / HLPURE
        CO3 = CO3 + DCO3
        DOH = - 2. * DCO3
        OH = OH + DOH
*       test whether ph dropped below 11, but keep t for FIRST time ph d
*        (note: oh is in moles/m3, not moles/liter)
        IF ((OH .LT. 1.) .AND. (TLIM .GT. 1.E29)) THEN
          TLIM = T
          CALL WARN('o','PH<11, RESULTS ARE NOT ACCURATE.              ')
        ENDIF
*       maximum value of dissolved co2 in the bulk (assuming that no rea
*         occurs in the film, but still assuming that the reaction in th
*         enhances the mass transfer: truly a worst case!)
        CO2MX = VG * CO2IN * X / (HLPURE * OH * XK2)
        CO2B = CO2MAX
        CO2MAX = AMAX1(CO2MX, CO2MAX)

1     CONTINUE
      CO3END = CO3
      OHEND = OH
      IF (OHEND .LE. 0.) THEN
        PHEND = 0.
       ELSE
*       note: oh is in moles/m3, not moles/liter
        PHEND = 14. + ALOG10(OHEND/1000)
      ENDIF

      CALL IO('o',OHRMIN,'minimum value of oh- ratio                ')
*     average enhancement factor
      EAVG = EAVG / FLOAT(NEAVG)
*     calculation of Schumpe's criterion (Schumpe A., Deckwer W.D., Chem
*      Eng. Sci., 35, 19809, 2221-2233
*     note that this criterion is not perfect since it assumes that Danc
*      conditions are verified.

*     take average oh- concentration, not the worse case!
*     (worse case approach would be to use largest oh- concentration,
*       i.e. at start of experiment)
*     pseudo-first order kinetic rate constant for average oh- concentra
      OH = 0.5 * (OHBEG + OHEND)
      XK1 = XK2 * OH
*     assume a temperature of 20 Celsius
      RT = 8.32 * 293
      HENRY = 1.013E5 / CO2SOL
      XKK1 = SQRT(XK1*DCO2) / HENRY
*     smallest bubbles
      TAUS = HDIS / UBS
      STS = XKK1 * RT * 6. * TAUS / DBS
      XS = 1 - EXP(-STS)
*     largest bubbles
      TAUL = HDIS / UBL
      STL = XKK1 * RT * 6. * TAUL / DBL
      XL = 1 - EXP(-STL)

      RETURN
      END
```

Appendix 24

Tabulated raw data

Batch Bubble Column:

Gas Holdup Data: Liquid: 30 vppm MIBK Solutions Gas: Air

Dist.: PR1		Dist.: PR2		Dist.: PR3		Dist.: SP1		Dist.: SP2	
V_g (m/s)	ϵ_g	V_g (m/s)	ϵ_g	V_g (m/s)	ϵ_g	V_g (m/s)	ϵ_g	V_g (m/s)	ϵ_g
0.033	0.195	0.029	0.15	0.028	0.107	0.03	0.094	0.028	0.065
0.046	0.28	0.044	0.23	0.038	0.114	0.045	0.13	0.0445	0.089
0.056	0.373	0.05	0.24	0.05	0.12	0.051	0.136	0.051	0.097
0.061	0.42	0.06	0.228	0.06	0.122	0.061	0.148	0.06	0.118
0.071	0.48	0.076	0.203	0.075	0.13	0.09	0.183	0.089	0.154
		0.087	0.197	0.0975	0.16	0.102	0.186	0.098	0.164
		0.10	0.195			0.117	0.205	0.116	0.18
		0.107	0.204						

Batch Bubble Column:

Gas Holdup Data: Liquid: Tap Water Gas: Air

Dist.: PR1		Dist.: PR2		Dist.: PR3		Dist.: SP1		Dist.: SP2	
V_g (m/s)	ϵ_g	V_g (m/s)	ϵ_g	V_g (m/s)	ϵ_g	V_g (m/s)	ϵ_g	V_g (m/s)	ϵ_g
0.031	0.14	0.02	0.1	0.015	0.064	0.03	0.076	0.03	0.063
0.04	0.2	0.03	0.136	0.025	0.093	0.04	0.096	0.037	0.075
0.05	0.23	0.043	0.167	0.04	0.103	0.05	0.11	0.045	0.085
0.072	0.29	0.05	0.17	0.05	0.105	0.06	0.124	0.055	0.098
0.086	0.35	0.073	0.16	0.057	0.106	0.07	0.134	0.061	0.106
0.104	0.38	0.098	0.162	0.073	0.125	0.08	0.135	0.078	0.121
0.126	0.388	0.117	0.178	0.088	0.135	0.09	0.144	0.089	0.132
0.148	0.41			0.1	0.15	0.1	0.154	0.1	0.14
0.168	0.39					0.11	0.167	0.112	0.148
0.194	0.36							0.118	0.153

Batch Bubble Column:

Gas-Liquid Mass Transfer Data: Liquid: Tap Water Gas: Air/N_2

Dist.: PR1			Dist.: PR2			Dist.: PR3			Dist.: SP1			Dist.: SP2		
V_g (m/s)	k_la (s^{-1})	. P (kPa)	V_g (m/s)	k_la (s^{-1})	. P (kPa)	V_g (m/s)	k_la (s^{-1})	. P (kPa)	V_g (m/s)	k_la (s^{-1})	. P (kPa)	V_g (m/s)	k_la (s^{-1})	. P (kPa)
0.028	0.058	6.57	0.029	0.053	8.43	0.0274	0.038	9.99	0.03	0.0296	7.15	0.0296	0.019	6.49
0.0445	0.079	5.65	0.043	0.07	8.5	0.036	0.039	10.68	0.04	0.031	7.24	0.037	0.025	6.68
0.07	0.102	5.78	0.05	0.072	8.6	0.044	0.0387	10.95	0.05	0.034	7.33	0.045	0.03	6.84
0.091	0.096	5.4	0.073	0.065	9.11	0.05	0.04	10.6	0.06	0.0385	7.45	0.055	0.033	7.0
0.107	0.1	5.5	0.089	0.065	9.5	0.057	0.0402	9.7	0.07	0.042	7.6	0.061	0.035	7.14
0.116	0.092	5.42	0.098	0.0653	9.8	0.0725	0.044	10.19	0.08	0.043	7.78	0.078	0.041	7.22
			0.1173	0.069	10.3	0.088	0.052	10.63	0.09	0.05	7.96	0.089	0.047	7.43
						0.0992	0.055	10.78	0.10	0.059	8.16	0.103	0.052	7.95
									0.11	0.062	8.4	0.112	0.055	8.1
												0.1184	0.061	8.28

Batch Bubble Column:

Gas-Liquid Mass Transfer Data: Liquid: 30 vppm MIBK Solution Gas: Air/N_2

Dist.: PR1		Dist.: PR2		Dist.: PR3		Dist.: SP1		Dist.: SP2	
V_g (m/s)	k_la (s^{-1})	V_g (m/s)	k_la (s^{-1})	V_g (m/s)	k_la (s^{-1})	V_g (m/s)	k_la (s^{-1})	V_g (m/s)	k_la (s^{-1})
0.03	0.102	0.029	0.09	0.028	0.058	0.03	0.037	0.028	0.027
0.044	0.09	0.044	0.091	0.038	0.062	0.045	0.054	0.0445	0.04
0.046	0.099	0.05	0.092	0.049	0.067	0.051	0.062	0.05	0.049
0.052	0.094	0.06	0.095	0.059	0.074	0.061	0.07	0.062	0.062
0.0645	0.09	0.076	0.096	0.075	0.088	0.089	0.092	0.089	0.092
		0.087	0.096			0.102	0.099	0.098	0.102
		0.1	0.099			0.117	0.10	0.1155	0.119
		0.117	0.1						

Batch Bubble Column:

Gas-Liquid Mass Transfer; Effect of different additives

Additive Conc.: 50 ppm; Gas Velocity: 0.065 m/s

Additive	Dist.: PR2		Dist.: SP1	
	k_la	ϵ_g	k_la	ϵ_g
Methyl Alcohol	0.082	0.173	0.058	0.118
Propanol	0.092	0.179	0.043	0.105
Butanol	0.104	0.214	0.057	0.12
Iso-Butanol	0.093	0.200	0.057	0.114
1-Pentanol	0.105	0.24	0.073	0.14
Iso-Amyl Alcohol	0.109	0.236	0.08	0.146
Ter-Amyl Alcohol	0.11	0.24	0.085	0.145
Acetone	0.092	0.19	0.063	0.13
MEK	0.096	0.20	0.068	0.127
MIBK	0.107	0.25	0.085	0.156
Di-isopropyl ether	0.077	0.155	0.05	0.106
Formaldehyde	0.083	0.174	0.055	0.128
Benzaldehyde	0.09	0.17	0.056	0.116
Hexanal	0.055	0.127	0.037	0.105
Cyclohexanone	0.107	0.25	0.07	0.138
2-hexanone	0.11	0.23	0.074	0.148
3-hexanone	0.103	0.22	0.083	0.157

Batch Bubble Column:

Gas-Liquid Mass Transfer; Effect of different additives

Additive Conc.: 50 ppm; Gas Velocity: 0.065 m/s

Additive	Dist.: PR2		Dist.: SP1	
	$k_l a$	ϵ_g	$k_l a$	ϵ_g
Acetophenone	0.078	0.174	0.056	0.127
Triethyl Amine	0.068	0.144	0.05	0.12
Hexanoic Acid	0.097	0.19	0.053	0.11
Cetric Acid	0.072	0.15	0.05	0.12
Adipic Acid	0.082	0.18	0.054	0.12
Benzoic Acid	0.055	0.12	0.036	0.09

Batch Bubble Column:

Gas-Liquid Mass Transfer; Effect of different additives

Additive Conc.: 50 ppm; Gas Velocity: 0.125 m/s

Additive	Dist.: PR2		Dist.: SP1	
	k_la	e_g	k_la	e_g
Methyl Alcohol	0.086	0.18	0.088	0.17
Propanol	0.08	0.17	0.066	0.168
Butanol	0.107	0.198	0.086	0.176
Iso-Butanol	0.1	0.19	0.09	0.186
1-Pentanol	0.114	0.21	0.114	0.194
Iso-Amyl Alcohol	0.115	0.22	0.112	0.197
Ter-Amyl Alcohol	0.118	0.21	0.113	0.213
Acetone	0.084	0.179	0.09	0.18
MEK	0.096	0.19	0.098	0.18
MIBK	0.12	0.21	0.117	0.21
Di-isopropyl ether	0.07	0.168	0.077	0.176
Formaldehyde	0.082	0.184	0.082	0.183
Benzaldehyde	0.086	0.177	0.086	0.173
Hexanal	0.065	0.166	0.058	0.166
Cyclohexanone	0.112	0.21	0.096	0.196
2-hexanone	0.113	0.21	0.116	0.21
3-hexanone	0.114	0.20	0.115	0.197

Batch Bubble Column:

Gas-Liquid Mass Transfer; Effect of different additives

Additive Conc.: 50 ppm; Gas Velocity: 0.125 m/s

Additive	Dist.: PR2		Dist.: SP1	
	$k_l a$	ϵ_g	$k_l a$	ϵ_g
Acetophenone	0.084	0.186	0.086	0.177
Triethyl Amine	0.066	0.172	0.084	0.174
Hexanoic Acid	0.10	0.20	0.078	0.186
Cetric Acid	0.075	0.177	0.076	0.173
Adipic Acid	0.078	0.18	0.09	0.174
Benzoic Acid	0.065	0.159	0.064	0.15

Batch Bubble Column:

Gas-Liquid Mass Transfer; Effect of different additives

Additive Conc.: 5 ppm; Gas Velocity: 0.125 m/s

Additive	Dist.: PR2		Dist.: SP1	
	k_la	ϵ_g	k_la	ϵ_g
Butanol	0.09	0.185	0.076	0.178
Iso-Amyl Alcohol	0.11	0.195	0.118	0.19
Ter-Amyl Alcohol	0.10	0.192	0.102	0.188
MIBK	0.095	0.194	0.076	0.18
Cyclohexanone	0.084	0.184	0.085	0.17
2-hexanone	0.095	0.19	0.09	0.18
3-hexanone	0.096	0.184	0.073	0.183

Batch Bubble Column:

Gas-Liquid Mass Transfer; Effect of different additives

Additive Conc.: 5 ppm; Gas Velocity: 0.065 m/s

Additive	Dist.: PR2		Dist.: SP1	
	k_la	ϵ_g	k_la	ϵ_g
Butanol	0.096	0.194	0.06	0.123
Iso-Amyl Alcohol	0.104	0.192	0.077	0.132
Ter-Amyl Alcohol	0.10	0.19	0.065	0.132
MIBK	0.095	0.183	0.07	0.137
Cyclohexanone	0.087	0.183	0.056	0.116
2-hexanone	0.1	0.197	0.06	0.126
3-hexanone	0.096	0.184	0.06	0.123

Batch Bubble Column:

Gas-Liquid Mass Transfer; Effect of different additives

Additive Conc.: 200 ppm; Gas Velocity: 0.125 m/s

Additive	Dist.: PR2		Dist.: SP1	
	k_la .	ϵ_g .	k_la .	ϵ_g .
Methyl Alcohol	0.084	0.184	0.084	0.176
Propanol	0.123	0.20	0.113	0.20
Iso-Butanol	0.11	0.214	0.105	0.21
Acetone	0.078	0.185	0.08	0.18
MEK	0.11	0.21	0.113	0.195
Di-isopropyl ether	0.074	0.175	0.076	0.171
Formaldehyde	0.07	0.168	0.072	0.164
Benzaldehyde	0.129	0.22	0.12	0.21
Hexanal	0.054	0.157	0.05	0.176
Acetophenone	0.114	0.21	0.104	0.20
Triethyl Amine	0.106	0.19	0.11	0.195
Hexanoic Acid	0.1	0.188	0.094	0.18
Cetric Acid	0.074	0.163	0.082	0.16
Adipic Acid	0.088	0.186	0.09	0.185

Batch Bubble Column:

Gas-Liquid Mass Transfer; Effect of different additives

Additive Conc.: 200 ppm; Gas Velocity: 0.065 m/s

Additive	Dist.: PR2		Dist.: SP1	
	k_la .	ϵ_g .	k_la .	ϵ_g .
Methyl Alcohol	0.092	0.20	0.058	0.125
Propanol	0.115	0.23	0.072	0.127
Iso-Butanol	0.112	0.23	0.072	0.14
Acetone	0.075	0.19	0.055	0.125
MEK	0.112	0.23	0.076	0.144
Di-isopropyl ether	0.074	0.133	0.068	0.13
Formaldehyde	0.066	0.137	0.049	0.107
Benzaldehyde	0.125	0.24	0.096	0.156
Hexanal	0.036	0.11	0.032	0.105
Acetophenone	0.115	0.257	0.076	0.13
Triethyl Amine	0.097	0.18	0.08	0.156
Hexanoic Acid	0.11	0.19	0.065	0.12
Cetric Acid	0.073	0.13	0.052	0.1
Adipic Acid	0.083	0.197	0.052	0.125

Continuous Bubble Column:

Gas-Liquid Mass Transfer and Phase Holdup data:

Column ID: 0.08 m Dist.: SP1

Liquid: Tap Water				Liquid: 30 vppm isoamyl alcohol solution			
V_l (m/s)	V_g (m/s)	ϵ_g	k_la (s^{-1})	V_l (m/s)	V_g (m/s)	ϵ_g	k_la (s^{-1})
0.037	0.03	0.072	0.02	0.037	0.03	0.081	0.028
0.037	0.04	0.084	0.027	0.037	0.04	0.089	0.04
0.037	0.048	0.082	0.033	0.037	0.048	0.105	0.05
0.037	0.062	0.087	0.037	0.037	0.062	0.118	0.057
0.037	0.078	0.105	-	0.037	0.078	0.133	0.069
0.048	0.03	0.075	0.026	0.048	0.03	0.079	0.028
0.048	0.04	0.076	0.034	0.048	0.04	0.095	0.037
0.048	0.048	0.081	0.037	0.048	0.048	0.105	0.051
0.048	0.062	0.093	0.04	0.048	0.062	0.114	0.06
0.048	0.078	0.11	0.05	0.048	0.078	0.13	
0.057	0.03	0.068	0.03	0.057	0.03	0.064	0.038
0.057	0.04	0.078	0.035	0.057	0.04	0.086	0.04
0.057	0.048	0.085	0.043	0.057	0.048	0.104	0.053
0.057	0.062	0.09	0.047	0.057	0.062	0.117	0.067
0.057	0.078	0.112	0.05	0.057	0.078	0.132	0.08

Continuous Bubble Column:

Gas-Liquid Mass Transfer and Phase Holdup data:

Column ID: 0.08 m Dist.: PR2

Liquid: Tap Water				Liquid: 30 vppm isoamyl alcohol solution			
V_l (m/s)	V_g (m/s)	ϵ_g	k_la (s^{-1})	V_l (m/s)	V_g (m/s)	ϵ_g	k_la (s^{-1})
0.037	0.03	0.1	0.067	0.037	0.03	0.116	0.108
0.037	0.04	0.11	0.072	0.037	0.04	0.152	0.11
0.037	0.048	0.14	0.074	0.037	0.048	0.164	0.108
0.037	0.062	0.14	0.069	0.037	0.062	0.174	0.109
0.037	0.078		0.062	0.037	0.078	0.162	0.094
0.048	0.03	0.086	0.06	0.048	0.03	0.117	0.106
0.048	0.04	0.12	0.064	0.048	0.04	0.142	0.117
0.048	0.048	0.13	0.067	0.048	0.048	0.157	0.113
0.048	0.062	0.133	0.063	0.048	0.062	0.173	0.106
0.048	0.078	0.129		0.048	0.078	0.17	0.102
0.057	0.03	0.09	0.06				
0.057	0.04	0.1	0.065				
0.057	0.048	0.112	0.069				
0.057	0.062	0.123	0.064				
0.057	0.078	0.126					

Three Phase Fluidized Bed:

Gas-Liquid Mass Transfer and Phase Holdup data:

Column ID: 0.08 m d_p = 0.0052 m Gas Dist.: SP1

Liquid: Tap Water							Liquid: 30 vppm isoamyl alcohol Solution						
V_l (m/s)	V_g (m/s)	ϵ_g	ϵ_l	$C_{o,in}$ (moles/m^3)	$C_{o,out}$ (moles/m^3)	k_la (s^{-1})	V_l (m/s)	V_g (m/s)	ϵ_g	ϵ_l	$C_{o,in}$ (moles/m^3)	$C_{o,out}$ (moles/m^3)	k_la (s^{-1})
0.048	0.04	0.1	0.285	0.2875	0.206	0.069	0.048	0.04	0.186	0.29	0.2875	0.186	0.089
0.048	0.05	0.11	0.33	0.2937	0.209	0.07	0.048	0.05	0.2	0.28	0.275	0.168	0.1
0.048	0.062	0.113	0.332	0.2934	0.204	0.075	0.048	0.062	0.21	0.26	0.291	0.173	0.107
0.048	0.078	0.15	0.26	0.2934	0.202	0.078	0.048	0.078	0.24	0.235	0.283	0.162	0.114
0.057	0.03	0.088	0.33	0.2925	0.226	0.063	0.057	0.03	0.18	0.33	0.298	0.219	0.076
0.057	0.04	0.11	0.32	0.2925	0.219	0.07	0.057	0.04	0.206	0.31	0.298	0.204	0.093
0.057	0.05	0.113	0.318	0.293	0.203	0.09	0.057	0.05	0.23	0.295	0.299	0.192	0.108
0.057	0.062	0.115	0.32	0.292	0.196	0.098	0.057	0.062	0.24	0.3	0.3	0.182	0.123
0.057	0.078	0.142	0.31	0.292	0.185	0.112	0.057	0.078	0.29	0.29	0.296	0.169	0.138
0.0676	0.03	0.118	0.34	0.2975	0.246	0.054	0.0676	0.03	0.206	0.31	0.312	0.245	0.07
0.0676	0.04	0.122	0.338	0.2975	0.202	0.063	0.0676	0.04	0.24	0.33	0.313	0.23	0.09
0.0676	0.05	0.12	0.35	0.305	0.234	0.076	0.0676	0.05	0.25	0.32	0.29	0.192	0.103
0.0676	0.062	0.119	0.344	0.3	0.222	0.087	0.0676	0.062	0.24	0.31	0.279	0.18	0.12
0.0676	0.078	0.124	0.34	0.298	0.19	0.115	0.0676	0.078					

Three Phase Fluidized Bed:

Gas-Liquid Mass Transfer and Phase Holdup data:

Column ID: 0.08 m d_p = 0.0052 m Gas Dist.: PR2

Liquid: Tap Water						Liquid: 30 vppm isoamyl alcohol Solution					
V_l (m/s)	V_g (m/s)	ϵ_g	$C_{o,in}$ (moles/m^3)	$C_{o,out}$ (moles/m^3)	k_la (s^{-1})	V_l (m/s)	V_g (m/s)	ϵ_g	$C_{o,in}$ (moles/m^3)	$C_{o,out}$ (moles/m^3)	k_la (s^{-1})
0.057	0.03	0.083	0.305	0.263	0.04	0.057	0.03	0.139	0.286	0.225	0.064
0.057	0.04	0.13	0.314	0.253	0.058	0.057	0.04	0.174	0.293	0.219	0.079
0.057	0.05	0.15	0.313	0.251	0.06	0.057	0.05	0.187	0.287	0.21	0.084
0.057	0.062	0.145	0.309	0.243	0.064	0.057	0.062	0.226	0.29	0.207	0.09
0.057	0.078	0.16	0.309	0.228	0.082	0.057	0.078	0.226	0.29	0.201	0.1

Column ID: 0.08 m d_p = 0.0032 m Gas Dist.: SP1

Liquid: Tap Water							Liquid: 30 vppm isoamyl alcohol Solution						
V_l (m/s)	V_g (m/s)	ϵ_g	ϵ_l	$C_{o,in}$ (moles/m^3)	$C_{o,out}$ (moles/m^3)	k_la (s^{-1})	V_l (m/s)	V_g (m/s)	ϵ_g	ϵ_l	$C_{o,in}$ (moles/m^3)	$C_{o,out}$ (moles/m^3)	k_la
0.057	0.03	0.09	0.41	0.3075	0.26	0.041	0.057	0.03	0.17	0.31	0.29	0.226	0.061
0.057	0.04	0.092	0.4	0.307	0.242	0.058	0.057	0.04	0.158	0.34	0.292	0.225	0.064
0.057	0.05	0.1	0.39	0.3075	0.238	0.063	0.057	0.05	0.157	0.34	-	-	-
0.057	0.062	0.097	0.4	0.306	0.236	0.066	0.057	0.062	0.17	0.33	0.291	0.214	0.076
0.057	0.078	0.111	0.35	0.306	0.222	0.078	0.057	0.078	0.174	0.33	0.292	0.201	0.091

Three Phase Fluidized Bed:

Liquid-Solid Mass Transfer and Phase Holdup data:

Column ID: 0.17 m d_p = 0.0052 m Dist.: Direct Gas Jets

Liquid: Tap Water					Liquid: Benzoic Acid Solution (100 - 150 vppm)				
V_l (m/s)	V_g (m/s)	ϵ_g	ϵ_l	k_s (m/s)	V_l (m/s)	V_g (m/s)	ϵ_g	ϵ_l	k_s (m/s)
0.06	0.00	0.0	0.42	0.007	0.06	0.025	0.142	0.31	0.102
0.06	0.025	0.072	0.397	0.0076	0.06	0.05	0.209	0.281	0.124
0.06	0.05	0.084	0.4	0.0078	0.06	0.1	0.248	0.255	0.136
0.06	0.1	0.138	0.376	0.008	0.06	0.15	0.268	0.246	0.142
0.06	0.2	0.163	0.367	0.0084	0.06	0.3	0.322	0.21	0.143
0.048	0.1	0.15	0.348	0.0085					
0.068	0.2	0.196	0.322	0.0086					

Three Phase Fluidized Bed:

Liquid-Solid Mass Transfer and Phase Holdup data:

Column ID: 0.17 m d_p = 0.0052 m Dist.: Packed Bed Distributor

Liquid: Tap Water					Liquid: Benzoic Acid Solution (100 - 150 vppm)				
V_l (m/s)	V_g (m/s)	ϵ_g	ϵ_l	k_s (m/s)	V_l (m/s)	V_g (m/s)	ϵ_g	ϵ_l	k_s (m/s)
0.06	0.05	0.092	0.372	0.0087	0.06	0.025	0.156	0.3	0.01
0.06	0.1	0.141	0.356	0.0091	0.06	0.05	0.238	0.245	0.0129
0.06	0.15	0.146	0.343	0.0093	0.06	0.1	0.286	0.23	0.0141
0.06	0.20	0.173	0.341	0.0092	0.06	0.3	0.32	0.223	0.0143
0.06	0.3	0.196	0.33	0.0093					

Liquid: MIBK Solution (200 vppm)

V_l (m/s)	V_g (m/s)	ϵ_g	ϵ_l	k_s (m/s)
0.06	0.05	0.212	0.28	0.0114
0.06	0.3	0.34	0.22	0.014

REFERENCES

Achwal, S.K. and Stepanek, J.B., "An Alternative Method of Determining Holdup in Gas-Liquid Systems", Chem. Eng.Sci., Vol. 30, p.1443 (1975).

Adamson, W.R.,"Physical Chemistry of Surfaces", Interscience Publishers, New York (1964).

Ade Bello, R., C.W. Robinson, M. Moo-Young, "Prediction of the Volumetric Mass Transfer Coefficient in Pneumatic Contactors", Chem. Eng. Sci., Vol. 40, p. 53-58 (1985).

Adlington, D., and Thompson, "Desulphurization in Fixed Fixed and Fluidized Bed Catalyst System," Proc. 3rd European Symp. Cem. React. Eng., 203, Pergamon press, Oxford (1965).

Akita, K. and Yoshida F., "Gas Holdup and Volumetric Mass Transfer Coefficient in Bubble Columns", Ind. Eng. Chem, Proc. Des. Dev., Vol. 12, p.76-80, (1973).

Akita, K., and Yoshida F., "Bubble Size, Interfacial Area and Liquid Phase Mass Transfer Coefficients in Bubble Columns", Ind. Eng. Chem. Proc. Des. Dev., Vol. 13, p. 84-91 (1974).

Alexander, B.F., and Shah, Y.T., "Axial Dispersion Coefficient in Bubble Columns", Chem. Eng. J., Vol. 11, p.153 (1976).

Alper, E., Wichtendahl, B., Deckwer, W.D., "Gas Absorption Mechanism in Catalytic Slurry Reactors", Chem. Eng. Sci., Vol. 65, p. 217-22 (1980).

Alvarez-Cuenca, M., "Oxygen Mass Transfer in Bubble Columns", Ph.D Thesis, University of Western Ontario, London, Canada (1979).

Alvarez-Cuenca, M., C.G.J Baker and M.A. Bergougnou,"Oxygen Mass Transfer in Three-Phase Fluidized Beds Working at Large Flow rates," Can. J. Chem. Eng., Vol.61, p.58 (1983).

Alvarez-Cuenca, M.A. Nerenberg, A.A. Asfour, "Mass Transfer Effects Near the Distributor of Three-phase Fluidized Beds," Ind. Eng. Chem. Fund. Vol.23, p.381 (1984).

Anderson, J.L. and Quinn, J.A., "The Transition to Slug Flow in Bubble Columns," Chem. Eng. Sci., Vol. 25, p. 338-45 (1970).

Andrews, G.F., J.P. Fonta, E.Marrotta and P.Stroeve,"The Effect of Cells on Oxygen Transfer Coefficients: Cell Accumulation Around Bubbles", The Chem. Eng. J., Vol. 29, p. B39-B46 (1984).

Aoyama, Y., Ogushi, K., Koide, K., and Kubota, H., "Liquid Mixing in Cocurrent Bubble Column", J. of Chem. Eng. of Japan, Vol. 1, p. 158 (1968).

Argo, W.B., and Cova, D.R., "Longitudinal Mixing in Gas-Sparged Tubular Reactor", Ind. Eng. Proc. Des., Vol. 13, p.292 (1974).

Armstrong, E.R., C.G.J. Baker, M.A. Bergougnou, "The Effects of Solid Wettability on the Characteristics of Three-phase Fluidization" in Fluidization Technology, Ed. D.L. Keairns, Hemisphere Publishing Vol 1, p.405 (1976)

Armstrong, E.R,. Baker, C.G.J., M.A. Bergougnou, "Heat Transfer and Hydrodynamic Studies on Three-phase Fluidized beds", in Fluidization Technology, Ed. D.L.Keairns, Hemisphere publishing Vol.1, p.453 (1978)

Arters, D.C. and Fan, L-S., "Solid-liquid Mass Transfer in Gas-liquid-solid Fluidized Beds", Chem. Eng. Sci., 41, p.107-115, (1986).

Arters, D.C. and Fan, L-S., "On The Correlation of Liquid-solid Mass Transfer in Gas-liquid-solid fluidized beds", A shorter communication submitted to Chem. Eng.Sci. (1987)

Astarita, G., "Diffusivity in Non-newtonian Liquids", Ind. Eng. Chem. Fundumentals, Vol.4, p.236 (1965).

Bach, H.F. and Pilhofer T., "Variation of Gas Holdup in Bubble Columns with Physical Properties of Liquid and Operating Parameters of Columns", Ger. Chem. Eng. Vol. 1, p. 270-75 (1978).

Baird, M.H.I., Rice, R.G., "Axial Distribution in Large Unbaffled Columns", Chem. Eng. J., Vol. 9, p. 171-74 (1975).

Baker, C.G.J., Kim, S.D., and Bergougnou, M.A., "Wake Characteristics of Three-Phase Fluidized Beds", Powder Technol., Vol. 18, p.201 (1977)

Baker, C.G.J., Armstrong, E.R., M.A.Bergougnou, "Heat Transfer in Three-phase Fluidized Beds", Powder Techn.,Vol.21, p.195 (1978).

Ballesteros, R. L., Riba, J.P. and Couderc, J.P., "Dissolution of Non-spherical particles in Solid-liquid Fluidization", Chem. Eng. Sci.,Vol.37, p.1639 (1982).

Begovich, J.M., and J.S. Watson, "Hydrodynamic Characteristics of Three-phase Fluidized beds" in "Fluidization", Ed. J.F.Davidson, D.L.Keairns, Cambridge Univ. Press, p.190, (1978a).

Begovich, J.M., and J.S. Watson, " An Electroconductivity Technique for the Measurement of Axial variation of Hold-ups in Three-phase Fluidized beds", AIChE J. Vol. 24,p.351,(1978b).

Berger, F.P., and Ziai, A., "Optimization of Experimental Conditions for Electrochemical Mass Transfer Measurements", Chem. Eng. Res. Des., Vol. 61, p.377-82 (1983)

Berk, D., L.A.Behie, A.Jones, B.H.Lesser, G.M.Gaucher "The Production of the Antibiotic Patulin in a Three-phase Fluidization Bed Reactor: Effect of Medium Composition ", Can. J. of Chem. Eng., Vol. 62, p.112 (1984a).

Berk, D., L.A.Behie, A.Jones, B.H.Lesser, G.M.Gaucher, "The Production of the Antibiotic Patulin in a Three-phase Fluidized Bed Reactor : Longivity of the Biocatalyst", Can. J. of Chem. Eng. Vol. 62, p.120 (1984b).

Bhatia, V.K., K.A.Evans, N.Epstein, "Effects of Solids Wettabilty on Expansion of Gas-liquid Fluidized Beds", Ind. Eng. Chem. Proc. Des. Dev., Vol.11, p.151 (1972).

Bhatia, V.K., and N. Epstein, "Three-phase Fluidization: A Generalized Wake Model", H. Angelino Eds., Cepadues-Editions, Toulouse, 372, (1974).

Bhavaraju, S.M., Russell, T.W.F. and Blanch, H.W., "The Design of Gas Sparged Devices for Viscous Liquid Systems", AIChE J.,Vol. 24, p. 454-66 (1978).

Bird, R.B., Stewart, W.E., and Lightfoot, E.N., "Transport Phenomena, New York, John Wiley and Sons Inc. (1960).

Blum,D.B.,and J.J.Toman, "Three-Phase Fluidization in a Liquid Methanator", AIChE symp. ser. No. 161, Vol.74, 115, (1977).

Bohm, U., "Maximum Mass Transfer to the Wall or Immersed Objects in Liquid Fluidized Bed", Ind. Eng. Chem. Proc. Des. Dev., Vol. 22, p. 339-41 (1983).

Botton, R. and Cosserat,D., "Influence of Column Diameter and High Gas Throuputs on the Operation of a Bubble Column", The Chem. Eng. Journal, Vol. 16 p. 107-15 (1978).

Bouman,H., C.W.J. Van Koppen and L.J. Raas,"Some Investigations of the influence of the heat flux on flow pattern in vertical boiler tubes", European Two-Phase Flow Group Meeting Harwell, paper A2 June 1974.

Bowonder, B. and Kumar R., "Studies in Bubble Formation - IV: Bubble Formation at Porous Discs", Chem. Eng. Sci., Vol. 25, p. 25-32 (1970).

Brian, P.L.T., Vivian, J.E., Mayr, S.T.,"Cellular Convection in Desorbing Surface Tension Lowering Solutes from Water", Ind. Eng. Chem. Fundam., Vol. 10, p.75 (1971).

Saberian-Broudjenni, M., Wild, G., Charpentier J.C., Fortin, Y., Euzen, J.P. and Patoux, R., "Contributions to the Hydrodynamic Study of Gas-Liquid-Solid Fluidized Bed Reactors", Int. Chem. Eng. Vol. 27, p.423-40, (1987)

Bruce, P.N. and Revel-Chion, L., "Bed Porosity in Three-Phase Fluidized Bed", Powder Technology, Vol. 10 p. 243-(1974).

Bruck, F.J., and H. Hammer, " Intensification of Mass Transfer in Bubble Column Reactors by Suspended Solids", Ger. Chem. Eng., Vol. 9, p. 382-90 (1986).

Buchholz, R., Zakrzewski, W., and Schuegerl, K., "Techniques for Determining the Properties of Bubbles in Bubble Columns", Int. Chem. Eng., Vol. 21, p. 180 (1981).

Buchholz, R., Tsepetonides J., Steinemann J. and Onken U., "Influence of Gas Distribution on Interfacial Area and Mass Transfer in Bubble Columns", Ger. Chem. Eng., Vol. 6, p.105-13, (1983).

Bukur, D.B., S.A.Patel and R. Mahheo, "Hydrodynamics Studies in Fischer Tropsch Derived Waxes in a Bubble Column", Chem. Eng. Comm., Vol. 60, p. 63-78 (1987).

Burckhart, R. and Deckwer, W.D., "Bubble Size Distribution and Interfacial Areas of Electrolyte Solutions in Bubble Columns", Chem. Eng. Sci., Vol. 30, p. 351 (1975).

Burgess, J.M. and Calderbank, P.H., "Bubble Size Distribution and Interfacial areas of Electrolyte Solutions in Bubble Columns", Chem. Eng. Sci., Vol. 30, p. 1107 (1975).

Burru, I.G., "Particle-Liquid Mass Transfer in Two and Three-Phase Fluidized Beds", MESc Thesis, University of Western Ontario, Canada (1988).

Burru, I.G., and Briens, C.L., "Particle-Liquid Mass Transfer in Three-Phase Fluidized Beds at High Velocities and with Non-Newtonian Liquids", Accepted for Publication at the 6th International Fluidization Confrence, Banff Alberta, Canada, May 7-12, (1988)

Calderbank, P.H., Trans. Inst. Chem. Engrs., Vol. 36, p. 443 (1958).

Calderbank, P.H., and M.B. Moo-Young, "The Continuous Phase Heat and Mass Transfer Properties of Dispersions", Chem. Eng. Sci., Vol. 16, p. 39-54 (1961).

Carleton, A.J., Flair, R.J., Rennie, J., and Valentin, F.H.H., "Some Properties of Packed Bubble Columns", Chem. Eng. Sci., Vol. 22, p. 1839 (1967).

Catros, A., Bernard, J.R., Briens, C.L., and Bergougnou, M.A., "Generalized Model for Gas-Liquid Mass Transfer in Three-Phase Fluidized Beds With and Without Horizontal Baffles", Powder Technology, Vol. 44, p. 159-68 (1985).

Catros, A. "Hydrodynamics and Mass Transfer in Bubble Columns and Three-phase Fluidized Beds With and Without Baffles", Ph. D. Thesis, University of Western Ontario, London (Canada), (1986).

Chang, S., "Determination of Diffusion Coefficients in Aqueous Solutions", M.S. Thesis, M.I.T. (1949).

Chang, S.K., Kang, Y., and Kim, S.D., "Mass Transfer in Two- and Three-Phase Fluidized Beds", J. of Chem. Eng. of Japan, Vol. 19, p.524-30 (1986).

Chen, J.J.J., "Comments on Improved Equation for the Calculation of Minimum Fluidization Velocity", Ind. Eng. Chem. Res., Vol. 26, p. 633 (1987).

Chervenak, M.C., Feigelman, S., R. Wolk, C.R.Byrd, L.R.Hellwig, R.P.Van Driesen , "Hy-C cracking", Chem Eng. Prog. Vol.59, No.2, p.53 (1963).

Chiu, T.M. anf Ziegler, E.N. , "Heat Transfer in Three-phase Fluidized Beds", AIChE J., Vol.29, p.677, (1983).

Chu, J.C., Kalil, J., and Wetteroth, W.A., "Mass Transfer in a Fluidized Bed", Chem. Eng. Prog., Vol.,49, p. 141 (1953).

Chuang, S.C., V.W. Goldschmidt, "The Response of a Hot-Wire Anemometer to a Bubble of Air in Water", Turbulence Measurement in Liquids, Patterson G.K., J.L. Zakin, eds., Dept. of Chem. Eng., University of Missouri-Rollo, Continuing Education Series, p. 88-95, (1971).

Cichy, P.T., Uitman, J.S. and Russel, T.W.F., Industrial Engineering Chemistry, Vol. 61, p.6 (1969).

Clark, N.N., R.L. Flemmer, "Gas-Liquid Contacting in Vertical Two-Phase Flow", Ind. Eng. Chem. Proc. Des. Dev., Vol. 24, p. 231-36 (1985).

Clift, R., Grace, J.R. and Weber, M.E., "Bubble Drops and Particles", Academic Press, N.Y., N.Y. (1978).

Colquhoun-Lee, I. and Stepanek, J.B., "Solid-Liquid Mass Transfer in Two-phase Cocurrent Up-flow in Packed Beds, Trans. Inst. Chem. Eng., Vol.56, p.136 (1978).

Costa, E., Lucas, A.D., and Garcia, P., "Fluid Dynamics of Gas-Liquid-Solid Fluidized Beds", Ind. Eng. Chem. Proc. Des. Dev., Vol. 25, p.849-54 (1986).

Couderc, J.P. Gibert, H. and Angelino, H., " Transfer de Matere par Diffusion en Fluidisation Liquide", Chem. Eng. Sci., Vol.7, p.11 (1972).

Cova, D.R., "Axial Mixing in the Liquid Phase in Gas-Sparged Columns", Ind. Eng. Chem. Proc. Des. Dev., Vol. 13, p. 292, (1974).

Curl, R.L., "Note on Light Transmission Through a Polydisperse Distribution", AIChE J., Vol. 20, p. 184, (1974).

Cussler, E.L." Diffusion : Mass Transfer in Fluid Systems", Cambridge univ.Press. , 282-288, (1984).

Dakshinamurty, P. K.V.Rao, R.V.Subrahmanyam, and V. Subrahmanyam, "Bed Porosities in Gas-liquid Fluidization" Ind. Eng. Chem. Process Des. Dev., 10, 322, (1971).

Dakshinamurty, P., Chiranjevi, C.,Subrahmanyam, V., and Kameswara Rao,"Studies of Gas-liquid Mass Transfer in Gas-liquid Fluidized beds", in Fluidization and its Applications, Ed. Cepadues, Toulouse, p.327, (1974).

Dakshinamurty, P., Veerabhadra Rao, K., "Gas-liquid Mass Transfer in Gas-Liquid Fluidized Beds: Part II", Indian J. Technology, Vol. 14, p.9, (1976).

Damranglerd, S., Couderc, J.P. and Angelino, H., "Mass Transfer in Fixed and Fluidized Beds', Ind. Eng. Chem. Process Des. Dev., Vol.16, p.157, (1977).

Danckwerts, P.V., "Significance of Liquid Film Coefficients in Gas Absorption", Ind. Eng. Chem., Vol.43, p.1460 (1951).

Danckwerts, P.V., and Sharma, M.M., "The Absorption of Carbon Dioxide with Solution of Alkalis and Amines", Chem. Eng. (London), Vol. 44, CE 244 (1966).

Danckwerts, P.V.,"Gas-Liquid Reactions", MacGraw Hill (1971).

Darton, R.C., and Harrison, D., "Gas and Liquid Holdup in Three-phase Fluidization",Chem. Eng. Sci., Vol. 30, p.581, (1975).

Davies, J.T., and Radial, E.K., "interfacial Phenomena", Academic Press, New York, (1963).

Davidson, J.F., and Schuler, O.G., "Bubble Formation at an Orifice in an Inviscid Liquid", Trans. Instn. Chem. Engrs, Vol. 38, p. 335-42 (1960).

Davidson, J.F. and Harrison, D., "The Behaviour of Continuily Bubbling Fluidized Beds," Chem. Eng. Sci., Vol. 21, p.731 (1966).

Davidson, J.F., and Harrison, D., "Fluidization", Academic Press, N.Y., (1971).

Davis, M.R., and B.Fungtamasan, "Large Scale Structures in Gas-Liquid Mixture Flows", Int. J. Multiphase Flow, Vol. 10, p. 663-76 (1984).

Dawson, D.A., and Trass, O., "Mass Transfer at Rough Surfaces", Int. J. Heat Mass Transfer, Vol. 15, p.1317 (1972).

Dayan, A. and Zalmovich, S., "Axial Dispersion and Entrainment of Particles in wakes of bubbles", Chem. Eng. Sci., Vol.37, p.1253, (1982).

Deckwer, W.D., U.Graeser, H. Langemann, Y. Serpemen,"Zones of Different Mixing in the Liquid Phase of Bubble Columns", Chem. Eng. Sci., Vol. 28, p. 1223-25 (1973).

Deckwer, W.D., Burckhart, R. and Zoll, G., "Mixing and Mass Transfer in Tall Bubble Columns", Chem. Eng. Sci., Vol. 29, p. 2177 (1974).

Deckwer, W.D. and I. Adler, "A Comprehensive study on CO_2 Interphase Mass Transfer in Vertical Cocurrent and Countercurrent Gas-Liquid Flow", Can. J. Chem. Eng., Vol. 56, p. 43-55 (1978)

Deckwer, W.D., Nguyen-tien, K., Schumpe, A. and Serpemen, Y., "Oxygen Mass Transfer into Aerated CMC Solutions in a Bubble Column", Biotechn. Bioengng., Vol. 24, p. 461-81 (1981).

DeCoursey, W.J.,"Absorption with Chemical Reaction: Development of a New Relation for the Danckwerts Model", Chem. Eng. Sci., Vol. 29, p. 1867-72 (1974).

Defay, R., and J.R. Hommelen, " Measurement of Dynamic Surface Tensions of Aqueous Solutions By the Oscillating Jet Method", J. of Colloid Sci., Vol. 13, p. 553-64 (1958).

de Lasa, H.I., Lee, S.L.P. and Bergougnou, M.A., "Bubble Measurement in Three-phase Fluidized Beds Using a U-shaped Optical Fiber", Can. J. Chem. Eng., Vol. 62, p.165, (1984).

Delaunay, G., Storck, A., Laurent, A., Charpentier, J.C., "Electrochemical Study of Liquid-Solid Mass Transfer in Packed Beds With Upward Co-current Gas-liquid Flow", Ind. Eng. Process Des. Dev., Vol. 19, p.515, (1980).

Delhaye, J.M., "Two-Phase Pipe Flow", Int. Chem. Eng., Vol.23, No. 3, p.385-410, (1983).

Devine, W.D., Y.T. Shah and B.I. Morsi, "Liquid Phase Axial Mixing in a Bubble Column with Viscous Non-Newtonian Liquids", Can. J. of Chem. Eng., Vol. 63, p. 195-201 (1985).

Dhanuka, V.R. and Stepanek, J.B., "Gas and Liquid Holdup and Pressure Drop Measurements in a Three-phase Fluidized Bed" in Fluidization", Ed. Davidson, J.F. and Keairns , D.L., Eds. Cambridge University press, p.179, (1978).

Dhanuka, V.R. amd Stepanek, J.B., "Simultaneous Measurement of Interfacial Area and Mass Transfer Coefficient in Three-phase Fluiidzed Beds', AIChE J., Vol. 26, p.1029, (1980).

Drogaris, G., and P. Weiland,"Coalescence Behaviour of Gas Bubbles in Aqueous Solutions of n-Alcohols and Fatty Acids", Chem. Eng. Sci., Vol. 18, p. 1501-1506 (1983).

Dudukovic, A.P., "Influence of the Turbulent Schmidt Number on Mass Transfer Rates Between Turbulent Fluid stream and a Solid Surface", AIChE J., Vol. 31, p. 1919-22 (1985).

Dwivedi, P.N., and Upadhyay, S.N., "Particle-fluid Mass Transfer in Fixed and Fluidized beds", Ind. Eng. Chem. Process Des. Dev., Vol.16, p.157 (1977).

Economou, D.J. and Alkre, R.C., "Two-phase Mass Transfer in Channel Electrolyzers with Gas-Liquid Flow", J. Electrochemical Soc., Vol. 132, p.601 (1985).

Eissa, S.H., El-Halwagi, M.M., and Saleh, M.A., "Axial and Radial Mixing in a Cocurrent Bubble Column", Ind. Eng. Chem. Proc. Des. Dev., Vol. 10, p. 31 (1971).

Efremov, G.I. and Vakhrushev, I. A., "A Study of the Hydrodynamics of Three-phase Fluidized beds", Int. Chem. Eng. Vol. 10, p.37 (1970).

Eissa, S.H., and Schuegerl, K., "Holdup and Backmixing Investigations in Cocurrent and Countercurrent Bubble Columns", Chem. Eng. Sci., Vol. 30, p. 1251 (1975).

El-Temtamy, S.A., and Epstein, N., "Bubble Wake Solid Content in Three-Phase Fluidized Beds", Int. J. Multiphase Flow, Vol.4, p.19 (1978)

El-Temtamy, S.A., Epstein, N., "Contraction or Expansion of Three-phase Fluidized Beds Containing Fine/Light Solids", Can. J. Chem. Eng., Vol.57, p.520 (1979).

El-Temtamy, S.A., El-Sharnoubi, Y.O and El-Halwagi, M.M., "Liquid Dispersion in Gas-Liquid Fluidized Beds Part I: Axial Dispersion. The Axially Dispersed Plug-Flow Model", The Chem. Eng. Journal, Vol. 18, p.151-59, (1979)

El-Temtamy, S.A., and Epstein,N., "Simultaneous Solids Entrainment and De-entrainment Above a Three-Phase Fluidized Bed", Fluidization, G.R. Grace and G.M. Matsen, Eds., 519, Plenum Press (1980).

Endo, I., Nagamune, T., Kato, N., Kobayaski, T., and M. Nishimura, paper 25C presented at the AIChE Ann. Mtg. Miami Beach, Nov. (1986) as quoted in Fan et al. (1986c).

Epstein, N., and Nicks, D., " Contraction or Expansion of Three- phase Fluidized Beds", in Fluidization Technology, I.D.L., Keairns, ed., Hemisphere, 389, (1976).

Epstein, N., "Three-Phase Fluidization: Some Knowledge Gaps," Can. J. Chem. Eng., Vol. 59 p.649- (1981).

Epstein, N., "Hydrodynamics of Three-Phase Fluidization", Handbook of Fluids in Motion, N.P. Cheremisinoff and R. Gupta, Eds., p.1165 Ann Arbor Science (1983).

Ermakova, A., Kuzmin, V.A. and Umbetov, A.S., "Investigation of Mass Tansfer from Individual Particles to a Liquid IV. Three-phase Systems: Fixed and Fluidized Beds. Derivation of a Generalized Mass Transfer Equation" Int. Chem. Eng., vol 28 , p 559-69, (1988).

Ergun, S., Chem. Engng. Prg., Vol. 48, p. 227 (1952).

Evans, G.C. and Gerald, C.F., "Mass Transfer from Benzoic Acid Granules to Water in Fixed and Fluidized Beds at Low Reynolds Numbers", Chem. Eng. Prog., Vol.49, p.135 (1953).

Fair, J.R., "Designing Gas-sparged Reactors, Chem. Eng., Vol. 74, p. 67 (1967).

Fan, L.S. and Yang, Yung-Chia, "Mass Transfer in Semi-fluidized beds on Liquid-Solid Systems", AICHE J., Vol. 6 p.482 (1960).

Fan, L.S., Fujie, K., and Long, T.R., "Some Remarks on Gas-Liquid Mass Transfer and Biological Phenol Degradation in a Draft Tube G-L-S Fluidized Bed Reactor", AIChE Symposium Series No. 241, Vol. 80, p.102 (1984).

Fan, L.S., Matsuura, A., and Chern, S.H., 'Hydrodynamic Characteristics of a Gas-Liquid-Solid Fluidized Bed Containing a Binary Mixture of Particles", AIChE J., Vol. 31, p.1801 (1985).

Fan, L-S., Satija, S. and Wisecarver, K., "Pressure Fluctuation Measurements and Flow Regime Transitions in Gas-liquid-solid Fluidized Beds", AIChE J., Vol.32, p.338, (1986a).

Fan, L-S., Bavarian, F., Gorawara, R., Kreischer, B., Buttke, R.D. and Peck, L.E. "Hydrodynamics of Gas-liquid-solid fluidization Under High Gas Hold-up Conditions", AIChE Mtg., Miami Beach, Fl. Nov 2-7,(1986b).

Fan, L-S., Kreicher, B.E., Tsuchiya, K., "Advances in Gas-liquid-solid Fluidization : Fundamentals and Application", paper presented at AIChE national Meeting, Miami Beach, Fl. Nov.2-7, (1986c).

Fan. L.S., and Tsuchiya, K., " paper presented at AIChE Ann. Mtg., Miami (1986) - as quoted in Fan et al. (1986c).

Fluid Meters, Their Theory and Applications, American Society of Mechanical Engineers Research Committee on Fluid Meters fifth ed., Published by ASME-345 East Forty seventh st. NY (1959).

Freedman, W. and Davidson, J.F., "Holdup and Liquid Circulation in Bubble Columns", Trans. Inst, Chem. Engrs., Vol. 47, p. T251-62 (1969).

Frössling, N., Beitr. Geophysik, Vol. 52, p. 170 (1938).

Fujie, K., Tasumota, T., Kubota, H., and S.Shibuya, J. of Japan Sewage Works Assoc., 20 (227), 25 (1983) as quoted in Fan et al. (1986c).

Fujie, K., and Fan, L.S., "Overall Gas-Liquid Mass Transfer Coefficients in a Draft Tube Gas-Liquid-Solid Fluidized Bed", in Fluidization V, eds. Ostergaard K., A.Sorenson, Engineering Foundation, N.Y. p. 369-76 (1986).

Fukuma, M., Sato,M., Muroyama, K. and Yasunishi, A., "Particle-To-Liquid Mass Transfer in Gas-Liquid-Solid Fluidization", J. of Chem. Eng. of Japan, Vol. 21, p 231-37, (1988).

Fukushima, S., "Gas-Liquid Mass Transfer in Three-Phase Fluidized Beds", J. Chem. Eng. Jpn., Vol. 12, p. 489 (1979).

Ganho, T., Gibert, H. and Angelino, H., "Cinetique de l'absorption du phenol en couche fluidisee de charbon actif", Chem. Eng. Sci., Vol.30,p.1231, (1975).

Garner, F.H. and Suckling, R.D., "Mass Transfer from a Soluble Solid Surface", AICHE, Vol. 4, p.114 (1958).

Garside, J., and Mulin, J.W., "The Crystallization of Aluminium Potassium Sulphate: a study in the assessment of Crystallizer Design Data", Trans. Inst. Chem. Engrs. Vol.6 p.T111 (1968).

Garside, J., and Al-Dibouni, "Velocity Voidage Relationships for Fluidization and Sedimentation in Solid-Liquid Systems", Ind. Eng. Chem. Proc. Des. Dev., Vol. 16, p. 206-10 (1977).

Goto, S., Levec, J., Smith, J.M., "Mass Transfer in Packed Beds With Two-phase Flow", Ind. Eng. Chem. Process Des. Dev., Vol.14, p.473 (1975a).

Goto, S., and Smith, J.M., " Trickle Bed Reactor Performance Part I.: Hold-up and Mass Transfer Effects", AIChE J., Vol.21, p.706 (1975b).

Godbole, S.P., M.F. Honath and Y.T.Shah, "Holdup Structure in Highly Viscous Newtonian and Newtonian Liquids in Bubble Columns", Chem. Eng. Commun., Vol. 16, p. 119-34 (1982).

Godbole, S.P., Schumpe, A., Shah, Y.T., "Hydrodynamics and Mass Transfer in Bubble Columns: Effects of Solids", Chem. Eng. Commun., Vol. 24, p. 235-58 (1983).

Godbole, S.P., Joseph, S., and Shah, Y.T., "Hydrodynamics and Mass Transfer in a Bubble Column with an Organic Liquid", Can. J. of Chem. Eng., Vol. 62, p. 440 (1984).

Gopal, J.S. and Sharma, M.M., "Mass Transfer Characteristics of Low H/D Bubble Columns", The Can. J. of Chem. Eng. Vol. 61, p. 517-26 (1983).

Goren, S.L. and Mani, R.V.S., "Mass Transfer Through Horizontal Liquid Films in Wavy Motion", AIChE J., Vol.14, p.57 (1968).

Govier, G.W. and Aziz, K., "The Flow of Complex Mixtures in Pipes," Van Nostrnd Rheinhold, New York, (1972).

Grace, J.R., "Handbook of Multiphase Systems", Chap. 8, Ed. G. Hetsroni, Mc Gra Hill, New york, (1980).

Grandjean, B.P.A., Carreau, P.J., and Paris, J., "Solid-Liquid Heat Transfer in a Three-Phase Fluidized Red", Conf. Proc. 37th Canadian Chem. Eng. Conf., Montreal, Quebec, May 18-22 (1987).

Griffith, P. and Wallis, G.B., "Two Phase Slug Flow", ASME Trans. J. of Heat Transfer, Vol. 83, p. 307 (1961).

Grover, G.S., Rode, C.V., and Chaudhari, R.V., "Effect of Temperature on Flow Regimes and Gas Holdup in a Bubble Column", Can. J. of Chem. Eng., Vol. 64, p. 501 (1986).

Gurol, M.D., and Nekouinaini, S., "Effect of Organic Substances on Mass Transfer in Bubble Aeration", Journal WPCF, Vol. 57, p. 235 (1985).

Guy, C., Carreau, P.J. and Paris, J., "Mixing Characteristics and Gas Holdup of a Bubble Column", The Can. J. of Chem. Eng. Vol. 64, p. 23-35 (1986).

Hamaker, H.C.,"Physica's Grav., Vol. 4, p. 1058 (1937).

Hansfor, G., and Litt, M., "Mass Transfer from a Rotating Disk into Power Law Liquids", Chem. Eng. Sci., Vol. 23, p.849-64 (1968).

Haque, M.W., Nigam, K.D.P. and Joshi, J.B., "Optimum Gas Sparger Design for Bubble Columns with a Low Height to Diameter Ratio", The Chem. Eng. J., Vol. 33, p. 63-69 (1986).

Hardy, J.E. and J.O. Hylton, "Electrical Impedence String Probes for Two-Phase Void and Velocity Measurements", Int. J. Multiphase Flow, Vol. 1, p. 541-56 (1984).

Hassanien , S, Delmas, H., and Riba, J.P., "Transfert de matere liquid-particles en fluidisation a trois phases", Entropie, No. 119,p 17-26, (1984).

Hatate, Y., Nomura, H., Fujita, T., Tajiri, S., Hidaka, N. and Ikari, A., "Gas Holdup and Pressure Drop in Three-Phase Vertical Flows of Gas-Liquid-Fine Solid Particles", J. of Chemical Engineering of Japan, Vol., 19, p 56-61, (1986).

Heijnen, J.J. and Vant Riet, K., "Mass Transfer Mixing and Heat Transfer Phenomena in Low Viscosity Bubble Column Reactors", The Chem. Eng. J. Vol. 28, p. B21-42 (1984).

Hellwig, K.C., Chevernak, H.C., Johanson, E.S., Stotler, H.H. and Wolk, R.H., "Convert Coal to Liquid Fuels with H-Coal", Chem. Eng. Progr. Symp. Ser., 64, p 85-98 (1966).

Henriksen, H. K. and Ostergaard, K. , "Characcerstics of Large Two-dimensional Air Bubbles in Liquids and Three-phase Fluidized Beds", Chem. Eng. J., Vol.7, p.141, (1974).

Hewitt,G.F., Chapter 10,"Handbook of Multiphase Systems", McGraw Hill Book Company, Ed. Hetsroni, G. (1982).

Hewitt, G.F., "Measurement of Two Phase Flow Parameters", Academic Press, New York (1978).

Hewitt, G.F., and Roberts, D.N., "Studies of Two Phase Flow Patterns by Simultaneous X-ray and Flash Photography AERE-M2159" quoted in Measurement of Two Phase Flow Parameters by Hewitt, G.F., Academic Press (1978).

Higbie, R., Trans. Am. Inst. Chem. Engrs., Vol. 31, p. 365 (1935).

Hikita, H., and Kikukawa, H., "Liquid Phase Mixing in Bubble Columns: Effect of Liquid Properties", Chem. Eng. J., Vol. 8, p. 191 (1974).

Hikita, H., Asai, S. Tanigawa, K., Segawa, K. and Kitao, M., "The Volumetric Liquid Phase Mass Transfer Coefficient in Bubble Columns", Chem. Eng. J., p. 61-69 (1980).

Hikita, H., Asai, S., Tanigawa, K., Segawa, K., and Kitano, M., "The Volumetric Liquid-Phase Mass Transfer Coefficient in Bubble Columns", Chem. Eng. J., Vol. 22, p. 61 (1981).

Hills, J.H., 'Radial Nonuniformity of velocity and Voidage in a Bubble Column", Trans. Inst. of Chem. Eng., Vol. 52, p. 1-8 (1974).

Hills, J.H., "The Operation of a Bubble Column at High Throughputs: Gas Holdup Measurements", chem. Eng. J., Vol. 12, p. 89 (1976).

Hinze, J.O., Turbulence, McGraw-Hill, New York (1958).

Hommelen, J.R., "The Elimination of Errors Due to Evaporation of the Solute in the Determination of Surface Tensions", J. of Colloid Sci., Vol. 14, p.385-400 (1959).

Houzelot, J.L., Thiebaut, M.F., Charpentier, J.C., and Schiber, J., "Contribution to the Hydrodynamic study of Bubble Columns", Int. Chem. Eng., Vol. 25, p.645 (1985).

Hu, Tsung-ting, Yu, Bao-Tien and Wang, Y-ping, "Holdups and models of Three-Phase Fluidized Beds", Fluidization, Proc. of the 5th Eng. Foun. Conf on Fluidization, May 18 - 23 , Elsinore, Denmark (1986).

Hung, G.W. and Dinius, R.H., " Diffusivity of oxygen in electrolye solution, J. Chem. Eng. Data. Vol.17, p.449, (1972).

Hwang, S.J. and Fan, L.S., "Some Design Considerations of Draft Tube Gas-Liquid-Solid Spouted Bed", The Chemical Engineering Journal, Vol. 33, p 49-56, (1986).

Idogawa, K., Ikeda, K., Fukuda, Y., and Morooka, S., "Behavior of Bubbles of the Air-Water System in a Column Under High Pressure", Int. Chem. Eng., Vol. 26, p. 468 (1986).

Idogawa, K., Ikeda, K., Fukuda, T., Morooka, S., "Effects of Gas and Liquid Properties on the Behavior of Bubbles in a Column Under High Pressure", Int. Chem. Eng., Vol. 27, p. 93 (1987).

Irandoust, S., and Andersson, B., "Concentration-Dependent Diffusivity of Benzoic Acid in Water and its Influence on the Liquid-Solid Mass Transfer", The Can. J. Chem. Eng., Vol., 64, p. 954-59 (1986).

Ishida, M., and H.Tanaka, "An Optical Probe to Detect Both Bubbles and Suspended Particles in a Three-phase fluidized bed", J. Chem. Eng. Japan.,15, 389 (1982).

Ivanov, M.E., and Bykov, V.P., "Frequency of the Passage of Bubbles and Gas Content in Bubble Beds", Theor. Found. Chem. Eng., Vol. 4, p. 119 (1970).

Jackson, M.L., James, D.R., and B.P. Leber, Jr., AIChE Symp. Ser., 71(151), p. 159-65 (1975).

Jagannadhraju, G.J.V. and Rao, C.V., Indian J. Technol. Vol. 3, p.201 (1965).

Joshi, J.B., and Sharma, M.M., "A Circulation Cell Model for Bubble Columns", Trans. Inst. Chem. Engrs., Vol. 57, p. 244, (1979).

Joshi, J.B., "Axial Mixing in Multiphase Contactors - A Unified Correlation", Trans IChemE, Vol. 58, p.155-86 (1980).

Kafarov, V.V., Klipinistser, V.A., Saks, O.I., "Solids Phase Distribution and Holdup in a Column-Type Reactor with a Gas-Liquid-Solid Three-Phase System", Theor. Found. Chem. Eng., Vol.1, p.742 (1973).

Kalogerakis, N., Behie, L.A., and Gaucher, G.M., in "Fluidization", K.Ostergaard and A. Sorensen, Eds. Engineering Foundation Press, 611 (1986).

Kang, Y., Suh, I.S., and Kim, S.D., "Heat Transfer Characteristics of Three-Phase Fluidized Beds", Chem. Eng. Commun., Vol. 34, p.1 (1985).

Kang, Y., and Kim, S.D., "Radial Dispersion Characteristics of Two- and Three-Phase Fluidized Beds", Ind. Eng. Chem. Proc. Des. Dev. Vol. 25, p.717 (1986).

Kara, S., Kelkar, B.G., Shah, Y.T., Carr, N.L., "Hydrodynamics and Axial Mixing in Three-Phase Bubble Column", Ind. Eng. Chem. Proc. Des. and Dev., Vol. 21, p.584 (1982).

Kataoka, H., H.Takeuchi, K.Nakao, H.Yagi, T.Tadaki, T.Otake, T.Miyauchi, K.Washimi, K.Watanabe and F.Yoshida,"Mass Transfer in a Large Bubble Column", J.Chem. Eng. Japan, Vol. 12, p. 105-10 (1979).

Kato, Y., and Nishikawa, A., "Longitudinal Dispersion Coefficient of a Liquid in a Bubble Column", Int. Chem. Eng., Vol. 12, p. 182 (1972).

Kato, Y., Nishiwaki, A., Kago, T., Fukuda, T., Tanaka, S., "Gas Holdup and Overall Volumetric Absorption Coefficient in Bubble Columns with Suspended Solid Particles: Absorption Rate of Oxygen by an Aqueous Solution of Sodium Sulfite, Int. Chem. Eng., Vol. 13, p. 562-76 (1973).

Kato, Y., Nishikawa, M., Morooka, S., "Distribution of Gas Holdup in a Bubble Column", Kagaku, Kogaku Ronbunshu, Vol. 1, p. 530 (1975).

Kato, Y., Uchida, K., Kago, T. and S. Morooka , "Liquid Hold-up and Heat Transfer Coefficient Between Bed and Wall

in Liquid-solid and Gas-liquid-solid Fluidized Beds", Powder Technology, Vol. 28, p.173 (1981).

Kato, Y., Morooka, S., Kago, T., Saruwatari, T., and Yang, S., "Axial Holdup Distribution of Gas and Solid Particles in Three-Phase Fluidized Bed for Gas-Liquid (slurry), Solid Systems", J. Chem. Eng. of Japan, Vol. 18, p.308 (1985).

Kawagoe, M., K.Nakao and T.Otake, "Liquid-Phase Mass Transfer Coefficient and Bubble Size in Gas Sparged Contactors", J. Chem. Eng. of Japan, Vol. 8, p. 254-56 (1975).

Kawagoe, K., Inoue, T., Nakao, K., and Otake, T., "Flow Pattern and Gas Holdup Conditions in Gas Sparged Contactors", Int. Chem. Eng., Vol. 16, p. 176-83 (1976).

Kawase, Y., Halard, B., and Moo-Yong, M., "Theoretical Prediction of Volumetric Mass Transfer Coefficients in Bubble Columns for Newtonian and Non-Newtonian Fluids', Chem. Eng. Sci., Vol. 42, p. 1609 (1987).

Kawecki, W., Reith, T., Van Heuven, J.W., "Bubble Size Distribution in the Impeller Region of a Stirred Vessel", Chem. Eng. Sci., Vol. 22, p. 1519 (1967).

Keitel,G., and U.Onken,"Inhibition of bubble Coalescence by Solutes in Air/Water Dispersions", Chem. Eng. Sci., Vol. 37, p. 1635-38 (1982).

Kelkar, B.G., Godbole, S.P., Honath, M.F., Shah, Y.T., Carr, N.L., Deckwer, W.D., "Effect of Addition of Alcohols on Gas Holdup and Backmixing in Bubble Columns", AIChE J., Vol. 29, No. 3 p. 361-69 (1983a).

Kelkar, B.G., Phulgaonkar, S.R., Shah, Y.T., "The Effects of Electrolyte Solutions on Hydrodynamics and backmixing Characteristics in Bubble Columns", The Chem. Eng. J., Vol. 27, p. 125-33 (1983b).

Kelkar, B.G., Y.T.Shah, N.L. Carr,"Hydrodynamics and Axial Mixing in a Three-Phase Bubble Column: Effects of Slurry Properties", Ind. Eng. Proc. Des. Dev., Vol. 23, p. 308-13 (1984).

Khang, S.J., Schwartz, J.G., and Buttke, R.D., "A Practical Wake Model for Estimating Bed Expansion and Holdup in Three-Phase Fluidized Systems", AIChE Symposium series No. 222, Vol. 79 (1983).

Kikuchi, K.J., Kono, H., Sugawane, T., Ohashi, H. "Mass Transfer Between Particles and Liquid in Dilute Fluidized beds in low Reynolds numbers", J. Chem. Eng. Japan, Vol.17, p.438 (1984).

Kikuchi, K., Tadakuma, Y., Sugawara, T., and Ohashi, H., "Effects of Inert Particle Concentration on Mass Transfer Between particles and Liquid in Solid-Liquid and Two-phase upflow through Vertical Tubes and in Stirred Tanks", J. of Chem. Eng. of Japan, Vol. 20, p.134 (1987).

Kim, S.D., Baker, C.G.J. and M.A. Bergougnou, "Hold-up and Axial Mixing Characterstics of Two- and Three-phase Fluidized Beds", Can. J. Chem. Eng., 50, 695, (1972).

Kim, S.D., Baker,C.G.J. and M.A. Bergougnou, "Phase Holdup Characterstics of Three-phase Fluidized Beds", Can. J. Chem. Eng., Vol.53, p.134, (1975).

Kim, S.D., Baker, C.G.J. and M.A. Bergougnou, " Bubble Characterstics in Three-phase Fluidized beds", Chem. Eng. Sci., Vol.32, p.1299, (1977).

Kim, S.D. and Kim, C.H., "Axial Dispersion Characteristics of Three-Phase Fluidized Beds", J. of Chem. Eng. of Japan, Vol.16, p.172-178 (1983).

Kim, J.W., and W.K. Lee,"Coalescence Behavior of Two Bubbles in Stagnant Liquids", J. Chem. eng. Japan. Vol. 20, p. 448-53 (1987).

King, D.H., and Smith, J.W., "Wall mass transfer in liquid fluidized beds", Can. J. Chem. Eng., Vol. 45, p.329, (1967).

Kirillov, V.A., Nasamanyan, M.A., "Mass Transfer Processes Between Liquid and Packing in a Three-phase Fixed bed", Int. Chem. Eng., Vol. 9, p.220, (1976).

Kito, M., Shimida, M., Sakai, T., Sugiyama, S., and Wen, C.Y., "Performance of Turbulent Bed Contactor, Gas Holdup and Interfacial Area Under liquid Stagnant Flow", Fluidization p. 411 (1976).

Koide,K., Hayashi, T., Sumino, K. and Iwamoto, S.,, "Mass Transfer from Single Bubbles in Aqueous Solutions of Surfactants", Chem. Eng. Sci., Vol. 31, p. 963-67 (1976).

Koide, K., Morooka, S., Ueyama, K., Matsuura, A., Yamashita, F., Iwamoto, S., Kato, Y., Inoue, H., Shigeta, M., Suzuki, S., Akehata, T., "Behavior of Bubbles in Large Scale Bubble Columns", J. Chem. Eng. of Japan, Vol. 12, p. 98 (1979).

Koide, K., Yasuda, T., Iwamato, S., Fukuda, A., "Critical Gas Velocity Required for Complete Suspension of Solid Particles in Solid-Suspended Bubble Columns", J. Chem. Eng. Japan, Vol. 16, p. 7-12 (1983).

Koide,K., A. Takazawa, M. Komura, and H. Matsunaga, "Gas Holdup and Volumetric Liquid-Phase Mass Transfer Coefficient in Solid-Suspended Bubble Columns", J. of Chem. Eng. of Japan, Vol.17, p. 459-66 (1984).

Koide, K., Sato, H. and Iwamoto, S., "Gas Holdup and Volumetric Liquid-Phase Mass Transfer Coefficient in Bubble Column with Draft Tube and with Gas Dispersion into Annulus", J. of Chem. Eng. Japan, Vol. 4, p. 287-92 (1985).

Koide, K., Yamazoe, S. and Harada, S., "Effects of Surface Active Substances on Gas Holdup and Gas-Liquid Mass Transfer in Bubble Columns", J. of Chem. Eng. Japan, Vol. 4, p. 287-92 (1985).

Koloni, T. Sopcic, M, and Zumer, M.Y., "Mass Trnasfer in Liquid Fluidized Beds at Low Reynolds Numbers", Chem. Eng. Sci. Vol.32, p.637 (1977).

Koenig, B., Buchholz, R., Luecke, J., Schuegerl, K., "Longitudinal Mixing of the liquid phase in bubble Columns", Ger. Chem. Eng., Vol. 1, p. 199 (1978).

Kumar, A., Dagaleesam, T.T., Laddha, G.S., Hoelscher, H.E., "Bubble Swarm Characteristics in Bubble Columns". Can. J. Chem. Eng., Vol. 54, p. 503. (1976).

Kumar, S., Upadhyay, S.N., and Mathur, V.K., "On the Solubility of Benzoic Acid in Aqueous Carboxymethylcellulose Solutions", J. Chem. Eng. Data, Vol., 23, p. 139-41 (1978).

Kumar, S., Upadhyay, S.N., "Laminar Flow Dissolution and Diffusion in Non-Newtonian Fluids", Ind. Eng. Chem. Fund., Vol. 19, p. 75-79 (1980).

Kumar. S., and Upadhyay, S.N., "Mass and Momentum Transfer in Newtonian and Non-newtonian Fluids in Fixed and Fluidized Beds", Ind. Eng. Chem. Fund., Vol. 20, p.186, (1981).

Kurten, H., and Zehner, P., "Slurry Reactors", Ger. Chem. Eng., Vol. 2, p. 220-7 (1979).

Kusakabe, K., Morooka, S. and Kato, Y. "Charge Transfer Rate in Liquid-solid and Gas-liquid-solid Fluidized Bed Bed Electrodes", J. Chem. Eng. Japan, Vol.14, p. 208, (1980).

Laguerie, C. and Angelino, H., "Comparaison entre la dissolution et la croissance de cristaux d'acide citrique monohydrate en lit fluidise", Chem. Engng. J., Vol.10, p.41 (1975).

Landau, J., Boyle, J., Gomma, H.G., Al Taweel, A.M., "Comparison of Methods for Measuring Interfacial Areas in Gas-Liquid Dispersions", Can. J. of Chem. Eng., Vol. 55, p.13 (1977).

Lapidus, L. and Elgin, J.C., "Mechanics of Vertical-Moving Fluidized Systems," AIChE Journal, Vol. 3 No. 1 p. 63-68, (1957).

Latifi, M.A., "Analyse globale et locale des phenomenes de tranfert de Matiere Liquide-Solide Dans Un Reacteur A Lit Five Fonctionnant A Co-Courant Vers Le Bas De Gaz Et De Liquide", Ph.D. Thesis , L' Institut National Polytechnique de Lorraine (1988).

Lee, J.C., "Discussion in the Paper of Adlington and Thompson", Proc. of 3rd Europ. Symp. Chem. React. Eng., 211 Pergamon Press, Oxford (1965).

Lee, J.C., and Meyrick, D.L., "Gas-Liquid Interfacial Area in Salt Solutions in an Agitated Tank", Trans. Instn. Chem. Engrs., Vol. 48, p. t37-45 (1970).

Lee, J.C., Sherrard, A.J., and Buckley, P.S., "Optimum Particle Size in Three-phase Fluidized bed Reactors", Pro. Int. Symp., Fluidization and its Applications Ed. Cepadues, 407, (1974).

Lee, J.C., and Worthington, H., " Gas-liquid Mass Transfer in Three-phase Fluidized beds", Inst. Chem. Engr. Symp. Series 38, B2, (1974).

Lee, J.C., and Al-Dabbagh, N., "Three-Phase Fluidized Beds: Onset of Fluidization', ed. J.F. Davidson, D.K. Keairns, Cambridge University Press, p.184 (1978).

Lee, S.L.P., de Lasa, H.I., M.A. Bergougnou, " Bubble Phenomenon in Three-phase Fluidized Beds as Viewed by a U-Shaped Fiber Optic Probe", AIChE sym. Ser. 80, vol. 241, 110, (1984).

Lee, S.L.P. "Bubble Dynamics in Three-phase Fluidized Beds", Ph. D. thesis, University of western Ontario, London, Canada, (1986).

Lee, S.L.P. and de Lasa, H. I., "Phase Hold-ups in Three-phase Fluidized beds", AIChE, Vol.33, p.1359, (1987).

Leibson, I., Holcombe, E.G., Carcass, A.G., and Jaenie, J.J., "Rate of Flow and Mechanics of Bubble Formation from Single Submerged Orifices", AIChE J., Vol. 2, p. 296 (1956).

Lemay, Y., Pineault, G. and Ruther J.A., "Particle-liquid Mass Transfer in a Three-phase Fixed Bed Reactor with Cocurrent Flow in Pulsing Regime", Ind. Eng. Chem. Process Des. Dev., Vol.14, p.280, (1975).

Letan, R. and Elgin, J.C., "Fluid Mixing in Particulate Fluidized Beds", Chem. Eng. J., Vol. 3, p.136 (1972)

Levish, I.P., Krainev, N.I., and Niyazov, M.I., "Calculation of the Pressure Drop and Heights of Three-phase Fluidized Beds", Int. Chem. Engng. Vol.8, p.311 (1968).

Lewis, D.A., R.S. Nical and J.W. Thompson, "Measurement of Bubble Sizes and Velocities in Gas-Liquid Dispersions", Chem. Eng. Res. Des., Vol. 62, p. 334-6 (1984).

Lin, C.S., Denton, E.B., Gaskil, H.S., and Putnam, G.L., "Diffusion-controlled Electrode Reactions", Ind. Eng. Chem., Vol. 43, p.2136 (1951).

Linek, V. and Vacek, V., "Dynamic Measurement of the Volumetric Mass Transfer Coefficient in Agitated Vessels: Effect of the Start-up Period on the Response of an Oxygen Electrode", Biotech.and Bioeng. XIX, p. 983-1008 (1977).

Linneweber, K.W., and Blass, E. " Local Gas and Solids Hold-up in Three-phase Bubble Flow," proc. 2nd, World Cong. Chem. Eng., Montreal, vol.3, 50, (1981).

Lockett, M.J. and Kirkpatrick, R.D., "Ideal Bubbly Flow and Actual Flow in Bubble Columns," Transactions Institution of Chemical Engineers," Vol. 53, p. 267-73 (1975).

Lockett, M.J., and Safekourdi, A.A., "Light Transmission Through BubbleSwarms", AIChE J., Vol. 23, p. 395 (1977).

Lozar, J., Laguerie, C., Couderc, J.P., "Diffusivite de l'acide benzoique dans l'eau: Influence de la temperature", Can. J. Chem. Eng., Vol., 53, p. 200-3 (1975).

Lucas, A., Arnaldos, J., Casal, J., and Pugjaner, L., "Improved Equation for the Calculation of Minimum Fluidization Velocity", Ind. Eng. Chem. Proc. Des. Dev., Vol. 25, p.426 (1986).

Mangartz, K.H., Pilhofer, T., "Interpretation of Mass Transfer Measurements in Bubble Columns Considering Dispersion of Both Phases", Chem. Eng. Sci., Vol. 36, p. 1069 (1981).

Marrone, G.M., and Kirwan, D.J., "Mass transfer to Suspended Particles in gas-Liquid Agitated Systems", AIChE J., Vol. 32, p.523 (1986).

Marrucci, G., "Rising Velocity of a Swarm of Spherical Bubbles", Ind. Eng. Chem. Fund., Vol. 4, p. 224 (1965).

Marrucci, G., and Nicodemo, "Coalescence of gas Bubbles in Aqueous Solutions of Inorganic Electrolytes", Chem. Eng. Sci., Vol. 22, p. 1257-65 (1967).

Marrucci, G.,"A Theory of Coalescence", Chem. Eng. Sci., Vol. 24, p. 975-85 (1969).

Maruyama, T., Yoshida, S. and Mizushina, T., "The Flow Transition in a Bubble Column", J. of Chem. Eng. of Japan, Vol. 14, p. 352-57, (1981).

Mashelkar, R.A., "Bubble Columns", Brit. Chem. Eng., Vol. 15, p. 1297 (1970).

Mashelkar, R.A., and Sharma, M.M., "Mass Transfer in Bubble and Packed Bubble Columns", Trans. Inst. Chem. Eng., Vol. 48, p. T-162 (1970).

Massimilla, L., Majuri, N. and Signorini, P., "Sull Assorbimento Di Gas in Sistema: Solido-Liquido-Fluidizzato," La Ricerca Scientifica, Vol. 29 (1959).

Massimilla, L., Solimanal, A., and E. Squillace, "Gas Dispersion in Solid-Liquid Fluidized Beds", Brit. Chem. Eng. Vol. 6, p.232 (1961).

Matsuura, A., and Fan, L.S., "Distribution of Bubble Properties in a Gas-Liquid-Solid Fluidized Bed", AIChE J., Vol. 30, p. 894 (1984).

McCune, L.K., and Wilhelm, R.H., "Mass and Momentum transfer in solid-liquid systems". Ind. Engng. Chem., 41, p.1124 (1949).

McLaughlin, C.M., and Rushton, J.H., "Interfacial Area of Liquid-Liquid Dispersion from Light Transmission Measurements, AIChE J., Vol. 19, p. 817 (1973).

McManamey, W.J., Wase, D.A.J., Raymahasay, S. and Thayanithy, K., "The Influence of Gas Inlet Design on Gas Holdup Values for Water and Various Solutions in a Loop-

type Air-Lift Fermenter", J. Chem. Tech. Biotechnol., 34b, p. 151-64 (1984).

Michelsen, M.L. and Ostergaard, K., "Hold-up and fluid mixing in gas-liquid fluidized beds", Chem. Eng. J. Vol.1, p.37, (1970).

Miller, D.N., "Gas Holdup and Pressure Drop in Bubble Column Reactor," Industrial Engineering Chemistry Process Design and Development, Vol. 19, p. 371-77, (1980).

Miyauchi, T., and Shyu, C.N., Kagaku Kogaku, Vol. 34, p. 958 (1970) quoted in Wachi et al. (1987).

Miyauchi, T., Furusaki, S., Morooka, S., Ikeda, Y., "Advances in Chemical Engineering", Vol. 11, p. 275-448, Academic Press, New York (1981).

Mochizuki, S., Matusi, T. "Liquid-solid mass transfer rate in liquid-gas upward cocurrent flow in packed beds", Chem, Eng. Sci., Vol.29, p.1328 (1974).

Morikawa, Y., Karube, I., Suzuki, S., "Continuous Production of Bacitraan by Immobilized Living Whole Cells of Bacillus Sp.", Biotech and Bioeng., Vol. 22, p. 1015 (1980).

Morita, S. and Smith, J.M., "Mass Transfer and Contacting Efficiency in a Trickle Bed Reactor", Ind. Eng. Chem. Fund., Vol. 17, p.113 (1978)

Morooka, S., Kusakabe, K., Kato, Y. "Mass transfer coefficient at the wall of a rectangular fluiized bed for liquid-solid and gas solid systems", Int. Chem. Eng. Vol.20, p.433,(1980).

Morooka, S., Koyama, and Kato, Y. , "Axial Mixing and internal recirculation flow in three-phase fluidized beds', in "Fluidization V" proc. of the 5th Eng. Found. Conf. on fluidization, May 18-23, Elsinore, Denmark, (1986).

Mounce, W., and Robin, R.S., "The H-oil Route for Hydroprocessing", Chem. Eng. Prog., Vol. 67, p.81 (1971).

Muir, L.A., Briens C.L., Bergougnou, M.A., "Entrainment of Particles from Three-phase Fluidized Beds", Proceedings of 37th Canadian Chemical Engineering Conference, Montreal, May 18-22, p. 149-51 (1987).

Mukherjee, R.N., Bhattacharya, P., and Taraphadar, D.K., "Studies on the dynamics of three-phase fluidization", Proc. Int. Symp. 'Fluidization and its Applications', Ed. Cepadues, Toulouse, 372, (1974).

Muroyama, K., M.Fukuma, and A.Yasunishi, "Heat Transfer in Three-phase Fluidized Beds", AIChE Symp. Ser. 308, 77, 385, (1981)

Muroyama, K., Hashimoto, K., Kawabata, T., and Shiota, M., Kagaku Kogaku Ronbunshu, Vol. 4, p. 622 (1978) as quoted in Kim and Kim (1983).

Muroyama, K., Fukuma, M., Yasunishi, A., "Wall-to-Bed Heat Transfer Coefficient in Gas-Liquid-Solid Fluidized Beds", The Can. J. of Chem. Eng., Vol. 62, p.199-208, (1984).

Muroyama, K., and Fan, L-S, "Fundamentals of Gas-liquid-solid Fluidization" AIChE J.,31, p 1-34 (1985).

Muroyama, K., M.Fukuma, and A.Yasunishi, "Heat Transfer in Three-phase Fluidized beds", Can. J. Chem. Eng., Vol. 64, p.399 (1986a).

Muroyama, K., M.Fukuma, and A. Yasunishi, "Heat Transfer in Three-phase Fluidized beds", Can. J. Chem. Eng., Vol.64, p.409, (1986b).

Nacef, C.G.J., Wild, G., Laurent,A., and Kim, S.D., "Effects D'Echelle EN Fluidization Gaz-Liquide-Solide", Submitted to Entropie (1988).

Nagel, O., Kuerten, H., and Hegner, B., "Design of Gas/Liquid Reactor: Mass Transfer Area and Input of Energy", Two-Phase Momentum heat and Mass Transfer in Chemical Process and Engineering Systems, ed. F. Durst, G.V. Tsiklauri, and N.H. Afgan, 2, 835, Hemisphere, Publ. Corp. Washington, D.C. (1979).

Nakanoh, M., and Yoshida, F., "Gas Absorption by Newtonian and Non-Newtonian Liquids in a Bubble Column", Ind. Eng. Chem. Proc. Des. Dev., Vol. 19 p. 190-95 (1980).

Nakao, K., H.Takeuchi, H.Kataoka, H.Kaji, T.Otake, T.Miyauchi,"Mass Transfer Characteristics of Bubble Columns in Recirculation Flow Regime", Ind. Eng. Chem. Proc. Des. Dev., Vol. 22, p.577-82 (1983).

Nguyen-Tien, K., Patwari, A.N., Schumpe, A., and Deckwer, W.D., "Gas-Liquid Mass Transfer in Fluidized Particle beds", AIChE J., Vol. 31, p.194 (1985a).

Nguyen-Tien, K., Schumpe, A., and Deckwer, W.D., "Effect of Reactor Diameter on Gas-Liquid Mass Transfer in Three-Phase Fluidized Beds", AIChE J., Vol. 31 p.1742 (1985b).

Nigam, K.D.P., and A.Schumpe, "Gas-Liquid Mass Transfer in a Bubble Column with Suspended Solids", AIChE J., Vol. 33, p. 328-30 (1987).

Nikov, I., and Delmas, H., "Solid-liquid Mass Transfer in Three-phase Fixed and Fluidized beds', Chem.Eng. Sci., Vol.42, p.1089, (1987).

Nishikawa, M., Inui, K., Yonezawa, Y. and Nagata, S., "Mass Transfer from Solid Particles in a Spouted Vessel", Int. Chem. Eng., Vol. 16, p.714-719 (1976).

Nishikawa, M., Kosaka, K., and Hashimoto, K., "Gas Absorption in Gas-Liquid or Solid-Liquid Spouted Vessels", Pacific Eng. Cong., Denver p.1389 (1977).

Nottenkaemper, R., A.Steiff and P.M.Weinspach, "Experimental Investigation of Hydrodynamics of Bubble Columns", Ger. Chem. Eng., Vol. 6, p. 147-55 (1983).

Oels, U., Luecke, J., Buchholz, R. and Schuegerl, K., "Influence of Gas Distributor Type and Composition of Liquid on the Behavior of a Bubble Column Bioreactor", Ger. Chem. Eng. Vol. 1, p. 115-29 (1978).

Ohki, Y. and Inoue, H., "Longitudinal Mixing of The Liquids Phase in Bubbles Columns", Chem. Eng. Sci., Vol. 25, p. 1-16 (1970).

Oosterhuis, N.M.G., A.P.J. Sweere, and N.W.F. Kossen, "Determination of the Liquid Side Oxygen Transfer Coefficient in a Biological Medium", Chem. Eng. Res. Des., Vol. 63, p.203-5 (1985).

Oshinowo, T. and Charles, M.E., "Vertical Two Phase Flow, Part 1: Flow Pattern Correlations," The Canadian Journal of Chemical Engineering, Vol. 52, p. 25-35 (1974).

Ostergaard, K.,"Discussion in the Paper of R.Turner, "Fluidization", 58, Soc. for the Chem. Ind. London (1964)

Ostergaard, K., "On the Growth of Air Bubbles Formed at a Single Orifice in a Water Fluidized Bed", Chem. Eng. Sci., Vol. 21, p.470 (1966)

Ostergaard, K., "Gas-liquid-particle operation in chemical reaction engineering", Adv. in Chem. Eng. T.B.Drew et al. Eds., Vol.7, p.71, Academic Press. (1968).

Ostergaard, K., and Michelsen, M.L., "On the Use of Imperfect Tracer Pulse Method for Determining of Holdup and Axial Mixing", Can. J. Chem. Eng., Vol. 47, p.107 (1969).

Ostergard, K., Suchozebrski, W., "Gas-Liquid Mass Transfer in Gas-Liquid Fluidized Beds", Proc. Eur. Symp. Chem. React. Eng., 21, Pergamon Press, Oxford (1969).

Ostergaard, K., "Three-phase Fluidization", in Fluidization, Davidson, J.F. Davidson and Harrison Eds. Chap.18, 751, Academic press, New york.(1971)

Ostergaard, K., and Fosbol, P. "Transfer of Oxygen Across the Gas-liquid Interface in Gas Liquid Fluidized Beds", Chem., Eng. J., Vol.3, p.105, (1972).

Ostergaard, K., "Holdup Mass Transfer and Mixing in Three-Phase Fluidization", AICHE Symp. Ser. Vol. 74, p.82-(1978).

Otake, T., S. Tone and K. Shinohara, "Gas Holdup in the Bubble Column with Cocurrent and Countercurrent Gas-Liquid Flow", J. Chem. Eng. of Japan, Vol. 14, p.338-40 (1981).

Özturk, S.S., Schumpe, A., Deckwer, W.D., "Organic Liquids in a Bubble Column: Holdups and Mass Transfer Coefficients", AIChE J., Vol. 33, p. 1473 (1987).

Page, R.E., and Harrison, D., "Particle entrainment from a three-phase fluidized bed", in Fluidization and its Applications, Eds. Cepadeus, Toulouse, 393, (1975).

Pal, S.S., Akita, A.K., and Roy, N.N., "Pressure Drop and Holdup in Vertical Two Phase Cocurrent Flow with Improved Gas-Liquid Mixing", Ind. Eng. Chem. proc. Des. Dev., Vol. 19, p. 67-75 (1980).

Pal, S.K., M.M. Sharma and V.A. Juvekar, " Fast Reactions in Slurry Reactors: Catalyst Particle Size Smaller Than Film Thickness: Oxidation of Aqueous Sodium Sulphide Solutions With Activated Carbon Particles as Catalyst at Elevated Temperatures", Chem. Eng. Sci., Vol. 37, p. 327-36 (1982).

Parkinson, G., Chem. Eng. 92 Vol. 19 p. 17 (1985).

Patwari, A.N., Nguyen-Tien, K., Schumpe, A., and Deckwer, W.D., "Three-Phase Fluidized Beds With Viscous Liquid: Hydrodynamics and Mass Transfer", Chem. Eng. Commun., Vol., p. 40-65 (1986).

Peschke, G., Franz, C., Lippert, J., Zakrzewski, W., and Schuegerl, "Blasenschwarmverhalten in Hochviskosen Fluessigkeiten", Chem. Ing. Tech., Vol. 52, p. 847 (1980).

Peterson, D., Tankin, R.S., and Bankoff, S.G., "Holographic Measurements of Bubble Size and Velocity in a Three-Phase System. IUTAM symposium, Measuring Techniques in Gas-Liquid Two-phase Flows, July 5-8 (1983) in Nancy.

Peterson, D.A., "Bubble Breakup and Coalescence in a Three-Phase Fluidized Bed", Ph.D. Thesis, Northwestern University, Evanston, Illinois, (1985).

Pinsent, B.R.W., Pearson, L., Roughton, F.J.W., " The Kinetics of Combination of Carbon Dioxide with Hydroxide ion", Trans Faraday Soc., Vol. 52, p. 1512 (1956).

Posarac, D. and Tekic, M.N., "Gas Holdup and Volumetric Mass Transfer Coefficient in Bubble Columns with Dilute Alcohol Solutions", AIChE Journal, Vol. 33, p. 497-99 (1987).

Pradhan, A.A., and Heideger, W.J., "On the Measurement of Liquid Phase Diffusivities for Slightly Soluble Solids", Can. J. Chem. Eng., Vol., 49, p. 10-13 (1971).

Prakash, A., C.L.Briens, and M.A. Bergougnou, "Mass Transfer transfer between solid particles and liquid in three-phase fluidized bed', Proc. of the 34th Can. Chem. Eng. conf. pp 478-81, (1984)

Prakash, A., C.L.Briens, and M.A. Bergougnou "Mass Transfer Between, Solid Particles and Liquid in a Three-phase Fluidized Bed", Can. J. Chem. Eng., Vol.65, p.228 (1987).

Prakash, A., Briens, C.L., "Gas-Liquid Mass Transfer in a Batch Bubble Column. Effects of Gas Distribution", Submitted to Can. J. of Chem. Eng. (1988).

Quicker, G., Deckwer, W.D., "Gasgehalt and Phasengrenzfaeche in Degasten Kohlenwasserstoffen", Chem. Ing. Tech., Vol. 53, p. 474 (1981).

Rabiger, N., Chem. Ing. Tech., Vol. 57, p. 248-49 (1985), quoted in Sauer and Hempel (1987).

Rahman, K., and Streat, M.,"Mass Transfer in Liquid Fluidized Beds of Ion Exchange Particles", Chem. Eng. Sci., Vol. 36, p. 293 (1981).

Ray, W.F., "Fundamentals of Transport Phenomena", McGraw Hill Book Company, N.Y., (1983).

Raymond, D.R., S.A. Zieminski,"Mass Transfer and Drag Coefficients of Bubbles Rising in Dilute Aqueous Solutions", AIChE J., Vol. 17, p. 57-65 (1971).

Razumov, I.M., Manshilin, V.V., Nemets, L.L., " The structure of three-phase fluidized beds", Int. Chem. Eng., Vol.13, p.57, (1973).

Reid, R.C., Prausnitz, J.M., Sherwood, T.K., "The Properties of Gases and Liquids", 3rd ed. McGraw Hill, NY (1977).

Reilly, I.G., Scott, D.S., De Bruijn, T., Jain, A. and Piskorz, J., "A Correlation for Gas Holdup in Turbulent Coalescing Bubble Columns", The Can. J. of Chem. Eng. Vol. 64, p. 705-17 (1986).

Reiss, L.P. and Harnatty, T.J., "An Experimental Study of the Unsteady Nature of the Viscous Sublayer", AICHE J., Vol. 9, p.154 (1963).

Reith, T., Renken, S., and Istael, B.A., "Gas Holdup and Axial Mixing in the Fluid Phase of Bubble Columns", Chem. Eng. Sci., Vol. 23, p. 619 (1968).

Riba, J.P., Routie, R., and Couderc, J.P., "Mass transfer from a fixed sphere to a liquid in a fluidized bed", in "Fluidizaion", Ed. Davidson, J.F., Keairns, D.L., Cambridge Univ. Press, Cambbridge, England, (1978).

Rice, R., J.M.I. Tupperainen, and R.M. Hedge, "Dispersion and Holdup in Bubble Columns, Comparison of Rigid and Flexible Spargers", Can. J. of Chem. Eng., Vol. 59, p. 677- 87 (1981).

Rice, R.G., Littlefield, M.R., "Dispersion Coefficients for Ideal Bubbly Flow in Truly Vertical Bubble Columns", Chem. Eng. Sci., Vol. 42, p. 2045-53 (1987).

Richardson, J.F. and Zaki, W.N., "Sedimentation and fluidization part 1. Trans. Ins. Chem. Engrs., Vol.32, p.35, (1954).

Richardson, J.F., and Da St. Jeronimo, M.A., "Velocity-Voidage Relations for Sedimentation and Fluidization", Chem. Eng. Sci., Vol. 34, p. 1419 (1979).

Rigby, G.R., Van Blockland, G.P., Park, W.H., and Capes, "Properties of Bubbles in Three-Phase Bed as Measured by an Electroresistivity Probe," Chem. Eng. Sci., Vol.25, p.1729, (1970a).

Rigby, G.R., and Capes, C.E., "Bed Expansion and Bubble Wakes in Three-Phase Fluidization", Can. J. Chem. Eng. Vol. 48, p.343 (1970b).

Rowe, P.N., and Claxton, K.T., " Heat and mass transfer from a single sphere to fluid flowing through an array", Trans. Inst. Chem. Engrs., Vol.43, p.T321, (1965).

Ruchti, G., Dunn, I.J. and Bourne, J.R., "Practical Guidelines for the Determination of Oxygen Transfer

Coefficient ($k_l a$) with the sulfite oxidation Method", The Chem. Eng. J. Vol 30, p. 29-38, (1985).

Saberian-Broudjenni, M., "Contribution a l'etude de l'hydrodynamique des reacteurs fluidise a troia phases : gas-liquide-solide" Ph. D. Thesis, Docteur Ingenieur, INPL, Nancy, France, (1984).

Saberian-Broudjenni, M., " Les reacteurs a lit fluidise gaz-liquide-solide: Hydrodynamique des ecoulements et transfert de chalcur a la paroi en milieu liquide organique", Docteur-Ingenieur thesis INPL, Nancy, France, (1985).

Sada,E., H.Kumazawa, C.Lee, and N. Fujiwara, "Gas-Liquid Mass Transfer Characteristics in a Bubble Column with Suspended Sparingly Soluble Fine Particles", Ind. Eng. Chem. Proc. Des. Dev., Vol. 21, p. 255-61 (1985).

Sada, E., H. Kumazawa, and C.H.Lee, "Influence of Suspended Fine Particles on Gas Holdup and Mass Transfer Characteristics in a Slurry Bubble Column", AIChE J., Vol. 32, p. 853-56 (1986).

Sagert, N.H., Quinn, M.J., "The Coalescence of Gas Bubbles in Dilute Aqueous Solutions ", Chem. Eng. Sci., Vol. 33, p. 1087-95 (1978).

Sänger, P. and Deckwer, W.D., "Liquid-solid mass transfer in aerated suspensions", Chem. Eng. J., Vol.22, p.179 (1981).

Sano, Y., Yamaguchi, N,. Adachi, T. "Mass transfer coefficients for suspended particles in agitated vessels and bubble columns", J. Chem. Eng. Japan, Vol. 7, p.255, (1974).

Satterfield, C.N., Vanelk, M.W., Bliss, G.S., "Liquid-solid mass transfer in packed beds with downflow cocurrent gas-liquid flow", AIChE, J., Vol.4, p.709, (1978).

Sauer, T., Hempel, D.C., "Fluid Dynamics and Mass Transfer in a Bubble Column with Suspended particles", Chem. Eng. Technol., Vol. 10, p. 180-9 (1987).

Saxena, S.C., and Vogel, G.J., "Trans. Inst. Chem. Eng., Vol. 55, p. 184 (1977).

Schügerl, K., Lucke, J., and Oels, U., "Bubble Column Bioreactors" Adv. Biochem. Eng., ed., T.K. Ghose, A. Fiechter and N. Blakeborogh, Vol. 7, p. 1-84, (1977).

Schumpe, A., and Deckwer, W.D., Chem. Ing. Technik, Vol. 50, p. 630 (1978) as quoted in Schumpe and Deckwer (1980).

Schumpe, A., and Deckwer, W.D., "Analysis of Chemical Methods for Determination of Interfacial Areas in Gas-in-Liquid Dispersions with Non-uniform Bubble Sizes", Chem. Eng. Sci., Vol. 35, p. 2221-33 (1980).

Schumpe, A., and W.D. Deckwer,"Gas Holdups, Specific Interfacial Areas and Mass Transfer Coefficients of Aerated Carboxy Methyl Cellulose Solutions in a bubble Column", Ind. Eng. Chem. Proc. Des. Dev., Vol. 21, p. 706-11 (1982).

Schumpe, A., and Grund, G., "The Gas Disengagement Technique for Studying Gas Holdup Structure in Bubble Columns", The Can. J. of Chem. Eng., Vol. 64, p. 891-96, (1986).

Schumpe, A., A.K. Saxena, K.D.P. Nigam, "Gas-Liquid Mass Transfer in a Bubble Column with Suspended Nonwettable Solids", AIChE J., Vol. 33, p. 1916-20 (1987).

Schutz, G., "Natural Convection Mass Transfer Measurements on Spheres and Horizontal Cylinders by an Electrochemical Method", Int. J. Heat and Mass Transfer, Vol.6, p.873, (1963).

Sedahmed, G.H., "Electrochemical Mass Transfer at a Fixed Bed of Spheres Under Forced Convection Induced by Counterelectrode Gas Bubbles", Can. J. of Chem. Eng., Vol. 64, P.75 (1986).

Sedelies, A., Steiff, A., Weinspach, P.M., "Mass Transfer Area in Different Gas-Liquid Reactors as a Function of Liquid Properties", Chem. Eng. Technol., Vol. 10, p. 1-15 (1987).

Selman, J.R., and Tobias, C.W., "Mass Transfer Measurements by the Limiting Current Technique", Advances in Chem. Eng., Vol.10, p. 211 Academic Press (1978).

Shah, Y.T., Stiegel, G.J., and Sharma, M.M., "Backmixing in Gas-Liquid-Solid Reactors", AIChE J., Vol. 24, p. 369 (1978).

Shah, Y.T., "Gas-liquid-solid reactor design", McGraw Hill, New York, (1979).

Shah, Y.Y., Kelkar, B.G., Godbole, S.P. and Deckwer, W.D., "Design Parameters Estimations for Bubble Column Reactors", AIChE J. Vol. 28, No. 3, p.353-79, (1982).

Shah, Y.T., S. Joseph, D.N. Smith and J.A. Ruether, "On the Behavior of the Gas Phase in a Bubble Column with Ethanol-Water Mixture", Ind. Eng. Chem. Proc. Des. Dev., Vol. 24, p. 1140-48 (1985).

Sharma, M.M., and Mashelkar, R.R., "Absorption with Reaction in Bubble Columns", Instn. Chem. Engrs. Symp. Ser., Vol. 28, p. 10 (1968).

Sharma, M.M., and Danckwerts, P.V., "Chemical Methods of Measuring Interfacial Area and Mass Transfer Coefficients in Two Fluid Systems", Brit. Chem. Eng., Vol. 15, p. 522 (1970).

Shen, G.C., Geankoplis, C.J., and Brodkey, R.S., "A Note on Particle-Liquid Mass Transfer in a Fluidized Bed of Small Irregular Shaped Benzoic Acid Particles", Chem. Eng. Sci., Vol. 40, p.1797 (1985).

Sigrist, L., O. Dossenbach and N.Ibl," Mass Transport in Electrolytic Cells with Gas Sparging", Int. J. Heat and Mass Transfer, Vol. 22, p.1393-99 (1979).

Sisak, C., and Ormos, ., "Investigation of Three-Phase Fluidized Systems II. The Effect of Distributor Type and Flow Conditions on the Parameters of Bubble Size Distribution", Hungarian Journal of Industrial Chemistry, Vol. 13, p. 503-19 (1985).

Snider , J.W., Perona, J.J., "Mass Transfer in Fixed Bed Gas Liquid Catalytic Reactor with Cocurrent Upflow", AIChE, J., Vol.6, p.1172, (1974).

Soung, W.Y., "Bed Expansion in Three-Phase Fluidization", Ind. Eng. Chem. Proc. Des. Dev., Vol. 17, p.33 (1978).

Specchia, V., Baldi, G. and Gianetto, A., "Solid-liquid Mass Transfer in Cocurrent Two-phase Flow Through Packed Beds", Ind. Eng. Chem. Process Des. Dev., Vol.17, p.362, (1978).

Sridhar, T., and Potter, O.E., "Interfacial Areas in Gas-Liquid Stirred Vessels", Chem. Eng. Sci., Vol. 35, p. 683-95 (1980).

Srirar, K., and Mann, R., "Dynamic Gas Disengagement A New Technique for Assessing the Behavior of Bubble Columns", Chem. Eng. Sci., Vol. 32, p. 571-80 (1977).

Stephen, H., and Stephen, T., "Solubilities of Inorganic and Organic Compounds", Vol. 1, Binary Systems Part 1, The Macmillan Company, New York (1963).

Stewart, P.S.B., and Davidson, J.F., "Three-Phase Fluidization: Water, Particles and Air", Chem. Eng. Sci., Vol.19, p.33 (1964).

Strimulo, C., Kudra, T. "Interfacial Area in Three-

Phase Fluidized Beds", Chem. eng. Sci., Vol. 32, p.229, (1977).

St. Dennis, C.E., and Fell, C.J.D., "Diffusivity of Oxygen in Water', Can. J. Chem. Engng. Vol. 49, p.885,(1971).

Steel, L.R., Geankoplis, C.J., "Mass Transfer from a Solid Sphere to Water in Highly Turbulent Flow", AIChE J., Vol. 5, p.178 (1959).

Steinberger, R.L. and Treybal, R.E., "Mass Transfer from a Solid Soluble Sphere to a Flowing Liquid Stream", AICHE J., Vol. 6, p.227-32 (1960)

Sun, Y., Nozawa, T. and Furusaki, S., "Gas Holdup and Volumetric Oxygen Transfer Coefficient in a Three-Phase Fluidized Bed Bioreactor", J. of Chem. Eng. of Japan, Vol.21, p.15-20, (1988).

Sutey, A.M. and Knudsen, G.J., "Effect of Dissolved Oxygen on the Redox Method for Measurement of Mass Transport Coefficients", Ind. Eng. Chem. Fund. Vol. 6, p.132-(1967).

Sutton,P.M., Shieh, W.K., Kos, P., Dunning, P.R., in "Biological Fluidized Bed Treatment of Water and Wastewater" P.F.Cooper and B. Atkinson, Eds., Ellis-Horwood, Chichester, p. 285 (1981).

Sylvester, N.D., Pitayagulson, P. " Mass Transfer for Two-Phase- Cocurrent Downflow in a Packed Bed', Ind. Eng. Chem. Process Des. Dev., Vol.14, p.421, (1975)

Tan, C.S., and Smith, J.M., "A Dynamic Method for Liquid-Particle Mass Transfer in Trickle Beds", AIChE J., Vol. 28, p.190 (1982).

Taweel, A.M., R.Divakarla and H.G. Gomma, "Measurement of Large Gas-Liquid Interfacial Areas", Can. J. of Chem. Eng., Vol. 62, p. 73-77 (1984).

Teng Jyh-Tong, "Experimental and Theoretical Studies in Convective Transport", Ph.D. Thesis, University of California, Berkley, U.S.A. (1978).

Thomas, W.J., and Adams, M.J., Trans. Faraday Soc., Vol. 61, p. 668 (1965).

Ting, J.T., and Drinkenburg, A.A.H., "The Influence of Slight Departures from Vertical Alignment on Liquid Dispersion and Gas Holdup in a Bubble Column", Chem. Eng. Sci., Vol. 41, p. 165- 69 (1986).

Tosyali, U.C. and Uysal, B.Z., "Chemical Reactor Design and Technology" Ed. H.I. de Lasa, Martinus Nijhoff Publishers, Boston, p.393-410 (1986).

Tournie. P., Laguerie, C., Couderc, J.P., "Mass Transfer in a Liquid Fluidized Bed at Low Reynolds Numbers, Chem. Eng. Sci., Vol.32, p.1259, (1977).

Towell, G.D., Strand, C.P., and Ackerman, G.H., "Mixing and Mass Transfer in Large Diameter Bubble Columns", AIChE- Inst. Chem. Eng. Symp. Ser., No. 10, p. 10-97 (1965).

Towell, G.D., Ackermann, G.H., "Axial Mixing of Liquid and Gas in Large Bubble Reactor", Proceeding of the Fifth European/Second International Symposium on Chemical Reaction Engineering, B3-1, Amsterdam, Elsevier, (1972).

Tsuge, H., and Hibino, S., "Bubble Formation From a Submerged Single Orifice, Accompanied by Pressure Fluctuations in Gas Chamber", J. Chem. Eng. Jpn., Vol 11, p.173 (1978).

Tsuge, H., "Hydrodynamics of Bubble Formation from Submerged Orifices", in Encyclopedia of Fluid Mechanics", Cheremisinoff, N.P. editor, Gulf Publish. Co., Vo. 3, p. 191-232 (1986).

Hu, T.H., Ying, Z., Hsuehmin, C.,Baotien, Y., and Yiping, W.,"A Study of Holdup and Liquid Mixing in a Three-Phase Fluidized Bed", in "Fluidization 85" Eds. Kwank, M., Kunii, D., Science Press Beijing China, Elsevier, Amsterdam, p.262 (1985).

Tucker, R.F., and Wragg, A.A., "Simulation of Heat Transfer to Horizontal Tubes in a Fluidized Bed Using the Electrochemical Mass Transfer Modelling Technique", Heat and Mass transfer in Fixed and Fluidized Beds", eds. Vanswaaj, W.P.M., Afgan, N.H., Hemisphere p.589 (1986).

Turner, J.C.R., "On Bubble Flow in Liquids in Fluidized Beds", Chem. Eng. Sci., Vol. 21, p. 971-74, (1966).

Turner, R., "Fluidization in the Petroleum Industry", Fluidization, Soc. Chem. Ind., London, 47 (1964).

Turner, J.C.R., "Two Phase Conductivity. The Electrical Conductance of Liquid-Fluidized Beds of Spheres", Chem. Eng. Sci., Vol. 31, p. 487-92 (1976).

Ueyama, K., Morooka, S., Koide, K., kaji, H., Miyauchi, T., "Behavior of Gas Bubbles in Bubble Columns", Ind. Eng. Proc. Des. Dev., Vol. 19, p. 592-99 (1980).

Upadhyay, S.N. and Tripathi, G., "Mass Transfer in Fixed and Fluidized Beds", J. Scient. Ind. Res. Vol. 34, p. 10-35, (1975).

Urua, I.J., and M.C.G. Del Cerro,"Measurement of Large Gas-Liquid Interfacial Areas by the Light Transmission Method", Can. J. of Chem. Eng., Vol. 665, p. 565-69 (1987).

Vail, Yu.K., Manokov, N.K., and Manshilin, V.V., "The Gas Contents of Three-Phase Fluidized Beds", Int. Chem. Eng., Vol. 10, p.204 (1970).

Vanadurongwan, V., Laguerie, C., and Couderc, J.P., "Influence des properties physiques sur le transport de matiere en fluidisation liquide", Chem. Eng. J. 12, 29,(1976).

Van Krevelen, D.W., and Hoftijzer, P.J., Chem. Eng. Prog., Vol. 46, p. 29, (1950).

Vasalos, I.A. Bild, E.M., Rundell, D.N. and Tatterson, D.R., "Experimental Techniques for Studying Fluid Dynamics of H-coal Reactor", Coal Processing Technology, CEP Technical Manual Vol. 6, p. 226 (1980).

Vasalos, I.A., et al., "Holdup Correlations in Slurry-Solid Fluidized Beds", AICHE J., Vol. 28, p.346 (1982).

Venkatasubramanian, K., and Karkare, S.B., in "Immobilized Cells and Organelles", B.Mattiasson, Ed. CRC Press Inc. II (1983).

Viswanathan, S., Kakar, A.S., Murti, P.S., "Effects of Dispersing Bubbles into Liquid Fluidized Beds on Heat Transfer Holdup at Constant Bed Expansion", Chem. Eng. Sci., Vol. 20, p.903 (1964)

Viswanathan, K., D.S. Rao, "Inviscid Liquid Circulation in Bubble Columns", Chem. Eng. Commun., Vol. 25, p. 133-55 (1984).

Vivian, J.E., and King, C.J., "Diffusivities of Slightly Soluble Gases in Water", AIChE J., Vol. 10, p. 220 (1964).

Voigt, J., and K. Schuegerl,"Absorption of Oxygen in Cocurrent Multistage Bubble Columns-1",Chem. Eng. Sci., Vol. 34, p. 1221-29 (1979).

Volpicelli, G., and Massimilla, L., "Three-phase Fluidized Bed Reactors : An Application to the Production of Calcium Bisulphite Acid Solution', Chem. Eng. Sci., Vol. 25,p.1361,(1970).

Voyer, R.D., and Miller, A.I., "Improved Gas-Liquid Contacting in Co-current Flow", Can. J. Chem. Eng., Vol. 40, p. 335 (1968).

Wachi, S., Morikawa, H., and Ueyama, K., "Gas Holdup and Axial Dispersion in Gas-Liquid Co-current Bubble Column", J. of Chem. Eng. of Japan, Vol. 20, p. 309-16 (1987).

Wallis, G.B., "One Dimensional Two Phase Flow", New York: McGraw Hill, (1969).

Walter, J.F., and N.W. Blanch,"Bubble Breakup in Gas-Liquid Bioreactors: Breakup in Turbulent Flow", The Chem. Eng. J., Vol. 32, p. b7-17 (1986).

Wassan, D.T., Lynch, M.A., Chad, K.J., Srinivasan, N., "Mass Transfer Into Dilute Polymeric Solutions", AIChE J., Vol. 18,p.928, (1972).

Weiland, P.,L. Brentrup, U.Onken," Measurement of Bubble Size Distribution in Fermentation Media Using a Photoelectric Probe", Ger. Chem. Eng., Vol. 3, p. 296-302 (1980).

Wen, C.Y., and Yu, U.H., "A Generalized Method for Predicting the Minimum Fluidization Velocity", AIChE J., Vol. 12, p.610 (1966).

Wendt, R., Steiff, A., and Weinspach, P.M., "Liquid Phase Dispersion in Bubble Columns", Ger. Chem. Eng., Vol. 7, p. 267-73 (1984).

Whitman, W.G., Chem. and Met Eng. 29, p.147, - as quoted in Skelland, A.H., 1974 p. 95.

Wild, G, et al., "Les reacteurs a lits fluidises gaz-liquide solide Etat de la et perspectives indutrieles", Entropie No 106 (1982).

Wild, G., Saberian, M., Schwartz, J-L, Charpentier, J-C., "Gas-liquid-solid Fluidized Bed Reactors. State of the Art and Industrial Possibilities", Int. Chem. Eng., Vol. 24,p.639 (1984).

Wild, G., Saberian-Broudjenni, M. and Chaepentier, C., "The Hydrodynamics of Gas-Liquid-Solid Fluidized Beds: The Bubble Wake Model Revisited", in Recent Trends in Chemical Reacion Engineering Eds. B.D. Kulkarni, M.A. Mashelkar and M.M. Sharma, Wiley Eastern Ltd., New Delhi (1987).

Wilson, E.J., and Geankoplis, C.J., "Liquid Mass Transfer at Very Low Reynolds Numbers in Packed Beds", Ind. Engng. Chem. Fundamentals, Vol. 5, p. 9-14 (1966).

Winstein, B., and Treybal, R.E., "Liquid-Liquid Contacting in Unbaffled Agitated Vessels", AIChE J., Vol. 19, p. 304 (1973).

Wolff, C., F.U. Briegleb, J. Bader, K. Hektor and H. Hammer,"Measurements with Multipoint Microprobes", Chem. Eng. Technol., Vol. 13, p. 172-80 (1990).

Yamashita, F. and Inoue, H., "Gas Holdup in Bubble Columns", J. of Chem. Eng. of Japan, Vol. 8, p. 334-36 (1975).

Yamashita, F., Mori, Y., and Fujita, S., "Sizes and Size Distributions of Bubbles in a Bubble Column", J. of Chem. Eng. Japan, Vol. 12, p. 5 (1979).

Yashunishi, A., Fukuma, M., and Muroyama, K., "Kagaku Kogaku Ronbunshu (1986)"- as quoted in Fan et al. (1987).

Yoshida, F., and Akita, K., "Performance of Gas Bubble Columns: Volumetric Liquid-Phase Mass Transfer Coefficient and Gas Holdup", AIChE J., Vol. 11, p. 9 (1965).

Zehner, P.,"Momentum Mass and Heat Transfer in Bubble Columns Part 2. Axial Blending and Heat Transfer", Int. Chem. Eng., Vol. 26, No. 1, p. 29-35 (1986).

Zieminski, S., Caron, M.M., and Blackmore, R.B., "Behavior of Air Bubbles in Dilute Aqueous Solutions", I & EC Fundamentals, Vol. 6, p. 233-42 (1967).

Zlokarnik, M., "Bioengineering Aspects of Aerobic Waste Water Purifications", Ger. Chem. Eng., Vol. 6, p. 183-97 (1983).

Zuber, N. and Findlay, J.A., "Average Volumetric Concentration in Two Phase Systems", Transactions American Society of Mechanical Engineering, Journal of Heat Transfer, Vol. 87, p. 453-67 (1963).